Joint Trajectory Generation and High-level Control for Patient-tailored Robotic Gait Rehabilitation

Santiago Focke Martínez

Universität Bremen 2017

Joint Trajectory Generation and High-level Control for Patient-tailored Robotic Gait Rehabilitation

Vom Fachbereich für Physik und Elektrotechnik
der Universität Bremen

zur Erlangung des akademischen Grades

Doktor–Ingenieur (Dr.-Ing.)

genehmigte Dissertation

von

MSc. Santiago Focke Martinez

aus Kolumbien

Referent:	Prof. Dr.-Ing. Axel Gräser
Korreferent:	Prof. Dr.-Ing. Udo Frese
Eingereicht am:	21. Februar 2017
Tag des Promotionskolloquiums:	23. Mai 2017

To my family, especially my mom and dad who, with their love and values, helped to forge the person that I am today, and Pita for being the foundation of this great family and an exemplary role model.

Para mi familia, especialmente mi mama y mi papa que con su amor y sus valores ayudaron a forjar la persona que soy hoy en día, y Pita por ser el cimiento de esta gran familia y un claro ejemplo de vida.

Acknowledgement

First of all I would like to thank Prof. Axel Graeser for giving me the opportunity to carry out my PhD studies and for his guidance and support during my years in the Institute of Automation (IAT). I would also like to thank Prof. Udo Frese for being the second reviewer of my dissertation, as well as Prof. Walter Lang and Prof. Walter Anheier for being my examiners.

I would like to express my special appreciation and gratitude to three of my IAT colleagues. First, to Dr. Olena Kuzmicheva for her constant and overwhelming assistance during my research, which include the review of most of my publications (including this dissertation) and the corresponding feedback. Second, to Dr. Danijela Ristic-Durrant for all her support and valuable feedback during my master's and doctoral studies. And finally, to Mr. Ulrich Krebs who, together with Dr. Kuzmicheva, was of constant help during the course of the *MOPASS* project.

I would also like to thank all the colleagues and ex-colleagues who, one way or the other, helped me during my years in the institute, especially Dr. Henning Kampe for his everlasting willingness to assist when facing programming-related difficulties, Dr. Sinisa Slavnic for his support during my master's thesis and first years of research, Mr. Michael Ehlen and Mr. Asis Niaz for their miscellaneous technical assistance, and Ms. Maren Hoffman for her help related to administrative and organization issues.

Moreover, I would like to thank all the technical and clinical partners that were involved in the *MOPASS* project, and all the people who took part in the experiments and testing of the *MOPASS* system. My thanks go as well to the Postgraduate International Programme (PIP) in Physics and Electrical Engineering from the University of Bremen for partially funding my participation in conferences.

Last but not least, I would like to thank all the people who stood by my side during this process. First and foremost, my family in Colombia (all four generations) for all their support and for always being there for me despite the distance. My mom and dad, for all the unconditional love, encouragement and self-sacrifice. My sister, for taking care of my parents and filling the hole I left in pursuit of my goals. And my grandmother, for her everlasting love and for all she represents; there are not enough words to thank for all she has given to this family and to the people surrounding her. I want to thank also Melora for her support, company and patience during this journey; and all my close friends in Colombia and Germany.

23. May 2017, Bremen *Santiago Focke Martinez*

Kurzfassung

In den vergangenen zwei Jahrzehnten haben Forscher verschiedene Robotersysteme entwickelt, um die Gangrehabilitation von Menschen zu verbessern, deren Gang aus medizinischen Gründen beeinträchtigt ist. Zu der Zielgruppe gehören Schlaganfallpatienten sowie Patienten unterschiedlichen Alters, die unter zerebralen Lähmungen, traumatischen Hirnverletzungen, Rückenmarksverletzungen und Multipler Sklerose leiden. Die Entwicklung dieser Art von Geräten wurde durch die offensichtlichen Vorteile der robotergestützten Rehabilitation gegenüber der traditionellen manuellen Therapie vorangetrieben, denn Robotersysteme sind in der Lage, das Bewegungstraining intensiv, präzise und reproduzierbar durchzuführen.

Es ist allerdings noch nicht ausreichend erforscht, wie genau diese Geräte eingesetzt werden müssen, um die bestmöglichen Rehabilitationsergebnisse zu erzielen. Es wurden bereits zahlreiche unterschiedliche Strategien zur Bestimmung des Unterstützungsgrads und des vom System zu verwendenden Referenzgangmuster vorgestellt, die sich an den aktuellen Therapiemodellen wie z.B. „*Assist as Needed*“ („Bedarfsgerechte Unterstützung“) orientieren. Allerdings schränken die meisten dieser Strategien die Einbindung der Therapeuten in die Therapieplanung stark ein. Die spezifischen Bedürfnisse und Einschränkungen der Patienten bleiben bei der Parametrierung der robotergestützten Therapie oftmals unberücksichtigt, was aber die Effektivität des Rehabilitationsprozesses mindert.

Die vorliegende Dissertation stellt eine Reihe von neuartigen Methoden für die roboterbasierte Gangrehabilitation vor, die mit dem Ziel entwickelt wurden, ausgehend vom spezifischen Zustand des Patienten stärker individualisierte Therapien anzubieten und hierdurch die gesamte Rehabilitationserfahrung sowohl für den Patienten als auch für den Therapeuten zu verbessern. Das erste Verfahren umfasst die Erzeugung und Anpassung von Trajektorien für Hüft- und Kniegelenke auf der Basis von gesunden Gangmustern. Die hier vorgeschlagene neuartige Methode zur Gangmustererzeugung ermöglicht es dem Therapeuten, die vom System für die Regelung herangezogenen Referenztrajektorien durch einfache grafische Manipulation der Gangkurven anzupassen, um somit die speziellen Bedürfnisse und Einschränkungen des Patienten besser berücksichtigen zu können.

Die zweite Gruppe von Methoden umfasst die Bewegungsregelung und die Synchronisation zwischen Roboter und Patient. Zunächst werden einige Strategien für die Bewegungsregelung vorgestellt, die für das mobile robotergestützte Gangrehabilitationssystem *MOPASS* entwickelt wurden. Das System *MOPASS* besteht aus einer mobilen Plattform, einer aktuierten Orthese mit aktiven Hüft- und Kniegelenken und einem Mechanismus zur aktiven Unterstützung des Beckens. Zu den vorgestellten Regelungsstrategien gehören die Bewegungsregelung für die Hüft- und Kniegelenke (sowohl der im *MOPASS* – System umgesetzte Positionsregler als auch der vorgeschlagene „*Assist as Needed*“-Impedanzregler), sowie die Bewegungssteuerung für die mobile Basis und den Beckenantrieb. Die Bewegungsregelung wird durch eine Reihe von Methoden zur Synchronisation zwischen dem Roboter und dem Patienten ergänzt. Probleme bei der Synchronisation zwischen dem vorgegebenen Referenzgangmuster und dem tatsächlichen Gangmuster des Patienten sind allen robotergestützten Gangrehabilitationssystemen inhärent, die sich nachgiebig verhalten und eine Abweichung von den Referenztrajektorien zulassen. Die vorgeschlagenen Methoden umfassen zwei Synchronisationsansätze sowie einen Algorithmus zur Online-Adaption der

Hüfttrajektorien, der obstruktive Kräfte während der Therapie mit nachgiebigen Robotersystemen reduziert.

Zum Schluss wird eine prototypische Umsetzung einer grafischen Benutzeroberfläche (Graphical User Interface – GUI) vorgestellt. Diese implementiert die neuartigen Funktionalitäten zur Erzeugung und Anpassung von Hüft- und Knietrajektorien, die vorgeschlagene Methode zur Anpassung des Unterstützungsgrades sowie andere Funktionalitäten, die sich speziell auf den Betrieb des *MOPASS*-Systems beziehen.

Zusätzlich zu den vorgeschlagenen neuartigen Methoden gibt die vorliegende Dissertation eine Übersicht über gesundes und pathologisches Gehen sowie eine Aufstellung der wichtigsten Gangrehabilitationsgeräte, um dem Leser die zu bewältigenden Herausforderungen der robotergestützten Gangrehabilitation zu verdeutlichen. Daneben werden detaillierte Informationen über das *MOPASS*-System präsentiert, einschließlich der mechanischen Konstruktion und Architektur.

Abstract

During the past two decades researches have been developing several robotic systems meant to improve the gait rehabilitation of people who are impaired in their lower limbs due to a medical condition. Target patients include stroke survivors and people who have suffered cerebral palsy, traumatic brain injury, spinal cord injury and multiple sclerosis, among other conditions, ranging from children to elderlies. The development of this kind of devices has been made thanks to the evident advantages of robotic systems over traditional, manual therapy approaches. Robotic systems are able to perform motion training in an intensive, precise, repetitive and reproducible way.

However, it is not yet clear what the most efficient way to utilize these devices is, in order to maximize the rehabilitation outcome. Several strategies to determine the level of assistance given by the robotic system to the patient and to set the reference walking patterns used by the system's controllers have been presented widely, following current therapy paradigms such as 'assist as needed'. Nevertheless, most of the current strategies limit the involvement of the therapist in the decision making and do not take into account the specific needs of the patients during the setting of the robot-assisted therapy, which would increase the effectiveness of the rehabilitation process.

This dissertation presents a group of novel methods for robot-based gait rehabilitation, which were developed with the objective of offering more individualized therapies based on the specific condition of each patient, aiming as well to improve the overall rehabilitation experience for both patient and therapist. The first method involves the generation and adaptation of hip and knee joint trajectories based on healthy walking patterns. The proposed novel methodology for gait pattern generation allows the therapist to easily and graphically adapt the reference trajectories, used by the system's controllers, in order to fit better the patient's needs and disabilities.

A second set of methods involving motion control and robot-patient synchronization is also presented. First, some strategies for the motion control are introduced, which were developed for the *MOPASS* system, a robotic device for over-ground gait rehabilitation consisting of a mobile platform, an actuated orthosis with active hip and knee joints, and a mechanism for active pelvic assistance. The presented control strategies include the motion controllers for the hip and knee actuated joints (namely a position controller implemented in the *MOPASS* system and a proposed impedance-based 'assist as needed' controller), as well as the motion controllers of the mobile platform and the pelvic mechanism. The motion control is complemented with a set of robot-patient synchronization methods. Problems regarding the synchronization between the reference gait pattern and the actual gait pattern of the patient are inherent of robotic gait rehabilitation systems that possess a compliant behavior which allows the patient to deviate from the reference trajectories. The proposed methods introduce two synchronization approaches, as well as an online hip trajectory adaptation algorithm developed to reduce obstructive forces during therapy with compliant robotic systems.

Finally, a prototype graphical user interface (GUI) is also presented, which implements the functionalities offered to the therapist including the hip and knee trajectories' generation and adaptation, a proposed method for the adjustment of support levels, and other functionalities specifically related to the operation of the *MOPASS* system.

Additional to the high-level methods, this dissertation includes also an overview of healthy and pathological walking to help the reader understand the problems faced by robot-based gait rehabilitation, as well as a summary of the most relevant state-of-the-art devices developed for gait rehabilitation. It presents as well detailed information about the *MOPASS* system, including the mechanical design and architecture.

Table of contents

1 Introduction

Physical impairment on adults and children is a health issue well known worldwide with millions of reported cases. The impairment in an affected person may include the inability to generate optimal motor response of the lower limbs to perform daily actions such as stand up/sit down, and walk. These physical disabilities can be caused by several medical conditions, including congenital diseases and injuries inflicted during the lifetime. Among the causes one can find strokes (or cerebrovascular accidents - CVA), cerebral palsy (CP), traumatic brain injuries (TBI), spinal cord injuries (SCI), multiple sclerosis (MS), and other different physical injuries that lead to the necessity of physical therapy to regain the motor skills, including falls, sport and car crash injuries, among others. These conditions are of big concern for physicians and researchers all around the world, showing considerable numbers of occurrence. There were over 15 million estimated cases of Stroke in 2010 worldwide, with prevalence of around 33 million [1], being the leading cause of acquired disability in adults [2]. The prevalence of cerebral palsy lies around 3 to 4 per 1000 live-births in the United States marked by a reduction of the mortality of children with CP result of improvements in obstetric and neonatal care, leading CP to be the most common motor disability in childhood [3]. Although population-based statistics for traumatic brain injury have been difficult to gather [4], the incidence rates in Europe are calculated to be around 235 per 100,000 inhabitants per year [5], whereas in the United States around 1.7 million people suffer a TBI every year from which 275,000 are hospitalized [6], making TBI a leading cause of death and disability for adolescents and young adults [7]. Spinal cord injury is another major cause of physical disability, where almost 300,000 people live with it only in United States and Canada, with a rate of new cases of around 11,000 per year, almost half of them resulting in incomplete SCI [8]. Multiple sclerosis affects approximately 350,000 individuals in the United States and around two million people around the world [9].

Due to the high incidence and prevalence rates of the aforementioned medical conditions, without disregarding other traumatic physical injuries that people may suffer on their daily lives or all the cases of prostheses holders (e.g. hip and knee replacement patients), researchers all over the world have been taking special attention on finding optimal treatments for the rehabilitation of the patients, including therapy approaches that can lead to a regain of the lost motor abilities or plausible enhancement of the ones that are left, improving therefore their lifestyle. This ideal is supported by several laws and statements such as the article 26 of the Convention on the Rights of Persons with Disabilities from the United Nations, which declares that “States Parties shall take effective and appropriate measures, including through peer support, to enable persons with disabilities to attain and maintain maximum independence, full physical, mental, social and vocational ability, and full inclusion and participation in all aspects of life” [10].

Moreover, since walking is one of the functionalities typically affected by these conditions and it influences directly the quality of life of people, many efforts have been put into gait rehabilitation. In stroke survivors, for instance, improving walking with respect to safety and speed is a major goal [11]. Independent walking is often a major objective after moderate to severe TBI [7]. In pediatric rehabilitation the goals are focused on the restoration of previous levels of ability and facilitation of the development of functionalities, including walking [12]. Consumer-based studies have reported that incomplete SCI patients consider the restoration of walking to be fundamental in the level of quality of life making it one of the ultimate goals of rehabilitation and hence making gait improvement a very important aspect in this population [13]. Studies on the impact of Multiple sclerosis have also reported that that

walking impairment is one of the most impactful symptoms on the quality of life of both patients and care partners [14].

There is no discussion that walking impairments affect the quality of life of the people suffering them and hindrance their day-to-day interaction with society. For instance, significantly decreased walking speed is one of the common manifestations present in pathological walking. It has been suggested that walking speeds over 0.80 m/s are necessary for effective community ambulation (e.g. to timely cross the street) [11], which normally is considerably higher than the walking speed in people whose gait is impaired (e.g. the preferred speed of chronic stroke patients ranges between 0.1m/s and 0.76 m/s [11]). Hence, the regain of normal walking speeds is a major goal in rehabilitation.

It is clear that efficient gait rehabilitation strategies are needed to increase the recovery level on the patients. Some of the therapy approaches nowadays include (and in some cases combine) functional electric stimulation (FES), muscle strength training, neuro-stimulation, mental imagery, task-oriented therapy, over-ground gait training, treadmill gait training, body-weight supported gait training, active and passive lower limb orthosis (e.g. knee-ankle-foot orthosis), constraint-induced movement therapy (CIMT), and virtual reality [11] [12] [15] [16]. In the last two decades, robot-based rehabilitation has emerged as an alternative strategy in gait rehabilitation thanks to the evident advantages of robotic systems over traditional, manual therapy approaches. Robotic systems are able to perform motion training in an intensive, repetitive and reproducible way. In conditions such as post-stroke and SCI, treatments focused on high-intensity and repetitive task-specific practices have shown promising results in the improvement of motor recovery [8] [17] [18]. These facts corroborate the idea that robot-based systems may improve significantly the recovery process of impaired patients. Moreover, robotic rehabilitation enables parameterized active, assistive, and resistive exercises, and facilitates the patient assessment process thanks to the feedback they offer (e.g. level of assistance used during training or actual trajectories of the joints). Additionally, robotic systems are not restricted by the physical limitations of the therapists and reduce the number of therapist needed for each training session, easing the therapists' job on the way.

Several devices have been designed throughout the last years [19] aiming to identify the most efficient way to conduct therapy and improve the rehabilitation outcomes. Many designs and control strategies have been developed and tested with both healthy and impaired people. Several strategies to determine the level of assistance given by the robotic system to the patient and to set the reference walking patterns used by the system's controllers have been presented widely, following current therapy paradigms such as 'assist as needed'. However, to this date it is not yet clear what the best approach for robotic gait rehabilitation is. Moreover, despite the efforts, many of the state of the art systems tend to automate many of the processes and decision making related to the therapy, leading in many cases to training approaches that assist the patients in a rather general manner instead of in a patient-specific way. These general approaches are not in line with some concepts of optimal rehabilitation: there exists the necessity to develop training strategies that are oriented towards specific needs of both the patient and the care giver, implying that the rehabilitation interventions should be customizable and adaptable [15].

From the point of view of the author, one of the hindrances to patient-specific robot-based training is the exclusion of the therapist from the loop of decision making. In many cases, several of the therapy parameters are set automatically by the high-level components of the robotic systems (e.g. joint trajectory estimators and adjusters), while the tasks of the therapist are reduced to set some very general parameters (such as the desired training walking speed or the anthropometric characteristics of the patient) and to oversee the training sessions with the system. Bearing this in mind, the primary objective in this research was to

find a middle point in which we could make use of the advantages brought by robotic systems and their high-level intelligent components without disregarding the experience and valuable input from the therapists.

The research focus point selected to achieve this objective was the generation of reference trajectories that included the therapist in the parametrization process in a higher degree. The selection of correct therapy (reference) gait patterns is a crucial step towards gait recovery [15]; hence the trajectory generation is a key element in robot-based therapy. The novel trajectory generator presented in this dissertation was developed aiming to achieve "patient-tailored' therapy by meeting two objectives. The first one was to provide the therapist with 'healthy-like' joint trajectories automatically generated based on some desired gait parameters (e.g. walking speed or cadence) and on the patient's features (e.g. height). These healthy-like trajectories are estimated based on experimental studies on over-ground walking of healthy subjects, and are used by the therapist as reference templates of healthy gait patterns. The second objective was to allow the therapist to adapt these joint trajectories in an easy, intuitive and graphical manner in order to address the patient's specific needs. This adaptation is done through the adjustment of a set of points that highly influence the trajectories' profile (curve shape), such as the joints' maximum flexion and extension points (extrema). With the proposed trajectory generator, the therapist is able to train with the patient not only healthy walking, but also, if desired, compensatory patterns that could be beneficial to the patient and might lead to better rehabilitation outcomes (e.g. independent walking) which may not be reached by using healthy walking patterns as reference. The trajectory generator was implemented and tested in the *MOPASS* system [20], a robotic device for over-ground gait rehabilitation consisting of a mobile platform, an actuated orthosis with active hip and knee joints, and a mechanism for active pelvic assistance. Both the estimation of healthy like trajectories and handling of the trajectories based on the adaptations made by the therapist were included in the final implementation.

Additional to the trajectory generation, this dissertation also presents the motion control strategies developed for the *MOPASS* system. This subject includes the development of the motion controllers of the active joints of *MOPASS* (i.e. hip, knee, pelvis and wheels) which were used during the practical tests and the initial clinical trials of the robotic system. It also includes a proposed 'assist as needed' control approach (for future use), which is based on impedance-based control strategies that have been used with success in other state of the art systems. The objective of 'assist as needed' approaches is to assist the patients only when needed, depending on their actual performance, instead of using approaches such as fixed position controllers. The aim of the presented 'assist as needed' approach was to enhance current strategies towards a more patient-specific therapy by introducing easily adaptable levels of assistance.

The inclusion of 'assist as needed' and 'patient-cooperative' therapy strategies in robot-assisted gait rehabilitation leads to the need of compliant systems to allow the patient to move more freely during the training. Systems that possess a compliant behavior (achieved, for instance, by implementing impedance control without high stiffness) allow the patient to deviate from the reference trajectories and therefore to walk with a cadence and walking speed different from those set as reference ones for the therapy (for example, selected by the therapist). This leads to problems of synchronization between the system's reference gait pattern and actual patient's gait pattern. Hence, a set of methods were also developed to overcome this synchronization problems that are inherent to compliant robotic systems. The robot-patient motion synchronization methods proposed in this dissertation are based on strategies that have been used successfully in other systems, but were enhanced to tackle the synchronization problems in a more favorable and effective manner. The proposed methods

introduce two synchronization approaches: one that performs cyclic phase-compensation, calculated every time that a new gait cycle is detected, to reduce the phase difference between the reference and the actual gait patterns; and a second one based on a phase controller that performs continues phase-compensation throughout the complete gait cycle. An online hip trajectory adaptation algorithm is also part of the proposed synchronization methods, which was developed to reduce obstructive forces during therapy with compliant robotic systems.

Finally, a prototype graphical user interface (GUI) was developed to put together the concepts and functionalities developed during this work, including the trajectory generation and adaptation, and the setting of assistance levels. The GUI comprises all the developed functionalities and offers them to the therapist as a set of tools to provide patient-tailored therapy.

1.1 Chapters' outline

Chapter 2 makes an introduction to human gait. It includes the basics of human locomotion during the walking process, focusing mostly in the kinematics of the lower-body joints and the gait-related spatiotemporal parameters. It also includes a review on the abnormalities characterizing pathological walking, examining some of the impairments affecting specifically the aforementioned medical conditions (i.e. stroke, cerebral palsy, traumatic brain injury, spinal cord injury and multiple sclerosis).

Chapter 3 includes a detailed introduction to the state of the art systems used in gait rehabilitation, classifying them depending on its mechanical design and giving some general information about each one of them. It also presents the *MOPASS* system, including specifics on its mechanical design and control architecture.

Chapter 4 is dedicated to the generation of reference hip and knee joint trajectories. First, the state of the art related specifically to trajectory generation in robotic gait rehabilitation devices is presented. Afterwards, the concept for trajectory parametrization and generation developed in this work is presented, followed by the explanation of the estimation methods used to obtain healthy-like joint motion profiles, including the experimental setup used to obtain the data to train the estimators, the corresponding data processing, and the specifics of the estimators (including performance and error measurements). Finally the evaluation of the complete trajectory generation concept and implementation, including the limitations, is presented.

Chapter 5 includes the explanation of the motion control strategies used in *MOPASS*, namely the motion control of the hip, knee, wheels and pelvis modules. It also includes a proposed control strategy based on impedance models yet to be implemented and tested in the *MOPASS* system. Finally, it presents some methods developed to overcome problems of desynchronization between the reference gait patterns from the system and the actual gait pattern from the patient, which are common during gait training when using compliant systems.

Chapter 6 introduces the design of the graphical user interface (GUI). It makes a quick review of the functionalities of the GUI. Additionally, it includes a detailed explanation of three of the functionalities offered to the therapists for patient-tailored therapy adjustments, namely the advanced options for trajectory generation, the tools for assistance-level adaptations, and the adjustments of the reference trajectories following an online change of gait parameters.

Finally the conclusions and open topics for future work are presented.

1.2 Main contributions

The most important contribution of this work is related to the trajectory generation of hip and knee joints. It presents a novel approach for parametrization and regeneration of hip and knee angular-motion profiles, aiming to an easy graphical adaptation by the therapists. Thanks to the adaptation features offered by the developed trajectory generator, the therapist can adjust as desired the joint trajectories that are used as reference by the control components of the robotic system. This type of direct manual adaptation of the reference motion profiles of the active joints is not seen in other state of the art approaches[1]. Additionally, it presents a novel trajectories' adjustment method used during online adaptation of the gait parameters (i.e. cadence) which takes into account the initial settings of the therapists (i.e. the manually adjusted reference trajectories). This type of online trajectory adaptation is also not present in other state of the art systems[1]. The generator also includes the generation and adaptation of the trajectories of the initial step, which are normally not treated in literature. Finally, a novel method for advanced manual shaping of the joint motion profiles was also developed, which is strongly related to the proposed trajectories' parametrization. This contribution allows the therapist to further adapt the shape of the joint trajectories and incorporate these adaptations in the following generation of gait patterns.

The second contribution is a set of synchronization methods designed for compliant rehabilitation therapy. Even though these methods were designed based on current strategies for synchronization developed for other systems, they contain improvements that enhance the performance of the synchronization process. Specifically, this work proposes different ways to implement some of the elements of the current methods, and includes a hip trajectory adaptation (not present in the current methods) that enhances the synergy between the system and the patient during robot-assisted walking. Additionally, it presents some methods for a comfortable and timely adaptation of the walking speed (i.e. the speed of the system's platform or the treadmill) during synchronization. This specific topic has not been treated in the literature[1].

The last contribution relates to the setting of assistance profiles in the graphical user interface. The GUI possesses methods for manual (graphical) adjustments of the assistance levels throughout the gait cycle targeting patient-tailored therapy. Although these methods are not presented as better than other strategies developed with similar objectives, they are introduced as a suggested way to interact with the therapist in order to facilitate the interplay between user and robot.

Secondary contributions, mostly related specifically to the proposed concepts or characteristics of the *MOPASS* system (and therefore with low applicability outside of this work), include the design of the position controller using the built-in controllers of the motor drives, the development of search algorithms to obtain some of the parameters of the joint trajectories (namely the shaping points' coefficients) and the design of the software architecture used in the controller computer of the *MOPASS* system.

[1] To the best of the author's knowledge

2 Theoretical background on human walking

The process of human walking comprises several control motor tasks, namely support of the body weight, maintenance of stability along the transverse plane (forward, backward and lateral stability) and maintenance of forward progression [11]. This chapter is dedicated to introduce the basics on human walking to have a better understanding of the problems faced during gait rehabilitation. It is more focused on the kinematics of walking (motion) and the spatiotemporal gait parameters, rather than on the kinetics (forces, powers and energies of the movements) and the behavior of the skeletomuscular, neural and nervous systems during gait. The chapter is divided in two: first, a quick review on the most important aspects of healthy walking are given; second, a review on the pathological gait patterns caused by some medical conditions is presented. The second part covers the generalities of pathological gait, but also introduces some specifics related to some of the most important medical conditions that affect walking.

It is important to understand that walking is a very complex process involving synchronization, balance, displacement of the center of mass of the body, muscle activation and synergies, and compensations, among other matters. This dissertation only presents a rough overview on the topic. For more detailed and complete explanation of the walking process, for both normal and pathological gait, please refer to specialized literature such as [21], [22], [23], [24] and [25].

2.1 Basics of human walking

Let us open this section by making an introduction of the different body planes, axis, joints and motions involved in the process of walking. There exist three different body planes perpendicular to each other: sagittal, frontal and transverse planes. Fig. 1 shows these planes, together with alternative names to each one of them. Each one of the planes possesses an axis perpendicular to it (depicted also in Fig. 1), namely coronal, sagittal and longitudinal axes. Several body parts are involved in the walking process, together with the different joints associated with them. In this manuscript, only some parts of the lower body will be taken into account for the following explanations because they are the ones that influence the most the process and are the ones to be part of the discussion in the following chapters. Four different

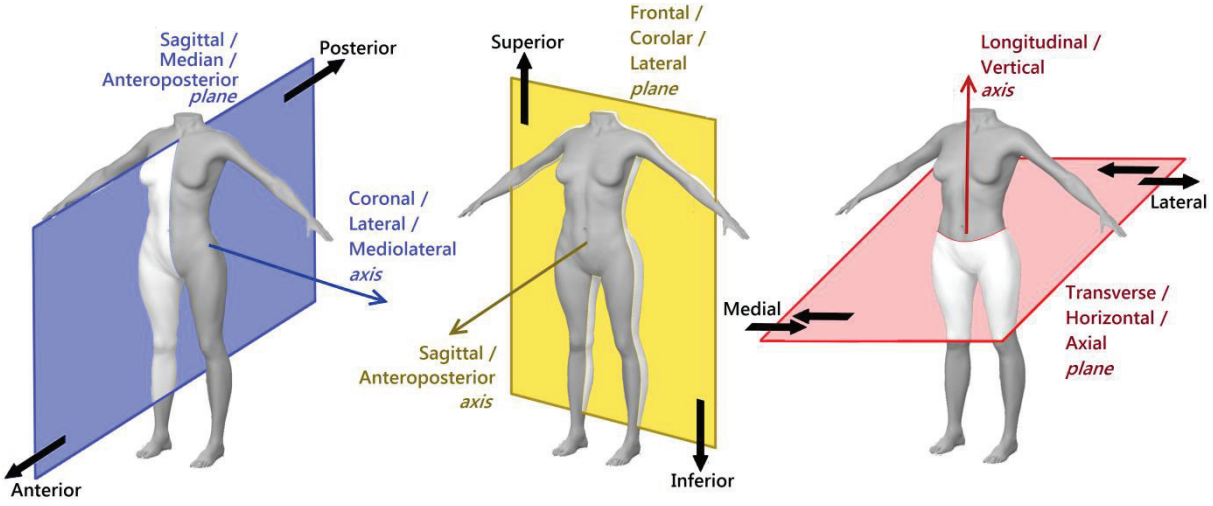

Fig. 1 Body planes, axis and translations

joints are analyzed: pelvis, hip, knee and ankle. The corresponding axis of rotations and the rotation themselves of the aforementioned joints are shown in Fig. 2. Because of the body symmetry, the internal/external rotations of hip, knee and ankle, the hip abduction/adduction and the ankle inversion/eversion are mirrored with respect to the sagittal plane, i.e. they are opposite for left and right joints.

To understand human walking, it is necessary to introduce some of the related terminology. It is important to make clear that the terminology presented in this section of the chapter was introduced for healthy walking. However, it could be inadequate to describe pathological gait patterns [26]. The first concept to be introduced is the *gait cycle* (GC). During walking, the body moves forward as a result of the motion of the two lower limbs (legs). During this motion, one of the limbs serves as a source of support while the other one advances towards a subsequent support location. Once it reaches this new support location, the limbs exchange their roles, while the body shifts its weight from one limb to the other. This sequence of events is repeated during the walking process. A single sequence is referred to as gait cycle [21]. The upper images in Fig. 3 show the single sequence for the right leg. Normally, the start of the gait cycle is considered to be the moment in which the foot makes the first contact with the ground (*initial contact*). In this case, the gait cycle would comprise the sequence of events following this moment until the next time the foot makes contact with the ground.

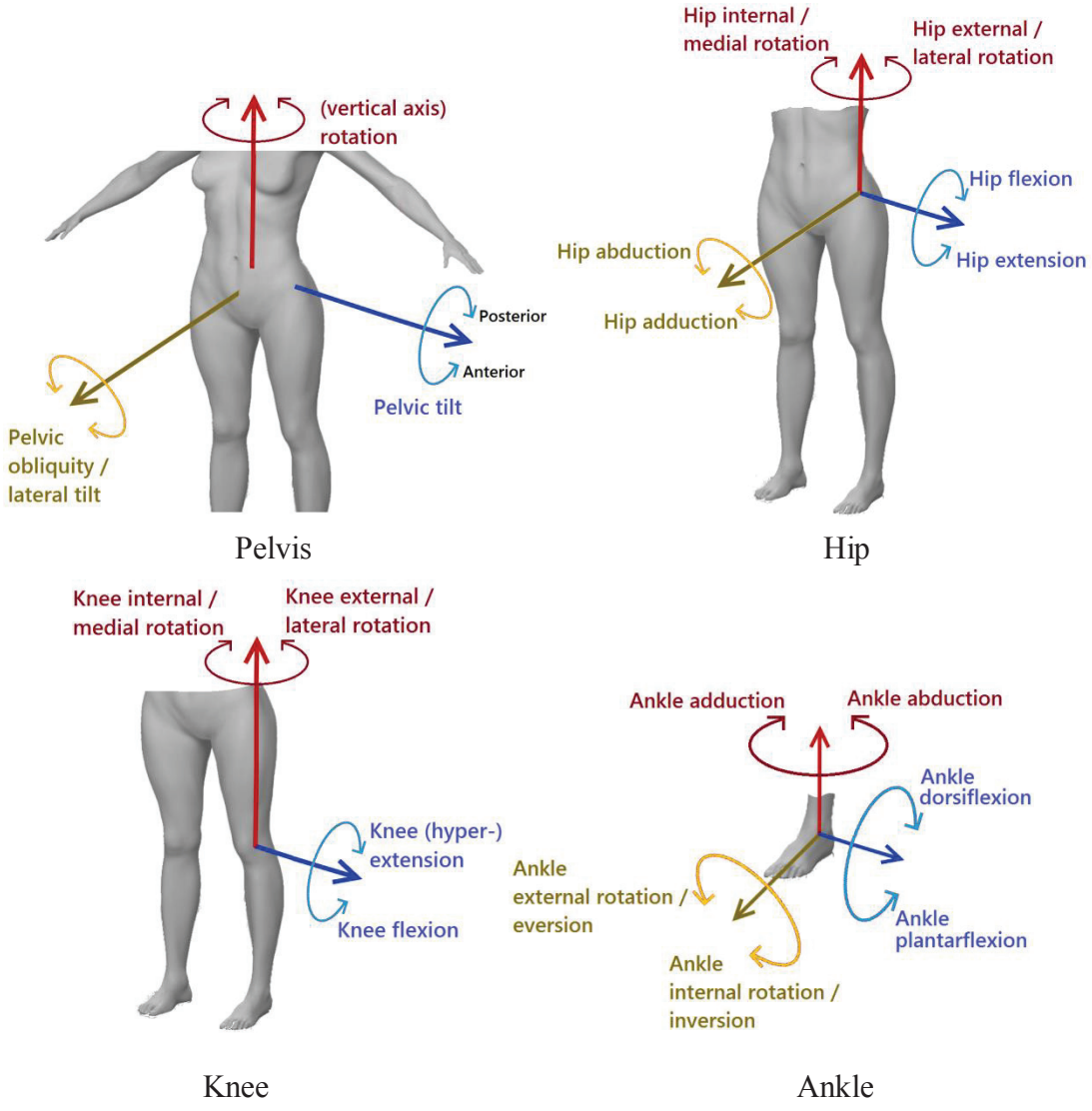

Fig. 2 Pelvis, hip, knee and ankle axis and rotations.

More generally, the GC is defined as the sequence of events between two successive occurrences of one of the repetitive events of walking [22].

Stride and *step* are terms that are often confused by people. Stride relates to the movement of one limb during the gait cycle, whereas the step relates to the motion of both legs. The stride duration is the time elapsed between consecutive initial contacts of one leg (i.e. the corresponding cycle duration). Hence, the stride length is the distance covered between two successive initial contacts of the same foot. On the other hand, the step duration refers to the time elapsed between the initial contact of one leg and the immediately next (or previous) initial contact of the other leg, and step length refers to the distance covered between successive initial contacts of different feet. Therefore, the stride length consists of two step lengths, and two steps are taken during one gait cycle period (also called stride period). Although it is possible that the lengths of two successive steps are different during forward walking with constant speed, the stride length from the left limb must be same as the one from the right one, even in the presence of marked gait asymmetry [25]. This fulfills unless there is turning involved [22].

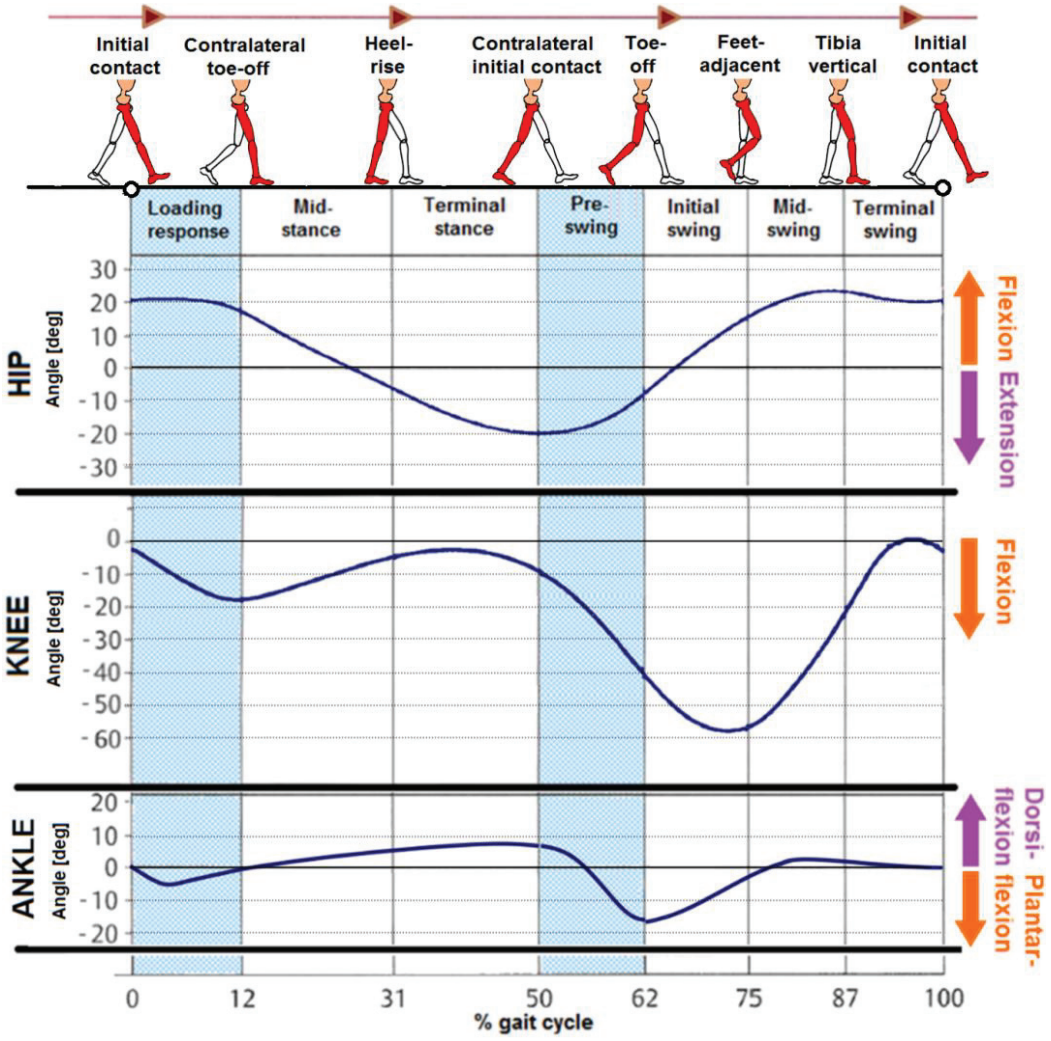

Fig. 3 Example angular trajectories in sagittal plane of hip, knee and ankle joints throughout a gait cycle during normal walking[2].

[2] Angles extracted from [24]

Other important concepts are *cadence* and *walking speed*. The cadence refers to the number of steps taken in a given period of time (i.e. step frequency), commonly given in steps per min. Notice that, because cadence measures steps and not strides, the cadence is two times higher than the gait cycle frequency (1 cycle /min = 1 stride / min = 2 steps/min). The walking speed corresponds to the distance covered by the whole body in a given period of time. Hence, it is equal to the stride length over the gait cycle period. Naturally, it can also be calculated from the step length and cadence. However, the walking speed is not constant throughout the gait cycle.

The gait cycle is divided into two phases: *stance* and *swing*. The stance phase corresponds to the period in which the foot is in contact with the floor starting in the moment of *initial contact* (*heel strike* in natural walking) and finishing when the foot is lifted from the ground (*toe-off*). Consequently, the swing phase is the period from the toe-off event until the next heel-strike event, i.e. when the foot is moving in the air. The duration of the stance phase during normal walking lies around 60% of the complete cycle duration, whereas the remaining 40% correspond to the swing phase [21] [22] [23] [24]. Naturally, the precise duration of each phase is subject-dependent. Moreover, these relative durations are also dependent on the walking speed. As the speed increases, the swing phase increases its relative duration, whereas the stance phase shortens its [27].

Each one of these gait phases is divided into sub-phases (or simply phases), also depicted in Fig. 3. The stance phase starts with the *loading response*[3], which has a duration of around 10% of the GC and where the shock absorption, body weight shifting (weight-bearing stability) and preservation of the progression happen. The second and third sub-phases of the stance phase are the *mid-stance* and *terminal-stance* sub-phases, which have durations of around 20% of the GC each. The mid-stance starts at the moment of toe-off of the opposite leg, whereas the terminal stance starts at the moment of *heel-rise*, which is the time when the heel begins to lift from the ground. The last sub-phase during stance is the *pre-swing,* where the weight is transferred back to the contralateral leg and the limb prepares for the rapid demands of the swing. It starts at the moment of initial contact of the opposite limb and its duration is around 10% of the GC. The swing phase starts with the *initial swing* sub-phase, which takes around one third of the swing period (13% of the GC), and is where the foot clearance from the ground and the advancement of the leg from the trailing position occur. The transition between this sub-phase and the next one (*mid swing*) happens when the swing limb passes the stance limb (event known as *feet adjacent*). The mid-swing endures around 14% of the GC, and is characterized by the further limb-advancement and foot-clearance from the ground. Finally, the swing motion ends with the *terminal swing* sub-phase, which takes around 13% of the GC and where the limb completes its advancement and prepares for the stance. It starts at the moment where the tibia of the swinging leg is perpendicular to the ground (*tibia vertical*).

Considering that there are two limbs during natural walking, and assuming periodicity during walking and symmetry in the motions of both legs[4], it is considered that the events of the opposite (contralateral) limb are offset by 50% of the GC [23], i.e. the initial contact of one leg happens 50% of the GC duration before/after the initial contact of the other leg. With

[3] Sometimes in literature the initial contact is considered the first sub-phase of the stance phase. Here, however, it is considered as the event that starts the stance phase and has no real duration.

[4] The assumption of periodicity is not completely true due to the fact that, even in healthy normal walking, there exist inter-stride variability between the joint angles. Likewise, a certain degree of asymmetry between legs is also present even during normal walking of unimpaired subjects [254].

this in mind, it is possible to divide the stance phase also in the following three sub-phases: initial double limb stance, single limb stance and terminal double limb stance. The first and latter ones correspond to the double stance phases of the gait cycle (shadowed areas in Fig. 3), where both limbs are in contact with the ground and the body weight shifting happens (loading response and pre-swing sub-phases). The single stance sub-phase is therefore the period in which the limb is in contact with the ground, and the opposite limb is swinging (mid- and terminal stance sub-phases). Hence, during the double stance phases, the body weight is resting in both limbs, whereas during single stance all the weigh is resting in the limb that is in contact with the ground. The duration of these three sub-phases is around 10%, 40% and 10% of the GC, respectively. Again, the duration of the sub-phases is dependent on the subject and on the walking speed. For instance, increasing the speed shortens the duration of the double stance sub-phases, and increases the one from the single stance [21], until the moment in which there is no double stance, marking the transition from walking to running.

Let us analyze now the behavior of the lower body joints in each one of the gait (sub) phases during normal walking at self-selected speed. Only the joint motions in sagittal plane will be analyzed in detail due to the fact that these are the most representative motions during walking.

An example of the hip joint angular displacement in sagittal plane during natural walking is depicted in Fig. 3, whereas Fig. 4 shows the relation between the measured angles and the leg segments[5]. During one gait cycle, the hip has one period of extension and one period of flexion. The maximum flexion is reached around mid-swing. The hip is kept highly flexed (i.e. minimal variations in the angle) until the moment of heel strike, following a higher degree extension movement during the loading response. The hip continues to extend during the mid-stance phase (where it passes from a flexion to an extension state) and terminal stance. Significant muscle activity about this joint occurs in the frontal plane throughout the

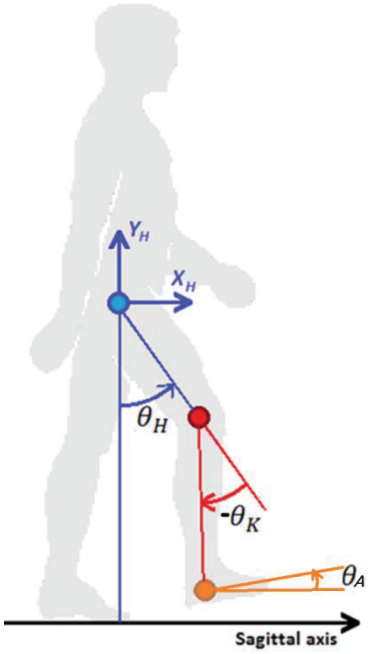

Fig. 4 Hip, knee and ankle angular measurements (H: hip, K: knee, A: ankle).

[5] Several approaches for hip angle measurement are taken by researchers. For more details, refer to [21].

single-stance sub-phase [22]. The maximum flexion is reached around the transition between terminal stance and pre-swing (or, in other words, around the moment of initial contact of the opposite limb). From this point, the hip performs a flexion movement, starting even before the foot leaves the ground (toe off). The flexion movement is continued throughout most of the pre-swing sub-phase and the swing phase, making the hip transition from extended to flexed state around the beginning of the swing phase, until the maximum flexion is again reached. The range of motion of the hip during normal walking averages 40° [21]. The peak extensor torque in the hip in sagittal plane is around 10 BWLL[6], and it is reached at the onset of limb loading, around the starting point of the pre-swing sub-phase. The peak flexor torque happens within the fist 2% of the GC (shortly after the initial contact) and it is around 8.2 BWLL [21]. Regarding the motion of the hip in coronal plane (ab/adduction), smaller deviations are made during the gait cycle, with ranges of motion of around 15°. Internal and external hip rotations are also present during the cycle, although in a much lower degree (the range of motion averages 8°).

Fig. 3 also shows an example of the knee displacement with respect to the upper leg segment. During healthy walking the knee always stays in the flexion state, normally having two flexion and two extension peaks per gait cycle at normal walking speed. The global peak flexion happens during the initial swing (*swing phase knee flexion*) before the feet are adjacent. After reaching the peak, it starts a fast extension motion that goes through the mid-swing and most of the terminal swing until reaching a fully extended (0°)[7] state. Before the initial contact, the knee starts a flexion motion that continues in the loading response sub-phase. This flexion is referred to as *knee stance flexion*. Around the moment of toe-off of the opposite limb the knee reaches the stance-phase peak flexion. The degree of flexion during stance is very dependent on the walking speed, even disappearing at very slow walking [21]. Moreover, its moment of occurrence is also subject- and speed- dependent. After the stance peak is reached, the knee starts again an extension motion though most of the mid-stance and part of the terminal stance, until it reaches an extension peak near the moment of heel-rise. A fast flexion motion starts and continues throughout the pre-swing sub-phase and part of the initial-swing, until it reaches the global maximum flexion. The range of motion of the knee is around 70°. The knee presents four torque peaks during the cycle. An initial extensor torque peak of around 2.6 BWLL happens at the initial contact as a result of the impulse of the foot-ground strike. The maximum flexor torque occurs by the end of the loading response, with a value around 7.8 BWLL. The maximum extensor torque is reached by the middle of the terminal stance and has a value of around 3.8 BWLL. Finally, by the middle of the pre-swing sub-phase a flexor peak torque of around 1.5 BWLL occurs [21].

Regarding the knee angles, it is important to make clear that, normally, the convention used in the literature for the direction of the angles in the knee joint is opposite to the one proposed in this dissertation (Fig. 3 and Fig. 4). Most of the medical references use positive values for the flexion stages of the hip and knee joints. Nevertheless, from the point of view of robotics and engineering, this will lead to a usage of rotation axis with opposite directions in each one of the joints. Therefore, to be more consistent and clear from the engineering point of view, the selected rotation axis for hip and knee joints have the same direction, and consequently the knee flexion angles are presented as negative.

The displacement of the ankle joint is not as high as the ones from the hip and knee joints (Fig. 3), with an average range of motion of around 30° (±10°). However, its motion is of

[6] Anatomical units (scaled for body weight and limb segment length): body weight / leg length [21]

[7] When talking about the knee, full extension refers to the moment when the leg is straight. Beyond this point (in the positive direction in our convention), it is referred to as hyper-extension.

great importance for progression and shock absorption during the stance phase. The ankle possesses four states during the GC: two plantarflexion (PF) and two dorsiflexion (DF) states. Three of this states happen during the stance phase (PF, DF, PF), and the remaining one (DF) in the swing phase. At the moment of initial contact, the ankle is near the neutral position (0°), where it starts its first stance phase plantarflexion motion. By the middle of the loading response it reaches the first PF peak, and subsequently starts moving in opposite direction throughout the mid-stance and most of the terminal stance until reaching the DF global peak before the pre-swing sub-phase starts. During a small part of the terminal stance and all the pre-swing the ankle performs a plantarflexion motion until reaching a PF global peak shortly after the moment of toe-off. Throughout the swing phase the ankle performs a dorsiflexion motion reaching a low DF peak and finally returns to an almost neutral position before the heel strike. The torque presents two peaks during the GC (more specifically, during the stance phase). The first, relatively low, in the first half of the loading response corresponding to a plantarflexion torque of around 1.5 BWLL. The second, much higher, occurs shortly before the pre-swing and corresponds to a dorsiflexion torque of around 17 BWLL [21]. During the swing phase, the torque in the ankle is almost zero [24].

The trunk and the head behave like a unit during normal gate, with very small deviations from each other. Throughout the gate cycle, this 'unit' experiences translation in all three body axes. The vertical displacement (longitudinal axis) is characterized by two superior (upwards) and two inferior (downwards) movements (see Fig. 5), and possesses a range of motion of around 4.55 cm at normal speed [21]. The two peak downward deviations occur at the beginning of the two double stance phases, i.e. in the first halves of the loading response and the pre-swing. The two upward peaks, on the other hand, occur during the single-stance phases of each leg, most precisely during the first half of the terminal stance (or, in other words, during the terminal stance and late mid-swing of one leg). The lateral displacement (coronal axis) is characterized by one movement to each side (left and right), as shown in Fig. 6, and has a range of motion of around 4.5 cm at normal speed. At the moment of initial contact the trunk and head are located in the neutral position. From this point, a motion in the direction of the stance leg is carried out, reaching a peak displacement around the onset of the terminal stance. After this point, the trunk starts moving gradually back to the neutral position, reaching it around the moment of initial contact from the opposite leg. The same sequence is repeated from this point with the opposite leg throughout the second half of the gait cycle. The lateral displacement is consistent with the body weight shifting during the

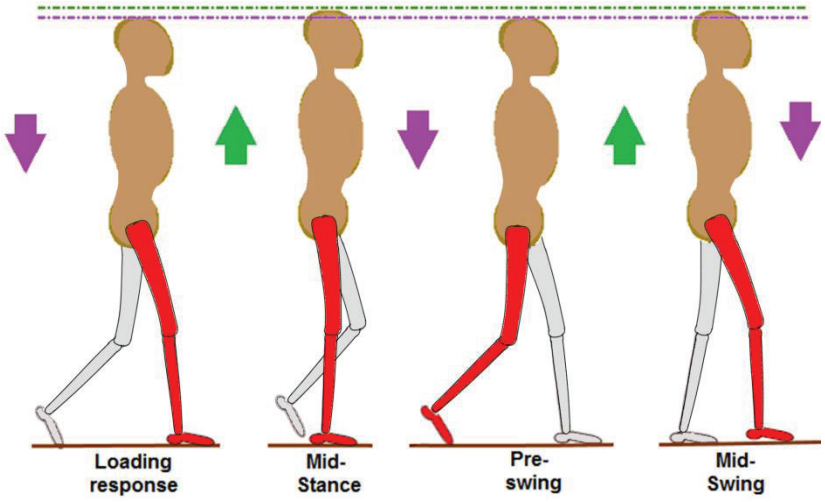

Fig. 5 Upper-body vertical displacement during normal walking

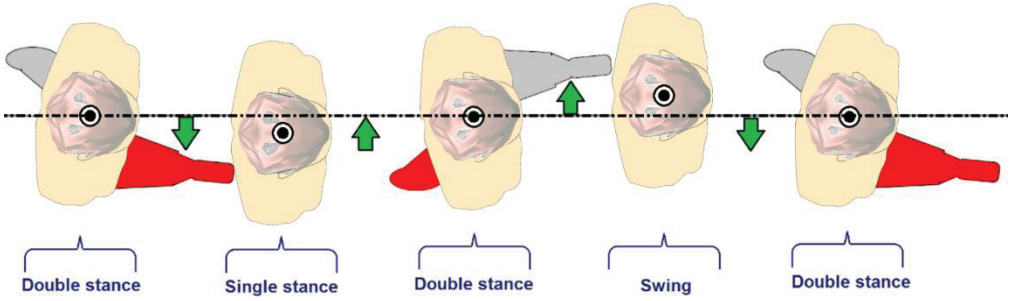

Fig. 6 Upper-body lateral displacement during normal walking

cycle. In the case of the anteroposterior displacement (sagittal axis), a relationship between the mean gait speed and the displacement is drawn. The speed of the upper body is variable during the GC. During the first third of the GC the speed of the trunk is higher than the mean walking speed; the trunk speed later decreases to be lower than the mean walking speed. In general, the upper body speed is lower than the mean speed in the middle of the stance and swing phases and higher in the double support sub-phases [22]. Consequently, the peak positive displacement of the upper body with respect to the average progression occurs shortly after the onset of the mid-stance and in the middle of the pre-swing, whereas the peak negative displacements occur in the late terminal stance and in the second half of the terminal swing [21]. At initial contact, the position of the trunk is about half stride length behind the location of the leading foot.

The pelvis, which behaves as a mobile link between the two lower limbs, also experiences some asynchronous motion patterns throughout the gait cycle, with peak values of pelvic obliquity (drop), tilt and rotation of around 4°, 4° and 10°, respectively [21]. It is important to notice that pelvic motion results in displacement of the hip with respect to the center of the pelvis, influencing the positions of the lower limb segments (e.g. feet) with respect to the centroids of the pelvis and trunk (or other reference frames/points). In the case of the rotation about the vertical axis, for instance, pelvic motion results in hip displacement in the transverse plane, which ultimately may contribute to the step length. Following the same idea, pelvic obliquity may contribute to foot clearance.

2.2 Overview of pathological walking

There exist a large amount of medical conditions that affect the ability to walk in patients, with pathologies that differ from disease to disease. However, the abnormalities imposed by them on the gait mechanics can be generally classified in four different categories: deformity, muscle weakness, pain and impaired control [21]. Functional deformity happens when body tissues put constrains that impede enough passive mobility to the person to achieve normal ranges of motion and postures characteristic of the walking process. Muscle weakness refers to the lack of sufficient muscle strength to fulfill the demands of gait. Muscular and skeletal pain alters as well the way people walk, and is related also with deformity and muscular weakness. Finally, impaired motor control is related with patients that suffered a central neurological lesion that caused paralysis (e.g. stroke, cerebral palsy, brain injury, incomplete spinal cord injury and multiple sclerosis). These patients suffer from spasticity (overreaction to stretch), lack of selective control (they cannot control the timing and intensity of the muscle activation), inappropriate phasing, primitive locomotor patterns and alteration of the muscle control due to limp positioning and body alignment. Other cause for pathological gait is the loss of sensory feedback, where the person is unable to reliably know, for instance, the actual

state of the limbs and joints or the type of contact with the ground, resulting in feelings of insecurity during walking.

The gait deviations resulting from anatomical and functional alterations due to a medical condition can be generally classified into primary and secondary [11]. The primary ones refer to the deviations that were caused directly by the pathology of the medical condition, commonly present in the early stages. The secondary ones comprise the passive deviations consequence of physical effects from the primary deviations, and the active deviations (also referred to as tertiary deviations) caused by the mechanisms used to compensate for the functional limitations and counteract primary and passive secondary deviations.

Each one of the lower limb joints is affected by the aforementioned dysfunctionalities. The following is a summary of the kinematic abnormalities in the joints, mostly obtained from [21].

The hip joint, because of its high mobility (degrees of freedom) is affected in all three planes. Several issues may rise in this joint depending on the pathology of the condition: inadequate (low, limited) flexion and extension, and excessive flexion, adduction, abduction, internal rotation and external rotation. Inadequate extension affects the weight-bearing stability and prevents progression. It causes modifications in the alignments of pelvis and thigh during mid-stance, resulting in abnormal postures such as trunk leaning and knee flexion. Abnormal postures are also present during the terminal stance due to limited hip extension. Excessive flexion normally results in high lower-limb posture alteration. It is present in pre-swing and initial swing sub-phases as a continuation of the inadequate hip extension in the previous sub-phases. During mid-swing, excessive flexion causes high pelvic tilting. Both inadequate extension and excessive flexion can be caused by contractures, spasticity, arthrodesis (fusion of bones via surgery to reduce or eliminate joint mobility) and pain, as well as deliberate movements done by the patient to compensate for other limitations (e.g. excessive hip flexion to increase the foot clearance and compensate for foot drop). Low angles from inadequate hip flexion during the initial swing can reduce the limb advancement and limit the knee flexion, and can also contribute to foot/ankle related issues such as toe-drag and abnormal plantarflexion. This abnormal motion may continue throughout the mid-swing, even being present in the terminal swing and loading response. Normally, this limitation in hip flexion is caused by the lack of active muscle control (e.g. insufficiencies in the hip flexor). Other cause can be arthrodesis. The excessive adduction can be present in both stance and swing phases, and can be caused by abductor weakness, contracture, spasticity and muscle substitution for functional purposes. In the case of excessive abduction, the high angles result in wider strides (walking base), which increase stability during stance and easier floor clearance. However, it also results in higher demands during the weight shifting. Causes of excessive abduction include contractions, discrepancy in the leg lengths, and voluntary abduction normally used as a substitution in the presence of inadequate hip flexion. Finally, excessive rotations in the transverse plane can be caused by muscle over-activity, excessive ankle plantarflexion in the ankle and muscle weakness.

In the case of the knee most of the abnormal displacements due to pathological walking are present in the sagittal plane rotations. Inadequate knee flexion might cause several problems during some of the gait sub-phases. In loading response, limited flexion reduces the quality of the shock absorption by the knees in the moments following (and including) the initial contact. Low flexion angles during pre-swing can hinder the toe-off, making more difficult the transition from stance to swing, whereas during the initial swing they can cause toe-drag and hinder the advancement of the limb, and might be continued to the mid-swing sub-phase. On the other hand, the knee can also have two types of excess in extension: extension thrust (which inhibits the knee flexion due to an excessive extensor force) and

hyperextension (positive knee angles in Fig. 3 that happened when the knee has the degree of mobility to reach such postures). Inadequate flexion and excessive extension in the knee joint can be caused by muscle weakness, spasticity, pain, excessive plantarflexion in the ankle and contractures. Likewise, there can also be excessive knee flexion and inadequate extension. The first one can be present in the loading response and mid-swing sub-phases; the latter can be seen in mid- and terminal stance (generally as a continuation of excessive flexion in loading response) and terminal swing. The causes of these two abnormal motions include muscle weakness, contractions, inappropriate hamstring activity and excessive plantarflexion in the ankle.

The ankle joint can present excessive plantarflexion and dorsiflexion. Excessive plantarflexion causes abnormal functions in both stance and swing phases. In the first one, generally put, it affects the progression by decreasing it, leading to shorter stride lengths. Moreover, it hinders the maintenance of an upright posture. In the case of the swing phase, it hinders the limb advancement. More specifically, it draws issues differently in each of the sub-phases, starting from the moment of initial contact. As stated before, in normal walking the initial contact corresponds to the heel strike. However, in pathological walking, the initial contact might be done with the frontal part of the foot (*forefoot contact*) caused by excessive plantarflexion. Other type of contact caused by this abnormal pattern is the low-heel contact, where even though the heel is the one making the first contact with the floor, the foot is in an almost horizontal position with respect to the ground level (*flat-foot contact*). In the loading response, the effects are related to the type of initial contact. Normal heel strike, for instance, can be followed by *foot-drop*, and fore-foot contact can lead to abnormal loading patterns. During mid-stance, excessive plantarflexion reduces the progression, causing shorter step lengths from the opposite leg. Normally, people experiencing this dysfunctionality appeal to three substitutions: premature heel rise, knee hyperextension (if mechanically possible) and forward trunk leaning. The effects in the terminal stand include hindrance of advancement and reduction of the step length. During pre- and initial swing, the effects are not that significant. During mid-swing excessive plantarflexion would cause toe drag, resulting in a hindrance to the limb advancement and premature termination of the swing phase. As stated before, one substitution for this case is the increase of hip flexion during this sub-phase. Finally, in the terminal swing there are no significant interferences caused by the excessive plantarflexion, and normally the toe-drag from the previous sub-phase is corrected in this sub-phase. Excessive plantarflexion can be caused by muscle weakness, contractures and spasticity.

While excessive ankle plantarflexion introduces significant abnormalities in four of the gait sub-phases, excessive dorsiflexion does it in five of them (all but mid- and terminal stance), although they might not be as significant as with the previous one. If present during the initial contact (very seldom), excessive dorsiflexion can be the cause of instability. During the loading response it can lead to greater knee flexion, whereas during the swing phase, no clinical significance exists related to high dorsiflexion except for the way the foot is positioned to perform the initial contact. Causes for excessive dorsiflexion include muscle weakness, lock of the ankle joint (e.g. by an orthosis) and persistent stance knee flexion.

Besides the hip, knee and ankle joints, abnormal motions can be also present in the pelvis and trunk. As with the hip, the pelvis motion can be altered by the pathologies in all three planes do to its high number of degrees of freedom. In the sagittal plane, the pelvis might present anterior tilting, caused by muscle weakness, contractures and spasticity. In the frontal plane the pelvis could expose pelvis hike (lateral elevation of the pelvis above the neutral position) during the swing phase, used deliberately to assist the foot clearance from the ground; and contralateral drop (descent of the opposite side of the pelvis) during stance phase,

which can be caused by muscle weakness, contractures and spasticity, among other reasons. Finally, in the transverse plane, the pelvis can present excessive forward and backward rotations, and insufficient pelvic rotation. The trunk, on the other hand, can present backward leaning, caused by muscle weakness and inadequate hip flexion; forward leaning, caused by muscle weakness or deliberate reduction of muscle activation during loading response, and abnormal ankle plantarflexion in mid- and terminal stance; lateral lean, caused by muscle weakness, contractions, significant differences in the length of the legs and scoliosis, among other causes; and excessive rotations about the vertical axis, which can be caused by trunk synergy with the pelvic motions or walking aids.

It is important to make clear that the aforementioned pathological joint motions affect directly the walking parameters. For example, it is common that the step lengths from both legs are significantly different during pathological gait [22], which results in lower walking speeds. Other matters such as energy consumption are also affected by pathologic walking (more specifically by the abnormal movements, spasticity and contraction of antagonistic muscles), being higher than during normal walking [22]. Rhythmic disturbances can also be present during pathological walking. These disturbances can come as asymmetric or irregular disturbances. Asymmetric disturbances refer to the cases when there exists difference in the gait timing of both limbs caused, for example, by the pursuit of a reducing of pain in one of the limbs or by differences in the legs' lengths; irregular disturbances refer to the alteration of the timing from one stride to the other, which is seen in some neurologic diseases [22]. Finally, other abnormalities observed during pathological gait include tremblers and abnormal movements of the head and upper limbs (e.g. hindered arms' swing).

As stated before, several clinical conditions affect, in a lower or higher degree, the walking ability of the people suffering from them. A quick review on the characteristics on the walking related abnormalities from stroke, cerebral palsy, brain injury and spinal cord injury will be presented next.

Stroke (cerebrovascular accident)

A stroke (or cerebrovascular accident – CVA) happens when the flow of blood to an area of the brain is poor (or blocked), causing cell death due to the privation of oxygen. When this happens, the abilities controlled by the affected brain area (including muscle control and memory) are compromised. In general, around 80% of the people that suffer stroke exhibit walking issues three months after the accident occur [11]. An extensive prospective study [28] on 804 stroke survivors in the acute phase showed that 51% of the participants were unable to walk following the accident onset, 12% could walk assisted and the remaining 37% could walk independently. After rehabilitation, 18% were unable to regain any walking capability, 11% were able to walk assisted and 50% regain the capabilities to walk independently. The study had a mortality rate of 21%.

The sensorimotor impairments caused by strokes include muscle weakness, impaired selective motor control, spasticity and proprioceptive deficits [29], resulting in hemi-paretic[8] gait. It is important to understand that the related hemiparesis is a consequence of a disruption in the neural system which does not cause direct lesions neither in the spinal network nor in the musculoskeletal system [11]. Hemiparesis affects the gait symmetry, the temporal and spatial parameters, the kinematics of the joints, and the kinetics of the body.

[8] Unilateral impaired movement, i.e. one side of the body

Asymmetry between the two lower limbs is characterized by an inadequate selective motor control, disturbed equilibrium reactions and a reduction of the weight support by the paretic leg [29]. This asymmetry compromises the smooth progression of the body, and is often partly caused by the compensation made to overcome the limitations of the paretic side of the body (e.g. adjustments in the pelvis and the non-paretic side). The recovery of normal symmetry during post-stroke rehabilitation is a point of discussion. Some specialists suggest that asymmetry plays an important role in the walking performance of chronic hemi-paretic patients, compensating for the neurologic deficits and being a source of gait functionalities [29]. Discussions about allowing compensation in the early post-stroke stages and its influence in suboptimal recovery have been also held [11].

One of the most critical effects of hemiparesis in the gait parameters is the reduction of the walking speed [30], although it is dependent on the motor recovery of the patients (higher motor recoveries have shown less reduction in the speed and less asymmetry [31]). Besides poor motor recovery, other causes for speed decrement include impaired balance and muscle weakness [29]. Significant temporal and spatial asymmetries between the two legs are also often present during hemi-paretic gait analysis: 48% to 82% of post-stroke patients show temporal asymmetries, whereas 44% to 62% show spatial asymmetries [11]. In a study involving 54 chronic post-stroke patients, 55.5% of the participants exhibited abnormal temporal asymmetry, whereas 33.3% exhibited significant spatial asymmetry [32]. Reported effects on the temporal features include reduction of the cadence [33], lower and higher (relative) durations of the stance phase in the paretic [34] and sound legs [33], respectively, higher durations of double-limb support sub-phases [31], reduction of the duration of single-limb support sub-phase in the paretic leg [29], and durations in the pre-swing higher than in the loading response in the paretic limb (mostly at low speed) [11]. Regarding the spatial gait parameters, the mostly compromised feature is the step length symmetry between both limbs, where generally the step length from the paretic length (the foot of the affected leg is ahead) is longer than the one from the sound leg, although cases where it is shorter have been also reported [11]. However, some studies have indicated that asymmetries in the step length do not necessarily cause limitations on the self-selected walking speed of the patients [29].

The kinematics of the lower limb joints are also affected [29]. The hip experiences a reduction of extension (caused in part by limited ankle dorsiflexion in the late stance) and flexion during the stance and swing phases, respectively. The knee shows different type of patterns during hemi-paretic walking. During stance phase the knee can experience an increment of flexion (particularly at initial contact), a reduction of flexion during the initial stance, hyperextension during the terminal stance, or high and prolonged hyperextension during most of the stance period. High hyperextension presents usually at very low speeds and is associated with abnormal initial contact (fore-foot or flat-foot), prolonged ankle plantarflexion and low knee flexion previous to the initial contact. Moderate hyperflexion presents typically in relatively normal to high walking speeds, and is caused by irregular initial contact and abnormal ankle plantar- and dorsiflexion during the stance. During the swing phase the knee can experience a decrement of knee flexion (causing stiff knee) and decrement of extension in the moments before the initial contact. In the case of the ankle, the joint can experience low plantarflexion prior to toe-off and decrements on the dorsiflexion (or continues plantarflexion) during swing-phase that hinders the ankle to reach the neutral position, normally achieved at mid-swing to prevent toe drag, which ultimately can cause an abnormal initial contact. As stated before, the patient might do some compensation to avoid the toe drag, including pelvic elevation. Moreover, the kinematics of the arms and trunk are also affected by the hemiparesis, presenting asymmetries in their motions [11]. Three examples of the affected joint kinematics in hemi-paretic gait can be seen in Fig. 7.

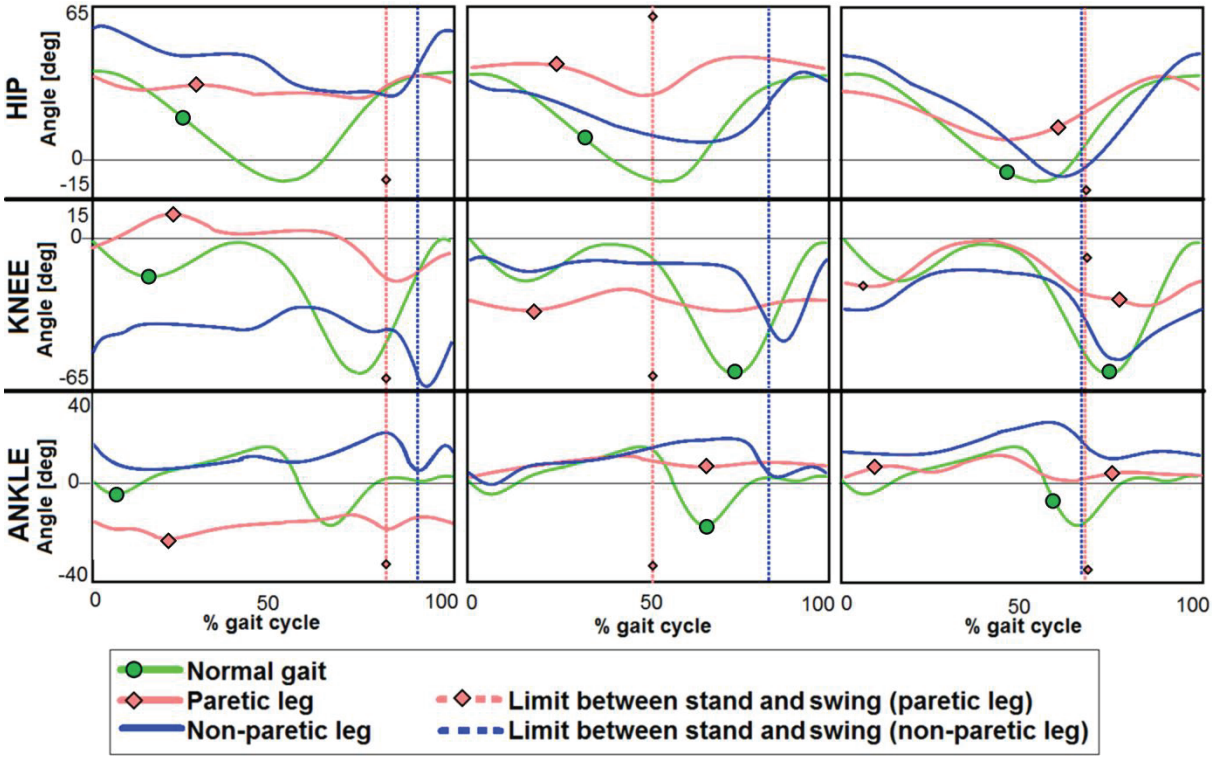

Fig. 7 Examples of joint angles in hemi-paretic gait[9]

Besides the spatial-temporal and kinematic abnormalities, hemi-paretic gait in stroke survivors is also characterized by high risk of falling [11] and higher energy consumption, the latter based on the level of oxygen spend during walking and varying depending on the degree of weakness, spasticity and training [29].

Cerebral Palsy

Cerebral palsy (CP) is caused by damage in the brain during its development, ultimately consequence of lack of oxygen that kills or damages developing neurons, and can affect different areas of the organ. Unlike stroke, it is of great difficulty to identify the area of the brain that is affected [12]. CP is not one disease, but rather a collection of diverse syndromes, and its severity and clinical effects possess a high inter-subject variability [22], where the clinical picture is based on the muscles that are affected and their contraction timing relative to the gait cycle. Because CP is related to damage in the immature brain, studies normally focus in the medical condition of children. However, the effects continue to the adulthood of the people who suffered it, where premature aging due to the stress and strain caused by the disability is characteristic [35]. The effects from the brain damage continue developing throughout the child up-growing and current treatments are unable to do anything for the damage itself. However, some treatments can help prevent or reduce some of the secondary effects.

The motion patterns caused by CP are diverse and include spastic, dyskinetic, hypotonic, ataxic, and mixed forms of movements, where spastic motions are the most common and the other types represent a minority of the cases [12]. Hence, spasticity is often the dominant clinical feature affecting most of the CP patients [22] and is one of the focus points in this

[9] Angles extracted from [11]

section. Primary abnormalities that are consequence of CP include loss of selective motor control, abnormal tone and problems with balance. Secondary abnormalities include abnormal bone growth, muscle growth, joint alignments (e.g. dislocation) and foot deformities. The emergence of primitive patterns of contraction is also characteristic of CP patients. In general, muscle weakness is not one of its primary effects. Compensations arise to overcome the primary and secondary abnormalities, although successful treatment of the secondary abnormalities (the primary are normally permanent and untreatable) may lead to an unnecessity of these compensations commonly leading to their disappearance.

Generally, CP can cause hemiplegia[10], spastic diplegia, spastic quadriplegia (also called double hemiplegia) and triplegia. As the names suggest, spastic diplegia is characterized by paralysis in both sides of the body but mostly affecting the lower limbs, quadriplegia affects all four limbs (more severely in the lower limbs) and triplegia refers to paralysis primarily involving the lower limbs and one of the arms [22]. The following explanations focus on hemiplegia and diplegia.

In the case of hemiparesis, and specifically referring to children and young adults, Winters *et al.* [36] conducted experiments with 46 young patients who had suffered CP, traumatic brain injury and stroke (mostly CP) and divided the group in four based on the level of disability: from group I (with the mildest deviation from normal gait) to group IV (the more severely impaired). Group I was characterized by foot drop (although the ankle dorsiflexion range during stance phase was adequate), increased knee flexion in terminal swing and loading response (including initial contact), hip hyperflexion (increased flexion) during swing phase and increased anterior pelvic tilt throughout the gait cycle. Group II also presented hip hyperflexion and increased anterior pelvic tilt, together with persistent plantarflexion throughout the gait cycle and knee full extension or hyperextension in stance phase. Group III showed more limited knee flexion than the previous group, as well as hip hyperflexion, increased anterior pelvic tilt and persistent plantarflexion. Finally, group IV showed the same limitation of group three, but in a higher degree. All groups presented walking speeds lower than the average speeds for the corresponding age. These findings concur with the kinematic analysis of hemiplegia presented in the previous section.

In spastic diplegia, as inferred from the name, spasticity plays a prominent role. The presence of spasticity during the muscle development can also lead to deformity. Patients suffering from spastic diplegia are normally characterized by a lack of stability in both standing and walking [22]. As stated before, the limitations and effects differ from patient to patient, but normally they include increased hip flexion (which leads to increased anterior pelvic tilt) and internal rotation, increased knee flexion, ankle eversion, and deformity of the foot, which causes forefoot contact and loss of plantarflexion in loading response, dorsiflexion in mid-stance and plantarflexion in pre-swing [22] [37]. Hyperextension of the knee and ‘stiff-leg’ are also present in some patients suffering from spastic diplegia. However, it is important to make clear that these are only some of the disabilities and abnormalities present in diplegic patients.

Some studies have focused strictly in the knee limitations in CP patients. Sutherland and Davids [38] identified four types of primary knee joint abnormalities after conducting gait analysis in over 588 CP patients: jump knee, crouch knee, recurvatum knee and stiff knee [37]. Jump knee is characterized by increased knee flexion in the initial stance with correction to almost normal in the mid-stance and terminal stance. Crouch knee presents increased

[10] Although strictly speaking hemiplegia refers to total paralysis, it is often used to refer to both total paralysis and partial paralysis (hemiparesis).

flexion in stance phase and variable motion in swing phase. Recurvatum knee was characterized by increased extension in mid-swing and terminal stance and variable motion in swing phase. Finally, stiff knee presented a highly decreased range of motion in swing phase. Some examples of lower joints' trajectories from diplegic CP patients are shown Fig. 8, including the cases of jump, crouch and recurvatum knee.

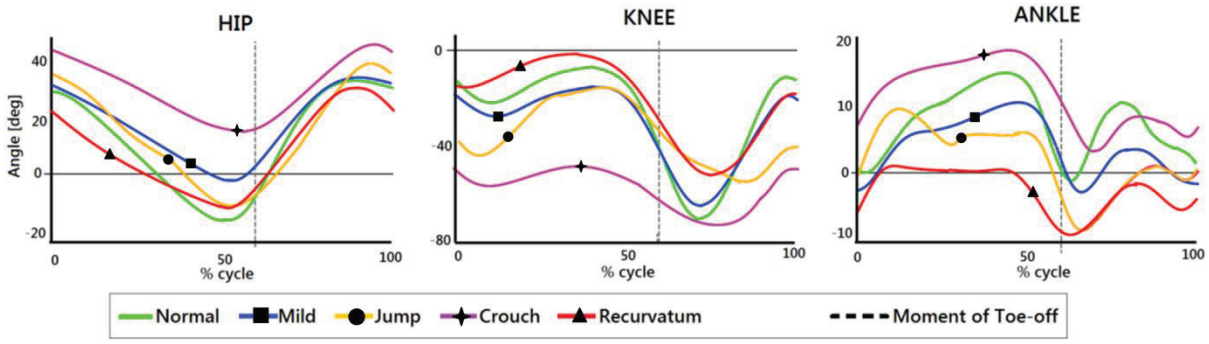

Fig. 8 Examples of hip, knee and ankle trajectories in diplegic CP patients[11]

Traumatic brain injury

The causes of traumatic brain injury (TBI) are very diverse, although the leading ones are car accidents, firearms and falls [39]. The effects of severe TBI include motoric, cognitive, behavioral and emotional dysfunctions, however not much is known on how gait patterns are affected by the neurophysiologic impairments caused by TBI [7]. A high amount of patients express problems with instability and balance [4], as well as spasticity [40]. Dysfunctional patterns in TBI patients that have been reported include persistent hip flexion throughout the stance phase (causing shortened steps in the contralateral leg and affecting the stability during single limb support), hip adduction during terminal swing (narrowing the support base potentially causing balance problems), persistent knee extension during pre- and initial swing (stiff knee), delay in the timing of the knee flexion (causing reduction of hip flexion and possible toe-drag), persistent knee flexion during stance and swing phases (inducing compensatory hip flexion in stance phase and increased contralateral hip and knee flexions in swing phase, hindering the advancement of the limb in both swing and stance phases, shortening the step length, and potentially affecting balance and energy efficiency), equinovarus foot (plantarflexion with inversion), higher hip flexion in foot clearance, excessive knee flexion at initial contact, abnormal trunk and pelvic movements, and decrease of the walking speed [7] [40] [41].

Spinal cord injury

As with TBI, the causes of spinal cord injury (SCI) are diverse, with the main ones being car accidents, falls, violence (mostly involving gun shuts) and sports [42]. TBI can be complete, where the damage to the spinal cord is absolute and leads to a permanent loss of functionality below the injury level; and incomplete, where the damage caused incomplete loss of feeling and functionalities leading to different types of incomplete paralysis (paraplegia, quadriplegia). Reported pathological patterns include inadequate hip extension during stance, excessive ankle plantarflexion during stance, contralateral vaulting of the foot, limited hip and knee flexion during swing, excessive plantarflexion during swing, abnormal

[11] Angles extracted from [37]

hip rotations during swing, impaired ankle eversion during swing, pelvic hiking, and impaired foot contact [13]. The first three contribute to impairments in stance instability, the latter to impairment in the foot positioning, and the remaining six to impairments in foot clearance.

Multiple sclerosis

Multiple sclerosis (MS) is a disease of the central nervous system that causes damages in the nerve tissues of the brain and spinal cord and is characterized by impairments in several neurologic functions [43]. Although the exact cause of MS is yet to be identified, it is known that something causes the immune system to attack the brain and spinal cord, typically causing sensory, cognitive and motor impairments [9]. Neurologic abnormalities commonly found in MS patients are spasticity, weakness and ataxia [44]. Other possible symptoms caused by MS include paralysis, pain, fatigue, memory problems, numbness, tingling, changes in the mood, and blindness, varying from person to person. These symptoms can be short or long lasting, and some patients can experience gradual loss of function (progressive MS) [45].

Although gait disorders are commonly present in MS patients, there exist a relatively low number of studies related to the gait patterns. Most of the studies report a decrease in the stride length and walking speed with respect to healthy subjects, which can be related to protective strategies towards balance and stability at the expense of speed [44]. Other findings include increased stance-to-swing ratios (longer double support times), higher step length difference between legs, wider base support, arrhythmic gait, increased hip flexion, knee flexion and ankle plantarflexion at initial contact, decreased hip and knee extension at toe-off, reduced ankle plantarflexion during swing, increased hip flexion during swing (leading to higher ranges of motion of the hip), reduced range of motion in the ankle, reduced cadence, reduced walking endurance, and increased metabolic cost during walking [43] [9] [44] [46]. Elevated variability in both joint kinematics and spatiotemporal gait parameters has also been reported by multiple studies, linking it with different possible causes including the level of disability, usage of walking aids, dual-task performance and fatigue [9]. Some of the walking abnormalities were found even in minimally disabled MS patients [47]. Additionally, falls are a recurrent issue faced by these patients, where several studies inform that 50%-70% of the people suffering from MS reported falls in the past two to six months [48].

Elderly

The walking patterns in the elderly population are subject to two factors: the effects of aging and the effects of pathologies such as osteoarthritis and Parkinsonism [22] (although some pathologies affecting walking could be also undiscovered by the patient or his/her doctors). If the second effects are excluded, the gait of healthy elderly generally resembles slow walking in younger adults [49]. Generally seen patterns include decreased stride length, variable and typically decreased cadence, increased walking base, and increased relative duration of the stance phase. It is suggested that these changes in the gait features are triggered by the need to improve the security during walking [49], characterized by lower times in which the weight is supported by only one limb, and making easier to keep balance by reducing the stride length and increasing the walking base.

3 Robotic gait rehabilitation systems

During the past two decades researches have been developing several robotic systems meant to improve the gait rehabilitation of people that are impaired in their lower limbs due to a medical condition. These efforts are made thanks to the evident advantages of robotic systems over traditional, manual therapy approaches. Robotic systems are able to perform motion training in an intensive, precise, repetitive and reproducible way, without being restricted by the physical limitations of the therapists and reducing the number of therapist needed for each training session, easing the therapists' job on the way. In the same way, robotic rehabilitation enables parameterized active, assistive, and resistive exercises.

This chapter presents an overview of the state of the art in robot-based gait rehabilitation. Additionally, it presents the robotic system for over-ground gait rehabilitation *MOPASS*, which was developed by a consortium composed of technical and clinical partners for the design, control and test of the system.

3.1 State of the art

The state of the art systems implement several therapy techniques, mechanical designs and control approaches. Most of them base their robotic-aided rehabilitation techniques on the idea of fomenting the active participation of the patient, assisting him/her depending on his/her performance during the training, avoiding the usage of full-assistance to closely track the desired joint trajectories, or implementing adaptive reference gait patterns. These techniques are referred to as 'assist-as-needed' or 'patient-cooperative' strategies.

Different types of systems have been built until now for both commercial and research purposes, with sundry designs and degrees of freedom (*DoF*). After a careful investigation, the robotic gait rehabilitation systems (*RGRS*) can be classified as follows: treadmill systems with lower-limb robotic orthoses, footplate systems, mobile platforms with lower-limb robotic orthoses and stand-alone systems.

Treadmill-based exoskeleton systems

Treadmill-based exoskeleton systems are the most common type of RGRS. These systems are usually characterized by big structures that include a treadmill and an attached robotic system assisting different joints and movements in the body. Due to their size and stationary operation, treadmill systems often include partial or complete body-weight support (*BWS*) for the patients.

Lokomat [50] [51] is the most known RGRS worldwide. It is commercially available and is the system that has undergone more clinical tests. It consists of a treadmill, a controlled BWS mechanism, a parallelogram for trunk stability and horizontal movement, a lower-limb exoskeleton for active assistance in hip and knee flexion/extension, and passive foot lifters to support dorsiflexion in both ankles. Although the commercial system implements a fixed position control, several researchers have presented assist-as-needed and patient-cooperative strategies to foment the active participation of the patients while using *Lokomat* [52] [53], for instance, by adjusting the trajectory or controller parameters in order to minimize the interaction forces between the device and the patient. A newer version of this system, the *LokomatPro* [54], offers new features, such as weight shift and balance activation through lateral and rotational movements of the pelvis and assist-as-needed support. However, no specifics on the design or implementation are given to this date.

Another widely researched RGRS is *LOPES* (*LOwer-extremity Powered ExoSkeleton*). The first version of the system [55] [56] [57] consists of an exoskeleton for the legs and an end-effector robot for the pelvis working together with a treadmill. It offers eight DoF, namely ab/adduction in hip joints, flexion/extension in hip and knee joints, and mediolateral and anteroposterior movements in the pelvis, together with a passive joint for longitudinal pelvic motion. *LOPES* implements different virtual physical models (*VM*) (such as inertias, springs and dumpers), to generate interaction forces between the robotic system and the patient. These VMs are activated and deactivated during the gait cycle, so that each VM is used during a specific gait (sub) phase. *LOPES II* [58], the latest version of the system, is composed of a treadmill, a harness, and a parallel 'shadow leg' structure located behind the patient and connected to the patient's joints with rods. It offers the same eight powered DoF from the previous version, whereas all the other DoF can be left free to enable quasi-unconstrained movement in the corresponding joints. This system implements an assist-as-needed approach together with an admittance controller. It enables the therapist to set desired support levels during different gait (sub) phases, and translates these desired support levels into stiffness profiles and adjustments of the reference joint trajectories.

PAM (*Pelvic Assist Manipulator*) and *POGO* (*Pneumatically Operated Gait Orthosis*) are two other known RGRS that work together with a treadmill and a controlled BWS mechanism [59] [60]. *PAM* is composed of two robotic mechanisms (each one with three pneumatic cylinders) for pelvic support, whereas *POGO* consists of two pneumatic cylinders, fixed to a telescoping rail system, that induce hip/knee joint flexion/extension movement. Together, they offer a wide range of active DoF: *POGO* offers two active DoF (flexion/extension in knee and hip joints) and two passive DoF (hip ab/adduction and ankle dorsiflexion) per leg; whereas *PAM* offers five active DoF on pelvis (the three translational DoF, pelvic rotation and pelvic obliquity) and one passive DoF (pelvic tilt).

Another well-known system is *ALEX* (*Active Leg EXoskeleton*), which to this date possesses three versions. The first version is composed of a treadmill together with a trunk and a leg orthosis attached to the patient. The trunk orthosis offers four DoF, namely mediolateral and longitudinal translations, and rotation in sagittal and transverse planes. The leg orthosis, on the other hand, offers active DoF for flexion/extension of the hip and knee joints, and passive DoF for hip ab/adduction and ankle dorsiflexion. It offers an assist-as-needed therapy approach by means of a force-field controller implemented in world space coordinates, which applies support forces in the foot composed by a force tangential to the foot trajectory (to help the patient when he/she has problems following the trajectory speed) and a force normal to the foot trajectory (to maintain the user near the desired trajectory). The latter force is calculated with respect to a virtual wall around the desired foot trajectory wherein no normal support forces are applied. The design of the second version, *ALEX II* [61], which consists of a back support and a leg orthosis, is similar to its predecessor, offering the same DoF and implementing the same force-field controller. ALEX III [62] [63], on the other hand, presents an enhanced design with 12 active DoF: four in the pelvis (rotation around the vertical axis, and anterior/posterior, superior/inferior and lateral translations) and four in each leg (hip adduction/abduction, hip and knee flexion/extension, and ankle plantar/dorsiflexion). Additionally, it implements an adaptive assist-as-needed controller which includes a force-field controller with an adjustable virtual wall.

A treadmill-based robotic gait rehabilitation trainer is also presented in [64] [65]. This system was designed to apply corrective force fields in pelvic obliquity, while trying to mimic the interaction between patient and therapist during traditional rehabilitation. The system consists of a stationary frame standing over a treadmill, and an actuated pelvic mechanism. It offers active assistance for pelvic rotation about the anteroposterior axis, while leaving free

the other DoF in the pelvis. The system is meant to work with a lower-limb exoskeleton in charge of transferring corrective moments to the pelvis, imparting forces onto the user's lower body, and altering the orientation of the pelvis in the frontal plane. The initial implementation of the system presented a legs' exoskeleton with passive DoF for hip ab-/adduction, hip internal/external rotation, hip and knee flexion/extension and ankle plantar-/dorsiflexion. However, the idea is to combine it with the *AndROS* lower-limbs exoskeleton [66]. *AndROS* offers active DoF for knee flexion/extension and passive DoF for hip ab/adduction and flexion/extension, and is originally designed to assist only one leg generating its reference trajectories from the unassisted leg. Both the pelvic mechanism and *AndROS* implement impedance controllers in their actuated joints to generate corrective force/torque fields.

Another commercially available system is the *AutoAmbulator* [67] [68], although not many details from this system are available. It consists of a treadmill, a BWS mechanism and a couple of robotic arms to assist flexion/extension of hip and knee joints. The *Walkbot* system [69] [70] is also commercial, comprising a treadmill, a lower-limbs orthosis, a gravity balancing orthosis and a BWS mechanism.

Although the aforementioned systems are the most know RGRS working with treadmills, there exist sundry devices that have been developed worldwide for research purposes. An out-of-the-box system is presented in [71] called *RGTW*. It consists of a pneumatic lower-limb orthosis that offers active DoF for hip and knee rotations in sagittal plane and passive DoF in the ankles, and works together with a treadmill to train the walking underwater. *COWALK* [72] comprises a treadmill, a lower-limb exoskeleton and a gravity compensator, offering three active DoF in pelvis (translational motion in the horizontal plane and rotational motion along the longitudinal axis), three active DoF per leg (hip and knee flexion-extension and ankle dorsi-/plantarflexion), and two passive DoF per leg (ankle inversion-eversion and hip ab/adduction). In [73], a soft-actuated exoskeleton for lower limbs designed to work together with a treadmill and BWS is presented. The exoskeleton is powered by Pneumatic Muscle Actuators (*pMA*), and offers four active DoF per leg, namely ab/adduction in hip, flexion/extension in hip and knee, and dorsi-/plantarflexion in ankle. In [74], a system consisting of treadmill, BWS and a lower-limbs' exoskeleton driven by pneumatic actuators is presented, which offers active DoF for flexion/extension in hip and knee, and dorsi-/plantarflexion in ankle. These are only some examples of research prototypes.

Footplates systems

Similar to the treadmill systems, footplates devices are stationary and often include BWS. The basic idea of these systems is to train the gait patterns of the patient by assisting the feet movement through programmable footplates, normally allowing the movement of the feet in the sagittal plane.

The first footplates-based system was the *Gait Trainer* [75], which offers assistance to the feet to perform walking-like movements in sagittal plane, whilst controlling the patient's center of mass in vertical and horizontal directions. It also offers partial or total support of the gait movements by adjusting the output torque according to the patient's active participation. The *HapticWalker* [76] [77] is another well-known system of this type. It consist of a programmable footplates device with three active DoF per foot, corresponding to the foot movements in the sagittal plane (two translational and one rotational). The *HapticWalker* implements virtual environments (e.g. walking and going up/down stairs) which might include perturbations (e.g. stumbling and sliding), and offers programmable trajectories to that end. Another interesting approach is presented in [78], where a system composed of a lower-limb mechanism (consisting of footplates and a sliding device that generates 3-DoF

spatial motions on the sagittal plane for each foot) conjunct with BWS and an upper-limb mechanism (which allows users to swing their arms naturally) is presented. The device is combined with a simple virtual reality component that allows the user to navigate in virtual environments while training. Additionally, the lower-limb mechanism can be used to simulate different terrain types, e.g. stairs and slopes. *LOKOIRAN* [79] and *LokoHelp* [80] are other systems that combine a footplates mechanism with BWS. The latter one also includes a treadmill in the therapy process.

Mobile systems for over-ground training

Unlike the previous groups, these devices are not stationary, letting the training to be performed on actual foot-ground interaction. In general, these systems comprise a motorized platform holding other complementary mechanisms, which may include lower-limb active orthoses and pelvic attachment systems. This type of RGRS may also have BWS mechanisms, leading to bulkier and heavier devices.

The *WalkTrainer* [81] [82] [83] is the first example of this type of systems. It consists of a motorized mobile platform, an active pelvic orthosis, an active leg orthosis, a controlled BWS mechanism and electrical muscle stimulators, offering six active DoF in the pelvis and three active DoF in each leg, namely hip and knee flexion-extension and ankle dorsi-/plantarflexion. The *WalkTrainer* uses a compliance controller and implements an assist-as-needed strategy that aims to automatically select the level of compliance of each one of the active DoF. Additionally, it uses EMG (Electromyography) to calculate the level of muscle stimulation given to the patient by means of CLEMS (Closed Loop Electrical Muscle Stimulation), aiming to minimize the forces that the patient is applying to the orthosis.

NaTUre-gaits (*NAtural and TUnable REhabilitation gait system*) [84] [85] [86] [87] [88] is another extensively researched RGRS. This system consists of three modules: a motorized platform, a pelvic assistance mechanism and leg robotic orthoses. The pelvic assistance mechanism includes BWS, and is composed by a couple of compound robotic arms (one in each side of the patient) which give active assistance to perform translational motion in the sagittal plane in each side of the pelvis (resulting as well in pelvic rotation about the vertical and sagittal axis), as well as mediolateral movements. Additionally, it offers passive rotation of the pelvis about the transverse axis. Thanks to this mechanism, the system is able to perform balance control. The leg orthoses offers active assistance for hip and knee flexion-extension and ankle dorsi-/plantarflexion. This assistance can be full or partial in order to compensate the patient's lower-limb muscle power.

Another mobile RGRS that offers a wide range of active DoF is *CORBYS* [89] [90] [91], whose development was based on the design and analysis of the *RoboWalker* concept [92] [93]. Besides incorporating an omnidirectional motorized mobile platform for over-ground therapy, the *CORBYS* system includes the option to also work with treadmill in cases when the space is an issue. Additionally, it includes a pelvic structure and two active leg orthoses. These three components offer a total of 16 DoF to the patient: 10 active, namely longitudinal and mediolateral translations of the pelvis, pelvic rotation in the frontal and transverse planes, flexion-extension in the hip and knee joints and dorsi-/plantarflexion in the ankle joints; and six passive, namely ab/adduction and internal/external rotation in hip joints, and eversion/inversion in the ankle joints. The system implements an impedance controller in joint space, that works together with a robot model compensator, a velocity limiter controller and the torque controllers of each drive.

An interesting design of a mobile RGRS can be found in [94], where a combination of a motorized wheel chair and a lower-limbs exoskeleton is presented. The exoskeleton offers

three active DoF per leg, namely hip and knee flexion-extension and ankle dorsi-/plantarflexion, and three passive (two in the hip joint and one in the ankle). This versatile approach enables training not only of over-ground walking, but also of motion for standing up, sitting down, and stair climbing. Some other more simple designs can also be found in literature, e.g. the system presented in [95], the *ARGO* prototype [96] and *EXPOS* [97]. For instance, *EXPOS* is a system consisting of a motorized walker and a legs' exoskeleton. It offers active flexion/extension in hips and knees, and passive dorsi-/plantarflexion in ankle. However, this simplistic approach with a walker (like the ones used by the elderly to support their weight while walking) does not provide enough safety (e.g. concerning balance and falling) which becomes an issue for patients that require high or medium assistance in most aspects of walking, like for example balance control.

The aforementioned systems are composed by a mobile platform and some kind of lower-limb active orthosis. Nevertheless, there exist also mobile RGRS that do not include orthosis for the legs. This type of systems is mainly used to train the balance of the patients during over-ground walking in a fall-safe scenario. Two of these systems are the *WHERE-I* and *WHERE-II* [98]. The *WHERE-I* consists of a motorized mobile platform with a one-link rotary arm used as attachment to the patient and as electric BWS mechanism, whereas the *WHERE-II* is composed of a mobile vehicle with two one-link manipulators and a pneumatic BWS mechanism. Additionally, both devices possess a safety system and an intention analysis system. The latter is used when the systems are set to follow the movement intentions of the patient, instead of having a set trajectory to be followed, which describes their second operation mode. Both systems offer longitudinal motion (controlled by the BWS mechanisms), anteroposterior movement and rotation in place. Another system for balance training is the *KineAssist* [99]. It consists of an omnidirectional motorized mobile platform with a partial BWS mechanism and a pelvis/torso harness, offering active trunk rotations around the frontal and sagittal axis, passive torso rotation around the longitudinal axis, passive anteroposterior, mediolateral and longitudinal trunk movements, and passive pelvic rotations in all three axes. *KineAssist* also offers different operation modes: free walking, challenge mode (balance, obstacles), strength training mode (resistance), stabilization mode (adjustable-stiffness forces on trunk and pelvis), postural control mode (forces applied to maintain pelvis/trunk in certain position), adjustable BWS mode, and perturbation mode (therapist can push patient). Finally, the *GaitEnable* system is presented in [100]. This system is composed by an omnidirectional mobile base, a passive BWS mechanism and a passive pelvic linkage. It implements an admittance controller for the platform to move depending on user's intentions, and offers the possibility to generate gentle gait perturbations to facilitate balance training and gait assessments.

Stand-alone systems

Stand-alone devices are referred here as exoskeleton systems that do not use a support structure such as a platform or a static base. In principle, this type of devices are not designed for gait rehabilitation, but rather to give full assistance to people that have lost the movement on the legs (e.g. paraplegics), or as devices for human augmentation utilized, for instance, to enhance the strength of a person to lift heavy objects or to achieve high endurance during physical activities. Although their main objective is not gait rehabilitation, these systems have the potential to be combined with support mechanisms and proper control algorithms to be used as RGRS, and thanks to their autonomy, could be suitable devices to train movements such as going up/down stairs and stand-up/sit-down. In general, stand-alone systems can be divided into two groups: systems to enable handicapped people to walk, which usually are complemented with crutches or canes, and human augmentation systems.

In the first group we find commercial systems such as the *ReWalk* [101] [102] and the *EKSO* [103] [104] systems. Another system of this kind is *MINA* [105] [106]. All three aforementioned devices possess an exoskeleton that offers active DoF for hip and knee flexion/extension, and the users may use either crutches or canes if needed. Another system belonging to this category that has been tested with complete SCI patients (paraplegics) is *MINDWALKER* [107]. This exoskeleton offers active DoF for hip and knee flexion/extension and hip ab/adduction, together with passive DoF for hip and ankle endo/exo-rotation and ankle dorsi/plantarflexion. It implements a finite-state machine (*FSM*) that defines different motion scenarios and the assistance given in each one of them, and a HMI that triggers the transition between the states of the FSM depending on the user's intentions. The joint reference trajectories are tracked by means of variable-impedance controllers (in joint space) which are supervised by the FSM. Although stable walking was achieved during tests with healthy subjects using the system without any kind of support, in the case of Spinal Cord Injury (*SCI*) paraplegics there was the need to use crutches. Another system that could be part of this group is the one presented in [108], where the system consists not only of elastic crutches and a lower-limb orthosis that offers active DoF for hip and knee rotation in sagittal plane, but also a sort of skates-like foot-platforms, which allows forward and backward movements and turning. However, this system appears to be design more to roll rather than to walk assisted by it.

In the second group, the *HAL* (*Hybrid Assistive Limb*) commercial systems [109] [110] [111] stand out. The *HAL* series comprises different versions of the system, including a full-body exoskeleton (for upper- and lower- limbs), a two-leg exoskeleton and a one-leg exoskeleton. The lower-limbs exoskeletons are offered with active assistance in hip and knee joints for rotation in sagittal plane, and either passive or active dorsi-plantarflexion on the ankle joints. At first, the HAL systems were designed to apply joint torques and generate motion based one bioelectrical signal from the user (e.g. EMG) by means of a 'voluntary' controller. This way, the system was able to assist the user and move based solely on the user's intentions. The HAL systems have been widely used to assist physically impaired people, and some approaches to rehabilitation have been made as well with some success. In [112] [113], the two-leg version of HAL was used to perform gait support for complete SCI patients. Because of the difficulty of severely impaired people to produce bioelectrical signals that are appropriate for the voluntary controller, an autonomous controller was designed to complement it. It bases its operation in three steps: a user-swing-intention estimation based on the behavior of the center of ground reaction force (*CoGRF*): an inference of the speed of the swing leg based on the relationship between the walking velocity and the duration of the double stance phase: and the trajectory generation dependent on the outputs of the previous state. As stated before, the HAL systems have also shown modularity capabilities, being able to be used as a one-leg exoskeleton. This configuration was implemented to assist hemiplegic people in their affected leg based on the performance of the sound leg [114] [115] [116]. For this implementation, the autonomous controller was adapted to fulfill the requirements of the new tasks at hand. The control strategy for the *HAL* systems using the autonomous mode is normally a position Proportional–Integral (PI) controller, sometimes complemented with dynamic-model-based feedforward torques (e.g. torques corresponding to the dynamics of the system or to the gravity terms of the model).

Other systems are more focused in human augmentation. The BLEEX [117] and XOS 2 [118] [119], for instance, are two exoskeleton systems developed for military purposes aiming to increase the user's strength, agility and endurance capabilities. In [120] [121] a 10-active-DoF body exoskeleton for assisting nurse labor is presented. Other examples of systems designed for load-transferring tasks can be found in [122], [123] and [124].

Other systems

Besides the systems that have been presented so far, there exist some devices that have been developed to assist only one or two leg joints, independent from a static or mobile frame. In this group we find the so-called AFO (Ankle-Foot Orthosis) and KAFO (Knee-Ankle-Foot Orthosis), as well as other single-joint orthoses (e.g. knee orthoses). These devices can be used to help the users to walk, similar to the first type of stand-alone devices presented above, or can be combined with some other mechanisms (e.g. BWS, mobile or static platforms, etc.) to assist the patients during rehabilitation therapy. Some examples of this type of devices are presented in [125] (*RoboKnee*), [126] (*TUPLEE*), [127] (*Tibion PK100*), [128], [129] and [130], among many others.

Additionally, there exist some treadmill-based gait rehabilitation systems that do not possess a lower-limb active orthosis. A very out-of-the-box design of treadmill-based RGRS is *StringMan* [131] [132], which is a string-based mechanism with partial BWS that allows posture control in six DoF, comprising seven wires attached to a trunk/pelvic harness. This system does not assist the legs of the patients, but rather helps the patients to correct their posture and balance. The *MIT-Skywalker* [133] is another example of this type of systems. This device consists of BWS mechanism and two separate treadmills (one per foot) with different DoF in them. It offers as well a vision system for gait analysis and position sensing for high level control. Three different training approaches are offered by the *MIT-Skywalker*: rhythmic training (moving the ground in swing phase), discrete training (to train step length) and balance training.

Other type of systems used in gait rehabilitation are simulation systems, which include some motion simulator and a virtual-reality training environment. In this group we find, for instance, the *Rutgers Mega-Ankle* [134], a system that simulates walking by moving some platforms where the feet are located while a virtual environment is displayed in front of the user; and the *Sarcos Treadport* [135], which comprises a tilting treadmill (designed to apply forces to the user's torso), a harness and a virtual environment.

Finally, there are sundry devices that have been developed for lower-limb physiotherapy but not for gait rehabilitation. Here we can find, for example, couch/bed-based devices, such as the *MotionMaker* [136] [137], and the *iLeg* [138]. These two systems offer active DoF for hip, knee and ankle rotation in sagittal plane. Other type of devices designed to perform other type of lower-limb training (e.g. stand-up/sit/down motion) are presented in [139] and [140], among others.

Assessment of robot-based gait rehabilitation

Several tests have been done using RGRS (mostly *LOKOMAT*) with both healthy and impaired subjects. Although the studies tend to favor robot-based rehabilitation, they have yielded mixed results regarding the effectiveness of their usage and benefits and deficiencies with respect to traditional physiotherapy.

Several studies have been carried out to assess the outcome of therapy after using RGRS. Most of these studies showed that robot-assisted therapy improved many gait-related parameters (e.g. [141], [142], [143] and [144]). However, a few studies showed abnormal measurements in some gait parameters when using RGRS by both healthy [145] [146] [147] and impaired [148] subjects. Nonetheless, it is important to take into account that abnormal measurements can also be present during other types of therapy and may not be exclusive of RGRS. Other studies focused on finding the difference between robot-based gait rehabilitation and conventional therapy. These studies showed more mixed findings than the

previously mentioned ones, although most of them favor robotic rehabilitation. Some studies have reported advantages of RGRS with respect to conventional methods (e.g. [149], [150], [151] and [152]); others did not find significant differences between the two (e.g. [153], [154] and [155]); and finally, some have reported disadvantages of robot-based rehabilitation (e.g. [156] and [146]). A summary of the findings of some studies can be found in Appendix A.

3.2 *MOPASS* system

The *MOPASS* system [20] is an over-ground gait rehabilitation system developed by the *MOPASS* consortium[12], composed by technical partners with expertise in actuation, mechanical design for medical purposes, control and information technologies, as well as medical partners with expertise in rehabilitation. This section will present the features of the *MOPASS* system, including mechanical design, components and software design.

3.2.1 Mechanical design

The *MOPASS* system consists of a motorized platform and a pair of actuated leg orthoses. The CAD design is shown in Fig. 9, including the active DoF (circles), the main mechanical parts (diamonds), and the computers and batteries (stars).

The mobile platform consists of a chassis *{A}* with adjustable height and width, two motorized wheels *{W},* and four caster wheels *{B}*. The patient display *{PPC},* controller computer *{CPC}* and two batteries *{B}* for power supply of the computers and drives are attached to the chassis. The orthotic legs are connected to the platform through the trunk support *{C},* which allows limited lateral displacement along the frontal axis, as well as limited trunk rotation in all axes. The trunk support contains a couple of waist holders/cuffs *{D}* and one motor on each side *{1}* used to perform pelvic active movement. The base of

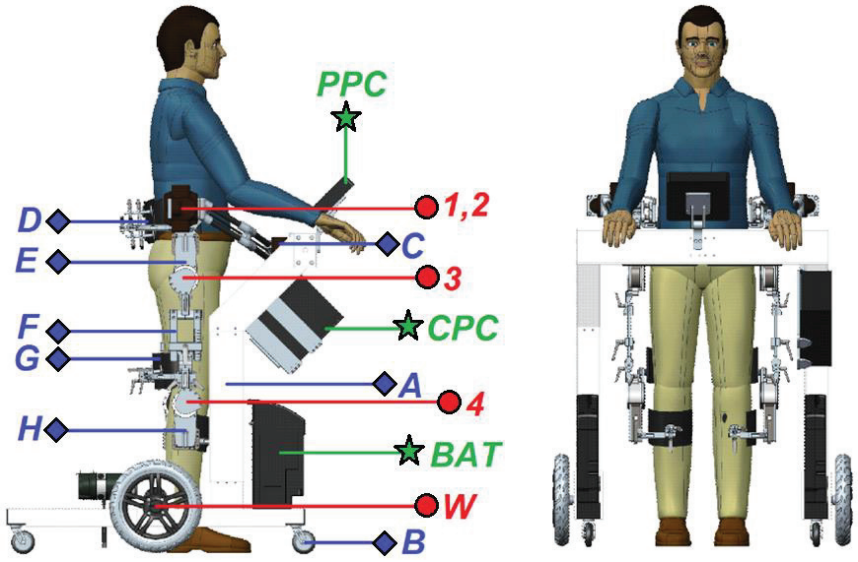

Fig. 9 *MOPASS* gait rehabilitation system

[12] Research supported by the German Federal Ministry of Education and Research as part of the MOPASS (**Mo**biles, dem Patienten ange**pass**tes,robotergestütztes Gangrehabilitationssystem) project under project number 13EZ1123A–E .

each leg orthosis *{E}* is attached to the trunk support by a mechanism that prevents rotation of the base in the sagittal plane regardless of the motion of the pelvis motors. Additionally, passive hip ab/adduction is introduced in this attachment between the leg base and the trunk support. The leg base and upper-leg link *{F}* of the orthosis are connected to a motor which allows hip active rotation in the sagittal plane *{3}*. The upper-leg link contains a thigh cuff, and permits length adjustments to adapt the link to the patient's leg. Finally, the lower- and upper-leg links are connected through a second motor that allows knee active rotation in the sagittal plane *{4}*. The lower-leg link *{H}* contains additionally a shin cuff.

The system offers several passive DoFs, briefly explained above, plus the active DoFs given by the eight motors installed on it. The active DoFs include hip *{3}* and knee *{4}* rotation in the sagittal plane, trunk/pelvis rotation *{1}*, and translation and rotation of the platform in the transverse plane given by the control of the powered wheels *{W}* (subject to the corresponding non-holonomic constraints introduced by the wheels). The pelvis active rotation is described by an eccentric movement that leads to circular motion of the leg's base. For simplicity, it can be described as two coupled DoFs, one active *{1}* and one passive *{2},* performing rotation in the sagittal plane. The active DoF is provided by the motor, and the passive DoF is enabled by the mechanical construction of the joint. The coupling is done so, that the angle of the virtual passive joint *{2}* has always the opposite sign of the angle of the active joint *{1}*. A list of all the passive and active DoFs of *MOPASS* system is given in Table 1. Additional information regarding the dynamic model of the system can be found in Appendix B.

The hip and knee joints are actuated using Maxon EC45 flat motors [157] with HFUS-2A harmonic drives [158] and Elmo Whistle Solo G-SOLWHI20/100SE servo-drives [159]. The mobile platform uses AMT SRG05 gear-motors [160] to actuate the wheels, together with the aforementioned Elmo servo-drives. Schunk PDU 70-101 servo motor drives [161] are used to actuate the pelvis modules. The position, velocity, current and torque limits of each one of the active joints are given in Table 2.

3.2.2 Architecture

This section will give a brief explanation of the overall architecture of the *MOPASS* system. The complete system consists of several components comprising computers, sensors and drives/motors.

Three computers are used in *MOPASS*: the therapist portable PC (Tablet), the patient PC

Table 1 Active and passive DoF in the *MOPASS* system

Degrees of Freedom	Active (A) / Passive (P)
2-dimensional translation of the platform in the transverse plane [a]	A
Rotation of the platform around the longitudinal axis	A
Hip and knee rotation in sagital plane (in each leg)	A
Trunk/pelvis rotation constrained to circular motions [b]	A
Hip ab-adduction (in each leg)	P
Trunk translation along the frontal axis	P
Limited trunk rotation around all axis	P

a. Subject to non-holonomic constraints

b. Given by the pelvis motors and mechanisms in each side of the body

Table 2 Limits of the active joints' in *MOPASS*

Joint	Maximum ang. position [deg]	Minimum ang. position [deg]	Maximum ang. velocity [deg/s]	Maximum current [amp]	Maximum torque [Nm]
Hip	-10	100	180	3.21 / 5	20
Knee	-90	0	180	3.21 / 5	20
Pelvis	unlimited	unlimited	---	4 / 8	15 / 30
Wheel	unlimited	unlimited	1200	---	---

attached to the mobile platform frame, and the controller PC. The therapist PC comprises the therapist user interface which is used by the therapists and doctors to give all the settings of the therapy, set and adjust the reference gait patterns, retrieve, show and save patient personal data, retrieve and save assessment and motion measurements and show them in real time, and handle the device operation. The Patient PC has two components: the server of the system and the patient graphical user interface. The server is the heart of the communication between all the components in the system. It is in charge of the network management and of retrieving and delivering the information between other components in the network. The patient interface offers a limited set of functions to the patient during training, such as stopping the device when desired or showing some therapy measurements for assessment and encouragement. Finally, the controller PC comprises all the control functionalities of the system (except for the low-level controller built in the motor drives). A detailed explanation of these functionalities is given in the next section.

The device is equipped with six motors with their corresponding drives. All of them communicate with the controller PC via CAN-bus, where the Elmo drives use CAN-Open as application layer protocol whereas the Schunk drives use a proprietary application protocol (Schunk Motion Protocol – SMP [162]). Additionally, *MOPASS* possesses heart-rate and foot-pressure sensors for assessment, which are optional to use and are not utilized by the system controllers.

The communication between all the components (except the drives and sensors of the motors, which communicate directly with the controller PC) is done through the server using Ethernet – TCP-IP. A proprietary application layer protocol was developed for this communication: Mopass Communication Protocol (MCP). This protocol included all the necessary functionalities to ensure a reliable and organized exchange of information between components aiming to have a high communication throughput. However, the details of the protocol are out of the scope of this manuscript. Fig. 10 shows the overall software architecture and communication network in the *MOPASS* system.

3.2.3 Controller computer

The control architecture of *MOPASS* is located in the controller computer, and it is based on the software framework offered by the Orocos project [163]. It consists of eight components in charge of management, communication and medium -level control of the eight actuated joints of the system, and three management components in charge of tasks such as general management, user commands handling and medium-level and synchronization control, additional to the build-in management and control tools in the Elmo and Schunk drives. The Orocos toolchain is a software tool to create real-time robotics applications using modular, run-time configurable software components. It offers real-time components, interacting scripting, state machines, distributed processes and code generation.

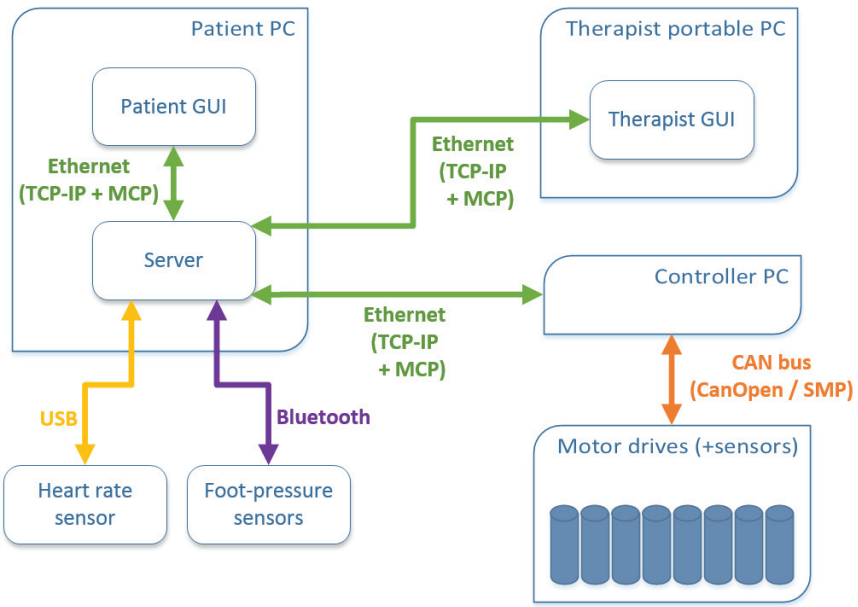

Fig. 10 Overall software architecture and communication in the *MOPASS* system

There are a total of eleven Orocos components in the *MOPASS* control network, namely *Guard*, *Therapist-Controller Interface (TCI)*, *Controller*, and the eight components in charge of the motor drives. A detailed diagram of this network is shown in Fig. 11. As it can be seen, the *Guard* component is connected to all the other components in the network. These connections appear as data flow connections and inter-component commands executions. Further connections are between the *TCI* component and the *Controller* component, and between the *Controller* component and the eight joint components. A brief explanation of each type of components is presented next.

Guard component:

As it can be inferred by the name, this component makes sure that all the components in the network are working without any problems, and takes action when that is not the case. Its thread runs at a relative low frequency of 10 Hz. Its main set of functions covers:

- Overall management of the Orocos components: it administrates what components are enabled, as well as it controls the Orocos components' state machines (Pre-Operational ←→ Stopped ←→ Running).
- Perform all the configuration on the components that must be done before they are run (i.e. in pre-operational and stopped states).
- Receive the error and warning messages from the components, handle them and take the corresponding administrative action.
- Act as the main interface between the user and the controller computer, publishing the errors and warnings to the higher layers, and handling the user commands that are not related with control and trajectory generation (e.g. enabling components, quitting program).

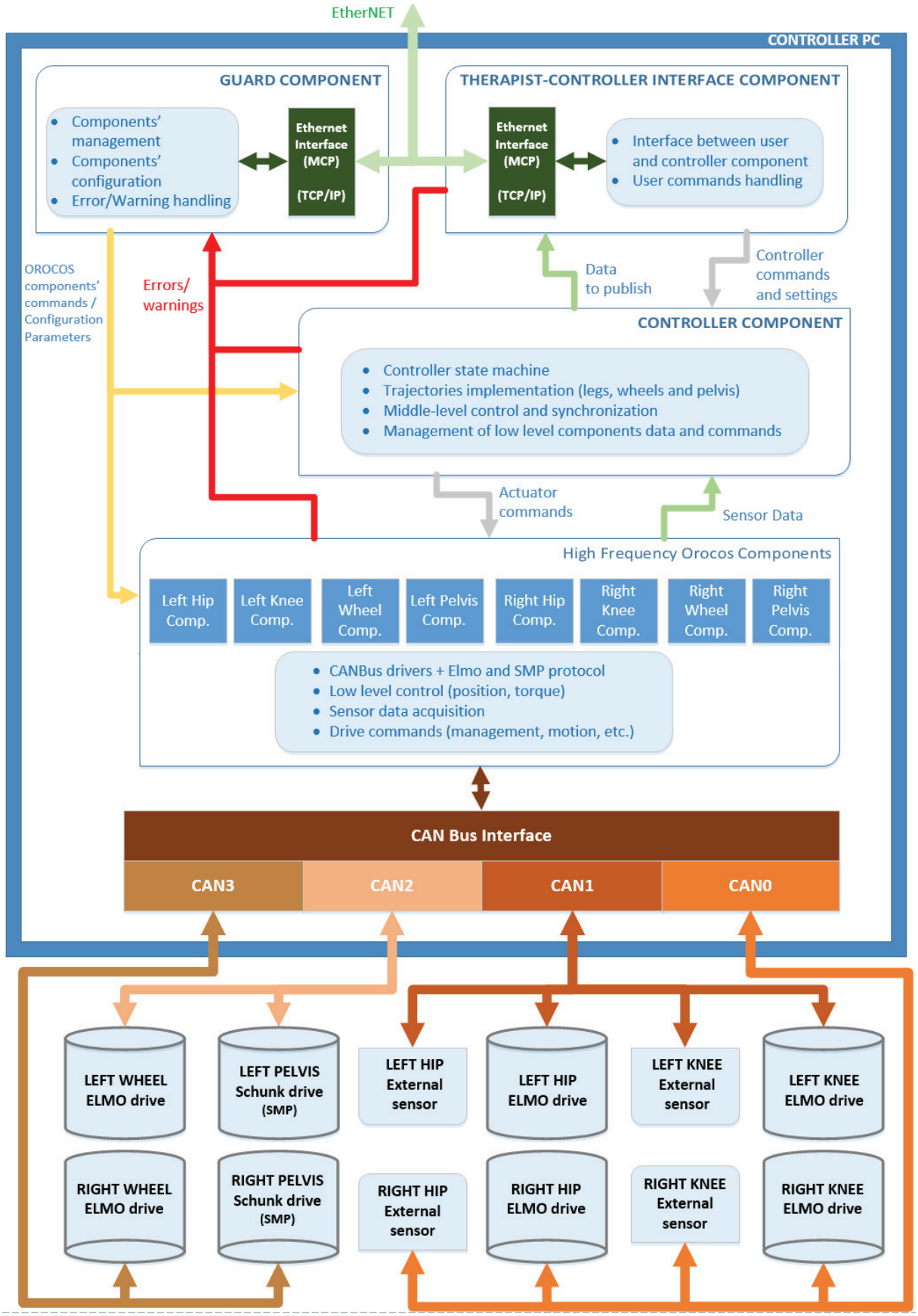

Fig. 11 Diagram of the controller PC architecture

Therapist-Controller Interface (TCI) component:

This component is the second interface between the user and the controller computer. It runs at a frequency of 20 Hz. Its main functions include:

- Handling the user commands that are related to control and trajectory generation (e.g. set joint trajectories, change velocity, change controller state). It verifies the input commands to make sure that they fulfill the controller specifications, such as motion limits and controller state machine allowed events. Once verified, they are passed to the *Controller* component to be executed.
- Publish the controller related data to the upper layers, e.g. joint positions and position errors.

Controller component:

This component is in charge of the control state machine, mid-level control and trajectory management. It runs at a frequency of 100 Hz and its functionality includes:

- Administration of the control state-machine: It performs an internal revision to allow or dismiss commanded state changes and setting modifications, and implements the functionality of each specific state. (The details about the controller state-machine will be given afterwards).
- Generates the trajectories for the hip and knee joints based on the curve parameters (points) and other gait parameters given by the *Generator* component.
- Generates the motion profiles of the pelvis and wheels joint so that they are synchronized with the hip and knee desired trajectories.
- Implements the first level of mid-control which involves the states of all joints in the system, such as synchronization and, if available, 'assist as needed' control.
- Send the specific control commands to the joint components, such as desired angular position or velocity.

Elmo components:

There are a total of six Elmo components in the network, one for each wheel, hip and knee joint. The hip and knee components run at a frequency of 333.33 Hz. whereas the wheel components do it at a frequency of 200 Hz. Their main functions are:

- Implementation of the CANOpen protocol and the Elmo-specific functionality to act as an interface between the Elmo-drives (plus external sensors) and the controller computer.
- Initialize the corresponding Elmo drive and external sensor by setting some CANOpen and control parameters.
- Send motion commands to the Elmo drives.
- Retrieve data from the Elmo drives and external sensors, such as actual position and current.
- Implements the second level of mid-level control which involves only the corresponding joint, e.g. the joint-space position control explained later on in section 5.1.1.
- General administration of the Elmo drives, including error handling.

SMP components:

There are two SMP (Schunk Motion Protocol) components in the network, one for each side of the pelvis (trunk). Each one of them runs at a frequency of 20 Hz. Their functions include:

- Implementation of the CAN-Bus protocol and the SMP-specific functionality to act as an interface between the Schunk-drives and the controller computer.
- Initialize the Schunk drives by setting protocol and control parameters.
- Send motion commands to the Schunk drives.
- Retrieve data from the Schunk drives and external sensors, such as actual position and velocity.
- General administration of the Schunk drives.

Additional to the controller computer and its mentioned components, the build-in control components of the Elmo and Schunk drives must be included in the overall control architecture. Each one of the drives counts with internal position and velocity controllers, among others. These drives communicate with the controller computer (more exactly with the respective Orocos components) via CAN-Bus. The complete CAN communication was distributed over four different buses in order to achieve better bandwidth usage, higher communication frequencies and therefore faster control components.

As stated above, the Orocos *Controller* component possesses a state machine in charge of avoiding invalid system state changes and user commands. The state machine was built for both, integrity of the usability and operation of the system, and safety measurements. It is the basis of the whole *MOPASS* operation, and was designed to give a high level of usability to the system, including features such as 'platform-driving' mode to move the platform without patient, turning mode to turn the platform and set its direction of walking before starting the walking training, therapy with position control for close tracking of the reference trajectories, enhanced therapy control strategies (e.g. 'assist as needed'), 'zero-force' control and spasticity detection. However, not all of these functionalities (namely the later three) have been implemented in the system because of the lack of appropriate user-intention feedback (e.g. torque sensors). Nonetheless, these functionalities can be easily added in future enhancements of the *MOPASS* system. The state machine consists of two layers: the outer layer, which corresponds to the generic Orocos component state machine (Pre-Operational ←→ Stopped ←→ Running); and the inner layer consisting of the operation states during training.

A diagram of the controller state machine is shown in Fig. 12. For safety reasons, the system will always start in 'Halt' state every time it is initialized. Additionally, states as 'Position control', 'Therapy control', 'Turning' and 'Drive' are only accessible if the system is in the home position, or if it is in halt and the previous state was the now commanded one (i.e. the user want to continue with the previous operation mode after a 'halt' command). Additionally, the states 'Zero-force control' (Follow-up mode) and 'Spasticity mode' can be activated from any of the other (Running) states, since these states are available to release pain or other uncomfortable situations. Furthermore, only some user commands are allowed in each of the controller states, for the same safety and operation related reasons. For instance, the leg with which the system will give the first step can only be set while 'at home'.

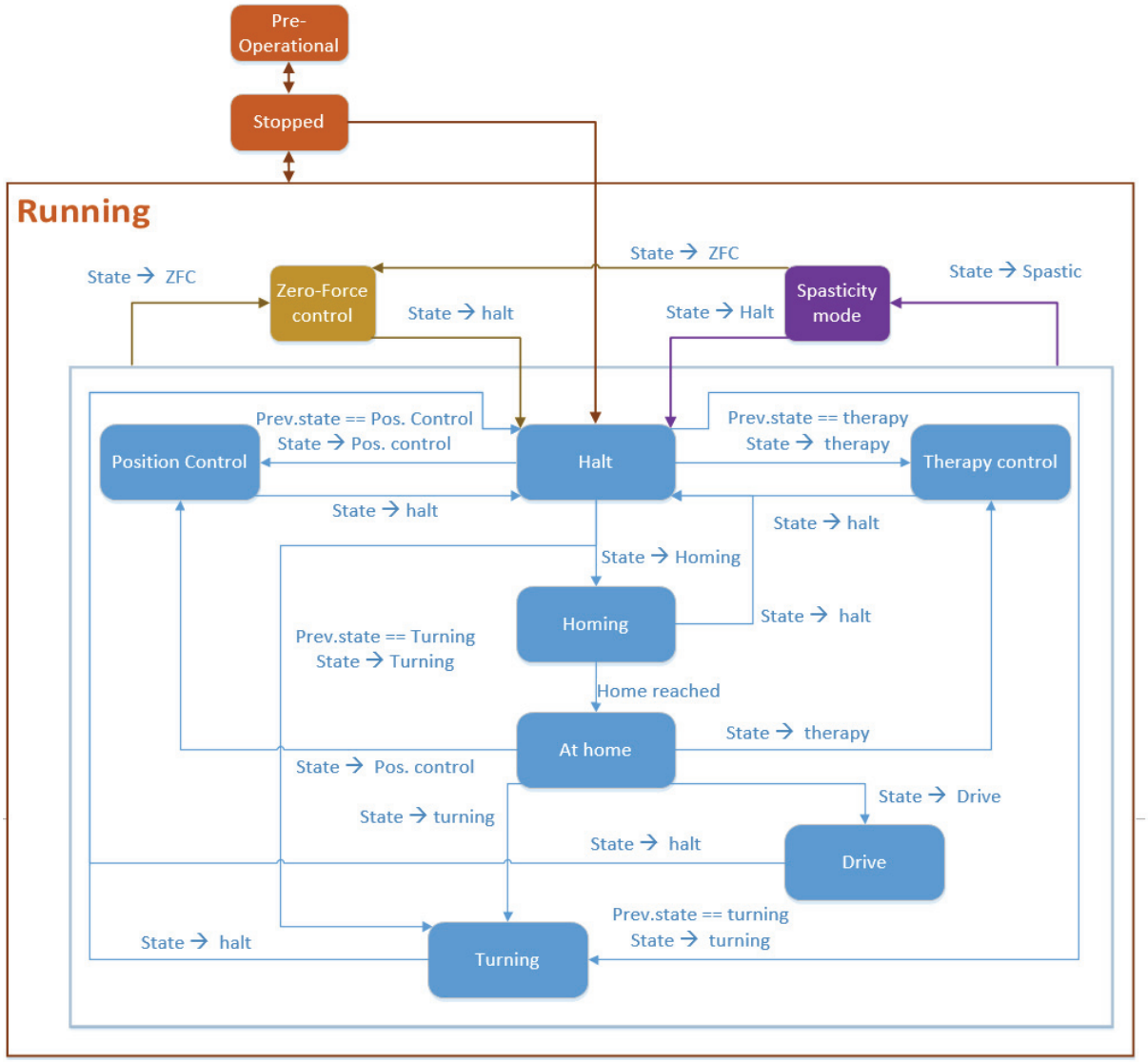

Fig. 12 Controller state-machine

4 Generation of reference gait patterns

This chapter presents the key contribution of the thesis and covers the theory behind the concept and implementation of the hip and knee joints trajectory generation for patient-tailored therapy. Initially, an overview of the state of the art regarding specifically trajectory generation for robot-based gait rehabilitation will be presented. Next, the specifics of the trajectory generator developed for the robotic system *MOPASS* will be explained. First, the concept for trajectory generation proposed in this work will be introduced. This concept is based on the generation and adaptation of joint trajectories through some points (also referred as knots) in the position curves, namely the characteristic points (which influence the most the motion pattern) and the shaping points (used for shaping the curve). The adjustment of these points is offered to the therapist in order to fit better the therapy reference trajectories to a specific patient and his/her (dis)abilities and preferences. The adaptation is done in a graphical way, so that it is easy and intuitive for the therapist to adjust the curves as desired. Besides the intuitive adaptation of the trajectories, the therapists are also offered healthy gait patterns' templates to be used as reference for the desired adaptations. The idea is that the therapist are able to see how would the joint trajectories of a healthy walking pattern look like depending on some desired therapy gait parameters, namely walking speed and cadence. Based on these healthy-like trajectories, the therapist will be able to adapt the patient-tailored therapy reference trajectories in a better manner.

To be able to automatically estimate the healthy-like trajectories, an experiment on healthy subjects performing over-ground walking was carried out in order to obtain the data that will be used to train the estimation algorithms. The specifics of the experiment are therefore presented in this chapter. Additionally, a detailed explanation of the raw data processing is given, including the cycle segmentation, the drift compensation and the automatic extraction of the characteristic points, walking speed and cadence. Next, the training and performance of the characteristic points' estimation algorithm are presented. In this case, Artificial Neural Networks (*ANN* or *NN*) were used to perform such estimation. The shaping knots' estimation process is presented afterwards, including the different methods that were used for the automatic extraction of the shaping knots' parameters from the processed data and the estimation of such parameters depending on the desired walking speed and cadence. This way, the complete process of reference trajectories' generation is covered. Ultimately, an evaluation of the final trajectories' estimation method is presented and the limitations of the proposed experiment and methods are introduced.

4.1 State of the art

Not many publications address in detail the issue of trajectory generation and manipulation for robotic gait rehabilitation systems. Some of the ones addressing this topic are presented below.

The *LOKOMAT* system, implements position control to track fixed angular trajectories of knee and hip joints based on recordings of healthy gait patterns. Not much information is given about the selection of these reference trajectories, but it is known that it is made based on the patient's height and the range of motion at the joints [146]. Some trajectory adaptation algorithms have also been presented which aim at 'patient-cooperative' therapy strategies using the *LOKOMAT* system. Three adaptation algorithms are presented in [52] which modify the hip and knee joint curves changing their period, amplitude and angular off-set based on the patience active participation. The first algorithm makes a model-based adaptation of the

trajectories by minimizing the estimated active forces exerted by the patient; the second one uses the direct dynamics formulation to perform a variation in the acceleration of the joint motions; and the third one modifies the trajectories based on an impedance controller and the interaction forces between the patient and the system.

The *NaTUre-Gaits* system incorporates the trajectory generator *GaitGen*. Several approaches have been studies and implemented by this research group. In [164], a healthy-gait database is used together with a mapping algorithm and a normalized formula for gait parameters to obtain the extrema points of the joint curves depending on desired gait parameters (namely walking speed, stride length and stance-phase timing) and the anthropometric features of the patients (Lower-limb segment length, height and physical constraints). These extrema points are later interpolated using cubic splines to generate the joint motion profiles. In [165] and [166], the authors used Multi-Layer Perceptron Neural Network (MLPNN) to predict natural values of cadence and stride length depending on the age, gender, height, and weight of the patient (*Stage 1*), which are used afterwards as inputs by a multiple linear regression model that delivers sets of Fourier coefficients, which are ultimately used to generate the hip, knee and ankle joint curves via discrete Fourier transform (*Stage 2*). In [167], MLPNN were used in *Stage 2* instead of the linear regression models to estimate the Fourier coefficients, with their inputs being the desired stride length and cadence (obtained in *Stage 1*), the patient's anterior superior iliac spine, and the lengths of the upper-leg, lower-leg and foot of the patient. Finally, in [168], two sets of Generalized Regression Neural Networks (GRNN) are used in *Stage 1*: one to predict suggested ranges of walking speed depending on the patients age, gender, height, and weight: and another one to predict the stride length based on the aforementioned physical characteristics of the patient and the selected walking speed. The selected walking speed and stride length are finally used by a gait parameters' calculator to obtain the final stride length and cadence which is used as input of *Stage 2*.

The *LOPES* group has also published some strategies for trajectory generation, including [169] where reference trajectories for hip ab-/adduction, and hip and knee flexion/extension are obtained, based on measurements done to unimpaired subjects, by predicting some key curve parameters using regression models with walking speed and the subjects' leg lengths as inputs. These key parameters correspond to normalized time, position, velocity and acceleration of the joint curves in some key events: the moments where the position and velocity reached a minimum or maximum, the starting and ending points of each trajectory (heel contact), and some additional fixed instants (fixed values of normalized time) to reduce fitting errors. Finally, these parameters were used to interpolate the time-position points (ordered pairs) corresponding to each event using 6th order B-splines. The *LOPES* team later presented an improvement of the previous method [170] adding one key parameter per joint and including a study in ankle dorsi-plantar flexion. In the new method, regression models based on walking speed (2nd degree polynomials) and subject's height (1st degree polynomials) were used to predict the key parameters, and piece-wise quintic splines were used to interpolate them. *LOPES II* [58] incorporates the previous method in its trajectory generator (only that it uses 3rd order splines to interpolate the key points), and combines it with an user interface that allows the therapist to indirectly change the joint trajectories by adjusting the level of support for each patient based on some gait sub-tasks.

Another detailed method is given in [171], where recorded data of healthy subjects walking at different speeds is used to build a database which is later utilized to obtain patient-specific joint trajectories depending on the patient's gender, age, height, weight, thigh length and shank length. The customization is made through a probability distribution model and the obtained trajectories can be further adapted by desired kinematic parameters such as walking

speed and step length. The *CORBYS* system [90] goes for a different approach for trajectory generation. This device allows the therapist to interact physically with the legs of the patients, as he/she would do in traditional therapy with BWS, while the system is in a full-compliant mode, allowing the therapist to move the legs as desired. This is a learning process for *CORBYS*, where it records the desired trajectories and corrections for each specific patient and, after some data processing, reconstructs periodic joint motion curves that are representative of the therapist's correction across all gait variables.

In [76], a special Fourier-based interpolation method is implemented to generate cyclic foot trajectories for the *HapticWalker*. In [172], a pattern adaptation approach is shown for the *ALEX* system, where the patient's pre-training pattern is initially acquired and then modified towards a healthy pattern depending on the patient's progress. In [173], a model-based adaptation tool is offered to be used in the *LERE* system, focused on deriving adaptive joint trajectories by minimizing the active torque exerted by the patient, with the help of the inverse dynamic model, a fuzzy adaptation algorithm, and a trajectory generator. Another attempt to generate hip and knee trajectories from recorded data from a healthy leg that takes into account desired gait characteristics such as walking speed, gait cycle period and gait phase changes can be found in [174], where Radial Basis Functions Neural Networks were used to fit the joint curves. In [112], quintic splines are used to generate the hip, knee and ankle trajectories in the *HAL* system during gait training with Spinal Cord Injury patients. This generation is done together with a swing-motion intention estimator and a swing-speed calculator, and is performed on the basis of minimizing the jerk related to the trajectories.

Some other approaches have been followed specifically for patients that present disabilities in only one leg, whilst the other leg has only mild impairments, as it is normally the case of patients with hemiplegia. The idea behind these approaches is to generate online the reference trajectory for the affected leg based on the actual movement of the sound leg, which moves unconstrained. One example can be seen in [175] [176], where the authors tested the generation of joint trajectories by means of Complementary Limb Motion Estimation (*CLME*). The objective of the CLME is to map the current position and velocities of the unaffected leg into reference angular positions and velocities for the affected leg. Inter-joint coordination patterns were extracted from recorded physiological gait patterns to this end. In this case, the authors implemented the CLME following two approaches: Principal Component Analysis (*PCA*) and Best Linear Unbiased Estimator (*BLUE*). Other examples can be seen in [114] [115], where a single-leg version of the *HAL* system is adapted to assist people with hemiplegia. In this case, the sound leg moves without constraints while recording the motion of its hip and knee joints during the swing phase. This recorded swing motion profiles are used as the reference trajectories for the hip and knee joints of the impaired leg during the subsequent swing phase. During the stance phase of the affected leg, its reference trajectory is fixed to a constant trajectory (no information about these trajectories is given).

From most of the aforementioned studies it can be seen that the freedom given by the systems to the doctors and therapists to adapt the gait patterns to fit a specific patient's capabilities is very constrained, limited to the setting of just very general parameters such as cadence and walking speed. Some others attempt to generate patient-specific trajectories incorporating more personal features as inputs, such as age and height, which at first glance might seem to tackle the customization problem, but the fact that people have personal walking patterns, that patients possess different disabilities, and that most methods lack enough freedom to change the proposed patterns to fit the patient's personal walking preferences and disabilities suggest that there is still place for improvement. Moreover, most of the trajectory-related handling is non-transparent and inaccessible to the users. The usage of not-intuitive trajectory parametrization methods, such as usage of Fourier coefficients and

joint accelerations, hinder the possibility of giving more freedom and decision power to the doctors and therapists during the trajectory generation process.

4.2 Concept for trajectory generation for hip and knee motion in sagittal plane

The idea in the *MOPASS* project was to design a user-friendly interface that allowed the therapist to adjust the hip and knee trajectories in an easy and intuitive way, as well as to select desired gait parameters such as walking speed and cadence, aiming to a more patient-specific therapy. This way, the doctors and therapist have more freedom to select and adjust the joint trajectories, instead of leaving most of the decision power to the trajectory estimators of the system. Consequently, the therapist can address in a more specific and effective way the different abnormalities present in the kinematics and spatiotemporal gait parameters of impaired patients (presented in 2.2) or set compensatory reference trajectories to cope with specific patient dysfunctions which, although they might be considered non-normal patterns, they might increase the chances to get better rehabilitation outcomes (e.g. independent walking).

The objective behind the adaptation of hip and knee motion profiles is to offer the therapist a way to adjust the joint trajectories in an intuitive and graphical way, so that the gait patterns that are taken as reference for the robot-assisted therapy could be adapted thinking on each patient's limitations and preferences. The proposed method was developed based on the adaptation of the joint trajectories through some characteristic points of the curves (the ones that influence the most their shapes and the gait pattern resulting from them), such as the extrema. To this end, an extensive research in literature regarding the shape of the hip and knee angular displacements in the sagittal plane during healthy walking was carried out in order to see which points from the joint trajectories should be taken as the characteristic points.

In the case of the knee joint, most of the curves showed a similar shape, with a clear presence of four extrema points during the complete gait cycle. An example, taken from [24], can be seen in Fig. 13, where the extrema $P_{M1}...P_{M4}$ are circled. Thanks to this, the selection of the four extrema points of the curve as the characteristic points that will rule the shape of the knee trajectories was straight forward. Referring to the theory behind human walking presented in section 2.1, these points correspond to the maximum knee flexion (P_{M1}) at the end of the loading response, a minimum flexion (P_{M2}) at the terminal stance, the global maximum extension (P_{M3}) at the end of the initial swing, and the minimum flexion (P_{M4}) present at the end of the terminal swing, near the moment of heel strike. In the case of the hip joint, the curve shapes extracted from the literature differ slightly from each other. In general, there were three different types of shapes: with clear presence of four extrema (Fig. 14-a); with only two extrema but a marked bending point near the maximum hip flexion (Fig. 14-b/c); and with only two extrema and no marked bending points (Fig. 14-d). These points are circled (with no shade) in Fig. 14. It was decided to take four characteristic points to rule the shape of the hip trajectory since it is possible to cover all three types of curves when they are conveniently set. For the first type of curves it is clear that the characteristic points correspond to the four extrema points. For the second type, the selected characteristic points would be the two extrema, together with the marked bending point and the point between the global maximum and bending points that influences the most the curve shape (e.g. a second bending point). For the third type, two points near the maximum extension can be taken as characteristic points, together with the global minimum and maximum points. Since there are no marked bending points in this curve, the selection doesn't affect significantly the shape of

the curve. For the latter two cases, the selection of the extra points as described (one point for the second type and two points for the third type) will conserve the shape and will not affect negatively the form of the curve, thanks to the interpolation method used to regenerate the trajectories, explained in the next section. Examples of these extra points can be seen in Fig. 14, circled with shade.

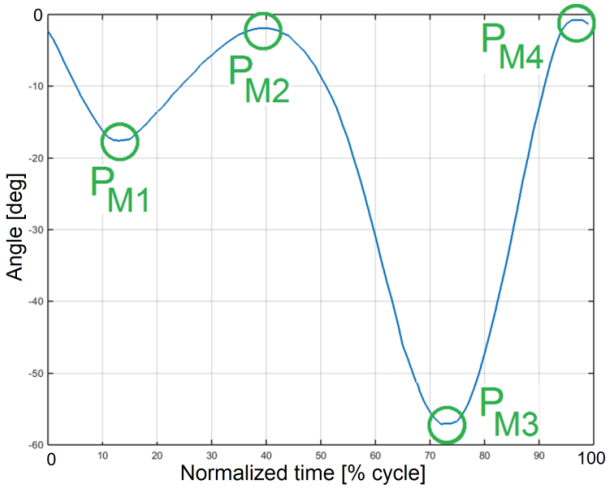

Fig. 13 Knee joint trajectory for healthy walking[13]

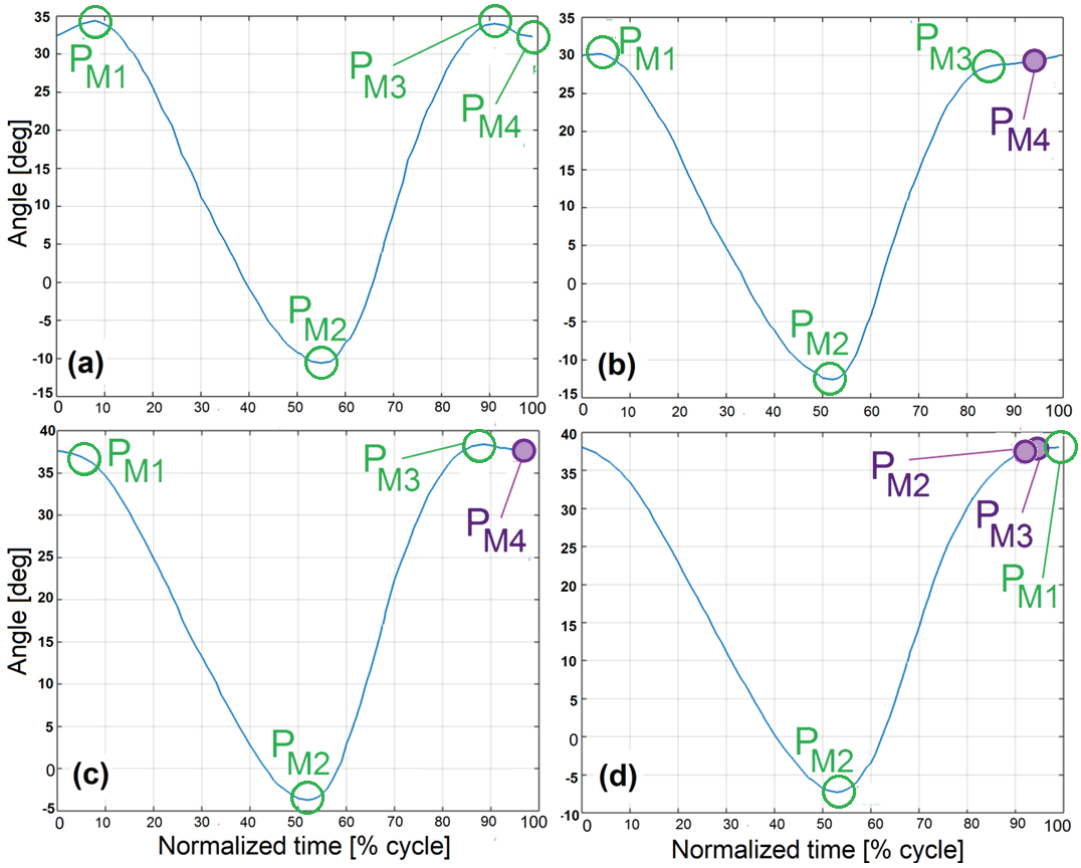

Fig. 14 Hip joint trajectories for healthy walking[14]

[13] Angles extracted from [24]

[14] Angles extracted from [195] (a), [196] (b), [197] (c) and [201] (d).

The spatio-temporal behavior of the hip and knee joints is completely governed by the selected characteristic points. Because of this, care must be taken when setting the limits in which the therapist can adapt these points. A slightly misplacement of any of these points can highly affect the resulting walking pattern. On the other hand, the right selection of these points can results in trajectories that tackle better the disability of a specific patient and help him/her achieve better results. For example, an increase in the swing maximum flexion of the knee (P_{M3}) could help in cases of foot drop. If the ankle is not fit enough to perform the dorsiflexion necessary to avoid contact of the foot with the floor during swing phase, a higher knee flexion can compensate that deficit. Because only the maximum flexion during swing phase has to be changed, the therapist must be able to change the parameters of that characteristic point alone, without disturbing the other ones, in a way that is simple and intuitive. In the same way, other specific disabilities can be tackled by adjusting only the part of the joint trajectories related to them (i.e. in the cycle phases where they are present), without disturbing the motion of the joints in the other phases.

Fitting methods for curve reconstruction

Several fitting methods were researched and tested in order to obtain the most appropriate one, able to fulfill the basic requirements given by the concept of generation and adaptation of joint trajectories via curve characteristic points. The researched methods were developed for curve generation on different areas, including computer graphics. Specifically, seven fitting methods were selected for a more detailed study:

1. Cubic spline interpolation from *MATLAB* [177] [178]
2. Piecewise Cubic Hermite Interpolating Polynomial (PCHIP) offered by *MATLAB* [179], based on [180].
3. Piecewise Quintic Hermite Interpolation (PQHI) taken from [181]
4. Boundary-Valued Shape-preserving Interpolating Spline (BVSIS), taken from [182] and explained on [183] [184] [185], based on Bernstein polynomials.
5. SDDEEL energy-minimization framework with strain energy optimization [186].
6. SDDEEL energy-minimization framework without strain energy optimization [186].
7. Periodic spline shared by *MATLAB* user Bruno Luong via *MATLAB* Central Newsreader [187].

Table 3 shows the main features of each one of the studied interpolation methods. The continuity degree is very important in this specific application since the first and second derivatives of the interpolation function correspond to the angular velocity and acceleration of the joint, respectively, and it influences directly the smoothness of the trajectories. Abrupt jumps on the velocity or acceleration on the joints are highly undesired in robotic applications and should be avoided. On the other hand, locality is important at the moment of computation, since local methods will search for the solutions fulfilling the desired constraints without revising all the data and recalculating all the function parameters, but doing it just in the vicinity of the knots where the constraints are not fulfilled. Locality is also important from the shape point of view because changes on one specific point will affect the shape only of the vicinity of that point, leaving the curve unchanged in the other areas. The polynomial degree is worth of taking into account because of the pros and cons related to it. The higher the degree, the more degrees of freedom one has, which might be useful when setting constraints

Table 3 Main features of the curve fitting methods

Method	Continuity degree	Locality	Polynomial Degree	Piecewise Monotonicity	Periodicity	Boundary constraints
(MATLAB) Spline	C^2	No	3th	No	No	No
PCHIP	C^1	Yes	3th	Yes	No	No
PQHI	C^2	Yes	5th	Yes	No	Yes
BVSIS	C^2	Yes	6th	Yes	No	Yes
SDDEEL	C^2 (if possible) Minimum C^1	No	3th	Yes	No	No
Periodic spline	C^2	No	3th	No	Yes	No

on the interpolation knots; but higher degrees imply also more complex polynomials and bring some other issues related to monotonicity that are explained afterwards.

Piecewise-monotonicity is not only a desired feature but a required one because of the concept of trajectory generation in the project, explained previously. To be able to ensure that the global and local minimum and maximum points selected by the therapist remain as the extrema of the curve after interpolation, it is necessary that the selected fitting method possesses a piecewise monotonic behavior. An example of non-desired interpolation behavior from fitting methods without piecewise monotonicity can be appreciated in Fig. 15-a. It is also desired that the only extrema present in the curve are the ones selected by the therapist. A problem on this regard might arise with interpolation methods that use high-degree polynomials (even with constraints in the higher derivatives (e.g. 1st and 2nd) in the interpolation points, although it is more unlikely to happen), due to the fact that there might exist a polynomial that fulfills the interpolation constraints for the given interpolation points, but has other local minimums and maximums between them. A trivial example can be seen in Fig. 15-b, where a quintic polynomial is plotted. This polynomial possesses two local minimum and two local maximum points. If it is desired to have only two extrema points, denoted in Fig. 15-b by the shaded points, a quintic spline that uses this polynomial would

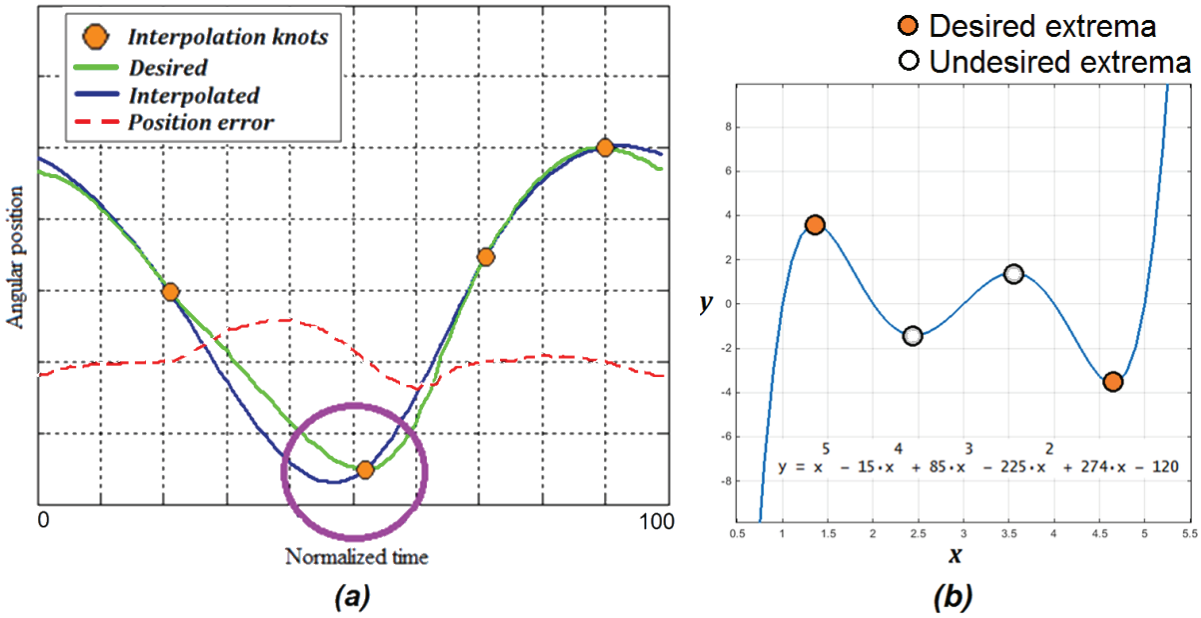

Fig. 15 Problems with non-monotonic interpolation

insert two undesired additional extrema points, denoted by the unshaded points.

Finally, periodicity is also a highly important feature due to the nature of the application. The joint trajectories are considered to be quasi-periodic: a pure periodicity is not present in real-life walking, but the gait cycles are considered to be periodic for analysis purposes. In the case of gait rehabilitation, the reference trajectories used for the therapy are normally periodic. Accordingly, it is needed that the generated trajectories possess periodic attributes with boundary continuity (i.e. continuity in the transition from cycle to cycle). If the interpolation method is not inherently periodic, some actions can be done to achieve a periodic behavior as smooth as possible.

If the fitting methods possess boundary constraints, they can be used as workaround. Boundary constraints refer to desired derivative values (e.g. angular velocity and acceleration) in the first and/or last interpolation point of a series. In our case, it is possible to duplicate the first extremum point from the curve and locate the duplicate one period ahead. Let's analyze the case where a joint trajectory with gait period T is to be generated, and a set of n interpolation knots $\boldsymbol{P} = \{P_1, \dots, P_n\}$ that includes m ($m \leq n$) extrema points $\{P_{M1}, \dots, P_{Mm}\} \in \boldsymbol{P}$ are used to generate it. Each point is represented as an ordered pair with a temporal and an angular value: $P_i = (t_i, \theta_i)$. Suppose that P_{M1} is the first extremum point, i.e. the time value t_{M1} is lower than the time values of $\{P_{M2} \dots P_{Mm}\}$. All the interpolation points P_k that have a time value lower than t_{M1} can be translated to the end of the curve by adding the period to their time values: $t_k^* = t_k + T$. Likewise, P_{M1} can be duplicated, and the duplicate knot P_{M1}^* can be located at the end of the set, with a time value $t_{M1}^* = t_{M1} + T$. Note that the new set $\boldsymbol{P}^*$ contains now $n+1$ knots, and that the relocated knots, as well as the duplicate, possess the same angular values as the original knots. Moreover, because the new initial and final knots of the set are in principle the same knot, the boundary constraints are equal for both ends. If the method offers non-separable boundary constraints (i.e. automatic selection of the derivative values for the first and last interpolation knots so that they are equal in both ends), periodicity and boundary continuity in the derivatives are ensured. When that is not the case and the values of the derivatives for the boundary knots have to be set, C^1 continuity can be ensured due to the fact that the desired velocity in the first and last knots is zero (they are either a minimum or a maximum point). Nevertheless, note that this method only ensures C^1 boundary continuity unless the acceleration is known for the extrema points, which is not the case in our application. A default acceleration (e.g. equal to zero) could be set to overcome this problem and obtain a non-ideal 2nd degree of continuity.

For the sake of understanding, suppose that the original set of interpolation knots were as follows: $\boldsymbol{P} = \{P_1 \dots P_8\}$, with $t_1 < \dots < t_8$. The set $\boldsymbol{P}$ contains four extrema knots: $P_{M1} = P_3$, $P_{M2} = P_4$, $P_{M3} = P_6$, $P_{M4} = P_7$. Therefore, it is possible to obtain a new ordered set $\boldsymbol{P}^* = \{P_1^*, \dots, P_9^*\} = \{P_{M1}, P_{M2}, P_4, P_5, P_{M3}, P_{M4}, P_8, P_1^*, P_2^*, P_{M1}^*\}$, where $t_{M1} + T = t_{M1}^*$, $\theta_{M1} = \theta_{M1}^*$, and $\dot{\theta}_{M1} = \dot{\theta}_{M1}^* = 0$. An illustration of the operation is shown in Fig. 16.

If there are no boundary constraints offered by the fitting method, a second method can be applied to obtain pseudo-periodic interpolation with C^1 continuity in the cycle-to-cycle transition. The ordered set of knots $\boldsymbol{P} = \{P_1, \dots, P_n\}$ can be triplicated, and the two sets of clone knots can be located one and two periods ahead in the curve, with the corresponding change in their time values, obtaining a final ordered set $\widetilde{\boldsymbol{P}} = \{P_1, \dots, P_n, P_1^*, \dots, P_n^*, P_1^{**}, \dots, P_n^{**}\}$ with $3n$ knots. This means that the extrema knots $\{P_{M1}, \dots, P_{Mm}\} \in \boldsymbol{P}$ are also triplicated and relocated, getting a new set of ordered set of extrema knots $\{P_{M1}, \dots, P_{Mm}, P_{M1}^*, \dots, P_{Mm}^*, P_{M1}^{**}, \dots, P_{Mm}^{**}\}$. One can now interpolate the whole set and extract the generated curve in the middle area, starting from P_{M1}^* and ending in P_{M1}^{**}. This way, we obtain a periodic curve with C^1 boundary continuity. The values of the

second derivative in the boundary knots will be set automatically by the fitting methods, but most likely will differ from each other. Nevertheless, the existing difference between $\ddot{\theta}_{M1}{}^{*}$ and $\ddot{\theta}_{M1}{}^{**}$ is not high. Note that this method increases the complexity of the fitting by triplicating the number of knots to be interpolated, which ultimately increases the computation time. An example of this method is depicted in Fig. 17.

Taking all the above into consideration, the Boundary-Valued Shape-preserving

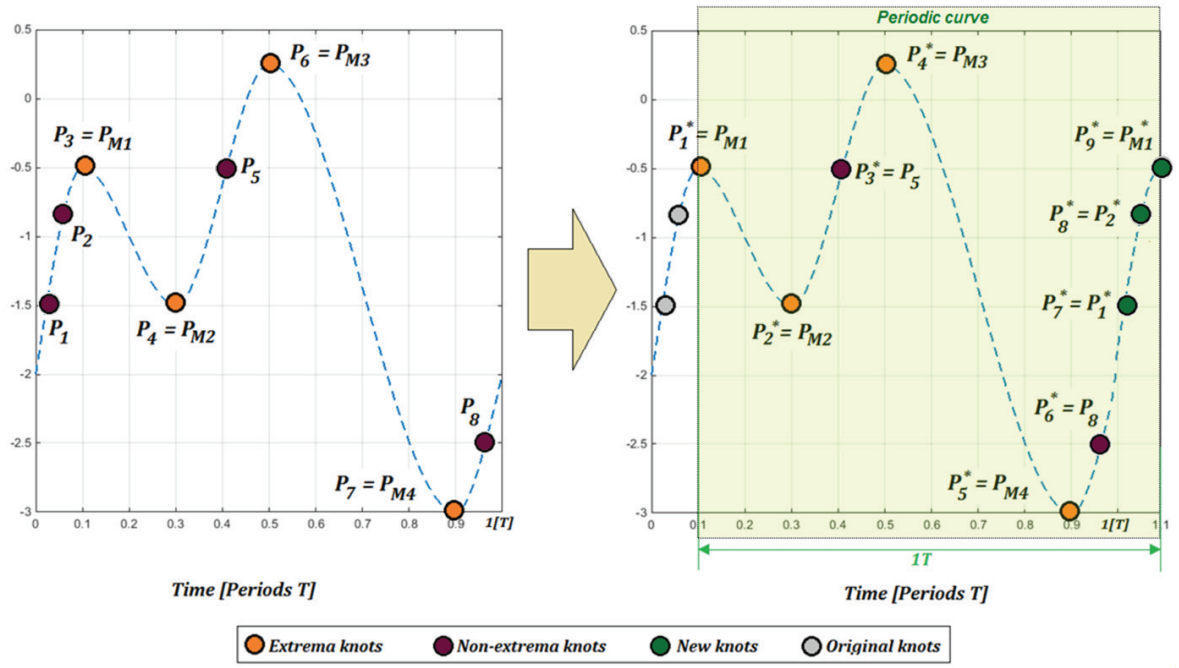

Fig. 16 Knots manipulation to achieve periodicity using boundary constraints

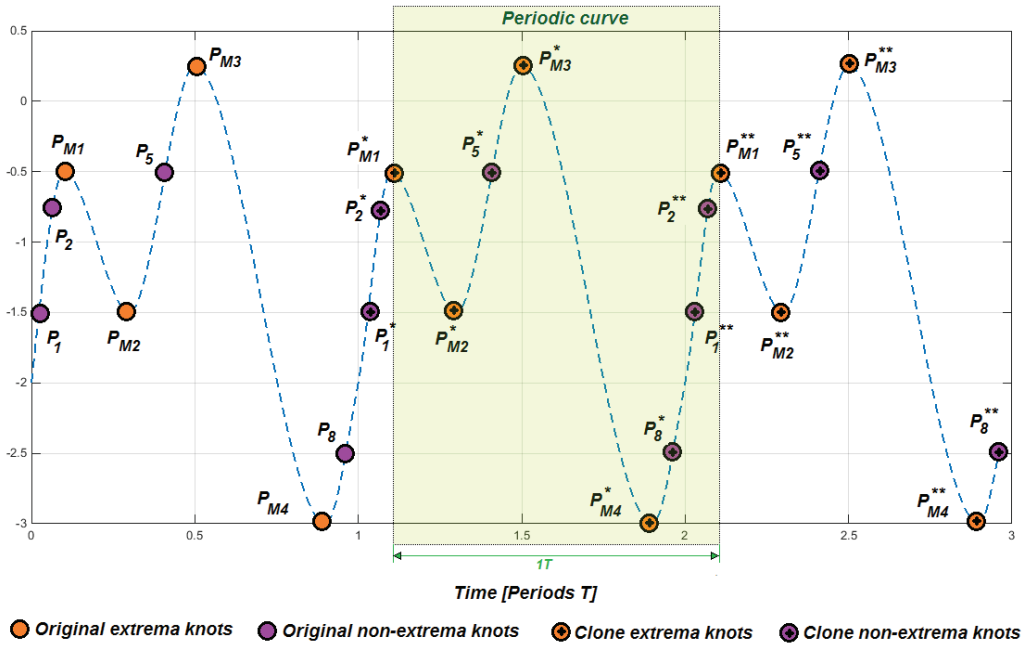

Fig. 17 Knots manipulation to achieve periodicity using knots multiplication

Interpolating Spline (BVSIS) [183] was finally selected as fitting method[15]. In summary, this method offers C^2 continuity degree, which means continuity in position, velocity and acceleration, and piece-wise monotonicity, which ensures preservation of selected extrema points and prevent undesired behaviors regarding the shape. Although this method is not inherently periodic, it offers the possibility to set separable and non-separable boundary constraints, therefore periodicity can be achieved. Also, if the non-separable constraints cannot be fulfilled, the two workarounds presented previously can be used to generate pseudo-periodic curves, which would be acceptable for the application.

It is important to stress that there exist other interpolation methods that allow setting of higher derivatives values in the points to be interpolated. In joint trajectory generation, it would mean to set desired angular velocity and acceleration values to the interpolation knots. An example of such methods can be seen in [170], where quantic splines are used to interpolate some given points constrained by desired time, position, velocity and acceleration. This will ensure both piecewise monotonicity and periodicity if the points are correctly handled. Nevertheless, this increases the complexity of the selection of the points since the derivative values of all knots must be known a priori. That is not the case of the method proposed here, since the therapist only interacts with the time and position values of the desired knots and only the desired velocities of the extrema are known (the velocities in these points are zero). Therefore these methods are not suitable for the proposed trajectory generation and adaptation method.

Curve-shaping principle

Although the characteristic points are the most influential regarding the shape of the joint trajectories and, ultimately, regarding the walking patterns resulting from them, it is necessary to include other curve parameters to obtain more healthy-like trajectories. In other words, it is necessary to influence the shape of the curves between the selected characteristic points, mostly in the area surrounding the maximum extension point in hip (P_{M2}) and the maximum flexion point during in the terminal stance in knee (P_{M3}). To this end, an inclusion of extra shaping knots is done. After an initial study with some reference joint trajectories extracted from the literature, it was decided to include four and six shaping knot for the hip and knee joint trajectories generation, respectively. In the case of the hip, two extra knots will be inserted between the maximum extension point (P_{M2}) and the previous characteristic point (P_{M1}), and two will be inserted between the maximum extension point (P_{M2}) and the next characteristic point (P_{M3}). For the knee, two extra knots will be inserted between the maximum flexion point (P_{M3}) and minimum flexion point in the terminal stance (P_{M2}); two will be inserted between the maximum flexion point (P_{M3}) and the minimum flexion point in the terminal swing (P_{M4}); one will be inserted between the maximum flexion point in the loading response (P_{M1}) and the minimum flexion point in the terminal stance (P_{M2}); and one will be inserted between the minimum flexion point in the terminal swing (P_{M4}) and the maximum flexion point in the loading response (P_{M1}). The selected areas for the placement of shaping knots can be seen Fig. 18, where an example with random shaping knots is shown.

Now, a selection of those ten shaping points must be done. To this end, the characteristic and extra shaping knots are expressed as ordered pairs of the form

[15] The code offered in [182] in *Fortran* programming language was translated into MATLAB and *C++* programming languages to be used throughout the study.

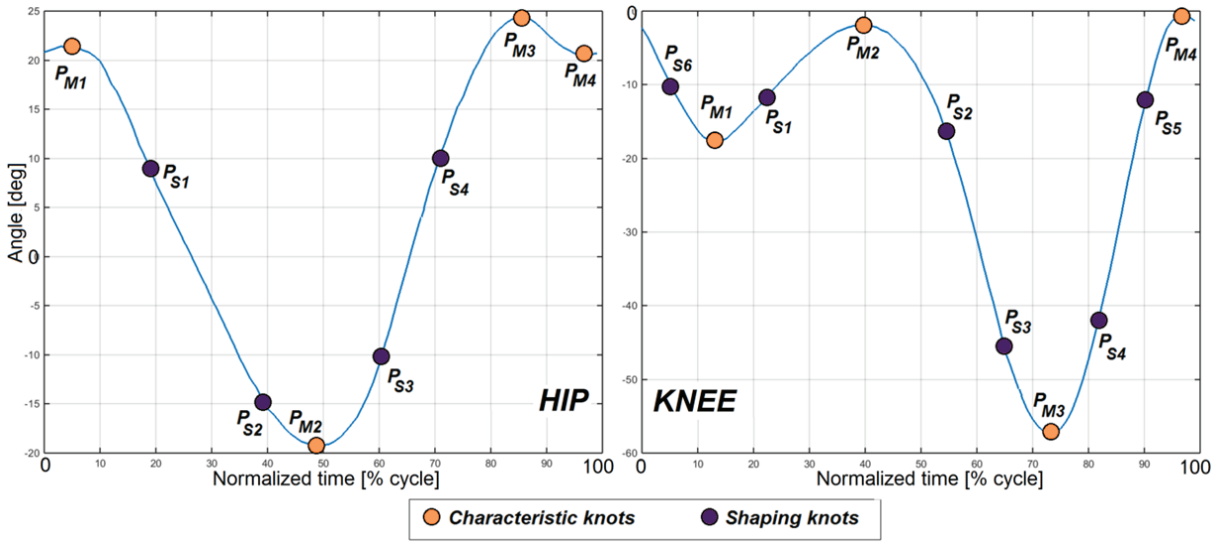

Fig. 18 Characteristic and shaping knots for hip and knee trajectories[16]

$$P = (t, \theta), \tag{1}$$

where $t = [0\ ,100)$ is the time value normalized with respect to the gait period and θ is the angular value. These two values are referred as the parameters of the points. The proposed method expresses the shaping knots as a normalized function of the characteristic points adjacent to them (i.e. the characteristic points are input parameters for the calculation of the shaping knots):

$$P_{Si} = (t_{Si}, \theta_{Si})$$

$$t_{Si} = f_t(\, t_{M+}\, , t_{M-}\,)$$

$$\theta_{Si} = f_\theta(\, \theta_{M+}, \theta_{M-}\,)\,, \tag{2}$$

where P_{Si} is a shaping knot ordered pair with the corresponding time and angular values, and the ordered pairs $P_{M+} = (t_{M+}, \theta_{S+})$ and $P_{M-} = (t_{M-}, \theta_{S-})$ correspond to the characteristic points located immediately after and before the shaping-point, respectively (i.e. the ones immediately surrounding it). The proposed functions are of the form

$$t_{Si} = \mathrm{mod}\big(\, t_{M-} + \alpha_{t_i} \cdot \big(t_{M+} + \gamma - t_{M-}\big)\,, 100\big) \qquad ;0 < \alpha_{t_i} < 1 \tag{3}$$

$$\theta_{Si} = \theta_{M+} \cdot \alpha_{\theta_i} + \theta_{M-} \cdot \big(1 - \alpha_{\theta_i}\big) \qquad ;0 \le \alpha_{\theta_i} \le 1 \tag{4}$$

where *mod* is the modulo operator, $\gamma = 0$ if $t_{M+} \geq t_{M-}$, and $\gamma = 100$ otherwise. The problem is now reduced to find suitable values of α_{t_i} and α_{θ_i} (referred as the shaping knots' coefficients or α-values) that characterize each one of the shaping knots. The automatic selection of these values is explained in section 4.3.3.

The manual selection of fixed values for the shaping points can also be offered to the therapist in an 'expert mode' in case they decide that a higher adaptation of the curve shape may benefit a certain patient, one that cannot be achieved only through the characteristic

[16] Angles extracted from [24]

points. In this case, α-values can be recalculated depending on this selection, and later be used to maintain the shape given by the therapist when the characteristic points are changed.

Trajectories for the initial step

The generation of the hip and knee trajectories for the initial step, starting from straight-standing position, is also covered in the study. For this, a short experiment was conducted with one subject performing over-ground walking to study the shape of these initial step trajectories and to revise the way they are related to the subsequent (quasi) periodic joint profiles. For the experiment, three markers were placed in one of the legs of the subject, as shown in Fig. 19: one on the hip, one on the knee, and one on the ankle. The subject was asked to start walking from a straight-standing position ten times: five swinging first the leg with the markers and five swinging first the leg with no markers. The movements were recorded with a RGB-D camera. Afterwards, the same markers were placed in the other leg in the same locations and the experiment was repeated to obtain the data from the second leg. Finally, marker-based joint detection and tracking was carried out using the *Kinovea* [188] software to extract the hip and knee joint trajectories from the recordings. For this study, the initial-step duration was considered as the time elapsed from the start of the step to the moment in which the knee of the swinging leg reached its minimum flexion point in the terminal swing (PM_4). After analyzing the raw data, it could be seen that the initial-step duration lied around 40%-50% of the gait cycle time. A default value of 50% was selected for the trajectory generator, but it can be manually changed by the therapist. Further analysis was done to each of the four trajectories at issue.

Regarding the knee joint of the leg performing the initial swing (referred as main leg in this report), the maximum flexion during this first step had an average normalized value of 60% of the maximum knee flexion (PM_3) angle of the subsequent step (i.e. the periodic trajectory). Likewise, this maximum flexion happened at around $0.6 \cdot T_{1s}$, where T_{1s} is the initial-step time. Taking this into account, an initial set of first-step characteristic knots was selected: one corresponding to the starting moment, with an angular value equal to the reference (standing) position, normally 0°; a second one corresponding to the maximum knee flexion during the first step, with a default angular value of $0.6 \cdot \theta_{M3}$; and one corresponding to the minimum flexion point in terminal swing (PM_4) from the periodic trajectory, where the connection between initial- and periodic- curves in done. Finally, an additional knot was

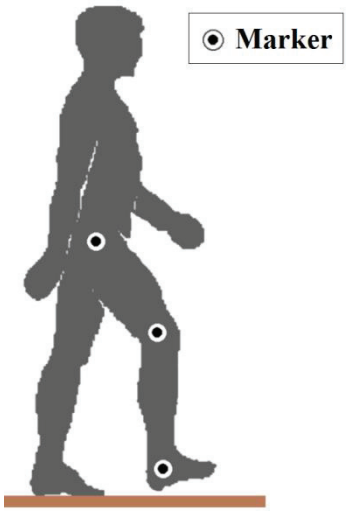

Fig. 19 Placement of markers for initial-step experiment

added to the curve between the first two characteristic points in order to shape it closer to the recorded ones. The angular and temporal values of this knot are relative to the values of the surrounding characteristic knots, following the same principle of the shaping knots from the periodic curve explained in the previous section. The temporal values of these four knots depend on the initial-step duration and are relative to the normalized time value of PM_4. An example of the knee curve for the main leg is shown in the lower-left plot of Fig. 20. A further manipulation of the maximum initial-step flexion knot is also offered to the therapist to adapt the initial-step trajectories to each patient to, for instance, exercise the foot clearance in this first step. Adaptation of the shaping knot can also be offered to the therapist as an extra feature for 'expert mode' trajectory adaptation.

For the other three trajectories (namely the curves of the hip and knee joints of the secondary leg and the curve of the hip joint of the main leg), a smooth transition between the given starting positions and a corresponding extrema point was performed with no extra shaping knots, as shown in Fig. 20. In the case of the main leg's hip, the curve connects the starting position with the maximum extension point (either PM_1 or PM_3 or PM_4) of the given periodic trajectory, whereas for the joints of the secondary leg, the transition is made from the starting positions to the hip maximum extension (PM_2) and the knee terminal stance minimum flexion (PM_3) points of the periodical curves. Notice that for these three joints, the time spent by these initial-step trajectories is not necessarily the same as the initial-step duration (i.e. the time spent by the main leg's knee to achieve the minimum point in the terminal swing). Instead, they are dependent on the time parameter of the characteristic points of the periodic curves.

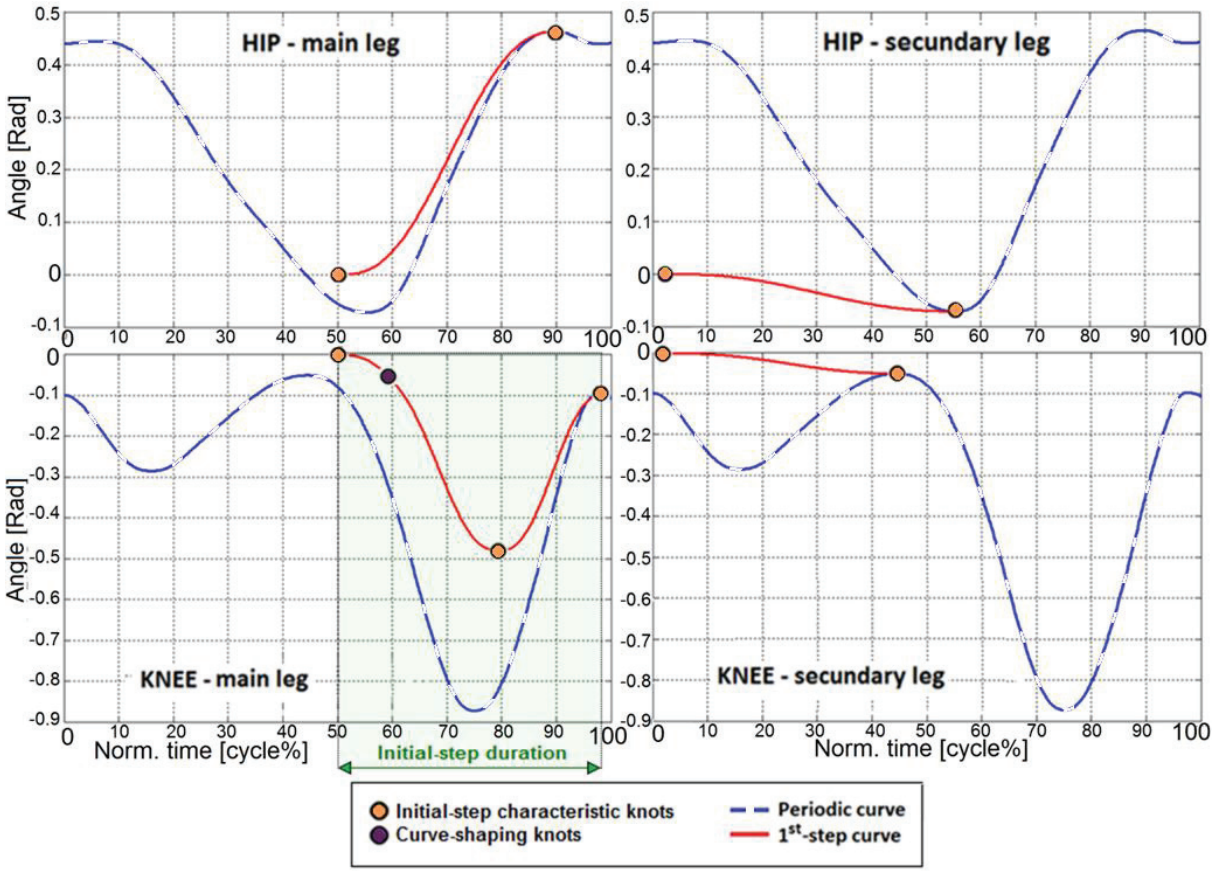

Fig. 20 Initial step trajectories

4.3 Automatic generation of hip and knee trajectories for therapy

As it is explained in the previous section, the generation of the periodic trajectories for hip and knee joints for the proposed method is parameterized by the characteristic and the shaping knots, together with the desired cycle period. Several studies have reported dependencies of the kinematic and spatiotemporal gait parameters on factors such as the walking speed[17-A], cadence[17-B], age[17-C] and gender[17-D]. Therefore, it is expected that these factors will directly influence the parameters of the knots used in the trajectory generation method, mostly the characteristic points. Accordingly, it is desired to give some of these factors as desired input parameters to the generator to automatically generate the trajectories based on them. More precisely, it is desired that the therapists are able to set some of these parameters and that the generator automatically creates healthy-like joint trajectories depending on them. This way, the therapist can use the estimated trajectories as reference patterns during the therapy sessions. To this end, a study on how the characteristic and shaping knots correlate to those input parameters is necessary. Because of the difficulty to obtain a large amount of subjects to cover a wide range of all four factors, the age and gender were not included in the study, leaving only the cycle period and walking speed as case study parameters.

Moreover, from a kinematic analysis of the leg's motion during walking, it can be seen that the leg segments' lengths have a direct influence on gait parameters such as step length and walking speed. In other words, if two persons have the same gait period and angular displacements in hip and knee, the person with larger leg segments will achieve a larger step length and, hence, a higher walking speed. A better insight to this fact can be appreciated in the following sub-section. This leg segment's lengths are tightly related to the height of the person. Hence, the height is also taken into account in the study. Normalization of stride/step length and walking speed with respect to the height is a common approach in gait analysis to scale these parameters [189].

To obtain the aforementioned correlations between input parameters (period, speed and height) and the knot parameters, a multi-task experiment on healthy subjects was conducted. The obtained data was later processed and fed to some learning algorithms in order to estimate the knots parameters based on the input parameters. The following sub-sections explain in detail the experiment and data processing, together with the implementation and results of the estimation algorithms for the characteristic and shaping knots.

4.3.1 Experimental study on healthy subjects

An experimental study was carried out in order to obtain healthy gait patterns' data during over-ground walking. These data, corresponding to hip and knee joint angular positions, was later processed to be used as input to the learning algorithms and further trajectory generation functionalities that will be explained in this section.

Experimental set-up

This section explains the details of the experiment that was carried out. A total of 18 subjects between 24 and 47 years old took part in the experiment. To the best of their knowledge, none of them possessed any health condition that would cause pathological

[17] **A)** [23] [25] [195] [255] [256] [194] [257] ; **B)** [23] [258] ; **C)** [25] [49] [195] [255] [256] [259] [260] [261] [262] ; **D)** [258] [260] [261]

walking. All the participants were informed about the scope of the experiment and gave their consent. From the study group, 7 of the subjects were female whereas 11 were male. The ranges of age, height and weight can be observed in Table 4, as well as their mean and standard deviation values. The lengths of the leg segments, namely upper-leg and lower-leg, were also obtained for each participant to be used in a later stage for kinematic analysis.

The joint angles were measured using the FMS-9 Inertial measurement units (IMUs) produced by *Hillcrest Labs* [190]. These 9-axis IMUs are low-cost modules with a dynamic accuracy of 2.5° that include a tri-axial accelerometer, a tri-axial gyroscope and a tri-axial magnetometer. Two IMUs where used in each leg, located in the frontal part of the upper and lower legs. Fig. 21 shows the sensors' placement. Special care was taken to place the sensors as aligned with the leg links as possible, since only data from one axis of rotation (corresponding to the sagittal plane) was used for the data processing. The sensor data was recorded with a sampling frequency of 50Hz by a graphical user interface developed in *C++* using the libraries offered by Hillcrest Labs, which also recorded the participants' relevant data in an anonymous manner. The hip angle θ_H corresponds to the rotation angle of the upper-leg IMU, whereas the knee angle θ_K corresponds to the angle formed by the upper- and lower- leg segments and was obtained following

$$\theta_K = \theta_{UL} - \theta_{LL}, \tag{5}$$

where θ_{UL} and θ_{LL} are the rotation angles given by the IMUs located in the upper- and lower-leg segments, respectively.

Once the subjects were explained the goals of the experiment and the IMUs were placed in their legs, they were asked to walk on the floor as comfortable as possible while avoiding strange (unnatural) walking and while following some given instructions related to desired gait parameters. The experiment was divided in three sections:

Ex1: The first exercise consisted in walking at different speeds. The subjects were asked to walk with the following speeds: as slow as possible, slow, medium, fast, and as fast as possible. For this exercise, unlike the next two exercises, the interpretation of the instructions was subjective, since no fixed target values were given to the participant. Likewise, no instructions on cadence or step length were given.

Ex2: For the second exercise, the participants were asked to walk while trying to maintain a given step length. The selected range of step lengths was 0.4 to 1 m, with increments of 0.1 meters between courses. To achieve this, several markers were placed in the floor equidistant from each other, depending on the desired step length of the course. The step frequency for this exercise was selected by each subject without any explicit instructions on this regard.

Ex3: Finally, the subjects were asked to walk trying to keep a given cadence, where the target step frequencies varied from 0.6 to 2 steps/s, increasing 0.2 steps/s in every course. For this, a periodic sound feedback was given to the subjects with the corresponding frequency. No instructions regarding step length were given to the participants.

Table 4 Age, height and weight of the study subjects

	Mean	**SD**	**Max**	**Min**
Age[years]	30.72	6.99	47	24
Height [m]	1.75	0.10	1.92	1.52
Weight [Kg]	68.83	15.03	100.00	48.00

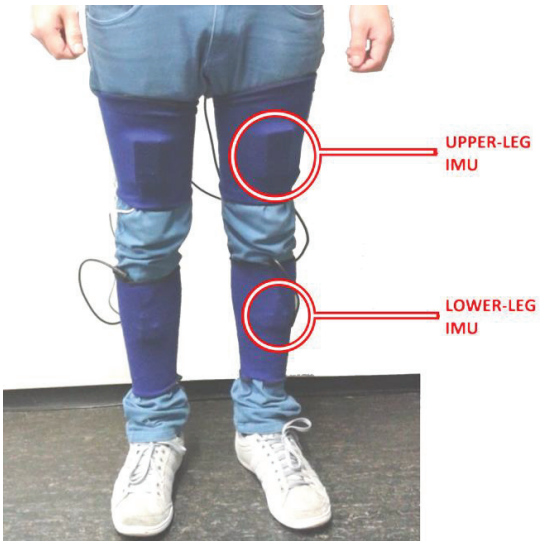

Fig. 21 Placement of the IMUs on the study subjects

Additionally, at the beginning and at the end of each one of the three sections, the subjects were asked to walk with their desired speed, step length and cadence, respectively. Taking this into account, a total of 26 courses were carried out by each subject (7 in *Ex1*, 9 in *Ex2* and 10 in *Ex3*), shown in Table 5, where they walked between 30 and 35 steps per course. In each one of the exercises, the subjects were given the chance to practice the walking with the desired parameters before the recording started, to get familiar with them and obtain the most comfortable and natural pattern possible. Likewise, they were able to repeat the exercise when they were not feeling comfortable or when their walking parameters were distant from the instructed ones. In the case of two subjects, one or more of the longest step lengths courses where discarded because of the difficulty to achieve the desired step length (*Ex2*) due to the subjects' leg lengths. Additionally, two subjects presented problems following the lower cadences of *Ex3*; hence these courses were also discarded.

Data processing

The raw data was processed by a program developed in MATLAB. The program was composed by different algorithms in charge of the gait cycles' segmentation, the drift corrections, the automatic extraction of the characteristic points (explained in section 4.2), and the calculation of gait parameters. The algorithms and program calculations are presented next.

Gait cycles segmentation

Initially, the raw data was filtered with a 2nd-order low-pass Butterworth filter with a normalized cutoff frequency of 0.35 to smooth the curves and remove high-frequency noise. Next, the filtered data of each course and of each leg was segmented into complete cycles. Since no ground-reaction forces were sensed during the experiment, the recognition of cycles was done solely with the hip and knee curves of the leg being analyzed. In this case, a recognition based on the horizontal position of the foot among the sagittal axis with respect to the hip was performed. This foot position is calculated straightforward using the kinematic relations of the subjects legs, based on the joint angles and the lengths of the upper and lower leg segments:

Table 5 Exercises of the experiment

Exercise	Instruction		Exercise	Instruction
P1-1	Walk with desired walking speed		P2-7	Walk with a step length of 0.9 meters
P1-2	Walk as slow as possible		P2-8	Walk with a step length of 1 meter
P1-3	Walk slow		P2-9	Walk with desired step length
P1-4	Walk with medium speed		P3-1	Walk with desired cadence
P1-5	Walk fast		P3-2	Walk with a cadence of 0.6 steps/s
P1-6	Walk as fast as possible		P3-3	Walk with a cadence of 0.8 steps/s
P1-7	Walk with desired walking speed		P3-4	Walk with a cadence of 1 step/s
P2-1	Walk with desired step length		P3-5	Walk with a cadence of 1.2 steps/s
P2-2	Walk with a step length of 0.4 meters		P3-6	Walk with a cadence of 1.4 steps/s
P2-3	Walk with a step length of 0.5 meters		P3-7	Walk with a cadence of 1.6 steps/s
P2-4	Walk with a step length of 0.6 meters		P3-8	Walk with a cadence of 1.8 steps/s
P2-5	Walk with a step length of 0.7 meters		P3-9	Walk with a cadence of 2 steps/s
P2-6	Walk with a step length of 0.8 meters		P3-10	Walk with desired cadence

$$x = l_{UL} \cdot sin(\theta_H) + l_{LL} \cdot sin(\theta_H + \theta_K) \tag{6}$$

where x is the i^{th} foot horizontal position, l_{UL} and l_{LL} are the upper and lower leg segment's lengths, respectively, and θ_H and θ_K are the hip and knee angles, respectively. Fig. 22(a) illustrates this relation between the foot displacement in the sagittal axis and the leg kinematics.

A new cycle was recognized every time the horizontal displacement achieved a local maximum value, but only if that value was higher than a selected threshold. An example of this procedure is depicted in Fig. 22(b) and Fig. 23. Following the convention for angles' directions used throughout this document, the hip flexion angles are positive and are measured with respect to the longitudinal axis, whereas the knee flexion angles are negative and measured with respect to the upper leg segment. Once the curves where segmented in cycles, it was decided to discard the first cycle and last cycle of each course to avoid the inclusion of atypical curves generated by the first and last steps. Additionally, the segmented data were manually checked in order to find and discard abnormal cycles, i.e. cycles where

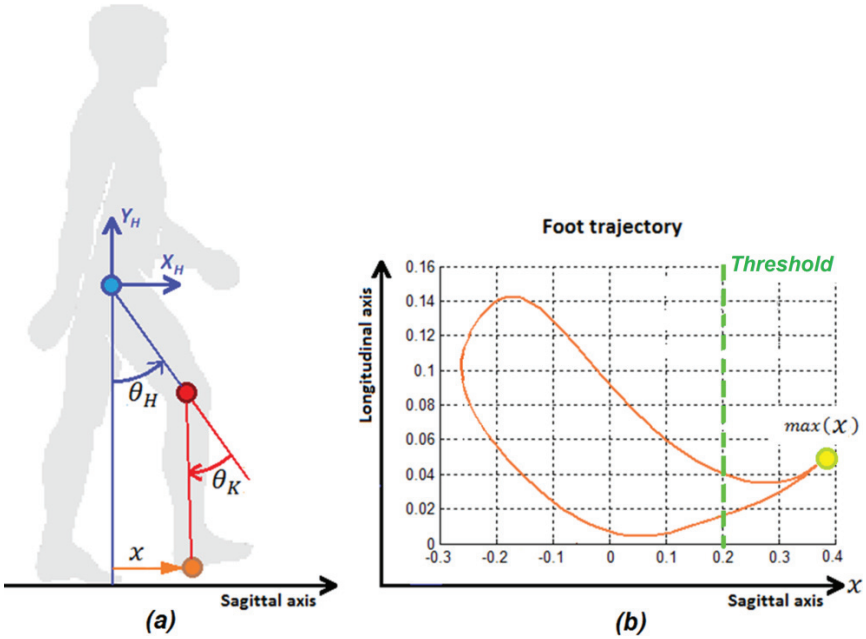

Fig. 22 Relation between the foot displacement in sagittal axis and the leg kinematics

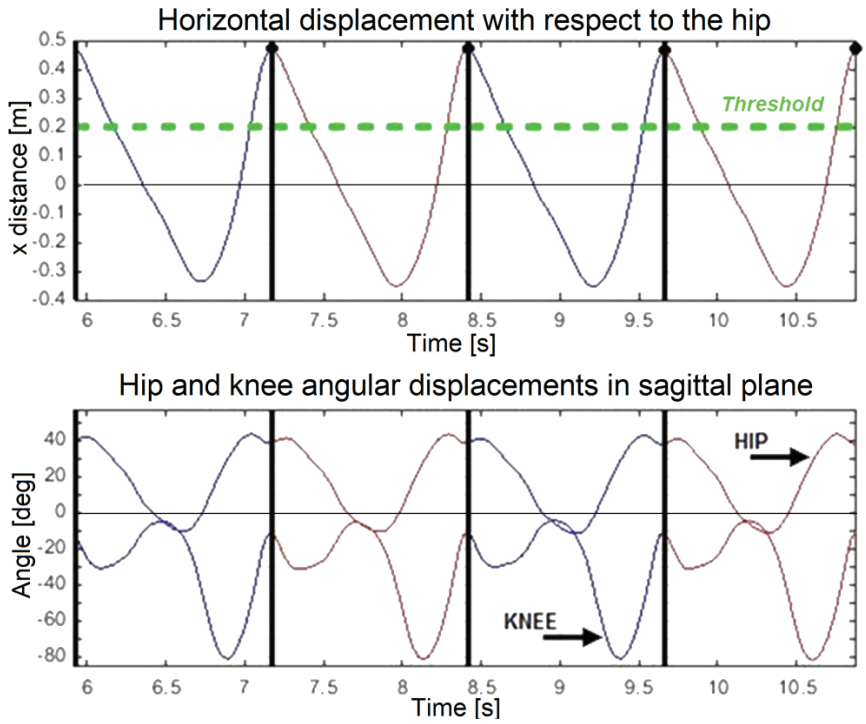

Fig. 23 Gait cycles recognition. Horizontal displacement of the foot with respect to the hip (up) and hip and knee angles (down)

the curves presented unusual behavior due to wrong operation of the sensors (e.g. loss of data or excessive drifting) or irregular steps (e.g. caused by loss of balance). Some examples of discarded cycles can be appreciated in Fig. 24, were the area corresponding to the discarded data is shadowed. In the upper four plots, it can be seen that the discarded cycles possess a rather atypical form. In the case of plots a, b, and d, it might have been caused by loss of data, either by the sensors or by the recording program. Regarding plot c, the causes of the strange curves could be the improper operation of the sensors or irregular walking from the subject. The plot in Fig. 24(e) shows a case of strange behavior occurring in the knee flexion during the swing phase. This behavior could be caused by the participants walking, but it could also be caused by drifting produced by the IMUs that affected the cycle data, therefore it was decided to also discard this type of cycles to avoid the inclusion of probably corrupted data. Finally, Fig. 24(f) shows a clear case of data drifting in the knee curve caused by the IMUs. Unlike the previous case, this couldn't have been caused by the subject's walking, because the data show hyperflexion angles of almost 10°.

Drift corrections

Some drifting behavior was spotted in the knee curves after the first data processing. Even though the curves with excessive drifting were manually discarded for the data analysis, it became clear that some drifting could be present in the accepted knee processed curves. Therefore, an algorithm was developed for the compensation of this lower drifting in the knee trajectories. This algorithm was developed with one assumption in mind: the global maximum and range of motion of the knee trajectory cycles from the same course do not change much from cycle to cycle, i.e. the gait pattern is almost uniform during the course. For this reason, the algorithm mas executed separately for each one of the courses.

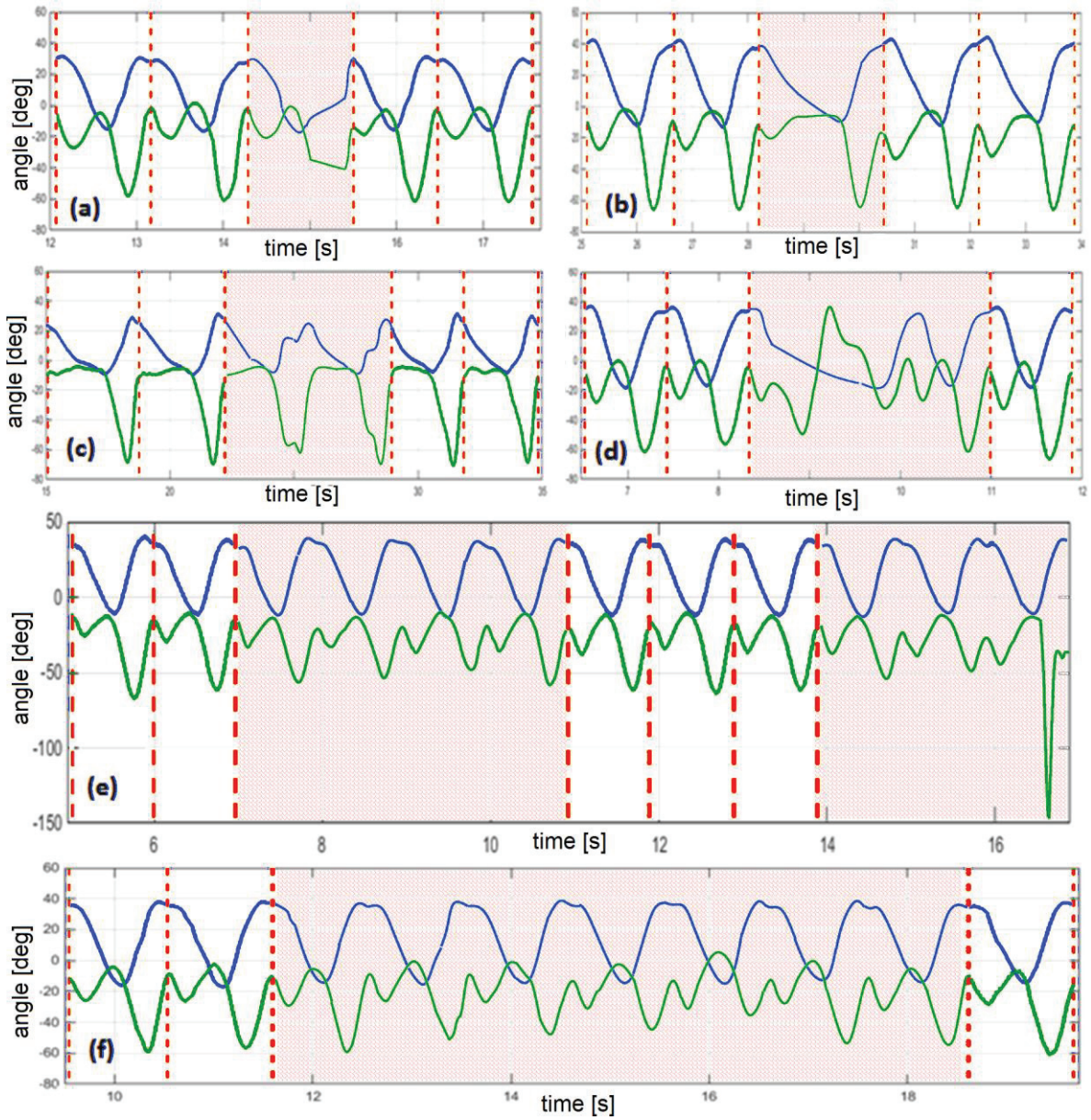

Fig. 24 Examples of discard of cycles due to corrupted recorded data (shaded area)

The algorithm is executed for every cycle of the course. The execution starts from the forth cycle, comparing the cycles in question with the first three cycles of the course, which are assumed to have no significant drifting. It initially checks if it is necessary to do drift corrections in the knee cycle being revised (cycle i) by comparing the angle of the cycle's global maximum ($\theta_{max,i}$) and the cycle's range of motion (ROM_i) with the average angle of the global maximums of the first three cycles ($\bar{\theta}_{max}$) and with the average ROM of the first three cycles ($\overline{ROM}$), respectively, and by checking if the differences surpass some defined thresholds (ε_θ and ε_{ROM}). If the thresholds are surpassed, then some drift correction must be done.

The overall correction done in each cycle is divided in three areas to be corrected (*A1*, *A2* and *A3*) based on two correction parameters (*C1* and *C2*). *A1* goes from the first sample of the cycle ($P_{0,i}$) to the cycle's global maximum point ($P_{max,i}$), where the samples in between are subject to a smooth dynamic compensation in their angular values ruled by *C1*, which is computed from the differences between the maximum angle and ROM with the respective

average values of the first cycles, and by a ROM correlation factor (K_{ROM}). The corrections on the areas *A2* and *A3* are done based also on the differences between the maximum angle and ROM of the next cycle, $\theta_{max,i+1}$ and ROM_{i+1}, with the average values from the first three cycles. In the case of *A2*, which covers the area from $P_{max,i}$ until the first sample of the next cycle ($P_{0,i+1}$), the smooth dynamic compensation is ruled by K_{ROM} and *C2*, which is based on the differences from the next cycle, and works together with a fixed offset compensation given by *C1*. Finally, all the remaining data from the course is located in *A3*, from $P_{0,i+1}$ until the last processed sample, and are subject to a fixed offset compensation given by *C1* and *C2*. It is important to clarify that the smooth compensation is presented as dynamic because it depends on the time value of the sample being corrected and its relation with the time values of other specific points, namely $P_{0,i}$, $P_{max,i}$ and $P_{max,i+1}$. On the other hand, the offset compensations are presented as fixed because their value is invariant, regardless of the time value of the sample. Fig. 25 shows an illustration to help understanding the main idea behind the process with an example of a curve with drifting, where the cycle $i=5$ is being checked. An elaborate flowchart of the algorithm is shown in Fig. 26, where a more detailed explanation regarding the computations made by the algorithm can be seen. After a careful revision of Fig. 26, it can be noticed that the corrected angles (θ^C_j) are continues at the three boundary points of the correction areas ($P_{0,i}$, $P_{max,i}$ and $P_{0,i+1}$) thanks to the appropriate handling of the correction parameters *C1* and *C2*. Note also that, although the algorithm is executed having a specific cycle under scope, it affects all the cycles following that cycle. Moreover, after the algorithm finishes with a given cycle (correcting as well the subsequent cycles), it continues with the next cycle and, if necessary, performs more corrections on it and its subsequent cycles. This must be done until the last cycle of the course is reached.

Albeit most of the knee trajectories were not affected or were only minimally affected by the algorithm, some curves showed a more significant correction. Fig. 27 shows an actual example of the performance of the algorithm. In this plot, the dashed line corresponds to the original curve which possesses an evident drifting problem, whereas the solid line corresponds to the corrected curve. The correction in this example can be observed in the 6th and 7th cycles, where the algorithm has performed a compensation to keep the curve close to the first cycles. The algorithm could also be used in the discarded curves that presented mayor drifting, but it was decided not to do it to protect the results from incorrect compensations and

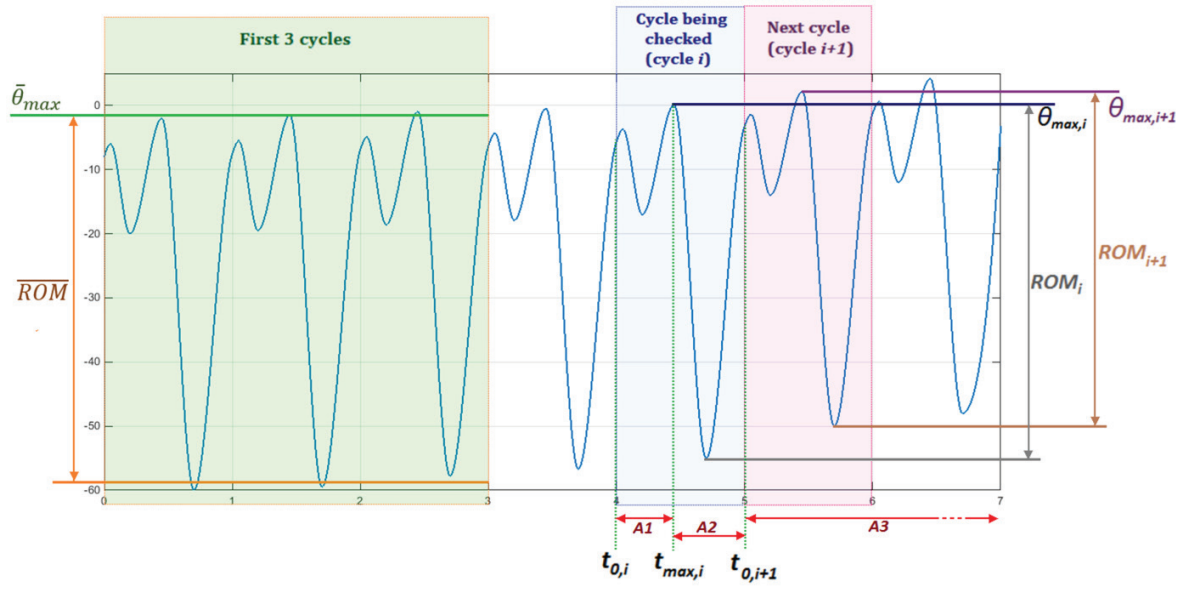

Fig. 25 Illustration of idea behind drift correction

corrupted data. This decision is backed up by Fig. 28, which shows the results of applying the drift correction algorithm to the discarded knee curve previously introduced in Fig. 24(f). Note how, although the algorithm manages to maintain the curves close to each other, the ROM of from the 6th to the 9th cycle show a rather unusual behavior.

Additionally, although the drift compensation algorithm was developed for the knee joint only, it was also applied to the hip curves to study their behavior. Almost all the hip curves remained unchanged by the algorithm, and, when the algorithm did alter them, almost all the changes were minimal, which suggests that the initial assumption applies in most of the cases. Nevertheless, some problems were spotted when the hip ROM was altered by the subject during the course, contradicting the initial assumption. In these cases, the alteration will be perceived as a drift caused by the IMU and make the corresponding corrections. These ill corrections will inflict drifting in the processed data, due to the fact that the algorithm corrects the differences between global maximum points and the influence of the global minimums in lower. Fig. 29 shows an example of such behavior. Notice how the high flexion angles of the first two cycles influence the wrong correction of the trajectories, making an ill adjustment to a curve that apparently possessed no drifting. If at some point it becomes necessary to perform also drifting corrections in the hip trajectories, it is recommended to use an algorithm specific for this joint, which wouldn't be based on the global maximums but on the angular value between the global extrema

$$\theta_{mid,i} = \frac{\theta_{max,i} + \theta_{min,i}}{2}. \tag{7}$$

Moreover, if drift compensation has to be done to the hip curves, a recalculation of the knee angles with respect to the upper leg segment must be done based on (5).

Extraction of characteristic points

Two separate algorithms, one for each joint, were developed to automatically obtain of characteristic points from the experimental data, based the concept explained in section 4.2. Both algorithms were executed for each extracted cycle. For the following explanations, consider that each cycle C possesses parameters that are specific to the cycle, e.g. the period T_C or the samples $(t_{C,i},\theta_{C,i})$. For simplicity, the subscript C will not be used in the subsequent formulations, but it must be understood that the data are already segmented by cycles, and that the values of parameters such as T, t_i, θ_i, among others, correspond to a specific cycle C.

The first steps of the process are the same for both algorithms. Initially, a resampling of the data is done for each cycle, bearing in mind that the amount of samples per cycle in the original data depends on the cycle period and it is not necessarily the same for all cycles. The resampling is done by interpolating the samples of each cycle using the *BVSIS* fitting method with $n = 401$ new samples that are equidistant in time. This way, all cycles will possess the same number of (fitted) samples. Now, we can consider that each cycle possesses a set of n samples which are expressed as ordered pairs $P_i = (t_i,\theta_i)$, with $i=0,1,\ldots,n-1$. For convenience, the time value of the first sample is subtracted from all the time values from the resampled data, so that $t_0 = 0$ *and* $t_{n-1} = T_C$. It is important not to forget that the curves in question are treated as periodic for the data analysis. This means that the first and last samples of a cycle are connected in a (pseudo-) continues manner and that any sample $(t_{C,j},\theta_{C,j})$, $j\neq i$, is considered to be both to the right and to the left of sample $(t_{C,i},\theta_{C,i})$. So, if it is necessary to check the samples to the right (ahead in time) of a certain point, one should not stop evaluating in sample P_{n-1}, but restart from sample P_0 until the evaluation criteria are met or until a complete cycle has been evaluated.

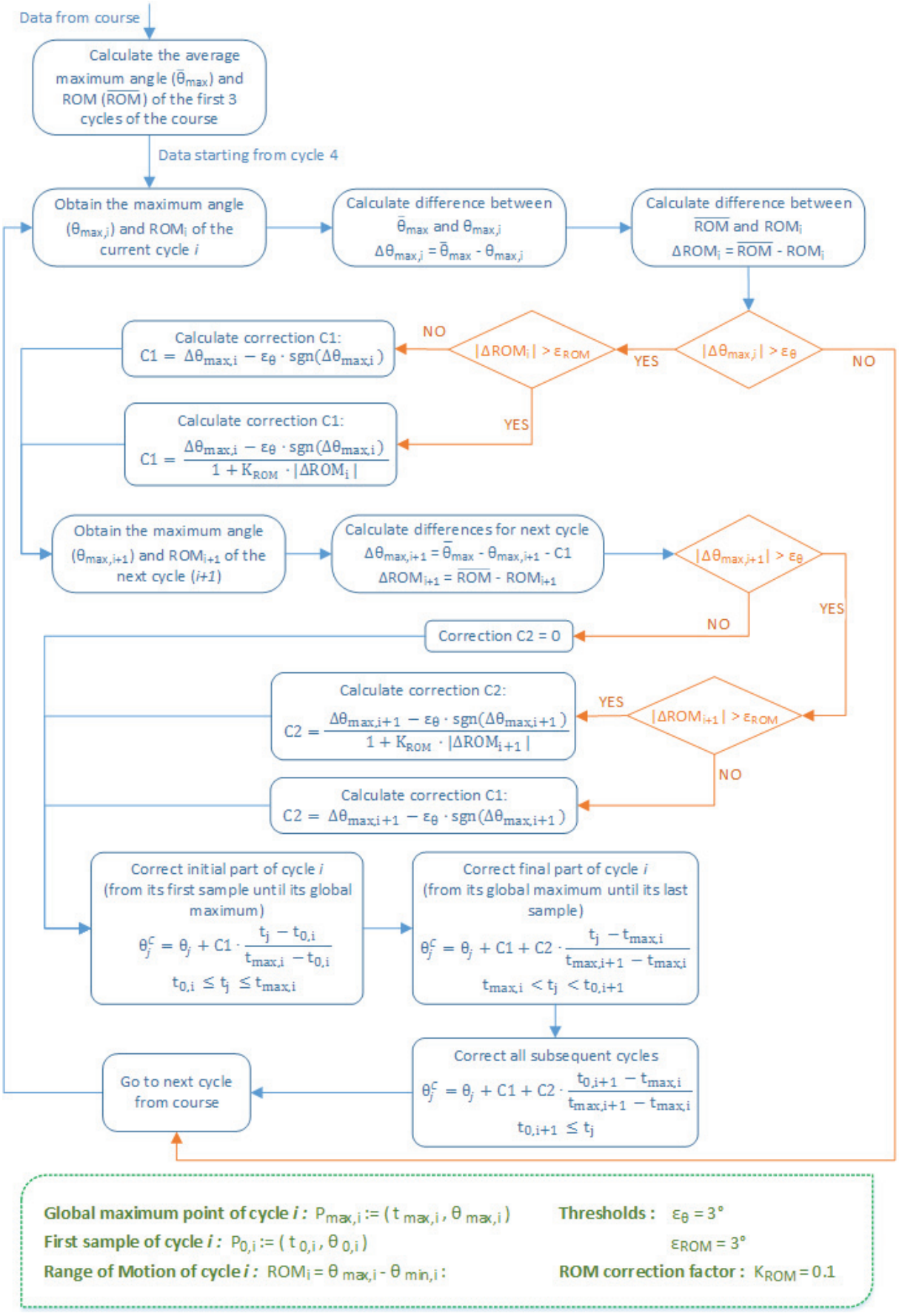

Fig. 26 Flowchart of the algorithm for drift correction

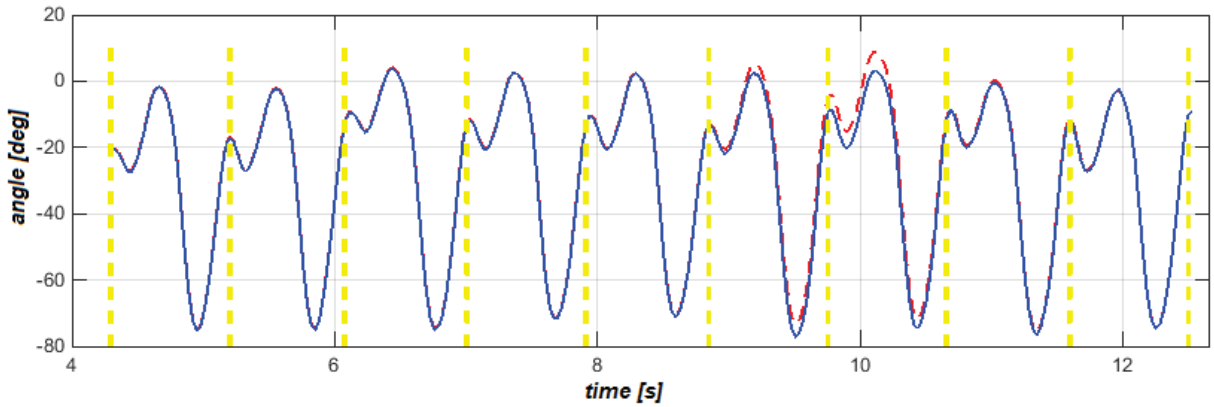

Fig. 27 Example of drift correction on knee curve

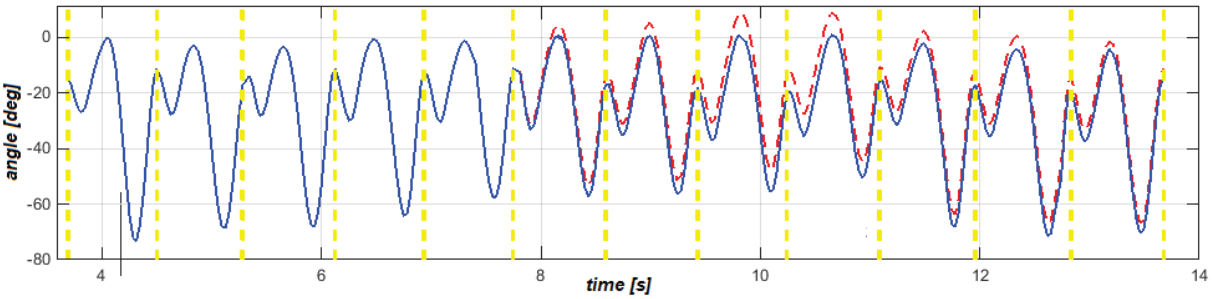

Fig. 28 Example of drift correction on discarded knee curve

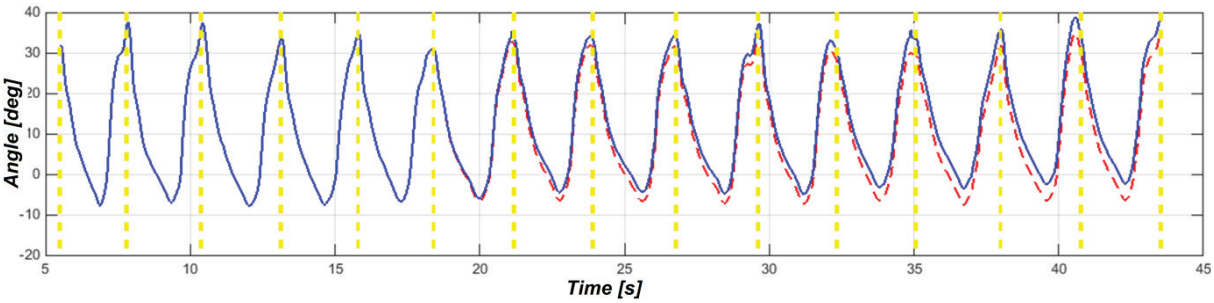

Fig. 29 Ill drift correction in hip curves

Once the cycles are resampled, the normalized time values of the samples are calculated, based on the period T_C of each cycle:

$$t_{i,norm} = t_i \cdot TF\ , \tag{8}$$

where $t_{i,norm}$ is the normalized time value of sample P_i, and $TF = 100/T_C$ is the time factor for a given cycle. This way, the normalized time values of all samples of a given cycle lay between the 0% and 100% of the cycle's period: $0 \leq t_{i,norm} \leq 100$. Likewise, the range of motion (*ROM*) and the ROM factor (*ROMF*) of each cycle are calculated:

$$ROM = \max(\{\theta_i\}) - \min(\{\theta_i\})\ , \tag{9}$$

$$ROMF = 100/ROM, \tag{10}$$

where $min(\{\theta_i\})$ and $max(\{\theta_i\})$ are the minimum and maximum angles is the cycle, respectively.

From this point, the process of extraction of characteristic points is different for each one of the joints. In the case of the hip, the curve forms acquired from the experimental data were similar to the expected ones, i.e. with two global extrema and either 1) two marked local extrema, 2) non-maxima points bending the curve or 3) neither additional extrema nor bending points (refer to section 4.2). The extraction of the characteristic points was done based on several time- and angle-based conditions in order to avoid an ill selection of the points. Fig. 30 depicts a simplified flowchart of the algorithm developed for the automatic extraction of the hip characteristic knots from the experimental data. A more detailed step-by-step procedure containing the different selection conditions can be found in Appendix C. Fig. 31 shows some examples of the output of the algorithm corresponding to the previous mentioned cases: Fig. 31(a) shows three cycles where a set of four marked extrema were selected as characteristic points; Fig. 31(b) shows two cycles where two bending points were selected as characteristic points, together with the global extrema; and Fig. 31(c) shows the case where no points, different from the global extrema, where found which influenced significantly the shape of the curve, therefore two samples near the maximum extension point were selected as the remaining pair of characteristic knots.

In the case of the knee, the behavior of some of the recoded curves was not the expected. Although most of the recorded knee curves possessed the general form obtained from

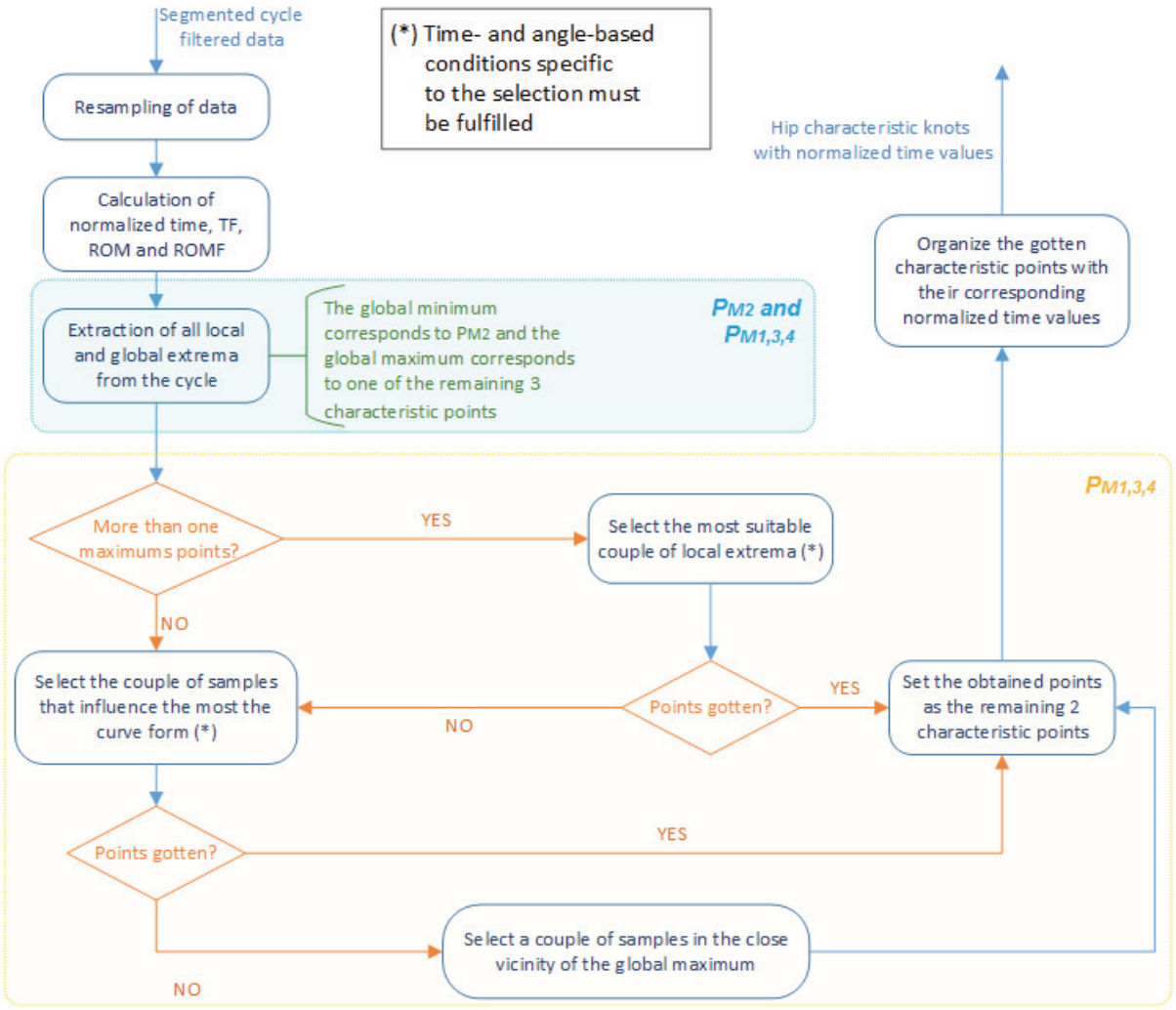

Fig. 30 Flowchart of the automatic extraction process of hip characteristic points from the experimental data

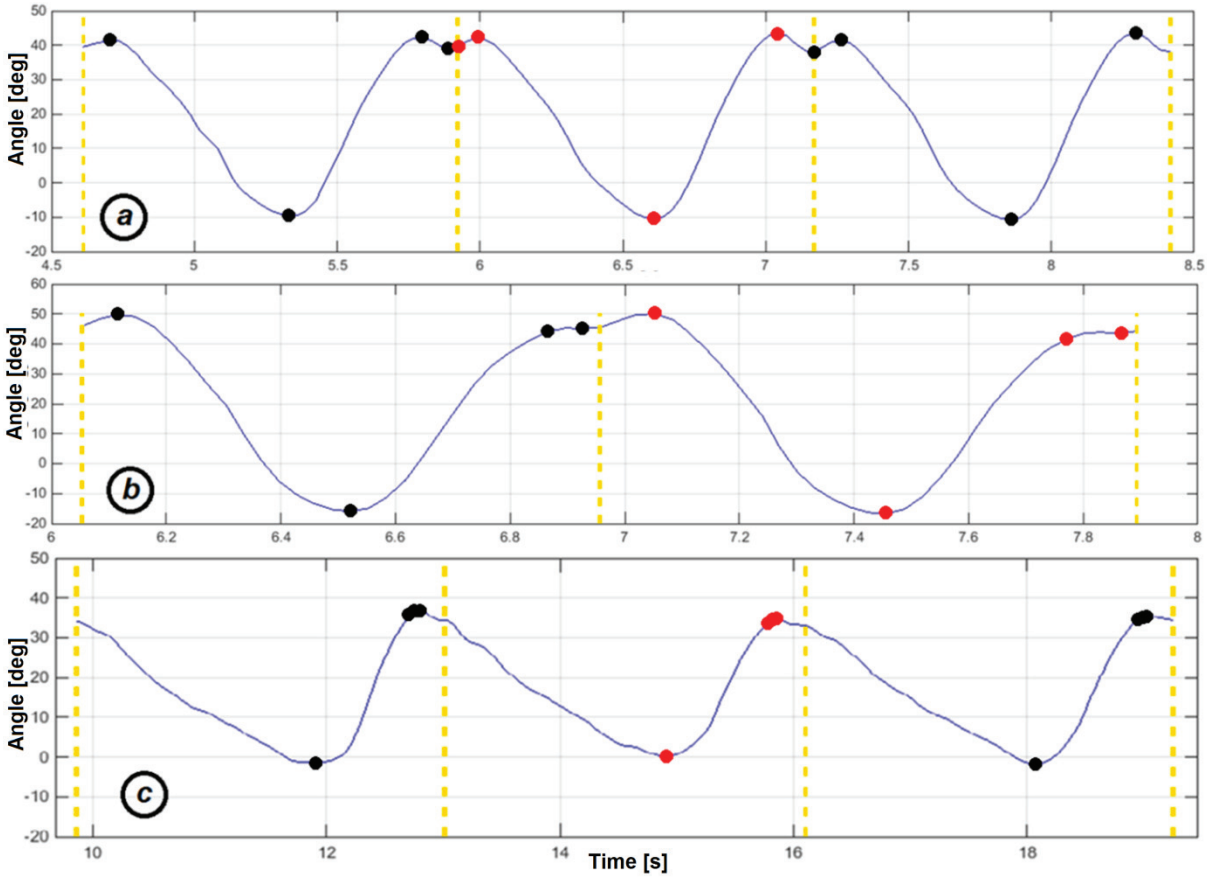

Fig. 31 Examples of the automatic extraction of hip characteristic points

literature (section 4.2), some curves differed significantly from it, mostly in the cases where the cadence and walking speed were low. The most significant differences appeared in the region corresponding to the stance phase, where no salient local extrema points were present, leading to an unclear selection of the characteristic points P_{M1}, P_{M2} and P_{M4} that suit the proposed trajectory generation method. Fig. 32 depicts a simplified flowchart of the automatic extraction process of the knee characteristic knots from the experimental data. As before, a more detailed step-by-step procedure containing the different selection conditions can be found in Appendix C.

Fig. 33 shows an example of the performance of the extraction algorithm with curves that had the expected form. As it can be seen, the four characteristic points could be extracted in a clear, straight-forward manner based on the local and global extrema. On the other hand, Fig. 34 shows some examples of unexpected behavior in the recorded knee curves. Fig. 34(a) shows an example of mild rippling in the stance phase, where more than one pair of local extrema appeared in the left side of the curve. Fig. 34(b) shows a case where no significant local maximum was located during the stance phase, whereas Fig. 34(c) depicts a similar behavior, only that in this case the angular profile during the stance phase is highly flattened. These three cases don't appear to be very critical regarding the shaping of the curve, but they might affect the performance of the estimation process.

The other cases (*d* to *j*) represent a potential cause of high error levels in both shaping and estimation performances. Fig. 34(d) shows a case of excessive rippling with several salient local extrema, being completely inconsistent with the curve form exhibited in literature and causing a rather random selection of point P_{M1}. This affects considerably the correlation performance of the estimation methods. Fig. 34(e) to Fig. 34(g) depicts a case where a point

causing a notable bending appears after P_{M3} and before the global/local minimum point, yielding an unclear selection of P_{M4}. Selecting the bending point as P_{M4} will preserve the curve shape in the second half of the swing phase but will affect the shape in part of the stance phase, whereas selecting the minimum point will preserve the shape in part of the stance phase but will affect not only the shape corresponding to the second half of the swing phase, but also the shape of the initial part of the stance phase. In these particular cases, the selection of the bending point as P_{M4} was preferred because it would affect the curve shape in a lower degree. Additionally, the time values of the bending points seem to be more consistent between cycles, which will affect positively the performance of the estimation methods. Nonetheless, the shape of the reconstructed curve will differ significantly in the area between P_{M4} and P_{M1}. Finally, Fig. 34(h) to Fig. 34(i) show some cases where the selection of the point P_{M2} was not clear, similar to the previous case, or where there was a presence of some additional salient extrema during the stance phase. Similarly, these cases will affect significantly the shape-related performance of the reconstructed curves and could have an important influence in the performance of the estimation algorithms.

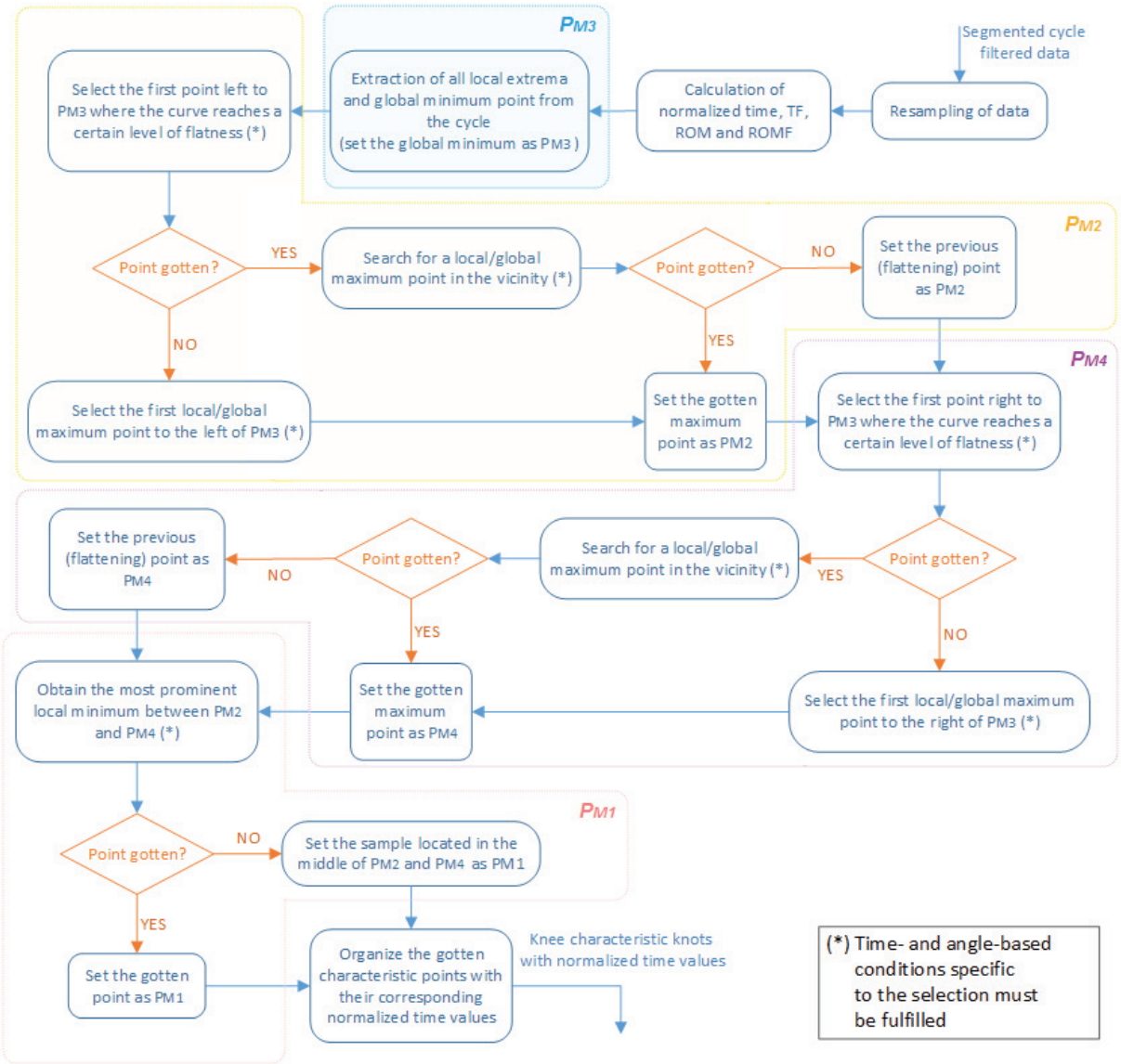

Fig. 32 Flowchart of the automatic extraction process of knee characteristic points from the experimental data

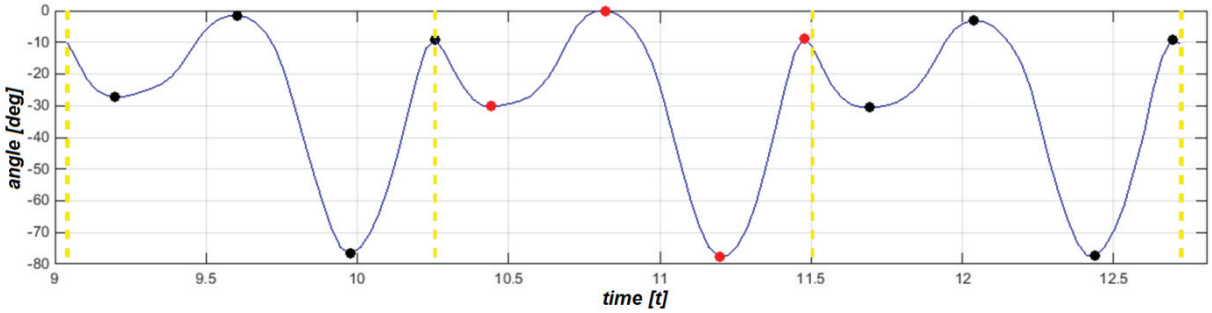

Fig. 33 Examples of the automatic extraction of knee characteristic points

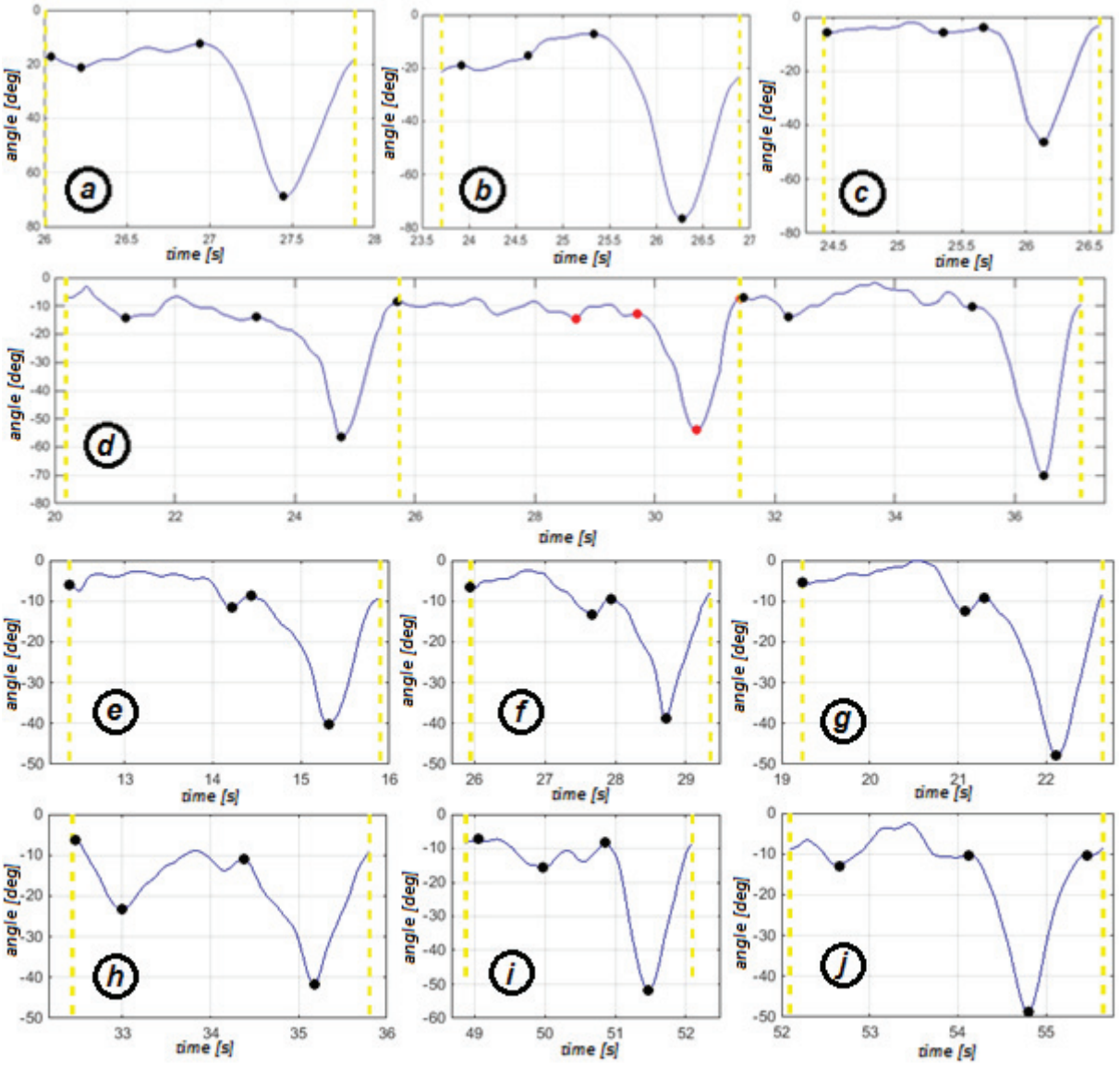

Fig. 34 Examples of the automatic extraction of knee characteristic points with unexpected curve shapes

Calculation of gait parameters

Besides the characteristic points, other gait parameters were extracted for each of the segmented cycles, namely cadence, step length and walking speed. The cadence (step frequency) is calculated directly from the cycle period T_C, which is known once the cycle is recognized. Note that each cycle covers two steps (one per leg), hence the cadence is given by

$$Cad = 2/T_C \,, \tag{11}$$

To obtain the walking speed, it is necessary to calculate the step length in order to know the distance covered by the subject during the duration of each cycle. Therefore, the problem is reduced to the obtainment of the step length of each cycle. The step length (*SL*) is considered here as the distance covered by the trunk between the moment of initial contact (IC) and the moment of toe-off, i.e. the distance covered while the foot was in contact with the ground. Because no external measurement system was used to identify the moments of foot contact and clearance (e.g. foot-pressure sensors or image-based systems), the calculation of the step length was done based on the horizontal displacement of the foot computed solely from the angular data from the hip and knee joints, following the same kinematic analysis used for the cycles segmentation explained at the beginning of the section and illustrated in Fig. 22. By finding the distance between the minimum and maximum horizontal displacement one can get the maximum distance (*FD*) covered by the foot with respect to the hip joint during a certain cycle. Nevertheless, this distance is not strictly equal to the length of the corresponding step. Normally, the heel strike happens shortly after the maximum horizontal position of the foot is reached, when the foot is already moving backwards. Therefore, *SL* is shorter than *FD*. On the other hand, pelvic rotations about the vertical axis during walking cause a slight translation of the hip joint in world space, contributing to the resulting horizontal displacement of the foot. The relation between the *FD* and *SL* is dependent on the subject. To estimate *SL* from the calculated *FD*, the following formulation is proposed:

$$SL = FD \cdot f_s(FD) = FD \cdot \sum_{i=0}^{n} k_{s,i} \cdot FD^i \,, \tag{12}$$

where $f_s(FD)$ is a polynomial function of order n ($1 \leq n \leq 3$) and k_i are constant values that are specific to each subject s. To obtain these constants, the data gotten from the experiment section *Ex2* where utilized. The *FD* calculated from the cycles from each course of *Ex2* was averaged and compared with the known target step length of each course. Having these values, the specific polynomial f_s was yielded for each subject via regression. Two examples of such regression for different subjects are shown in Fig. 35. It is important to bear in mind

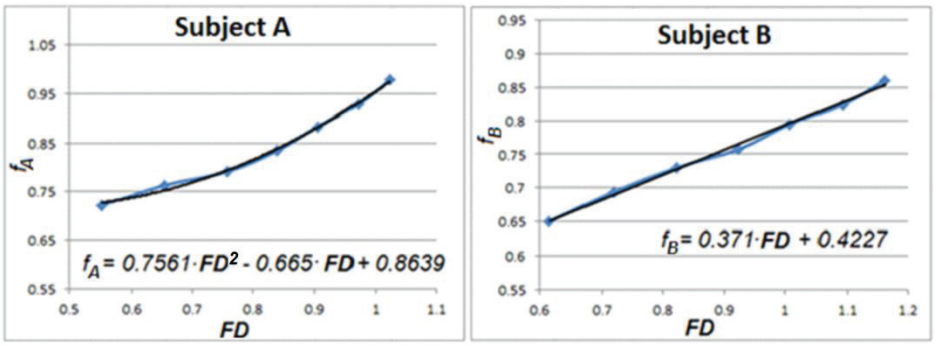

Fig. 35 Examples of regression to obtain $f_s(FD)$ of two different subjects

that this is only an estimation of the real step length and as so is not free of error.

Once the step length and period are obtained for each cycle, it possible to estimate the walking speed in that cycle:

$$WS = SL \cdot Cad\,, \tag{13}$$

where *WS* is the walking speed, given normally in *m/s* of *Km/h*. Nevertheless, because the step length (and consequently the walking speed) are dependent on the subject's height (or, more specifically, on the length of the leg segments), it is necessary to include the subject's height in the estimation process. Normalization of spatial parameters is a common practice in gait analysis, where some measurements are divided by some aspect of the body size (e.g. height or leg length), particularly when analyzing gait in children [22]. In this work, the inclusion of the subject's height is made by normalizing the step length and walking speed with respect to the height. Consequently, two new gait parameters are introduced:

$$SL_{s,norm} = SL/h_s\,, \tag{14}$$

$$WS_{s,norm} = WS/h_s\,, \tag{15}$$

where $SL_{s,norm}$ and $WS_{s,norm}$ are the normalized step length and normalized walking speed of subject *s* with respect to his/her height h_s. Notice that $SL_{s,norm}$ and $WS_{s,norm}$ are given in subject' heights and heights/s, respectively.

4.3.2 Automatic estimation of characteristic curve points

The outputs acquired from the data collection and processing are the characteristic points, cadence, normalized step length and normalized walking speed of each cycle. The later three were potential inputs to the estimation algorithm, whereas the characteristic points are the variables to be estimated based on the inputs. The objective now was to study which of the input variables should be used to get the best correlation between the experimental values of the characteristic points and the predicted ones. In this case, six different sets of outputs were tested: normalized walking speed ($WS_{s,norm}$), cadence (*cad*), normalized step length ($SL_{s,norm}$), and a combination of the previous inputs, namely $WS_{s,norm}\&cad$, $WS_{s,norm}\&\ SL_{s,norm}$, and $cad\&SL_{s,norm}$. The combination of all the three variables was not taken into account due to the fact that the one of them is always a function of the other two, based on (13). Moreover, based on the same fact, it is expected that the performances of the estimation process using the input sets consisting of combined variables are almost the same. The ranges and mean values of normalized walking speed (in heights/s), cadence (in steps/min) and normalized step length (in heights) were [0.066, 1.359] (mean = 0.58), [20.24, 174.93] (mean = 91.38), [0.11, 0.65] (mean = 0.37), respectively.

The estimation method selected for this task was the Artificial Neural Network (NN). Two different training algorithms were tested: Levenberg-Marquardt [191] and Bayesian regularization [192]. The Bayesian regularization algorithm usually improves the performance of the NN in terms of estimating the target values, but the training time spent by it is considerably higher than the one needed by the Levenberg-Marquardt algorithm. Each tested neural network had one hidden layer with ten neurons and started with random initial weight values. The outputs of the neural networks were the characteristic points, more specifically, the (normalized) time and angular values of each of the eight characteristic points of both joints. One neural network was used for each of the output variables. This way, the complete configuration for the learning process contains 16 neural networks, each one receiving a set of

inputs (consisting of one or two input variables) and estimating 16 output values. The configurations with only one input will be referred as *1I1O*, whereas the ones with combined input values will be *2I1O*. Fig. 36 shows the diagram of the neural network configuration. The MATLAB Neural Network Toolbox [193] was used for the training of the neural networks. A total of 11399 processed gait cycles were used for the NNs training, from which 70% were used for the training itself, 15% for validation and 15% for testing. The selection of these three sets was done randomly.

To test the performance of the trained neural networks, the Pearson cross-correlation coefficients (R) were calculated for each output to measure the linear dependency between the measured and the fitted values of each of the 16 outputs. The correlation coefficient of two sets of random variables is defined as

$$R = \frac{cov(y, \hat{y})}{\sigma_y \cdot \sigma_{\hat{y}}}, \tag{16}$$

where y is the set of measured values, $\hat{y}$ is the set of fitted values, cov is the covariance between the two set of values, and σ_y and $\sigma_{\hat{y}}$ are the standard deviations of the measured and fitted values, respectively. The covariance between the two sets of variables is defined as

$$cov = \frac{1}{N} \sum_{i=0}^{N-1} \left((y_i - \mu_y) \cdot (\hat{y}_i - \mu_{\hat{y}}) \right), \tag{17}$$

where N is number of elements in sets y and $\hat{y}$ (i.e. number of processed cycles), y_i and $\hat{y}_i$ are corresponding elements of the sets, and μ is the mean value of a set. The definitions of the mean and standard deviation values are

$$\mu_x = \frac{1}{N} \sum_{i=0}^{N-1} x_i, \tag{18}$$

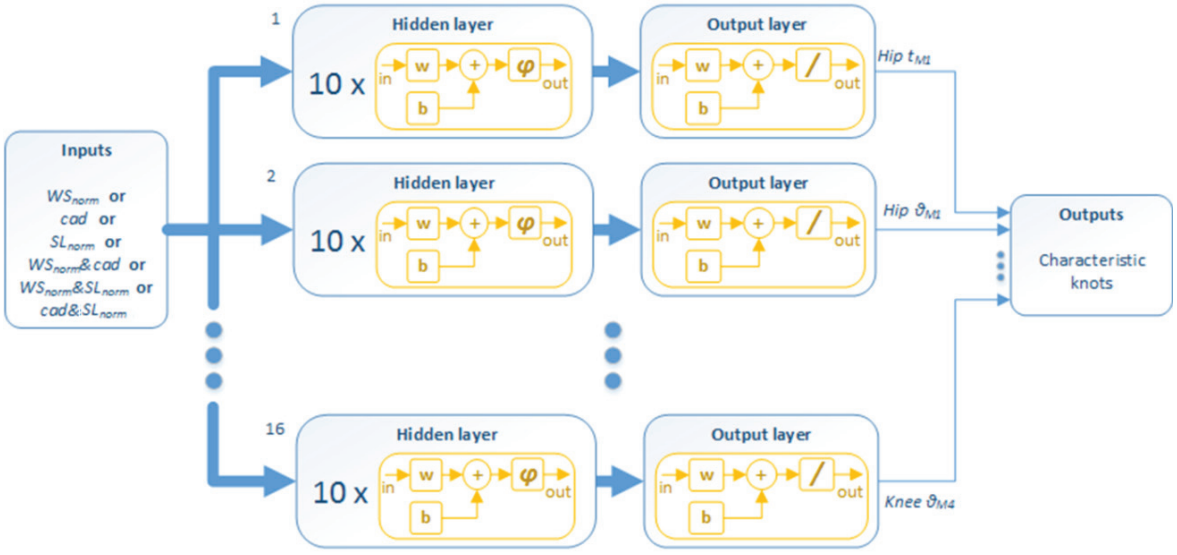

Fig. 36 Neural networks' configuration

$$\sigma_x = \sqrt{\frac{1}{N}\sum_{i=0}^{N-1}(x_i - \mu(x))^2}. \quad (19)$$

The correlation coefficients given by each one of the networks with each one of the input sets are shown in Table 6. Values of *R* close to one mean close relationships between the two sets whereas values close to zero mean random relationships. Contrary to what was expected, the resulting coefficients from using Bayesian regularization were only slightly better than the ones using the Levenberg-Marquardt algorithm, thus, from this point, the results presented will be the ones corresponding to the NNs trained with Bayesian regularization. Unfortunately, most of the correlation coefficients are relatively low. One reason for this is the fact that this study deals with human behavior and the intra-subject preferences when walking might have affected considerably the performance of the estimation. Related poor predictability results were also reported by other studies [194]. Complementary measurements of the mean absolute errors (MAE), standard deviation of the absolute errors and root mean square errors (RMSE) can be found in Appendix D.

Some additional observations can be made from Table 6. First of all, it is easy to note how close the correlation coefficients for the combined-inputs (2I1O) neural networks are. As explained previously, this is expected since the walking speed is calculated directly from the step length and cadence, deriving in a tight relationship between them. Second, note that the results using combined inputs are in most of the cases better than the ones using just one input. This shows how variable can human walking be, where, for instance, the same walking speed can be achieved with different cadences. Finally, it can be seen that the best correlation results were achieved for the maximum hip extension points (t_2, a_2 in hip), whereas some parameters from the points of the knee motion during the stance phase (a_1, t_2, t_3, a_3 in knee) scored lower. These low values might be consequence of the sundry and unexpected curve shapes of the knee trajectories presented in section 4.3.1, mostly while walking with some gait parameters such as low cadence and very slow walking. As explained in the previous section, these sundry knee curve shapes lead to an unclear automatic selection of the points during the data processing stage and, consequently, to a lower performance of the neural networks' estimation.

To have a better look on the behavior of the characteristic point's parameters obtained after training the neural networks with the data from all subjects, the trained NNs were used to predict different sets of characteristic points with different input values. The predicted

Table 6 Resulting correlation coefficients using Bayesian regularization with all processed data

	Correlation Coefficient (R)															
	HIP								***KNEE***							
	t_{M1}	θ_{M1}	t_{M2}	θ_{M2}	t_{M3}	θ_{M3}	t_{M4}	θ_{M4}	t_{M1}	θ_{M1}	t_{M2}	θ_{M2}	t_{M3}	θ_{M3}	t_{M4}	θ_{M4}
WS_{norm}	0.42	0.61	0.75	0.66	0.36	0.62	0.33	0.57	0.49	0.25	0.30	0.68	0.13	0.18	0.63	0.52
cad	0.33	0.42	0.81	0.50	0.25	0.47	0.18	0.39	0.48	0.23	0.26	0.54	0.10	0.18	0.60	0.50
SL_{norm}	0.43	0.68	0.52	0.72	0.36	0.67	0.38	0.63	0.40	0.21	0.28	0.68	0.20	0.18	0.52	0.44
WS_{norm} & *cad*	0.46	0.69	0.81	0.73	0.54	0.69	0.43	0.65	0.51	0.33	0.32	0.71	0.26	0.29	0.65	0.52
WS_{norm} & SL_{norm}	0.46	0.69	0.81	0.73	0.53	0.69	0.42	0.65	0.51	0.33	0.32	0.72	0.26	0.26	0.65	0.54
cad & SL_{norm}	0.46	0.69	0.80	0.73	0.54	0.69	0.43	0.66	0.51	0.33	0.31	0.71	0.26	0.28	0.65	0.53

characteristic points were then interpolated, together with corresponding shaping knots, using *BVSIS* splines. The selection of the α-values of the shaping knots' was done based on the results of *Method 1* for coefficients computation, explained in the following section (4.3.3). Because of the nature of the NNs, it is important to stay within the ranges of the input values that were used during the training. Stepping outside these limits during the prediction process is likely to cause very poor results. Moreover, this kind of undesired behavior is also caused by stepping outside the regions of combined input values used during the training of the NNs with multiple inputs. An example of the regions for multiple inputs can be seen in Fig. 37(a), where the combined inputs $WS_{s,norm}$&*cad* are analyzed. The figure shows the plot of $WS_{s,norm}$ vs *cad* with the data used to train the NNs. It is recommended therefore to stay inside a region such as the one delimited by the orange perimeter to avoid potential poor results. This way one not just prevents a poor performance of the neural network, but also avoids unrealistic inputs' combinations, such as a high walking speed with a low cadence. An example of curves generated without taking into account the inputs' limit region is depicted in Fig. 37(b). There, the value of the input variable $WS_{s,norm}$ was left fixed at 0.685[Heights/s] (purple line in Fig. 37.a) whereas the values for the second input *cad* varied between the minimum and maximum cadence values registered in the experiment. Note how only the curves corresponding to the region with training samples (more or less from 91 to 118 steps/min) appear to be normal walking patterns. Most of the other cadence values generate either completely non-sense trajectories or trajectories that at first sight show normal shapes, but they present flexion/extension values too high or too low to be considered normal. This shows that it is not recommended to rely in the extrapolation capabilities of the NNs.

Fig. 38 shows some examples of joint curves that were generated using the characteristic points predicted by the NNs. The curves generated with the outputs from the NNs with only $WS_{s,norm}$ as input are shown in Fig. 38(a), whereas some curves generated with the combined input $WS_{s,norm}$&*cad* are shown in Fig. 38(b-d). For the later ones the walking speed was varying, whereas a specific cadence value was selected for each normalized walking speed. Fig. 39 shows the plot of *cad* vs $WS_{s,norm}$, where the solid line corresponds to the selected

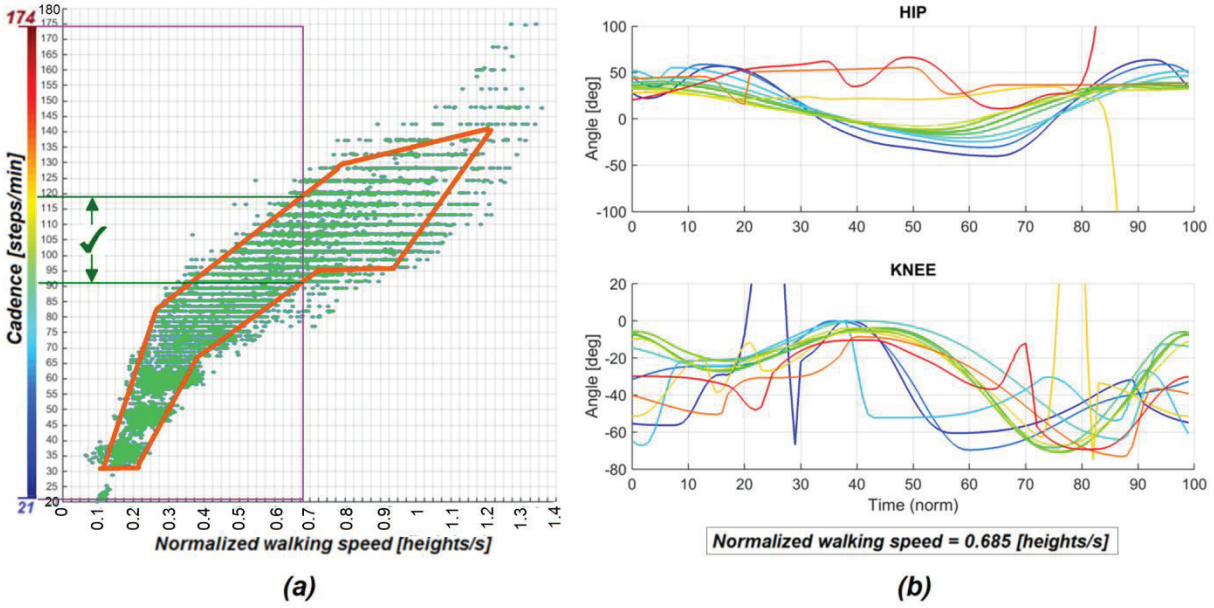

Fig. 37 (a) $WS_{s,norm}$ vs *cad* plotting the processed data used for training (light green points) with an example of a recommended application region (orange perimeter), plus **(b)** an example of regenerated curves with incorrect input selection out of the region

cadence used to plot Fig. 38(b), whereas the upper and lower dashed lines correspond to the plots in Fig. 38(c) and Fig. 38(d), respectively. From these figures, it can be seen that the generation of smooth curves is possible employing 1I1O and 2I1O neural networks. Only when using very small inputs (e.g. darkest blue curves in Fig. 38), the curves showed some unnatural behavior. This suggests that problems may arise when considering very low values of cadence, speed and step length as inputs of these NNs, which would be better to avoid in the final application. Notice as well how the curves in the four plots defer depending on the cadence (or the absence of it as input), even if the input value of normalized speed was the same for all. Example of generated curves using other sets of inputs can be found in Appendix E.

A second correlation analysis was done, but this time by training the neural networks for each subject independently using only the corresponding subject's processed data. The predictability of most of the parameters increased considerably for most of the subjects compared to the one using the complete data set, showing an average improvement higher than 0.18 in the correlation coefficients. The level of improvement was subject-dependent, though. The subject that presented the higher amelioration had an average improvement of 0.3, whereas the lowest average improvement was of just 0.1. These results show that the gait

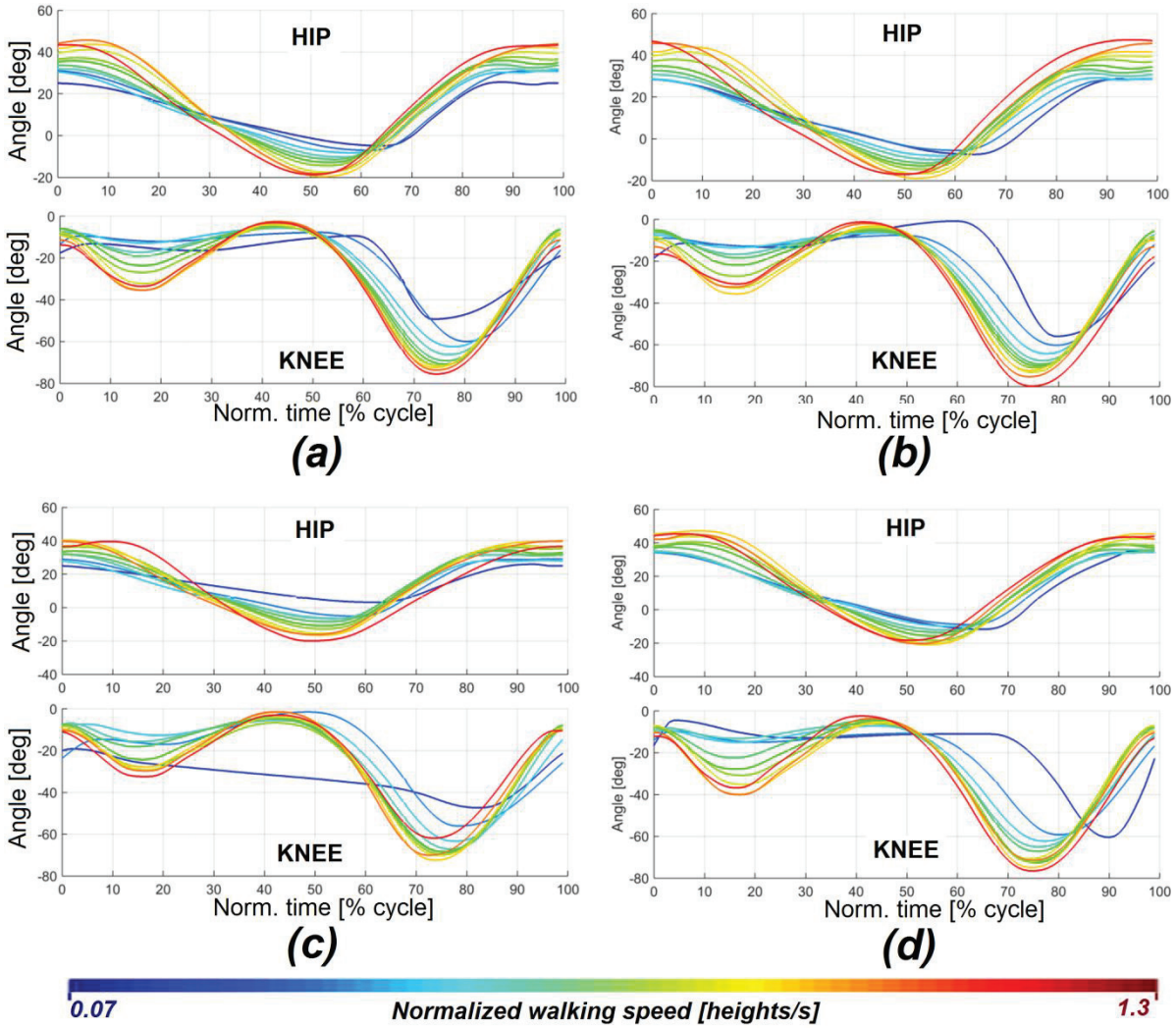

Fig. 38 Generation of hip and knee trajectories depending on $WS_{s,norm}$ (a) and $WS_{s,norm}$&cad (b,c,d)

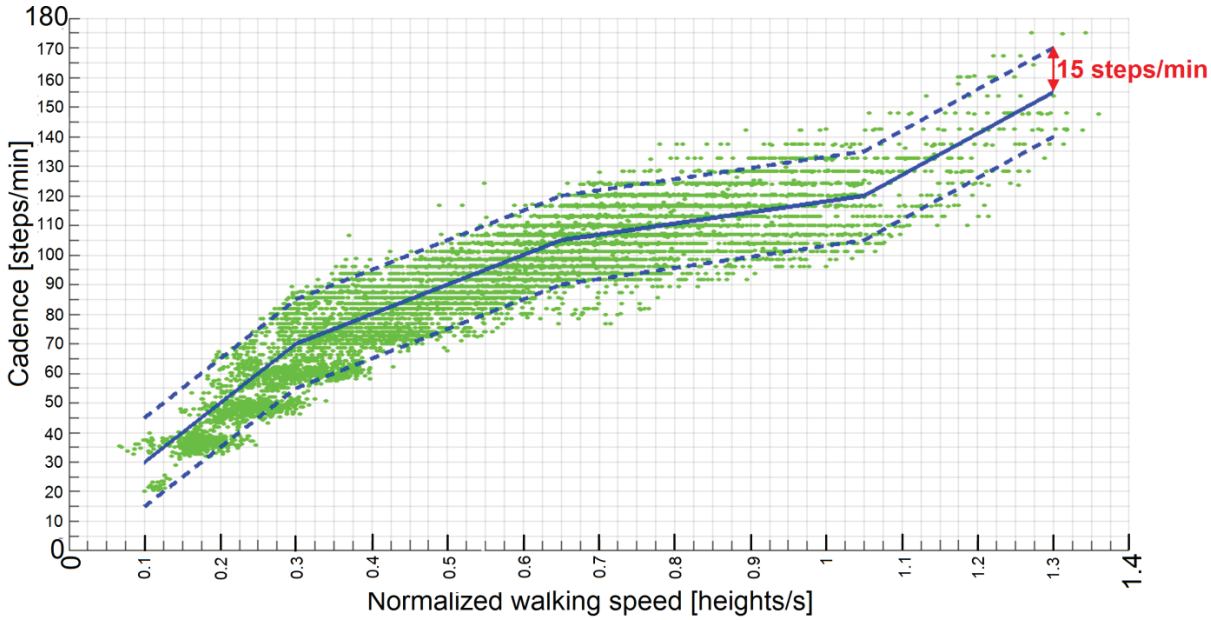

Fig. 39 *cad* vs $WS_{s,norm}$ input values for curve generation using all subjects' data

patterns possess a high inter-subject variability even when people are asked to maintain similar gait parameters, e.g. step length. Nevertheless, the difference between the two sets of results and the low predictability shown in Table 6 might have been also influenced by the sensors' accuracy and the experimental setup, for example, if the placement of the sensors was not exactly the same for all subjects.

After looking at the improvements on the correlation coefficients using only one subject's data, it was decided to use the NNs from the subject that scored higher correlation for the final trajectory generator. The reason of that decision is that it is preferred to present the therapists reference curves that fit better real curves, than curves 'averaged' for all subjects that have higher probabilities to be farther from natural patterns. The obtained trajectories will be based on the walking preferences of only one subject, but this drawback can be compensated by the possibility given to the therapist to adjust them to fit better the preferences of the patient. This problem would be anyway present if using the data from all subjects, as it was seen that the intra-subject walking preferences are significant. Nevertheless, the usage of NN trained only with the data of one subject presented high differences when compared to the experimental data from all the other subjects. This will be exposed ahead in this section and must be taken into account as a limitation of this selection. Future studies including more inputs (e.g. age and gender) might improve the correlation coefficients and allow a trajectory generation that fits better the patient's characteristic.

The data from the selected subject contained 628 cycles, and the ranges and mean values of normalized walking speed (in heights/s), cadence (in steps/min) and normalized step length (in heights) were [0.145, 1.21] (mean = 0.59), [34.97, 137.14] (mean = 85.62), [0.221, 0.601] (mean = 0.39), respectively. Table 7 shows the correlation coefficient from the neural networks that were trained with the selected data. Mean absolute error and root mean square error measurements are presented in Appendix D, where the estimated values are compared to the experimental data from the selected subject. The correlation coefficients are considerably better that the ones shown in Table 6. There still exist some low correlation values, though, mostly regarding the time values (t_{M3} and t_{M2} in hip, and t_{M1} and t_{M2} in knee). The improvements are also visible in the MAE and RMSE measurements in Appendix D when computed with respect to the selected subject's data.

Table 7 Resulting correlation coefficients using the selected-subject NNs, calculated with respect to the selected subject's experimental data

	Correlation Coefficient (R)															
	HIP								*KNEE*							
	t_{M1}	θ_{M1}	t_{M2}	θ_{M2}	t_{M3}	θ_{M3}	t_{M4}	θ_{M4}	t_{M1}	θ_{M1}	t_{M2}	θ_{M2}	t_{M3}	θ_{M3}	t_{M4}	θ_{M4}
WS_{norm}	0.80	0.93	0.88	0.94	0.55	0.88	0.66	0.87	0.70	0.88	0.41	0.93	0.77	0.80	0.82	0.80
cad	0.81	0.90	0.89	0.91	0.50	0.86	0.66	0.81	0.71	0.86	0.42	0.90	0.76	0.79	0.81	0.81
SL_{norm}	0.78	0.94	0.84	0.94	0.54	0.89	0.65	0.88	0.67	0.84	0.37	0.92	0.74	0.78	0.77	0.80
WS_{norm} & *cad*	0.81	0.95	0.88	0.95	0.50	0.92	0.66	0.92	0.69	0.86	0.41	0.93	0.77	0.80	0.83	0.82
WS_{norm} & SL_{norm}	0.82	0.95	0.88	0.94	0.63	0.91	0.68	0.92	0.69	0.87	0.41	0.93	0.78	0.79	0.83	0.82
cad & SL_{norm}	0.82	0.95	0.88	0.95	0.50	0.92	0.68	0.91	0.69	0.88	0.42	0.93	0.77	0.79	0.84	0.82

The one-subject-based neural networks were also evaluated with respect to the data from all the other subjects, i.e. the data that was not used for the training. The values of the characteristic knots were estimated for each gait cycle (based on the corresponding gait parameters of the cycle) and then evaluated by calculating the correlation coefficients, mean absolute errors (MAE) and root mean square errors (RMSE) between the estimated values and the experimental ones. As explained before, to avoid an ill estimation from the NNs, the values of the gait parameters used as inputs for the NNs were limited to a perimeter based on the input data used to train the NNs (Fig. 40). When the gait parameters from the experimental data from the other subjects lied outside these limits, the limit values were selected as the inputs for the estimators. Table 8 shows the correlation coefficients of this evaluation, whereas the MAE and RMSE measurements are presented in Appendix D. As expected, these results show low correlation coefficients, although comparing them with the ones obtained with the all-subjects-based NNs (Table 6) shows an average deterioration of only 0.1 in the coefficients.

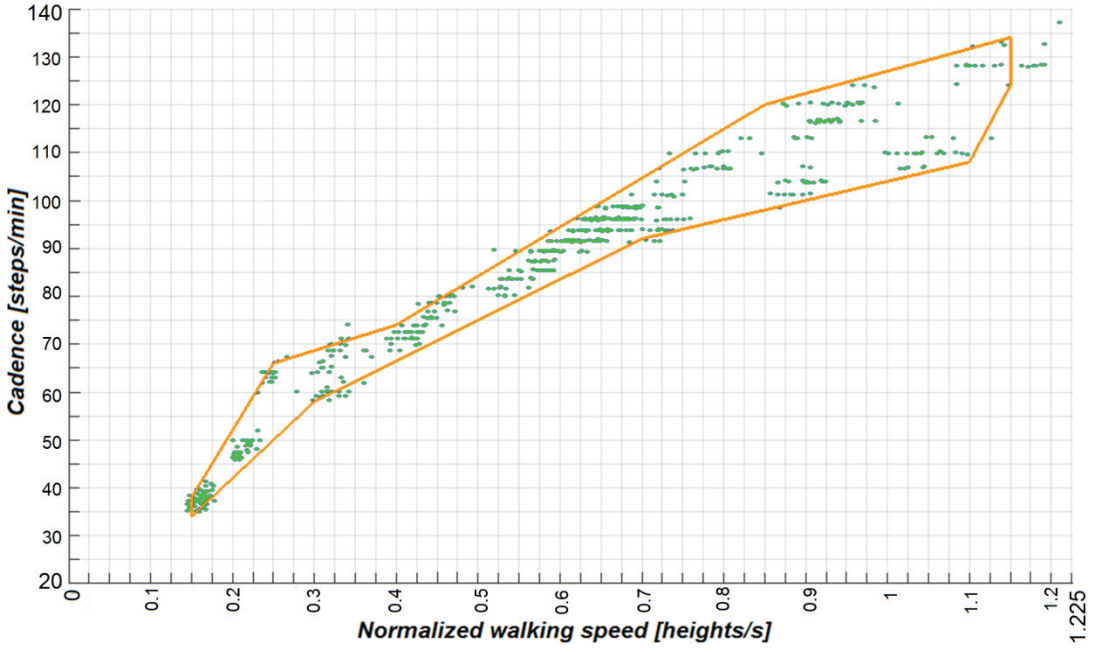

Fig. 40 Inputs' admissible area for $WS_{s,norm}$&*cad* neural networks of the selected subject

Table 8 Resulting correlation coefficients using the selected-subject NNs, calculated with respect to the other subjects' experimental data

	Correlation Coefficient (R)															
	HIP								*KNEE*							
	t_{M1}	θ_{M1}	t_{M2}	θ_{M2}	t_{M3}	θ_{M3}	t_{M4}	θ_{M4}	t_{M1}	θ_{M1}	t_{M2}	θ_{M2}	t_{M3}	θ_{M3}	t_{M4}	θ_{M4}
WS_{norm}	0.33	0.57	0.68	0.59	0.24	0.58	0.18	0.52	0.29	0.13	0.18	0.67	0.39	0.18	0.60	0.49
cad	0.27	0.39	0.78	0.43	0.06	0.44	0.09	0.36	0.27	0.13	0.18	0.52	0.40	0.19	0.55	0.46
SL_{norm}	0.35	0.64	0.43	0.68	0.21	0.66	0.25	0.60	0.24	0.02	0.08	0.66	0.22	0.09	0.47	0.42
WS_{norm} & *cad*	0.29	0.54	0.71	0.56	0.40	0.55	0.15	0.51	0.31	0.17	0.19	0.63	0.38	0.15	0.58	0.44
WS_{norm} & SL_{norm}	0.25	0.57	0.69	0.59	0.32	0.60	0.10	0.54	0.28	0.18	0.18	0.60	0.37	0.15	0.54	0.47
cad & SL_{norm}	0.26	0.51	0.73	0.52	0.35	0.50	0.13	0.45	0.27	0.17	0.18	0.58	0.38	0.16	0.54	0.47

Fig. 41 shows some examples of joint curves that were generated by interpolating the characteristic points predicted by the NNs and some shaping knots, as done before. The curves generated with the outputs from the NNs with only $WS_{s,norm}$ as input are shown in Fig. 41 (a), whereas some curves generated with the combined input $WS_{s,norm}$&*cad* are shown in Fig. 41 (b-d). The values of cadence depending on the normalized walking speed are depicted in Fig. 42. Note that the range of valid values for the second input given a specific first input is lower than before. Therefore, the differences between figures (a) to (d) are not as noticeable as when using the data from all subjects. For the final application, it is recommended that the combined inputs' neural networks are used to estimate the characteristic points, although now the differences between the performance of 1I1O and 2I1O NN are much lower than before. In this case, the ones using $WS_{s,norm}$&*cad* were selected for further explanation. The admissible area for the selected set of combined inputs lays inside the perimeter depicted in Fig. 40. It is important to understand that these are the input limits to make sure that the NNs will not generate undesired outputs due to extrapolation, but the limits that will be finally set for the therapist might be much stricter. For example, high velocities are not used for rehabilitation, therefore they would not be allowed. Anyway, the final admissible inputs' area set for the therapy must not lie neither completely nor partially outside of the admissible area set for the good performance of the neural networks.

4.3.3 Curve-shaping implementation

As explained in section 4.2, the generation of hip and knee trajectories is based not only on the desired cadence and the characteristic points of the curves. To obtain a more healthy-like shape of the trajectories, a set of shaping-knots is also introduced in the generation. The hip possesses four shaping-points, whereas the knee has six. The shaping-knots' time and angle values are calculated relative to the surrounding characteristic points following (2), (3) and (4), based on some coefficients α_{t_i} and α_{θ_i}. As stated before, the selected set of inputs for the automatic generation of trajectories were the normalized walking speed and the cadence. Consequently, apart from one of the methods that uses reference curves from the literature, all the methods presented next are based on these two gait parameters. Same as with the characteristic points, the problem is basically divided in two steps: first, getting the shaping-knots (or more specifically their α-coefficients) from the reference data; and second, developing an algorithm that delivers the estimated shaping-knots depending on the desired gait parameters. For the first step, several methods were designed and tested, whereas for the second step a simple mapping function was implemented.

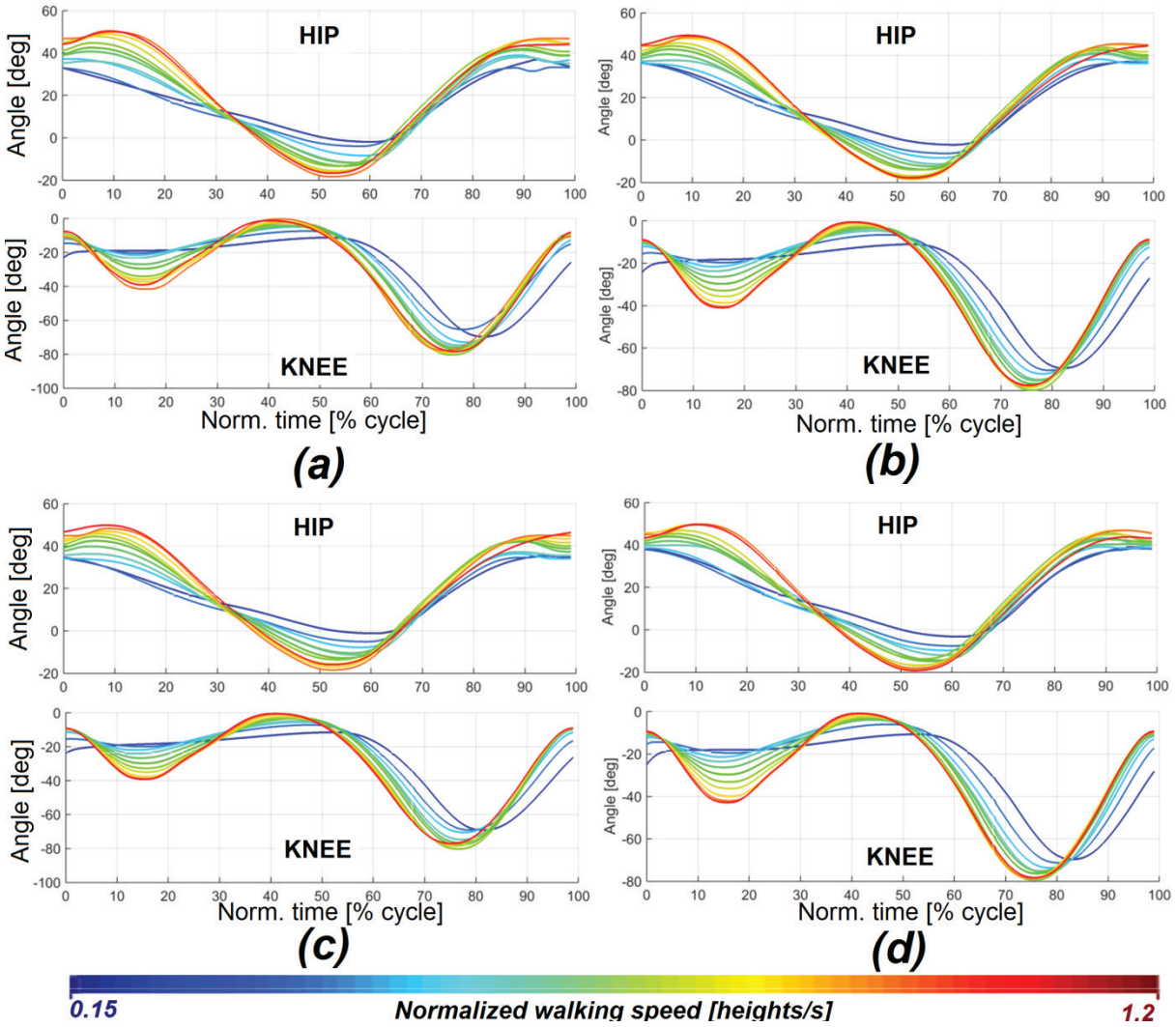

Fig. 41 Generation of hip and knee trajectories depending on $WS_{s,norm}$ (a) and $WS_{s,norm}$&cad (b,c,d) for the selected subject

This section is divided in five sub-sections, where the first three sub-sections relate specifically to the first step, and the fourth sub-section to the second step. Initially, the search algorithms that were developed to be used by each one of the first-step methods are introduced. Second, an explanation of the type of curves that were used during the search process is presented. Next, all the methods are explained in detail, including their training results and initial evaluation. Subsequently, the mapping of input gait parameters into the corresponding shaping knots is presented. At the end of the section, an overview of all the methods is given, including evaluations, comparisons and limitations of each one of them.

Search algorithms for shaping-knots coefficients

Three search algorithms were developed during this study to obtain the shaping knots from the reference joint trajectories. The objective behind all three is to find suitable sets of shaping knots' coefficients (α_t and α_θ) aiming to minimize a given cost function over all the samples of all the training reference curves that are fed to them. This way, the resulting shaping knots will be the ones that generate the trajectories that are closest to the reference curves.

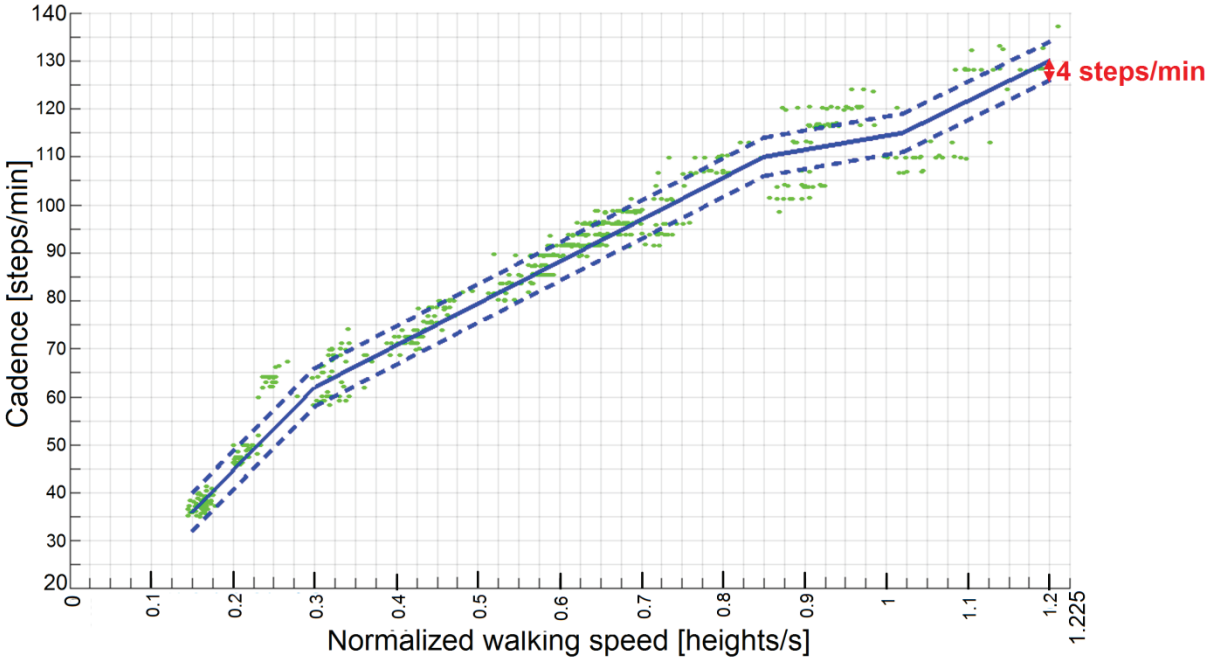

Fig. 42 *cad* vs $WS_{s,norm}$ input values for the generation of example curves using the selected subject's data

Full-Curve-Scanning Search Algorithm (FCSSA)

The first algorithm that was developed was the Full-Curve-Scanning Search Algorithm (*FCSSA*). The FCSSA goes over each gap between two consecutive characteristic points of the curve where at least one shaping knot is located, calculating the cost over all samples of all the curves while changing the time and angular values of the shaping knot(s) located in the current gap, controlling that the time-value difference between two knots is not lower than 20% of the time between the two characteristic points in each gap. The algorithm makes a complete scan of the possible values in each coefficient with a resolution of 0.01 (1%). In other words, it checks all the values in the range ($0<\alpha<1$) with steps of 0.01, and selects the set of coefficients that fulfill the given constraints and that generate the lowest cost measurement. A simplified state diagram of the algorithm can be seen in Fig. 43. Note that for each shaping point, two values must be analyzed. This means that for each value of α_{ti} being analyzed, 100 values of $\alpha_{\theta i}$ must be checked. Moreover, notice that the search is performed gap by gap. In the cases where the gap has two shaping points, a total of 100^4 different sets of those two points must be analyzed in that gap. With this in mind, a total of around 400 million sets of $\boldsymbol{\alpha}'$s were used at each iteration to search for the set that minimized the error. For this reason, the algorithm was designed for methods that use a very low number of training curves.

Dynamic-Clustering Search Algorithm (DCSA)

When the amount of curves used during the search increases, the time required by the FCSSA increases as well, due to the fact that this algorithm must perform a big amount of computations. A second search algorithm was developed in order to perform the search in a more time-efficient way: the Dynamic-Clustering Search Algorithm (DCSA).

The main idea behind the DCSA is to calculate the error (cost-function) checking only some α values between 0 and 1, equidistant from each other, instead of checking the whole

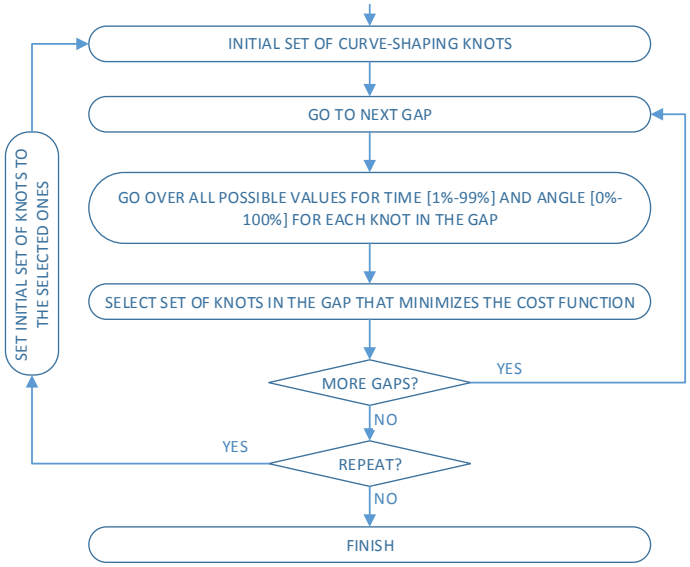

Fig. 43 Diagram of the error minimization in the FCSSA

range every 1%, as it was done before in the FCSSA. In this case, instead of working with 100 α values, the algorithm works only with k values, distant $\Delta d^1 = 1/(k-1)$ from each other. The value that generates the lowest error is taken as cluster centroid (or pivot) c for the next iteration of the algorithm. At each iteration, k α-values around the centroid are checked to search for the one that generates the lowest error. The range covered by the cluster is equal to the difference between working values from the last iteration (Δd^{i-1}), and consequently, the α values to be checked in the iteration range from $c^i - \Delta d^{i-1}/2$ to $c^i + \Delta d^{i-1}/2$. If k is even, $k/2$ values will be lower than c and $k/2$ values will be higher. If k is odd, $(k-1)/2$ values will lower than c, $(k-1)/2$ values will be higher than c, and one value will be equal to c. Note that the first iteration of the algorithm has a cluster range from 0 to 1, with a centroid in 0.5. For the final implementation of the algorithm a $k = 6$ was selected, and the number of iterations per coefficient was three. This way, the resolution in the final iteration is equal to 0.8%. Fig. 44 shows how the algorithm works for one α value with one simple example. The first iteration starts with a centroid located in 0.5 in a cluster that ranges from 0 to 1. In this iteration, the

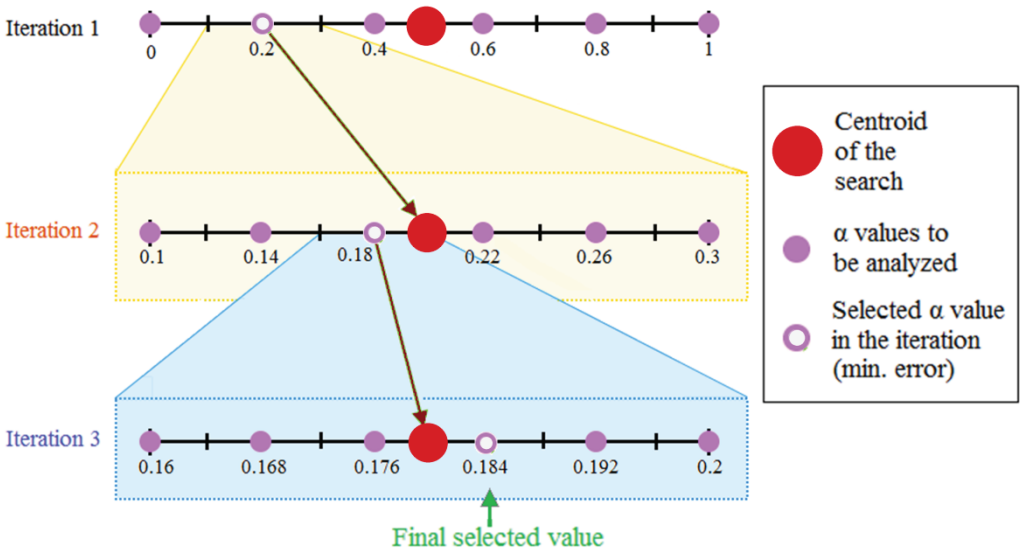

Fig. 44 Clustering and evaluation method for the DCSA

lowest error was obtained when using an $\alpha = 0.2$. This value is taken as the centroid of the cluster in iteration 2. This cluster ranges from 0.1 to 0.3. In this second iteration, an $\alpha = 0.18$ generated the lowest error, therefore that value is selected as the centroid for the 3^{rth} and last cluster. In the final iteration, an $\alpha = 0.184$ generated the lowest error, thus it is taken as the final α value.

As with the previous method, the search was done from gap to gap. With the selected k and number of iterations, $3 \cdot 6 = 18$ values were analyzed for each α. In the gaps with two shaping points, 18^4 values were checked. Finally a total of around 420000 sets of α values are used in each search. Fig. 45 shows the diagram of the DCSA. During the calculations, the α values from the gaps that had not been yet analyzed had to be set to some default initial values. In practice, these values were set to the resulting values of one of the methods that implemented the FCSSA (*Method 1*, presented in a subsequent section).

As with the FCSSA, some limits were set to the shaping knots coefficients during the search. The angular values of the points in the gap had to be apart from each other at least 1% of the range of motion in the gap, whereas the time values had to be apart at least 15% of the time between the two characteristic knots surrounding the gap.

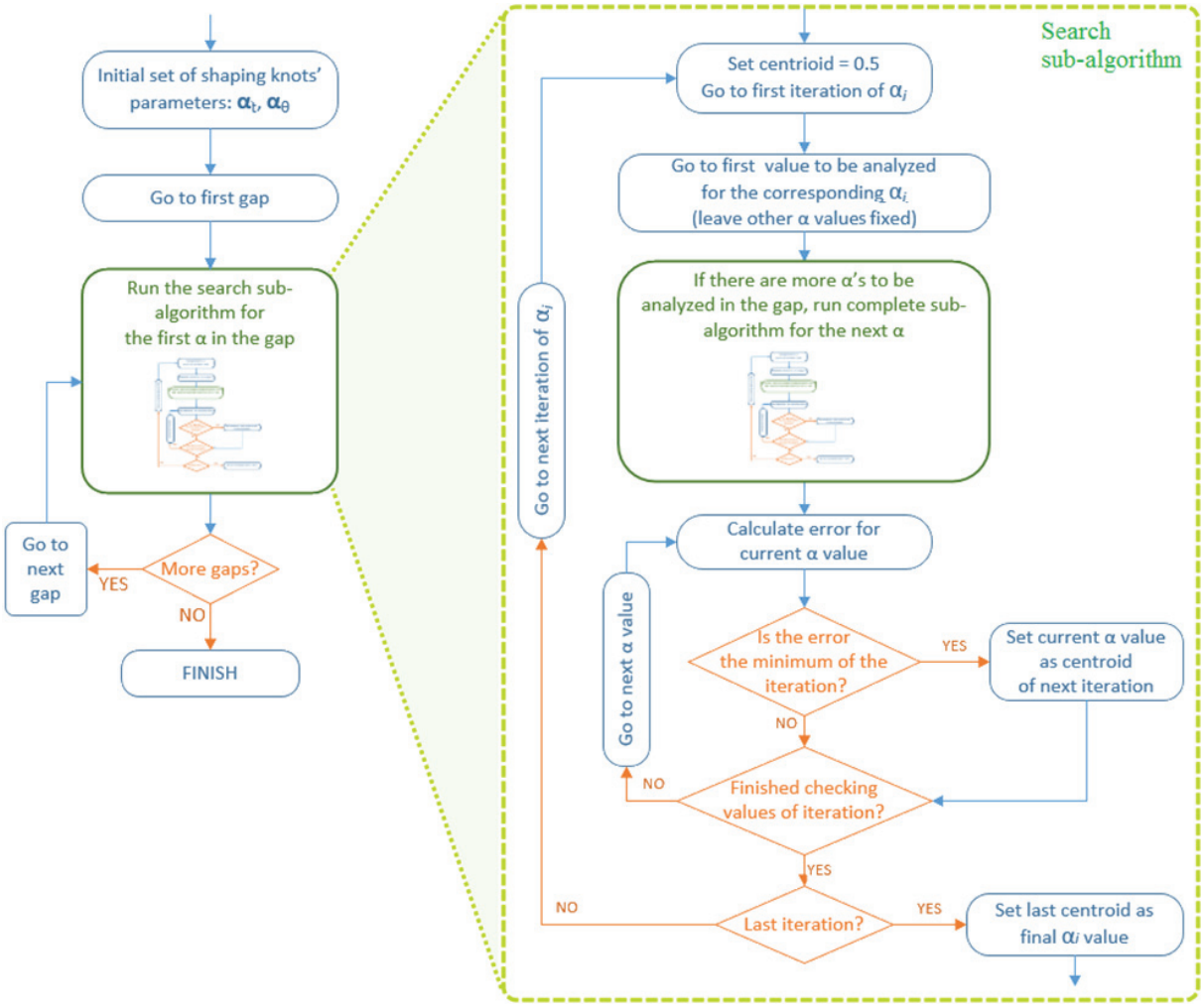

Fig. 45 Diagram of the error minimization in the DCSA

Progressive-Refinement Search Algorithm (PRSA)

Although the improvement in time-performance achieved with the DCSA was substantial compared to the FCSSA, it is not enough when a large amount of curves are utilized during the coefficients' search. For this reason, a third search algorithm was developed to further improve the processing time required by the search process: the Progressive-Refinement Search Algorithm (PRSA).

This search method is based on the concept that by adjusting progressively the actual shaping knots, the error between the reference and the reconstructed curves can be decreased. The idea is to set some initial α-values for all the shaping knots in the curve[18] and then move the shaping knots one by one (by means of their coefficients) in the direction that decreases the error. The shaping knot that is being adjusted is referred as the working point P_W, with coefficients $\{\alpha_{tw}, \alpha_{\theta w}\}$. The algorithm checks what would be the error if the working point changed its coefficients in four different ways:

$$
\begin{aligned}
(\alpha_t\ ,\ \alpha_\theta)^1 &= (\alpha_{tw} + \Delta t\ ,\ \alpha_{\theta w}) \\
(\alpha_t\ ,\ \alpha_\theta)^2 &= (\alpha_{tw}\ ,\ \alpha_{\theta w} + \Delta\theta) \\
(\alpha_t\ ,\ \alpha_\theta)^3 &= (\alpha_{tw} - \Delta t\ ,\ \alpha_{\theta w}) \\
(\alpha_t\ ,\ \alpha_\theta)^4 &= (\alpha_{tw}\ ,\ \alpha_{\theta w} - \Delta\theta)
\end{aligned}
\tag{20}
$$

where $\Delta t = \Delta\theta = 0.001$. The set of α-values that generates the lowest error is set to the corresponding working point and the operation is repeated. Once the working point cannot move to a state that generates an error lower than the actual one, the PRSA starts adjusting the next shaping point in the gap (if there is any). This procedure can be repeated several times per gap when there are more than one shaping points in it, starting again from the first point. The selected number of iterations in this case was five per gap. This process is done until all gaps have been analyzed. The constraints used in the DCSA regarding the closeness between the angle and time coefficient of two consecutive points was also applied in the PRSA.

The general concept behind the PRSA is depicted in Fig. 46, where a trivial example shows how the adjustment of shaping knot P_{S1} decreases the difference between a reference curve (pale line) and the regenerated curve (dark line). In the example, the working point first moved upward (*a*), by increasing the angle-coefficient value by $\Delta\theta$, and afterwards it moved to the right (*b*), by increasing the time-coefficient value by Δt, so that the final regenerated curve (*c*) fits better the reference one. The diagram of the PRSA is shown in Fig. 47.

Reference curves used in the search process

Two basic sets of references curves were used by the methods presented in the next sub-section. The first one contains twenty healthy curves (for each joint) extracted from study results of several publications. Since the original measurements were not available, these curves were obtained from the figures of the publications and manually sampled every 1% of the gait cycle period. The curves include gait trajectories (mostly averaged) of adult subjects [24] [195] [196] [197] [198] [23] [199] [21] [200] [22] [25] walking at normal, fast and slow speed, and of children [201] [198] [37] [202] walking at normal speed.

[18] In our case, all the α_t started with a value of 0.2, whereas all the α_θ started with a value of 0.8

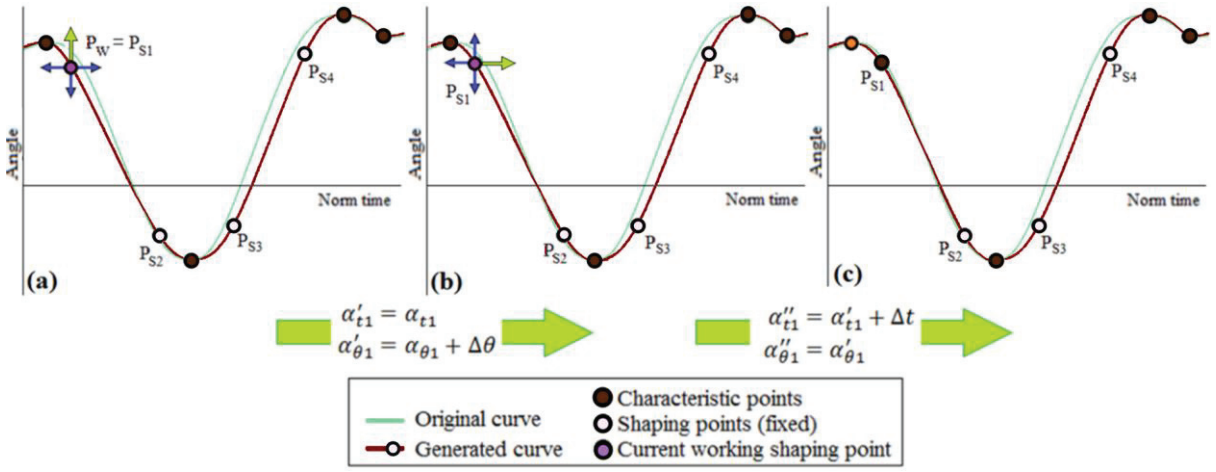

Fig. 46 Progressive adjustment of shaping knots in the PRSA

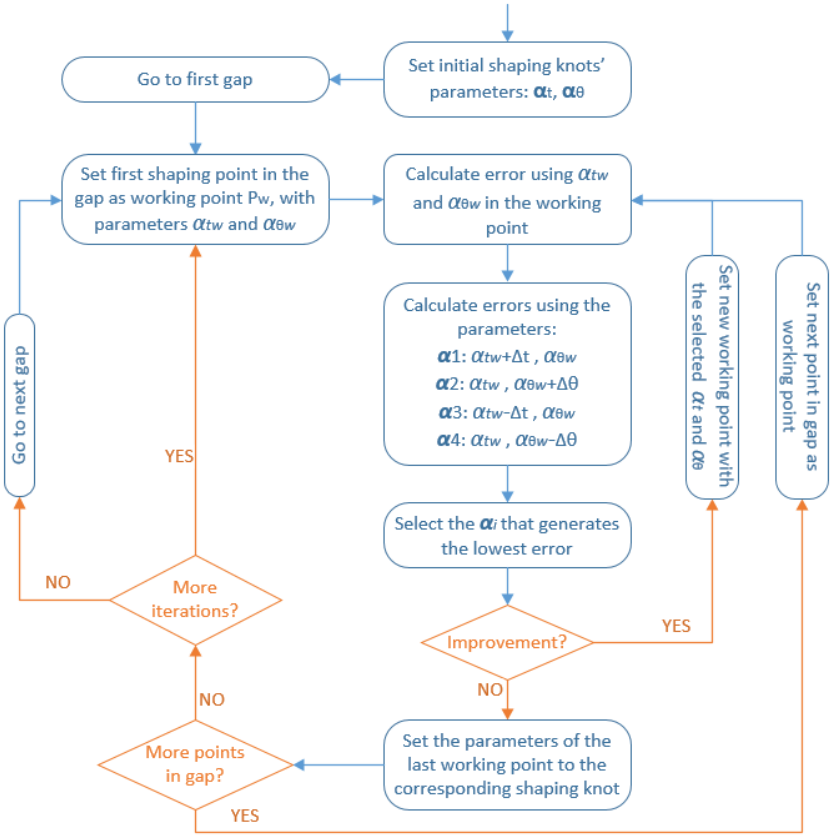

Fig. 47 Diagram of the Progressive Refinement Search Algorithm

After conducting the experiment presented in section 4.3.1 it was decided to study the dependency of the shaping points' coefficient values on the normalized walking speed and cadence of each cycle. To this end, a second set of reference curves was taken into account for the calculation of the α-values, corresponding to the segmented cycles gotten from the experimental data from the selected subject. These data were used to obtain the new sets of α_t and α_θ dependent on the aforementioned gait parameters. Because the objective is to get the coefficients based on the selected WS_{norm} and *cad*, it was necessary to group the reference set of curves based on their specific gait parameters and perform the search for each group separately. Two different grouping strategies were used: by exercise (*Gr1*), taking into

account that it is expected that the walking speed and cadence throughout each exercise do not vary significantly; and by clustering the cycles based on their WS_{norm} and *cad* (*Gr2*). The first grouping is done in a straight forward manner: there exist 26 different groups, each one corresponding to one of the exercises done during the experiment. For the second grouping strategy, the cycles' data were divided in 28 clusters[19]. Fig. 48 shows the map of normalized walking speed and cadence of all the processed cycles with the aforementioned clustering.

Because of the big amount of available curves in the second set of reference trajectories, some of the methods were developed to use smaller sets of curves, obtained from each group, to feed the search algorithms. Two selection strategies were elaborated to this end: selection of the most representative curves in the group (*p-MRep*); and average curve (*AvC*).

For the *p-MRep* strategy the *p* most representative curves of hip and knee joints were selected to be used in the search process. To obtain the most representative curves from each group, all the curves were subject to a weighted time-warping operation. This operation lined up in time some characteristic points (P_{M1}, P_{M2} and P_{M3} in hip; P_{M2}, P_{M3} and P_{M4} in knee) and resampled the angle values proportionally based on the time-warping and the original time and angular values of the samples of each curve. Besides the time-warping, all the curves' angles were normalized with respect to the range of motion of each curve. Fig. 49 shows an example of the time-warping operation. The time-warping was not done randomly, but rather following some weighting rules. In the case of the hip, the sections of the curves between P_{M1} and P_{M2}, and P_{M2} and P_{M3} were resampled to cover 46% of the cycle period each, whereas the region between P_{M3} and P_{M1} covers only 8% of the cycle. For the knee curves, the sections between P_{M2} and P_{M3}, and P_{M3} and P_{M4} were resampled to cover 40% of the cycle period each, whereas the region between P_{M4} and P_{M2} covers 20% of the cycle. This procedure was done to give more weight to the samples in the sections surrounding the global minimums of the curves, where the shaping knots influence the most the curve shape and the error between the original and the reconstructed curves.

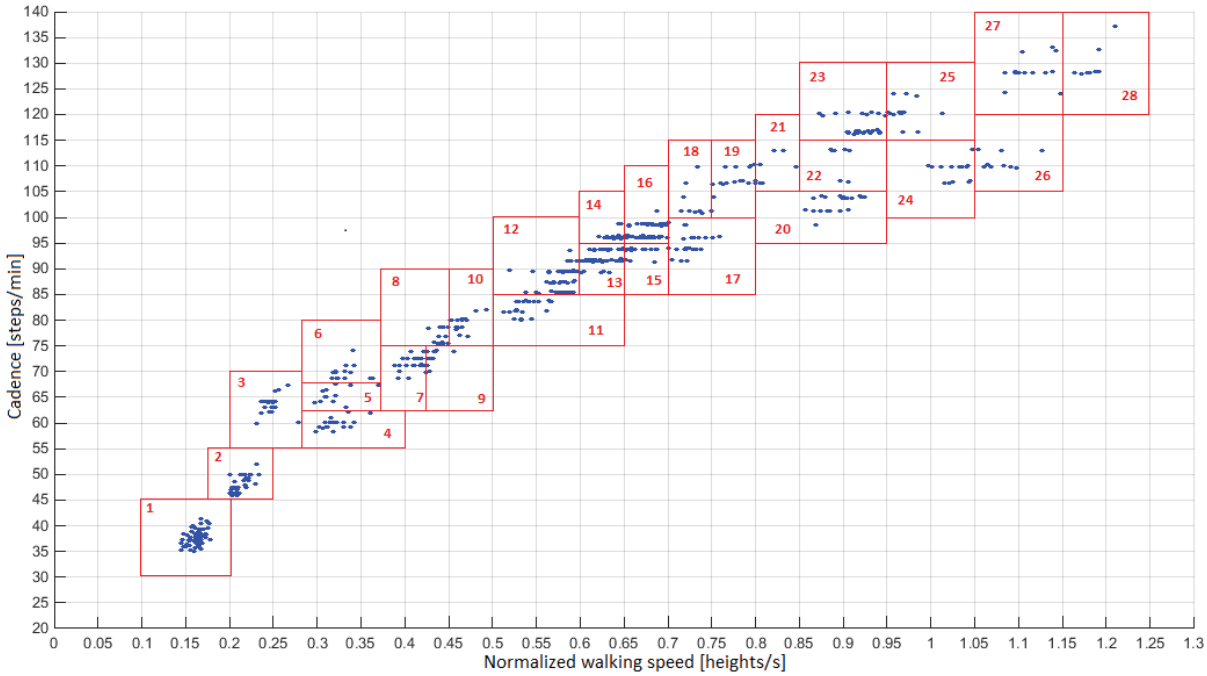

Fig. 48 Map of normalized walking speed and cadence by cluster

[19] Not to be confused with the clusters from the DCSA

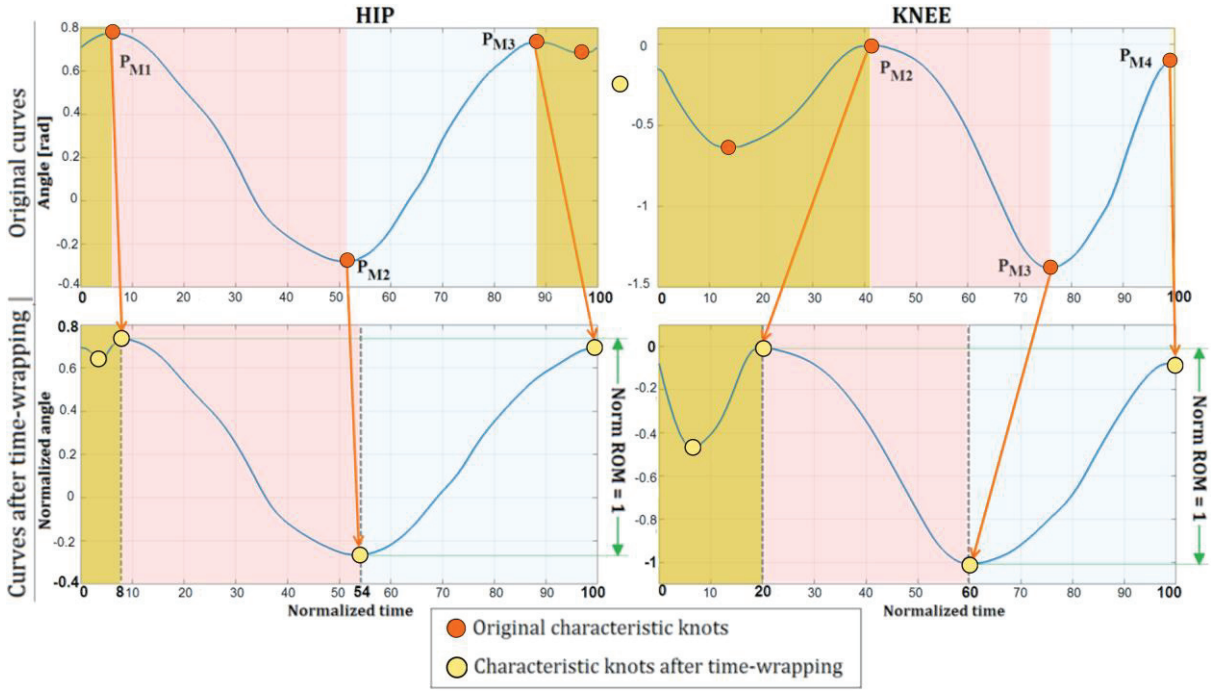

Fig. 49 Weighted time-warping operation

Once all the curves were warped in time and resampled, the cross-correlation coefficients between the obtained curves were used to select the curve that represented better the trajectories from the group. As explained before, the correlation coefficient is given by

$$R_{xy} = \frac{cov(x,y)}{\sigma_x \cdot \sigma_y}, \tag{21}$$

only that this time, the x and y values correspond to the normalized angular values from 100 resampled points (each) from two different time-warped curves. The correlation coefficient was calculated for each curve against all the other curves in the group and was placed in a cross-correlation coefficients' matrix similar to the one used in [171]:

$$\boldsymbol{R} = \begin{bmatrix} - & R_{12} & \cdots & R_{1n} \\ R_{21} & - & \ldots & R_{2n} \\ \vdots & \vdots & \ddots & \vdots \\ R_{n1} & R_{n2} & \ldots & - \end{bmatrix} \tag{22}$$

where n is the number of trajectories in the group. Note that the autocorrelation coefficients are not taken into account because they are always equal to one. Afterwards, the correlation coefficients of each row were added up and the p rows that possessed the highest summed values were extracted. These rows correspond to the p most representative curves in the group. An example is depicted in Fig. 50, where the orange and green lines correspond to the knee trajectories from the left and right legs, respectively, from a specific exercise, and the blue lines correspond to the most representative curve in the group (i.e. $p=1$). The figure in the left shows the normalized curves before the time-warping, whereas the figure in the right shows the time-warped curves with the normalized angles shifted to appear between 0 and 1.

For the *AvC* strategy the averaged normalized time-warped curve was the one used for the search process. To obtain this average trajectory, the angles of each curve were initially

normalized with respect to its range of motion; afterwards, all the curves were shifted in the angle axis so that all their values lay between 0 and 1; and finally, the aforementioned time-warping operation was applied to all trajectories. The resulting normalized time-warped curves were ultimately averaged, sample by sample, to obtain the desired mean curve, whose angle values are given by

$$\breve{\theta}(k) = \frac{1}{N}\sum_{i=1}^{N} \tilde{\theta}_i(k) \qquad ;k = 0,1,2,\dots,99 \tag{23}$$

where $\breve{\theta}(k)$ is the angle of the average curve corresponding to the normalized (warped) time k, $\tilde{\theta}_i(k)$ is the normalized angle value of the i^{th} resulting time-warped curve, and N is the number of curves in the group. An example of the average curve yielded by this operation is depicted in Fig. 51, where the original knee trajectories from cluster 13 are shown in the left

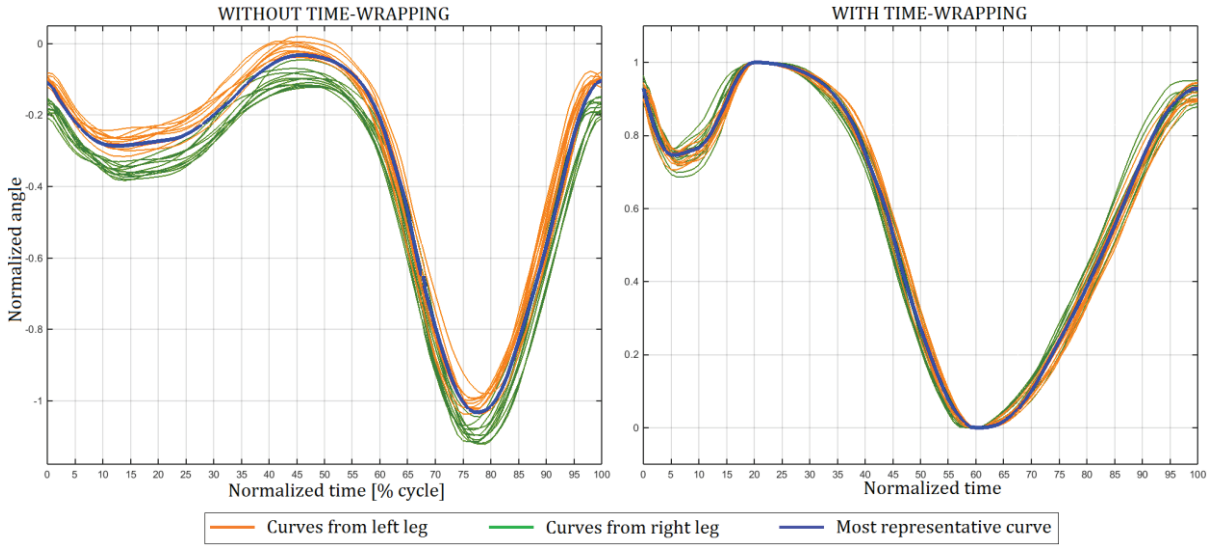

Fig. 50 Example of most representative curve from an exercise

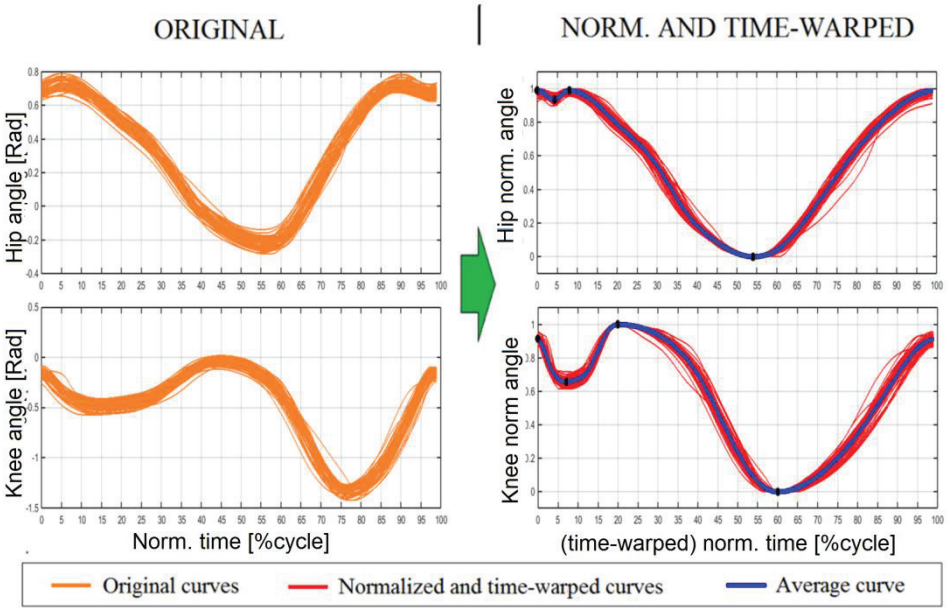

Fig. 51 Example of cluster average curve

plots, and the normalized, shifted and time-warped curves are shown in the right plots, together with the average curve (blue line).

Methods for shaping-knots coefficients' obtainment

Several methods were developed in the search for the best α-values obtainment procedure. Each one of the methods implements one of the aforementioned search algorithms, feeding it with specific sets of reference curves. This sub-section presents eight different methods with the corresponding initial evaluation.

Method 1: Using reference trajectories from the literature and the FCSSA [Lit+FCSAA]

This was the first developed method. Fifteen of the 20 reference curves obtained from the literature where randomly selected to feed the search algorithm, while the remaining five where used to test the results. This is the only method that uses the reference curves obtained from the literature and, hence, the only one that doesn't take into account the input walking speed and cadence to calculate the shaping knots' coefficients (i.e. the coefficients are fixed for all values of WS_{norm} and cad). Because of the small amount of training curves, the FCSSA was used to obtain the sets of α-values, aiming to minimize the sum of normalized position squared errors over all the samples of all the training reference curves. The general formulation of the minimization problem is as follows

$$\arg\min_{\{\boldsymbol{\alpha}_t,\boldsymbol{\alpha}_\theta\}}\left(\sum_{i=1}^{N_{REF}}\sum_{j=1}^{n}\left(\frac{\theta_{REF\,(i,j)}-\theta_C(\{\boldsymbol{\alpha}_t,\boldsymbol{\alpha}_\theta\})_{(j)}}{max\left(\left\{\theta_{REF\,(i)}\right\}\right)-min\left(\left\{\theta_{REF\,(i)}\right\}\right)}\right)^2\right) \tag{24}$$

where $N_{REF}=15$ is the number of training reference curves, $n=100$ is the number of samples per curve, $\theta_{REF\,(i,j)}$ is the angular value of the reference curve i in the sample j, $\theta_C(\{\boldsymbol{\alpha}_t,\boldsymbol{\alpha}_\theta\})$ is the angular value calculated from the interpolation using the shaping knots described by a given set of $\{\alpha_t,\alpha_\theta\}$, and $min\left(\left\{\theta_{REF\,(i)}\right\}\right)$ and $max\left(\left\{\theta_{REF\,(i)}\right\}\right)$ are the minimum and maximum angular values of the reference curve i, respectively. Note that the errors are normalized with respect to the range of motion of each curve.

The algorithm was run three times for each joint[20]. The resulting set of knots given by the first algorithm yielded a mean normalized position error (per sample) of 0.029 and 0.03 for the training set and the test set, respectively, for the hip joint, and 0.023 and 0.02 for the knee joint. The mean squared errors, standard deviations and mean absolute errors of the obtained results for the training and test sets can be seen in Table 9, as well as the overall results for the complete set of 20 reference curves. These results showed that with the given method it is possible to reconstruct joint trajectories by using the proposed number of characteristic and shaping knots. Fig. 52 shows an example comparing the hip and knee curves of a reference pattern (taken from the test set) and the curves generated with the results yielded by the FCSSA.

[20] No significant changes were reported between the results of the 2nd and 3rd runs, indicating that the algorithm had converged to a desired result.

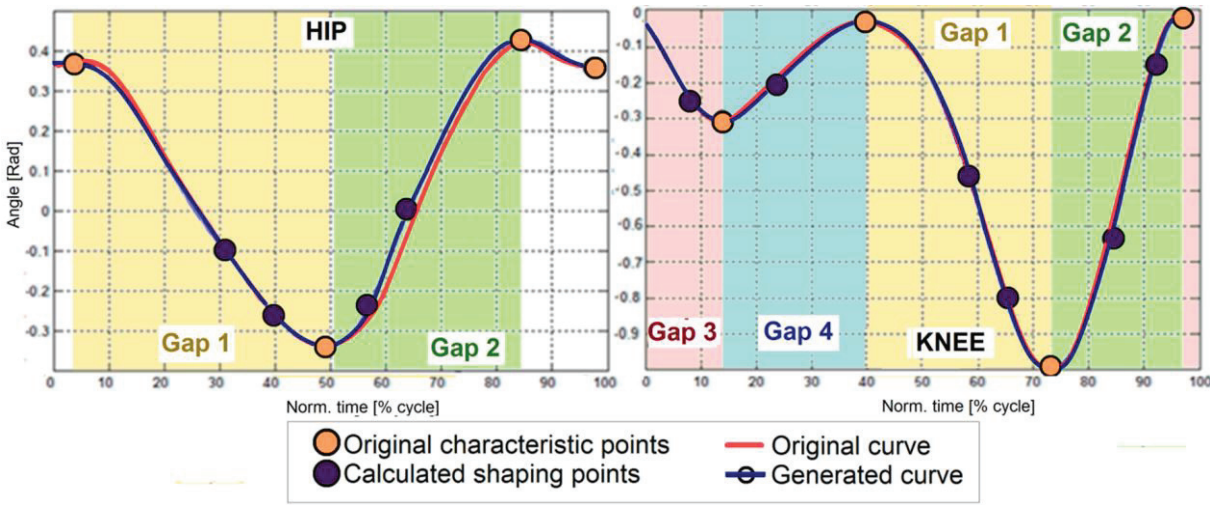

Fig. 52 Example of hip and knee generated curves vs original curves using the FCSSA

Method 2: Using all the curves from each exercise with the DCSA [Gr1+All+DCSA]

This method grouped the selected subject's processed data by exercise. Afterwards, it fed all the curves from each exercise to the search algorithm to obtain the set of α-values that represented better each group. Due to the substantial increment in the training curves, the FCSSA was not an option because of the huge amount of time it would need to go over all the trajectories. At this point, the DCSA was developed and used by this method. As explained before, the initial (default) α-values in the DCSA were set to the resulting coefficients from *Method 1*. The formulation of the cost-minimization problem implemented in the DCSA for this method is defined as

$$\arg\min_{\{\boldsymbol{\alpha}_{t,E},\boldsymbol{\alpha}_{\theta,E}\}}\left(\sum_{i=1}^{N_E}\sum_{j=1}^{n}\left(e_{p}^{2}{}_{(i,j)}+w_v\cdot\left|e_{v(i,j)}\right|\right)\right)$$

$$e_{p_{(i,j)}}=\theta_{REF\,(i,j)}-\theta_C\left(\{\boldsymbol{\alpha}_{t,E},\boldsymbol{\alpha}_{\theta,E}\}\right)_{(j)}$$

$$e_{v(i,j)}=\dot{\theta}_{REF\,(i,j)}-\dot{\theta}_C\left(\{\boldsymbol{\alpha}_{t,E},\boldsymbol{\alpha}_{\theta,E}\}\right)_{(j)} \tag{25}$$

where $n=100$ is the number of samples per curve, N_E is the number of curves in the exercise E, $e_{p_{(i,j)}}$ and $e_{v(i,j)}$ are the position and velocity error measurements in sample j when comparing the regenerated curve and the i^{th} curve of the exercise, $\theta_{REF\,(i,j)}$ and $\dot{\theta}_{REF\,(i,j)}$

Table 9 Results of the FCSSA

MNSE: Mean Normalized Squared Error (per sample). SD: Standard Deviation. MNAE: Mean Normalized Absolute Error (per sample)

		Training	Test	ALL
HIP	MNSE	0.0008	0.0009	0.0008
	SD	0.0013	0.0007	0.0021
	MNAE	0.0283	0.03	0.0283
KNEE	MNSE	0.0005	0.0004	0.0005
	SD	0.0015	0.0008	0.0013
	MNAE	0.0224	0.02	0.0224

are the position and velocity values of the i^{th} reference curve in the sample j, $\theta_C(\{\boldsymbol{\alpha}_{t,E}, \boldsymbol{\alpha}_{\theta,E}\})$ and $\dot{\theta}_C(\{\boldsymbol{\alpha}_{t,E}, \boldsymbol{\alpha}_{\theta,E}\})$ are the position and velocity values calculated from the interpolation using the shaping knots described by a given set of $\{\alpha_{t,E}, \alpha_{\theta,E}\}$ (specific to exercise E), and $w_v = 0.02$ is the weight of the velocity error in the cost function.

Because all the curves are used for the coefficients' search, the average normalized speed and average cadence of each exercise were selected as the reference pairs to be used by the radial-basis selection process during the input gait parameters mapping (explained in a forthcoming section). These reference pairs ($WS_{norm,E}$, cad_E) will be referred as the centroids of the groups. The centroids are calculated by averaging the gait parameters of each group

$$WS_{norm,E} = \frac{1}{n_E}\sum_{i=1}^{n_E} WS_{norm,i}$$

$$cad_E = \frac{1}{n_E}\sum_{i=1}^{n_E} cad_i \tag{26}$$

where n_E is the number of curves in exercise E. Fig. 53 shows the map of normalized walking speed and cadence with the 26 reference pairs of the exercises.

The results accomplished with this method can be seen in Table 10, where the Averaged Mean Absolute Errors (*AMAE*), Averaged Root Mean Squared Error (*ARMSE*) and Averaged Standard deviation of the Absolute Errors (*ASDAE*) calculated between all the original curves in each exercise, and the curves that were regenerated using the characteristic points of the corresponding original curve and the shaping knots calculated using the resulting coefficients of the exercise, are shown. These calculations were done by calculating the Mean Absolute Errors (*MAE*), Root Mean Squared Error (*RMSE*) and Standard deviation of the Absolute

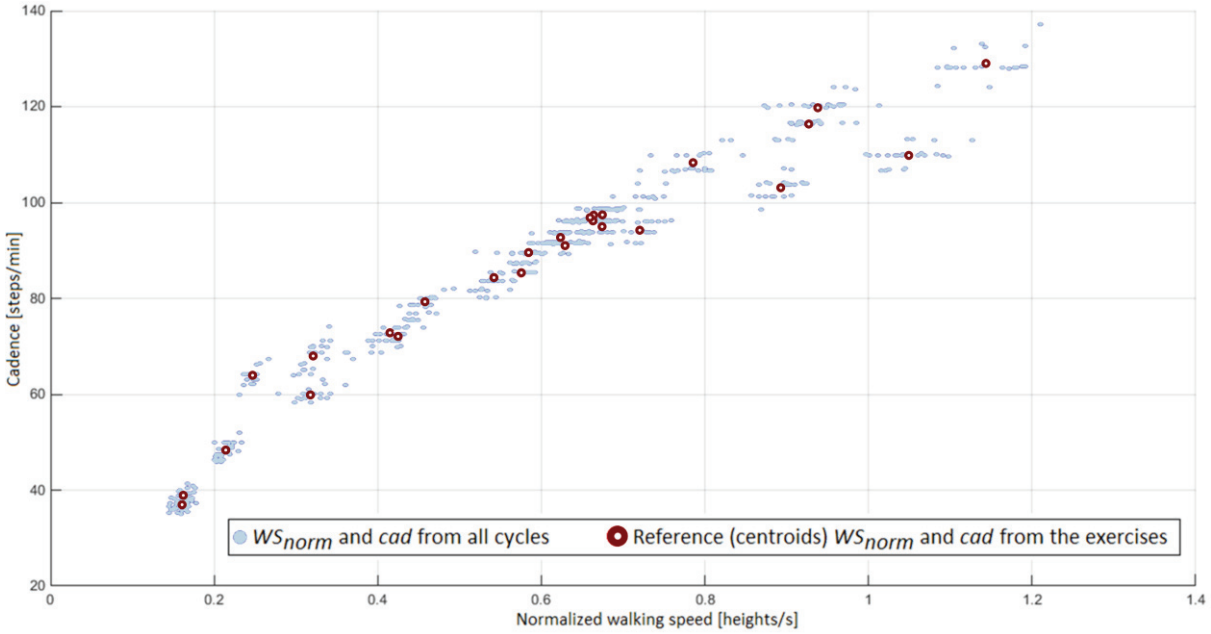

Fig. 53 Map of normalized walking speed and cadence with the exercises' reference gait parameters' pairs

Errors (*SDAE*) from each curve of an exercise and then averaging the resulting values, thus the values are averages per exercise. Table 10 also shows the corresponding reference WS_{norm} and *cad* for each group. Notice that the highest errors took place in the exercises with high walking speeds (e.g. *P1-6* and *P3-9*) and low cadences (e.g. *P3-2* and *P3-3*), whereas the best results were achieved for the exercises related to normal (desired) walking (e.g. *P1-1* and *P2-4*). An example of the generation using the resulting shaping-knots' coefficients is depicted in Fig. 54, where the position and velocity of the most representative curve from exercise P3-2 are compared to the ones from the reconstructed one. Although the results yielded by this method are good regarding the error-performance, the time spent by the DCSA to go through all the training curves was excessively high.

Method 3: Using the most representative curve from each exercise with the DCSA [Gr1+1-MRep+DCSA]

To reduce the amount of time needed by the DCSA to obtain suitable set of coefficients, it was decided to decrease the number of curves fed to the search algorithm. This method runs the DCSA only using one curve per exercise: the most representative (i.e. *p_MRep* with *p=1*). The curve fed to the DCSA is the original curve (the time-warped curves were only used to get the most representative one). The cost minimization formulation is similar to the one in (25), but with a reduction in the number of analyzed curves:

$$\arg\min_{\{\boldsymbol{\alpha}_{t,E},\boldsymbol{\alpha}_{\theta,E}\}}\left(\sum_{j=1}^{n}\left(e_{p,j}^{2}+w_v\cdot\left|e_{v,j}\right|\right)\right)$$

$$e_{p,j}=\theta_{REF\,(j)}-\theta_C\left(\{\boldsymbol{\alpha}_{t,E},\boldsymbol{\alpha}_{\theta,E}\}\right)_{(j)}$$

$$e_{v,j}=\dot{\theta}_{REF\,(j)}-\dot{\theta}_C\left(\{\boldsymbol{\alpha}_{t,E},\boldsymbol{\alpha}_{\theta,E}\}\right)_{(j)} \tag{27}$$

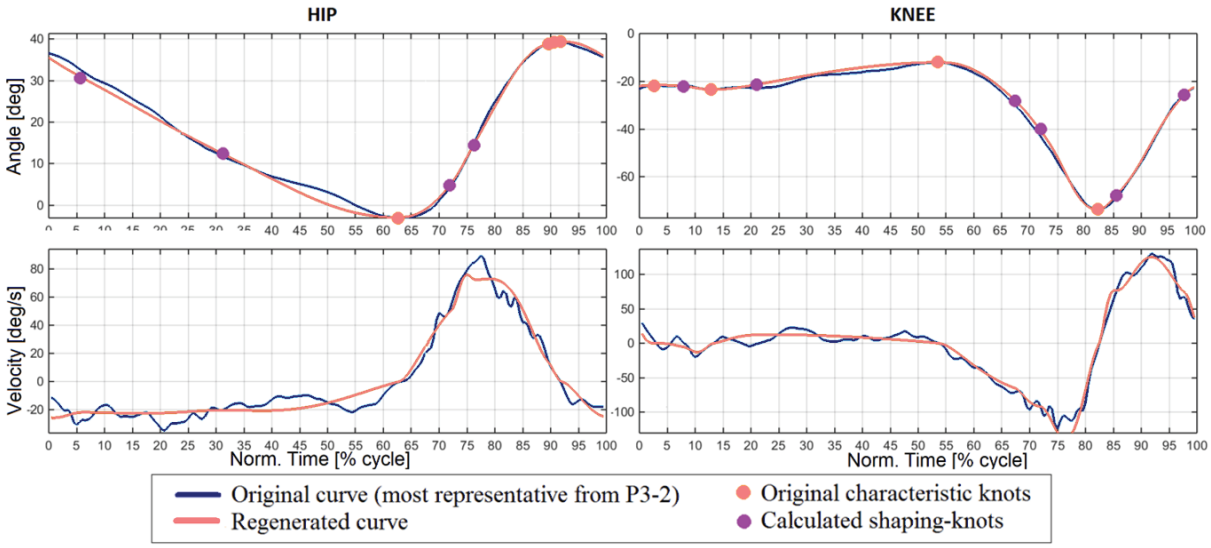

Fig. 54 Original curve (most representative from exercise P3-2) vs regenerated curve using the calculated shaping-knots coefficients

Table 10 Results of *Method 2* with respect to all the curves in the exercise

AMAE: Averaged MAE. ARMSE: Averaged RMSE. AR: Averaged SD of the Absolute Errors.

			HIP						KNEE					
			Position			Velocity			Position			Velocity		
Ex.	**WS norm**	**Cad**	**AMAE (±SD) [deg]**	**ASDAE (±SD) [deg]**	**ARMSE (±SD) [deg]**	**AMAE (±SD) [deg/s]**	**ASDAE (±SD) [deg/s]**	**ARMSE (±SD) [deg/s]**	**AMAE (±SD) [deg]**	**ASDAE (±SD) [deg]**	**ARMSE (±SD) [deg]**	**AMAE (±SD) [deg/s]**	**ASDAE (±SD) [deg/s]**	**ARMSE (±SD) [deg/s]**
P1-1	0.66	97.2	0.8 (±0.26)	0.79 (±0.24)	1.13 (±0.34)	14.43 (±2.03)	11.99 (±1.81)	18.76 (±2.55)	1.01 (±0.34)	1.01 (±0.38)	1.43 (±0.5)	20.6 (±3.78)	19.88 (±5.94)	28.66 (±6.75)
P1-2	0.16	39.0	1.26 (±0.34)	1.07 (±0.35)	1.66 (±0.46)	6.58 (±1.16)	5.49 (±1.19)	8.58 (±1.59)	1.39 (±0.5)	1.5 (±0.84)	2.06 (±0.95)	9.54 (±2.33)	9.81 (±4.02)	13.71 (±4.49)
P1-3	0.41	72.8	0.87 (±0.43)	0.81 (±0.45)	1.19 (±0.61)	9.71 (±1.93)	8.11 (±2.48)	12.66 (±3.05)	1.18 (±0.46)	1.25 (±0.53)	1.73 (±0.68)	14.72 (±2.83)	13.59 (±2.63)	20.04 (±3.67)
P1-4	0.58	89.5	0.89 (±0.26)	0.85 (±0.3)	1.23 (±0.39)	13.35 (±1.48)	10.59 (±1.59)	17.04 (±2.03)	1.03 (±0.36)	1.04 (±0.38)	1.46 (±0.52)	19.92 (±3.33)	19.41 (±4.34)	27.82 (±5.22)
P1-5	0.93	116.3	1.29 (±0.81)	1.37 (±0.94)	1.88 (±1.24)	22.22 (±5.12)	18.34 (±5.09)	28.85 (±6.93)	1.56 (±0.61)	1.65 (±0.79)	2.27 (±0.97)	31.25 (±9.63)	31.39 (±12.25)	44.45 (±14.91)
P1-6	1.14	129.0	2.08 (±0.52)	2.04 (±0.53)	2.92 (±0.7)	29.63 (±4.4)	25.18 (±4.88)	38.9 (±6.22)	1.34 (±0.45)	1.18 (±0.38)	1.79 (±0.58)	30.7 (±5.39)	26.91 (±5.97)	40.85 (±7.65)
P1-7	0.62	92.6	0.84 (±0.24)	0.81 (±0.25)	1.17 (±0.34)	14.07 (±1.43)	11.01 (±1.52)	17.86 (±1.95)	1.14 (±0.43)	1.2 (±0.51)	1.66 (±0.65)	21.53 (±5.3)	20.73 (±7.32)	29.96 (±8.67)
P2-1	0.67	97.4	0.95 (±0.31)	0.9 (±0.43)	1.32 (±0.52)	16.44 (±2.91)	13.87 (±5.02)	21.59 (±5.41)	1.23 (±0.39)	1.28 (±0.44)	1.78 (±0.57)	25.2 (±6.45)	27.35 (±9.01)	37.29 (±10.52)
P2-2	0.25	63.9	1.18 (±0.65)	1.07 (±0.61)	1.59 (±0.88)	10.18 (±3.05)	8.68 (±3.28)	13.49 (±4.06)	1.05 (±0.41)	1.14 (±0.53)	1.55 (±0.66)	11.79 (±2.53)	11.24 (±3.07)	16.31 (±3.78)
P2-3	0.32	68.0	1.08 (±0.46)	0.97 (±0.34)	1.46 (±0.55)	9.63 (±1.85)	8.6 (±1.98)	12.92 (±2.61)	1.03 (±0.54)	1.07 (±0.65)	1.49 (±0.83)	13.21 (±3.76)	12 (±3.65)	17.85 (±5.15)
P2-4	0.46	79.2	0.76 (±0.33)	0.68 (±0.3)	1.02 (±0.44)	10.05 (±2.36)	8.13 (±2.34)	12.92 (±3.29)	1 (±0.31)	0.94 (±0.29)	1.38 (±0.42)	15.61 (±2.08)	14.28 (±2.81)	21.17 (±3.23)
P2-5	0.58	85.3	0.73 (±0.16)	0.71 (±0.19)	1.02 (±0.24)	11.08 (±1.36)	8.97 (±1.28)	14.27 (±1.69)	1.02 (±0.23)	1.01 (±0.27)	1.44 (±0.34)	18.01 (±2.75)	17.57 (±3.5)	25.16 (±4.22)
P2-6	0.72	94.1	1.15 (±0.3)	1.13 (±0.35)	1.62 (±0.45)	16.57 (±3.14)	13.94 (±3.78)	21.68 (±4.72)	1.1 (±0.41)	1.11 (±0.4)	1.56 (±0.56)	21.68 (±5.15)	21.55 (±5.75)	30.57 (±7.56)
P2-7	0.89	103.2	1.47 (±0.92)	1.52 (±1.05)	2.11 (±1.38)	20.24 (±5.47)	16.88 (±4.93)	26.36 (±7.23)	1.08 (±0.3)	1.07 (±0.33)	1.52 (±0.43)	24.2 (±4.09)	23.84 (±6.73)	34.05 (±7.32)
P2-8	1.05	109.8	1.8 (±1.03)	1.96 (±1.3)	2.66 (±1.65)	24.6 (±6.22)	19.86 (±4.34)	31.61 (±7.45)	1.36 (±0.41)	1.22 (±0.43)	1.83 (±0.57)	28.15 (±5.71)	26.11 (±7.07)	38.42 (±8.76)
P2-9	0.63	91.1	0.74 (±0.25)	0.75 (±0.27)	1.06 (±0.37)	12.9 (±2.02)	10.82 (±2.05)	16.84 (±2.75)	1.22 (±0.48)	1.26 (±0.6)	1.76 (±0.76)	21.27 (±5.45)	20.22 (±6.4)	29.37 (±8.15)
P3-1	0.67	94.9	0.84 (±0.27)	0.83 (±0.23)	1.18 (±0.34)	14.58 (±1.94)	12.43 (±1.87)	19.18 (±2.33)	1.29 (±0.43)	1.35 (±0.46)	1.87 (±0.61)	23.79 (±3.73)	25.03 (±5.7)	34.55 (±6.46)
P3-2	0.16	36.8	1.58 (±0.62)	1.37 (±0.59)	2.1 (±0.84)	6.81 (±1.65)	5.53 (±1.68)	8.77 (±2.3)	1.39 (±0.37)	1.32 (±0.44)	1.92 (±0.56)	9.22 (±1.75)	8.27 (±1.93)	12.4 (±2.49)
P3-3	0.21	48.3	1.55 (±0.7)	1.29 (±0.57)	2.02 (±0.88)	9.25 (±2.27)	8.01 (±2.92)	12.26 (±3.55)	1.4 (±0.56)	1.49 (±0.68)	2.05 (±0.86)	12.83 (±4)	13.18 (±6.65)	18.47 (±7.49)
P3-4	0.32	60.0	1.42 (±0.77)	1.32 (±0.92)	1.95 (±1.19)	10.87 (±2.81)	8.47 (±2.22)	13.79 (±3.51)	1.4 (±0.55)	1.51 (±0.63)	2.06 (±0.82)	15.23 (±2.95)	14.11 (±2.81)	20.77 (±3.89)
P3-5	0.42	72.1	0.95 (±0.52)	0.89 (±0.49)	1.3 (±0.71)	11.04 (±3.74)	9.89 (±4.64)	14.85 (±5.82)	1.14 (±0.45)	1.22 (±0.63)	1.67 (±0.76)	16.46 (±5.02)	16.58 (±8.04)	23.43 (±9.22)
P3-6	0.54	84.3	0.88 (±0.31)	0.89 (±0.26)	1.25 (±0.39)	13.33 (±2.73)	12.48 (±4.23)	18.31 (±4.73)	1.17 (±0.39)	1.16 (±0.41)	1.65 (±0.55)	21.03 (±5.2)	21.94 (±7.94)	30.46 (±9.11)
P3-7	0.66	96.2	0.86 (±0.43)	0.87 (±0.47)	1.23 (±0.63)	16.52 (±4.39)	14.63 (±5.91)	22.12 (±7.11)	1.37 (±0.49)	1.46 (±0.68)	2.01 (±0.82)	26.29 (±6.23)	28.7 (±8.72)	38.99 (±10.22)
P3-8	0.78	108.2	1.08 (±0.63)	1.1 (±0.62)	1.55 (±0.87)	21.16 (±5.74)	18.92 (±7.24)	28.44 (±8.96)	1.49 (±0.53)	1.61 (±0.79)	2.21 (±0.92)	31.31 (±7.82)	32.4 (±11.2)	45.11 (±13.23)
P3-9	0.94	119.7	1.51 (±0.81)	1.59 (±0.93)	2.2 (±1.22)	27.48 (±7.82)	25.56 (±10.01)	37.64 (±12.22)	1.61 (±0.69)	1.69 (±0.74)	2.34 (±0.99)	35.66 (±10.24)	36.87 (±11.04)	51.42 (±14.36)
P3 -10	0.66	96.7	1.03 (±0.45)	1.09 (±0.62)	1.51 (±0.75)	18.61 (±6.87)	16.49 (±7.16)	24.91 (±9.72)	1.43 (±0.45)	1.51 (±0.55)	2.09 (±0.69)	29.19 (±8.05)	31.31 (±11.06)	42.86 (±13.29)
Average			1.14 (±0.49)	1.1 (±0.52)	1.59 (±0.71)	15.05 (±3.3)	12.8 (±3.67)	19.79 (±4.76)	1.25 (±0.44)	1.28 (±0.53)	1.79 (±0.68)	21.09 (±4.83)	20.93 (±6.37)	29.77 (±7.68)

where $e_{p,j}$ and $e_{v,j}$ are the errors in angular position and angular velocity, respectively, between the most representative curve in the exercise and the regenerated curve in the sample j, $\theta_{REF\,j}$ and $\dot{\theta}_{REF\,j}$ are the position and velocity values of the reference curve in the sample j, and n, $\theta_C(\{\boldsymbol{\alpha}_{t,E}, \boldsymbol{\alpha}_{\theta,E}\})_{(j)}$, $\dot{\theta}_C(\{\boldsymbol{\alpha}_{t,E}, \boldsymbol{\alpha}_{\theta,E}\})_{(j)}$ and w_v=*0.02* have the same definitions as in (25). In this method, the reference pair of gait parameters to be used by the radial-basis selection corresponds to the WS_{norm} and *cad* of each most-representative curve.

The results achieved from this method can be seen in Table 11 and Table 12. Table 11 shows the position and velocity Mean Absolute Errors (*MAE*) and the Standard Deviation of the Absolute Errors (*SDAE*) between the most representative curves in each exercise and the curves regenerated with the corresponding set of characteristic and shaping knots. It also shows the corresponding WS_{norm} and *cad* of each one of the representative curves, which are taken as the reference gait parameters' pairs of each group. Note that the representative curves for hip and knee joints for a specific exercise do not necessarily belong to the same cycle. On the other hand, Table 12 shows the AMAE, ARMSE and ASDAE calculated comparing all the original curves in each exercise and the curves that were regenerated using the characteristic points of the corresponding original curve and the shaping knots calculated using the resulting coefficients in each exercise. A visible deterioration in the error-performance in hip and knee joints can be seen which, although it might not be too big, could be considerable taking into account the range of motion of the curves dealt with in the study. In general, the regeneration yielded good looking curves, as the one presented in Fig. 55, where a hip and a knee trajectory from exercise *P2-6* are compared with the corresponding regenerated curve. In this case, the MAE and SDAE were equal to 1.78° and 1.54°, respectively, for the hip, and 1.61° and 1.67° for the knee. However, some of the regenerated curves yielded rather undesirable curves, like the one depicted in left plot of Fig. 56, which corresponds to a curve from exercise *P1-2*. The reconstruction produced a MAE of 2.9° and a SDAE of 2.68°. It is possible to compare the ill results from this method looking at the plot in the right, where the same curve was regenerated with the coefficients obtained in *Method 2*, where the MAE was 1.43° and the SDAE was 1.19°. One possible cause of this behavior is the usage of only one curve for the training when, despite the efforts, the selected curve is not very representative of some of the other curves in the group, caused probably by high differences between the trajectories in the group.

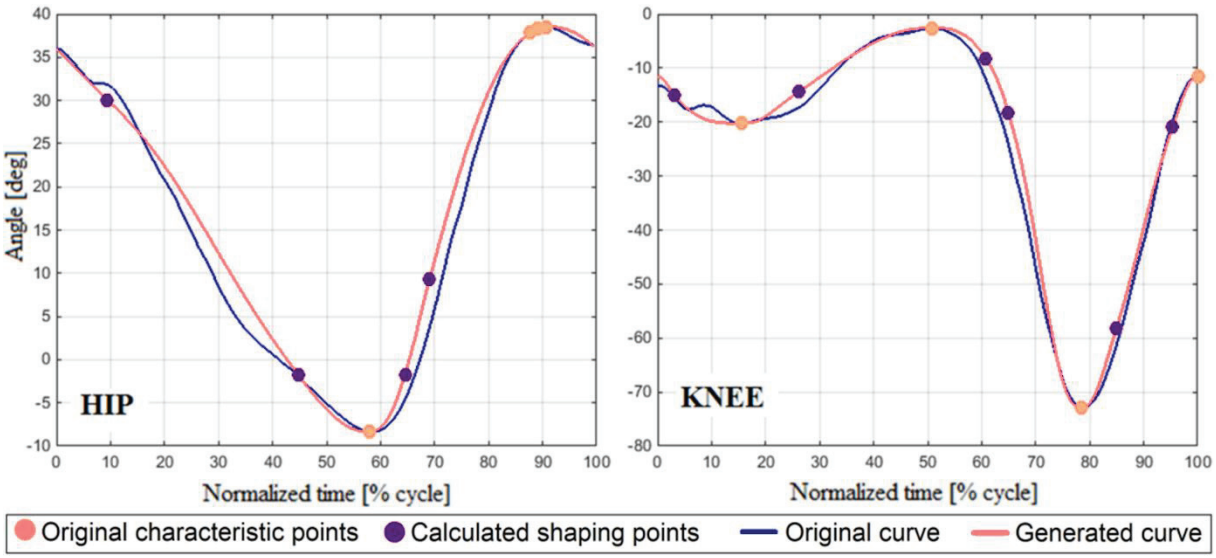

Fig. 55 Example of regenerated curves with *Method 3*

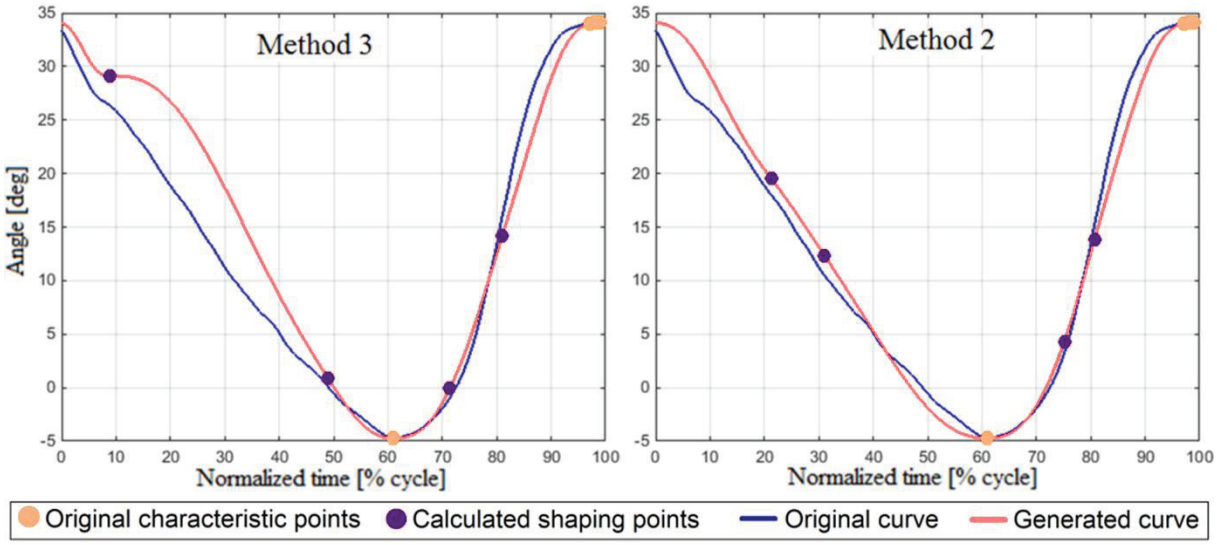

Fig. 56 Comparison of a hip curve from *P1-2* with the generated curves obtained by *Method 3* (left) and *Method 2* (right)

Table 11 Results of *Method 3* with respect to the most representative curves

MAE: Mean Absolute Error. SDAE: Standard Deviation of the Absolute Errors.

	HIP						KNEE					
Exercise	**WSnorm**	**Cad**	**MAE (pos) [deg]**	**SDAE (pos) [deg]**	**MAE (vel) [deg/s]**	**SDAE (vel) [deg/s]**	**WSnorm**	**Cad**	**MAE (pos) [deg]**	**SDAE (pos) [deg]**	**MAE (vel) [deg/s]**	**SDAE (vel) [deg/s]**
P1-1	98.68	0.70	0.47	0.51	13.60	11.98	0.70	98.68	0.33	0.29	11.65	8.95
P1-2	38.10	0.15	0.41	0.35	4.06	3.36	0.15	38.10	0.39	0.54	5.47	6.65
P1-3	73.98	0.42	0.43	0.34	9.32	8.34	0.42	73.98	0.30	0.28	10.80	11.70
P1-4	89.42	0.59	0.37	0.47	9.98	9.18	0.59	89.42	0.29	0.28	10.97	11.24
P1-5	112.99	0.91	0.45	0.61	18.14	17.81	0.91	112.99	0.28	0.24	13.81	10.91
P1-6	128.21	1.11	0.59	0.54	19.70	16.90	1.11	128.21	0.32	0.34	19.04	20.37
P1-7	93.90	0.65	0.38	0.43	10.90	9.76	0.65	93.90	0.27	0.29	12.17	13.32
P2-1	96.15	0.68	0.46	0.59	13.25	15.09	0.68	96.15	0.30	0.38	13.65	25.05
P2-2	62.08	0.25	0.27	0.29	5.52	5.44	0.25	62.08	0.38	0.56	9.36	11.41
P2-3	67.38	0.34	0.21	0.25	6.53	9.45	0.34	67.38	0.25	0.38	6.67	7.92
P2-4	78.48	0.43	0.20	0.17	6.95	5.55	0.43	78.48	0.23	0.20	9.09	8.78
P2-5	87.27	0.59	0.35	0.45	11.00	9.05	0.59	87.27	0.32	0.33	12.81	10.78
P2-6	93.97	0.72	0.39	0.43	12.00	10.72	0.72	93.97	0.30	0.34	12.43	13.36
P2-7	103.72	0.90	0.45	0.59	12.55	13.42	0.90	103.72	0.37	0.35	15.58	12.31
P2-8	109.59	1.10	0.51	0.68	15.47	17.89	1.10	109.59	0.24	0.26	14.37	12.81
P2-9	89.29	0.63	0.31	0.40	9.40	8.90	0.63	89.29	0.48	0.39	16.04	14.60
P3-1	94.04	0.65	0.46	0.58	12.11	12.29	0.65	94.04	0.29	0.36	14.73	18.43
P3-2	35.93	0.15	0.60	0.62	4.13	2.98	0.15	35.93	0.36	0.38	5.41	4.16
P3-3	51.97	0.23	0.33	0.37	4.84	4.02	0.23	51.97	0.24	0.33	4.74	4.55
P3-4	60.12	0.31	0.47	0.48	7.82	6.49	0.31	60.12	0.33	0.40	9.84	9.59
P3-5	72.55	0.42	0.25	0.21	5.95	4.59	0.42	72.55	0.29	0.33	10.27	9.99
P3-6	85.47	0.57	0.26	0.32	6.34	6.41	0.57	85.47	0.26	0.30	9.54	9.60
P3-7	96.23	0.68	0.43	0.42	13.05	12.59	0.68	96.23	0.30	0.28	13.32	15.54
P3-8	112.89	0.83	0.42	0.44	13.23	11.62	0.83	112.89	0.24	0.28	16.70	20.68
P3-9	120.12	0.87	0.46	0.46	14.30	13.59	0.87	120.12	0.30	0.29	17.86	20.21
P3-10	96.39	0.65	0.42	0.44	13.76	9.59	0.65	96.39	0.48	0.48	17.12	14.86
Average			0.40	0.44	10.53	9.89			0.31	0.34	12.06	12.61

Table 12 Results of *Method 3* with respect to all the curves in the exercise

	HIP						KNEE					
	Position			Velocity			Position			Velocity		
Exercise	**AMAE (±SD) [deg]**	**ASDAE (±SD) [deg]**	**ARMSE (±SD) [deg]**	**AMAE (±SD) [deg/s]**	**ASDAE (±SD) [deg/s]**	**ARMSE (±SD) [deg/s]**	**AMAE (±SD) [deg]**	**ASDAE (±SD) [deg]**	**ARMSE (±SD) [deg]**	**AMAE (±SD) [deg/s]**	**ASDAE (±SD) [deg/s]**	**ARMSE (±SD) [deg/s]**
P1-1	0.89 (±0.27)	0.91 (±0.31)	1.28 (±0.4)	15.37 (±2.44)	12.5 (±2.71)	19.83 (±3.39)	1.05 (±0.35)	1.04 (±0.41)	1.48 (±0.53)	21.6 (±4.63)	20.61 (±6.4)	29.87 (±7.7)
P1-2	1.8 (±0.9)	1.68 (±0.86)	2.47 (±1.23)	7.48 (±2.01)	5.83 (±1.24)	9.49 (±2.3)	1.56 (±0.61)	1.65 (±0.84)	2.28 (±1.01)	10.93 (±2.8)	11.17 (±3.63)	15.65 (±4.44)
P1-3	1.04 (±0.84)	0.96 (±0.88)	1.42 (±1.21)	10.6 (±2.47)	8.54 (±2.7)	13.63 (±3.56)	1.45 (±0.54)	1.33 (±0.5)	1.97 (±0.72)	18.63 (±4.29)	17.37 (±3.51)	25.51 (±5.19)
P1-4	0.98 (±0.35)	0.91 (±0.32)	1.34 (±0.47)	13.96 (±2.11)	11.21 (±1.83)	17.9 (±2.69)	1.18 (±0.36)	1.14 (±0.41)	1.65 (±0.53)	22.79 (±4.29)	22.84 (±5.43)	32.29 (±6.58)
P1-5	1.43 (±0.87)	1.44 (±0.85)	2.03 (±1.21)	22.72 (±5.41)	19.14 (±5.19)	29.75 (±7.22)	1.62 (±0.64)	1.71 (±0.81)	2.35 (±1.02)	32.64 (±10.36)	32.99 (±12.4)	46.5 (±15.68)
P1-6	2.2 (±0.82)	2.26 (±0.87)	3.16 (±1.17)	31.2 (±5.06)	25.12 (±4.34)	40.06 (±6.44)	1.52 (±0.52)	1.41 (±0.45)	2.08 (±0.67)	40.45 (±7.85)	35.98 (±6.98)	54.15 (±10.13)
P1-7	0.92 (±0.31)	0.84 (±0.27)	1.25 (±0.41)	14.72 (±1.7)	12.04 (±1.52)	19.01 (±2.19)	1.22 (±0.47)	1.32 (±0.62)	1.8 (±0.76)	22.65 (±5.91)	21.59 (±7.37)	31.34 (±9.13)
P2-1	1.06 (±0.4)	1.06 (±0.45)	1.5 (±0.6)	17.22 (±3.42)	15.02 (±4.92)	22.89 (±5.7)	1.44 (±0.6)	1.65 (±0.64)	2.19 (±0.84)	31.96 (±9.35)	43.1 (±11.15)	53.83 (±13.5)
P2-2	1.44 (±0.68)	1.29 (±0.6)	1.93 (±0.9)	10.47 (±2.82)	8.07 (±3.19)	13.36 (±3.71)	1.28 (±0.46)	1.28 (±0.52)	1.81 (±0.68)	14.01 (±2.67)	13.71 (±2.76)	19.63 (±3.57)
P2-3	1.67 (±0.97)	1.49 (±0.79)	2.24 (±1.24)	11.49 (±2.5)	9.78 (±2.12)	15.1 (±3.14)	1.14 (±0.61)	1.11 (±0.64)	1.59 (±0.88)	14.04 (±4.35)	12.66 (±3.92)	18.92 (±5.72)
P2-4	0.82 (±0.44)	0.71 (±0.38)	1.09 (±0.57)	10.42 (±3.38)	8.73 (±3.27)	13.59 (±4.66)	1.09 (±0.39)	0.99 (±0.31)	1.47 (±0.48)	17.14 (±3.21)	15.97 (±3.37)	23.46 (±4.33)
P2-5	0.76 (±0.19)	0.74 (±0.19)	1.06 (±0.26)	11.57 (±1.54)	9.45 (±1.35)	14.94 (±1.91)	1.17 (±0.34)	1.13 (±0.33)	1.63 (±0.46)	19.89 (±4.18)	18.85 (±3.98)	27.4 (±5.62)
P2-6	1.26 (±0.35)	1.18 (±0.38)	1.73 (±0.5)	16.86 (±3.33)	13.78 (±3.74)	21.79 (±4.85)	1.23 (±0.47)	1.19 (±0.44)	1.71 (±0.63)	24.89 (±6.46)	24.66 (±7.76)	35.1 (±9.66)
P2-7	1.56 (±0.85)	1.62 (±0.89)	2.25 (±1.22)	20.75 (±4.83)	17.85 (±4.23)	27.38 (±6.26)	1.21 (±0.29)	1.12 (±0.29)	1.65 (±0.4)	26.46 (±4.01)	25.31 (±5.37)	36.62 (±6.39)
P2-8	1.94 (±1.13)	2.03 (±1.32)	2.81 (±1.73)	24.52 (±7.06)	19.63 (±4.89)	31.44 (±8.34)	1.55 (±0.53)	1.4 (±0.5)	2.09 (±0.71)	31.7 (±7.32)	27.02 (±7.25)	41.65 (±10.09)
P2-9	0.77 (±0.29)	0.76 (±0.3)	1.08 (±0.41)	12.78 (±1.89)	10.42 (±1.49)	16.49 (±2.24)	1.3 (±0.51)	1.37 (±0.64)	1.89 (±0.8)	23.87 (±5.53)	24.66 (±6.74)	34.36 (±8.36)
P3-1	0.84 (±0.27)	0.83 (±0.22)	1.18 (±0.33)	14.42 (±1.94)	12.4 (±1.76)	19.04 (±2.25)	1.42 (±0.46)	1.43 (±0.51)	2.02 (±0.67)	26.41 (±4.14)	28.89 (±6.2)	39.24 (±6.57)
P3-2	1.66 (±0.73)	1.42 (±0.65)	2.19 (±0.96)	6.62 (±1.65)	5.38 (±1.6)	8.54 (±2.24)	1.57 (±0.5)	1.61 (±0.54)	2.25 (±0.7)	9.53 (±1.92)	8.74 (±2.17)	12.95 (±2.77)
P3-3	1.88 (±0.79)	1.49 (±0.64)	2.4 (±1)	10.64 (±2.9)	8.87 (±3.07)	13.91 (±3.97)	1.59 (±0.59)	1.64 (±0.72)	2.3 (±0.9)	13.89 (±3.83)	13.75 (±6.51)	19.62 (±7.25)
P3-4	1.79 (±0.89)	1.82 (±1.07)	2.56 (±1.38)	12.65 (±3.07)	9.98 (±2.04)	16.12 (±3.59)	1.52 (±0.55)	1.51 (±0.59)	2.15 (±0.79)	16.88 (±3.29)	15.13 (±2.8)	22.67 (±4.18)
P3-5	1.24 (±0.91)	1.1 (±0.69)	1.67 (±1.13)	11.88 (±4.19)	10.27 (±5.24)	15.73 (±6.59)	1.3 (±0.45)	1.34 (±0.63)	1.87 (±0.76)	18.5 (±4.54)	18.4 (±7.54)	26.15 (±8.5)
P3-6	1.13 (±0.4)	1.09 (±0.36)	1.58 (±0.52)	14.48 (±3.14)	13.25 (±4.07)	19.68 (±4.82)	1.25 (±0.46)	1.24 (±0.49)	1.77 (±0.66)	21.42 (±5.78)	22.12 (±9.08)	30.88 (±10.36)
P3-7	0.97 (±0.49)	0.89 (±0.56)	1.32 (±0.73)	17.26 (±4.92)	14.47 (±6)	22.58 (±7.49)	1.58 (±0.59)	1.63 (±0.65)	2.27 (±0.86)	30.19 (±7.79)	32.62 (±8.44)	44.46 (±11.18)
P3-8	1.15 (±0.62)	1.17 (±0.61)	1.64 (±0.86)	22.37 (±6.18)	20.52 (±7.72)	30.42 (±9.55)	1.55 (±0.63)	1.64 (±0.81)	2.27 (±1)	32.99 (±10.06)	34.13 (±11.74)	47.53 (±15.04)
P3-9	1.56 (±0.79)	1.64 (±0.93)	2.26 (±1.21)	27.32 (±7.89)	26.47 (±9.96)	38.12 (±12.28)	1.9 (±0.77)	1.95 (±0.75)	2.73 (±1.05)	40.77 (±9.83)	40.57 (±10.17)	57.6 (±13.43)
P3-10	1.09 (±0.41)	1.13 (±0.56)	1.57 (±0.68)	18.99 (±5.91)	16.21 (±6.4)	25.01 (±8.5)	1.51 (±0.49)	1.53 (±0.54)	2.16 (±0.71)	30.27 (±6.95)	32.18 (±10.73)	44.25 (±12.31)
Average	1.3 (±0.61)	1.25 (±0.61)	1.81 (±0.86)	15.72 (±3.61)	13.27 (±3.72)	20.61 (±5)	1.39 (±0.51)	1.4 (±0.56)	1.98 (±0.74)	23.64 (±5.59)	23.65 (±6.67)	33.52 (±8.37)

Method 4: Using the averaged curve from each cluster with the DCSA [Gr2+AvC+DCSA]

A second method feeding only one curve per group to the DCSA was developed expecting to get a better error-performance. This time, the clustering was done based on the WS_{norm} and *cad* of each processed cycle (*Gr2*), and instead of feeding the most representative curve to the algorithm, the average curve was used. Unlike the previous method, the curves fed to the search algorithm are now time-warped and normalized in angle, which means that any velocity measurements done to the fed curve are corrupted by the warping; therefore a new cost function must be introduced. The new formulation of the cost-minimization problem is

$$\arg\min_{\{\boldsymbol{\alpha}_{t,C},\boldsymbol{\alpha}_{\theta,C}\}}\left(\sum_{j=1}^{n}\left(\breve{\theta}_{REF_j}-\theta_C\left(\{\boldsymbol{\alpha}_{t,C},\boldsymbol{\alpha}_{\theta,C}\}\right)_j\right)^2\right) \tag{28}$$

where $n = 100$ is the number of samples per curve, $\breve{\theta}_{REF_j}$ is the (normalized) angle value of the average time-warped curve from cluster *C* in the sample j, and $\theta_C(\{\boldsymbol{\alpha}_{t,C},\boldsymbol{\alpha}_{\theta,C}\})$ is angle value calculated from the interpolation using the shaping knots described by a given set of $\{\alpha_{t,C},\alpha_{\theta,C}\}$, specific to cluster *C*. Similarly as in *Method 2*, because all the curves from the cluster are used for the obtainment of the average curve, the average normalized speed and average cadence of each cluster were selected as the reference pairs to be used by the radial-basis selection process during the input gait parameters mapping.

The results accomplished by this method can be seen in Table 13 and Table 14. Table 13 shows the normalized-position Mean Absolute Errors (*MAE*), the Standard Deviation of the Absolute Errors (*SDAE*), and the Root Mean Squared Error (*RMSE*) between the average curves in each cluster and the curves regenerated with the corresponding set of characteristic and shaping knots. It also shows the WS_{norm} and *cad* corresponding to the centroids of each cluster. Note that the error measurements are not measured neither in degrees nor Radians, but in normalized ranges of motion (*RoM* = 1). On the other hand, Table 14 shows the AMAE, ARMSE and AR calculated between all the original curves in each cluster and the curves that were regenerated using the characteristic points of the corresponding original curve and the shaping knots calculated using the resulting coefficients in each cluster. Comparing these results with the ones from the previous method (shown in Table 12) no visible improvement can be seen: this method brings a small improvement in the knee joint errors, but deterioration in similar magnitude in the hip joint. Apparently, some problems regarding the usage of only one curve appeared in this method, similar to the one explained in *Method 3*. An example of the generally good behavior of the regeneration is shown in Fig. 57, where the original hip and knee curves were selected from cluster 24. The hip trajectory reconstruction yielded a MAE and SDAE of 2.09° and 2.07°, respectively, whereas the knee trajectory yielded 1.74° and 1.5°. Note how the hip trajectory has a healthy-like form even if the MAE is relatively high. Fig. 58 shows an example of a possibly-undesired regeneration of a hip trajectory using this method. The original curve was taken from cluster 4, and the reconstruction yielded a MAE and SDAE of 1.8° and 1.7°, respectively. Notice how the MAE error in this generated curve is lower than the one from the curve in Fig. 57, and yet the shape of the latter is relatively closer to the original. The reason of this behavior is that normally the ranges of motion of the joint movements increase with the speed, causing higher errors in higher speeds (Cluster 4 has a lower walking speed than cluster 24).

Table 13 Results of *Method 4* with respect to the (normalized and time-warped) average curves of each cluster

			HIP			KNEE		
Cluster	**WSnorm**	**Cad**	**MAE (norm pos) [RoM]**	**SDAE (norm pos) [RoM]**	**RMSE (norm pos) [RoM]**	**MAE (norm pos) [RoM]**	**SDAE (norm pos) [RoM]**	**RMSE (norm pos) [RoM]**
1	0.16	37.75	0.0083	0.0089	0.0121	0.0031	0.0032	0.0045
2	0.21	48.32	0.0074	0.0072	0.0103	0.0041	0.0042	0.0058
3	0.25	63.73	0.0047	0.0043	0.0064	0.0041	0.0049	0.0064
4	0.32	59.81	0.0059	0.0043	0.0073	0.0042	0.0043	0.0060
5	0.32	65.29	0.0054	0.0058	0.0079	0.0038	0.0036	0.0052
6	0.33	69.66	0.0056	0.0061	0.0082	0.0037	0.0042	0.0056
7	0.41	71.65	0.0043	0.0035	0.0055	0.0039	0.0044	0.0058
8	0.44	76.89	0.0045	0.0038	0.0059	0.0033	0.0027	0.0043
9	0.43	72.83	0.0042	0.0044	0.0060	0.0041	0.0066	0.0077
10	0.46	79.41	0.0041	0.0043	0.0060	0.0042	0.0041	0.0058
11	0.54	82.46	0.0056	0.0072	0.0091	0.0033	0.0031	0.0045
12	0.58	88.08	0.0072	0.0071	0.0100	0.0040	0.0036	0.0053
13	0.63	92.28	0.0064	0.0076	0.0099	0.0041	0.0031	0.0051
14	0.64	96.41	0.0066	0.0068	0.0095	0.0035	0.0027	0.0045
15	0.67	93.33	0.0066	0.0086	0.0108	0.0033	0.0032	0.0046
16	0.68	97.20	0.0076	0.0069	0.0102	0.0045	0.0032	0.0055
17	0.72	94.87	0.0071	0.0095	0.0119	0.0035	0.0034	0.0049
18	0.73	103.05	0.0077	0.0086	0.0115	0.0035	0.0031	0.0047
19	0.78	107.61	0.0074	0.0080	0.0109	0.0038	0.0029	0.0048
20	0.89	102.79	0.0066	0.0060	0.0089	0.0045	0.0044	0.0063
21	0.82	109.88	0.0086	0.0094	0.0127	0.0035	0.0036	0.0051
22	0.90	111.33	0.0061	0.0061	0.0086	0.0038	0.0043	0.0057
23	0.92	117.65	0.0082	0.0086	0.0119	0.0031	0.0026	0.0040
24	1.03	109.04	0.0069	0.0058	0.0090	0.0035	0.0032	0.0047
25	0.97	120.49	0.0075	0.0086	0.0114	0.0030	0.0027	0.0041
26	1.08	110.98	0.0061	0.0059	0.0084	0.0042	0.0032	0.0053
27	1.11	128.61	0.0062	0.0047	0.0078	0.0027	0.0025	0.0036
28	1.18	129.53	0.0078	0.0075	0.0108	0.0031	0.0033	0.0045
Average			0.0064	0.0066	0.0093	0.0037	0.0036	0.0052

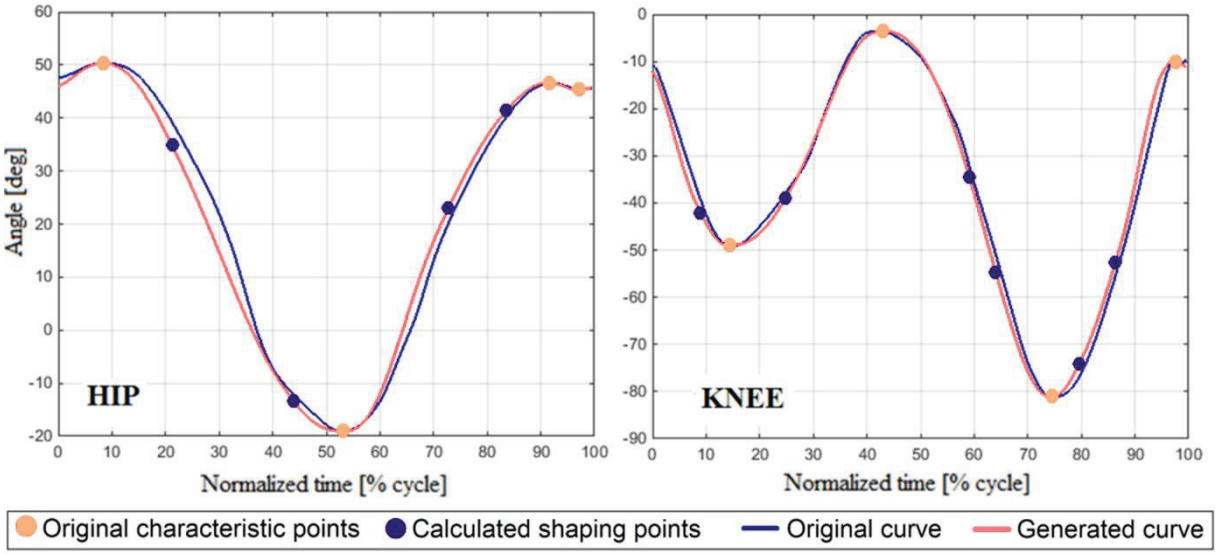

Fig. 57 Example of regenerated curves with *Method 4*

Table 14 Results of *Method 4* with respect to all the curves in the cluster

	HIP						KNEE					
	Position			Velocity			Position			Velocity		
Cluster	AMAE (±SD) [deg]	ASDAE (±SD) [deg]	ARMSE (±SD) [deg]	AMAE (±SD) [deg/s]	ASDAE (±SD) [deg/s]	ARMSE (±SD) [deg/s]	AMAE (±SD) [deg]	ASDAE (±SD) [deg]	ARMSE (±SD) [deg]	AMAE (±SD) [deg/s]	ASDAE (±SD) [deg/s]	ARMSE (±SD) [deg/s]
1	2.31 (±0.57)	2.15 (±0.64)	3.16 (±0.84)	9.81 (±1.5)	7.65 (±1.04)	12.44 (±1.69)	1.59 (±0.47)	1.63 (±0.59)	2.28 (±0.72)	10.09 (±2.08)	9.53 (±2.79)	13.89 (±3.34)
2	1.96 (±0.92)	1.73 (±0.75)	2.62 (±1.16)	11.22 (±3.38)	9.59 (±2.77)	14.81 (±4.13)	1.45 (±0.54)	1.5 (±0.68)	2.1 (±0.84)	13.15 (±3.91)	13.3 (±6.74)	18.79 (±7.49)
3	1.78 (±0.71)	1.62 (±0.68)	2.41 (±0.97)	11.11 (±2.89)	9.1 (±3.13)	14.47 (±3.77)	1.09 (±0.42)	1.13 (±0.49)	1.57 (±0.64)	12.64 (±2.17)	12.15 (±2.72)	17.54 (±3.29)
4	2.29 (±0.6)	2.16 (±0.7)	3.16 (±0.9)	14.3 (±2.54)	10.24 (±1.62)	17.58 (±2.96)	1.46 (±0.56)	1.53 (±0.62)	2.12 (±0.82)	15.7 (±3.01)	14.43 (±2.74)	21.32 (±3.92)
5	1.76 (±0.54)	1.56 (±0.63)	2.36 (±0.81)	12.04 (±2.14)	9.41 (±1.73)	15.28 (±2.64)	1.11 (±0.58)	1.08 (±0.62)	1.55 (±0.85)	13.38 (±3.54)	11.55 (±3.33)	17.68 (±4.79)
6	1.36 (±0.37)	1.21 (±0.36)	1.82 (±0.5)	10.83 (±1.89)	8.47 (±1.57)	13.74 (±2.43)	1.02 (±0.46)	1.08 (±0.59)	1.49 (±0.74)	13.52 (±3.01)	12.92 (±3.18)	18.69 (±4.3)
7	1.05 (±0.49)	0.99 (±0.56)	1.45 (±0.74)	11.07 (±3.19)	9.33 (±4.04)	14.52 (±4.98)	1.22 (±0.37)	1.3 (±0.42)	1.78 (±0.55)	16.72 (±4.12)	16.61 (±5.21)	23.57 (±6.49)
8	0.9 (±0.31)	0.82 (±0.23)	1.22 (±0.37)	10.18 (±2.19)	8.11 (±1.81)	13.01 (±2.8)	0.9 (±0.27)	0.87 (±0.25)	1.25 (±0.36)	14.12 (±1.83)	12.73 (±1.96)	19.01 (±2.47)
9	1.01 (±0.27)	0.95 (±0.23)	1.38 (±0.35)	12.05 (±2.6)	10.56 (±3.73)	16.04 (±4.38)	1.09 (±0.54)	1.15 (±0.85)	1.59 (±0.99)	15.1 (±4.41)	15.24 (±9.2)	21.6 (±9.77)
10	0.74 (±0.22)	0.69 (±0.27)	1.02 (±0.34)	10.3 (±1.22)	8.16 (±1.02)	13.13 (±1.47)	1.03 (±0.26)	0.98 (±0.29)	1.42 (±0.37)	16.36 (±2.03)	15.17 (±2.65)	22.3 (±3.21)
11	0.88 (±0.31)	0.88 (±0.31)	1.24 (±0.42)	12.54 (±3.1)	11.45 (±4.26)	17.02 (±5.06)	1.2 (±0.4)	1.12 (±0.33)	1.65 (±0.5)	19.85 (±5.04)	19.81 (±6.92)	28.11 (±8.21)
12	0.93 (±0.32)	0.9 (±0.32)	1.3 (±0.44)	13.7 (±1.88)	10.87 (±2.09)	17.5 (±2.61)	1.11 (±0.37)	1.13 (±0.41)	1.59 (±0.54)	21.01 (±4.61)	22.21 (±6.7)	30.62 (±7.78)
13	0.9 (±0.28)	0.88 (±0.31)	1.26 (±0.41)	14.74 (±2.57)	12.31 (±3.7)	19.24 (±4.29)	1.24 (±0.46)	1.29 (±0.58)	1.79 (±0.72)	23.42 (±6.24)	24.53 (±8.98)	33.97 (±10.59)
14	0.97 (±0.4)	0.98 (±0.43)	1.38 (±0.58)	16.27 (±4.1)	13.46 (±4.88)	21.13 (±6.25)	1.12 (±0.34)	1.17 (±0.46)	1.63 (±0.56)	24.61 (±5.46)	27.19 (±9.99)	36.76 (±10.89)
15	0.88 (±0.28)	0.92 (±0.3)	1.27 (±0.4)	15.15 (±3.95)	13.32 (±4.78)	20.2 (±6.03)	1.34 (±0.51)	1.41 (±0.55)	1.95 (±0.74)	25.73 (±6.5)	27.74 (±8.11)	37.84 (±10.16)
16	0.89 (±0.27)	0.86 (±0.31)	1.24 (±0.4)	16.93 (±2.79)	13.98 (±4.42)	22.02 (±4.87)	1.26 (±0.42)	1.25 (±0.44)	1.77 (±0.6)	26.51 (±5.43)	28.42 (±8.56)	38.97 (±9.49)
17	1.18 (±0.25)	1.16 (±0.27)	1.65 (±0.36)	17.44 (±3.33)	14.6 (±3.06)	22.75 (±4.34)	1.21 (±0.47)	1.18 (±0.46)	1.69 (±0.65)	24.12 (±5.93)	23.7 (±6.34)	33.84 (±8.41)
18	1.19 (±0.48)	1.31 (±0.65)	1.77 (±0.79)	23.19 (±7.53)	19.93 (±6.59)	30.59 (±9.84)	1.37 (±0.46)	1.46 (±0.63)	2.02 (±0.73)	32 (±8.95)	35.47 (±12.59)	47.91 (±14.72)
19	1.19 (±0.71)	1.21 (±0.66)	1.7 (±0.97)	22.64 (±5.53)	20.16 (±6.49)	30.34 (±8.31)	1.6 (±0.55)	1.68 (±0.87)	2.33 (±0.99)	33.61 (±8.03)	34.52 (±10.83)	48.2 (±13.13)
20	1.54 (±0.85)	1.58 (±0.92)	2.21 (±1.24)	20.66 (±4.61)	16.79 (±4.14)	26.65 (±5.94)	1.1 (±0.3)	1.07 (±0.33)	1.53 (±0.44)	25.11 (±3.63)	25.33 (±5.98)	35.73 (±6.42)
21	0.93 (±0.2)	0.93 (±0.21)	1.31 (±0.28)	22.29 (±5.37)	20.87 (±8.09)	30.62 (±9.24)	1.62 (±0.59)	1.61 (±0.73)	2.29 (±0.93)	35.44 (±7.05)	39.66 (±9.27)	53.17 (±11.32)
22	1.07 (±0.16)	1.09 (±0.25)	1.53 (±0.29)	22.24 (±2.79)	19.37 (±4.4)	29.56 (±4.54)	1.63 (±0.55)	1.83 (±0.63)	2.45 (±0.84)	33.47 (±6.58)	39.17 (±7.48)	51.49 (±9.7)
23	1.67 (±0.91)	1.77 (±1.03)	2.43 (±1.37)	26.32 (±6.38)	23.48 (±7.99)	35.29 (±9.97)	1.58 (±0.66)	1.61 (±0.72)	2.25 (±0.96)	33.92 (±11.09)	33.48 (±11.4)	47.75 (±15.41)
24	2.03 (±0.99)	2.06 (±1.06)	2.89 (±1.44)	24.8 (±5.07)	20.56 (±3.61)	32.2 (±6.09)	1.2 (±0.35)	1.15 (±0.36)	1.66 (±0.49)	26.92 (±5.7)	24.06 (±6.53)	36.14 (±8.34)
25	1.23 (±0.37)	1.31 (±0.47)	1.79 (±0.58)	26.9 (±5.74)	25.02 (±9.25)	36.85 (±10.3)	1.54 (±0.43)	1.53 (±0.4)	2.18 (±0.56)	33.52 (±8.78)	35.25 (±12.11)	48.81 (±14.13)
26	1.27 (±0.52)	1.24 (±0.57)	1.78 (±0.76)	22.73 (±3.24)	17.77 (±2.49)	28.87 (±3.7)	1.68 (±0.36)	1.52 (±0.52)	2.28 (±0.59)	33.91 (±6.2)	35.64 (±8.95)	49.2 (±10.5)
27	2.09 (±0.43)	1.97 (±0.66)	2.88 (±0.71)	26.87 (±6.2)	22.49 (±6.1)	35.02 (±8.58)	1.44 (±0.42)	1.24 (±0.4)	1.91 (±0.56)	32.63 (±6.38)	29.5 (±7.55)	44 (±9.54)
28	1.7 (±1.03)	1.73 (±1.24)	2.43 (±1.61)	28.45 (±5.6)	22.69 (±5.29)	36.38 (±7.6)	1.1 (±0.28)	0.92 (±0.28)	1.44 (±0.38)	28.25 (±3.21)	25.48 (±3.27)	38.08 (±3.77)
Average	1.35 (±0.49)	1.31 (±0.54)	1.88 (±0.72)	17.38 (±3.69)	14.63 (±4.08)	22.76 (±5.31)	1.3 (±0.44)	1.3 (±0.52)	1.84 (±0.67)	23.39 (±5.17)	23.74 (±6.86)	33.39 (±8.27)

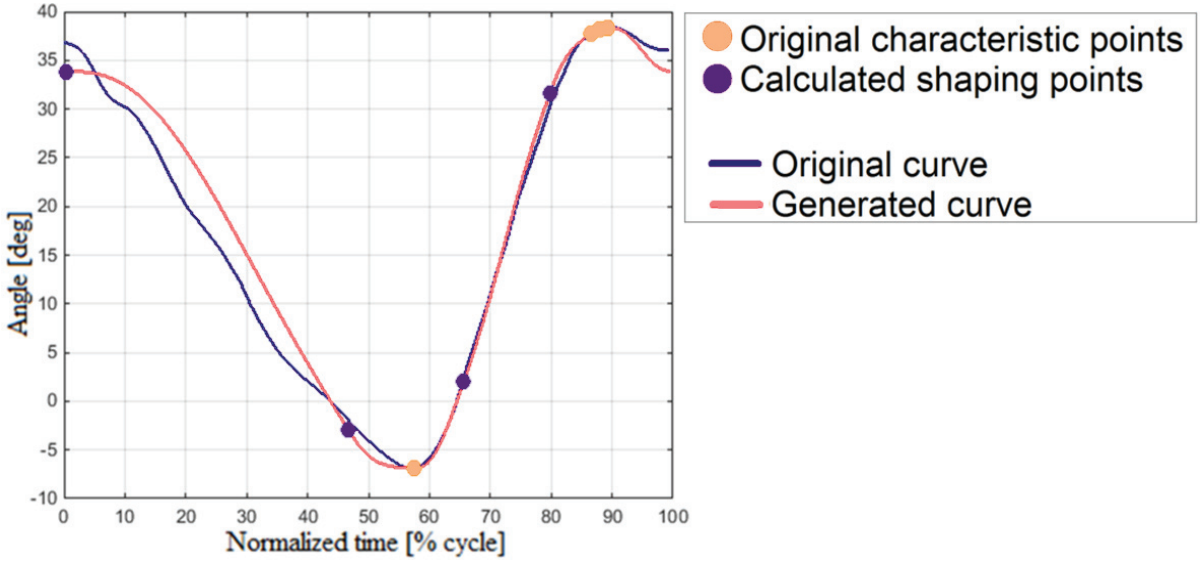

Fig. 58 Example of a possibly undesired generation of hip trajectory with *Method 4*

Method 5: Using the averaged curve from each cluster with the PRSA [Gr2+AvC+PRSA]

This method has the same settings as the previous one, except for the search algorithm. In this case, the PRSA was used in order to check its capabilities in both time- and error-performance. The results from this method are available in Table 15 and Table 16, and are comparable to the ones from *Method 4* shown in Table 13 and Table 14. Again, no significant changes in the error-performance can be noted (only a slight deterioration in the knee joint). Nevertheless, a considerable reduction in the processing time was achieved. An example of the generally good behavior of the regeneration is shown in Fig. 59, where the original hip and knee curves were selected from cluster 20. The hip trajectory reconstruction yielded a MAE and SDAE of 1.59° and 1.48°, respectively, whereas the knee trajectory yielded 0.98° and 1.03°. Fig. 60 shows the reconstruction of the same curve from cluster 4 showed in Fig. 58. Note how the undesired shape persists with this method, although the MAE and SDAE scored relatively low (1.49° and 1.41°, respectively).

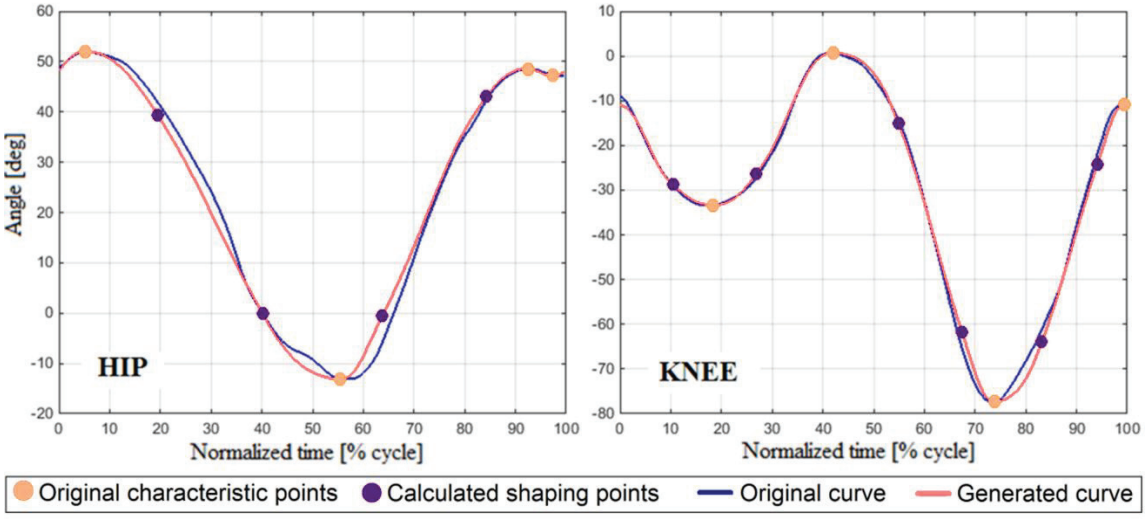

Fig. 59 Example of regenerated curves with *Method 5*

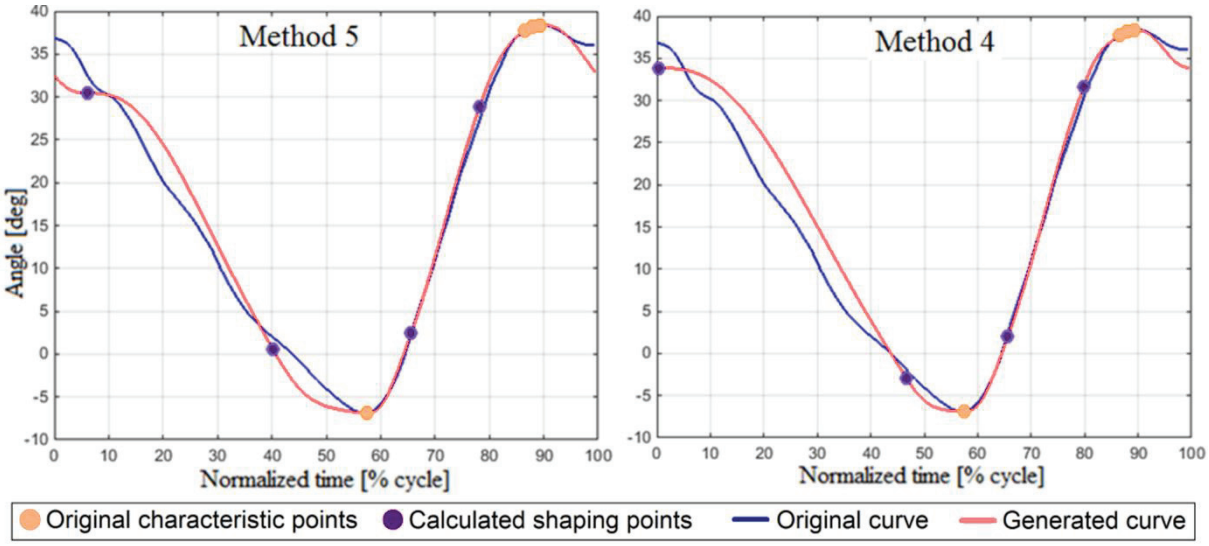

Fig. 60 Example of a possibly undesired generation of hip trajectory with *Method 5* (left) and *Method 4* (right)

Table 15 **Results of *Method 5* with respect to the (normalized and time-warped) average curves of each cluster**

			HIP			KNEE		
Cluster	**WSnorm**	**Cad**	**MAE (norm pos) [RoM]**	**SDAE (norm pos) [RoM]**	**RMSE (norm pos) [RoM]**	**MAE (norm pos) [RoM]**	**SDAE (norm pos) [RoM]**	**RMSE (norm pos) [RoM]**
1	0.16	37.75	0.009	0.008	0.012	0.006	0.010	0.012
2	0.21	48.32	0.010	0.008	0.013	0.010	0.009	0.013
3	0.25	63.73	0.006	0.005	0.008	0.007	0.006	0.009
4	0.32	59.81	0.008	0.007	0.011	0.007	0.006	0.009
5	0.32	65.29	0.007	0.006	0.009	0.007	0.007	0.010
6	0.33	69.66	0.007	0.006	0.009	0.006	0.005	0.008
7	0.41	71.65	0.007	0.004	0.008	0.007	0.007	0.010
8	0.44	76.89	0.008	0.005	0.009	0.007	0.006	0.009
9	0.43	72.83	0.007	0.007	0.010	0.006	0.005	0.008
10	0.46	79.41	0.006	0.006	0.009	0.006	0.006	0.008
11	0.54	82.46	0.008	0.007	0.011	0.007	0.008	0.011
12	0.58	88.08	0.009	0.010	0.013	0.009	0.009	0.012
13	0.63	92.28	0.010	0.011	0.015	0.009	0.009	0.012
14	0.64	96.41	0.011	0.012	0.016	0.011	0.009	0.015
15	0.67	93.33	0.011	0.011	0.016	0.010	0.009	0.013
16	0.68	97.20	0.011	0.011	0.015	0.009	0.008	0.012
17	0.72	94.87	0.012	0.012	0.017	0.010	0.009	0.013
18	0.73	103.05	0.011	0.010	0.015	0.011	0.010	0.015
19	0.78	107.61	0.012	0.010	0.015	0.008	0.007	0.011
20	0.89	102.79	0.011	0.011	0.016	0.013	0.010	0.017
21	0.82	109.88	0.011	0.011	0.015	0.008	0.008	0.011
22	0.90	111.33	0.011	0.010	0.014	0.012	0.009	0.015
23	0.92	117.65	0.012	0.009	0.014	0.009	0.008	0.012
24	1.03	109.04	0.008	0.008	0.011	0.010	0.007	0.013
25	0.97	120.49	0.011	0.011	0.015	0.010	0.008	0.013
26	1.08	110.98	0.010	0.008	0.013	0.011	0.008	0.014
27	1.11	128.61	0.007	0.005	0.009	0.009	0.007	0.012
28	1.18	129.53	0.008	0.006	0.011	0.011	0.009	0.014
Average			0.009	0.008	0.013	0.009	0.008	0.012

Table 16 Results of *Method 5* with respect to all the curves in the cluster

	HIP						KNEE					
	Position			Velocity			Position			Velocity		
Cluster	AMAE (±SD) [deg]	ASDAE (±SD) [deg]	ARMSE (±SD) [deg]	AMAE (±SD) [deg/s]	ASDAE (±SD) [deg/s]	ARMSE (±SD) [deg/s]	AMAE (±SD) [deg]	ASDAE (±SD) [deg]	ARMSE (±SD) [deg]	AMAE (±SD) [deg/s]	ASDAE (±SD) [deg/s]	ARMSE (±SD) [deg/s]
1	2.19 (±0.53)	2.03 (±0.61)	2.99 (±0.78)	9.83 (±1.46)	7.61 (±1)	12.43 (±1.65)	1.69 (±0.5)	1.63 (±0.56)	2.35 (±0.72)	11.07 (±2)	11.2 (±2.32)	15.75 (±2.92)
2	2.36 (±0.56)	2.03 (±0.49)	3.11 (±0.72)	13.46 (±2.21)	10.1 (±2)	16.85 (±2.78)	1.58 (±0.54)	1.6 (±0.7)	2.26 (±0.84)	14.51 (±3.86)	14.65 (±6.75)	20.7 (±7.45)
3	1.59 (±0.62)	1.43 (±0.58)	2.14 (±0.83)	11.7 (±3.18)	9.4 (±3.19)	15.12 (±4.01)	1.12 (±0.39)	1.16 (±0.49)	1.61 (±0.62)	13.17 (±2.5)	11.89 (±3.01)	17.78 (±3.63)
4	2.01 (±0.46)	1.79 (±0.63)	2.69 (±0.74)	15.45 (±2.35)	11.45 (±1.95)	19.23 (±2.96)	1.49 (±0.47)	1.54 (±0.65)	2.15 (±0.78)	15.94 (±2.99)	14.75 (±2.96)	21.72 (±4.05)
5	1.6 (±0.41)	1.44 (±0.41)	2.15 (±0.55)	12.35 (±2.38)	9.93 (±2.13)	15.84 (±3.12)	1.21 (±0.55)	1.09 (±0.64)	1.63 (±0.83)	14.81 (±3.48)	12.62 (±3.86)	19.48 (±5)
6	1.25 (±0.26)	1.11 (±0.26)	1.67 (±0.36)	10.75 (±1.68)	8.42 (±1.42)	13.65 (±2.16)	1.07 (±0.46)	1.06 (±0.57)	1.51 (±0.72)	13.96 (±3.04)	12.66 (±2.95)	18.85 (±4.1)
7	1.18 (±0.77)	1.02 (±0.61)	1.57 (±0.97)	11.73 (±3.77)	9.87 (±4.03)	15.34 (±5.42)	1.28 (±0.38)	1.3 (±0.45)	1.83 (±0.57)	16.84 (±4.16)	16.6 (±5.7)	23.67 (±6.87)
8	0.88 (±0.38)	0.82 (±0.29)	1.2 (±0.46)	11.01 (±3.5)	9.13 (±2.68)	14.3 (±4.36)	0.99 (±0.3)	0.86 (±0.28)	1.32 (±0.4)	15.42 (±2.26)	13.44 (±2.52)	20.46 (±3.21)
9	0.98 (±0.31)	0.87 (±0.3)	1.31 (±0.43)	11.84 (±2.56)	10.84 (±4.12)	16.09 (±4.63)	1.12 (±0.49)	1.16 (±0.78)	1.62 (±0.9)	16.1 (±4.11)	15.46 (±7.16)	22.4 (±7.92)
10	0.72 (±0.19)	0.67 (±0.24)	0.98 (±0.3)	10.26 (±1)	8.35 (±0.87)	13.22 (±1.21)	1.07 (±0.27)	0.99 (±0.29)	1.46 (±0.39)	17.07 (±2.39)	15.57 (±2.99)	23.13 (±3.52)
11	0.83 (±0.27)	0.85 (±0.27)	1.19 (±0.37)	13.14 (±3.12)	12.4 (±4.55)	18.11 (±5.3)	1.3 (±0.43)	1.13 (±0.31)	1.73 (±0.5)	21.18 (±4.78)	20.36 (±7.66)	29.47 (±8.57)
12	0.89 (±0.28)	0.87 (±0.27)	1.24 (±0.38)	13.85 (±2)	11.72 (±2.23)	18.14 (±2.84)	1.25 (±0.36)	1.19 (±0.39)	1.73 (±0.52)	23.44 (±4.32)	21.74 (±5.4)	31.97 (±6.68)
13	0.93 (±0.29)	0.89 (±0.31)	1.29 (±0.42)	15.46 (±2.78)	13.27 (±3.61)	20.39 (±4.35)	1.36 (±0.45)	1.36 (±0.55)	1.93 (±0.69)	26.17 (±6.06)	25.22 (±7.76)	36.38 (±9.53)
14	1.03 (±0.43)	1.02 (±0.44)	1.45 (±0.61)	17.26 (±4.43)	14.65 (±4.96)	22.65 (±6.51)	1.29 (±0.3)	1.27 (±0.47)	1.82 (±0.52)	29.24 (±4.24)	30.11 (±8.76)	42.05 (±9.11)
15	0.92 (±0.31)	0.96 (±0.36)	1.33 (±0.46)	16.49 (±4.37)	14.56 (±5.43)	22.01 (±6.82)	1.48 (±0.49)	1.45 (±0.54)	2.08 (±0.71)	28.87 (±6.78)	29.37 (±8.3)	41.23 (±10.3)
16	0.93 (±0.28)	0.91 (±0.27)	1.3 (±0.38)	17.42 (±2.92)	14.91 (±4.21)	22.96 (±4.83)	1.36 (±0.41)	1.29 (±0.41)	1.88 (±0.56)	28.05 (±4.75)	27.96 (±6.37)	39.64 (±7.5)
17	1.19 (±0.27)	1.2 (±0.29)	1.69 (±0.38)	18.89 (±3.48)	15.96 (±2.94)	24.74 (±4.34)	1.36 (±0.49)	1.26 (±0.39)	1.86 (±0.61)	26.99 (±6.1)	25.17 (±6.22)	36.92 (±8.43)
18	1.24 (±0.45)	1.32 (±0.65)	1.81 (±0.78)	23.62 (±6.86)	19.75 (±6.39)	30.8 (±9.19)	1.47 (±0.45)	1.48 (±0.67)	2.11 (±0.75)	35.01 (±9.25)	37.47 (±15.17)	51.4 (±17.12)
19	1.2 (±0.68)	1.25 (±0.67)	1.73 (±0.94)	23.25 (±6.22)	20.57 (±6.85)	31.06 (±9.05)	1.64 (±0.55)	1.7 (±0.88)	2.38 (±1)	35.25 (±9.08)	34.76 (±11.15)	49.54 (±14)
20	1.6 (±0.76)	1.71 (±0.86)	2.34 (±1.14)	23 (±4.45)	20.75 (±3.67)	30.98 (±5.59)	1.2 (±0.3)	1.21 (±0.29)	1.71 (±0.4)	30.31 (±3.82)	29.35 (±4.38)	42.21 (±5.21)
21	0.97 (±0.22)	0.99 (±0.36)	1.38 (±0.41)	23.13 (±5.81)	21.03 (±7.78)	31.28 (±9.49)	1.71 (±0.61)	1.64 (±0.72)	2.37 (±0.93)	38.22 (±5.92)	39.36 (±7.18)	54.87 (±8.73)
22	1.07 (±0.22)	1.11 (±0.29)	1.54 (±0.34)	22.33 (±3.53)	20.17 (±5.12)	30.14 (±5.7)	1.72 (±0.52)	1.81 (±0.62)	2.49 (±0.8)	37.68 (±4.52)	39.4 (±8.6)	54.59 (±8.74)
23	1.64 (±0.86)	1.72 (±0.98)	2.38 (±1.3)	26.94 (±7.07)	22.86 (±7.84)	35.36 (±10.28)	1.6 (±0.65)	1.63 (±0.74)	2.29 (±0.96)	35.4 (±10.1)	35.02 (±13)	49.95 (±15.75)
24	2.05 (±1)	2.09 (±1.06)	2.93 (±1.45)	25.71 (±5.39)	21.67 (±3.52)	33.63 (±6.23)	1.28 (±0.33)	1.16 (±0.31)	1.72 (±0.44)	29.33 (±5.03)	25.78 (±4.25)	39.06 (±6.27)
25	1.24 (±0.3)	1.35 (±0.38)	1.83 (±0.48)	27.72 (±5.58)	25.91 (±8.68)	38.02 (±9.82)	1.6 (±0.38)	1.6 (±0.37)	2.26 (±0.51)	38.63 (±6.6)	38.99 (±7.13)	54.93 (±8.97)
26	1.27 (±0.52)	1.26 (±0.57)	1.78 (±0.76)	22.34 (±3.29)	17.8 (±2.47)	28.57 (±3.77)	1.61 (±0.27)	1.45 (±0.38)	2.17 (±0.43)	35.08 (±5.69)	32.63 (±10.13)	48.06 (±10.59)
27	2.06 (±0.42)	1.99 (±0.7)	2.87 (±0.74)	28.28 (±6.43)	23.18 (±6.52)	36.55 (±9.03)	1.46 (±0.4)	1.38 (±0.39)	2 (±0.55)	37.21 (±4.68)	34.85 (±7.27)	51.03 (±7.94)
28	1.71 (±0.98)	1.76 (±1.18)	2.46 (±1.52)	29.83 (±5.35)	23.55 (±5.18)	38.02 (±7.13)	1.19 (±0.22)	1.03 (±0.26)	1.58 (±0.33)	35.17 (±2.4)	30.02 (±4.29)	46.25 (±4.16)
Average	1.34 (±0.47)	1.3 (±0.51)	1.87 (±0.68)	18.11 (±3.83)	15.35 (±4.12)	23.77 (±5.45)	1.38 (±0.43)	1.34 (±0.5)	1.92 (±0.64)	25.72 (±4.82)	24.87 (±6.54)	35.84 (±7.72)

Method 6: Using all the curves from the exercise with the PRSA [Gr1+All+PRSA]

Because of the good time-related results achieved with the PRSA in *Method 5,* it was decided to run the algorithm feeding it with all the curves after they were grouped by exercise (*Gr1*). In other words, the settings of this method are the same as the ones from *Method 2* with the difference of the search algorithm. The results from this method are shown in Table 17. Comparing these results with the ones in Table 10, it can be seen that the performance of the DCSA is slightly better than the one from the PRSA, although the improvement in processing time accomplished with the PRSA is significantly higher than the worsening in the results. An example of the generation using the resulting shaping-knots' coefficients is depicted in Fig. 61, where the position and velocity of the most representative curve from exercise P3-2 are compared to the ones from the reconstructed one, as it was done for *Method 2*. Likewise, Fig. 62 shows the regeneration of the curve from exercise P1-2 previously depicted in Fig. 56, using *Method 6*, *Method 2* and *Method 3*. In the case of *Method 6* the MAE and SDAE were 2.35° and 2.01°, respectively. In both Fig. 61 and Fig. 62 a small deterioration in the shape produced by this method can be seen compared to *Method 2.*

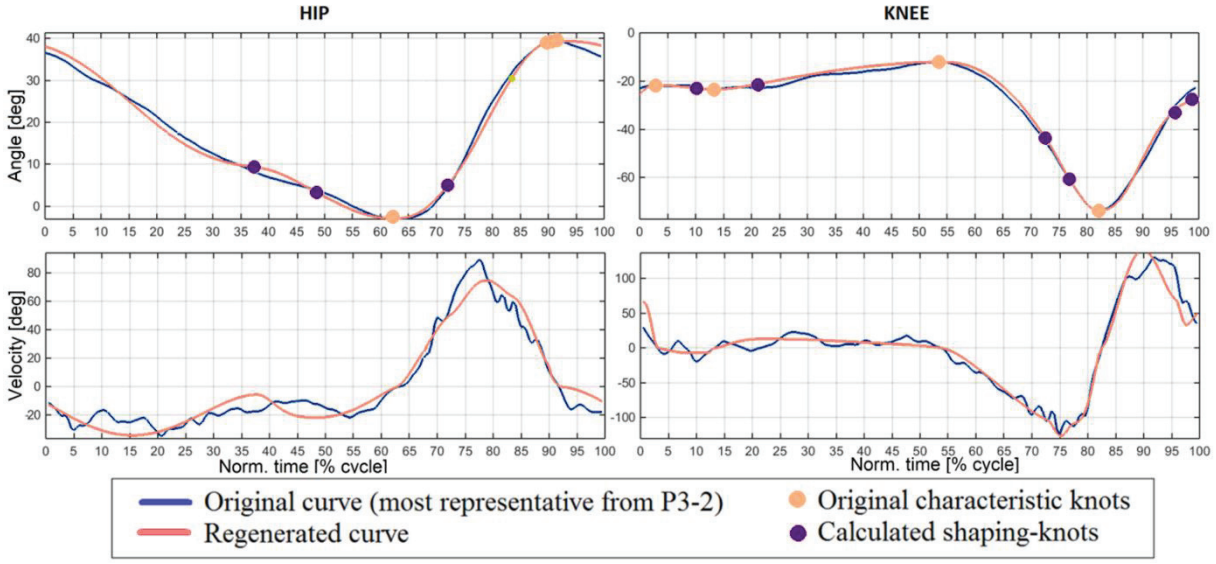

Fig. 61 Original curve (most representative from exercise P3-2) vs regenerated curve using the calculated shaping-knots coefficients

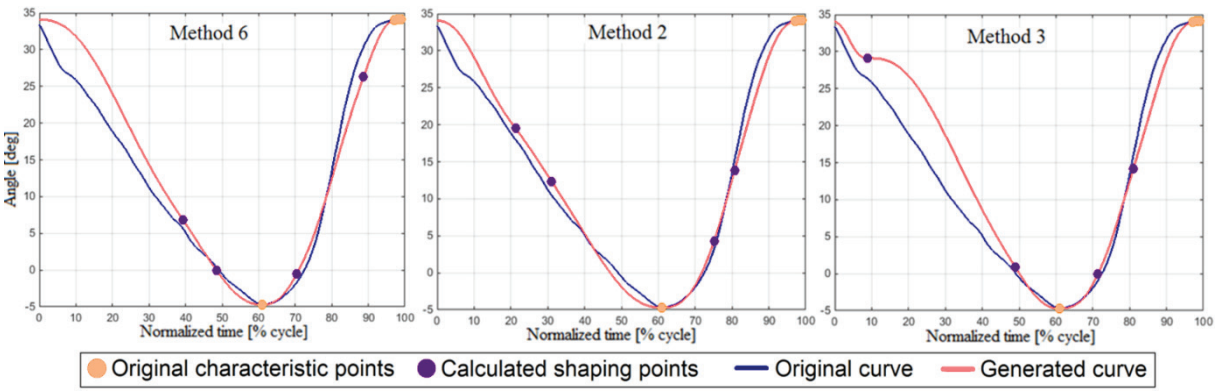

Fig. 62 Comparison of a curve from *P1-2* with the generated curves obtained by *Method 6 (left), Method 2* (center) and *Method 3* (right)

Table 17 Results of *Method 6* with respect to all the curves in the exercise

			HIP						KNEE					
			Position			Velocity			Position			Velocity		
Ex.	**WS norm**	**Cad**	**AMAE (±SD) [deg]**	**ASDAE (±SD) [deg]**	**ARMSE (±SD) [deg]**	**AMAE (±SD) [deg/s]**	**ASDAE (±SD) [deg/s]**	**ARMSE (±SD) [deg/s]**	**AMAE (±SD) [deg]**	**ASDAE (±SD) [deg]**	**ARMSE (±SD) [deg]**	**AMAE (±SD) [deg/s]**	**ASDAE (±SD) [deg/s]**	**ARMSE (±SD) [deg/s]**
P1-1	0.66	97.2	0.84 (±0.23)	0.87 (±0.22)	1.21 (±0.31)	15.21 (±1.83)	12.72 (±1.71)	19.83 (±2.38)	1.12 (±0.3)	1.05 (±0.34)	1.54 (±0.44)	24.44 (±4.08)	23.35 (±5.05)	33.83 (±6.14)
P1-2	0.16	39.0	1.61 (±0.63)	1.34 (±0.48)	2.1 (±0.78)	6.77 (±1.27)	5.72 (±1.39)	8.87 (±1.79)	1.63 (±0.56)	1.78 (±0.71)	2.42 (±0.87)	13.25 (±2.15)	15.83 (±2.67)	20.66 (±3.11)
P1-3	0.41	72.8	0.9 (±0.47)	0.79 (±0.42)	1.19 (±0.63)	9.95 (±1.76)	8.22 (±2.37)	12.92 (±2.84)	1.22 (±0.42)	1.25 (±0.54)	1.75 (±0.65)	15.66 (±3.15)	14.28 (±3.64)	21.21 (±4.64)
P1-4	0.58	89.5	0.91 (±0.27)	0.88 (±0.31)	1.27 (±0.39)	13.66 (±1.55)	11.02 (±1.8)	17.56 (±2.2)	1.06 (±0.34)	1.06 (±0.36)	1.5 (±0.49)	21.08 (±2.91)	21.91 (±4.3)	30.42 (±4.83)
P1-5	0.93	116.3	1.31 (±0.71)	1.39 (±0.85)	1.91 (±1.1)	22.59 (±4.65)	19.41 (±4.78)	29.81 (±6.38)	1.64 (±0.58)	1.7 (±0.77)	2.37 (±0.94)	34.63 (±7.45)	36.67 (±12.86)	50.7 (±13.63)
P1-6	1.14	129.0	2.19 (±0.49)	2.21 (±0.56)	3.12 (±0.7)	34.39 (±5.09)	26.96 (±5.7)	43.7 (±7.34)	1.38 (±0.41)	1.25 (±0.36)	1.86 (±0.53)	33.65 (±4.43)	28.32 (±5.72)	44.01 (±6.76)
P1-7	0.62	92.6	0.89 (±0.27)	0.86 (±0.32)	1.24 (±0.41)	14.23 (±1.68)	11.61 (±1.57)	18.37 (±2.14)	1.16 (±0.42)	1.21 (±0.49)	1.68 (±0.62)	22.98 (±5.05)	22.95 (±7.05)	32.53 (±8.27)
P2-1	0.67	97.4	1.02 (±0.34)	1.01 (±0.45)	1.44 (±0.56)	17.35 (±3.2)	15.43 (±5.16)	23.26 (±5.76)	1.31 (±0.37)	1.33 (±0.45)	1.87 (±0.57)	28.24 (±5.92)	30.18 (±7.78)	41.38 (±9.3)
P2-2	0.25	63.9	1.46 (±0.7)	1.31 (±0.64)	1.96 (±0.94)	9.97 (±2.65)	8.44 (±3.37)	13.14 (±3.98)	1.08 (±0.4)	1.17 (±0.53)	1.6 (±0.65)	12.91 (±2.48)	12.12 (±3.14)	17.74 (±3.78)
P2-3	0.32	68.0	1.12 (±0.49)	0.99 (±0.37)	1.5 (±0.6)	10.21 (±2.08)	8.86 (±2.08)	13.52 (±2.85)	1.06 (±0.53)	1.08 (±0.65)	1.51 (±0.83)	13.66 (±3.85)	12.25 (±3.9)	18.36 (±5.36)
P2-4	0.46	79.2	0.78 (±0.39)	0.71 (±0.31)	1.06 (±0.49)	10.52 (±2.29)	8.67 (±2.42)	13.64 (±3.25)	1.03 (±0.3)	0.94 (±0.3)	1.4 (±0.41)	15.95 (±2.5)	14.47 (±3.07)	21.57 (±3.63)
P2-5	0.58	85.3	0.76 (±0.14)	0.75 (±0.18)	1.07 (±0.21)	11.41 (±1.37)	9.24 (±1.36)	14.68 (±1.8)	1.03 (±0.21)	1.06 (±0.3)	1.48 (±0.35)	18.88 (±2.49)	18.4 (±3.89)	26.38 (±4.29)
P2-6	0.72	94.1	1.19 (±0.31)	1.19 (±0.33)	1.69 (±0.44)	17.38 (±3.38)	14.97 (±3.9)	22.95 (±4.96)	1.13 (±0.41)	1.12 (±0.38)	1.59 (±0.54)	22.61 (±5.12)	22.96 (±5.84)	32.24 (±7.51)
P2-7	0.89	103.2	1.47 (±0.92)	1.56 (±1.03)	2.14 (±1.37)	20.66 (±4.81)	17.54 (±4.91)	27.12 (±6.66)	1.1 (±0.29)	1.07 (±0.31)	1.54 (±0.41)	24.72 (±3.68)	24.24 (±5.32)	34.68 (±5.83)
P2-8	1.05	109.8	1.78 (±1.15)	1.97 (±1.32)	2.66 (±1.74)	24.1 (±6.68)	20.15 (±4.65)	31.44 (±7.9)	1.39 (±0.4)	1.24 (±0.44)	1.87 (±0.58)	30.67 (±5.75)	27.1 (±7.49)	40.97 (±9.02)
P2-9	0.63	91.1	0.79 (±0.25)	0.81 (±0.25)	1.13 (±0.33)	13.36 (±2)	11.13 (±1.76)	17.39 (±2.51)	1.24 (±0.46)	1.32 (±0.59)	1.81 (±0.73)	23.07 (±5.52)	23.47 (±6.18)	32.92 (±8.02)
P3-1	0.67	94.9	0.88 (±0.29)	0.88 (±0.26)	1.24 (±0.36)	15.03 (±2.25)	13.26 (±1.99)	20.06 (±2.7)	1.38 (±0.38)	1.41 (±0.46)	1.98 (±0.57)	27.17 (±3.65)	28.23 (±5.52)	39.25 (±5.81)
P3-2	0.16	36.8	1.76 (±0.77)	1.52 (±0.72)	2.33 (±1.03)	7.21 (±1.76)	5.98 (±2.1)	9.38 (±2.65)	1.63 (±0.39)	1.6 (±0.45)	2.29 (±0.56)	11.03 (±1.62)	10.96 (±2.66)	15.59 (±2.79)
P3-3	0.21	48.3	1.84 (±0.86)	1.48 (±0.58)	2.37 (±1.02)	10.2 (±2.23)	8.55 (±2.8)	13.33 (±3.42)	1.48 (±0.56)	1.56 (±0.74)	2.16 (±0.89)	13.66 (±3.91)	14.11 (±6.52)	19.7 (±7.35)
P3-4	0.32	60.0	1.77 (±0.82)	1.62 (±1)	2.4 (±1.27)	13.16 (±2.99)	9.97 (±2.08)	16.51 (±3.57)	1.43 (±0.51)	1.49 (±0.66)	2.07 (±0.82)	15.5 (±3.05)	13.83 (±3.08)	20.78 (±4.17)
P3-5	0.42	72.1	0.99 (±0.59)	0.91 (±0.54)	1.34 (±0.79)	11.5 (±4.07)	10.51 (±5.52)	15.63 (±6.67)	1.2 (±0.43)	1.22 (±0.63)	1.71 (±0.74)	16.89 (±4.57)	16.82 (±7.25)	23.89 (±8.33)
P3-6	0.54	84.3	0.89 (±0.3)	0.91 (±0.26)	1.28 (±0.38)	13.84 (±2.67)	12.59 (±3.84)	18.75 (±4.39)	1.18 (±0.39)	1.19 (±0.43)	1.68 (±0.56)	21.83 (±5.07)	22.52 (±7.91)	31.42 (±9.04)
P3-7	0.66	96.2	0.89 (±0.45)	0.89 (±0.46)	1.26 (±0.63)	16.71 (±4.8)	15.22 (±6.16)	22.65 (±7.58)	1.43 (±0.46)	1.54 (±0.67)	2.11 (±0.79)	30.12 (±5.35)	33.64 (±8.67)	45.22 (±9.53)
P3-8	0.78	108.2	1.14 (±0.61)	1.19 (±0.61)	1.65 (±0.85)	22.47 (±5.65)	20.12 (±7.27)	30.24 (±8.77)	1.55 (±0.56)	1.65 (±0.83)	2.27 (±0.97)	33.84 (±8.2)	34.92 (±11.02)	48.67 (±13.31)
P3-9	0.94	119.7	1.54 (±0.76)	1.66 (±0.9)	2.27 (±1.17)	28.75 (±7.56)	27.18 (±10.33)	39.67 (±12.26)	1.64 (±0.67)	1.73 (±0.74)	2.39 (±0.98)	38.44 (±10.22)	39.56 (±13.1)	55.3 (±15.82)
P3 -10	0.66	96.7	1.06 (±0.4)	1.13 (±0.61)	1.56 (±0.71)	19.25 (±6.83)	17.25 (±7.31)	25.89 (±9.79)	1.49 (±0.41)	1.6 (±0.51)	2.19 (±0.63)	32.2 (±7.39)	34.49 (±11.83)	47.24 (±13.48)
Average			1.22 (±0.52)	1.18 (±0.54)	1.71 (±0.74)	15.76 (±3.35)	13.49 (±3.78)	20.78 (±4.87)	1.31 (±0.43)	1.33 (±0.52)	1.87 (±0.66)	22.97 (±4.6)	22.98 (±6.36)	32.56 (±7.45)

Method 7: Using all the curves from the clusters with the PRSA [Gr2+All+PRSA]

The PRSA was also run feeding it with all the processed cycles after they were clustered based on its normalized walking speed and the cadence (*Gr2*). The search algorithm was executed using the following cost-minimization formulation:

$$\arg\min_{\{\boldsymbol{\alpha}_{t,C},\boldsymbol{\alpha}_{\theta,C}\}}\left(\sum_{i=1}^{N_C}\sum_{j=1}^{n}\left(e_{p_{(i,j)}}^2+w_v\cdot\left|e_{v_{(i,j)}}\right|\right)\right)$$

$$e_{p_{(i,j)}}=\theta_{REF\,(i,j)}-\theta_C\left(\left\{\boldsymbol{\alpha}_{t,C},\boldsymbol{\alpha}_{\theta,C}\right\}\right)_{(j)}$$

$$e_{v_{(i,j)}}=\dot{\theta}_{REF\,(i,j)}-\dot{\theta}_C\left(\left\{\boldsymbol{\alpha}_{t,C},\boldsymbol{\alpha}_{\theta,C}\right\}\right)_{(j)} \tag{29}$$

where n is the number of samples per curve, N_C is the number of curves in the cluster, $e_{p_{(i,j)}}$ and $e_{v_{(i,j)}}$ are the position and velocity error measurements in sample j when comparing the regenerated curve and the i^{th} curve of the cluster, $\theta_{REF\,(i,j)}$ and $\dot{\theta}_{REF\,(i,j)}$ are the position and velocity values of the i^{th} reference curve in sample j, $\theta_C(\{\boldsymbol{\alpha}_{t,C},\boldsymbol{\alpha}_{\theta,C}\})$ and $\dot{\theta}_C(\{\boldsymbol{\alpha}_{t,C},\boldsymbol{\alpha}_{\theta,C}\})$ are the position and velocity values calculated from the interpolation using the shaping knots described by a given set of $\{\alpha_{t,C},\alpha_{\theta,C}\}$ (specific to cluster *C*), and $w_v=0.02$ is the weight of the velocity error in the cost function.

Table 18 shows the results accomplished with this method, including the WS_{norm} and *cad* corresponding to each cluster centroid, and the AMAE, ARMSE and AR calculated between all the original curves in each cluster and the corresponding regenerated curve. Comparing Table 18 and Table 17, no significant differences in the performance can be spotted. This doesn't mean that both grouping methods are equally suited for the final application, just that they have to be evaluated and compared with different data to get a better insight. An example of the generally good behavior of the regeneration is shown in Fig. 63, where the depicted original hip and knee curves are the same as the ones shown in Fig. 59. The hip trajectory reconstruction yielded a MAE and SDAE of 1.35° and 1.42°, respectively, whereas the knee trajectory yielded 0.76° and 0.79°. Likewise, Fig. 64 shows the regeneration of the curve from cluster 4 previously depicted in Fig. 60, using *Method 7, Method 5* and *Method 4*. In the case of *Method 7* the MAE and SDAE were 0.95° and 0.85°, respectively. A clear improvement can be seen in the shape of the reconstructed curve using this method in comparison to *Method 4* and *Method 5*.

Table 18 Results of *Method 7* with respect to all the curves in the cluster

			HIP						KNEE					
			Position			Velocity			Position			Velocity		
Cl.	WS norm	Cad	AMAE (±SD) [deg]	ASDAE (±SD) [deg]	ARMSE (±SD) [deg]	AMAE (±SD) [deg/s]	ASDAE (±SD) [deg/s]	ARMSE (±SD) [deg/s]	AMAE (±SD) [deg]	ASDAE (±SD) [deg]	ARMSE (±SD) [deg]	AMAE (±SD) [deg/s]	ASDAE (±SD) [deg/s]	ARMSE (±SD) [deg/s]
1	0.16	37.75	1.81 (±0.76)	1.48 (±0.65)	2.34 (±0.98)	7.03 (±1.7)	5.84 (±1.72)	9.15 (±2.36)	1.65 (±0.46)	1.69 (±0.55)	2.37 (±0.68)	11.81 (±1.98)	12.44 (±2.96)	17.19 (±3.26)
2	0.21	48.32	1.84 (±0.86)	1.48 (±0.58)	2.37 (±1.02)	10.2 (±2.23)	8.55 (±2.8)	13.33 (±3.42)	1.48 (±0.56)	1.56 (±0.74)	2.16 (±0.89)	13.66 (±3.91)	14.11 (±6.52)	19.7 (±7.35)
3	0.25	63.73	1.44 (±0.68)	1.28 (±0.64)	1.93 (±0.92)	9.94 (±2.61)	8.33 (±3.3)	13.06 (±3.85)	1.04 (±0.37)	1.12 (±0.49)	1.53 (±0.6)	12.18 (±2.23)	11.48 (±3)	16.77 (±3.47)
4	0.32	59.81	1.82 (±0.8)	1.68 (±1)	2.49 (±1.26)	13.41 (±3)	10.08 (±2.02)	16.77 (±3.56)	1.47 (±0.49)	1.54 (±0.66)	2.13 (±0.8)	15.79 (±2.98)	14.22 (±3.09)	21.26 (±4.12)
5	0.32	65.29	1.23 (±0.47)	1.13 (±0.33)	1.67 (±0.54)	11.07 (±2.43)	9.33 (±2.01)	14.48 (±3.03)	1.12 (±0.57)	1.1 (±0.68)	1.58 (±0.87)	13.99 (±4.35)	11.88 (±4.52)	18.37 (±6.17)
6	0.33	69.66	0.98 (±0.41)	0.88 (±0.36)	1.33 (±0.53)	9.67 (±1.9)	8.4 (±1.84)	12.8 (±2.6)	1.04 (±0.47)	1.1 (±0.56)	1.52 (±0.72)	13.67 (±2.96)	12.6 (±2.99)	18.61 (±4)
7	0.41	71.65	0.96 (±0.57)	0.91 (±0.6)	1.32 (±0.82)	10.99 (±3.62)	9.63 (±4.62)	14.65 (±5.72)	1.26 (±0.39)	1.3 (±0.45)	1.82 (±0.57)	16.71 (±4.26)	16.4 (±5.67)	23.42 (±6.94)
8	0.44	76.89	0.85 (±0.42)	0.78 (±0.3)	1.15 (±0.5)	10.29 (±2.85)	8.35 (±2.91)	13.25 (±4.03)	0.88 (±0.31)	0.88 (±0.34)	1.25 (±0.45)	14.11 (±1.76)	13.07 (±1.79)	19.25 (±2.17)
9	0.43	72.83	0.94 (±0.26)	0.88 (±0.3)	1.29 (±0.39)	11.27 (±3.13)	10.26 (±5.74)	15.33 (±6.23)	1.09 (±0.54)	1.17 (±0.85)	1.61 (±0.98)	15.48 (±4.69)	15.01 (±8)	21.66 (±8.92)
10	0.46	79.41	0.73 (±0.22)	0.69 (±0.26)	1 (±0.34)	10.36 (±1.32)	8.46 (±1.14)	13.37 (±1.65)	1.03 (±0.27)	0.98 (±0.3)	1.42 (±0.4)	16.19 (±2.38)	14.68 (±3.4)	21.88 (±3.84)
11	0.54	82.46	0.81 (±0.27)	0.85 (±0.28)	1.18 (±0.37)	12.84 (±2.84)	11.87 (±4.24)	17.53 (±4.86)	1.11 (±0.37)	1.13 (±0.35)	1.59 (±0.49)	19.78 (±4.4)	20.27 (±7.53)	28.4 (±8.3)
12	0.58	88.08	0.87 (±0.27)	0.83 (±0.29)	1.2 (±0.38)	13.06 (±1.9)	10.57 (±2.02)	16.8 (±2.63)	1.12 (±0.37)	1.14 (±0.42)	1.6 (±0.55)	21.29 (±4.24)	21.82 (±5.35)	30.5 (±6.59)
13	0.63	92.28	0.92 (±0.29)	0.88 (±0.33)	1.28 (±0.43)	14.66 (±2.98)	12.34 (±4.04)	19.19 (±4.82)	1.25 (±0.44)	1.31 (±0.56)	1.82 (±0.69)	23.93 (±5.87)	24.63 (±7.87)	34.39 (±9.47)
14	0.64	96.41	0.96 (±0.42)	1.02 (±0.47)	1.4 (±0.62)	15.75 (±4.44)	13.8 (±4.42)	20.94 (±6.19)	1.21 (±0.35)	1.23 (±0.58)	1.73 (±0.65)	28.16 (±5.41)	29.5 (±10.14)	40.87 (±10.94)
15	0.67	93.33	0.9 (±0.27)	0.96 (±0.37)	1.32 (±0.44)	15.47 (±4.28)	13.84 (±4.82)	20.77 (±6.31)	1.41 (±0.47)	1.44 (±0.6)	2.02 (±0.74)	27.65 (±6.18)	29.16 (±8.77)	40.28 (±10.11)
16	0.68	97.20	0.9 (±0.29)	0.89 (±0.3)	1.27 (±0.4)	16.31 (±2.86)	14.33 (±4.1)	21.75 (±4.75)	1.31 (±0.39)	1.29 (±0.43)	1.84 (±0.57)	27.46 (±4.74)	28.53 (±6.66)	39.63 (±7.72)
17	0.72	94.87	1.2 (±0.38)	1.19 (±0.39)	1.69 (±0.54)	18 (±3.33)	15.52 (±3.4)	23.79 (±4.47)	1.3 (±0.52)	1.25 (±0.42)	1.81 (±0.65)	26 (±6.3)	25.36 (±6.93)	36.33 (±9.13)
18	0.73	103.05	1.22 (±0.46)	1.33 (±0.76)	1.81 (±0.88)	23.04 (±7.67)	19.99 (±7.93)	30.51 (±10.89)	1.42 (±0.46)	1.53 (±0.78)	2.1 (±0.86)	35.02 (±9.34)	37.49 (±15.97)	51.42 (±17.86)
19	0.78	107.61	1.18 (±0.71)	1.28 (±0.71)	1.74 (±0.98)	22.58 (±5.97)	20.29 (±7.07)	30.43 (±8.85)	1.53 (±0.55)	1.72 (±0.96)	2.31 (±1.08)	34.28 (±9.55)	35.71 (±13.05)	49.6 (±15.6)
20	0.89	102.79	1.53 (±0.93)	1.62 (±1.05)	2.23 (±1.4)	21.07 (±4.88)	17.97 (±4.96)	27.72 (±6.72)	1.12 (±0.28)	1.12 (±0.29)	1.58 (±0.39)	26.62 (±3.28)	26.7 (±4.75)	37.74 (±5.16)
21	0.82	109.88	0.91 (±0.21)	0.95 (±0.34)	1.32 (±0.38)	22.4 (±5.96)	21.06 (±8.8)	30.79 (±10.31)	1.61 (±0.68)	1.72 (±0.73)	2.35 (±0.99)	37.5 (±5.18)	39.39 (±6.18)	54.38 (±7.48)
22	0.90	111.33	1.03 (±0.17)	1.08 (±0.22)	1.49 (±0.25)	21.03 (±4.04)	19.64 (±5.59)	28.82 (±6.46)	1.51 (±0.78)	1.85 (±0.95)	2.39 (±1.21)	33.35 (±10.08)	41.98 (±19.15)	53.87 (±20.6)
23	0.92	117.65	1.62 (±0.88)	1.73 (±1.03)	2.37 (±1.34)	26.63 (±6.98)	23.32 (±8.41)	35.44 (±10.66)	1.62 (±0.67)	1.63 (±0.71)	2.3 (±0.96)	35.43 (±10.58)	35 (±13.18)	49.99 (±16.08)
24	1.03	109.04	1.98 (±1.36)	2.14 (±1.49)	2.91 (±2.01)	24.55 (±8.15)	20.86 (±4.94)	32.25 (±9.29)	1.22 (±0.34)	1.14 (±0.35)	1.67 (±0.48)	27.75 (±4.9)	23.79 (±5.19)	36.54 (±6.99)
25	0.97	120.49	1.2 (±0.38)	1.33 (±0.51)	1.79 (±0.62)	26.96 (±7.02)	26.22 (±10.53)	37.75 (±12.02)	1.56 (±0.4)	1.59 (±0.37)	2.23 (±0.52)	36.8 (±6.44)	38.32 (±6.66)	53.23 (±8.12)
26	1.08	110.98	1.23 (±0.52)	1.21 (±0.55)	1.73 (±0.75)	21.85 (±3.01)	17.08 (±1.89)	27.74 (±3.23)	1.58 (±0.26)	1.43 (±0.52)	2.14 (±0.52)	34.7 (±6.21)	32.94 (±11.32)	48 (±11.97)
27	1.11	128.61	1.94 (±0.74)	2.12 (±1.17)	2.88 (±1.35)	32 (±9.06)	27.08 (±9.76)	41.93 (±13.1)	1.41 (±0.42)	1.4 (±0.41)	1.99 (±0.58)	36.81 (±4.84)	35.03 (±7.22)	50.86 (±7.96)
28	1.18	129.53	1.7 (±0.94)	1.78 (±1.17)	2.46 (±1.49)	30.11 (±6.03)	23.69 (±5.09)	38.3 (±7.73)	1.09 (±0.37)	0.99 (±0.33)	1.47 (±0.49)	32.88 (±4.87)	26.9 (±4.84)	42.47 (±6.58)
Average			1.24 (±0.53)	1.23 (±0.59)	1.75 (±0.78)	17.23 (±4.15)	14.88 (±4.65)	22.81 (±6.06)	1.3 (±0.45)	1.33 (±0.55)	1.87 (±0.69)	24.61 (±5.14)	24.59 (±7.24)	34.88 (±8.46)

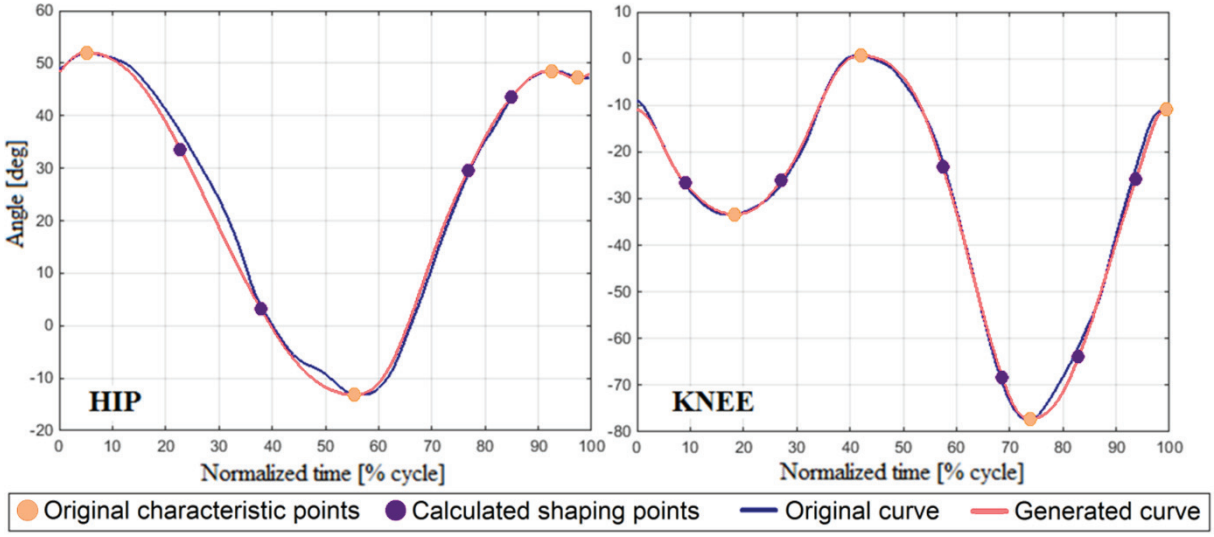

Fig. 63 Example of regenerated curves with *Method 7*

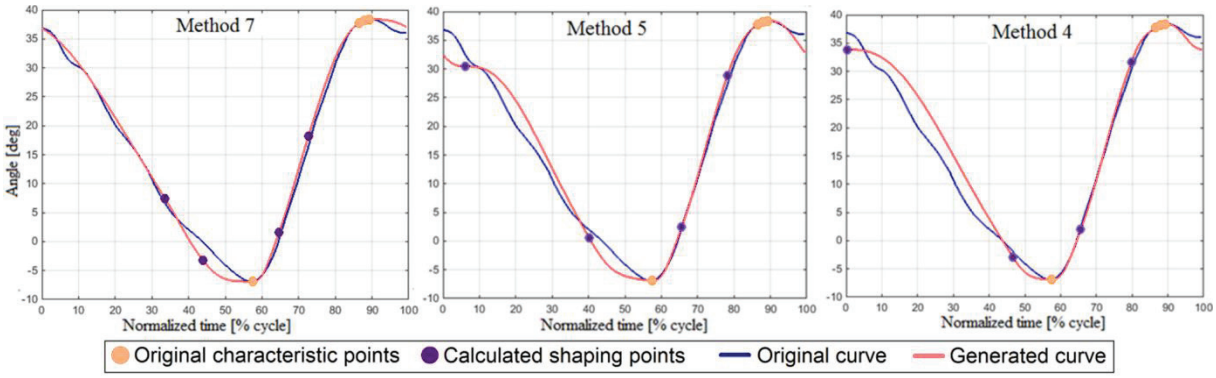

Fig. 64 Comparison of a hip curve from cluster 4 with the generated curves obtained by *Method 7* (left), *Method 5* (center) and *Method 4* (right)

Method 8: Using the 5 more representative curves from each cluster with the PRSA [Gr2+5-MRep+PRSA]

Finally, based on the experience gathered from the previous methods, it was decided to run the PRSA feeding it not with all the curves of each cluster, but with the p=5 most representative ones based on the cross-correlation coefficients' matrix. This way, a significant reduction in the processing time needed by the PRSA to go over all the clusters is accomplished compared to *Method 7*. The cost minimization problem will be defined as in (29), with the difference that $N_C = p = 5$ is the number of most representative curves in the cluster.

The results achieved from this method can be seen in Table 19 and Table 20. Table 19 shows position and velocity MAE and SDAE between the regenerated and the p most representative curves in the clusters. Table 20 shows AMAE, ARMSE and ASDAE between the reconstructed curves and all the curves in each cluster. Comparing the results with the ones in Table 18, it can be seen that a considerable reduction in the number of curves fed to the algorithm, although it reduced the processing time, led to a slight deterioration in the error performance in both joints. An example of the generally good behavior of the regeneration is shown in Fig. 65, where the depicted original hip and knee curves are the same as the ones

shown in Fig. 59 and Fig. 63. The hip trajectory reconstruction yielded a MAE and SDAE of 1.39° and 1.64°, respectively, whereas the knee trajectory yielded 0.85° and 0.77°. Likewise, Fig. 66 shows the regeneration of the curve from cluster 4 previously depicted in Fig. 60, using *Method 8, Method 7*and *Method 5*. In the case of *Method 8* the MAE and SDAE were 1.16° and 1.12°, respectively. An improvement can be seen in the shape of the reconstructed curve using this method in comparison to *Method 5*, but a visible deterioration took place with respect to *Method 7*. This suggests that the more curves are used by the search algorithm, the better resulting shapes are achieved after regeneration.

Table 19 Results *Method 8* with respect to the cluster's most representative curves

	HIP						KNEE					
Cluster	**WSnorm**	**Cad**	**MAE (pos) [deg]**	**SDAE (pos) [deg]**	**MAE (vel) [deg/s]**	**SDAE (vel) [deg/s]**	**WSnorm**	**Cad**	**MAE (pos) [deg]**	**SDAE (pos) [deg]**	**MAE (vel) [deg/s]**	**SDAE (vel) [deg/s]**
1	0.163	38.82	1.27	0.22	6.25	0.69	0.163	37.40	1.27	0.40	8.02	1.43
2	0.212	48.84	1.70	1.08	8.92	2.30	0.210	48.24	1.19	0.43	12.28	4.65
3	0.249	64.16	1.03	0.54	9.73	2.27	0.245	63.07	1.16	0.33	13.94	2.54
4	0.317	60.09	1.59	0.33	12.70	1.92	0.321	59.90	1.53	1.01	15.92	5.61
5	0.317	65.86	1.31	0.52	10.93	1.47	0.323	65.16	0.81	0.52	11.40	2.21
6	0.324	68.96	0.91	0.28	10.00	1.66	0.327	68.68	0.97	0.49	12.36	2.35
7	0.419	71.48	0.53	0.13	8.97	0.99	0.418	72.31	1.10	0.38	14.08	2.47
8	0.441	77.38	0.77	0.56	10.63	2.81	0.445	77.97	0.90	0.43	14.74	2.67
9	0.428	72.81	0.73	0.36	9.47	1.89	0.430	73.40	0.93	0.57	13.77	3.33
10	0.462	79.07	0.54	0.17	9.76	1.77	0.468	80.46	0.72	0.31	15.06	3.29
11	0.549	82.90	0.65	0.18	10.83	1.61	0.549	82.87	0.79	0.29	17.49	4.21
12	0.583	88.64	0.75	0.23	13.24	1.47	0.580	88.30	0.92	0.14	22.79	4.62
13	0.632	91.57	0.66	0.16	13.12	2.07	0.627	91.51	1.40	0.71	25.56	3.78
14	0.644	96.12	0.70	0.19	13.65	1.65	0.643	96.11	1.11	0.36	27.95	6.28
15	0.670	93.74	0.67	0.07	14.70	0.62	0.665	93.75	0.98	0.15	25.20	1.23
16	0.669	96.12	0.60	0.11	13.36	1.76	0.667	96.66	1.23	0.26	25.52	3.46
17	0.728	94.78	0.85	0.49	15.96	3.41	0.736	94.74	1.03	0.35	24.15	4.04
18	0.728	102.31	1.03	0.19	19.02	3.13	0.729	104.02	1.06	0.27	27.18	5.02
19	0.782	108.09	0.71	0.20	17.55	1.81	0.775	107.50	1.33	0.44	29.80	8.09
20	0.897	103.32	0.74	0.21	15.44	1.32	0.901	103.82	1.08	0.12	29.58	4.46
21	0.817	109.28	0.96	0.15	23.28	6.20	0.817	109.28	1.63	0.81	37.05	5.55
22	0.896	111.91	0.97	0.24	22.26	5.04	0.896	111.91	1.52	1.15	34.32	14.94
23	0.920	116.55	1.11	0.39	21.47	3.43	0.919	117.39	0.90	0.34	27.88	4.09
24	1.015	108.62	1.34	1.11	21.18	6.60	1.020	107.97	1.01	0.33	24.74	7.09
25	0.975	119.47	0.87	0.32	21.53	2.60	0.974	120.22	1.25	0.24	30.14	5.22
26	1.087	110.61	1.16	0.41	21.69	2.79	1.086	111.15	1.53	0.37	33.59	6.34
27	1.112	129.03	1.95	0.54	31.22	5.19	1.117	128.20	1.14	0.21	34.65	4.07
28	1.179	128.21	1.42	0.90	32.82	5.92	1.185	129.11	0.78	0.18	30.30	1.46
Average			0.98	0.37	15.70	2.66			1.12	0.41	22.84	4.45

Table 20 Results of *Method 8* with respect to all the curves in the cluster

	HIP						KNEE					
	Position			Velocity			Position			Velocity		
Cluster	**AMAE (±SD) [deg]**	**ASDAE (±SD) [deg]**	**ARMSE (±SD) [deg]**	**AMAE (±SD) [deg/s]**	**ASDAE (±SD) [deg/s]**	**ARMSE (±SD) [deg/s]**	**AMAE (±SD) [deg]**	**ASDAE (±SD) [deg]**	**ARMSE (±SD) [deg]**	**AMAE (±SD) [deg/s]**	**ASDAE (±SD) [deg/s]**	**ARMSE (±SD) [deg/s]**
1	1.75 (±0.65)	1.46 (±0.53)	2.29 (±0.82)	7.28 (±1.4)	5.94 (±1.51)	9.4 (±1.98)	1.75 (±0.56)	1.76 (±0.6)	2.48 (±0.79)	10.95 (±2.48)	10.32 (±2.35)	15.05 (±3.29)
2	1.85 (±0.94)	1.5 (±0.69)	2.38 (±1.15)	10.33 (±2.36)	8.82 (±2.79)	13.61 (±3.51)	1.71 (±0.62)	1.84 (±0.87)	2.52 (±1.03)	14.09 (±4.42)	14.65 (±7.94)	20.42 (±8.78)
3	1.39 (±0.68)	1.26 (±0.74)	1.88 (±0.99)	11.13 (±3.27)	9.15 (±3.37)	14.53 (±4.24)	1.23 (±0.45)	1.34 (±0.58)	1.82 (±0.73)	14.32 (±3.05)	13.62 (±3.15)	19.78 (±4.22)
4	2.29 (±1.09)	2.1 (±1.16)	3.11 (±1.57)	14.6 (±3.57)	10.87 (±2.17)	18.2 (±4.1)	1.81 (±0.65)	1.99 (±0.82)	2.69 (±1.02)	18.27 (±4.07)	17.32 (±3.98)	25.18 (±5.52)
5	1.39 (±0.37)	1.16 (±0.2)	1.81 (±0.41)	11.03 (±1.87)	9.04 (±1.83)	14.26 (±2.54)	1.12 (±0.59)	1.13 (±0.68)	1.59 (±0.89)	14.25 (±4.28)	12.27 (±4.38)	18.82 (±6)
6	1.11 (±0.68)	1.01 (±0.67)	1.5 (±0.95)	10.08 (±1.93)	8.65 (±1.83)	13.28 (±2.62)	1.11 (±0.54)	1.12 (±0.65)	1.58 (±0.84)	13.73 (±3.25)	12.38 (±3.59)	18.5 (±4.68)
7	1.17 (±1.13)	0.95 (±0.79)	1.51 (±1.37)	11.35 (±4.84)	9.85 (±5.26)	15.05 (±7.06)	1.31 (±0.38)	1.4 (±0.59)	1.93 (±0.66)	17.31 (±4.54)	16.79 (±6.27)	24.14 (±7.55)
8	1.04 (±0.51)	0.9 (±0.48)	1.37 (±0.7)	10.88 (±1.88)	9.05 (±2.59)	14.16 (±3.07)	1.02 (±0.34)	0.97 (±0.38)	1.41 (±0.5)	16.32 (±3.1)	14.7 (±3.06)	21.99 (±4.09)
9	1.03 (±0.44)	0.95 (±0.43)	1.4 (±0.59)	11.67 (±3.66)	10.55 (±5.61)	15.79 (±6.47)	1.1 (±0.54)	1.18 (±0.85)	1.63 (±0.98)	15.68 (±4.38)	15.76 (±7.38)	22.31 (±8.26)
10	0.8 (±0.32)	0.77 (±0.35)	1.11 (±0.47)	10.8 (±1.6)	8.68 (±1.32)	13.86 (±1.99)	1.07 (±0.36)	1.01 (±0.35)	1.47 (±0.5)	17.19 (±3.1)	15.84 (±3.96)	23.38 (±4.82)
11	0.81 (±0.27)	0.85 (±0.29)	1.18 (±0.38)	12.65 (±2.87)	11.82 (±4.3)	17.35 (±4.94)	1.14 (±0.38)	1.16 (±0.35)	1.63 (±0.49)	20.47 (±4.5)	20.7 (±7.7)	29.2 (±8.44)
12	0.91 (±0.32)	0.87 (±0.3)	1.26 (±0.43)	13.05 (±1.92)	10.57 (±2.02)	16.8 (±2.62)	1.27 (±0.37)	1.27 (±0.41)	1.79 (±0.54)	25.63 (±4.39)	25.92 (±5.87)	36.46 (±7.03)
13	0.93 (±0.29)	0.9 (±0.33)	1.29 (±0.43)	14.95 (±2.99)	12.44 (±4.04)	19.48 (±4.82)	1.5 (±0.57)	1.51 (±0.6)	2.13 (±0.81)	26.77 (±5.55)	28.46 (±6.76)	39.11 (±8.3)
14	1.03 (±0.45)	1.1 (±0.53)	1.5 (±0.69)	15.88 (±4.4)	14.05 (±4.34)	21.19 (±6.13)	1.29 (±0.35)	1.33 (±0.53)	1.86 (±0.61)	29.62 (±6.18)	32.5 (±9.79)	44.01 (±11.13)
15	1 (±0.37)	1.04 (±0.45)	1.45 (±0.57)	16.89 (±4.68)	15.34 (±5.44)	22.82 (±7.06)	1.47 (±0.55)	1.47 (±0.58)	2.08 (±0.78)	28.76 (±5.14)	32.07 (±8.89)	43.16 (±9.59)
16	0.92 (±0.28)	0.92 (±0.3)	1.31 (±0.4)	16.51 (±2.92)	14.41 (±4.07)	21.95 (±4.74)	1.44 (±0.42)	1.48 (±0.49)	2.07 (±0.63)	29.66 (±5.07)	30.09 (±5.98)	42.27 (±7.38)
17	1.26 (±0.55)	1.28 (±0.53)	1.79 (±0.77)	18.52 (±3.87)	15.82 (±3.43)	24.37 (±4.97)	1.31 (±0.64)	1.31 (±0.54)	1.85 (±0.82)	25.87 (±7.31)	26.71 (±8.04)	37.18 (±10.7)
18	1.24 (±0.55)	1.36 (±0.87)	1.85 (±1.01)	23.31 (±8.33)	20.11 (±8.31)	30.8 (±11.62)	1.4 (±0.5)	1.55 (±0.72)	2.1 (±0.84)	34.09 (±11.19)	36.44 (±17.22)	50.04 (±19.93)
19	1.19 (±0.73)	1.27 (±0.7)	1.75 (±1)	22.7 (±6.06)	20.33 (±7.04)	30.55 (±8.88)	1.66 (±0.6)	1.83 (±0.88)	2.48 (±1.04)	37.01 (±11.08)	38.82 (±13.56)	53.79 (±16.73)
20	1.6 (±1.14)	1.65 (±1.29)	2.3 (±1.71)	21.08 (±6.51)	17.61 (±5.83)	27.46 (±8.65)	1.15 (±0.29)	1.15 (±0.27)	1.63 (±0.39)	28.45 (±3.54)	26.95 (±4.26)	39.22 (±4.84)
21	0.92 (±0.17)	0.95 (±0.32)	1.32 (±0.33)	22.37 (±5.98)	21.04 (±8.74)	30.75 (±10.31)	1.6 (±0.73)	1.71 (±0.8)	2.34 (±1.08)	36.31 (±5.29)	38.34 (±7.22)	52.83 (±8.2)
22	1.01 (±0.23)	1.08 (±0.39)	1.49 (±0.44)	21.52 (±4.74)	19.98 (±5.98)	29.42 (±7.21)	1.53 (±0.96)	1.87 (±1.14)	2.43 (±1.46)	35.66 (±12.91)	43.66 (±22.13)	56.74 (±24.39)
23	1.76 (±0.92)	1.84 (±0.95)	2.55 (±1.31)	28.2 (±7.44)	23.92 (±8.66)	37.02 (±11.12)	1.76 (±0.8)	1.82 (±0.77)	2.54 (±1.09)	38.2 (±11.59)	36.68 (±12.36)	53.14 (±16.09)
24	2.03 (±1.41)	2.16 (±1.49)	2.97 (±2.05)	25.35 (±7.98)	21.92 (±5)	33.54 (±9.18)	1.36 (±0.51)	1.26 (±0.46)	1.86 (±0.67)	28.8 (±7.11)	24.25 (±7)	37.66 (±9.75)
25	1.2 (±0.43)	1.31 (±0.55)	1.77 (±0.68)	26.08 (±6.98)	25.48 (±10.44)	36.6 (±11.94)	1.66 (±0.44)	1.64 (±0.36)	2.34 (±0.53)	37.11 (±8.34)	40.23 (±8.49)	54.9 (±10.65)
26	1.3 (±0.63)	1.24 (±0.58)	1.79 (±0.85)	21.98 (±3.31)	17.18 (±2.32)	27.9 (±3.84)	1.62 (±0.42)	1.46 (±0.54)	2.18 (±0.66)	34.59 (±8.01)	33.87 (±12.44)	48.51 (±14.19)
27	2 (±0.58)	2.13 (±0.91)	2.93 (±1.03)	31.32 (±8.1)	26.32 (±7.56)	40.89 (±10.99)	1.46 (±0.51)	1.46 (±0.49)	2.06 (±0.7)	37.41 (±5.5)	34.74 (±6.99)	51.12 (±8.06)
28	1.84 (±0.93)	1.83 (±1.01)	2.6 (±1.36)	34.23 (±5.33)	26.28 (±4.17)	43.13 (±6.6)	1.15 (±0.51)	1.05 (±0.47)	1.55 (±0.68)	34.23 (±6.32)	28.72 (±5.58)	44.66 (±8.27)
Average	1.31 (±0.61)	1.28 (±0.64)	1.84 (±0.87)	17.71 (±4.31)	15.19 (±4.64)	23.36 (±6.19)	1.39 (±0.52)	1.43 (±0.6)	2 (±0.78)	25.74 (±5.92)	25.81 (±7.73)	36.56 (±9.32)

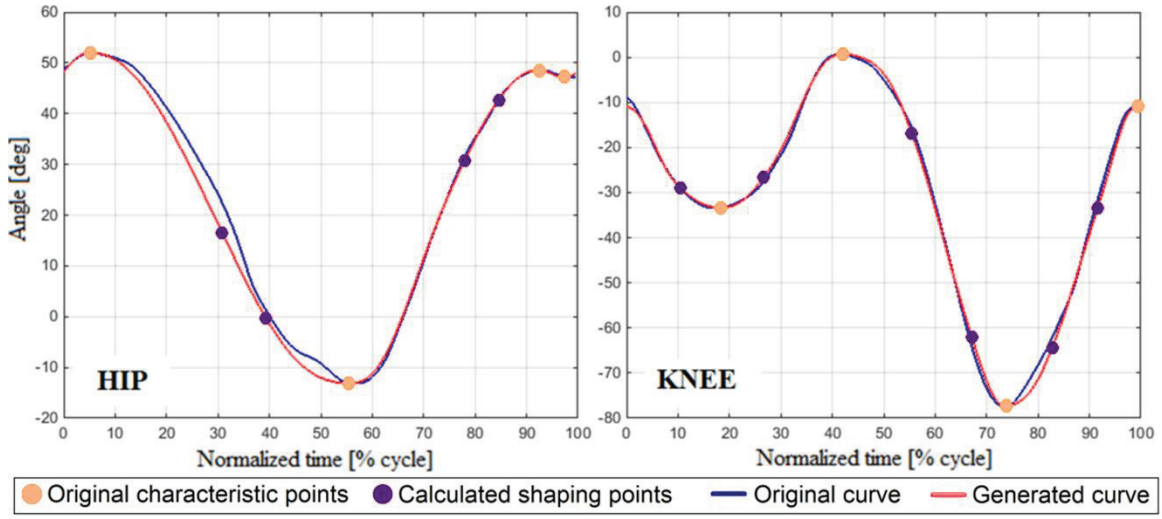

Fig. 65 Example of regenerated curves with *Method 8*

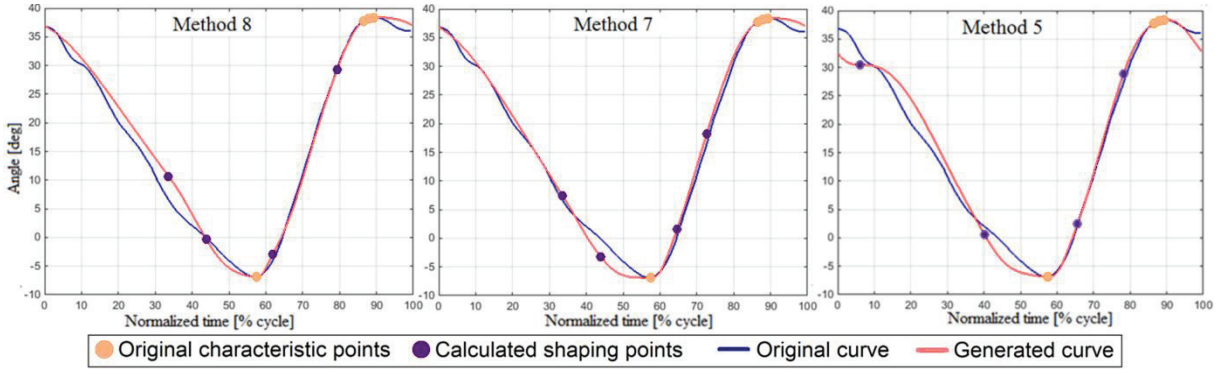

Fig. 66 Comparison of a hip curve from cluster 4 with the generated curves obtained by *Method 8* (left), *Method 7* (center) and *Method 5* (right)

Mapping of input gait parameters into the corresponding shaping knots

When a method implements cycles' grouping (*Gr1* or *Gr2*), each one of the groups will possess a pair of reference normalized walking speed and cadence values that represents it (referred also as centroids of the group). To evaluate which shaping knots' coefficients should be used for a given pair of input gait parameters $WS_{norm,in}$ and Cad_{in}, a radial basis selection was implemented, which calculates a 2-dimensional distance between the input pair and each one of the groups' reference pair, and finally selects the shaping knots' coefficients from the group with the reference gait parameters that generated the lowest distance. The selection process has the following formulation:

$$\arg\min_{\{G\}}\Big(d\big(\{WS_{norm,in}, cad_{in}\}, \{WS_{norm,G}, cad_G\}\big)\Big)$$

$$d(\dots) = \left(\frac{\left(WS_{norm,in} - WS_{norm,G}\right)}{\max(\{WS_{norm,G}\})}\right)^2 + \left(\frac{(cad_{in} - cad_G)}{\max(\{cad_G\})}\right)^2, \tag{30}$$

where $d(...)$ is the distance function, $WS_{norm,in}$ and Cad_{in} are the input pair of gait parameters, $WS_{norm,G}$ and Cad_G are the reference pair of gait parameters from group G, and $max(\{WS_{norm,G}\})$ and $max(\{Cad_G\})$ are the maximum normalized walking speed and cadence from all the reference pairs of the joint, respectively.

Fig. 67 shows an example of the selection when grouping following strategy *Gr2*, most specifically for *Method 4*. The figure shows the centroids of each cluster as well as two examples of input gait parameter pairs. The cluster centroid selection for each one of the input pairs is shown with the shaded area. Note that the selected centroid for a given pair of inputs does not necessarily belong to the cluster where the input pair is located. Take into account that the clustering was made only to train the algorithms and get the centroid, but not for the cluster selection itself.

Overview on the shaping parameters' acquisition methods

First, let us make a summary of the error-performances gotten from each one of the methods. Table 21 shows the overall average results of the seven methods that grouped their training data, depicting the error measurement obtained with respect to all the curves in the respective group. Note that *Method 1* is not included in the table because it was not trained with the data obtained from the experiment. At first glance the best method appears to be *Method 2,* delivering the lowest position errors in both hip and knee joints. The methods that used the (normalized time-warped) average curves to train the algorithm showed the worst results in the hip joint. In the case of the knee, besides *Method 2* all the methods performed similarly. It can also be noted that the DCSA delivered better results than the PRSA.

Next, a detailed analysis about the searching algorithms used to obtain the most appropriate sets of shaping knots coefficients is done. Three algorithms were presented: the Full-Curve-Scanning Search Algorithm (FCSSA), the Dynamic-Clustering Search Algorithm (DCSA) and the Progressive-Refinement Search Algorithm (PRSA). Regarding the best performance errorwise, it is clear that the FCSSA is the best, because it performs a full scanning in each one of the gaps, checking all possible values of α_t *and* α_θ of the shaping knots in the gap, with a real resolution of 0.01 (1%). This algorithm will surely deliver the set of knots that correspond to the global minimum error in the gap.

The performance of the DCSA is highly dependent on the behavior of the errors

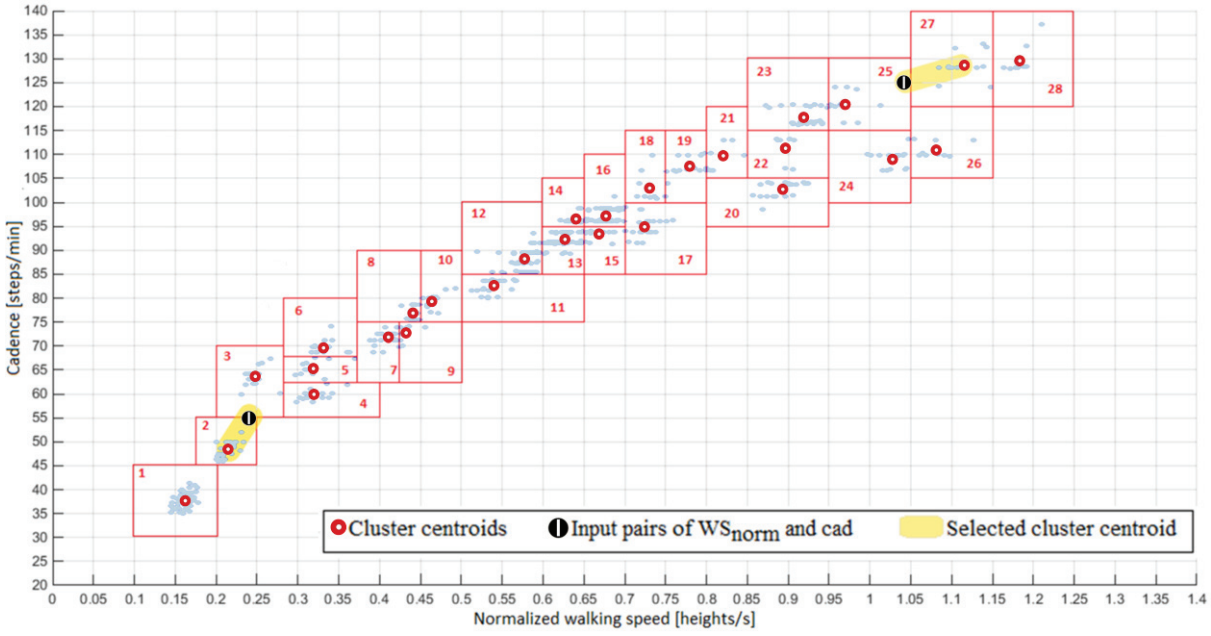

Fig. 67 Map of normalized walking speed and cadence by cluster with the respective cluster centroids

Table 21 Overall average results of the methods that grouped the training data, with respect to all the curves in the respective group

	HIP						KNEE					
	Position			Velocity			Position			Velocity		
Method	AMAE (±SD) [deg]	ASDAE (±SD) [deg]	ARMSE (±SD) [deg]	AMAE (±SD) [deg/s]	ASDAE (±SD) [deg/s]	ARMSE (±SD) [deg/s]	AMAE (±SD) [deg]	ASDAE (±SD) [deg]	ARMSE (±SD) [deg]	AMAE (±SD) [deg/s]	ASDAE (±SD) [deg/s]	ARMSE (±SD) [deg/s]
2	1.14 (±0.49)	1.1 (±0.52)	1.59 (±0.71)	15.05 (±3.3)	12.8 (±3.67)	19.79 (±4.76)	1.25 (±0.44)	1.28 (±0.53)	1.79 (±0.68)	21.09 (±4.83)	20.93 (±6.37)	29.77 (±7.68)
3	1.3 (±0.61)	1.25 (±0.61)	1.81 (±0.86)	15.72 (±3.61)	13.27 (±3.72)	20.61 (±5)	1.39 (±0.51)	1.4 (±0.56)	1.98 (±0.74)	23.64 (±5.59)	23.65 (±6.67)	33.52 (±8.37)
4	1.35 (±0.49)	1.31 (±0.54)	1.88 (±0.72)	17.38 (±3.69)	14.63 (±4.08)	22.76 (±5.31)	1.3 (±0.44)	1.3 (±0.52)	1.84 (±0.67)	23.39 (±5.17)	23.74 (±6.86)	33.39 (±8.27)
5	1.34 (±0.47)	1.3 (±0.51)	1.87 (±0.68)	18.11 (±3.83)	15.35 (±4.12)	23.77 (±5.45)	1.38 (±0.43)	1.34 (±0.5)	1.92 (±0.64)	25.72 (±4.82)	24.87 (±6.54)	35.84 (±7.72)
6	1.22 (±0.52)	1.18 (±0.54)	1.71 (±0.74)	15.76 (±3.35)	13.49 (±3.78)	20.78 (±4.87)	1.31 (±0.43)	1.33 (±0.52)	1.87 (±0.66)	22.97 (±4.6)	22.98 (±6.36)	32.56 (±7.45)
7	1.24 (±0.53)	1.23 (±0.59)	1.75 (±0.78)	17.23 (±4.15)	14.88 (±4.65)	22.81 (±6.06)	1.3 (±0.45)	1.33 (±0.55)	1.87 (±0.69)	24.61 (±5.14)	24.59 (±7.24)	34.88 (±8.46)
8	1.31 (±0.61)	1.28 (±0.64)	1.84 (±0.87)	17.71 (±4.31)	15.19 (±4.64)	23.36 (±6.19)	1.39 (±0.52)	1.43 (±0.6)	2 (±0.78)	25.74 (±5.92)	25.81 (±7.73)	36.56 (±9.32)

throughout the α-values' ranges, i.e. to the amount and location of the local and global minimums of the cost function. The algorithm will have a good performance if the selected centroids lay in the vicinity of the values that generate the global minimum error. But it must be clear that the DCSA cannot ensure that the obtained shaping knots' coefficients correspond to a global minimum. It is possible that the α-value that generates the global minimum error measurement is inconveniently close to values that generate relatively high errors. If, for example, $\alpha=0.72$ generate the minimum error, but $\alpha=0.2$ generates a lower error than $\alpha=0.8$, the algorithm will search for the best coefficient value in the vicinity of *0.2*, never checking *0.72*. This problem arises mostly during the first iteration. Increasing the number of working values per iteration will also increase the chances to end up with the global minimum error, but the processing time will also increase significantly.

The PRSA possesses similar problems regarding local minimum errors and it is entirely dependent on the initial set of α-values chosen to run the algorithm. In general, the PRSA has a probability of having poor performance when applied only over one curve, because the chances of getting stuck in a local minimum that generates high errors are higher than when calculating the errors over more than one curve. If several curves are used, when a specific curve achieves a poor local minimum with some set of parameters, the error produced in the other curves might make the parameters change until the process leaves that specific local-minimum region in that curve. At the end, although it is likely that the final parameters will generate an error different from the global minimum, it is unlikely that they generate high errors and undesired curve shapes. After comparing the results between the PRSA and the DCSA in similar conditions, relatively low differences were spotted between the error performances of both algorithms, which suggests that the concept behind the PRSA is not far from being truth, i.e. the curves can be adjusted to fit better a given reference curve just by slightly moving the shaping-knots.

Regarding the time performance of the algorithms, the differences are much more evident and significant. *Method 2* and *Method 6* were both implemented in MATLAB and had all the same settings except for the used search algorithm, so it is suitable to make a comparison. While the method running the DCSA needed more than 12 hours per exercise, the one running the PRSA needed 16 hours to complete the whole set of 26 exercises. It is expected that if the methods are implemented in other programing language (e.g. C++) the process will be done faster, but the big differences between the two algorithms will persist. Regarding the

FCSSA, because it revises the error for a much higher amount of α-values than the DCSA, it is evident that the difference in the processing time between the two of them is also extremely high, making the FCSSA completely inconvenient when the amount of curves to be analyzed increases. With this in mind, it is clearer that, although the DCSA delivers slightly better results than the PRSA, they are not very significant compared to the improvements in processing time brought by the PRSA. Table 22 shows a simple summary regarding the difference between the search algorithms.

Although the error-performance of the PRSA was good, the time needed by the algorithm is still relatively high, thus there is still some room for improvement in this regard. The reduction of the number of curves fed to the search algorithm done in *Method 8* resulted in a reduction of the overall processing time, but also affected slightly the performance of the algorithm. Additionally, if the number of clusters increases, the processing time needed to go through all of them will become again an issue. Model-based cost-minimization algorithms could be an option, but because of the difficulty to obtain the complete model and the complexity of the model itself (mostly related to the piece-wise manner of interpolation of the points and the complexity of the interpolation method) the solution would be far from trivial and difficult to formulate and implement.

Evaluation with familiar data

All the previously presented methods were evaluated again with respect to the data of the selected subject, but this time the gait parameters of each one of the cycles were taken as input pairs for the radial-basis selection of reference gait parameters (WS_{norm} and *cad*), which ultimately decides which set of α-values should be used in each shaping knot. This differs from the previous evaluations, where the performance was done by comparing the curves inside their groups, and not by mapping the respective walking speed and cadence to obtain the corresponding set of shaping knots coefficients utilizing the radial-basis selection. Since this section is related only to the shaping knots' calculation, the original characteristic points of the subject's curves were used for the regeneration of the trajectories that are utilized to compute the error measurements and correlation between reference and reconstructed curves. Table 23 shows the average values of MAE, SDAE, RMSE and correlation coefficients (R) for each one of the methods:

As expected, the best results were achieved with the methods that fed all the curves to the search algorithms, whereas the worst ones were gotten from the method that used the reference curves from the literature. Surprisingly, the method using the averaged time-warped curves with the DCSA had one of the best performances in the knee joint. From the methods that used the experimental data, the one that presented the worst results (in both joints) was *Method 3*, differing from the initial results shown in Table 21. It is also important to compare the results from *Method 6* and *Method 7*, which, although only slightly, presented a better performance for the method that grouped the cycles by walking speed and cadence. This

Table 22 Comparison between search algorithms

Search algorithm	Amount of checked α-values	Processing time	Error-performance
FCSSA	++++++++++	☹☹☹☹☹☹☹	☺☺☺☺☺
DCSA	+++	☹☹	☺☺☺☺
PRSA	+**	☺	☺☺☺☺

** The number of values checked by the algorithm is dependent on the curves and the initial α-values, but the resulting processing times suggest that it is much lower than the one from DCSA

Table 23 **Shaping-knots evaluation comparing the generated curves yielded by all the methods with respect to the selected subject's original curves**

Method	HIP							
	Position				Velocity			
	AR (±SD)	ARMSE (±SD) [deg]	AMAE (±SD) [deg]	ASDAE (±SD) [deg]	AR (±SD)	ARMSE (±SD) [deg/s]	AMAE (±SD) [deg/s]	ASDAE (±SD) [deg/s]
1	0.994 (±0.007)	2.1 (±1.05)	1.5 (±0.75)	1.46 (±0.76)	0.994 (±0.007)	24.52 (±11.4)	18.57 (±8.6)	15.95 (±7.73)
2	0.996 (±0.006)	1.62 (±0.92)	1.17 (±0.64)	1.12 (±0.68)	0.996 (±0.006)	19.58 (±9.64)	15.05 (±7.13)	12.48 (±6.67)
3	0.994 (±0.009)	1.88 (±1.1)	1.36 (±0.78)	1.3 (±0.79)	0.994 (±0.009)	20.46 (±9.76)	15.76 (±7.22)	12.99 (±6.78)
4	0.994 (±0.01)	1.87 (±1.03)	1.35 (±0.73)	1.29 (±0.74)	0.994 (±0.01)	20.59 (±8.82)	15.93 (±6.44)	12.99 (±6.23)
5	0.994 (±0.009)	1.86 (±0.97)	1.34 (±0.7)	1.28 (±0.69)	0.994 (±0.009)	21.6 (±9.04)	16.62 (±6.67)	13.74 (±6.31)
6	0.995 (±0.008)	1.74 (±0.99)	1.25 (±0.71)	1.2 (±0.72)	0.995 (±0.008)	20.49 (±10.12)	15.7 (±7.51)	13.11 (±6.97)
7	0.995 (±0.008)	1.71 (±0.99)	1.23 (±0.7)	1.18 (±0.72)	0.995 (±0.008)	20.34 (±10)	15.53 (±7.3)	13.07 (±7.02)
8	0.995 (±0.008)	1.79 (±1.06)	1.3 (±0.77)	1.23 (±0.75)	0.995 (±0.008)	20.77 (±10.08)	15.91 (±7.45)	13.3 (±6.98)

Method	KNEE							
	Position				Velocity			
	AR (±SD)	ARMSE (±SD) [deg]	AMAE (±SD) [deg]	ASDAE (±SD) [deg]	AR (±SD)	ARMSE (±SD) [deg/s]	AMAE (±SD) [deg/s]	ASDAE (±SD) [deg/s]
1	0.989 (±0.007)	3.44 (±1.01)	2.42 (±0.68)	2.43 (±0.8)	0.989 (±0.007)	41.25 (±14.65)	32.11 (±11.63)	25.81 (±9.37)
2	0.996 (±0.003)	1.83 (±0.76)	1.29 (±0.51)	1.3 (±0.59)	0.996 (±0.003)	29.38 (±13.25)	21.23 (±9.25)	20.21 (±9.81)
3	0.996 (±0.004)	2.04 (±0.83)	1.45 (±0.57)	1.43 (±0.63)	0.996 (±0.004)	33.6 (±15.06)	24.02 (±10.59)	23.34 (±11.17)
4	0.996 (±0.003)	1.84 (±0.72)	1.3 (±0.49)	1.29 (±0.56)	0.996 (±0.003)	30.22 (±13.18)	21.69 (±9.05)	20.97 (±9.89)
5	0.996 (±0.003)	1.93 (±0.7)	1.39 (±0.48)	1.33 (±0.55)	0.996 (±0.003)	32.09 (±13.47)	23.66 (±9.56)	21.6 (±9.81)
6	0.996 (±0.004)	1.91 (±0.76)	1.35 (±0.51)	1.35 (±0.6)	0.996 (±0.004)	31.42 (±13.46)	22.77 (±9.41)	21.54 (±10.01)
7	0.996 (±0.003)	1.88 (±0.73)	1.32 (±0.48)	1.33 (±0.57)	0.996 (±0.003)	31.26 (±13.45)	22.65 (±9.34)	21.44 (±10.04)
8	0.995 (±0.004)	2.05 (±0.82)	1.44 (±0.55)	1.45 (±0.63)	0.995 (±0.004)	33.42 (±14.3)	24.15 (±9.98)	23 (±10.62)

appears to be a more natural selection for grouping than the one that does it by exercise.

Fig. 68 shows the plots of the position MAE in both joints with respect to the normalized walking speed for three of the methods. It can be seen that, in all cases, the highest errors for the hip joint were located in the high and low walking speeds, with most of the errors from the medium velocities located below the average errors. However, it must be taken into consideration that the ranges of motion normally increase with the walking speed, hence higher errors are expected in high speeds even if the generated trajectories are relatively close to the original ones. With this in mind, higher errors in low speeds imply higher differences between the original and the reconstructed curves with respect to the range of motion than in medium and high speeds. In the case of the knee, the errors seem to be more evenly distributed throughout all the walking speed range. Fig. 69 shows the position and velocity MAE histograms of the method that scored better in error-performance (*Method 2*).

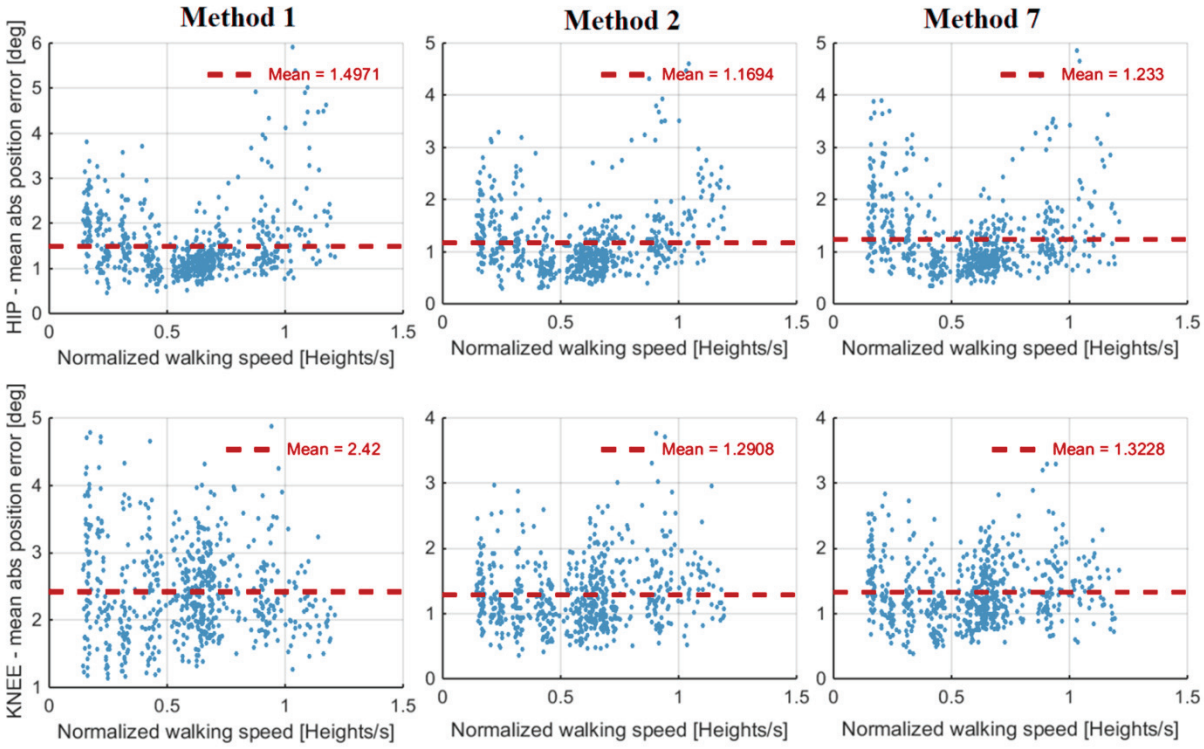

Fig. 68 MAE vs normalized walking speed: comparing the shaping knots' performance with respect to the selected subject's data

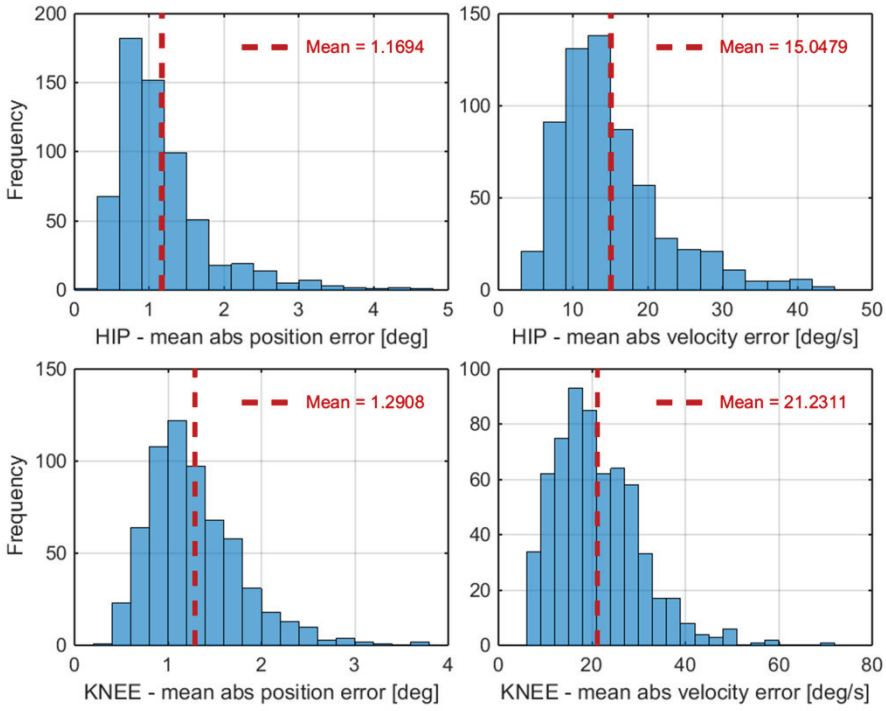

Fig. 69 MAE histogram for *Method 2*: comparing the shaping knots' performance with respect to the selected subject data

Evaluation with unfamiliar data

The same evaluation was done using the processed gait cycles from all the subjects that participated in the experiment (different from the selected one). This second evaluation gives

some insight on the inter-subject behavior of the trajectories' shape governed by the shaping points. Table 24 shows the performance of each method in this evaluation.

As expected, deterioration in the performance can be seen compared to Table 23, due to the fact that the previous evaluation was done using the curves that were used, to some extent, during the training process of the methods. In this case, not only the data were not used during the training, but also they belong to different subjects. One important fact to remark is the improvement of *Method 1* with respect to the other methods. As before, the best results for both joints were accomplished with *Method 2*.

The plots of the position MAE in both joints with respect to the normalized walking speed for three of the methods are depicted in Fig. 70. Although the highest errors for the hip joint are again located in the high and low walking speeds, the distribution of errors is more even than before. In the case of the knee, on the other hand, the highest errors are evidently present in the lowest walking speed for all methods, unlike the previous results. Again, the position and velocity MAE histograms of *Method 2* are shown in Fig. 71.

Table 24 Shaping-knots evaluation comparing the generated curves yielded by all the methods with respect to original curves of all subjects

Method	HIP							
	Position				Velocity			
	AR (±SD)	ARMSE (±SD) [deg]	AMAE (±SD) [deg]	ASDAE (±SD) [deg]	AR (±SD)	ARMSE (±SD) [deg/s]	AMAE (±SD) [deg/s]	ASDAE (±SD) [deg/s]
1	0.987 (±0.016)	2.7 (±1.55)	1.97 (±1.13)	1.83 (±1.09)	0.987 (±0.016)	24.36 (±11.9)	18.75 (±9.09)	15.45 (±7.94)
2	0.987 (±0.016)	2.66 (±1.49)	1.96 (±1.09)	1.8 (±1.04)	0.987 (±0.016)	24.05 (±11.26)	18.62 (±8.61)	15.12 (±7.55)
3	0.986 (±0.018)	2.76 (±1.54)	2.02 (±1.13)	1.87 (±1.09)	0.986 (±0.018)	24.72 (±11.33)	19.22 (±8.78)	15.45 (±7.49)
4	0.984 (±0.02)	2.85 (±1.59)	2.07 (±1.16)	1.95 (±1.12)	0.984 (±0.02)	24.82 (±10.46)	19.26 (±7.95)	15.56 (±7.13)
5	0.984 (±0.019)	2.81 (±1.51)	2.06 (±1.11)	1.89 (±1.05)	0.984 (±0.019)	25.24 (±10.36)	19.64 (±7.9)	15.76 (±7.04)
6	0.986 (±0.017)	2.7 (±1.5)	2.01 (±1.12)	1.8 (±1.02)	0.986 (±0.017)	24.02 (±11.16)	18.59 (±8.51)	15.1 (±7.52)
7	0.986 (±0.018)	2.72 (±1.53)	2.02 (±1.14)	1.81 (±1.05)	0.986 (±0.018)	24.1 (±11.29)	18.65 (±8.57)	15.16 (±7.64)
8	0.986 (±0.019)	2.77 (±1.6)	2.06 (±1.2)	1.84 (±1.09)	0.986 (±0.019)	24.46 (±11.68)	18.92 (±8.97)	15.39 (±7.79)

Method	KNEE							
	Position				Velocity			
	AR (±SD)	ARMSE (±SD) [deg]	AMAE (±SD) [deg]	ASDAE (±SD) [deg]	AR (±SD)	ARMSE (±SD) [deg/s]	AMAE (±SD) [deg/s]	ASDAE (±SD) [deg/s]
1	0.989 (±0.016)	3.08 (±1.92)	2.05 (±1.19)	2.29 (±1.54)	0.989 (±0.016)	35.92 (±14.23)	26.6 (±10.06)	23.98 (±10.6)
2	0.989 (±0.014)	2.97 (±1.53)	2.04 (±0.94)	2.15 (±1.25)	0.989 (±0.014)	38.23 (±15.14)	28.67 (±11.17)	25.11 (±10.82)
3	0.988 (±0.017)	3.12 (±1.6)	2.15 (±0.97)	2.24 (±1.3)	0.988 (±0.017)	42.05 (±17.58)	31.23 (±12.49)	27.97 (±13)
4	0.989 (±0.014)	3 (±1.54)	2.05 (±0.93)	2.17 (±1.27)	0.989 (±0.014)	40.22 (±16.71)	29.66 (±11.61)	26.98 (±12.6)
5	0.988 (±0.015)	3.06 (±1.56)	2.13 (±0.96)	2.18 (±1.27)	0.988 (±0.015)	39.97 (±15.58)	30.17 (±11.58)	26.05 (±11.01)
6	0.989 (±0.015)	3.01 (±1.55)	2.08 (±0.95)	2.15 (±1.26)	0.989 (±0.015)	39.1 (±15.34)	29.45 (±11.25)	25.54 (±11.04)
7	0.989 (±0.014)	3.02 (±1.57)	2.09 (±0.96)	2.17 (±1.28)	0.989 (±0.014)	39.65 (±15.71)	29.75 (±11.54)	26.04 (±11.25)
8	0.988 (±0.015)	3.11 (±1.57)	2.16 (±0.97)	2.22 (±1.28)	0.988 (±0.015)	40.93 (±16.31)	30.77 (±12.05)	26.82 (±11.59)

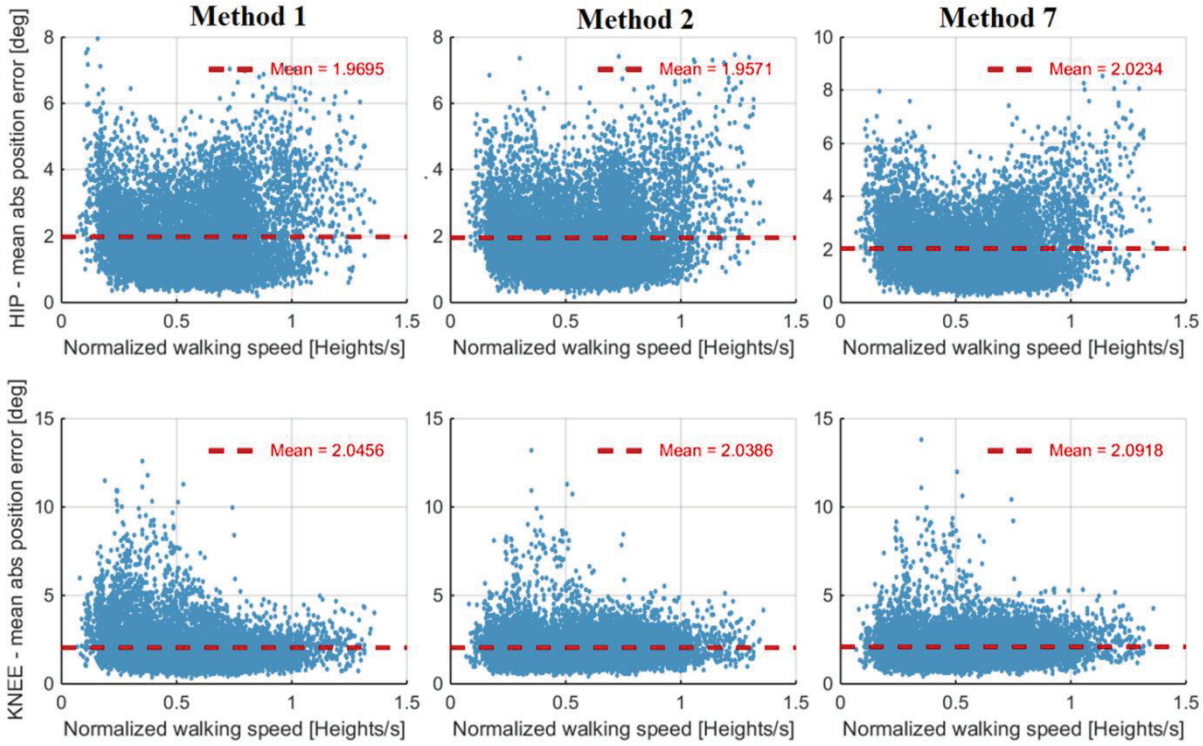

Fig. 70 MAE vs normalized walking speed: comparing the shaping knots' performance with respect to the data from all the subjects

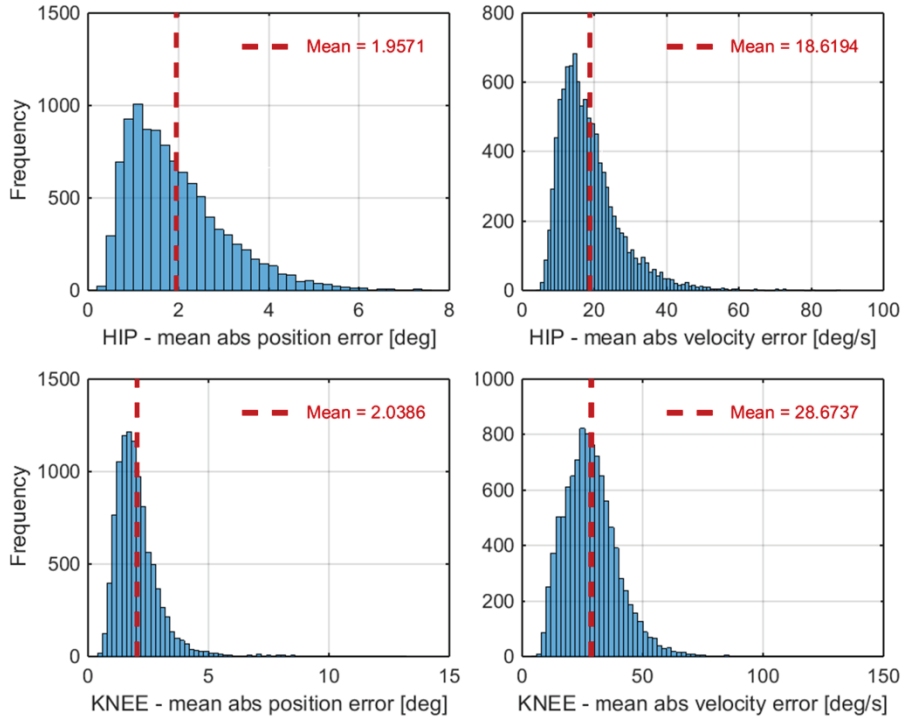

Fig. 71 MAE histogram for *Method 2*: comparing the shaping knots' performance with respect to the data from all the subjects

4.3.4 Evaluation of the trajectory generation process

This final evaluation combines the results of the automatic estimation of characteristic points and the calculation of the shaping knot's coefficients presented in the previous sections. The last evaluations presented in section 4.3.3 were done using the original characteristic knots from the processed cycles. Now, the curves will be generated with the characteristic points delivered by the neural networks (trained with the data of the selected subject), using the original gait parameters of each cycle as inputs for the NNs and for the radial-basis selector used to get the α-values of the shaping points. As explained previously, to avoid an ill behavior of the NNs, the inputs must lay inside the perimeter depicted in Fig. 40. In this case, many of the original gait parameters from the processed cycles lay outside this perimeter. For this evaluation, if the original WS_{norm} and/or *cad* are higher/lower than the limit, they will be replaced by the closest limit values before being used as inputs for the estimation process.

As it was done before, the evaluation is divided in two: using only the data from the selected subject and using the data from all the other subjects. For completeness, all the methods developed for the acquisition of the shaping-knots' coefficients were taken into account for the evaluation. Table 25 shows the results obtained after comparing the generated curves and the original curves from the selected subject. The method with better performance was again *Method 2* for both joints. The worst results in knee were seen again with *Method 1*, but surprisingly its performance for the hip joint was very close to the methods that didn't use all the curves during the training. Regarding *Method 2*, although a worsening in the results can be seen with respect to Table 23, the performance of the overall generation (characteristic and shaping knots) is still very good for the hip joint, with an average MAE of 1.67°. In the case of the knee, a more visible deterioration in the performance can be spotted, with an average MAE of 2.39°. Taking into account the results from the previous section, it is evident that the cause of such worsening is the characteristic points' predictability issues in this joint.

To have a better insight of the performance of *Method 2* using the estimated characteristic knots, the reference gait parameters of this method (centroids) were used to regenerate some sample curves (left plot in Fig. 72). All the trajectories, in both joints, had a healthy-like appearance except for two in the hip joint, which corresponded to exercises *P2-2* and *P2-3* (black and magenta curves in the figure, respectively). Because of this, it was decided to make an adjustment to the method in the region corresponding to these two exercises. The methods that reported better performance in the previous evaluations (namely *Method 6* and *Method 7*) were analyzed in this region. In the case of *P2-2*, the resulting curve using the coefficients from *Method 6* yielded a healthy-like curve; hence the hip α-values from *Method 2* for this exercise were replaced by the ones from *Method 6*. For exercise *P2-3*, both *Method 6* and *Method 7* yielded similar undesired curve shapes. Therefore, it was decided to avoid these coefficients from the generation, i.e. the centroid from exercise *P2-3* was removed from the radial-basis selection. Finally, the resulting adjusted method, referred as *Method 2**, was also evaluated. The right plot in Fig. 72 shows the curves generated with *Method 2**, depicting with a black and magenta lines the curves corresponding to the centroids from exercises *P2-2* and *P2-3*. An improvement in the trajectories' shapes with respect to the left plot is evident. Table 25 also shows the results after using *Method 2**.

Fig. 73 shows the plots of the position MAE in both joints with respect to the normalized walking speed for three of the methods. Although the hip error distribution shows a higher contribution from the low and high walking speeds, the difference is not very visible as in the previous section's evaluation. The knee, on the other hand, keeps showing a more even distribution of errors throughout the walking speed, although the high speeds report slightly

Table 25 **Trajectory generation evaluation comparing the generated curves yielded by all the methods with respect to the selected subject's original curves**

Method	HIP							
	Position				Velocity			
	AR (±SD)	ARMSE (±SD) [deg]	AMAE (±SD) [deg]	ASDAE (±SD) [deg]	AR (±SD)	ARMSE (±SD) [deg/s]	AMAE (±SD) [deg/s]	ASDAE (±SD) [deg/s]
1	0.994 (±0.006)	2.34 (±0.89)	1.88 (±0.74)	1.37 (±0.56)	0.994 (±0.006)	25.19 (±10.66)	19.49 (±8.17)	15.87 (±7.14)
2	0.996 (±0.004)	2.02 (±0.83)	1.67 (±0.72)	1.12 (±0.48)	0.996 (±0.004)	20.43 (±8.91)	16.12 (±6.84)	12.5 (±5.89)
3	0.994 (±0.008)	2.24 (±1)	1.82 (±0.81)	1.28 (±0.65)	0.994 (±0.008)	21.03 (±8.6)	16.56 (±6.41)	12.91 (±5.96)
4	0.992 (±0.01)	2.35 (±1.01)	1.9 (±0.81)	1.36 (±0.65)	0.992 (±0.01)	21.83 (±8.14)	17.34 (±6.19)	13.21 (±5.51)
5	0.993 (±0.008)	2.27 (±0.92)	1.84 (±0.74)	1.3 (±0.6)	0.993 (±0.008)	22.45 (±8.46)	17.62 (±6.43)	13.86 (±5.73)
6	0.996 (±0.005)	2.1 (±0.82)	1.73 (±0.71)	1.17 (±0.49)	0.996 (±0.005)	20.99 (±9.29)	16.52 (±7.13)	12.88 (±6.17)
7	0.995 (±0.005)	2.13 (±0.84)	1.75 (±0.72)	1.18 (±0.52)	0.995 (±0.005)	21.11 (±9.53)	16.57 (±7.27)	13.02 (±6.37)
8	0.995 (±0.006)	2.21 (±0.91)	1.81 (±0.77)	1.24 (±0.56)	0.995 (±0.006)	21.62 (±9.42)	16.98 (±7.21)	13.34 (±6.28)
2*	0.996 (±0.004)	2.01 (±0.83)	1.66 (±0.72)	1.11 (±0.48)	0.975 (±0.016)	20.17 (±9.04)	15.93 (±6.95)	12.34 (±5.96)

Method	KNEE							
	Position				Velocity			
	AR (±SD)	ARMSE (±SD) [deg]	AMAE (±SD) [deg]	ASDAE (±SD) [deg]	AR (±SD)	ARMSE (±SD) [deg/s]	AMAE (±SD) [deg/s]	ASDAE (±SD) [deg/s]
1	0.987 (±0.01)	4.11 (±1.26)	3.25 (±1)	2.49 (±0.87)	0.987 (±0.01)	43.98 (±15.58)	34.5 (±12.46)	27.16 (±9.88)
2	0.993 (±0.008)	2.94 (±1.11)	2.39 (±0.91)	1.68 (±0.73)	0.993 (±0.008)	32.54 (±14.03)	24.04 (±10.1)	21.82 (±10.13)
3	0.992 (±0.008)	3.09 (±1.12)	2.5 (±0.91)	1.78 (±0.75)	0.992 (±0.008)	36.71 (±15.72)	26.78 (±11.22)	24.96 (±11.51)
4	0.993 (±0.008)	2.95 (±1.1)	2.4 (±0.9)	1.69 (±0.72)	0.993 (±0.008)	33.51 (±14.35)	24.57 (±10.3)	22.68 (±10.4)
5	0.993 (±0.008)	3.01 (±1.09)	2.44 (±0.89)	1.73 (±0.71)	0.993 (±0.008)	34.91 (±14.36)	25.97 (±10.44)	23.22 (±10.29)
6	0.993 (±0.008)	2.98 (±1.1)	2.41 (±0.9)	1.71 (±0.72)	0.993 (±0.008)	34.25 (±14.12)	25.17 (±10.09)	23.11 (±10.31)
7	0.993 (±0.008)	2.99 (±1.09)	2.43 (±0.9)	1.72 (±0.72)	0.993 (±0.008)	34.55 (±14.47)	25.43 (±10.37)	23.26 (±10.52)
8	0.992 (±0.008)	3.09 (±1.14)	2.49 (±0.92)	1.79 (±0.76)	0.992 (±0.008)	36.38 (±15.32)	26.75 (±11.15)	24.52 (±10.95)
2*	0.993 (±0.008)	2.95 (±1.11)	2.39 (±0.91)	1.69 (±0.73)	0.977 (±0.022)	32.6 (±14)	24.1 (±10.08)	21.85 (±10.11)

lower errors than the low and medium speeds. Fig. 74 shows the position and velocity MAE histograms of the method that scored better in error-performance (*Method 2**).

Table 26 presents the results after comparing the generated curves with the curves from all the other participants. As expected, due to the inter-subject variability, a considerable worsening in the performance can be seen, mostly caused by the prediction of the characteristic points. Surprisingly, *Method 1* yielded the best results in the knee joint; in the hip joint all the methods scored similarly. These results also sustain the decision of using the curves of only one subject with high predictability to train the estimators of the curve points' parameters. They bring also one discussion to the table: the correlation coefficients calculated from the samples of two curves should not be used to evaluate the performance of trajectory

generation. Note that high values of *R* were accomplished in all cases, even when the error measurements were considerably high.

Fig. 75 shows the plots of the position MAE in both joints with respect to the normalized walking speed for three of the methods. The error distribution is even throughout the range of walking speed for the hip and knee joints, except for *Method 1* that shows an evident distribution of high errors for the low velocities. The similarity in the scattering of the errors in all plots also exhibits that the highest contribution of errors is made by the characteristic

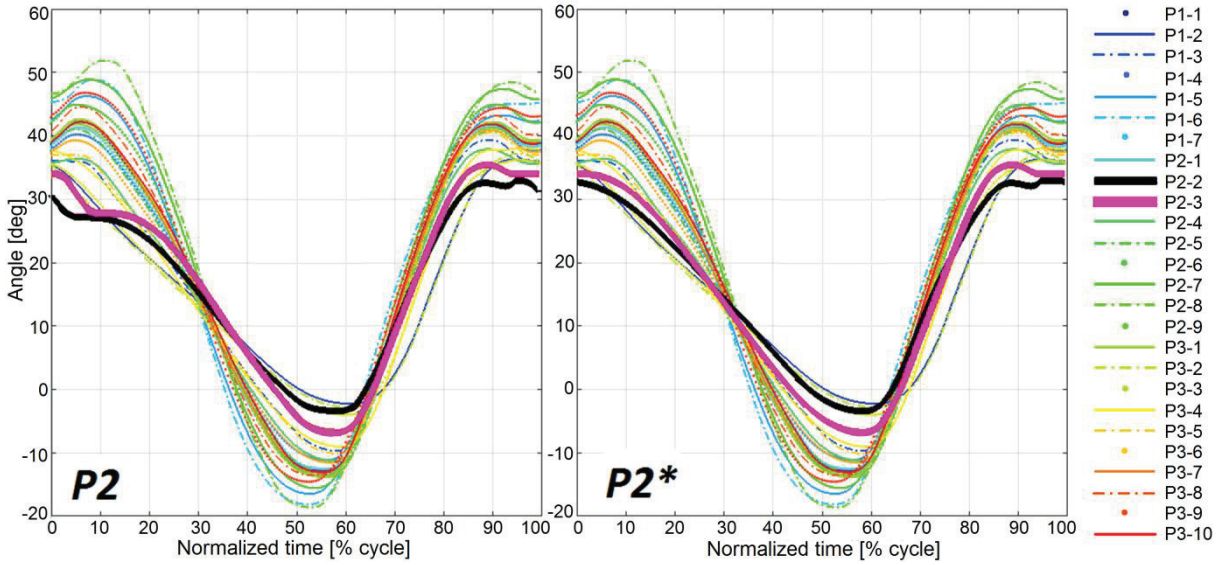

Fig. 72 Generation of trajectories using the centroids of *Method 2* as input gait parameters for the characteristic point's estimation and shaping knots' coefficients calculation using *Method 2* and *Method 2**.

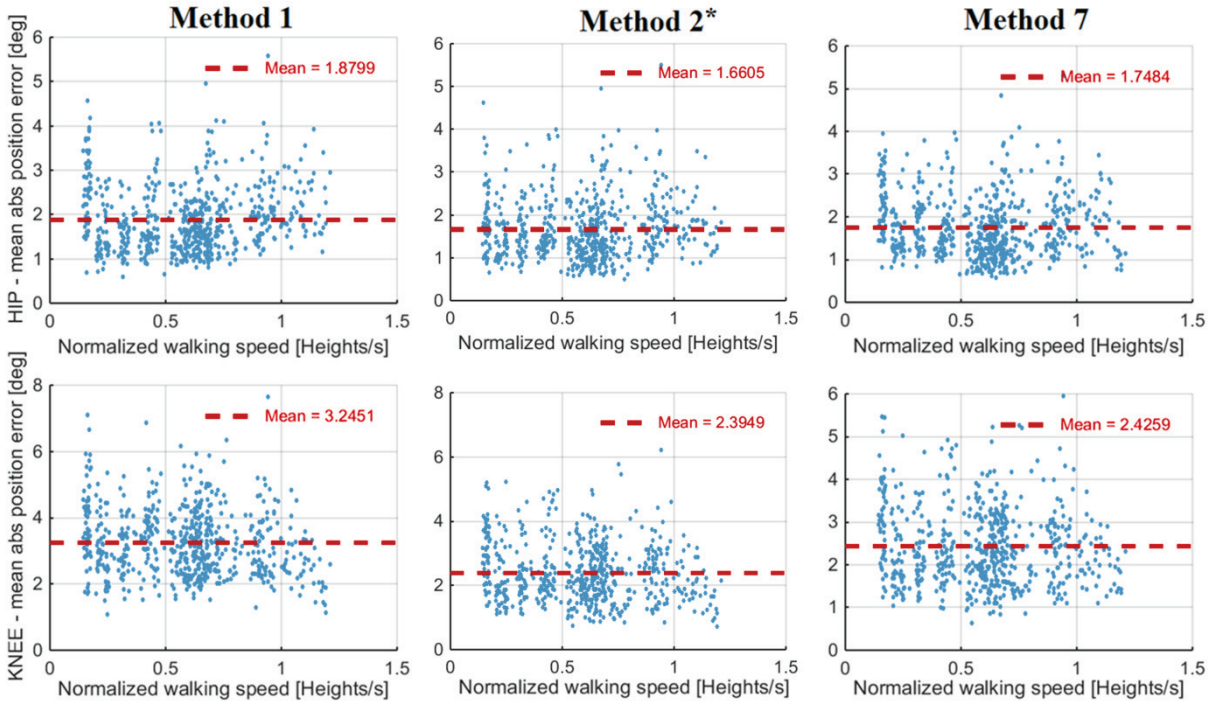

Fig. 73 MAE vs normalized walking speed: comparing the trajectory generator performance with respect to the selected subject's data

knots estimation, and not by the shaping-knots coefficients calculation, mostly in the medium and high walking speeds. Fig. 76 shows the position and velocity MAE histograms of *Method 2**.

Table 26 Trajectory generation evaluation comparing the generated curves yielded by all the methods with respect to original curves of all subjects

Method	HIP							
	Position				Velocity			
	AR (±SD)	ARMSE (±SD) [deg]	AMAE (±SD) [deg]	ASDAE (±SD) [deg]	AR (±SD)	ARMSE (±SD) [deg/s]	AMAE (±SD) [deg/s]	ASDAE (±SD) [deg/s]
1	0.98 (±0.027)	6.76 (±2.65)	5.85 (±2.47)	3.31 (±1.23)	0.98 (±0.027)	32.47 (±11.62)	26.58 (±9.83)	18.51 (±6.78)
2	0.98 (±0.026)	6.71 (±2.63)	5.81 (±2.43)	3.28 (±1.25)	0.98 (±0.026)	32.18 (±11.5)	26.23 (±9.68)	18.53 (±6.71)
3	0.979 (±0.028)	6.79 (±2.65)	5.87 (±2.44)	3.34 (±1.27)	0.979 (±0.028)	32.72 (±11.53)	26.69 (±9.72)	18.81 (±6.72)
4	0.975 (±0.031)	6.99 (±2.7)	6.06 (±2.49)	3.41 (±1.29)	0.975 (±0.031)	33.21 (±10.96)	27.06 (±9.05)	19.14 (±6.69)
5	0.977 (±0.029)	6.89 (±2.69)	5.95 (±2.49)	3.39 (±1.29)	0.977 (±0.029)	32.59 (±10.48)	26.55 (±8.63)	18.79 (±6.42)
6	0.98 (±0.027)	6.72 (±2.63)	5.81 (±2.43)	3.3 (±1.25)	0.98 (±0.027)	32.04 (±11.49)	26.16 (±9.73)	18.35 (±6.66)
7	0.98 (±0.027)	6.73 (±2.64)	5.82 (±2.45)	3.31 (±1.25)	0.98 (±0.027)	32.14 (±11.61)	26.22 (±9.78)	18.46 (±6.8)
8	0.98 (±0.027)	6.7 (±2.64)	5.79 (±2.44)	3.3 (±1.25)	0.98 (±0.027)	32.38 (±11.53)	26.39 (±9.72)	18.64 (±6.74)
2*	0.98 (±0.027)	6.73 (±2.63)	5.83 (±2.43)	3.3 (±1.26)	0.944 (±0.042)	32.04 (±11.62)	26.1 (±9.77)	18.45 (±6.77)

Method	KNEE							
	Position				Velocity			
	AR (±SD)	ARMSE (±SD) [deg]	AMAE (±SD) [deg]	ASDAE (±SD) [deg]	AR (±SD)	ARMSE (±SD) [deg/s]	AMAE (±SD) [deg/s]	ASDAE (±SD) [deg/s]
1	0.97 (±0.028)	8.12 (±3.07)	6.69 (±2.65)	4.52 (±1.8)	0.97 (±0.028)	55.74 (±19.46)	44.26 (±15.75)	33.69 (±12.27)
2	0.962 (±0.034)	8.49 (±2.88)	7.06 (±2.49)	4.65 (±1.7)	0.962 (±0.034)	61.16 (±22.25)	47.03 (±17.62)	38.9 (±14.41)
3	0.96 (±0.034)	8.61 (±2.91)	7.18 (±2.52)	4.69 (±1.7)	0.96 (±0.034)	64.66 (±23.84)	48.94 (±18.19)	42.02 (±16.35)
4	0.961 (±0.034)	8.51 (±2.89)	7.07 (±2.49)	4.66 (±1.7)	0.961 (±0.034)	63.14 (±23.13)	47.83 (±17.8)	41 (±15.66)
5	0.96 (±0.035)	8.58 (±2.86)	7.13 (±2.47)	4.7 (±1.69)	0.96 (±0.035)	62.11 (±22.55)	48.39 (±18.09)	38.76 (±14.29)
6	0.961 (±0.034)	8.52 (±2.89)	7.09 (±2.49)	4.66 (±1.7)	0.961 (±0.034)	60.48 (±21.8)	46.91 (±17.49)	37.99 (±13.82)
7	0.961 (±0.034)	8.49 (±2.88)	7.06 (±2.48)	4.65 (±1.7)	0.961 (±0.034)	60.81 (±21.97)	47.05 (±17.55)	38.34 (±14.04)
8	0.96 (±0.035)	8.58 (±2.9)	7.13 (±2.5)	4.7 (±1.71)	0.96 (±0.035)	62.2 (±22.67)	48.15 (±18.14)	39.19 (±14.39)
2*	0.962 (±0.034)	8.49 (±2.88)	7.06 (±2.49)	4.65 (±1.7)	0.935 (±0.062)	61.2 (±22.23)	47.06 (±17.61)	38.94 (±14.39)

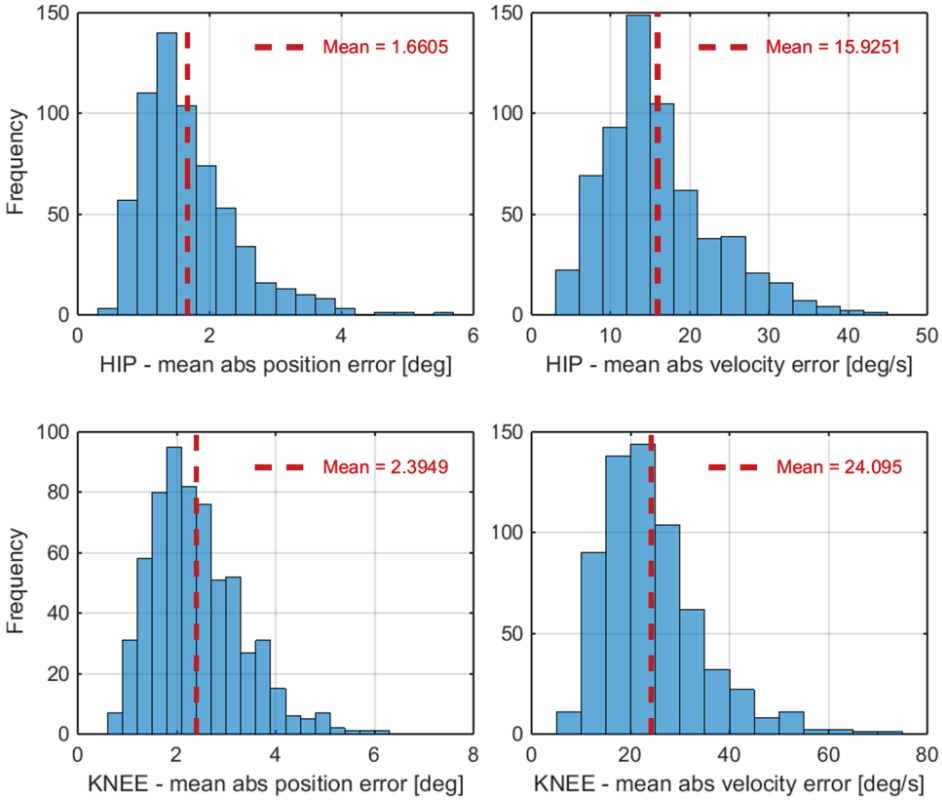

Fig. 74 MAE histogram for *Method 2**: comparing the trajectory generator performance with respect to the selected subject's data

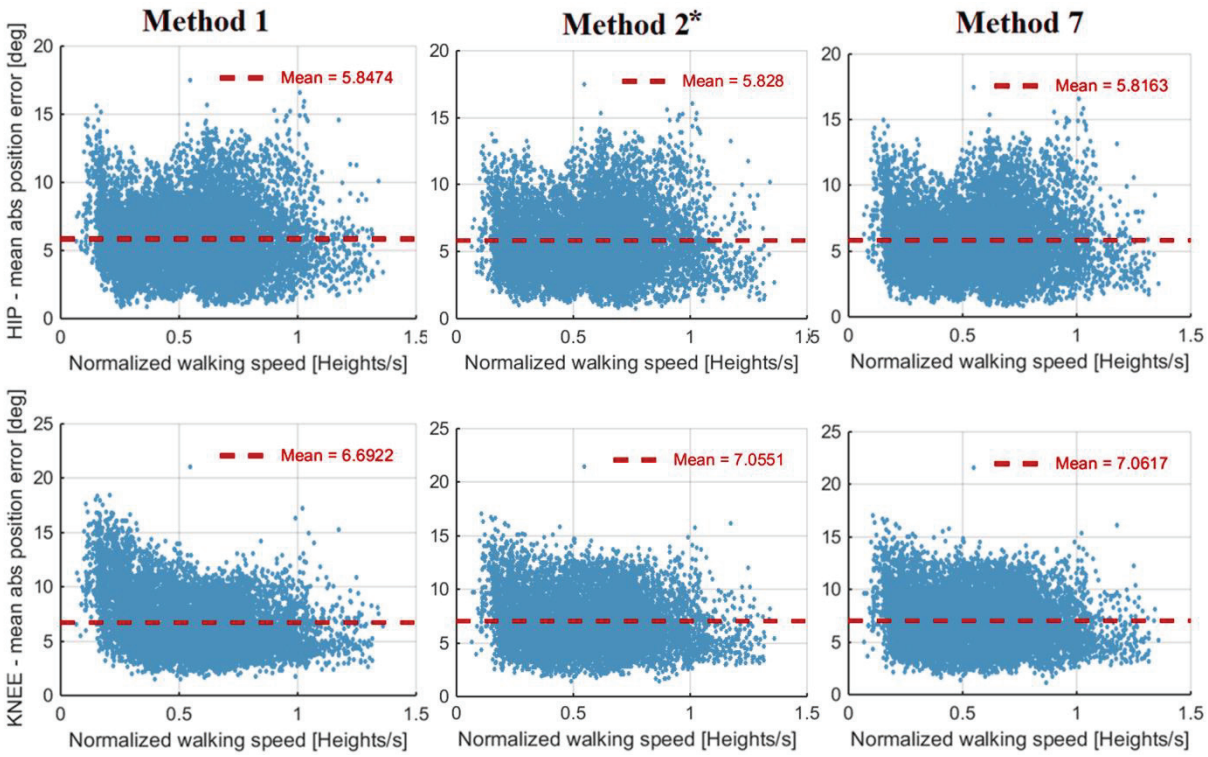

Fig. 75 MAE vs normalized walking speed: comparing the trajectory generator performance with respect to the data from all the subjects

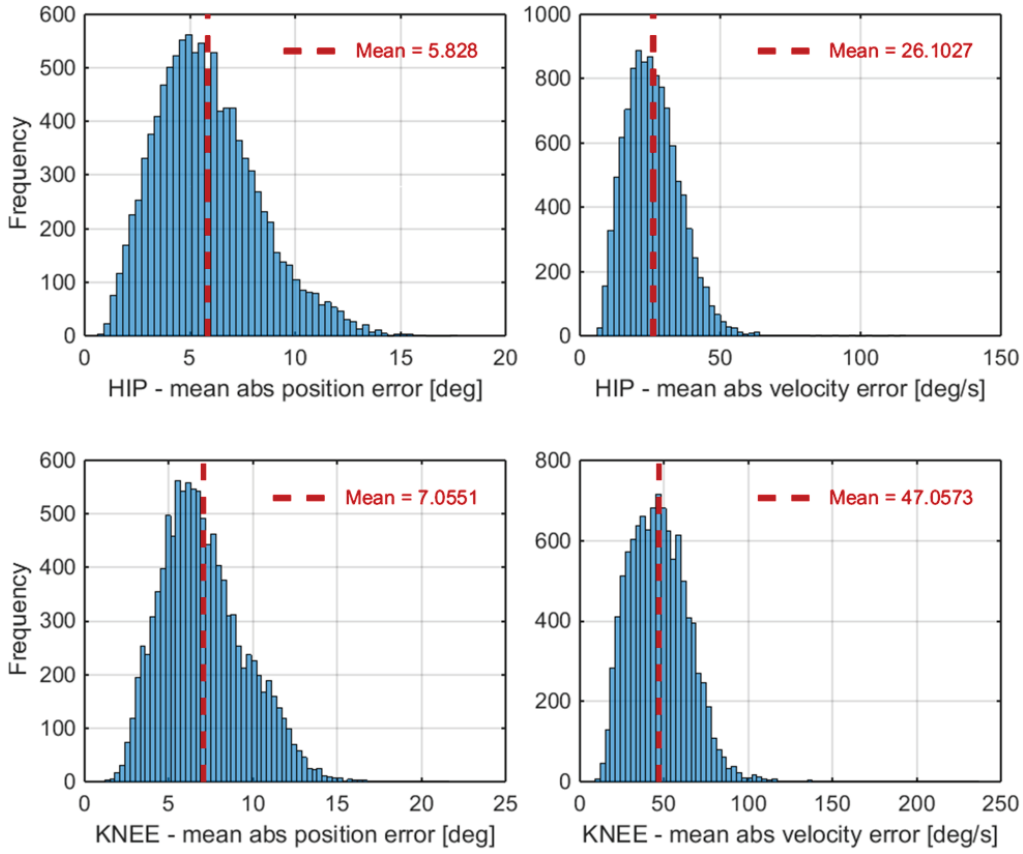

Fig. 76 MAE histogram for *Method 2**: comparing the shaping knots' performance with respect to the data from all the subjects

All in all, it is evident that the best method to calculate the coefficients of the shaping points throughout all the evaluations was *Method 2**. Hence, the resulting α-values from this method are the ones used in the final version of the trajectory generator, although the option to change this selection if preferred could be also given. Fig. 77 shows some examples of curves that were generated using the characteristic points predicted by the NNs and the resulting shaping knots' coefficients from *Method 2**. The inputs pairs for the generator were sets of WS_{norm} and *cad* that, although lying inside the perimeter shown in Fig. 40 (section 4.3.2), are located in a region where no training data were present, in order to evaluate the behavior of the trajectory generator in such circumstances. Likewise, a comparison between some examples of regenerated curves and some original curves from the selected subject, as well as from the other subjects, are depicted in Fig. 78 (hip) and Fig. 79 (knee). For these examples, 12 different sets of input gait parameters were selected to generate the trajectories. Two original curves, one extracted from the processed data of the selected subject and the other one from the data of the other subjects, with approximately the same values of WS_{norm} and *cad* are also shown in each one of the plots. Table 27 shows the information related to each one of the original trajectories depicted in the figure, including the exercise, leg, WS_{norm} and *cad*. Table 28 shows the MAE, SDAE, RMSE and correlation coefficients computed between the original curves and the generated ones.

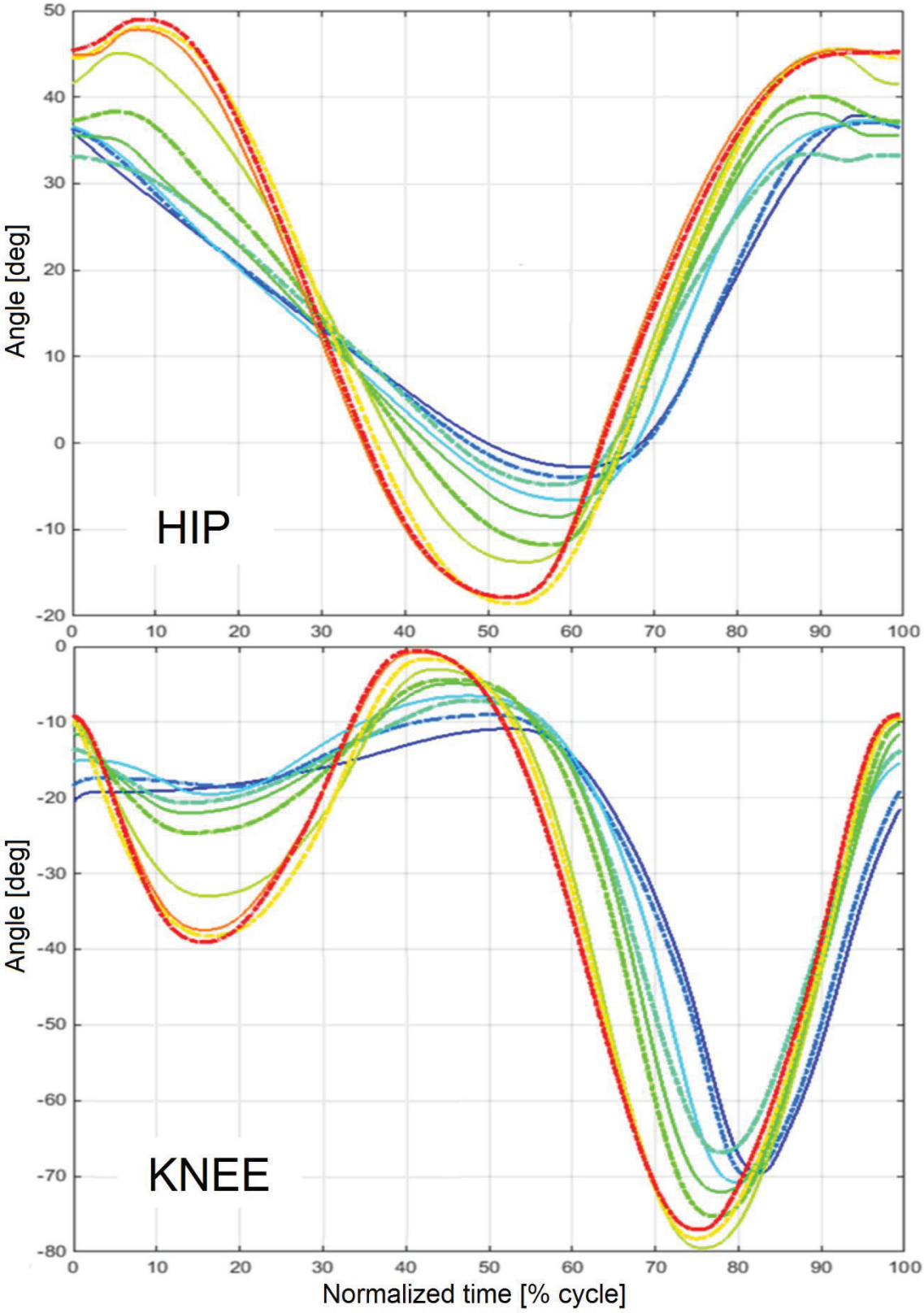

	WS_{norm}	Cad
	0.15	34
	0.19	42
	0.25	52
	0.275	65

	WS_{norm}	Cad
	0.375	70
	0.5	80
	0.775	100
	0.95	110

	WS_{norm}	Cad
	1.05	125
	1.15	130

WS_{norm} in heights/s
Cad in steps/min

Fig. 77 Examples of generation of trajectories using the NNs for the characteristic point's estimation and the resulting α-values from *Method 2**

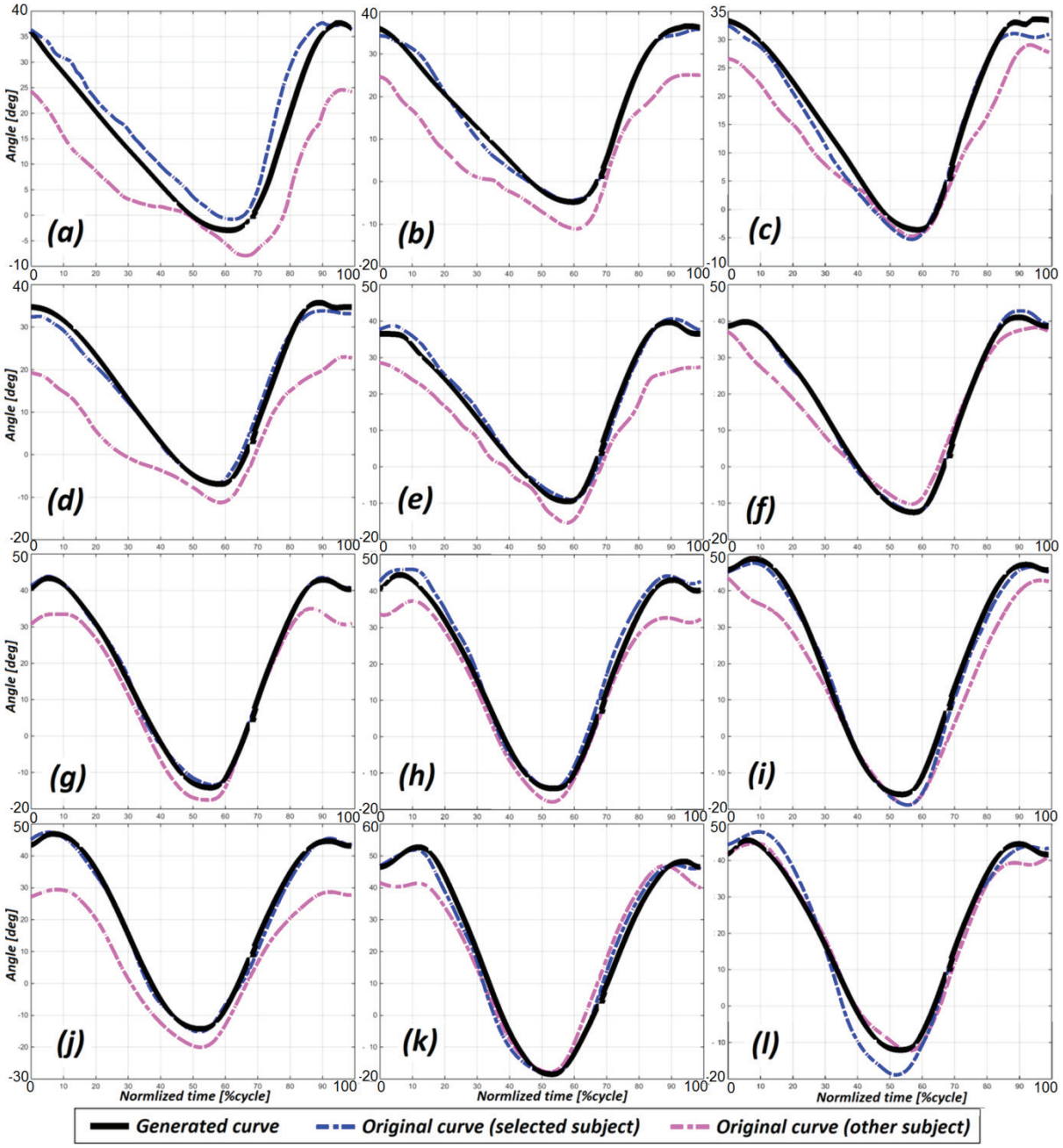

Fig. 78 Examples of regenerated and original hip trajectories for different set of input gait parameters

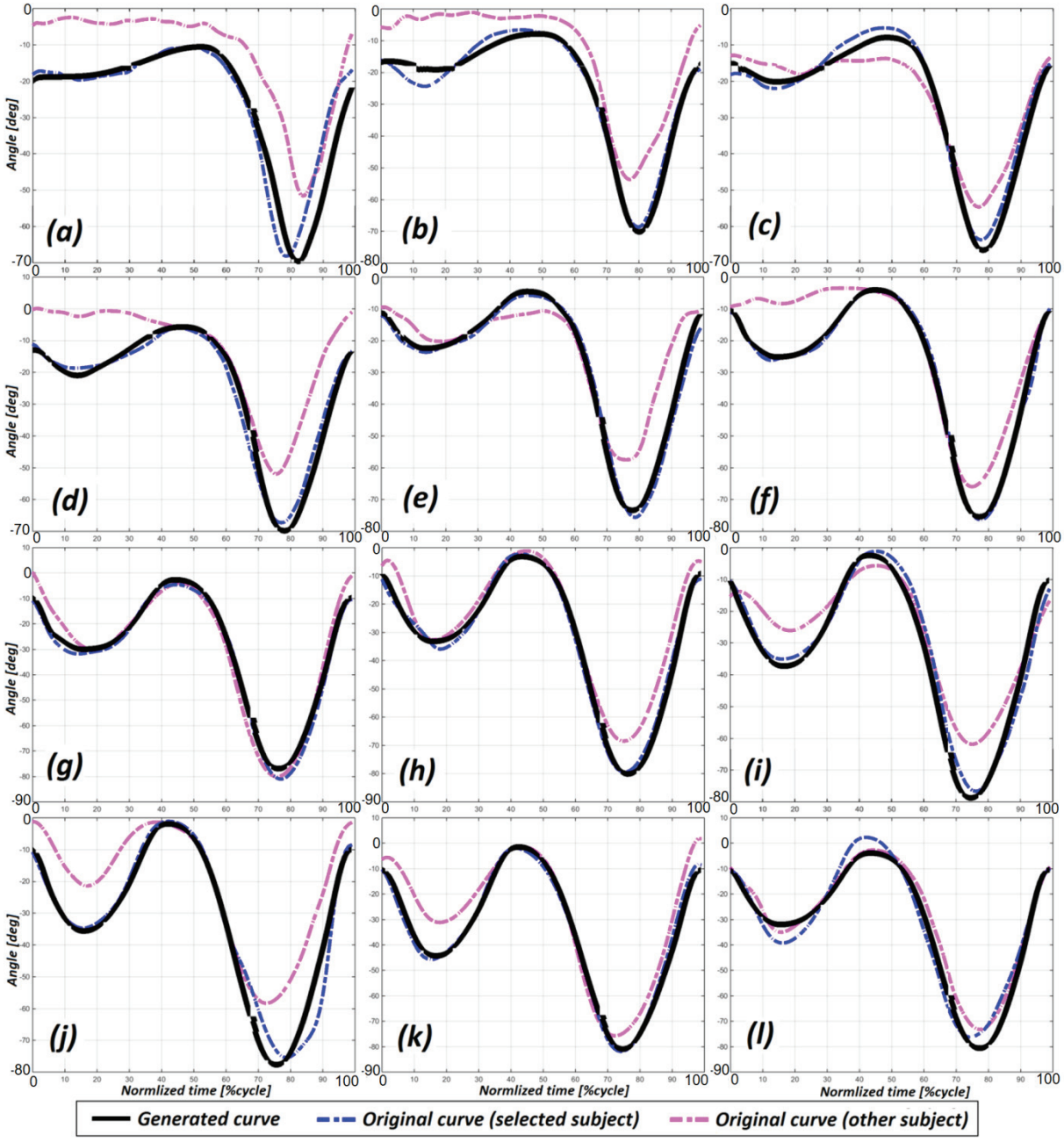

Fig. 79 Examples of regenerated and original knee trajectories for different set of input gait parameters

Table 27 Gait parameters of the original trajectories in Fig. 78 and Fig. 79

Fig	Subject	Ex.	Leg	Cycle Period [s]	Cadence [steps/min]	Step Length[m]	Normalized Step Length [heights]	Walking speed[m/s]	Normalized walking speed [heights/s]
(a)	selected	P3-2	left	3.4	35.29	0.467	0.27	0.27	0.158
	1	P3-2	left	3.4	35.29	0.440	0.27	0.26	0.157
(b)	selected	P3-3	right	2.43	49.32	0.476	0.27	0.39	0.225
	1	P3-3	left	2.434	49.3	0.450	0.27	0.37	0.222
(c)	selected	P2-2	right	1.93	62.08	0.415	0.24	0.43	0.247
	12	P3-4	right	1.935	62.02	0.360	0.24	0.38	0.248
(d)	selected	P2-3	right	1.84	65.15	0.483	0.28	0.52	0.301
	13	P3-4	right	1.841	65.18	0.510	0.29	0.56	0.314
(e)	selected	P1-3	right	1.68	71.26	0.581	0.33	0.69	0.397
	10	P3-5	right	1.685	71.22	0.610	0.34	0.73	0.403
(f)	selected	P3-6	left	1.5	80.16	0.650	0.37	0.87	0.499
	9	P3-6	left	1.498	80.11	0.750	0.39	1.00	0.525
(g)	selected	P3-1	left	1.28	93.75	0.698	0.4	1.09	0.627
	14	P2-6	left	1.28	93.75	0.790	0.44	1.24	0.684
(h)	selected	P3-8	right	1.12	106.76	0.704	0.4	1.25	0.720
	8	P1-5	right	1.123	106.86	0.830	0.45	1.48	0.793
(i)	selected	P2-7	right	1.16	103.9	0.823	0.47	1.42	0.819
	9	P2-8	right	1.155	103.9	0.990	0.52	1.71	0.896
(j)	selected	P3-9	right	1.00	120.24	0.872	0.5	1.75	1.005
	13	P1-6	right	0.999	120.12	0.840	0.47	1.67	0.941
(k)	selected	P2-8	left	1.09	109.99	0.910	0.52	1.67	0.959
	14	P2-8	right	1.092	109.89	1.070	0.59	1.96	1.082
(l)	selected	P1-6	right	0.94	128.07	0.800	0.46	1.71	0.982
	11	P3-8	left	1.09	110.09	0.760	0.41	1.40	0.754

Table 28 Comparison between the generated and original trajectories in Fig. 78 and Fig. 79

		HIP				KNEE			
Fig	Sub.	MAE [deg]	SDAE [deg]	RMSE [deg]	R	MAE [deg]	SDAE [deg]	RMSE [deg]	R
(a)	sel.	3.47	2.16	4.08	0.987	3.64	4.71	5.93	0.944
	1	9.22	4.92	10.44	0.961	13.49	5.24	14.47	0.967
(b)	sel.	1.04	0.88	1.36	0.996	2.01	1.47	2.48	0.991
	1	9.33	3.20	9.86	0.987	11.33	4.7	12.26	0.971
(c)	sel.	1.70	0.93	1.93	0.995	2.09	1.2	2.41	0.993
	12	5.02	2.93	5.81	0.989	4.86	3.42	5.93	0.975
(d)	sel.	2.06	1.42	2.50	0.989	2.09	1.73	2.70	0.992
	13	11.54	5.31	12.69	0.956	12.6	8.62	15.25	0.904
(e)	sel.	1.46	0.78	1.66	0.997	1.87	1.31	2.28	0.995
	10	7.63	3.38	8.34	0.992	6.89	7.06	9.84	0.936
(f)	sel.	0.61	0.52	0.8	0.999	0.99	1.07	1.45	0.998
	9	4.18	3.08	5.18	0.98	7.79	6.39	10.05	0.951
(g)	sel.	0.62	0.45	0.76	0.999	1.91	1.24	2.28	0.998
	14	4.86	3.00	5.70	0.993	3.54	2.78	4.49	0.985
(h)	sel.	2.18	1.37	2.57	0.998	1.82	1.02	2.09	0.996
	8	4.64	2.88	5.46	0.995	5.53	4.75	7.27	0.986
(i)	sel.	1.86	1.29	2.27	0.997	3.16	2.34	3.93	0.987
	9	6.37	3.97	7.49	0.989	7.75	5.00	9.21	0.977
(j)	sel.	1.30	1.00	1.64	0.998	3.11	3.84	4.93	0.978
	13	11.87	4.71	12.76	0.996	11.04	7.43	13.29	0.956
(k)	sel.	2.31	1.86	2.96	0.994	1.82	1.32	2.24	0.996
	14	5.47	3.36	6.41	0.973	7.14	5.09	8.76	0.968
(l)	sel.	3.38	2.42	4.15	0.994	4.22	2.61	4.95	0.979
	11	2.15	1.50	2.62	0.994	3.45	2.91	4.51	0.994

Finally, a comparison between the input (desired) gait parameters and the ones resulting from the generated joint trajectories was done. Twenty-five equidistant values of normalized walking speed between the input limits were selected to feed the generator. For each one of these values, five corresponding equidistant values of cadence, also inside the limiting perimeter, were also selected. Therefore, a total of 125 input pairs were used to generate the hip and knee trajectories for the analysis. Subsequently, the walking speed resulting from these trajectories was calculated using the anthropometric features of all the participants following (12) and (13), in order to evaluate the relation between the desired walking speed and the output one, given a desired cadence. Two different calculations were done: using the $f_s(FD)$ of each subject with the corresponding subject's height and leg segments' lengths; and using the f_s from the selected subject (which is the default in the final application) together with the anthropometric features of each one of the subjects. Table 29 shows the anthropometric measurements of each one of the subjects, as well as the correlation coefficients between the input and output walking speeds using the individual *fs* of each subject and the default *fs*. It also shows the coefficients of the 1st degree polynomials that relate the input and output speeds, given as

$$WS_O = WS_I \cdot \beta_1 + \beta_0, \tag{31}$$

where WS_O is the walking speed resulting from the generated trajectories, WS_I is the input walking speed, and β_0 and $\beta_1$are the polynomial coefficients. Ideally, $\beta_0=0$ and $\beta_1=1$. Fig. 80 depicts some examples of the relation between the input and output speeds. In these examples, the default f_S was used, and the upper right and lower plots correspond to the subjects with the minimum, median and maximum height from the set of participants.

4.3.5 Limitations

The experiment and data processing are not free of limitations that affect the results obtained from them. First of all, the recording setup based on IMUs may introduce some

Table 29 Comparison between the input and output walking speeds

				Individual fs(FD)			Default fs(FD)		
Sub.	**Height [m]**	**Upper-leg Length [m]**	**Lower-leg Length [m]**	**R**	**βo**	**β1**	**R**	**βo**	**β1**
sel.	1.74	0.4	0.48	0.9961	-0.0007	1.0002	0.9961	-0.0007	1.0002
1	1.67	0.38	0.5	0.9961	0.0540	0.9920	0.9964	0.0017	1.0569
2	1.74	0.42	0.48	0.9925	-0.1388	1.2747	0.9960	-0.0101	1.0398
3	1.92	0.465	0.555	0.9962	0.0270	1.0379	0.9954	-0.0791	1.2466
4	1.73	0.415	0.505	0.9963	0.0098	1.0566	0.9960	-0.0195	1.1057
5	1.65	0.42	0.49	0.9962	0.0460	0.9324	0.9960	-0.0149	1.1255
6	1.72	0.48	0.55	0.9939	-0.0244	1.0645	0.9953	-0.0859	1.4133
7	1.68	0.47	0.48	0.9960	0.0227	1.0956	0.9957	-0.0344	1.1871
8	1.86	0.46	0.58	0.9962	0.0374	1.0543	0.9954	-0.0925	1.3587
9	1.91	0.47	0.57	0.9961	0.0447	1.0431	0.9953	-0.0930	1.3141
10	1.8	0.425	0.535	0.9961	0.0475	0.9913	0.9959	-0.0405	1.1712
11	1.86	0.41	0.545	0.9961	-0.0012	1.0030	0.9961	-0.0357	1.1308
12	1.52	0.37	0.445	0.9961	0.0318	1.0091	0.9963	0.0248	0.9844
13	1.78	0.41	0.525	0.9958	-0.0352	1.1773	0.9961	-0.0262	1.1215
14	1.81	0.445	0.52	0.9945	0.0041	1.0178	0.9957	-0.0443	1.1638
15	1.72	0.43	0.52	0.9963	0.0004	1.1120	0.9959	-0.0355	1.1901
16	1.68	0.37	0.495	0.9963	0.0394	0.9961	0.9964	0.0088	1.0171
17	1.65	0.385	0.505	0.9961	0.0543	1.0217	0.9963	-0.0030	1.0944
Average				0.9957	0.0122	1.0489	0.9959	-0.0322	1.1512

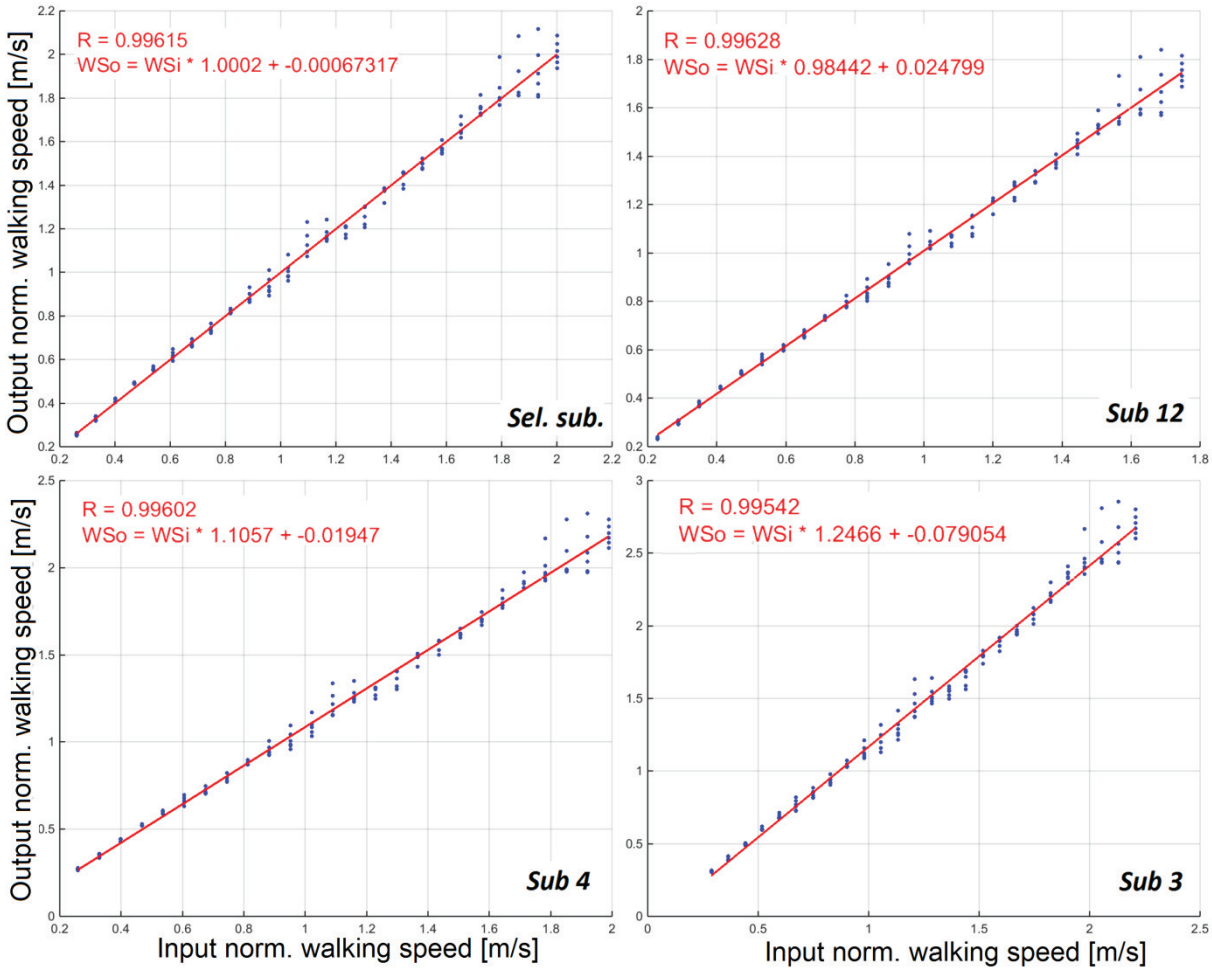

Fig. 80 Examples of output walking speed vs input walking speed

measurement errors. Some of the problems that arise from the usage of the selected IMUs include drifting and relatively low accuracy. Other issues concern the location of the sensors in the legs. For intra-subject experiment consistency, the placement of the sensors must be the same for all subjects. Moreover, to obtain the correct angle measurements, the axis of rotation of the sensors must be parallel to the joint axis of rotation. Bearing these two facts in mind, the impossibility of manually placing the sensor in the perfect position will introduce some errors to the measurements. It must be noticed as well that this experiment didn't take into account the rotation of the trunk during walking, due to the fact that the needed measurement of the hip angles where with respect to the transverse plane and not to the trunk segment. Other applications could need these measurements, thus for these cases, the inclination of the trunk must be included in the measurement process. The aforementioned problems can be reduced by using more sophisticated motion sensor systems (e.g. commercial marker-based motion systems), although this would increase considerably the complexity of the experimental setup and the costs of the study.

Other limitations are related to number of subjects that participated in the study. Increasing the number of participants, as well as their diversity regarding personal and anthropometric characteristics, will lead to more significant results. The inclusion of subjects that cover a higher spectrum of heights, weights and ages will give better insights on the prediction problem (mostly regarding ages, due to the fact that most of the target patients are elderly people). Similarly, a second limitation in the study concept is associated with the selected gait parameters used for the predictors. As explained at the beginning of this section

(4.3), there exist other personal parameters that have shown a degree of influence in the motion of the hip and knee joints during walking, namely gender and age. Including these two features as input parameters for the study and generation process might increase the predictability scores.

The data processing is also not free of limitations. Several assumptions were taken during the cycles' segmentation and the extraction of gait parameters and characteristic knots. The first one is regarding the step length of each cycle, or more specifically, the estimation of the step length for each one of the subjects. It was assumed that the relation between the covered distance by the foot and the actual step length, obtained from *Ex2*, is the same for all exercises. Additionally, the cycle segmentation was done based on the horizontal displacement of the foot and not on the foot contact with the floor. Using the exact moment of heel contact to segment the cycles might improve the predictability of the time parameters of the characteristic points. The drifting correction might have also introduced some errors in the angular processed values. This correction was done with the assumption that the gait patterns does not change considerably during an exercise. In the cases where the subjects made adjustments in their pattern during the execution of one exercise, the drifting correction process will compensate for inexistent drifting. This issue is not very crucial in this case due to the fact that the trajectories that (seemingly) presented high drifting were not included in the study's data processing and the correction in the remaining curves was minimal, but it must be taken into account during the evaluation of the prediction. Another cause of errors is the inexact measurement of the body segments, which is used in the computation of the step lengths and, consequently, affects all the prediction process. Finally, the study and prediction process is very susceptible to the extraction of the characteristic knots from the experimental data. An ill selection of these points, or the presence of unexpected behavior in the joints motion (as seen with the knee joints), will introduce a noisy data set for the training algorithms and will directly affect the prediction, not only of the parameters of the characteristic points, but also the calculation of the shaping knots' coefficients, which are strongly associated with the characteristic points surrounding the shaping points. One example of the bad effects of the wrong selection of characteristic points on the α-values' calculations can be observed in the example curve from Fig. 60, where undesired curve shapes were obtained from *Method 4* and *Method 5*.

The curve shaping though the shaping points is also not free of limitations. Due to the proposed parametrization of the angular and temporal values of the shaping points, and because the search of the shaping points' coefficients is based on the minimization of position and velocity errors (mostly position), the mapping of the desired gait parameters into α-values had to be done in a discrete manner. Moreover, the search process to obtain these α-values resulted to be challenging and very time consuming. Setting the temporal parameters of the shaping points to fixed values could allow the implementation of continues mapping strategies (i.e. regression methods or neural networks) and would reduce significantly the complexity and time-consumption of the angular coefficients search. However, that would yield higher discrepancies between the experimental and regenerated curves. Increasing the number of shaping points would decrease the difference between reference and regenerated curves, although this would increase the complexity of a possible manual adjustment of the shaping points. However, despite these limitations, the current approach resulted in the generation of healthy-like curves as desired.

At last, it is vital to remark that, because of the bad inter-subject predictability of the characteristic points' parameters, only the data from one subject was used in the final implementation of the generator. This was done to avoid the generation of 'averaged' curves lying between walking patterns, or in other words, the generation of curves that minimized the

errors, but might not be really close to real patterns or simply do not reflect properly the walking characteristics of the people that participated in the experiment. However, this decision leads to the usage of reference trajectories that fit a specific person. So, although we make sure these patterns are very close to real healthy patterns, they might differ, considerably or not, from the patient's walking preferences (e.g. the pre-stroke patterns). Nevertheless, this would be an issue, to some extent, even if the data from all the subjects would have been taken into account.

5 Motion control for robot-based gait rehabilitation

This chapter will present the motion control strategies proposed for the *MOPASS* system, which in principle could be partially implemented in other over-ground and treadmill-based rehabilitation devices. Specifically, it will present the motion control of the active joints offered by the *MOPASS* system, namely the hip, knee and pelvis joints, and the platform wheels. The hip and knee are the main joints in the rehabilitation process, hence different control strategies can be implemented on them depending on the mechanical components at hand (e.g. sensors) and the desired therapy strategies and goals. In this case, two approaches are proposed: one for joint reference position tracking and another one for 'assist as needed' therapy. On the other hand, the obtainment and further control of the motion profiles of the mobile platform and pelvis modules must be carried out depending on the motion of the hip and knee joints. Thanks to the rather simple motion profiles of the wheels' and pelvis modules, some straight forward position and velocity controllers were designed.

The motion control of all active joints in *MOPASS* was designed taking into account the built-in controllers from the motor drives, which include all or some of the following operation modes: profiled position, interpolated position, profiled velocity and profiled torque (current). These will be referred to as the low-level controllers, and their explanation is not included in this manuscript. For detailed explanations on the different operation modes and built-in controllers refer to [203] [204] (Elmo servo drives) and [162] (Schunk drives). Because of the access to the already-designed or automatically-designed built-in controllers of the used drives and the impossibility to properly design own controllers inside the drives (e.g. own hard real-time position controllers using the torque/current controllers of the drives), it was decided to design the corresponding motion controllers of *MOPASS* to work together with the drives' built-in controllers in the cases where the latter ones were not sufficient to fulfill the control goals of the therapy.

First, the control strategies proposed for the hip and knee joints, which include position and impedance controllers, are presented, followed by the controllers handling of the motion and control of the mobile platform. Next, the obtainment and control of the motion profiles of the pelvis modules are introduced. Finally, some methods to deal with synchronization between the reference gait patterns and the actual patterns from the patient are presented.

5.1 Therapy control strategies for hip and knee joints

This segment will present two different approaches for control to be used during robot-based gait rehabilitation. The first one is the position control used in the *MOPASS* system during the trials with healthy and impaired subjects. The second approach is an impedance controller developed thinking in an 'assist as needed' and 'patient cooperative' strategy. Although the latter approach was not tested with *MOPASS* due to the lack of a reliable feedback of the user's intention (e.g. torque sensors), it is presented as a 'next step' for the system, backed up by simulations that show the potential performance of the control strategy in real conditions.

5.1.1 Position control

Several approaches for motion control in robotic gait rehabilitation systems possess a stiff position controller in order to make the device track the given reference trajectories with minimal deviations, and therefore assist completely the movement of the patients, as it is the

case of the first version of the *LOKOMAT* system. In the case of the *MOPASS* system, for the hip and knee joints, an impedance-based control scheme was used in combination with the built-in position and velocity controllers of the drives, running in the corresponding Elmo Orocos component in the system. The controller models each one of the joints as a mass-spring-damper system following Newton's second law of motion, yielding the following equation

$$\tau = I \cdot \alpha = K \cdot \Delta\theta + B \cdot \Delta\dot{\theta} + K_i \cdot \int \Delta\theta \cdot dt \ , \tag{32}$$

where τ is the torque present in the joint, I is the virtual inertia of the link connected to the joint, α is the angular acceleration of the link, $\Delta\theta$ and $\Delta\dot{\theta}$ are the position and velocity errors, respectively, and K, B and K_i are the spring, damper and integral coefficients of the system. The influence of K_i is very small, hence it could be neglected leaving a pure mass-spring-damper virtual system. An inertia $I = 1\,[Kg \cdot m^2]$ was defined for the virtual system. Replacing this value in (32) and integrating the angular acceleration one can obtain the link's angular velocity

$$\omega = \int \alpha \cdot dt = \int \left(K \cdot \Delta\theta + B \cdot \Delta\dot{\theta} + K_i \cdot \int \Delta\theta \cdot dt \right) \cdot dt \, . \tag{33}$$

The diagram of the impedance controller of the virtual mass-spring-damper system is shown in Fig. 81. The output of this controller can be now used as the input of the profile velocity controller in the Elmo drives. The selected coefficient values for the controller were $K = 5$, $B = 20$ and $K_i = 0.1$. The open-loop virtual model in Laplace domain is given by

$$\begin{aligned} G_o &= \frac{\theta_{act}}{\Delta\theta} = \frac{\theta_{act}}{e} \\ &= \left(5 \cdot +20 \cdot s + \frac{0.1}{s} \right) \cdot \frac{1}{s^2} \ , \end{aligned} \tag{34}$$

where θ_{act} is the actual joint position and $\Delta\theta = e$ is the position error. The closed loop transfer function would be given by

$$\begin{aligned} G_c &= \frac{G_o}{1 + G_o} \\ &= \frac{200s^2 + 20s + 1}{10s^3 + 200s^2 + 20s + 1} \ , \end{aligned} \tag{35}$$

with poles in (-19.7471), (-0. 2310) and (-0. 0219), and zeros in (-0. 2281) and (-0.0219). As it can be seen, the real part of the poles are negative, therefore the virtual model is stable. The plot of the zeros and poles of the closed-loop system and the step response are shown in Fig. 82 and Fig. 83, respectively.

This approach is useful for lower range of reference trajectories' velocities, which is the particular case in our rehabilitation application. However, due to the nature of the controller and current limits in the motors, the performance of the controller with non-compliant patients and high speed reference trajectories decreases. For this reason a combination of the virtual impedance-based controller with the profiled position controller of the Elmo drives was done. The profiled position controller tries to achieve a given position using some specified acceleration/deceleration and maximum profile velocities; therefore it is a combination of velocity and position control working at a much higher sample frequency than the impedance-based controller running in the *MOPASS* computer. When the impedance-based controller

starts presenting (absolute) position errors higher than a given tolerance, the control switches to the profile position scheme. Once the error returns to lie within the given tolerance, the control switches back to the impedance-based approach.

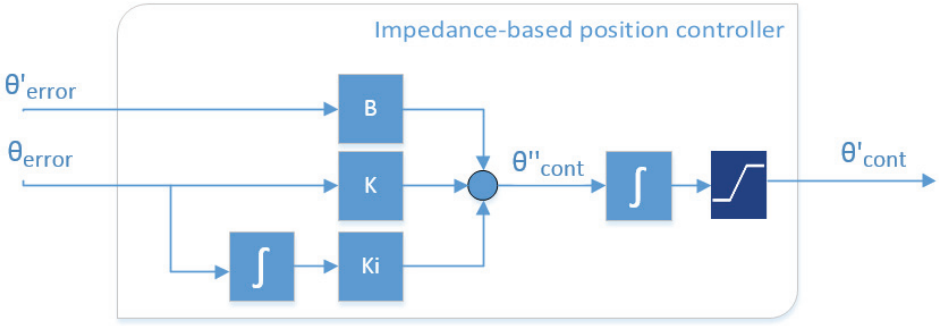

Fig. 81 Diagram of the impedance-based controller

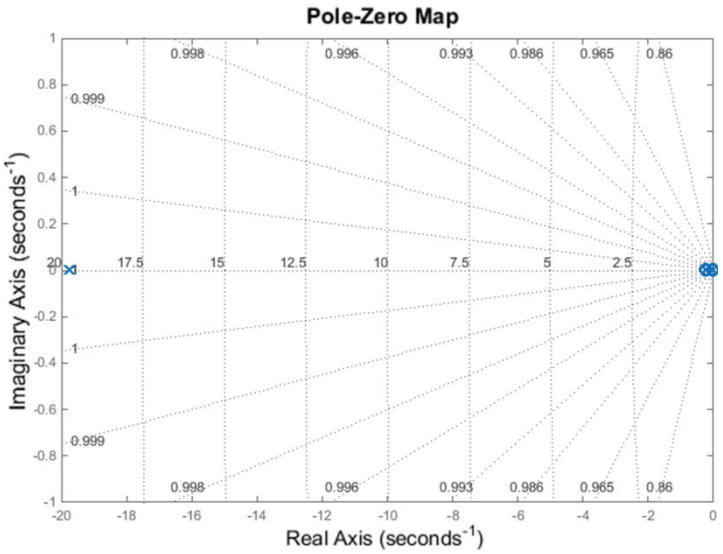

Fig. 82 Poles/Zeros map of the closed loop system

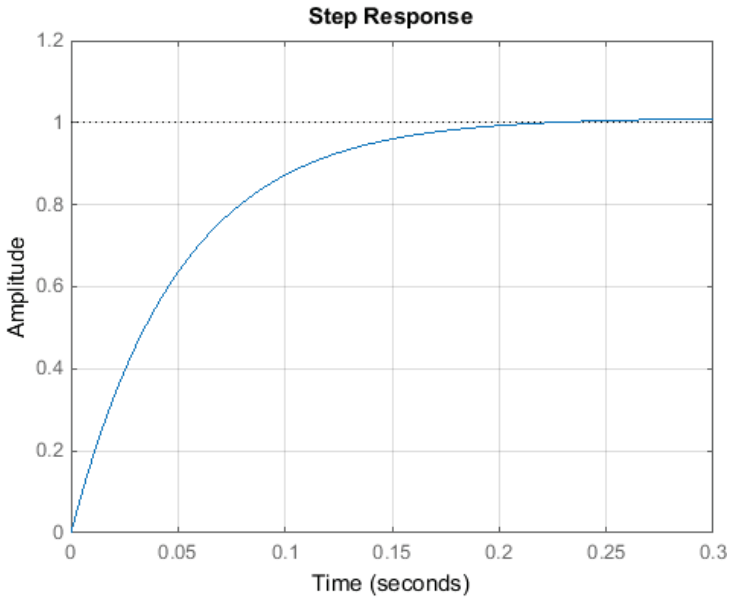

Fig. 83 Step response of the closed loop system

To improve the tracking capabilities of the impedance-based controller, a velocity feed-forward was added to the control scheme. A diagram of the implemented operation is shown in Fig. 84. Note that the controller component supplies the target position and velocity values to the hip and knee joint components (Elmo components), which are in charge of the control process. The reason the profiled position controller is not used always is that it is meant to achieve the target positions with a start-stop operation, causing undesired motions in the joints.

The position control was tested with a compliant healthy subject, i.e. the subject followed the reference trajectories without exerting significant opposition forces to the system that would cause the current limits to be reached. Fig. 85 shows the performance of the position controller using three different values of K_{vfw}, namely 0 (no velocity feed-forward), 0.2 and 0.5. Although the differences between the three plots are not evident, it can be seen that there exists a slight improvement in the tracking, regarding the lag of the actual trajectory with respect to the reference one, with higher velocity feed-forward contributions. However, the higher the feed-forward is, the more susceptible the controller is to the behavior of the velocity of the reference gait patterns, even reaching the point in which the controller barely tries to compensate for the position error and acts more as an open-loop velocity controller, which could result in undesired behaviors leading to poor tracking. Hence, high values of K_{vfw} are not recommended. After several tests, values between 0 and 0.2 yielded good results.

The controller was also tested during the clinical trials of the system with impaired patients. For these trials, no velocity feed-forward was introduced. Fig. 86 shows the performance of the controller with a compliant patient. Although the controller managed to track the trajectories successfully when the patients were capable to follow the reference walking patterns, patients with higher impairment levels often exerted forces into the system higher than the ones the joint motors were able to compensate, resulting in the motors working with the current limits unable to fulfill the low-level controller targets. This problem also happened during tests with healthy subjects that forced their personal walking pattern instead of following the suggested one. Even though this is not a problem of the controller but of the power limitations of the joint motors, it resulted in poor tracking, uncomfortable walking and desynchronization between reference and actual gait patterns. More details about this problem will be exposed in section 5.4.

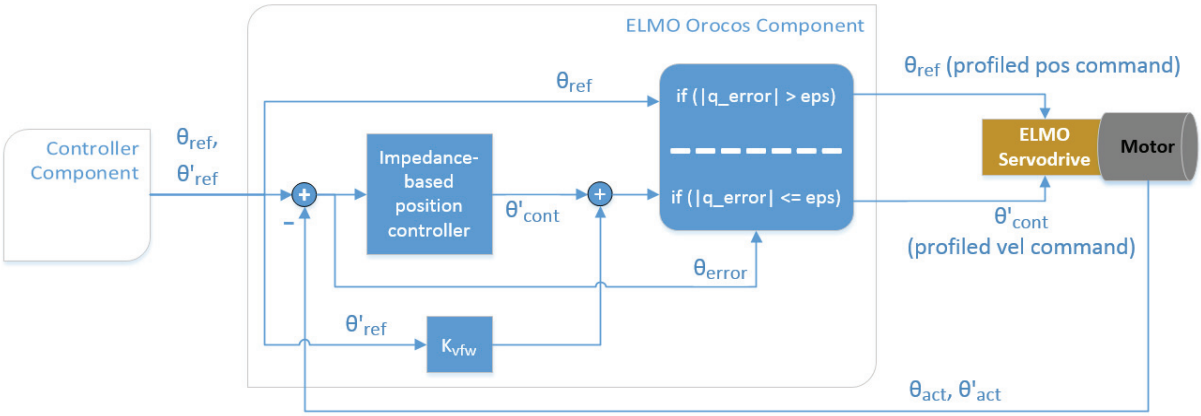

Fig. 84 Position control scheme for hip and knee joints

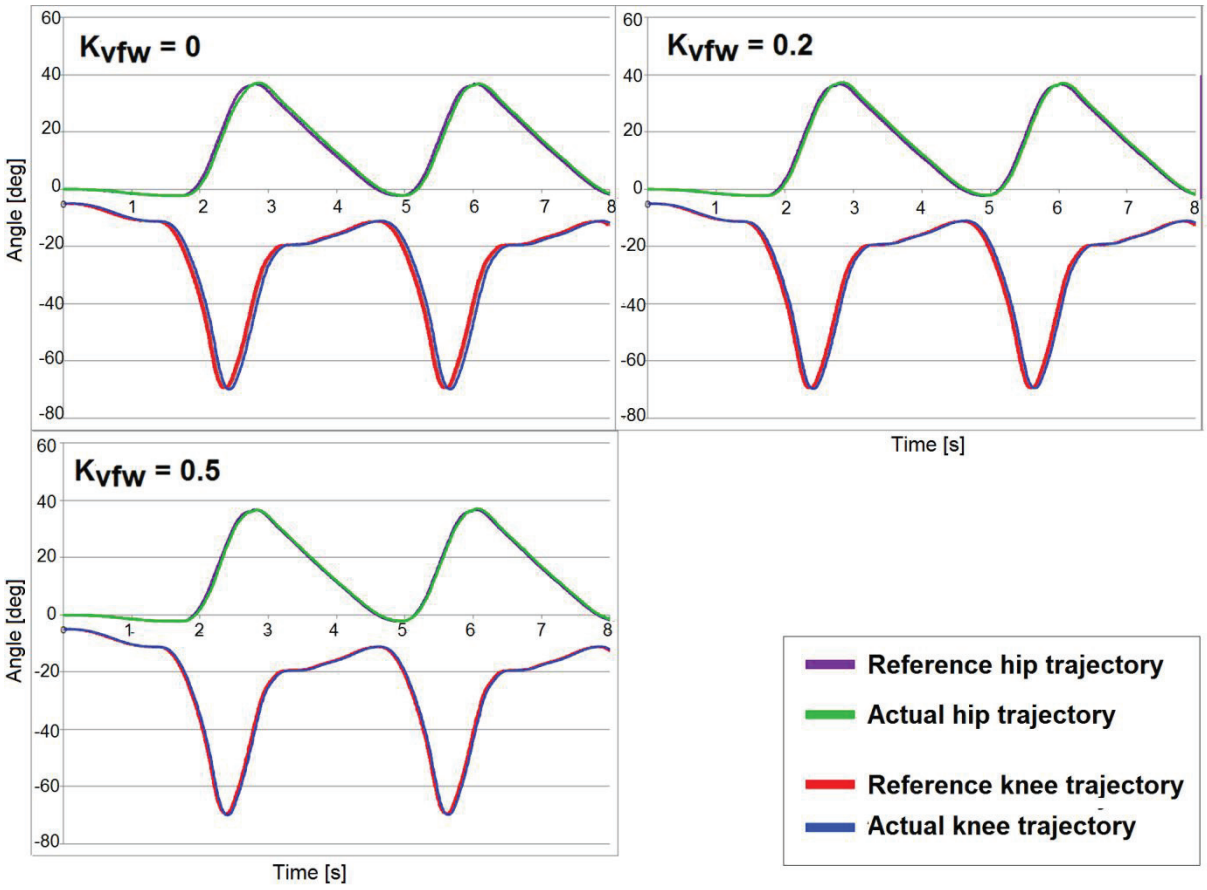

Fig. 85 Performance of the *MOPASS* position controller with a compliant healthy subject

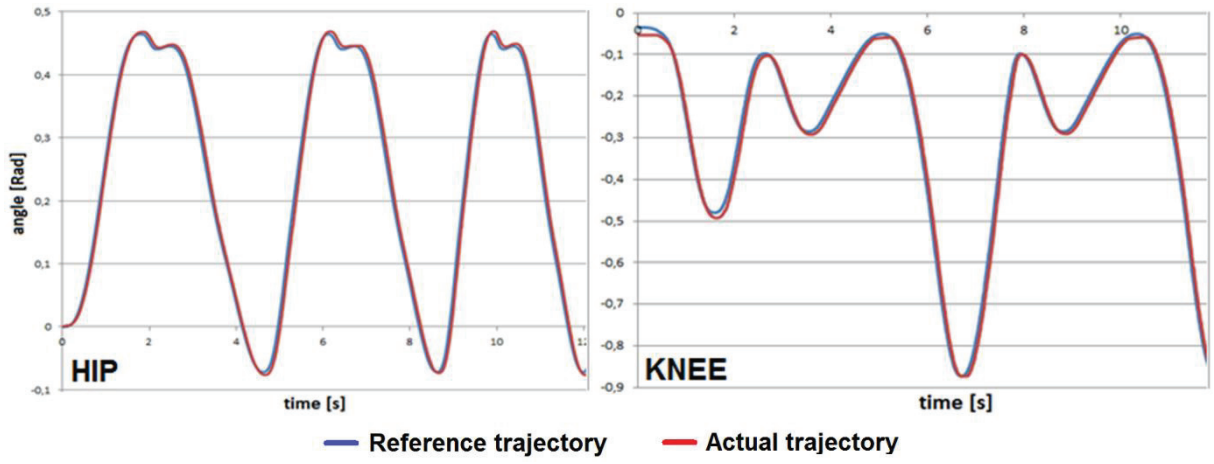

Fig. 86 Performance of the *MOPASS* position controller with a compliant patient during clinical trials

5.1.2 Impedance control

The mechanical impedance defines how a system reacts to an imposed motion. The notion of impedance control was first introduced by Hogan [205] to design control strategies comprising interaction between robots and the environment. Hogan argued that, commonly, the environment behaves as an admittance (i.e. it accepts force inputs and determines corresponding motion in response to them), and because of that, to ensure physical

compatibility, the robotic system must behave as an impedance in interaction tasks with such environments, implementing functions that specify the force produced by the mechanism in response to the motion imposed to it by the environment. These functions could be linear, non-linear, dynamic, or even discontinuous. Hence, when the task at hand includes reference trajectories to be followed by the robotic system, as it is the case in gait rehabilitation, the impedance controller will define the relationship between the force exerted by the robot and the deviation of the actual position from the reference one.

Impedance controllers have been normally implemented with non-linear control laws, often associated with stability problems, or by control schemes that combine an inner-loop for position control and an outer-loop for force-based compensations [52] [206] [207]. Other implementations use simpler schemes with controllers using linear relationships defined as zero or higher order functions of the position deviation (and its derivatives), although typically the implemented functions are of order zero (stiffness), one or two.

Impedance control has had a great reception in rehabilitation robotics because of its simple and natural concept, and because of its stability when interacting with stiff environments [66]. The upper-limbs rehabilitation system *MIT-MANUS* [208], for instance, started using impedance-control schemes long time ago to help the patient track some trajectories with their hands/arms during goal-directed therapy. In gait rehabilitation, including impedance controllers instead of stiff position controllers allows a variable deviation from the reference trajectories instead of imposing a rigid gait pattern, and these deviations will be dependent on the active efforts and participation of the patients. Because of their nature, impedance controllers present themselves as a basic, easy to understand 'assist as needed' strategy that aims to encourage the active participation of the patients in the therapy. Several state of the art devices and research groups implement impedance-control-based strategies. Researchers using *LOKOMAT* implement different impedance control schemes based on fixed reference trajectories [209] or adaptive ones [52]. In [132], the *STRING-MAN* system is designed with a second-order impedance controller included in a control scheme with an inner-loop impedance-based position control and an outer-loop that includes an admittance module used to shape the relation between the contact forces and the corresponding modifications of the reference position. The *ANdROS* system implements a first-order (spring–damper) impedance controller for the calculation of knee joint support torques [66]. Other devices also implement control strategies similar to or based on the impedance concept. The LOPES device realizes different virtual physical models (VM), such as springs and dampers, to define physical interactions of the robot with the subject [55], which can be activated or de-activated in different moments of the gait cycle. These VM are not restricted to linear models, and they can be a function not only of the position but also of the time. The *ALEX* system also uses some non-linear relations between the support-force field and the position deviation, and works in world space instead of joint space [172]. It also includes the concept of virtual wall, which behaves as a haptic tunnel, normal to the ankle's trajectory, where the component of the force field normal to the ankle reference trajectory is zero (no normal forces are exerted by the system to the patient). The force-field applied by *ALEX* to the patient's ankle has three components: a normal force, which is proportional to the square of the position error (with respect to the virtual wall) normal to the ankle's reference trajectory; a tangential force, which is applied only when the ankle's position normal to the trajectory is close to the reference position, and is stronger the lower the distance between these two positions is; and a damping force proportional to the linear velocity of the ankle.

Impedance control, in principle, also helps to tackle some problems specific to gait rehabilitation. In optimal therapy, the behavior of the robotic system must depend on the level

of impairment of the patients. Patients suffering of severe impairments need a system with high impedance that assists them to track the reference trajectories. The lower the impairment is, the more compliant the behavior of the system is desired. This way, patients with minor to moderate motor deficits who still have some motion capabilities are able to train the walking actively influencing the motion of the device, whilst the robot exerts correction forces just when needed. Hence, it is normally desired to have a system able to switch from high impedance (full support) to low impedance (low or no support) and vice versa [58]. However, the mechanic and power limitations of the device might hindrance this goal. On the other hand, implementing impedance controllers separately for each joint (or leg) with different levels of compliance might suit very well in therapy with hemiplegic patients because of the possibility of treating the impaired leg with different impedance values than the sound (or less impaired) leg [209]. However, these impedance controllers must be complemented with appropriate control modules to handle, for instance, the synchronization between the legs.

Even though the concept of impedance control was thought for interaction tasks, it not only provides a reliable unified approach for controlling robotic systems whilst in contact with the environment, but also during free-space operation [206]. However, it possesses an important drawback regarding its inability to control interaction forces when the environment is not in contact with the robot and its location and parameters are unknown by the system. In the case of gait rehabilitation, it is assumed that the patient will be always attached to the system whilst in impedance control operation and there won't be cases of free-space (contactless) operation, hence the aforementioned problems are not present in this specific implementation. However, it is important to understand that contactless situation would affect significantly the performance of the controller. If, for example, the overall control scheme is designed to control interaction forces, the controller would move the device aiming to reach a desired interaction force, but actually that interaction force is always zero[21], causing even instability. Moreover, in case the system manages to contact the environment, the transition from free-space-to-contact could introduce some undesired reaction of the control efforts.

The impedance control scheme proposed here combines a simple spring-damper impedance model with a haptic tunnel based on the virtual wall proposed by the *ALEX* group [172], all applied in joint space. Similar to the *ALEX*'s approach, the haptic tunnel refers to a tolerance area around the desired position at a certain time where the system doesn't exert assistive forces to the patient (i.e. the patient moves freely). Once the patient leaves this area, a support torque is exerted to help the patient's joint to return to the desired path. This torque is a function of the position error (with respect to the haptic tunnel wall and not to the desired trajectory) and the velocity error. The support torque calculated by the system for a certain joint would be therefore

$$\tau_{sup} = \begin{cases} K_{IC} \cdot \Delta\theta + B_{IC} \cdot \left(\dot{\theta}_{ref} - \dot{\theta}\right) & ; \left|\theta_{ref} - \theta\right| < r_{HT} \\ 0 & ; otherwise \end{cases}$$

$$\Delta\theta = \begin{cases} \theta_{ref} + r_{HT} - \theta & ; \theta > \theta_{ref} \\ \theta_{ref} - r_{HT} - \theta & ; \theta < \theta_{ref} \end{cases}, \tag{36}$$

where K_{IC} and B_{IC} are the spring and damper coefficients, $r_{HT} \geq 0$ is the radius of the haptic tunnel, θ and $\dot{\theta}_{ref}$ are the reference position and velocity given by the trajectory generator, and θ and $\dot{\theta}$ are the actual position and velocity in the joint. The general concept of the

[21] Assuming a perfect sensing or estimation of the interaction force. In practice, that might not be the case due to errors in the model compensation or simply noise in the measured data.

proposed impedance controller can be better understood with Fig. 87. For this proposal, it is advised that the damper coefficient B_{IC} is not too high if using high tunnel radius and high reference velocities, due to the fact that high contributions caused by velocity errors and the usage of the haptic tunnel generate discontinuities in the resulting support force. Even though these discontinuities are, to some extent, filtered by the dynamics of the subsequent torque controllers, the forces caused by high values of B_{IC} might be uncomfortable to the patient and are hence undesired.

To have a better idea of the potential of the proposed impedance controller, take a look to the simulation results depicted in Fig. 88. Initially, a pathological trajectory was set to the knee joint and then simulated using a human model in Adams [210] to obtain the torque necessary to track it. Afterwards, the same model was simulated, but this time the torque exerted in the joint was the sum of the previously calculated torque (original torque) and the support torque computed by the impedance controller using a healthy-like trajectory as reference. The upper plot in Fig. 88 shows the knee joint angles of the pathological trajectory (dark dashed line), the healthy-like reference trajectory (pale dashed line) and the resulting trajectories after applying the support torque with three different impedance and haptic tunnel parameters[22] (solid lines): K_{IC}=5, B_{IC} =5, r_{HT} =2°; K_{IC} =50, B_{IC} =5, r_{HT} =2°; and K_{IC} =300, B_{IC}=15, r_{HT} =0°. The latter set of parameters corresponds to a stiff behavior of the system aiming to a close tracking of the reference trajectory, whereas the first set corresponds to a more compliant behavior. The left lower plot in Fig. 88 shows the torques necessary to move the knee with the pathological and the reference trajectories. The lower right plot shows the support torques exerted with each one of the sets of impedance controller parameters. Although this is only a simulation and during real interaction with patients it is expected that the patients react to the support torques differently (e.g. resisting the support or complying to it) meaning that the torque applied by the patient during supportive therapy is different from the originally calculated one, we can observe how, depending on the selected controller parameters, the impedance controller can compute support torques aiming for a closer tracking of the reference trajectories.

As stated before, in gait rehabilitation it is desired to be able to set different levels of impedance separately for each joint. Moreover, it could be beneficial to set different impedance levels in different stages of the gait cycle (variable impedance throughout the cycle). This could be achieved by computing continuous and periodic profiles of impedance

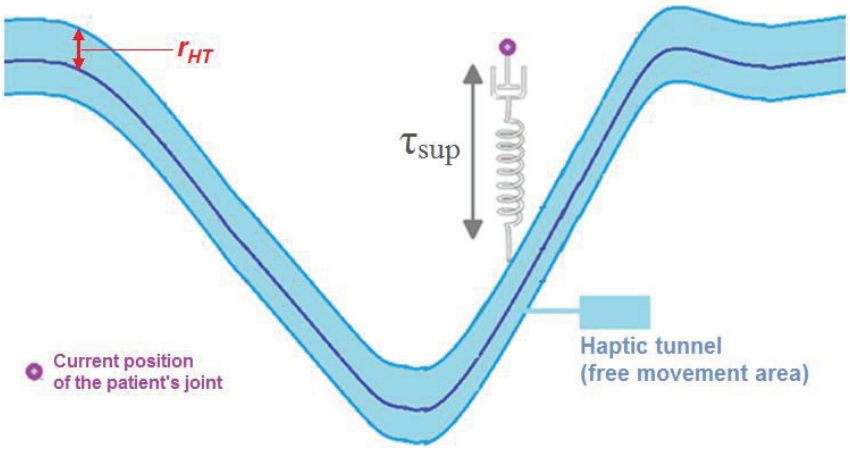

Fig. 87 Concept of the impedance controller

[22] With the inputs to the impedance controller being in Radians and Radians/s.

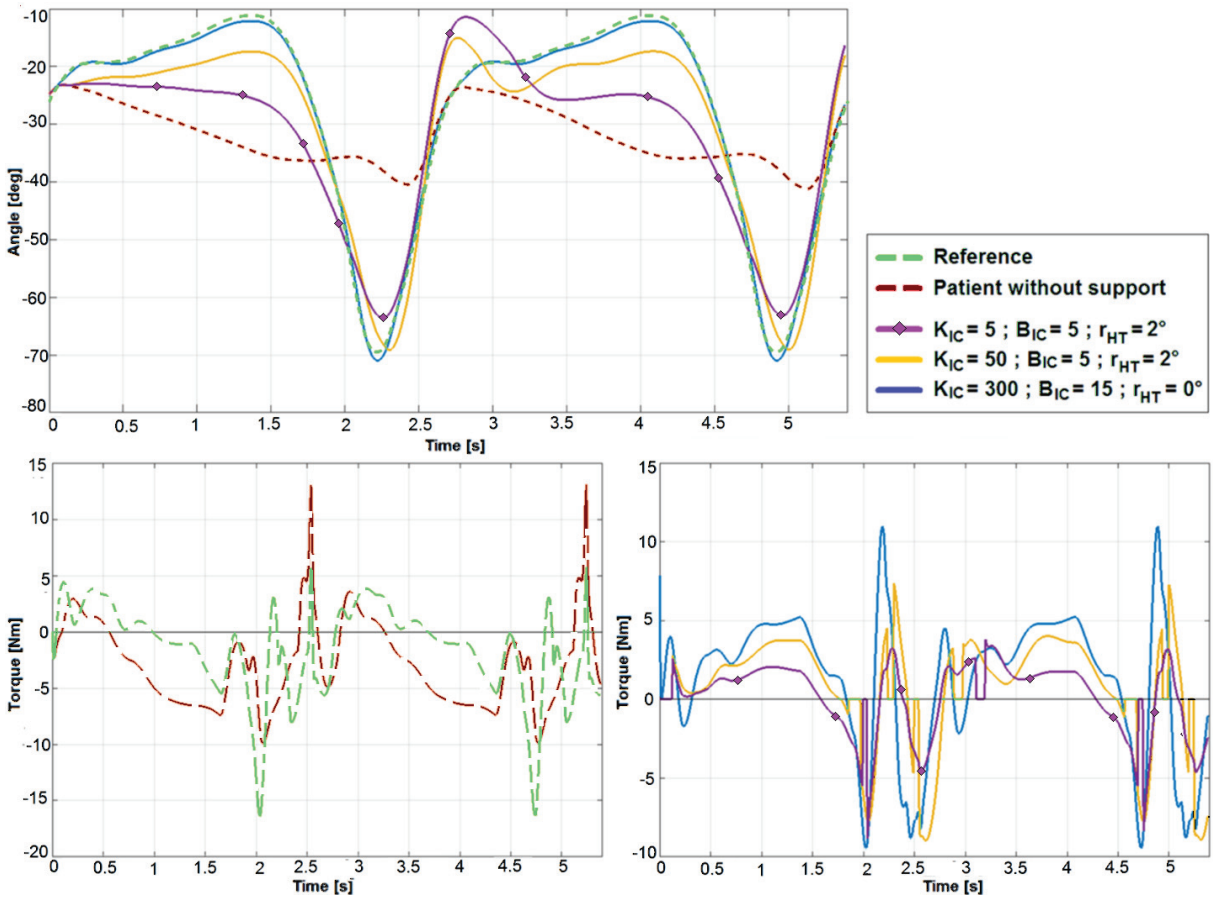

Fig. 88 Example of the impedance controller in the knee joint using different impedance and haptic tunnel values

and haptic tunnel parameters throughout the gait cycle. For instance, the system could have a stiff behavior in the vicinity of the moment of initial contact and be more compliant in the rest of the cycle to ensure that the patient keeps a desired cadence but allowing him/her to deviate from the reference gait pattern. Take a look to Fig. 89, where the simulation results of such case are depicted. For this example, a stiffness level profile (lower plots) was used to obtain the impedance controller parameters (proportional to the stiffness level) and the radius of the haptic tunnel (inversely proportional to the stiffness level). The left upper plot in Fig. 89 shows the reference trajectory (dashed lines) and the resulting trajectories gotten when using the stiffness level profiles (bright solid lines) and fixed highly-compliant impedance and haptic tunnel parameters (dark solid lines). The right upper plot shows the corresponding support torques. Note how when using the stiffness level profile, in the vicinity of the initial contact the actual trajectory is very close to the reference, whereas in the rest of the cycle it is deviated due to the compliant behavior of the system. The specific implementation of this variable support level through a graphical user interface can be seen later in section 6.3.

The complete control scheme implementing the impedance controller with haptic tunnel is shown in Fig. 90. This scheme is based on the usage of an interaction torque controller, although other implementation approaches can be used. This controller will compute control efforts u (e.g. motor current or voltage) in order to match the desired interaction torque (i.e. the support torque) with the actual one, which normally must be estimated because of the difficulty to decouple it from the rest of the toque measurements. The interaction torque

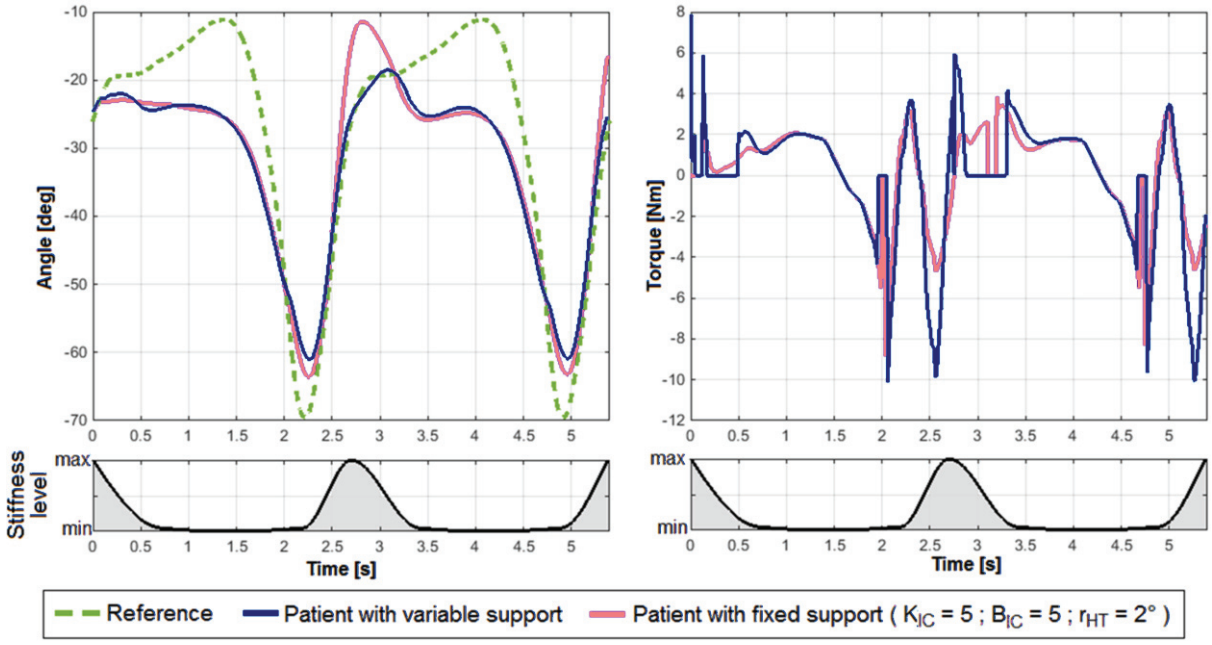

Fig. 89 Example of the impedance controller in the knee joint using variable stiffness levels.

estimator is dependent on the available measurements. In the presented scheme, it is assumed that the system possesses torque sensors able to reliably measure the torques present in the joints. With these torques and the position and velocity measurements, it is possible to estimate the interaction torques using the dynamic model of the system (presented in Appendix B). Although the complete dynamic model is governed by the equations of motion (refer to equations (78) and (71) in Appendix B), a simplified model could be used in practice taking into account the low values of some of the generalized positions, velocities and accelerations that contribute minimally to the forces in the system. In some cases, it might be enough to use the dynamic models of the legs separately disregarding the contributions related to the motion of the platform (e.g. when the motion of the platform is very smooth and its rotations about the longitudinal axis are not significant). Moreover, the contributions made by the Coriolis and centripetal forces can often be neglected. In many applications it is enough to estimate the gravitational forces and to neglect the remaining ones. The interaction torque controller could implement commonly used approaches such as *PI* control, as well as model based control with system dynamics' compensation. As before, this compensation could disregard some of the elements of the system's dynamic model.

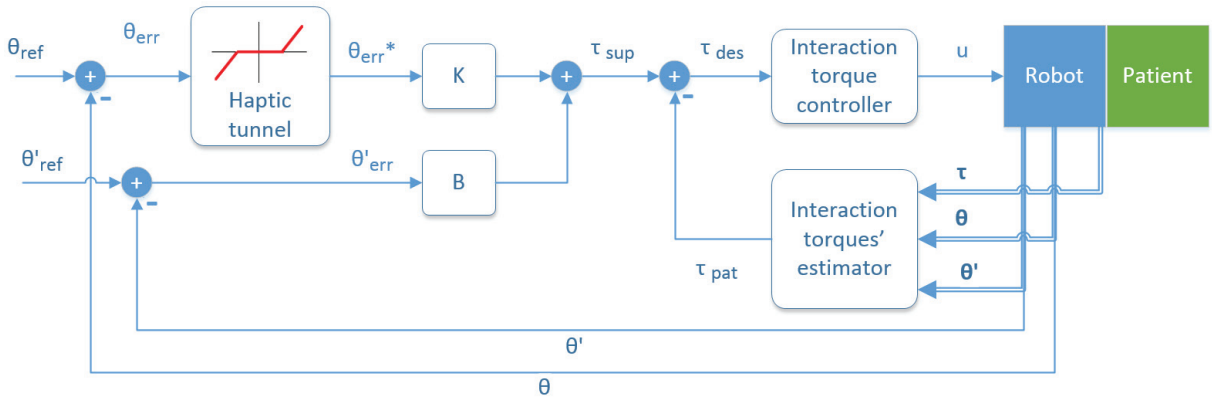

Fig. 90 Scheme of the proposed impedance controller with haptic tunnel

Other control schemes different from the one in Fig. 90 can be used together with the impedance controller. If the dynamic model of the system is well known, the scheme shown in Fig. 91 can be another option. In this case, the computed support torque is supplied to a torque controller together with the model-based compensation torques τ_{comp} (i.e. the torques that the system needs to generate in order to achieve the current positions, velocities and accelerations, and is calculated using the system's equation of motion (refer to equation (78) in Appendix B). Another option could be a control scheme based on pressure sensors located between the robotic structure and the patient limbs. This scheme would have a similar design as the one shown in in Fig. 90, but instead of controlling the interaction torques, the controller would control the pressure between robot and patient, and consequently, the impedance controller would not deliver support torque values, but rather pressure set-points following the same principle. This scheme is shown in Fig. 92, where ***P*** is a vector containing the measurements of all the pressure sensors used for the corresponding joint calculations. These values are used by the 'data fusion' block to deliver a single pressure value for the corresponding joint used for the control.

5.2 Mobile platform motion

In the case of the platform, its motion is completely governed by the desired walking speed of the therapy. This speed is obtained from the estimated value of the step lengths of the

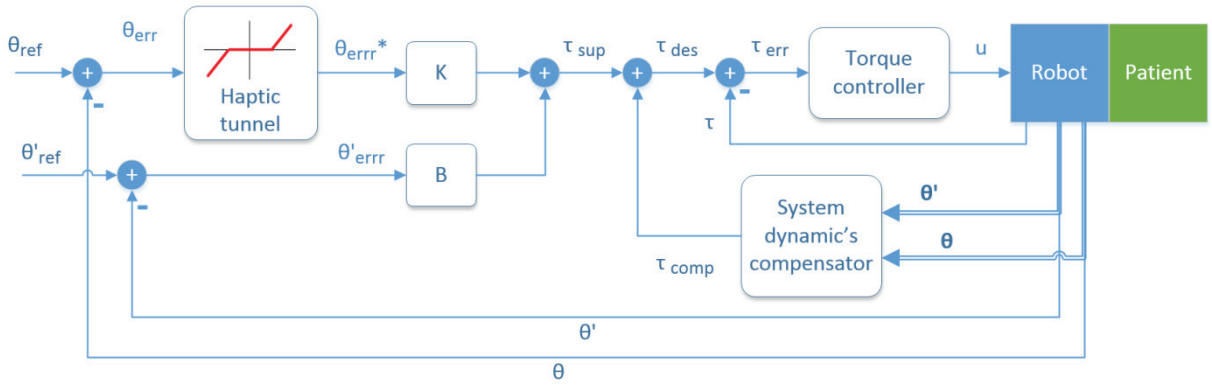

Fig. 91 Another scheme of the proposed impedance controller with haptic tunnel

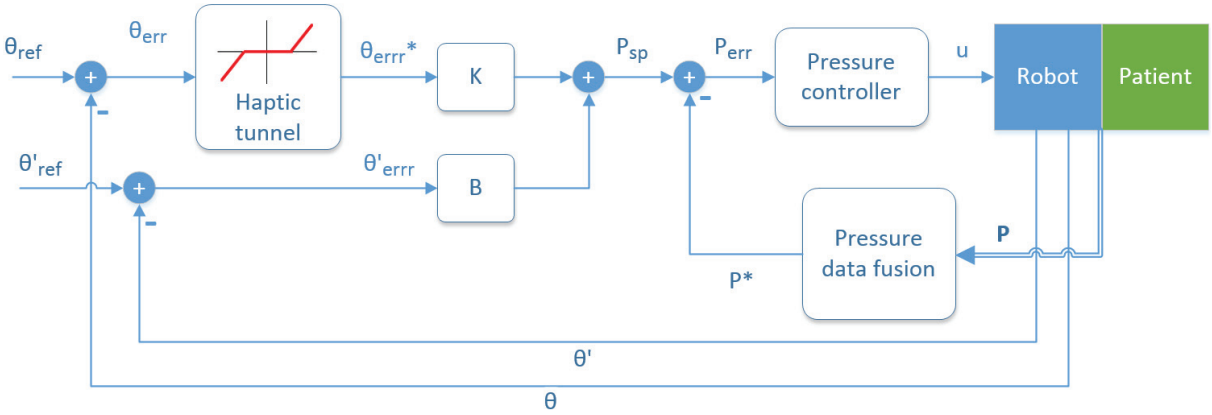

Fig. 92 Yet another scheme of the proposed impedance controller with haptic tunnel – based on pressure feedback

right and left legs, based on the horizontal displacement of the feet corresponding to the current reference trajectories, where the speed is equal to the addition of both step lengths divided by the reference gait cycle period. The proposed estimation of the step length is given by

$$SL = K_{SL} \cdot FD, \tag{37}$$

where FD is the foot horizontal displacement and K_{SL} is a proportional multiplier. Initially, K_{SL} was obtained following the equation (12) used during the data processing of the experimental data for hip and knee joints' trajectory generation ($K_{SL} = f_s(FD)$). However, during the practical tests with the *MOPASS* system at low speeds it was seen that these values generated a speed lower than the desired, resulting in a lagging behavior from the platform. Because of this, it was decided to test the platform speed performance with constant values of K_{SL}. After some tests, a $K_{SL} = 0.85$ resulted in a comfortable platform motion. However, the value of K_{SL} can be offered to the therapists as a selectable value ($K_{min} <= K_{SL} <= 1$) so that they can choose the proportion multiplier that feels better to each patient.

Once the estimated step length is obtained, the corresponding wheels' velocity can be calculated and set as the reference velocity for the low-level velocity controllers. This will lead to a forward motion of the platform equal to the estimated walking speed of the reference walking patterns. However, the therapists are also offered the option to introduce turning of the platform. During therapy, this turning will be minimal (and limited) and is meant to make corrections in the direction of movement of the platform that are necessary, for instance, when there is slipping of one of the wheels and the platform deviates slightly from the initial path. It can also be used when it is desired to practice higher-level turning, in case there exists an appropriate hip and knee trajectory generation for turning to complement it. Moreover, the therapist can use the turning feature to move the platform when no patient is using the system, or to adjust the direction of walking before starting the walking exercises with the patients. Taking this into account, the reference wheel velocities given to the low-level controllers are

$$\omega_i = \frac{2 \cdot SL}{T_{ref}} \cdot \frac{1}{r} + \varphi_i \ , \tag{38}$$

where i = *{R: right wheel, L: left wheel}*, ω is the desired angular velocity of the wheel which is set as the input of the low level profiled velocity controllers of the motors' drives, T_{ref} is the reference gait cycle period, r is the radius of the wheels, and φ_i corresponds to the turning deviation applied to each wheel, which is proportional to the desired turning set by the therapist. In practice, $\varphi_L = -\varphi_R$. Note that in (38) it is assumed that the hip and knee periodic trajectories are equal for both legs (with a phase of 50% of the gait cycle), hence $SL_R = SL_L$. A simple diagram of the procedure is shown in Fig. 93, where the low level control process carried out by the Elmo servo-drives is not depicted for simplicity.

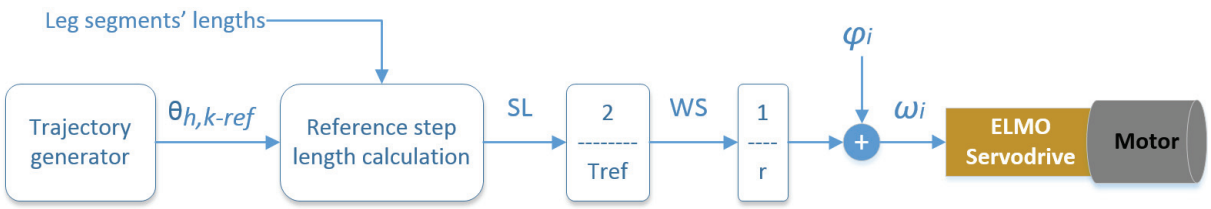

Fig. 93 Diagram of the mobile platform motion control

5.3 Pelvis modules' motion

As stated in section 3.2.1, a novel pelvis mechanism was designed for the *MOPASS* system by one of the technical partners with the objective of assisting the patient pelvis with movements constrained to circular motions in the sagittal plane. The initial intended movement of these active modules was a synchronized motion between the right and left modules during the periodic walking, maintaining the same velocity in each module but keeping an angular phase of 180° between them. A process to synchronize these movements with the periodic hip and knee trajectories was implemented to be done automatically by the *Controller* component. Additionally, a transition between the initial position and the periodic trajectories during the first step was also implemented. Such overall synchronization can be seen in Fig. 94 and Fig. 95.

The pelvis position control follows the same basis of the hip and knee position control scheme. There are only four basic differences: 1) the drives used are Schunk drives instead of Elmo drives, but they possess profiled position and velocity controllers as well; 2) the problem with current limits and position errors was not present in these joints, hence only the impedance-based control scheme was used; 3) no velocity feed-forward was used; 4) the control process was done in the controller component and not in the pelvis SMP components, which were only used as a bypass-interface between the controller component and the Schunk drives. The control scheme is shown in Fig. 96, whereas an example of its performance is shown in Fig. 97.

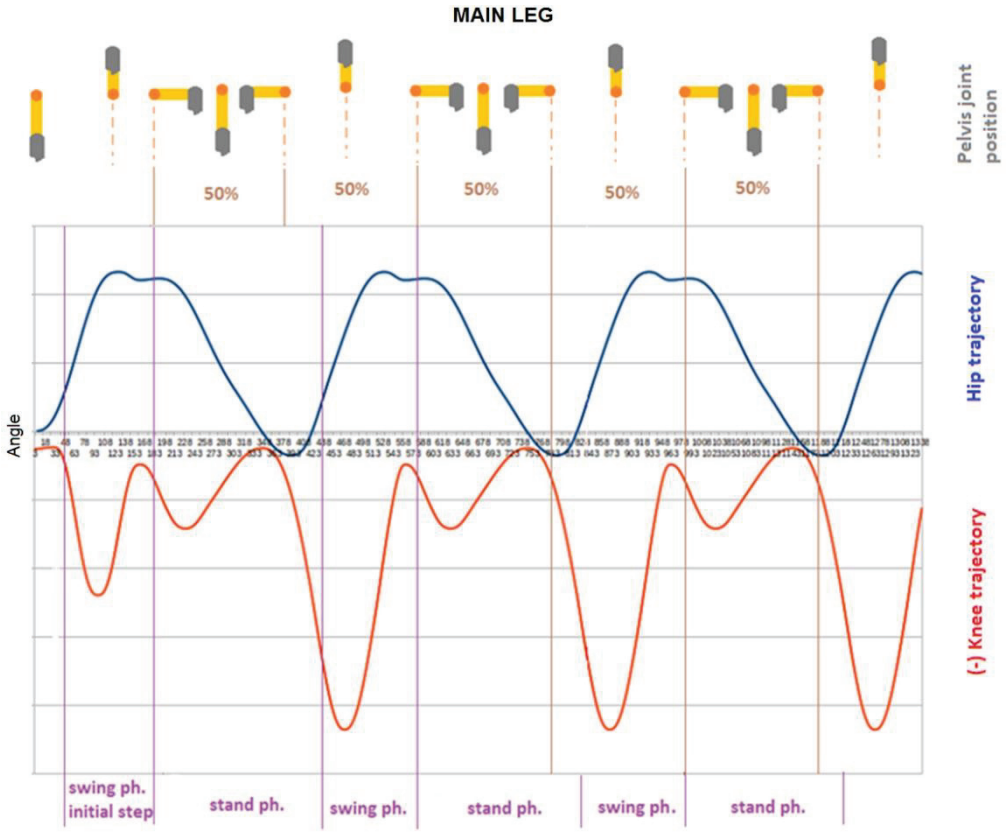

Fig. 94 Synchronization of the pelvis joints with the initial step and periodic trajectories of the hip and knee joints (main leg)

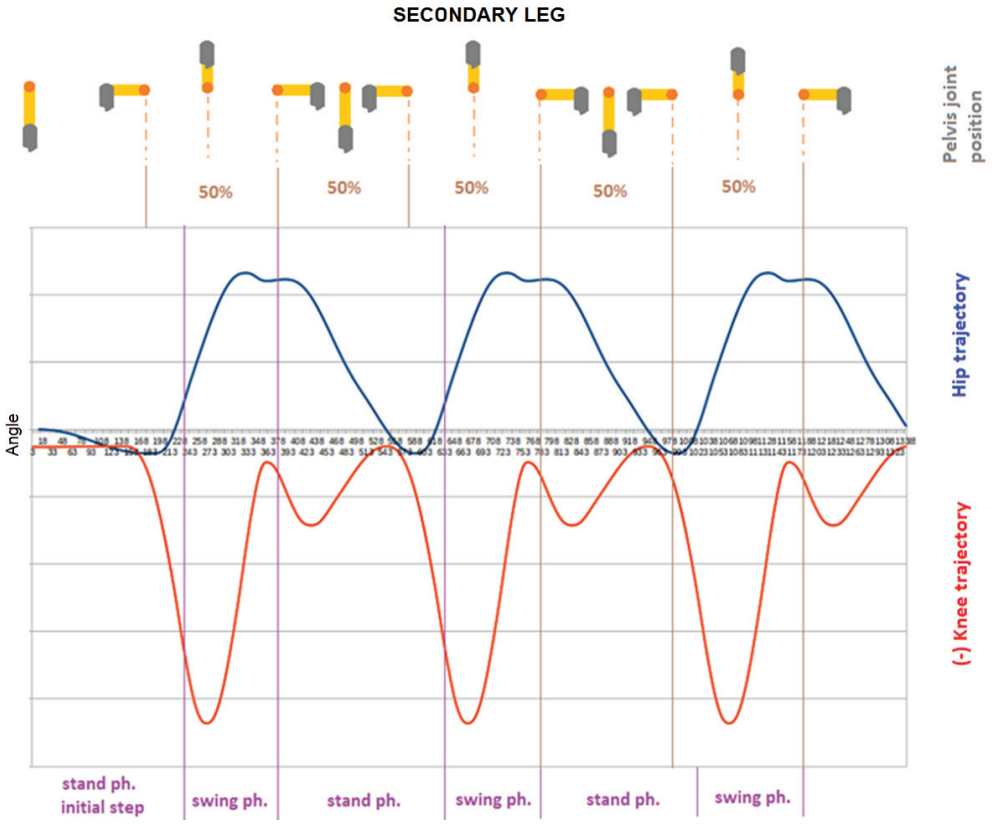

Fig. 95 Synchronization of the pelvis joints with the initial step and periodic trajectories of the hip and knee joints (secondary leg)

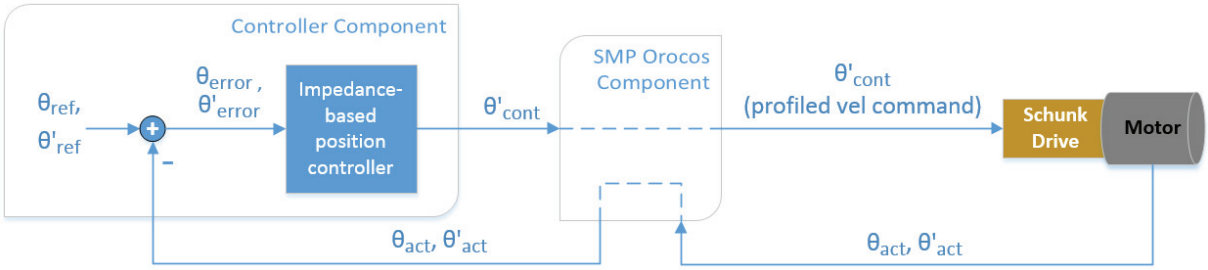

Fig. 96 Position control scheme for trunk/pelvis joints

Even though the implementation of the desired motion profiles was done and controlled successfully, initial tests with healthy subjects and further studies of the pelvis movement in the sagittal plane during walking showed that this particular motion doesn't reflect a general pattern throughout the population. Instead, the pelvis movements in this plane show great variability inter- and intra-subject. Thus, it was decided not to include this pelvic motion in the clinical trials and further development of the *MOPASS* system, and the active pelvis modules were set to a fixed position.

5.4 Robot-patient synchronization

Gait rehabilitation systems that possess some level of compliance, either because of its mechanical and electrical characteristics or the control strategies implemented in it, such as impedance controllers without high stiffness, are susceptible to have problems regarding the synchronization between the therapy reference trajectories and the actual gait patterns of the

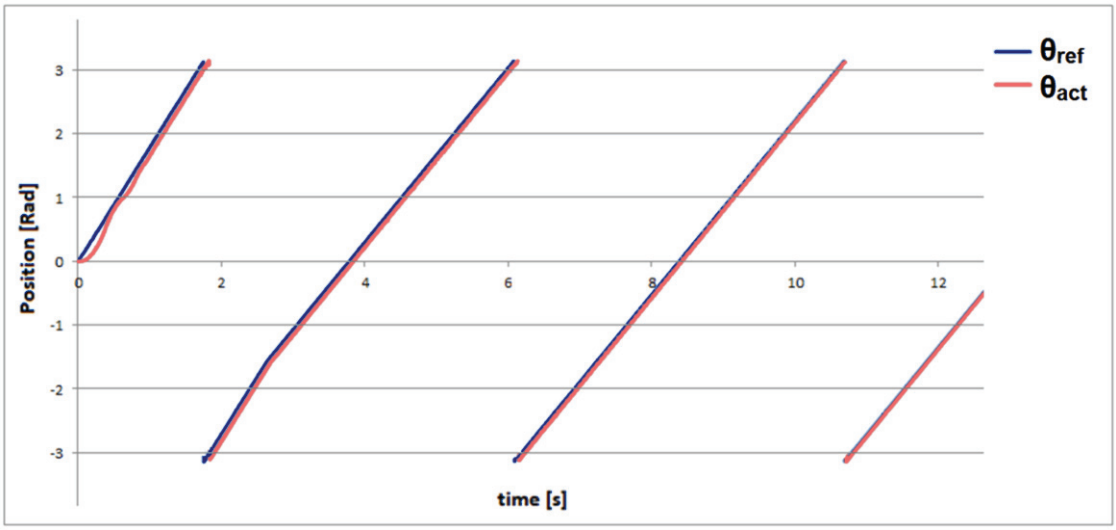

Fig. 97 Performance of the pelvis position controllers

patient. When a system is compliant, it allows the patient to influence the motion of the robot and to deviate from the reference patterns, hence allowing the patient to walk at speeds different from the one set by the therapist. Ultimately, this issue causes that the system applies corrective forces corresponding to a walking phase that is different from the actual walking phase of the patient, exerting forces that obstruct the patient's gait in a unfavorable manner rather that a supportive one. In other words, the patient will feel that the system is a source of impediment instead of assistance. Two different cases are present during desynchronization: the reference pattern is ahead of the patient (phase lead) and the patient pattern is ahead of the reference (phase lag). It is important here not to confuse the term 'phase' with the gait phases and sub-phases. In this context, phase refers to the normalized time and phase error refers to the difference in time between two periodic signals, or more specifically, the difference between the current relative times (with respect to the gait cycle period) between two walking patterns. If, for example, we say that the reference has a phase-lag of 40% (or 0.4), it means that while the patient is already making the initial contact of the foot with the ground, the reference is in the area of the pre-swing gait phase.

As stated before, during the initial clinical trials with *MOPASS*, this sort of synchronization issues arose during the therapy of some patients who had a high level of impairment and were not able to follow the trajectories suggested by the system. Because of the power limits of the joint motors, the system was unable to ensure a close tracking of the joint reference trajectories, resulting in an undesired compliant behavior of the system. Consequently, shorter/longer steps and changes in the walking speed and cadence from these patients caused the system to apply obstructive torques to them in some parts of the therapy, forcing the patients to resynchronize with the robot in a rather unpleasant way. An example of such behavior can be seen in Fig. 98, where the position tracking of the hip trajectory is shown, together with the current used by the motor while trying to fulfill the controller demands. The joint drives had a peak current limit of (+/-) 5 Amp, and a stall current limit (triggered when the drive has been in the peak current limit for some specific time) of 3.2 Amp. In this specific case, it can be observed that the patient was walking with a cadence higher than the reference one and sometimes with shorter step lengths (as seen in the 5th cycle) exerting high torques to the joint motor, making it reach the current limits and being unable to perform a close reference tracking, causing a case of phase lag (patient ahead) desynchronization. While the system was applying torques corresponding to the area

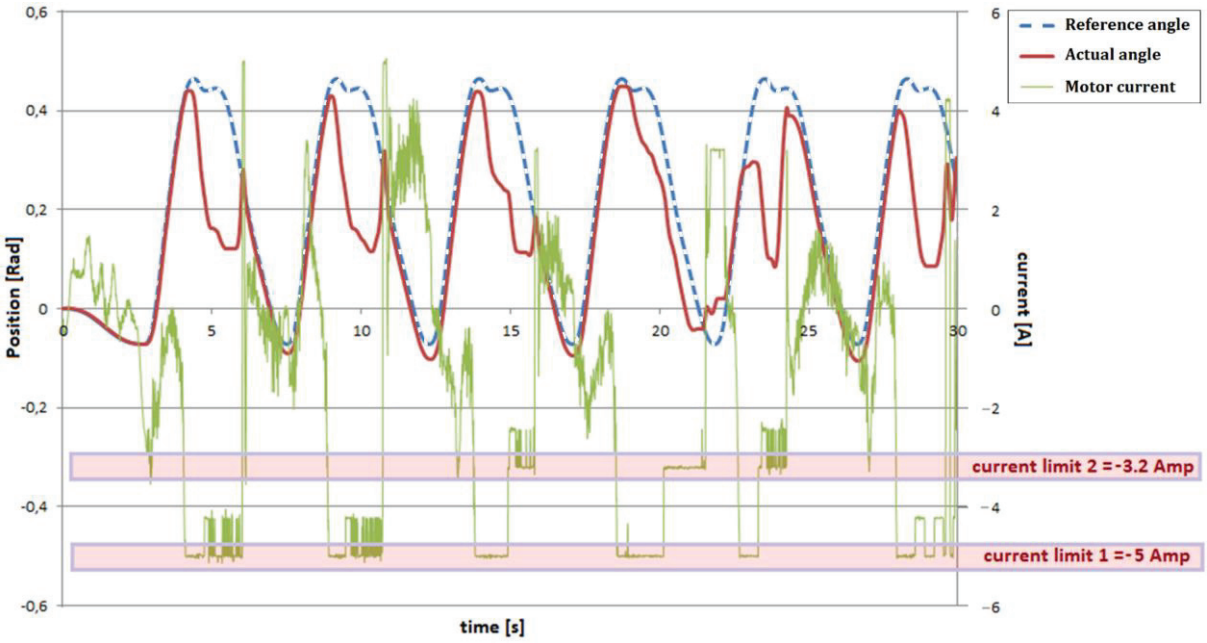

Fig. 98 Example of hip trajectory tracking during therapy with a non-compliant patient

surrounding the terminal swing and initial contact, the patient was already in stance phase moving his/her foot backwards. After some point, the patient had to do an abnormal step in order to resynchronize with the device, caused by the obstructive forces being applied by the system and the discomfort consequence of them.

Aoyagi *et al.* have openly referred to the synchronization problem and have presented two methods to overcome it. In [211], a synchronization strategy based on the cyclic adaptation of the playback speed of the reference trajectories is implemented in the *PAM* device. By using foot switches, the system recognizes the moment of heel contact in the actual pattern. This way, it is possible to measure the actual gait cycle period and therefore the real gait frequency. With this value and the value of the reference frequency, the system compensates for the frequency error and speeds up or down the walking speed to come close to or match the actual one. Additionally, it also compensates for the phase error between reference and actual patterns using the information gotten from the foot switches. Therefore, every time the system recognizes a heel strike from the patient, it measures the time elapsed between the current and the last heel strike to obtain the actual gait cycle period, and analyzes if the patient is ahead of the reference. If the patient is ahead, it compensates by further increasing the replay speed of the reference trajectories. In case the reference gait pattern has reached the moment of heel strike but the signal from the foot switches hasn't indicated an actual heel contact (reference ahead), the system holds the reference in its current state to wait for the patient to catch up with the device. The synchronization method is governed by

$$t_{ref} = \begin{cases} mod\left(\int^{t}\left(f_{ref} + K_1\left(f_{ref} - f_{act}\right) + \Delta f_{ph}\right)dt\,,1\right) & ;pat\ ahead \\ same\ as\ the\ last\ t_{ref}\ (no\ change) & ;ref\ ahead \end{cases} \quad (39)$$

where *mod* refers to de modulus operand, $f_{ref} = 1/T_{ref}$ is the original frequency of the reference trajectory which has a gait cycle period of T_{ref}, $f_{act} = 1/T_{act}$ is the actual frequency corresponding to the measured gait cycle period T_{act}, $K_1 < 0$ (usually $K_1 = -1$) is the feedback gain, Δf_{ph} is a constant value (e.g. *0.1*) corresponding to the compensation for the phase lag

error, and t_{ref} = [0, 1) is the input to the look-up table in charge of yielding the reference trajectories. Note that, in this case, the convention for normalized time between 0 and 1 is different from the one used in this manuscript (from 0 to 100%). Even though the frequency compensation manages to follow the actual walking speed present in the therapy, the way of implementing the phase lag compensation might not tackle the problem is a correct manner due to the fact that the value of Δf_{ph} should be dependent of the phase error instead of being constant. If the Δf_{ph} is too low, the system might never be able to correct the phase difference; if Δf_{ph} is too high, the reference would surpass the patient pattern passing from a phase lag to a phase lead.

The second synchronization method from Aoyagi *et al.* was presented in [60], this time applied to both *PAM* and *POGO* devices. Unlike the previous method that performed the synchronization efforts every heel strike, this strategy makes a continuous change in the playback speed of the reference throughout all the gait cycle. The algorithm consists of an actual phase estimator and a proportional phase controller. For the phase estimator, the system makes use of the current position and velocity of nine DoF of *PAM-POGO*. It obtains the 18 actual measured values and compares them to the positions and velocities of the reference trajectories in several moments of the gait cycle, obtaining the relative time where the actual and reference trajectories are closest (i.e. the estimated actual phase). To this end, they propose a cost function *C* of the form

$$C(t_i) = \left| \boldsymbol{W}^T \cdot \left(\boldsymbol{X}_{ref}(t_i) - \boldsymbol{X}_{act} \right) \right| \quad ; \quad 0 \leq t_i < 1 \,, \tag{40}$$

where $\boldsymbol{X}_{act}$ is the matrix of actual states composed by the measured positions and velocities in the nine DoF, $\boldsymbol{X}_{ref}$ is the matrix composed by positions and velocities of the reference trajectories in a given relative time (phase) t_i, and $\boldsymbol{W}^T$ is the transpose of the matrix of error weights. Note that $\boldsymbol{X}_{act}$, $\boldsymbol{X}_{ref}$ and $\boldsymbol{W}$ are matrices with dimensions 18×1. By calculating the cost using several values of t_i it is possible to obtain the t_i that generates the minimum cost value, which ultimately is taken as the value of the estimated actual phase (t_{act}). Once the estimated phase is obtained, the phase error between the reference and the actual patterns can be calculated and fed to the proportional controller. The output of this controller is finally integrated to obtain the phase-error compensation. The input of the reference trajectories' look-up table is therefore acquired following

$$t_{ref} = mod\left(\int^t \left(f_{ref} + K_2 (t_{ref} - t_{act}) \right) dt \,, 1 \right), \tag{41}$$

where K_2 = 2.5 is the proportional coefficient of the phase controller. Synchronization algorithms based on this method have been implemented in other systems such as the robotic devices presented in [64] and [66].

Jezernik *et al.* deal also the synchronization problems in [52], although not exclusively. Their 'patient-cooperative' therapy strategies implemented in the *LOKOMAT* system adapt the period, amplitude and angular off-set of the original joint reference trajectories based on the interaction forces between the device and the patient. This way, the period of the reference trajectories (and therefore the walking speed) is influenced by the patient's movements and efforts, hence tackling the synchronization problem. However, this approach is highly dependent on their therapy control strategy and hence is difficult to implement in other systems.

Other popular approaches have included adaptive oscillators to adjust the intrinsic frequency of the periodic reference trajectories (and therefore the reference cadence) towards the actual frequency of the patient's gait, as well as to eliminate the phase difference between actual and reference patterns. The first ones to implement adaptive oscillators in gait

rehabilitation were Ronsse *et al.* in the *LOPES* system [212] [213]. Their synchronization method is based on an estimated hip trajectory expressed as a Fourier series and a set of oscillators corresponding to different harmonics in the estimated hip trajectory. Their adaptation algorithm progressively adjusts the frequency of the reference pattern and eliminates phase errors depending on the difference between the (estimated) reference and actual angles, while adjusting the Fourier amplitude parameters of the estimated hip trajectory. Additionally, this method includes a non-linear filter based on Gaussian-like kernel functions which is applied to the Fourier-based estimated trajectory to obtain the final filtered estimated trajectory. This way, the system allows the patient to adapt the reference pattern's frequency through the adaptive oscillators, and the reference trajectory's shape through the estimation and filtering process.

Chen *et al.* have also implemented an adaptive oscillator in a knee-ankle-foot robotic device for rehabilitation purposes [214]. Their algorithm detects the gait sub-phases (or more specifically, the events that mark the gait phase transitions) by means of a hidden Markov model, and utilizes one or more of the detected events (e.g. initial contact and tibia vertical) to obtain the frequency of the actual trajectories and to compute the phase error between the reference and actual gait patterns. With this information, the algorithm adjusts the frequency of the reference patterns towards the actual gait pattern's frequency eliminating the phase error on the way. Unlike the previous method used in *LOPES*, this method only adapts the reference frequency to achieve synchronization and does not adjust the shape of the trajectories in order to keep healthy-like curves as references. Another example of synchronization by means of an adaptive oscillator is mentioned in [215], in this case using the *ALEX II* system, where the oscillator is combined with foot pressure sensor signals (used to detect the initial contact and toe-off events) to estimate the cadence and phase of the actual pattern. Rather than to adapt reference angular trajectories, these values are used to estimate the assistance torque that should be provided in the hip joint based on nominal torque profiles.

The state-of-the-art approaches for synchronization, and generally for reference pattern adaptation, can be classified depending on the degree to which the patient is allowed to adapt the reference gait pattern with his/her movements. In the case of the methods presented by Jezernik [52] and Ronsse [212] [213], the patient is able to adapt the shape (angular properties) of the reference trajectories and the cadence. Chen's method [214] allows the patient to adapt only the cadence. Aoyagi's first method [211] makes cyclic frequency compensation by setting a new reference frequency at every initial contact of the foot with the ground, which is kept for the subsequent gait cycle. Hence it ultimately also allows the patient to adapt the cadence. In the case of Aoyagi's second method [60], although the reference cadence is not directly adapted, the continuous compensation applied to the playback speed allows the patient to impose, to some extent, his/her desired cadence. Neither of Aoyagi's methods allows the patient to influence the shape of the trajectories.

The synchronization methods presented hereafter were designed intending to provide a low level of adaptability of the reference gait pattern. First, it is not desired that reference trajectories are adapted based on the patient's motion. When this is allowed, not only the walking preferences of the patients are part of the adaptation process, but also any pathological movements present in the current state of the patient. Hence, the system would be learning potentially undesired patterns which are ultimately used to assist the patient. A similar consideration was also stated by Chen *et al.* [214]. Methods allowing the adaptation of the reference trajectories should be able to filter the patient's pathologies not to include them in the adaptation process. This filtering is not a trivial task and, to the author's knowledge, is not addressed in the methods that include a reference pattern adaptation. However, the author found it necessary to implement an online hip trajectory adaptation in order to further

decrease obstructive forces applied by the system to the patient during the initial part of the stance phase and so to improve the synergy between the robot and the patient. Regarding the adaptation of the cadence (or reference frequency) two different approaches are contemplated: the first one intends to impose the reference cadence on the patient's gait allowing only minimal changes in the time-related behavior of the trajectory generation in order to tackle the synchronization problems; the second one allows the patient to influence the replay speed of the reference gait pattern, following the concept of Aoyagi's second method [60].

In the next sub-sections, three synchronization methods implemented in the *MOPASS* system are presented, which include novel approaches, extensions and improvements to the strategies proposed by Aoyagi *et al*., as well as the aforementioned hip trajectory adaptation.

5.4.1 Cyclic synchronization with hip-trajectory adaptation (CSHTA)

The first method was designed to synchronize the reference and actual patient's gait pattern every time an initial contact (IC) is recognized, either on the reference or on the actual gait pattern. The IC marks the transition of a leg from swing to stance phase. In the presented implementation, the moment of IC is approximated by the moment the patient's foot (or "virtual" foot, in the case of the reference gait patterns), reaches its maximum horizontal displacement (*FMHD*) along the sagittal axis. When the system identifies an IC in any of the walking motion profiles, it is able to recognize if there exist a phase-lag or phase-lead and perform the respective compensations either by speeding up or slowing down the reference trajectory. To this end, a gait phase detector was developed, capable of recognizing the moment in which the foot reached the FMHD, using some elements such as time- and angle-based thresholds to avoid false positives.

Contrary to Aoyagi's procedure, this method interacts directly with the time fed to the trajectory generator, instead of dealing with the frequencies to later integrate them. When no synchronization efforts are included in the reference trajectory generation process, the input time value for the generator would be equal to the real time that has elapsed since the beginning of the exercise. Since we are dealing with a discrete controller component that works at a certain frequency f_c, the time in a moment k can be calculated from the time at moment $k-1$

$$t[k] = t[k-1] + \Delta t, \tag{42}$$

where $\Delta t = 1/f_c$ is the time elapsed between the two intervals and $t[k]$ corresponds to the input given to the trajectory generator. By inserting a third element Δt_{comp} in (42), it is possible to manipulate the playback speed of the reference trajectories and, consequently, the walking speed. Therefore, a new equation for the input of the generator is yielded:

$$t[k] = t[k-1] + \Delta t + \Delta t_{comp}, \tag{43}$$

where the term Δt_{comp} corresponds to the time compensation element. Note that a $\Delta t_{comp} = -\Delta t$ would hold the reference positions to the values from the last iteration; a $\Delta t_{comp} = (-\Delta t, 0)$ will slow down the normal playback speed, a $\Delta t_{comp} > 0$ will speed up the normal playback speed, a $\Delta t_{comp} = 0$ will keep the normal playback speed; and a $\Delta t_{comp} < -\Delta t$, would generate a 'backwards- walking' situation, which in practice is avoided.

As stated before, there are two cases during desynchronization: phase-lead (reference ahead) and phase-lag (patient ahead). When the system recognizes a phase lead in leg i, it slows down the playback speed of the reference generation by setting $\Delta t_{comp,i}$ to $-0.9 \cdot \Delta t$. Thus, the reference is able to wait for the patient to catch-up without completely pausing the

reference playback speed. In the case of phase lag, the system is able to calculate the lag-time Δt_{lag}, i.e. the time that the reference needs to reach the moment of IC in leg i. The time compensation in this case would be defined by

$$\Delta t_{comp,i} = \begin{cases} v_{TC} \cdot \Delta t & ;\ t - t_{HS,i} \leq \Delta t_{lag} \\ 0 & ;\ t - t_{HS.i} > \Delta t_{lag} \end{cases}, \tag{44}$$

where $t - t_{HS}$ is the time elapsed since the IC from the actual trajectory and $v_{TC} = 25$ is the time compensation rate. This way the system will increase de value of Δt_{comp} smoothly with a rate v_{TC} until the total amount of compensated time is equal to the calculated phase error. Once this happens, the value of Δt_{comp} is reset to zero. It is important to clarify that, because the phase error analysis is done for each leg, there will be two different time compensations: $\Delta t_{comp,L}$ and $\Delta t_{comp,R}$. In situations where the phase error is not very high, these two values do not overlap (i.e. the complete time compensation of one leg will be achieved before the other leg reaches the IC). However, there might be occasions in which each leg will contribute with a non-zero compensation value (e.g. when the phase error is higher than 50% of the gait cycle period). The final value will be therefore equal to the sum of the two single compensations:

$$\Delta t_{comp} = \Delta t_{comp,L} + \Delta t_{comp,R}\ . \tag{45}$$

Fig. 99 shows two simple examples of the time compensation done during phase lead (A) and phase lag (B). In the phase lead example, the actual trajectory is the same as the reference one, but with a period 1.15 times lower. It is possible to observe how the reference trajectory almost holds its positions until the actual trajectory reaches the moment of IC, not only for the leg been analyzed, but also for the other leg. Similarly, in the phase lag example, both trajectories are the same, except for the period which is 1.15 times higher for the reference trajectory. In this case, it can be observed that the reference speeds up to compensate for the measured phase error in both legs. In the lower plot of Fig. 99(B), the total compensated time is shown for every phase-lag occurrence in the leg under scope. In this case, Δt_{lag} is approximately equal to 0.27 seconds (approx. 7.5% of the reference gait period). Note how in both (A) and (B) cases, the compensations correspondent to the contralateral leg also contribute to the overall time-compensation, and therefore also affect the motion profile of the joint trajectories of the leg under consideration, as shown in Fig. 99.

Additional to the time compensation used to synchronize the walking patterns, this method offers a complementary adaptation to the hip trajectories to deal with the cases where the actual step length differs from the reference one in a way that benefits the training process. From the kinematic point of view, the step length during walking is mostly dependent on the hip range of motion, namely the hip maximum flexion and extension. This adaptation was designed based on the following conception: once the patient has done the IC and has started the stance phase, it is counterproductive to force him/her to achieve the step length governed by the original reference pattern. Take as an example the fifth cycle shown in Fig. 98, where the actual step length of the patient was significantly shorter than the reference one (the actual maximum hip flexion was lower than the reference one). In this case, the device was forcing the patient to achieve a higher hip flexion, and therefore trying to move the patient's foot forward, while the patient had already his/her foot on the ground. Although applying the aforementioned time compensation would speed up the reference trajectory and decrease the time in which the system is applying this obstructive forces, it would be still trying to make the patient achieve a position that can't be reached unless he/she makes a very unnatural movement.

To tackle this problem, a cyclic adaptation of the reference hip trajectories based on the actual hip motion was developed. The basic idea is that, every time the system recognizes an

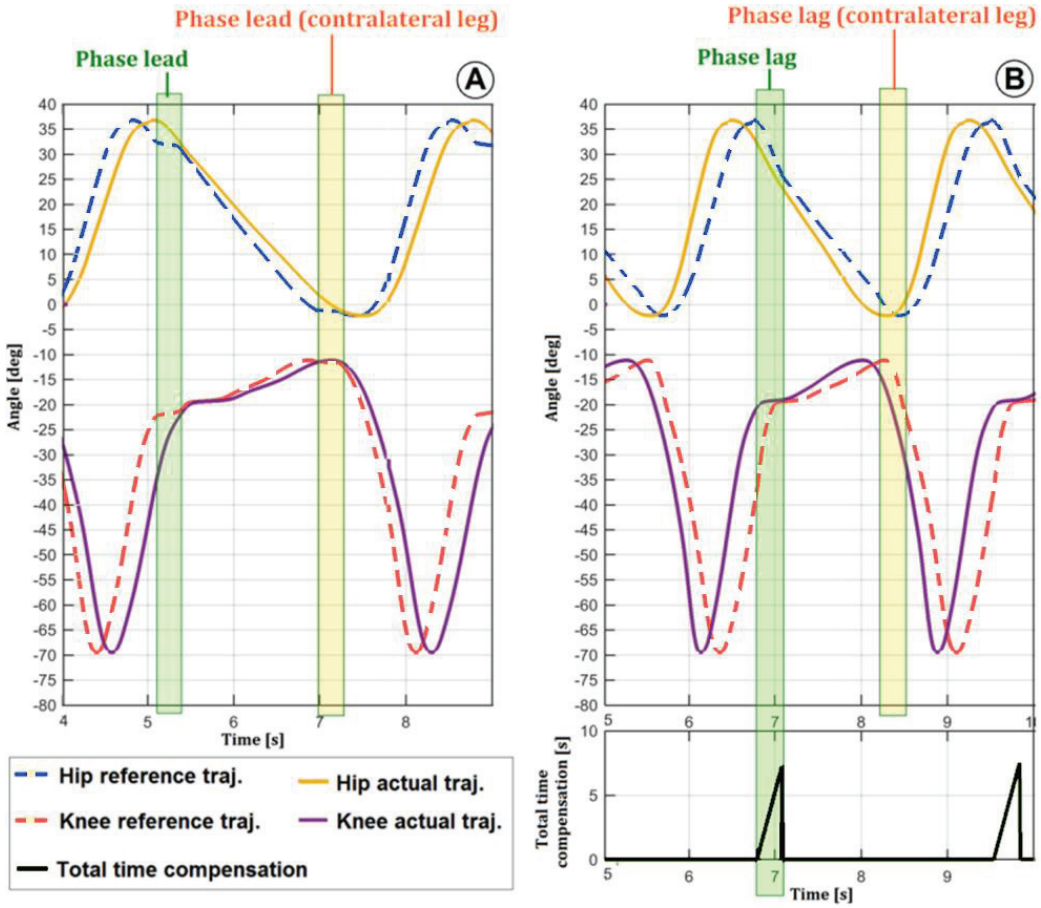

Fig. 99 Examples of time compensation during CSHTA synchronization

IC from the actual walking pattern, it will check which was the actual hip flexion angle in that specific moment and will compare it with the hip flexion angle in the moment of IC from the reference trajectories in order to perform a smooth adaptation of the hip reference trajectory that will reduce the difference between these two flexion angles. Such adaptation is governed by the following equation

$$\theta^*_{h-ref} = \theta_{h-ref} \cdot m_{adj} + b_{adj}$$

$$m_{adj} = \frac{\theta^*_{target} + \Delta\theta_{hh-ref} - \theta_{hh-ref}}{\Delta\theta_{hh-ref}}$$

$$b_{adj} = \frac{\theta^2_{hh-ref} - \theta_{hh-ref}\left(\Delta\theta_{hh-ref} + \theta^*_{target}\right) + \Delta\theta_{hh-ref} \cdot \theta^*_{target}}{\Delta\theta_{hh-ref}}$$

$$\Delta\theta_{hh-ref} = \theta_{hh-ref} - \theta_{min-h-ref} \ , \tag{46}$$

where θ^*_{h-ref} is the adjusted hip reference angle, $\theta_{h,ref}$ is the original hip reference angle, θ_{hh-ref} is the hip angle of the reference trajectory in the moment of FMHD (i.e. IC), $\theta_{min-h-ref}$ is the minimum hip angle from the reference trajectory (angle of maximum extension), and θ^*_{target} is the value of hip angle of the adjusted reference trajectory in the moment of FMHD. To have a better understanding of this adaptation refer to Fig. 100 where a simple example is depicted. Notice how the original trajectory is proportionally adjusted

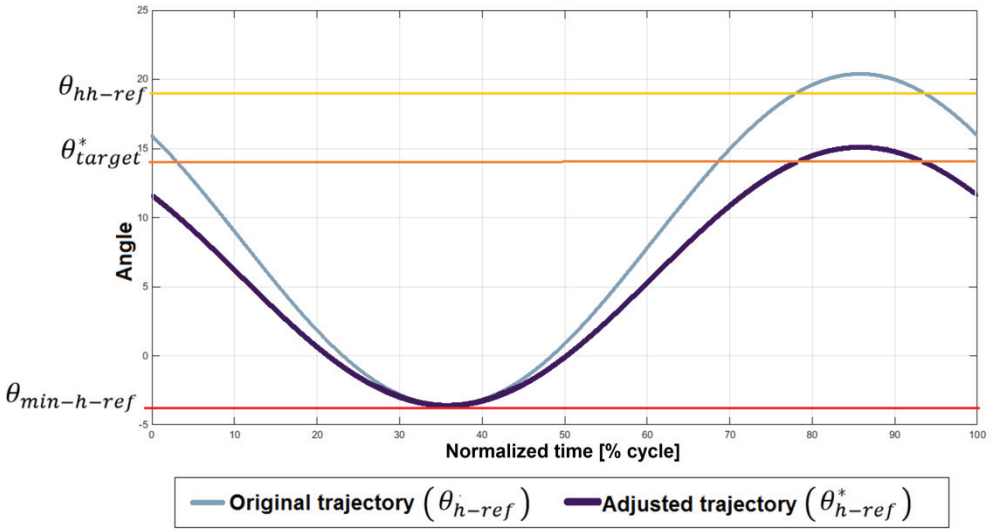

Fig. 100 Cyclic trajectory adaptation during synchronization process

based on the difference between the original and the target angular value during the IC. Notice as well that, the more the phase (normalized time) approaches the moment of global minimum, the more the adaptation level decreases, until reaching a level of no-adjustment in that global minimum moment. This means that the adaptation affects the maximum flexion but not the maximum extension.

So, once the system recognized an IC it measures the actual hip angle in the moment of FMHD (θ_{hh-act}) and sets it as the new adaptation target θ_{target}. It subsequently adapts the reference hip trajectory so that the hip angle in the moment of FMDF of the adjusted reference trajectory matches θ_{target}. However, this matching is not done instantly, but rather in a smooth manner. The angular adjustments in an instant k are done following (46) and

$$\theta^*_{target}[k] = \begin{cases} \theta^*_{target}[k-1] + k_{dir} \cdot v_{HA} \cdot \Delta t \;\; ; \;\; \theta^*_{target}[k] < \theta_{target} \,, k_{dir} > 0 \\ \theta^*_{target}[k-1] + k_{dir} \cdot v_{HA} \cdot \Delta t \;\; ; \;\; \theta^*_{target}[k] > \theta_{target} \,, k_{dir} < 0 \\ \theta_{target} \qquad\qquad\qquad\qquad ; \; otherwise \end{cases}, \quad (47)$$

where v_{HA} =50[deg/s] is the rate (velocity) of angular adjustment and k_{dir}={1,-1} corresponds to the direction of the angular adjustment (positive or negative) determined every time a new θ_{target} is set, following

$$k_{dir} = \begin{cases} 1 \;\; ; \;\; \theta^*_{target}[k-1] < \theta_{target} \\ -1 \;\; ; \;\; \theta^*_{target}[k-1] > \theta_{target} \end{cases}. \quad (48)$$

Once the reference hip trajectory reaches the moment of maximum extension, the adjustment is reset ($\theta_{target} = \theta_{hh-ref}$) and the reference trajectory returns to its original profile. Note that the value of θ_{target} is set (if necessary) every time an actual IC or reset command happens. The system will smoothly change the value of θ^*_{target} until it reaches the current θ_{target} and then it will maintain that value until θ_{target} is set again. An example of hip trajectory adaptation and subsequent reset of the θ_{target} is shown in Fig. 101, where the hip angle in the actual IC (θ_{hh-act}) is higher than the reference angle θ_{hh-ref}. Notice how, despite the adaptations, the hip and knee reference trajectories remain continues.

Taking into account the time compensation and the hip trajectory adaptation, the diagram of the complete procedure is depicted in Fig. 102. For simplicity, the diagram only shows the

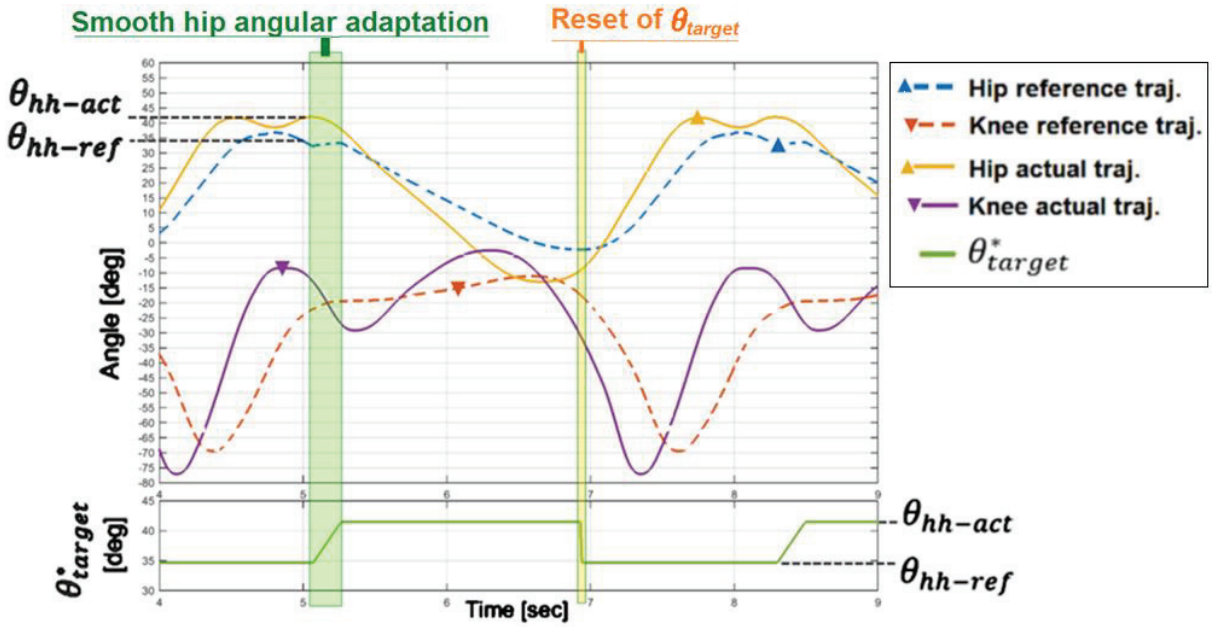

Fig. 101 Example of cyclic trajectory adaptation during synchronization process

hip and knee angles of one leg. In reality, the phase detection, hip trajectory calibration and hip adaptation function are applied separately to each leg. However, as explained before, the time compensator works together with the results of both legs.

To assess the behavior of the synchronization method, several simulations were run which include different cases of desynchronization (phase lag and lead) and hip trajectory adaptation. Table 30 contains the details of each one of the simulation cases whereas the simulation results are shown in **Fig. 103**. The *'TrajGen_0.35'* trajectory corresponds to the joint trajectories yielded by the generator from section 4.3 with the following inputs: $length_{LowerLeg}$ = 0.48 m, $length_{UpperLeg}$ = 0.40 m, *height* = 1.74 m, *WS* = 0.35 m/s, *Cad* = 47 steps/min, and *gait period* = 2.55 s. The *'Lit_GN'* trajectory corresponds to the gait patterns obtained from [24], with a period proportional to the period of the *'TrajGen_0.35'* trajectory (see table).The simulations also include a predefined initial phase difference between the reference and the actual (simulated) patterns (see table). Note that, besides the reference and actual hip and knee trajectories, **Fig. 103** shows the synchronization state of the leg under scope (green lines) with the following values: 0 if they are in-synch; 10 if there is a case of phase lag (patient ahead); and 20 if there is a case of phase lead (reference ahead). However, these states should not be considered as the real synchronization states. In this specific scenario, it is considered that the walking patterns are again in-synch when they are both in stance phase, although in reality there could be a phase error and therefore they could be still out-of-synch. Moreover, because the synchronization analysis is done only in between the moments of IC from the reference and actual trajectories, the real synchronization state throughout the rest of the gait cycle is unknown and therefore not represented by the states shown in **Fig. 103**. The depicted states are only used as a reference for the time compensator and hip trajectory calibrator to know when and how to make their compensations and adjustments.

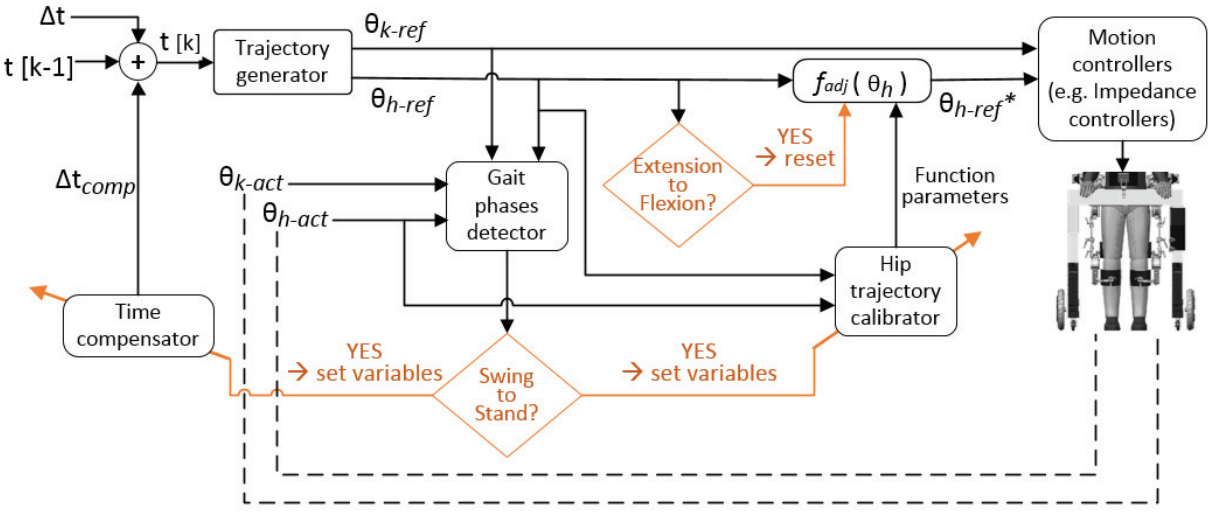

Fig. 102 Diagram of the cyclic synchronization algorithm with hip-trajectory adaptation

Table 30 Simulation cases for assessment of the synchronization methods

Case	Reference trajectory	(Simulated) Actual trajectory	Walking periods	Initial phase error
A	TrajGen_0.35	TrajGen_0.35	$T_{act} = T_{ref}$	Phase-lag = 15% (patient ahead)
B	TrajGen_0.35	TrajGen_0.35	$T_{act} = 0.85 \cdot T_{ref}$	In phase (no error)
C	TrajGen_0.35	TrajGen_0.35	$T_{act} = 1.15 \cdot T_{ref}$	In phase (no error)
D	TrajGen_0.35	Lit_GN	$T_{act} = T_{ref}$	Phase-lag = 15% (patient ahead)
E	TrajGen_0.35	Lit_GN	$T_{act} = 0.85 \cdot T_{ref}$	In phase (no error)
F	TrajGen_0.35	Lit_GN	$T_{act} = 1.15 \cdot T_{ref}$	In phase (no error)
G	TrajGen_0.35	Lit_GN	$T_{act} = T_{ref}$	In phase (no error)
H	Lit_GN	TrajGen_0.35	$T_{act} = T_{ref}$	Phase-lag = 15% (patient ahead)
I	Lit_GN	TrajGen_0.35	$T_{act} = 0.85 \cdot T_{ref}$	In phase (no error)
J	Lit_GN	TrajGen_0.35	$T_{act} = 1.15 \cdot T_{ref}$	In phase (no error)
K	Lit_GN	TrajGen_0.35	$T_{act} = T_{ref}$	In phase (no error)
L	TrajGen_0.35	Lit_GN	$T_{act} = 0.45 \cdot T_{ref}$	In phase (no error)

The simulation results show that the method manages to deal with the synchronization issues in a proper manner, although it is limited by the time compensation rate v_{TC}. If the difference between reference and actual walking speeds is too high, the method will struggle to catch up with the actual patterns (as seen in case *L*). Increasing v_{TC} would help in these circumstances, but will affect the smoothness of the reference walking patterns. However, such high differences in walking speeds are not expected during therapy. If they actually happen, it means that the reference speed is not appropriate for the specific patient and must be adjusted by the therapist. On the other hand, the hip trajectory adaptation behaved as expected, helping the reference patterns to come closer to the actual ones when necessary, decreasing the interference of the reference trajectories during the beginning of the stance phase.

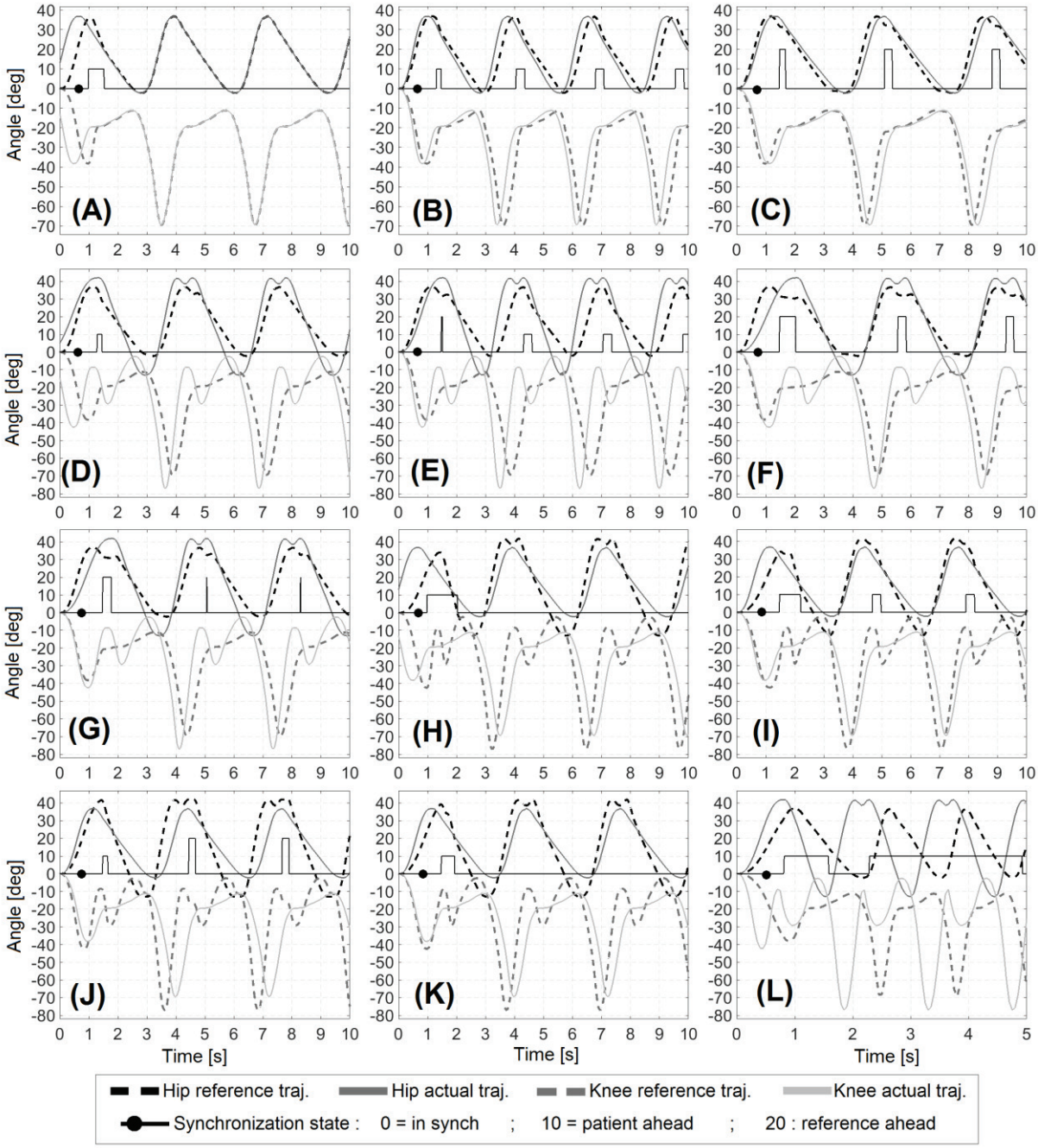

Fig. 103 Simulation results of the cyclic synchronization algorithm with hip-trajectory adaptation

Additional to the simulations, the synchronization method was tested with a healthy subject using the powered orthosis of the *MOPASS* system together with a treadmill. For these tests, the current limits of the joint drives were set to 1 Amp to allow a more compliant behavior of the system and more mobility freedom to the subject. The reference trajectory was set to *'TrajGen_0.35'*. Three exercises were carried out: in the first exercise (A) the subject was asked to walk very slow at the beginning and then increase considerably the speed; for the second exercise (B), the subject was asked to walk simulating lack of strength in the lower limbs; and for the last exercise (C), the subject was asked to walk simulating limping. The results of these exercises are depicted in Fig. 104, showing the proposed method managed to stay in-synch in all three cases, even when the actual gait patterns had abnormal trajectories.

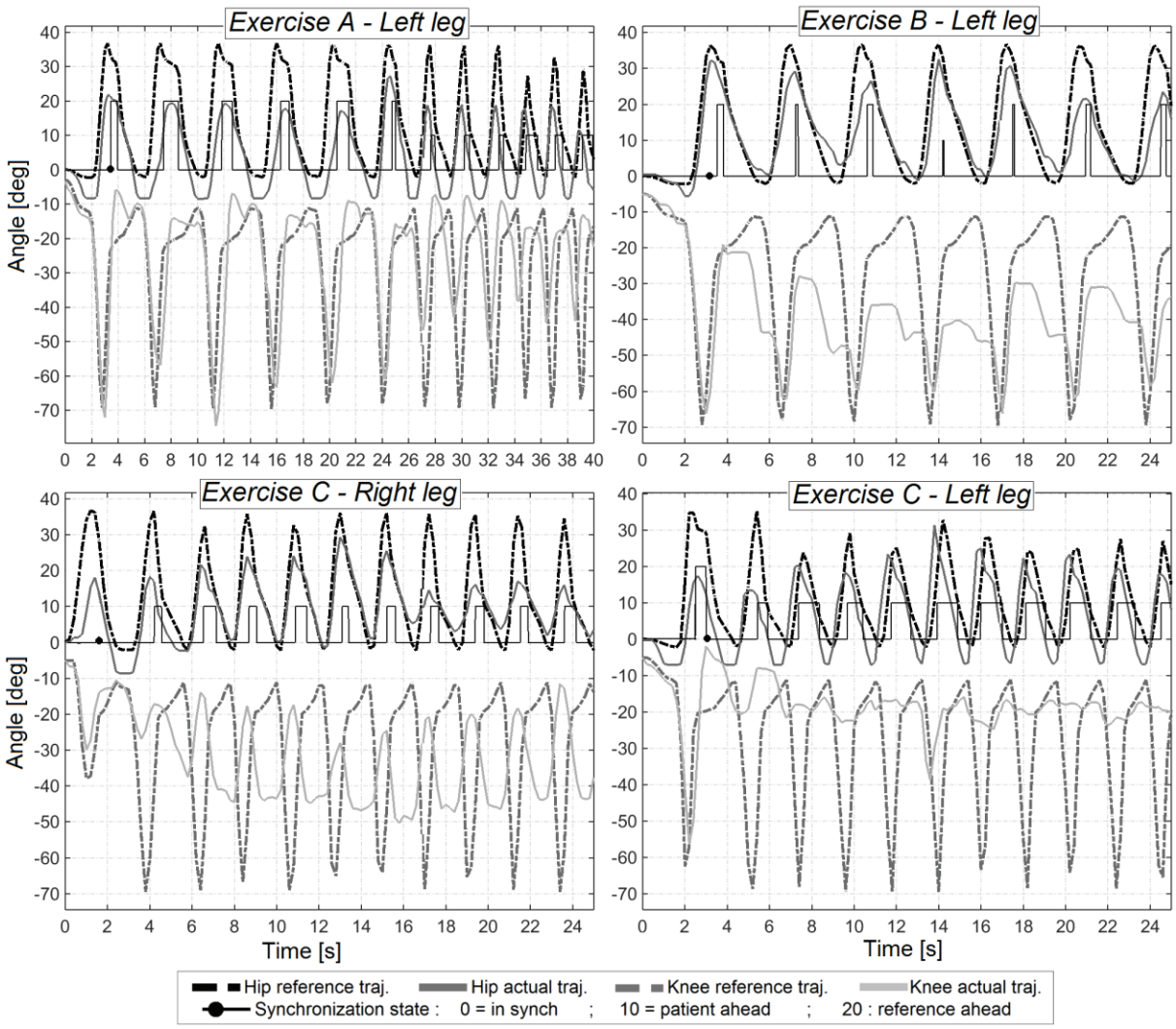

Fig. 104 Results of the cyclic synchronization algorithm with hip-trajectory adaptation using *MOPASS* and a treadmill

Regarding the hip trajectory adaptation, it also shown good results, mostly when the phase-lag error was high and the system had enough time to adjust timely the hip maximum extension angles.

Adjustment of platform speed

In the methods proposed by Aoyagi *et al.* it is not explicitly expressed how the adjustment in the treadmill speed is done, which leads to the assumption that such adjustment is governed directly by the resulting frequency and phase compensations. In their first method [211], it is assumed that the adjustments in the playback speed are implemented directly to the treadmill speed with changes every IC, whereas for the second method [60] the adjustments would be applied instantly (continuously) proportionally to the phase error. Whether filters are applied or not to the resulting treadmill speed to avoid undesired oscillations (which might appear as an inherited problem mostly in their second method) is, to our knowledge, not mentioned.

In this subsection, four different methods to adjust the platform velocity based on the compensations and adjustments done during the synchronization process are presented. These methods were developed aiming to obtain a smooth, yet timely adaptation of the speed of the

platform, trying to avoid lag feelings (the platforms is staying behind), pushing feelings (the platform is pushing forward faster than it is supposed to), and uncomfortable speed oscillations.

Method 1:

The first method gets the time compensation Δt_{comp} in each iteration of the synchronization component, calculates the corresponding platform speed compensation and applies a simple Butterworth low-pass filter to reduce the oscillations in the speed. The diagram of this method is depicted in Fig. 105, where WS_{ref} is the original walking speed (i.e. platform speed) of the reference pattern, r is the radius of the wheels, and K_{WSC} is the compensation constant. To get a full influence of the time compensations in the platform speed compensation, a $K_{WSC} = 1$ was selected. Note that the turning feature presented previously was neglected for a better understanding.

Method 2:

The second method adds a second low pass filter to work together with the Butterworth low-pass filter of *Method 1* (Fig. 106). This second filter is a simple 'average' filter used to further reduce the oscillations of the resulting platform speed: it takes the last n values of the compensated speed and calculates the average, before feeding it to the Butterworth filter. In this case, n corresponds to the amount of iterations happening during 75% of a gait cycle period:

$$n = 0.75 \cdot \frac{T_{ref}}{\Delta t} \ . \tag{49}$$

Method 3:

The third method includes a cyclic average filter to complement the two other filters of *Method 2*. Contrary to *Method 2*, the n from the initial average filter corresponds to the amount of iterations happening during 30% of a gait cycle period. The cyclic average filter works together with the gait phases' detector, and supplies the average compensated platform speed from the whole last gait cycle (calculated every time the reference trajectory of the main leg reaches a moment of FMHD) to the initial average filter. The cyclic average filter

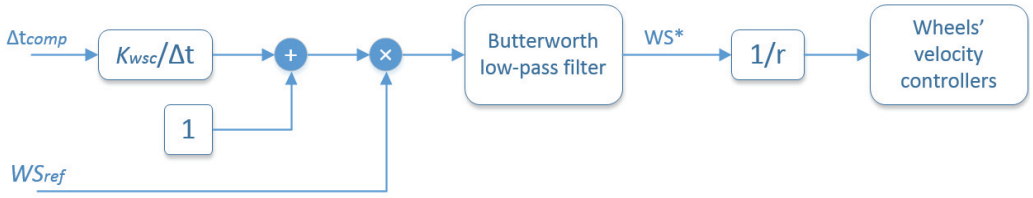

Fig. 105 *Method 1* for adjustment of platform speed during synchronization

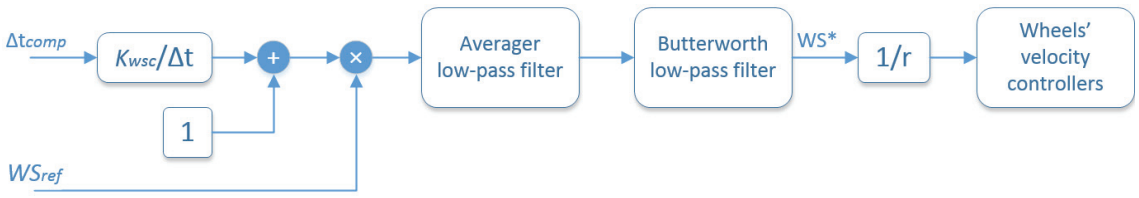

Fig. 106 *Method 2* for adjustment of platform speed during synchronization

keeps its output unchanged until the next moment of FMHD in the main leg happens. The diagram of this method is depicted in Fig. 107.

Method 4:

The fourth method intends to recalculate the walking speed taking into account the time compensations and hip angular adjustments done during the synchronization process, and based on that, to calculate the compensation value of the platform speed. The initial average and Butterworth filters from *Method 3* are kept, whereas the cyclic average filter is replaced by a 'flip-flop'-like component which bypasses the input value to the output when the moment of FMHD in the main leg happens and, similar to the cyclic average filter, retains the last fed value in its output until the next main leg's FMHD occurrence. The diagram of this method is depicted in Fig. 108. As it can be observed, the platform speed compensation in this method is governed by the multiplier

$$K_{WS} = \frac{SL_{ref} \cdot T_{ref} + K_{WSC} \cdot \Delta_{SL} \cdot T_{ref}}{SL_{ref} \cdot T_{ref} + K_{WSC} \cdot SL_{ref} \cdot \Delta_T}$$

$$\Delta_{SL} = SL^*_{ref} - SL_{ref}$$

$$\Delta_T = T^*_{ref} - T_{ref} \ , \qquad (50)$$

where SL_{ref} and T_{ref} are the calculated step length and period of the original reference patterns, respectively, T^*_{ref} is the time elapsed between the previous and the current moment of FMHD in the main leg (i.e. the reference gait period after applying the time compensations throughout the last cycle), and SL^*_{ref} is the calculated step length taking into account the hip trajectory adaptations. As with the previous methods, a K_{WSC} = 1 was selected to get a full influence of the time compensations and trajectory adaptations in the platform speed compensation calculations. Note that with this value of K_{WSC}, after multiplying by the original $WS_{ref} = 2\,SL_{ref}/T_{ref}$, the resulting compensated speed (before filters) is equal to the new measured reference speed ($2\,SL^*_{ref}/T^*_{ref}$). Because the method needs to calculate the adjusted period and step lengths from both legs, it only starts operating after a complete gait cycle is recognized, disregarding the initial step.

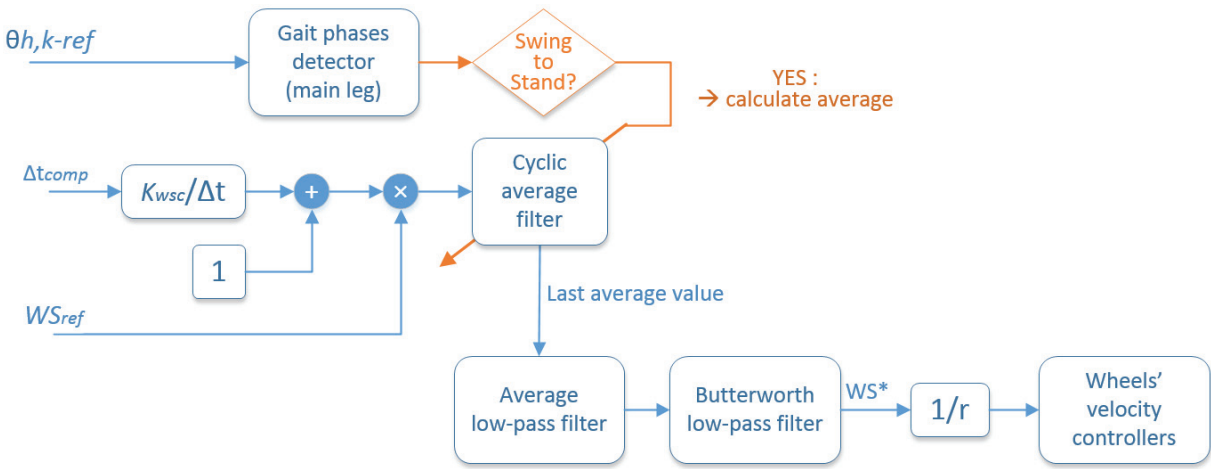

Fig. 107 *Method 3* for adjustment of platform speed during synchronization

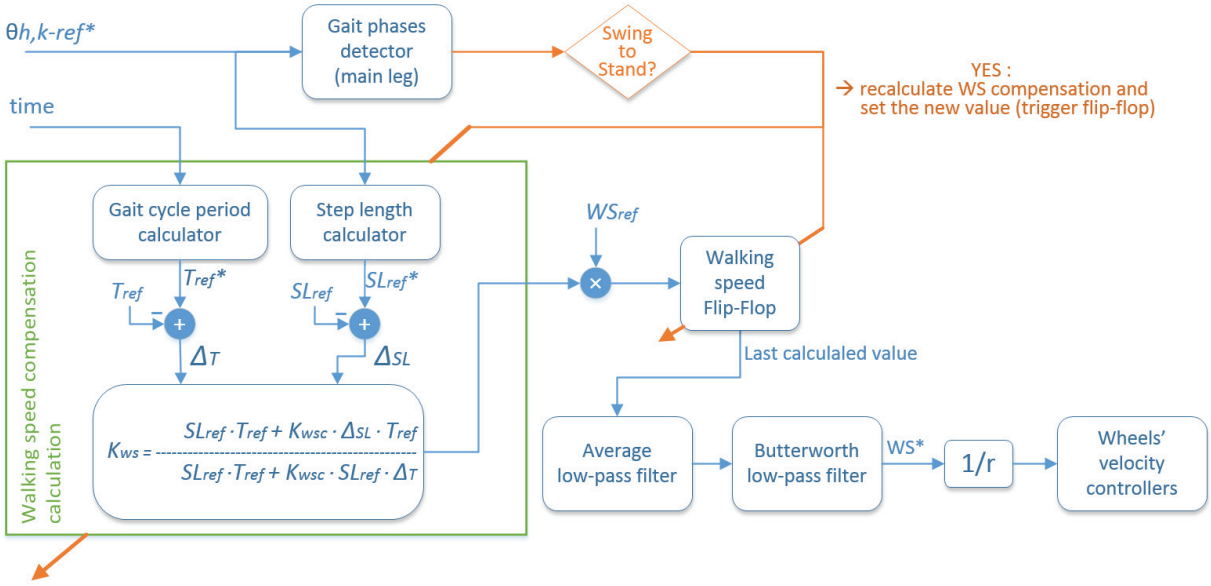

Fig. 108 *Method 4* for adjustment of platform speed during synchronization

Assessment of the methods

An initial revision of the behavior of the four methods was carried out by running the same simulations exposed in Table 30 and observing how the platform speed compensation reacted in each situation. The simulation results are depicted in **Fig. 109**. The first thing to note is that, in the cases where the actual gait cycle period is different from the reference one, the time compensation causes the output of *Method 1* to oscillate considerably. Lower oscillations are observed with *Method 2*, although the remaining ones could still be uncomfortable for the patient. These fluctuations do not affect methods 3 and 4, which appear to have very smooth changes. The second thing to notice is how the platform speeds delivered by *Method 4* are very different from the ones from the other three methods which, disregarding the oscillations, tend to settle in similar values. These differences are caused by the inclusion of the angular adjustments in the hip trajectory and recalculation of the walking speed. A final assessment on the reaction time of each method can be done. As expected, *Method 1* is the one that reacts the fastest followed by methods 2, 3 and 4. Regarding *Method 4*, it can be observed how, in some cases (*D*, *H* and *K*), its response is considerably slow compared to *Method 3*.

A second assessment was done with a healthy subject using the *MOPASS* system during over-ground walking. As before, the current limits of the hip and knee joints were set to 1 Amp to increase the compliance of the device and the reference trajectory was set to *'TrajGen_0.35'*. The subject was asked to walk naturally changing the speed in between the exercise. The results of these exercises can be seen in Fig. 110. When using *Method 1*, the subject felt that the platform speed was increasing and decreasing constantly during a gait cycle in an unpleasant manner. These drastic speed changes were significantly reduced with *Method 2*, leading to a more pleasant adjustment. Nevertheless, the subject felt that the platform was slightly pushing when he was walking at very low speed. *Method 3* presented no speed oscillations, as expected. Compared to the previous two methods, *Method 3* gave less freedom to the subject to influence the velocity of the platform, trying to make him maintain the velocity from his last gait cycle. This was also the case using *Method 4*, but in a higher

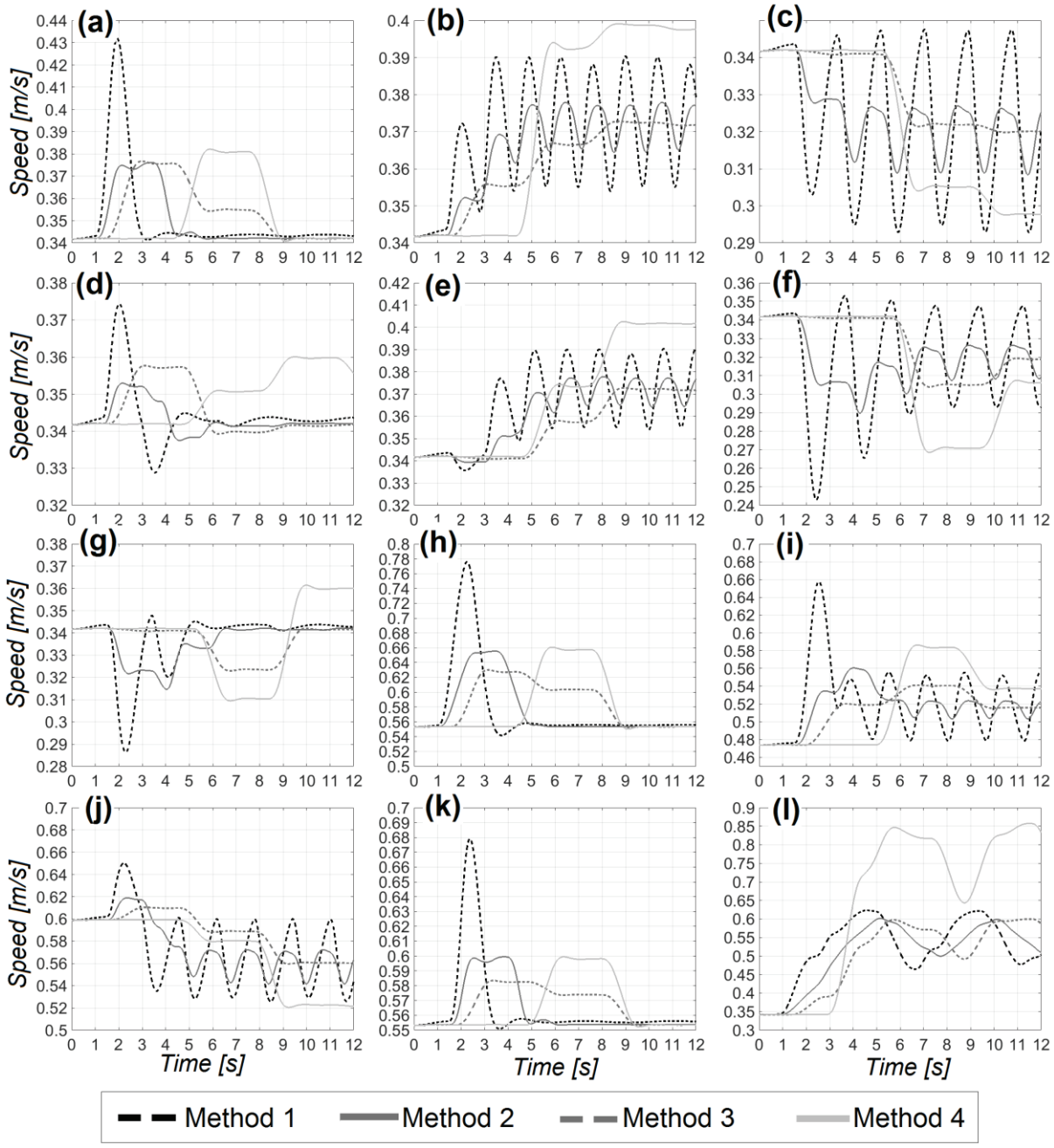

Fig. 109 Simulation results for adjustment of platform speed using the cyclic synchronization algorithm with hip-trajectory adaptation

degree; moreover, the subject felt that the platform was slightly lagging and not keeping up with his speed changes. At the end, methods 2 and 3 got the best feedback from the participant. Whether it is desired if the patient has more or less freedom to influence the platform speed during training can be judged by the therapist depending on the patient and the objectives at hand.

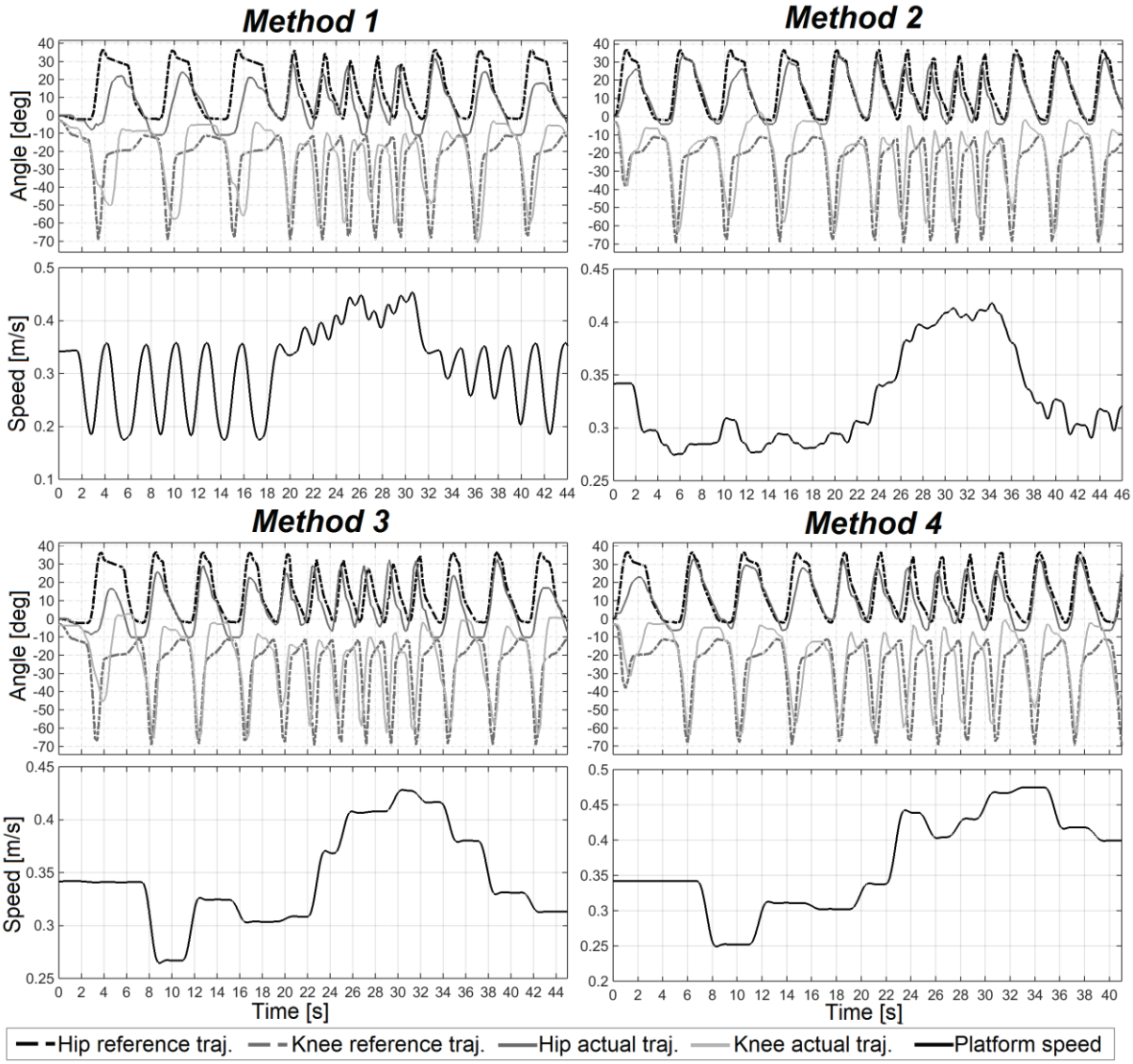

Fig. 110 Results for adjustment of platform speed using the cyclic synchronization algorithm with hip-trajectory adaptation during experiments with MOPASS system

5.4.2 Phase-control synchronization (PCS)

The phase-control synchronization (PCS) was the second method that was developed to tackle the synchronization issues. The PCS is based on concept of Aoyagi's second method [60]. The algorithm is composed basically of two components: the trajectory comparator and a phase controller. The trajectory comparator, which is actually a service offered by the same trajectory generator component, takes the actual joint angles and compares them with the reference ones in order to obtain the estimated actual phase (again, not to be confused with the gait phase). To this end, a cost function is introduced

$$C_{PC}(t_i) = \boldsymbol{W}_{PC}^T \cdot [e_\theta \quad e_h \quad e_d \quad e_{t1}^2 \quad e_{t2}]^T$$

$$e_\theta = \sum_{j=1}^{n} \left|\theta_{j,ref}(t_i) - \theta_{j,act}\right|$$

$$e_h = \left|h_{L,ref}(t_i) - h_{L,act}\right| + \left|h_{R,ref}(t_i) - h_{R,act}\right|$$

$$e_d = \left|d_{L,ref}(t_i) - d_{L,act}\right| + \left|d_{R,ref}(t_i) - d_{R,act}\right|$$

$$e_{t1} = |t_n - t_i|$$

$$e_{t2} = |t_n^*[k-1] - t_i|. \tag{51}$$

where $n = 4$ is the number of joints, $\theta_{j,act}$ is the actual position of joint j, $\theta_{j,ref}(t_i)$ is the reference position of joint j at a given normalized time (phase) t_i, $h_{p,act}$ and $d_{p,act}$ are the actual vertical and horizontal positions of the foot from the leg $p = \{L$:left, R:right$\}$ with respect to the hip joint calculated from the actual joint angles, $h_{p,ref}(t_i)$ and $d_{p,ref}(t_i)$ are the vertical and horizontal positions of the foot from the leg p calculated from the reference joint angles at a given normalized time t_i, t_n is the normalized time value corresponding to the current input of the generator, t_n*[k-1] is the estimated normalized time (phase) from the previous iteration and $\boldsymbol{W}_{CP}$ is the vector of weights. In the cases of e_{t1} and e_{t2}, special considerations must be taken during the error calculations due to the fact that we are dealing with periodic trajectories. The errors correspond to the minimum distance between the values under scope taking into consideration the period which, after normalization, is equal to 100%. If, for example, t_n = 90% and t_i = 10%, the value of e_{t1} will be 20% and not 80%.

The task of the phase comparator is to check several values of t_i (in practice, 200 values are checked) and find the one that minimizes the cost function. This value will be taken as the estimated phase (t_n*) of the actual walking pattern. Note that, unlike Aoyagi's cost function, C_{PC} includes phase- (time-) based error measurements, meant to give more stability and robustness to the phase comparator.

The phase controller component, on the other hand, is the one in charge of speeding up and slowing down the playback speed of the reference pattern to synchronize it with the actual walking pattern. It receives the phase error calculated from the generator's current phase and the estimated phase and yields a normalized-time rate compensation value. The controller is designed as a PI-controller of the form

$$\upsilon_{nt-comp}(s) = \left(K_{P-PC} + \frac{K_{I-PC}}{s}\right) \cdot e_{PC}(s). \tag{52}$$

where $e_{PC} = t_n$*- t_n is the phase error, $\upsilon_{nt\text{-}comp}$ is the normalized-time compensation rate, and $K_{P\text{-}PC} = 2$ and $K_{I\text{-}PC} = 0.02$ are the PI coefficients. After computing the normalized-time compensation rate, it can be saturated to avoid undesired high changes in the playback speed. In this case, the saturation limits were set to ±100. Note that the trajectory comparator, the phase controller and the saturator work with normalized time values, and because of this, normalization and de-normalization operations with respect to the reference gait cycle period must be performed to handle the normal and normalized values. Following this idea, $\upsilon_{nt\text{-}comp}$ must be de-normalized to obtain the time compensation rate

$$\upsilon_{t-comp} = \upsilon_{nt-comp} \cdot \frac{T_{ref}}{100}\ , \tag{53}$$

which is finally used to calculate the compensation time following

$$\Delta t_{comp} = v_{t-comp} \cdot \Delta t \ . \tag{54}$$

A second saturation is applied to the time compensation value to avoid negative playback speeds. In this case, the lower saturation value is equal to $-\Delta t$. The higher saturation can be set to a desired maximum compensation value, although the first compensation rate saturator should be designed in a way that there is no further need for a positive saturation of Δt_{comp}. Once Δt_{comp} is obtained, it is used to get the input value of the generator following (43).

The complete diagram of the phase-control synchronization method is depicted in Fig. 111. Again, for simplicity, only the trajectories corresponding to one leg are included in the diagram. However, as explained before, the trajectory comparator uses the angles of the joints of both legs.

The same procedure used to assess the previous synchronization method was carried out for the PCS method. Initially, the simulation cases exposed in Table 30 were analyzed. The simulation results are shown in Fig. 112. It can be seen that the phase controller manages to maintain the simulated and reference patterns in-synch, within the limitations given by the controller PI coefficients and the first saturator. If the actual walking speed is much higher that the reference one, the control efforts will not be enough to keep the reference pattern close to the actual one, as shown by case *L*. Moreover, if the actual walking speed is even much higher, the controller might end up causing unreliable changes in the reference trajectories. Nevertheless, as stated previously, these cases should not occur during training. Comparing with the results from the CSHTA method, the reference was able to follow the simulated patterns in a closer manner, due to the fact that the PCS is compensating for the phase difference continuously throughout the complete period, instead of doing it every IC. This does not directly mean that this method is better or worse than the CSHTA, only that it gives more freedom to the patient to influence the walking speed (and indirectly the reference trajectories), whereas the cyclic method intends to force more the patient into following the reference parameters and only perform the synchronization actions when strictly necessary. This difference can be seen more clearly when comparing the support torques that would be

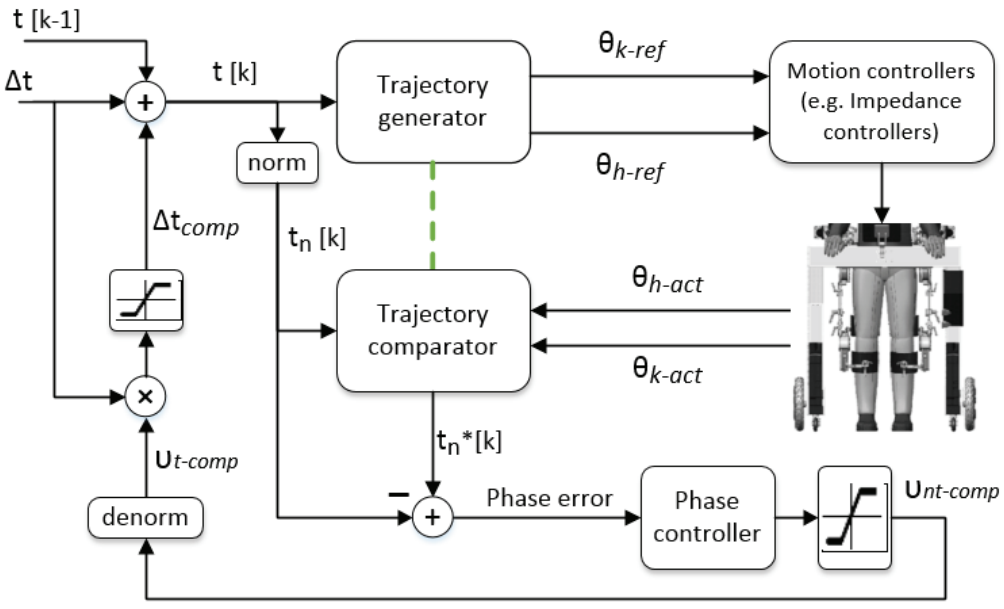

Fig. 111 Diagram of the phase-control synchronization method

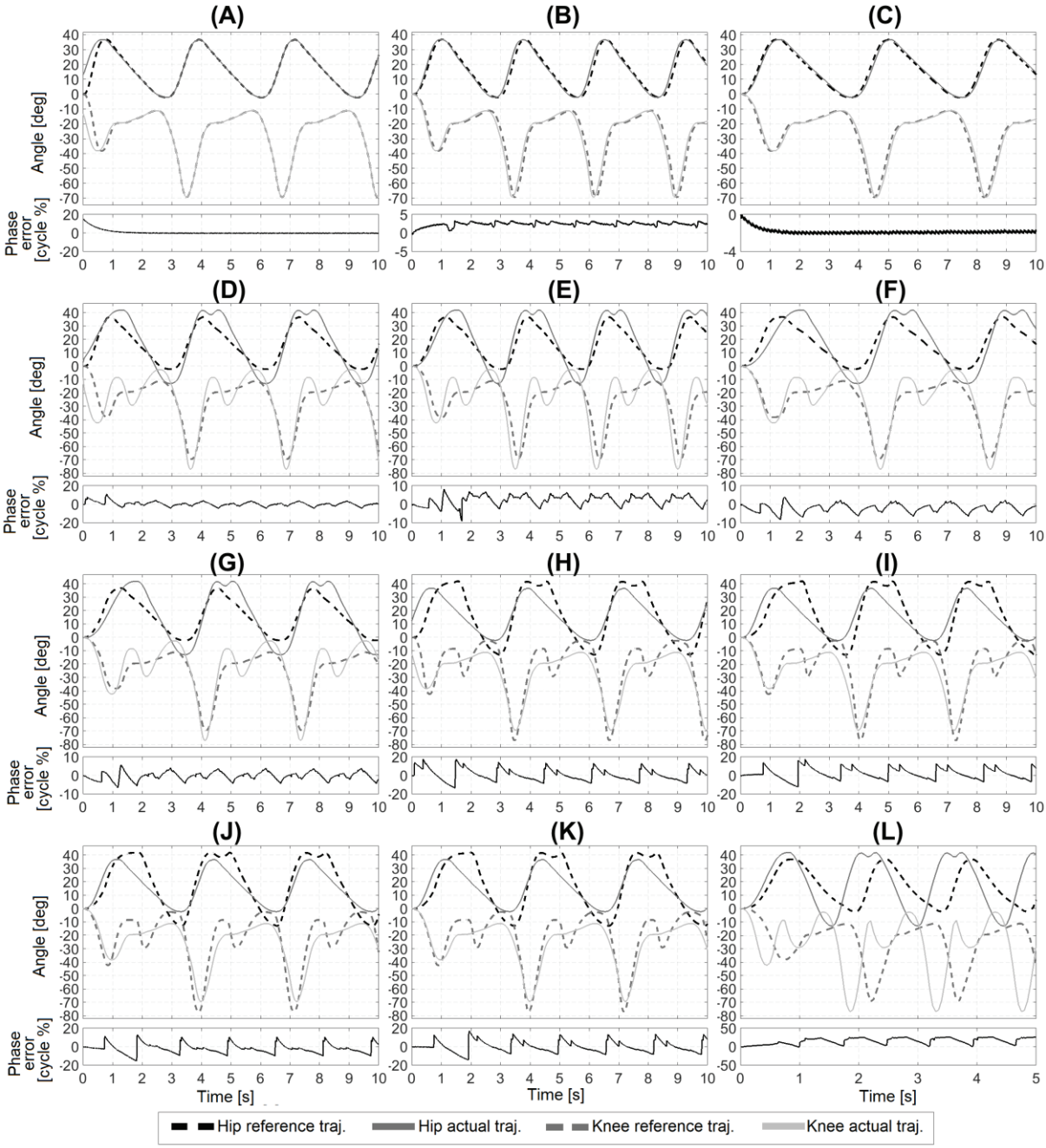

Fig. 112 Simulation results of the phase-control synchronization method

yielded when using an impedance controller in each of the simulation cases. This comparison is done in a forthcoming subsection.

The second analysis to the synchronization method was done using the *MOPASS* system with a treadmill where a healthy subject was asked to do the same three exercises as with the CSHTA method: (A) natural walking starting very slow and then increasing the speed; (B) simulation of lack of strength in the lower limbs; and (C) simulation of limping. The results of these exercises are depicted in Fig. 113. As with the CSHTA method, this method managed to stay in-synch in all three cases, although it sometimes struggled to follow the actual pattern during the initial step. It also showed a good performance when the actual gait patterns had abnormal trajectories, even though, at first glance, the results gotten from CSHTA method

(Fig. 104) seem slightly better. Because of the practical nature of these tests, a proper comparison between the methods cannot be carried out in this context because of the impossibility of the participant to exactly repeat the motion efforts during the tests.

Adjustment of platform speed

Because the time compensation follows also (43), the same principles for the adaptation of the platform speed from the CSHTA method apply for the PCS method. Hence, the four adaptation methods presented in section 5.4.1 were also implemented and tested with the phase-controller synchronization strategy. The results concerning the platform speed from the simulation cases exposed in Table 30 are shown in Fig. 114. Similar conclusions to the ones from the CSHTA method about the performance of each of the speed adjustment methods can be drawn. However, the differences in the time compensation strategies from both synchronization methods are reflected in the behavior of the platform speed. In some cases the CSHTA method presented stronger oscillations in the speed, whereas in other cases the stronger oscillations belonged to the PCS method.

A second set of practical tests was also carried out with the healthy subject walking over-ground with the *MOPASS* system and changing the walking speed during the exercises, same as with the previous synchronization method. The results of these tests are depicted in Fig. 115. The feedback gotten from the participant about how each of the speed adjustment

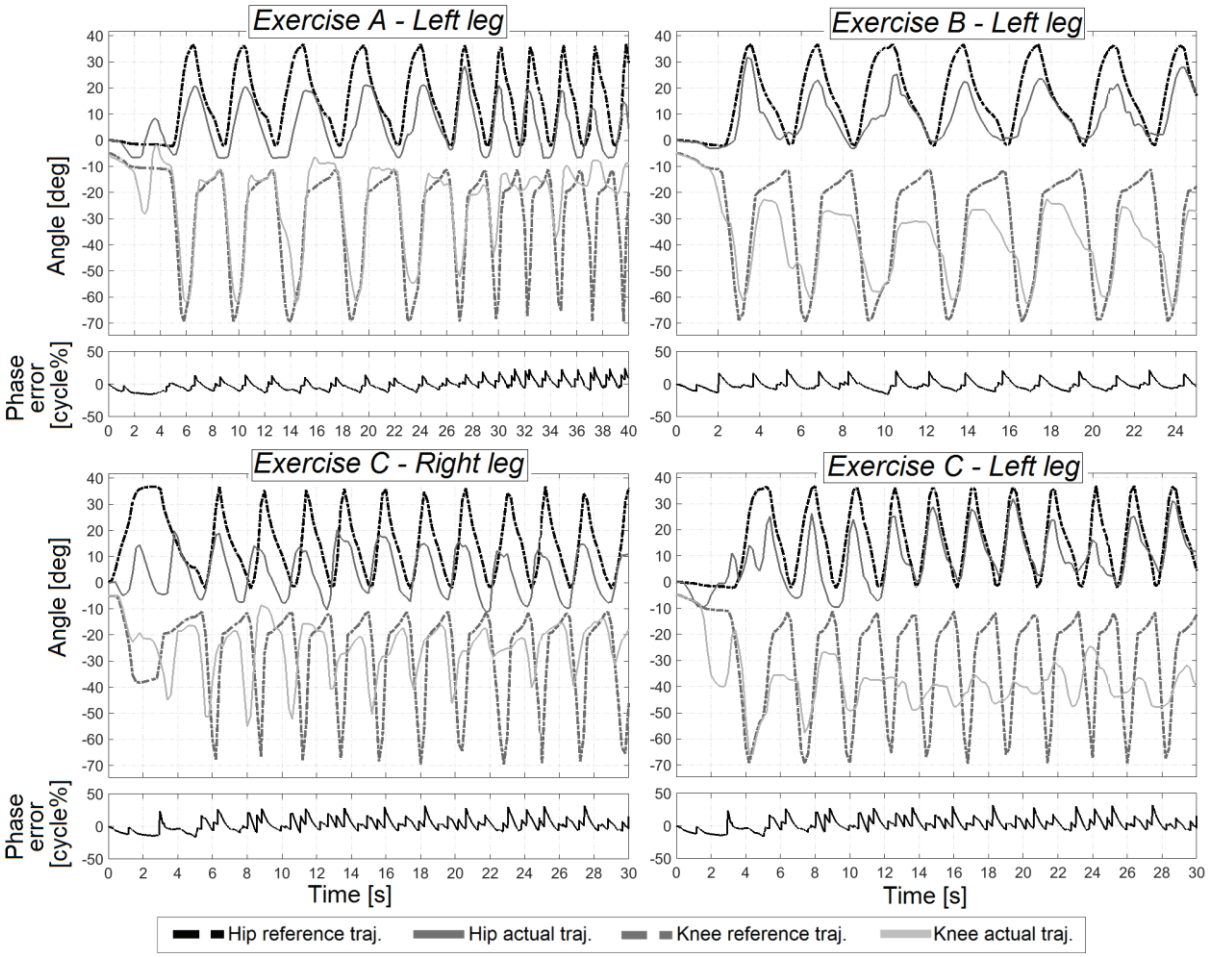

Fig. 113 Results of the phase-control synchronization using *MOPASS* and a treadmill

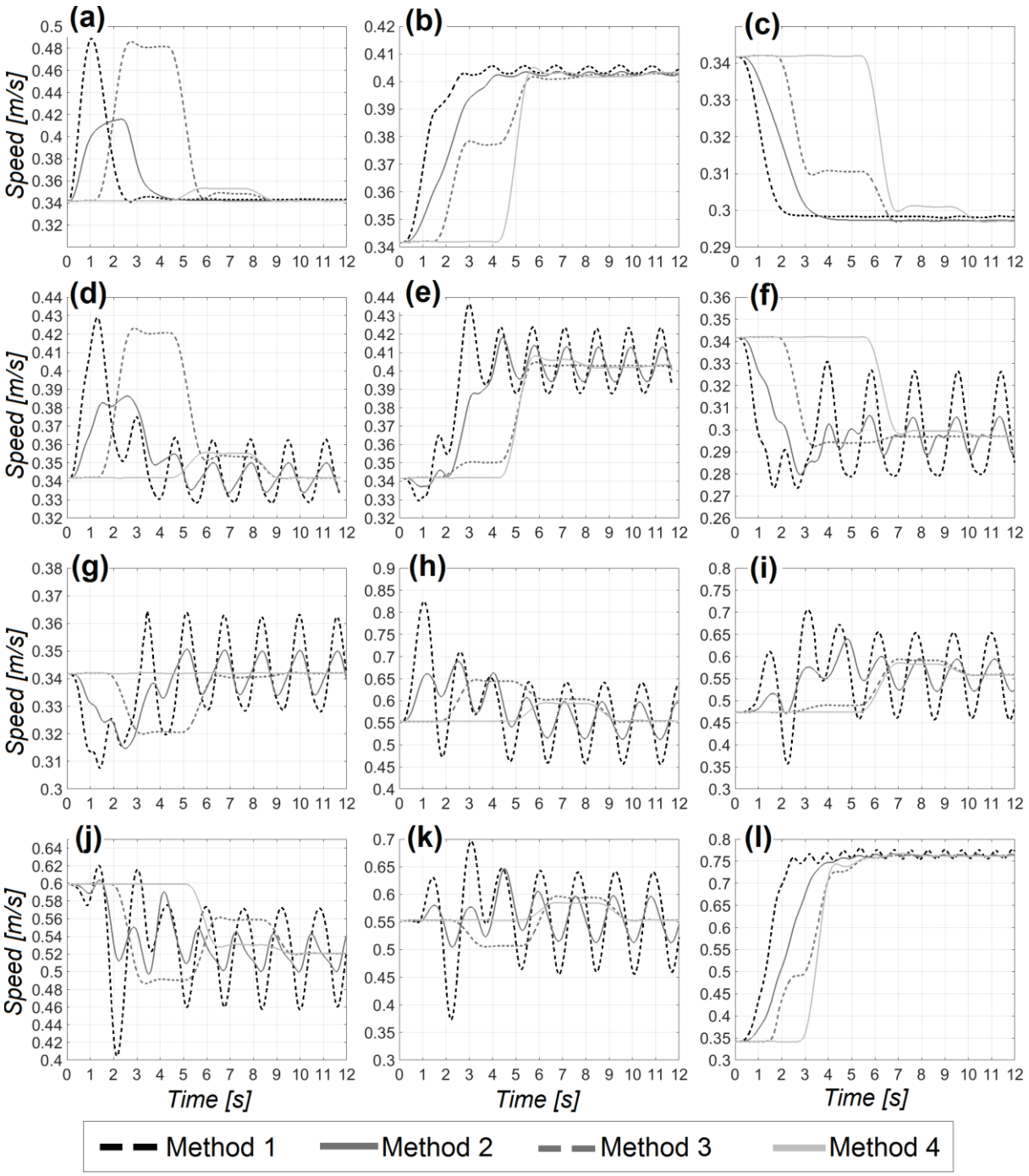

Fig. 114 Simulation results for adjustment of platform speed using the phase-control synchronization method

methods felt was the same as for the CSHTA method: drastic and uncomfortable changes in the speed with *Method 1*, a platform-lag feeling with *Method 4*, and good outcomes with methods 2 and 3. The only difference in the perception from the test subject was that the platform didn't present the 'pushing' behavior at very low speed when using *Method 3* that occurred with the CSHTA method.

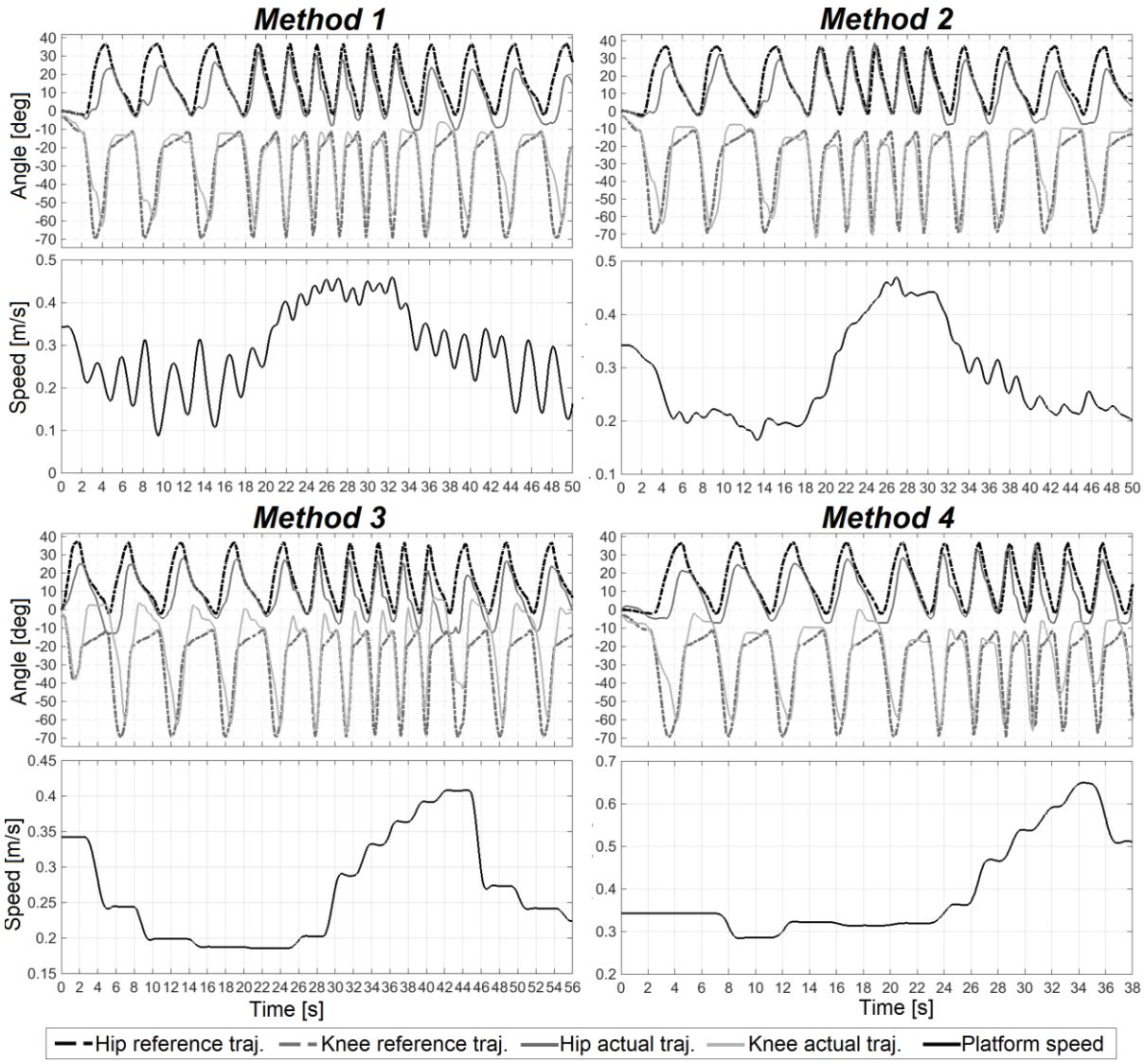

Fig. 115 Results for adjustment of platform speed using the phase-control synchronization method during experiments with the MOPASS system

5.4.3 Phase-control with hip-trajectory adaptation (PCHTA)

A third synchronization algorithm was designed by combining the PCS and the CSHTA methods. Simply put, the method possesses continuous time compensation, governed by the trajectory comparator and the phase controller, and a cyclic adaptation of the hip trajectory. The diagram of such combination is shown in Fig. 116.

The results from the simulation and practical tests of the PCHTA method are shown in Fig. 117 and Fig. 118, respectively. The method managed to maintain the reference trajectories in-synch with the actual walking pattern in all simulation cases (except for case L) and most of the practical ones. However, notice how this time the trajectory comparator had some struggle identifying correctly the actual phase during the exercise *C* of practical tests with the *MOPASS* system. This was caused by the highly unnatural curves in the walking

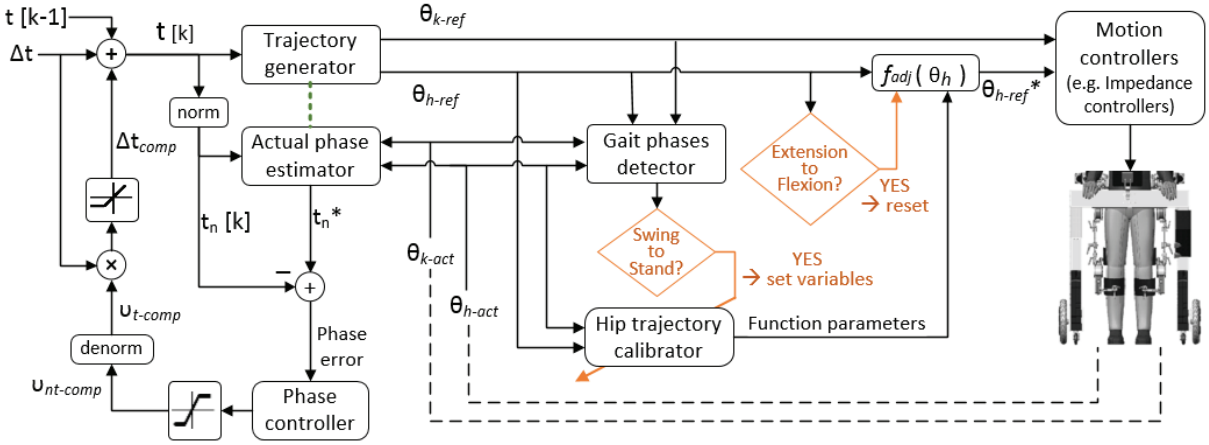

Fig. 116 Diagram of the phase-control synchronization method with hip trajectory adaptation

patterns. Here we can see one of the drawbacks from the phase controller-based time compensation: the trajectory comparator assumes that the actual walking pattern is close to a healthy pattern (or, more precisely, to the reference pattern). Highly unnatural patterns lead to ill estimations of the current phase. However, such unnatural patterns are only expected during therapy with highly impaired patients where therapy strategies based on low system compliance are implemented. Therefore, this type of patients is meant to be assisted with high torques in order to ensure a good tracking of the reference trajectories and, consequently, wouldn't have enough freedom to deviate from them. On the other hand, the cyclic hip trajectory adaptation worked as expected as with the CSHTA method, adapting the step lengths even when the time compensator had struggles synchronizing the gait patterns.

Adjustment of platform speed

As before, the methods for platform speed adjustment introduced in section 5.4.1 were implemented and tested using the new synchronization method. The simulation and practical results are shown in Fig. 119 and Fig. 120, respectively. Because of the nature of this synchronization method, only differences in the platform speed using *Method 4* can be observed in the simulation results compared to the results gotten with the PCS method, although in most of the cases the differences are very low or inexistent. Nevertheless, it is interesting to see how the recalculation of walking speed behaves when complementing the PCS with the hip trajectory adaptation. Because of the same reason, the feedback from the test subject about how the speed adjustments felt with methods 1, 2 and 3 was the same as with the PCS strategy, as expected. Moreover, no significant differences were felt with *Method 4* when using the PCS with and without the hip trajectory adaptation: a platform-lag feeling is still present.

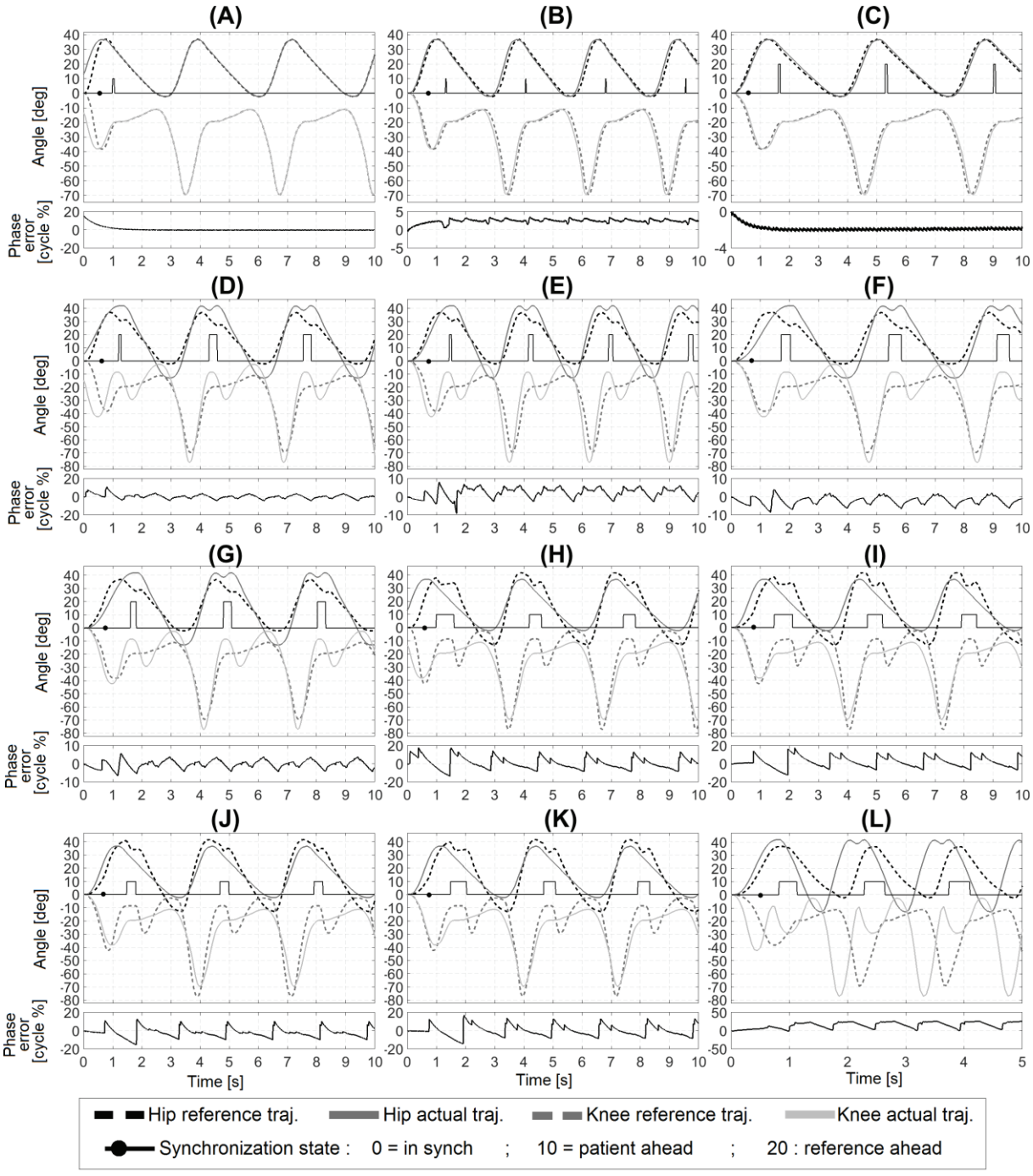

Fig. 117 Simulation results of the phase-control synchronization method with hip trajectory adaptation

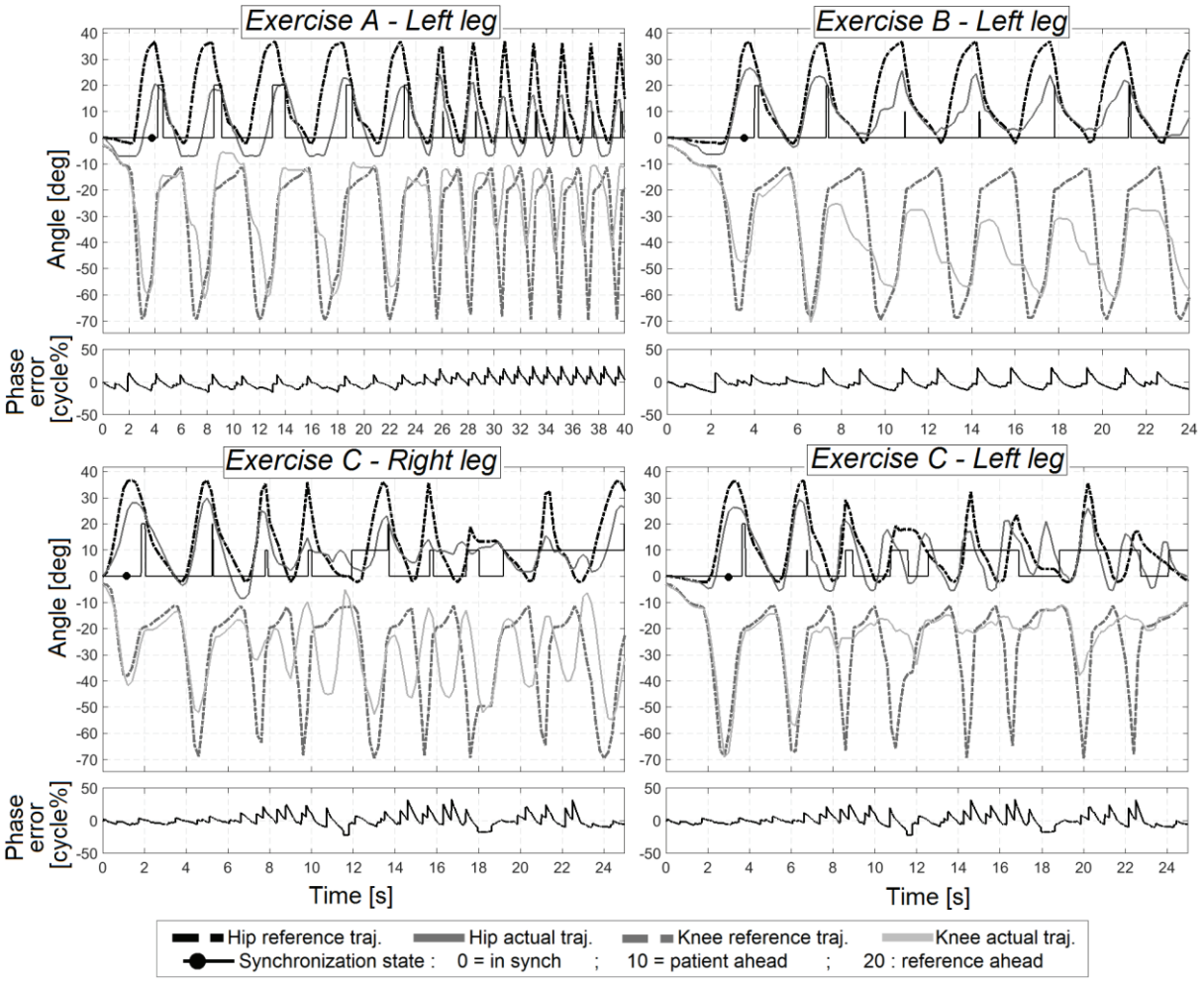

Fig. 118 Results of the phase-control synchronization with hip trajectory adaptation using *MOPASS* and a treadmill

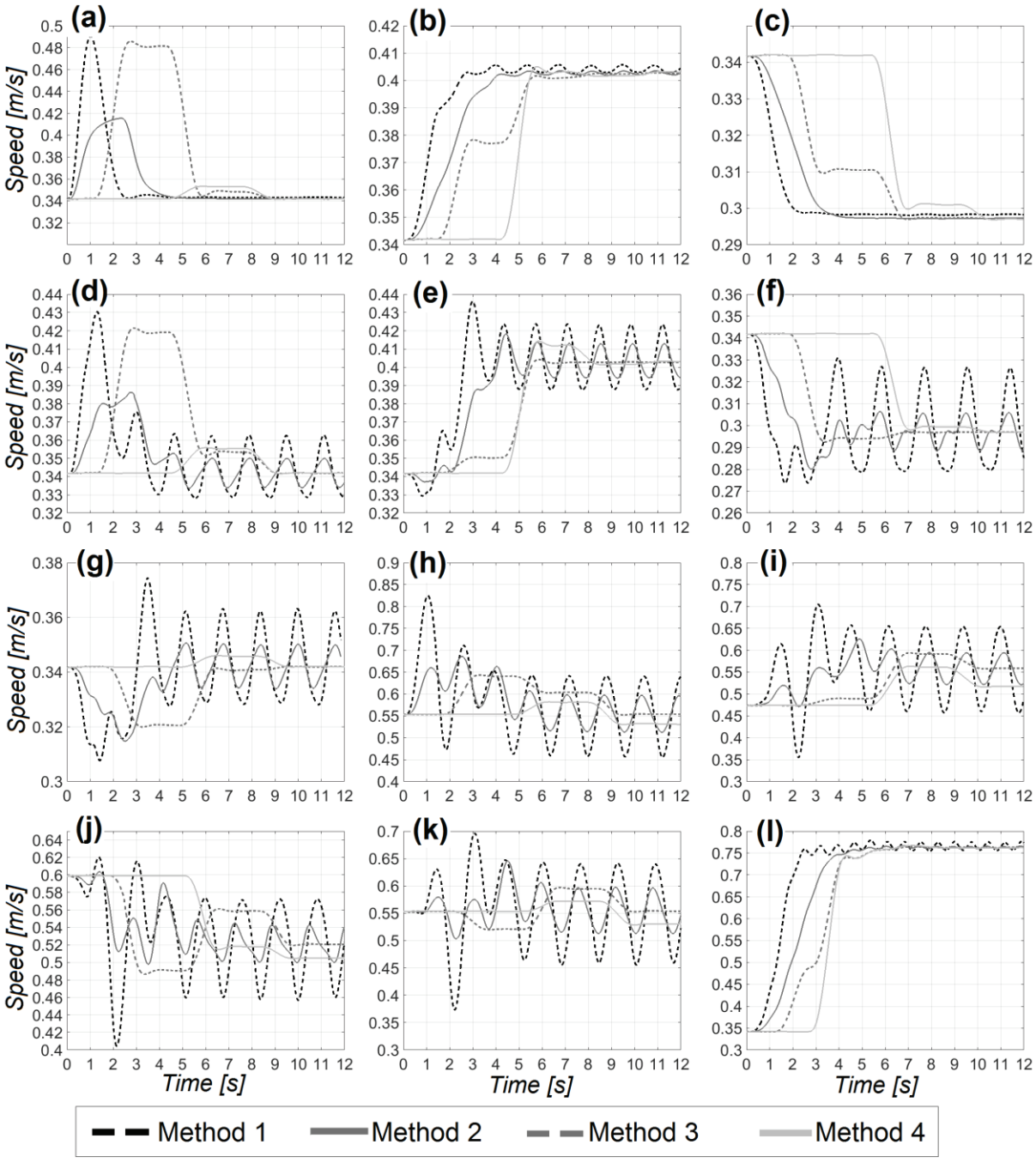

Fig. 119 Simulation results for adjustment of platform speed using the phase-control synchronization method with hip trajectory adaptation

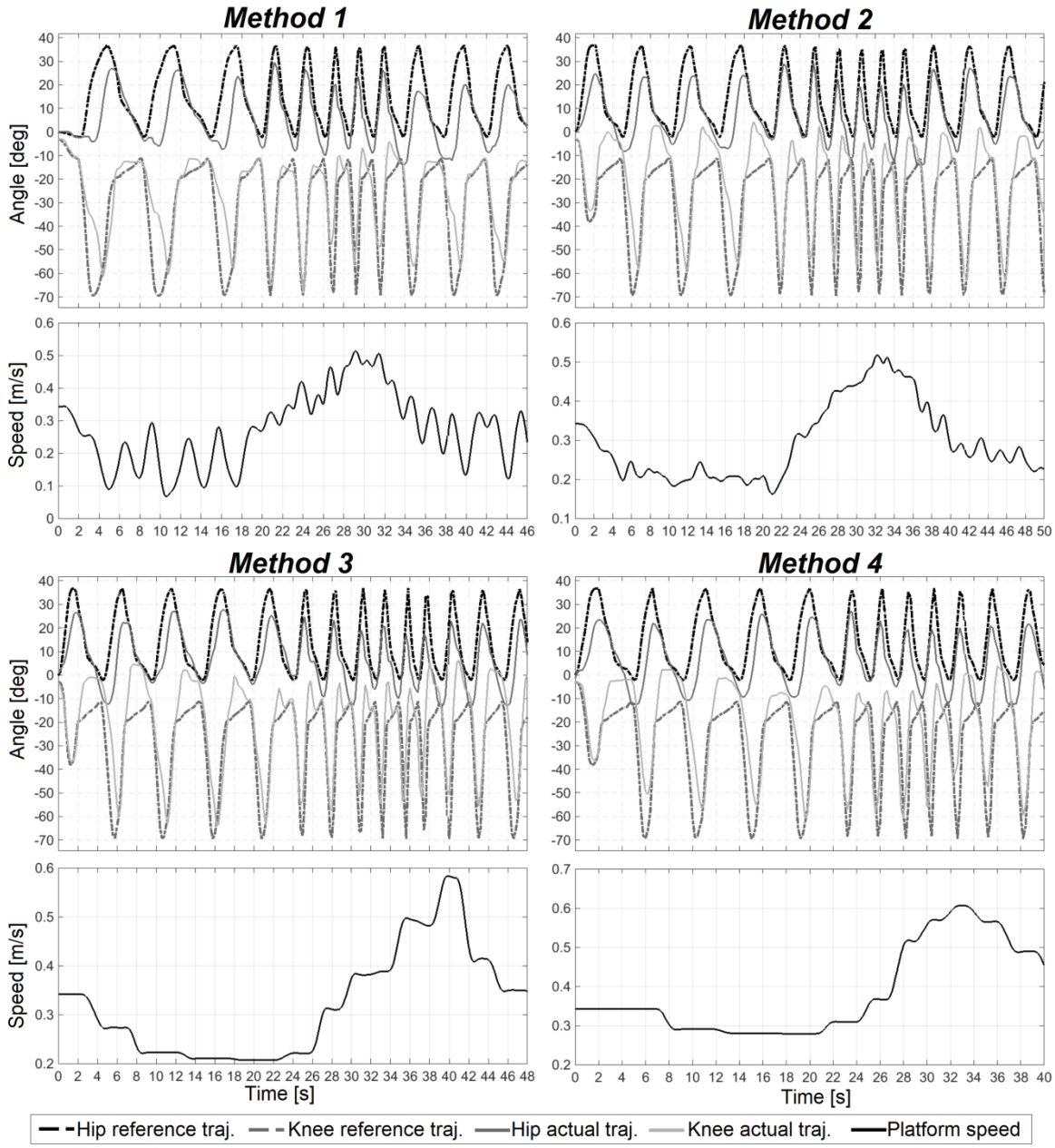

Fig. 120 Results for adjustment of platform speed using the phase-control synchronization method with hip trajectory adaptation during experiments with the MOPASS system

5.4.4 Comparison between the synchronization methods

The comparison between the synchronization strategies can be done from two distinct outlooks: the behavior of the trajectory generator and its dependencies when using the two different time compensation approaches (cyclic and phase control), and the behavior with and without the hip trajectory adaptation.

Regarding the time compensation, from the theoretical point of view, the phase-control approach gives more freedom to the patient to influence the walking speed during the therapy, leading to a closer phase-tracking. This higher freedom translates indirectly into higher changes in the instant reference joint angles perceived by the patient, which results in a decrement of the overall angular errors throughout all the gait cycle. The cyclic time

compensation, on the other hand, intends to reduce the phase error every cycle, but only enough to avoid considerable synchronization issues. Once the corresponding cyclic compensation is done, it returns to the original reference playback speed with the objective of inducing the patient to synchronize with the reference pattern in a natural way (i.e. speeding up or slowing down rather than performing unnatural steps). The selection between the two time compensation approaches is dependent on the objectives of the therapy. If the patient doesn't have a high impairment and the therapy goals invite to a compliant system behavior, including letting the patient influence freely the therapy cadence, the continues compensation delivered by the PCS might feel more comfortable to the patient. In the cases where a compliant system behavior is wanted but it is desired that the patient walks with a selected cadence, the cyclic time compensation might be better suited to achieve the therapy goals.

However, both time compensation strategies have their limitations. The cyclic approach is highly dependent on a proper identification of the moment of initial contact (IC). In this implementation, it is based solely on the hip and knee trajectories; hence, in cases where the actual patterns possess an unnatural motion, the inputs may appear insufficient to perform a proper and prompt identification avoiding false positive IC detections. The addition of other sensor inputs, such as foot-switches, can help to overcome this limitation and achieve a more robust and timely identification. On the other hand, the PCS is highly dependent on the proper estimation of the actual phase and, consequently, on how natural is the current walking pattern of the patient. If the estimation is not stable, the time compensation might end up having a random-like behavior, affecting the outcomes of the therapy.

Regarding the hip trajectory adjustment, the methods that implement it and complement it with a proper synchronization algorithm will deliver more meaningful reference trajectories to the therapy, mostly when the phase-error and the difference between step lengths are high. However, the trajectory adjustment algorithm possesses the same limitation from the cyclic time compensation: it is highly dependent on the proper and timely detection of the moment of IC.

Another aspect to take into account for the comparison of the methods is the effect that the time compensation and the direct and indirect reference trajectory adaptations would have on an impedance controller in charge of delivering the support torques during 'assist as needed' therapy. As explained in a previous section, this impedance controller calculates the assistive torques from the difference between the reference and actual positions and velocities, and because of that it is directly affected by any changes applied to the reference patterns. To analyze this specific scenario, an impedance controller with haptic tunnel was designed and fed with the result values obtained from the simulations that were carried out for each one of the synchronization strategies (Table 30). The coefficients of the controller selected for the simulation were $K_{IC} = 50$ and $B_{IC} = 1$, whereas the radius of the haptic tunnel was $r_{HT} = 2°$. The resulting support torques for the hip and knee joints can be seen in Fig. 121 and Fig. 122. Table 31 shows the absolute mean values of the support toques for each of the cases, where the average was calculated over the first six seconds of simulation.

Two main conclusions can be drawn from these results. First, in most of the cases, CHSTA yielded significantly higher torques that the other two methods. This is caused by the non-continues time compensation performed by the method and the fact that the phase controller tries to make the reference phase come close to a value where the position errors between reference and actual trajectories is lower (i.e. the estimated phase). These measurements corroborate the statements presented above: the cyclic time compensation keeps the reference pattern synchronized with the actual one while intending to influence the patient into following the reference cadence, giving the patient less freedom to train at a self-selected step frequency.

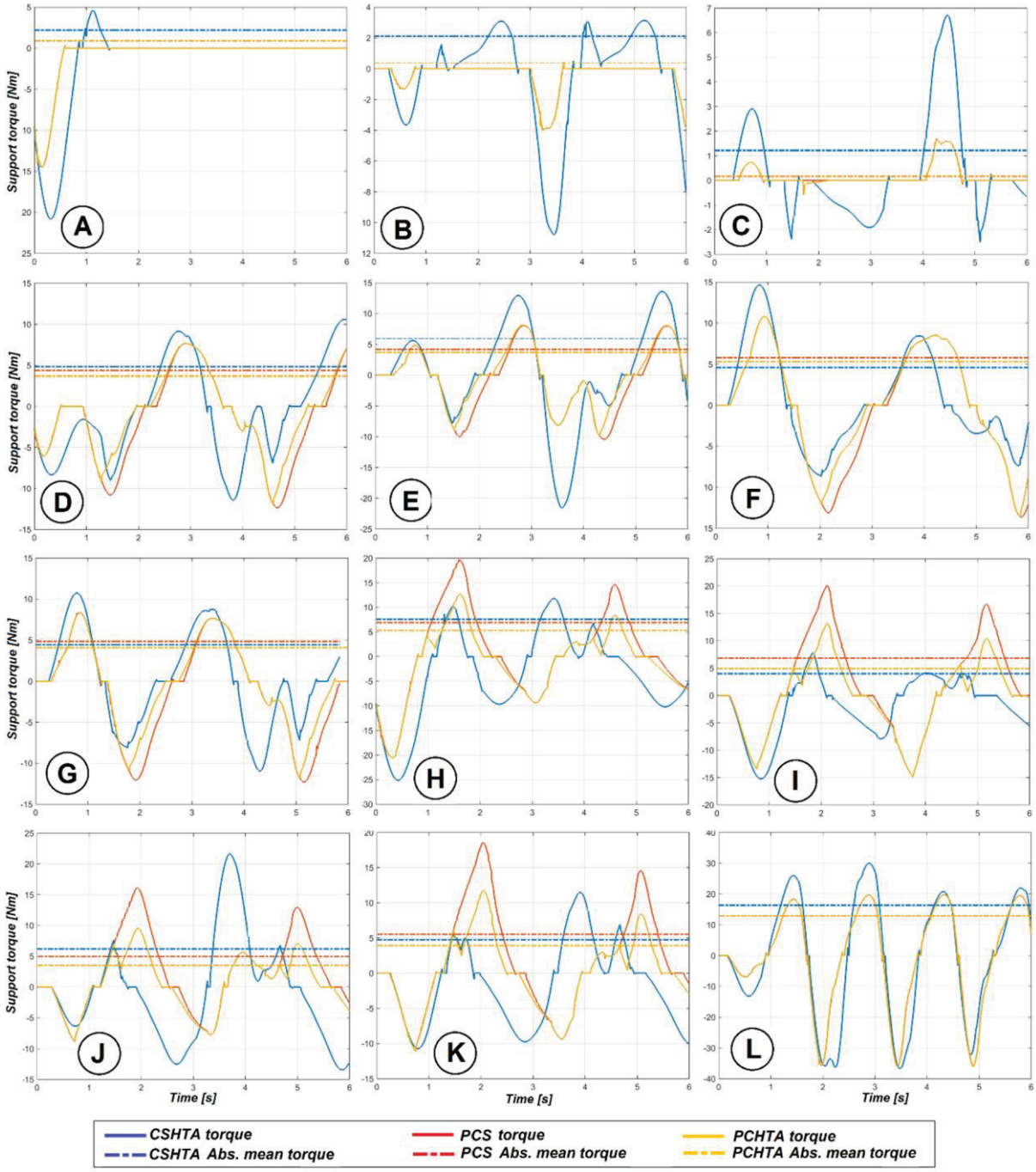

Fig. 121 Hip joint support torques of an impedance controller using the three synchronization methods during simulated therapy

The second conclusion can be reached by comparing the PCS and the PCHTA methods. The hip support torques in the simulation cases where two different trajectories were taken as reference and actual (cases *D* to *K*)[23] where significantly lower when using the PCHTA method. These lower values correspond to the reduction in the obstructive torques generated in the vicinity of swing-to-stance transition, achieved thanks to the hip trajectory adaptation strategy. Notice that there are no differences between the support torques yielded by these two

[23] In case *L*, the trajectory adaptation was so low that there were no visible differences between the two methods.

methods for the knee joint. This is because no adaptation of the knee trajectory is done and the time compensation is the same for both of them. Note as well that in the cases *A* to *C* the same trajectory was used as reference and actual, hence no trajectory adaptation resulted from the CSHTA and the PCHTA methods, and therefore there were no difference in the support torques between the methods using phase control.

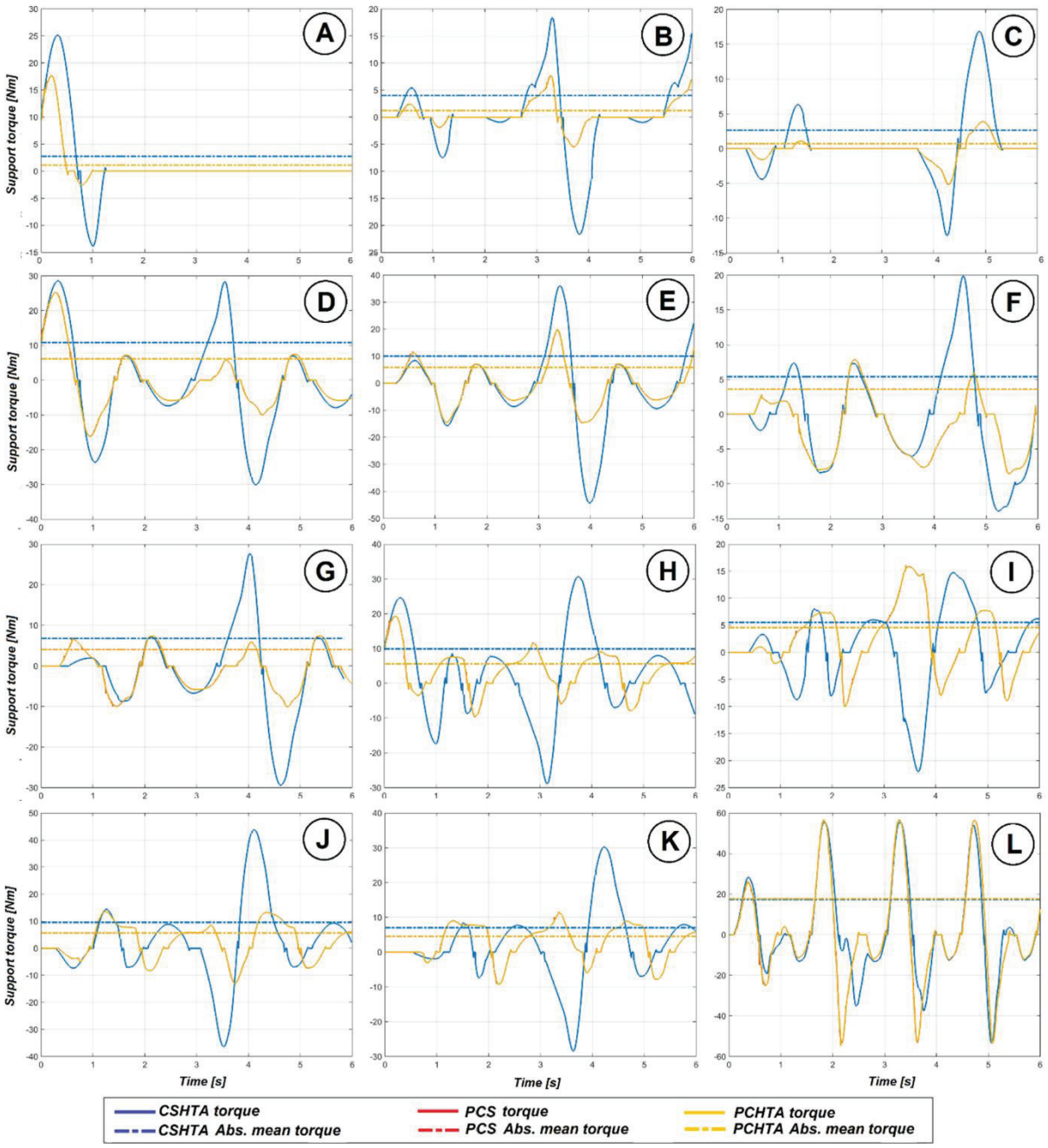

Fig. 122 Knee joint support torques of an impedance controller using the three synchronization methods during simulated therapy

Table 31 **Mean values of joint support torques of an impedance controller using the three synchronization methods during simulated therapy**

	Absolute mean support torque [Nm] HIP			Absolute mean support torque [Nm] KNEE		
Sim. case	**CSHTA**	**Phase cont.**	**PCHTA**	**CSHTA**	**Phase cont.**	**PCHTA**
A	2.20	0.88	0.88	2.75	1.10	1.10
B	2.12	0.41	0.41	4.04	1.24	1.24
C	1.21	0.17	0.18	2.63	0.72	0.72
D	4.85	4.37	3.69	10.78	6.14	6.14
E	6.03	4.19	3.68	9.96	5.81	5.81
F	4.58	5.78	5.30	5.40	3.61	3.61
G	4.43	4.84	4.10	6.76	4.01	3.96
H	7.56	6.90	5.26	9.84	5.61	5.61
I	4.00	6.84	4.92	5.55	4.61	4.60
J	6.17	4.95	3.54	9.57	5.65	5.65
K	4.74	5.52	3.93	7.03	4.51	4.51
L	16.40	12.92	12.92	17.30	17.78	17.75

As stated before, the CSHTA method was designed to let the system influence the cadence of the patient (and not the other way around) while decreasing the synchronization issues brought by the compliance of the system. In case it is desired to let the patient influence the reference cadence in a higher degree, it is possible to complement this method with an adaptation of the reference cadence, e.g. by means of a simple adaptive oscillator. However, this adaptation must be accompanied by the corresponding adjustment of the reference trajectories in case the trajectories are dependent on the cadence, as it is the case in *MOPASS*. Such an adaptation can follow the same procedure presented in section 6.4.

6 Graphical User Interface

This chapter is dedicated to the design of the therapist/doctor graphical user interface (GUI) and to the implementation of some features that are offered to the therapists through the interface to enhance the therapy outcome, namely the online adaptation of gait parameters (and corresponding automatic adjustment of the gait patterns), the advanced options for curve shaping and the adjustment of support control parameters.

6.1 Prototype design

The first version of the *MOPASS* therapist GUI was developed by the Institute of Automation (IAT) of the University of Bremen for the initial clinical trials. It included a basic trajectory generator that allowed the selection of characteristic points, together with an advanced option to manually adjust the curve-shaping points of the hip and knee trajectories, following the concept of trajectory generation presented in section 4.2. It also included an online display of the heart-rate and foot pressure sensors used by the therapist for assessment, additional to the handling of personal and therapy-related data (e.g. patient-specific characteristic points) of each patient. After the clinical trials, several new features were developed to improve the user experience and the rehabilitation outcomes, including the aforementioned estimator of healthy-like gait patterns, the handling of online adaptation of the gait parameters of the therapy, some extra advanced options for hip and knee trajectory generation, and handling of support-control parameters. A prototype GUI was designed to implement all these new features and carry out their proof of concept. An overview of the design and usability of the new GUI (from now referred only as GUI) is presented next.

The GUI is basically divided in five sections, each one dedicated to specific features offered by the interface, namely patient's data and system modules' monitoring, trajectory generation, gait pattern motion simulation, support level setting, and therapy setting and monitoring. The first section dedicated to the patient's personal data handling and monitoring of the system modules and devices is shown in Fig. 123. Here, the therapist can introduce the personal data of the patient into the system (*A*), as well as save it to or retrieve it from the data base of *MOPASS* (*B*). Additionally, it is possible for the therapist to monitor the connection state of each one of the software components of the system, as well as monitor the current state of the controller state machine (*C*).

The section for trajectory generation and adaptation is shown in Fig. 124. In the right (*A*) there are two plots to display the hip and knee trajectories together with their characteristic and shaping points. These points can be easily moved by the therapist in a graphical way by dragging them with the finger (touchscreen) or mouse. Fig. 124(*A*) shows the basic graphical trajectory adaptation mode, where the therapist can adjust only the characteristic points. Notice how, in the GUI, the knee flexion angles are treated as positive, contrary to the convention used so far. The reason for this depiction is that it comes more natural and understandable to the medical personnel. The healthy-like trajectories' estimator is offered in (*B*), where the therapist can decide which type of estimation to use (i.e. which sets of one-input or two-input neural networks, and which inputs to use)[24]. In this case, the set of neural networks with walking speed and cadence as inputs is utilized. Note that the values of

[24] In a final version it is recommended to fix 'normalized walking speed and cadence' as the only available input set.

walking speed and step lengths handled by the therapist are not normalized. The corresponding normalization is done transparently by the GUI based on the patient's anthropometric data. The selection of gait cycle period or cadence to be used during the therapy is offered in (*C*). The generation and adaptation of the initial steps is done through (*D*). If activated (Fig. 125), this feature allows the therapist to see the initial step trajectories and their characteristic and shaping points. It also allows him/her to adapt the knee curve of the main leg and the duration of the first step by moving these points. The advanced options for curve shaping are given in (*E*). The details on this feature are given in the next subsection. The therapist is also offered the option to save current patterns in the data base or retrieve previously saved ones (*F*). The GUI also makes an estimation of the gait parameters associated to the current joint trajectories and patient's anthropometric data (*G*), namely walking speed, step length and heel clearance (step height). Finally, once the therapist has finished setting the desired reference trajectories, he/she can download them to the controller PC (*H*).

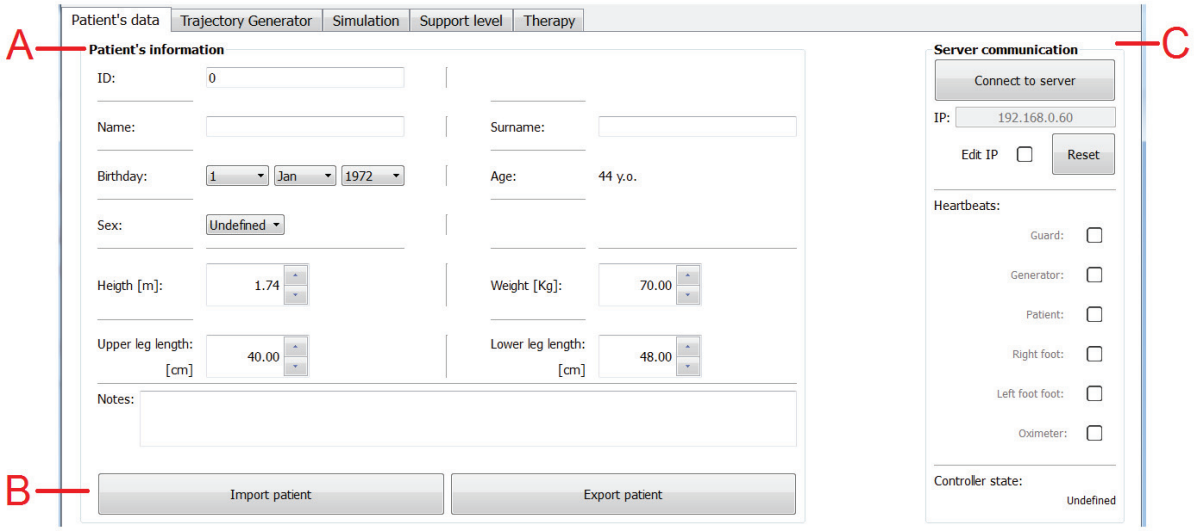

Fig. 123 GUI: patient's data and system modules' monitoring

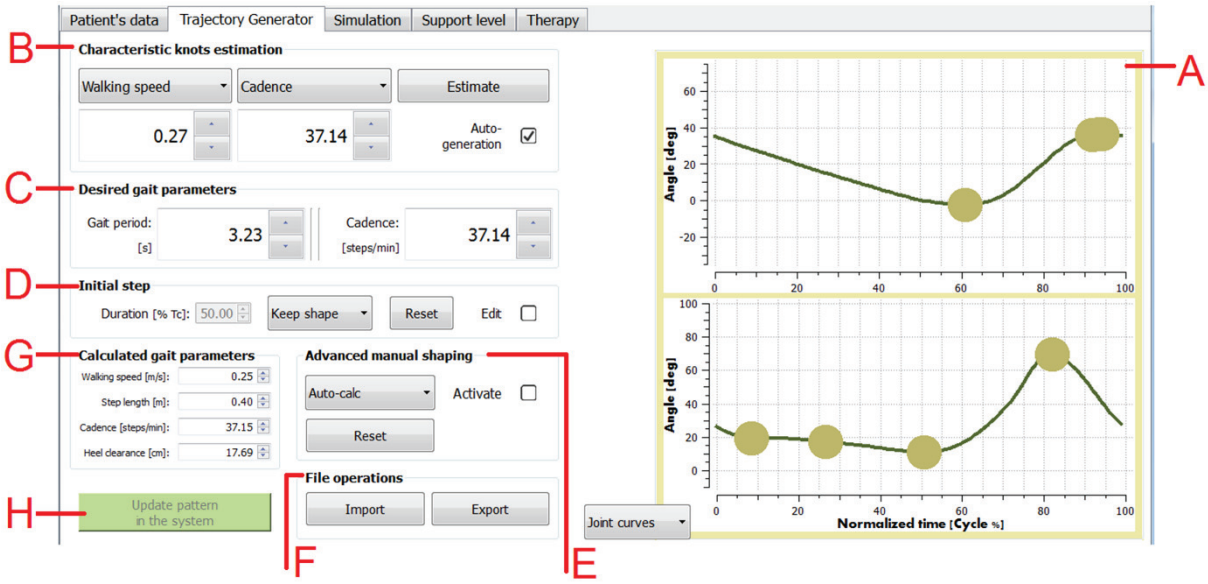

Fig. 124 GUI: trajectory generation and adaptation

The third section of the GUI, depicted in Fig. 126, is reserved for the motion simulation of the gait patterns that were set in the previous GUI section. This way, the therapist is able to observe the motion generated by the joint trajectories before starting the therapy and do the corresponding changes if needed or desired. This section offers again the display and graphical adaptation of the joint trajectories (*A*) so that the therapist sees directly how the changes in the trajectories affect the final gait pattern. Two different simulations are offered in (*B*): the legs' motion (as depicted in Fig. 126) and the heel trajectory (Fig. 127). The therapist can select between the two of them via (*C*). Additionally, the plots in (*A*) depict a couple of diamond-shaped markers (*D*) corresponding to the simulation time so that the therapists can relate the temporal parameters of the trajectories and the resulting motions, and hence perform adequate adaptations.

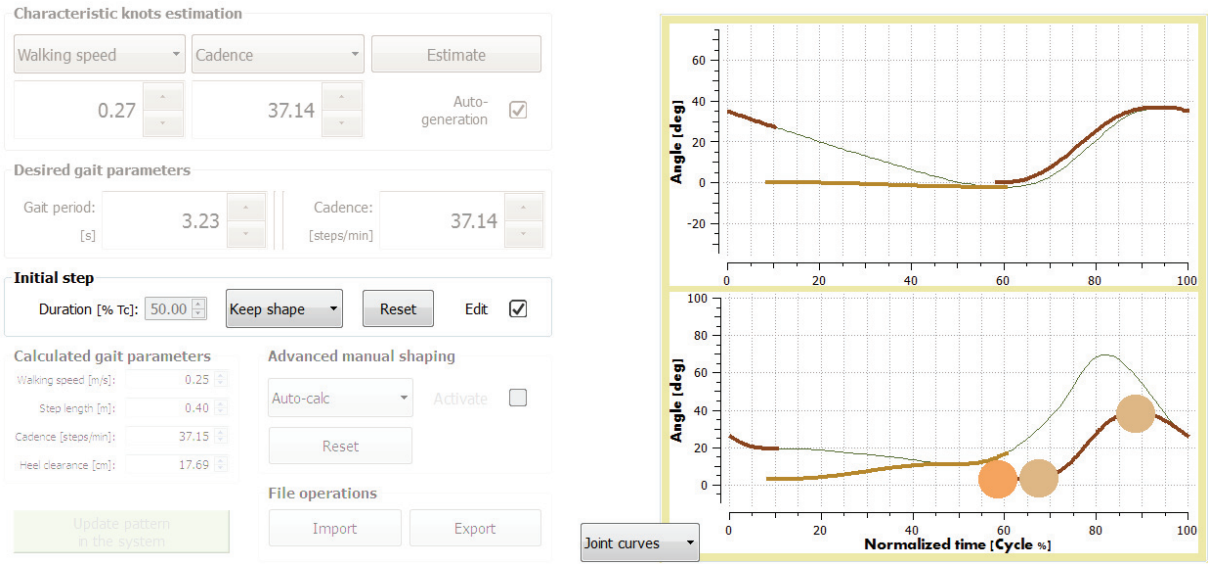

Fig. 125 GUI: initial step trajectories

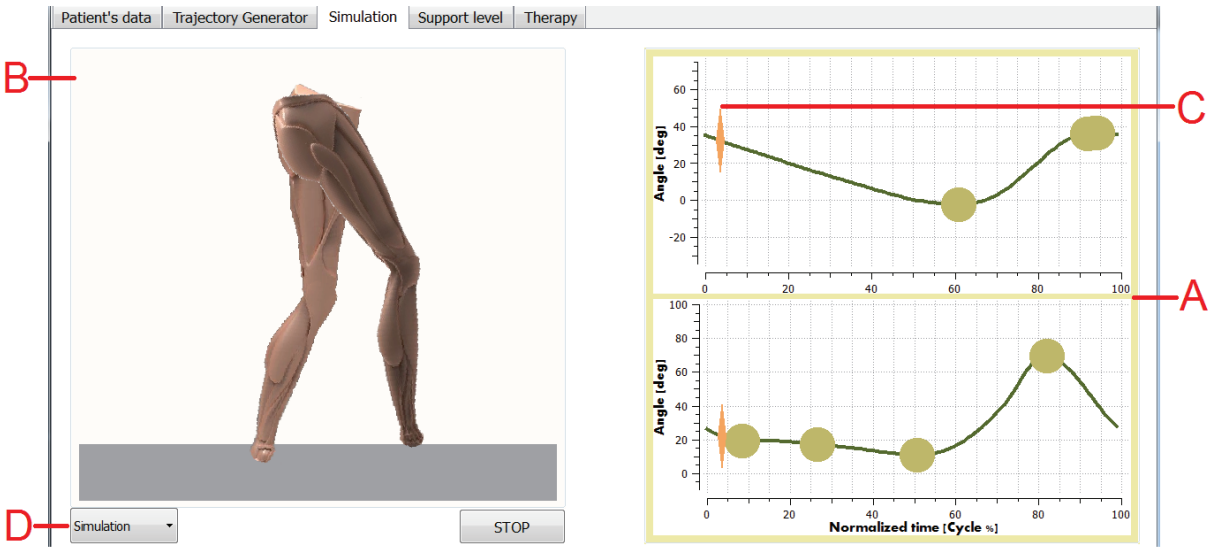

Fig. 126 GUI: gait pattern simulation

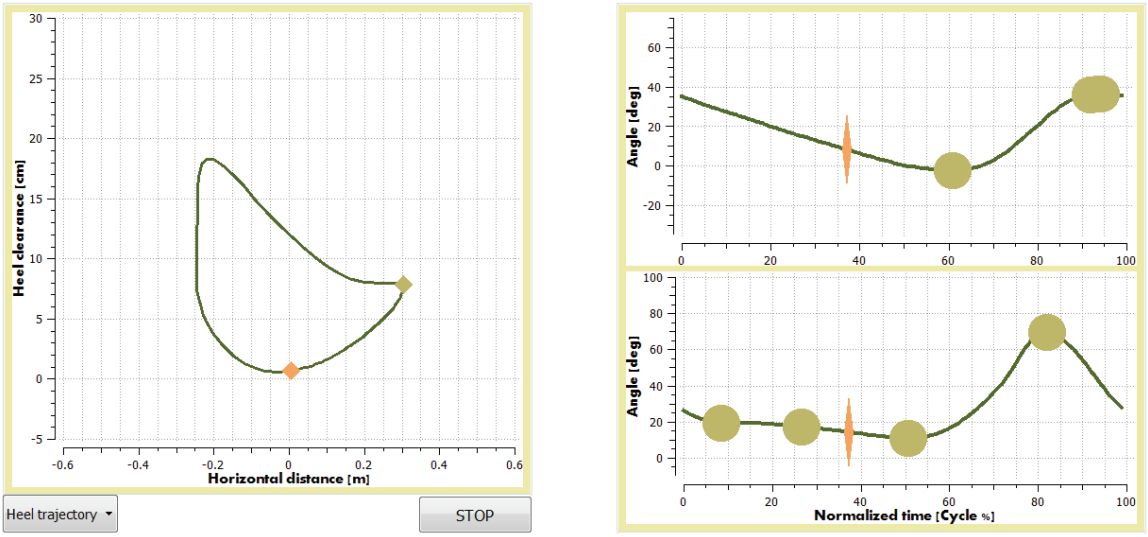

Fig. 127 GUI: simulation – heel trajectory

The Fourth section includes the tools to set adaptive patient support parameters, namely impedance parameters and size of the haptic wall. As stated before, these features were not tested in the actual *MOPASS* system. Details on these tools are given in a forthcoming section.

Finally, the last GUI section contains the tools for carrying out the exercises with the device and to display online the corresponding measurements. This section is shown in Fig. 128. The therapist is able to activate/deactivate the different active modules from the device (*A*) in case, for example, he/she wants to include the trunk/pelvis support or wants to deactivate the wheels to do the therapy using a treadmill. This feature can also be used in the future when only one of the orthotic legs is attached to the system. This would give the opportunity to offer assistive rehabilitation specifically for hemiplegic patients, with unconstrained movement in the sound leg. However, it would be imperative to include external motion sensors in the system, and to design and implement appropriate high- and medium-level control strategies (such as synchronization algorithms) to work together with this one-leg version of the system. Once the active modules have been selected, the system can be commanded to make the proper initialization of the modules (*B*) by the controller PC. The therapist can also select with what leg to perform the first step (*C*) (before the exercise starts). The selection of the operation mode is done through (*D*), where the therapist can choose between, for instance, therapy with position control, 'assist as needed' therapy (impedance control), 'follow-up' mode, platform free driving and platform in-site turning. The states of the controller can also be selected (respecting the allowed state changes of the controller state-machine) via (*E*), allowing the therapist to start the exercise, stop the exercise and send the device to the home position. Once the device is running (and depending on the selected operation mode), the therapist can variate online the exercise's reference cadence (*F*) and the level of platform turning (*G*). Details on the online adaptation of the cadence and the corresponding adjustments of the reference trajectories are given in a forthcoming section. The measurements obtained during the exercises are also depicted in the GUI. The reference and actual hip and knee trajectories are shown in the central plots (*H*), whereas the left plot (*I*) can be reserved for assessment measurements such as blood pressure, actual step length of both legs and foot-pressure. Finally, the therapist can execute an emergency stop of the device (*J*) and turn-off the controller PC once the therapy is over (*K*).

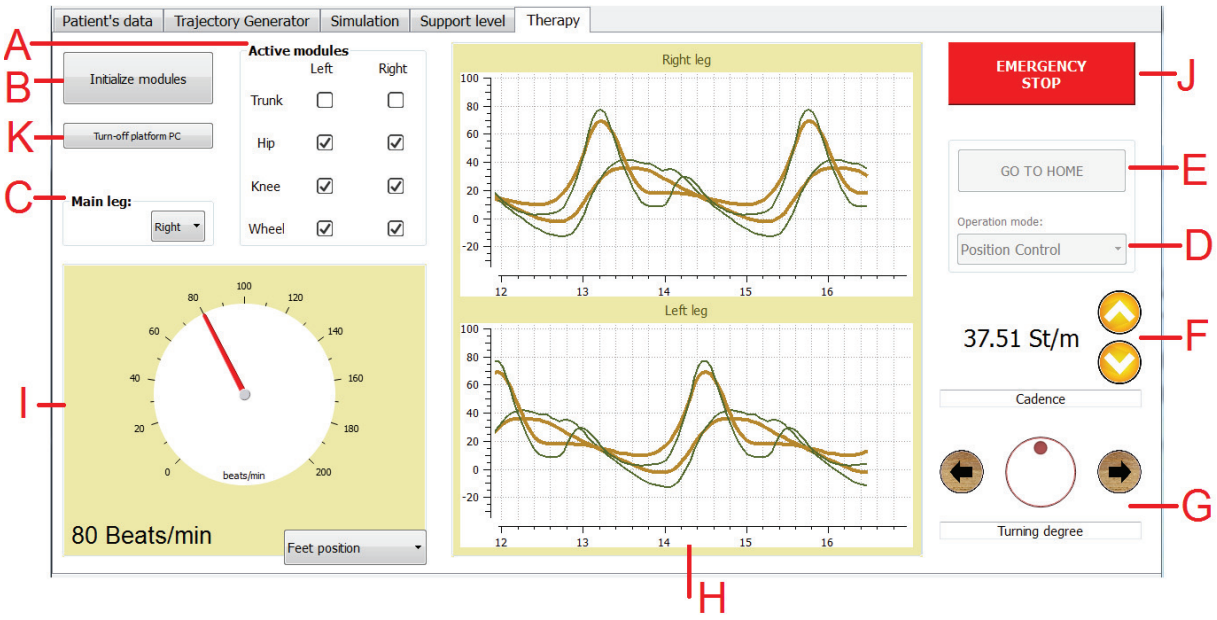

Fig. 128 GUI: therapy

6.2 Trajectory generation advanced options

In the basic mode of trajectory generation and adaptation, the therapist is able to adjust only the characteristic points of the hip and knee trajectories, whereas the shaping points are automatically calculated following the concept presented in section 4.2 and the methods presented in section 4.3.3. However, in the advanced mode, the therapist is able also to adjust the shaping points to further adapt the joint trajectories towards a desired curve shape, as shown in Fig. 129. The system offers three different options of this advanced feature, namely *Option 1* (keep shape in the given area), *Option 2* (keep shape always), and *Option 3* (force shaping points).

Option 1 allows the therapist to select the desired shaping points for a given operation area (i.e. a given pair of walking speed and cadence, and its surrounding area). This way the shaping points coefficients (α-values) corresponding to the actual pair of normalized walking speed and cadence will be used in the vicinity of the pair, outranking the mapping process previously presented in section 4.3.3 in this specific area. Outside the area, the selection of coefficients will return to the mapping method. The idea behind *Option 1* is depicted in Fig. 130, where the current pair of normalized walking speed and cadence is shown as a new centroid together with the area where the selected shaping coefficients will be used. In the case of *Option 2*, the α-values corresponding to the selected shaping points will be used over all the operation area disregarding the walking speed or cadence, completely avoiding the previously mentioned mapping process. Finally, *Option 3* fixes the time and angle values of the shaping knots, eliminating their relative relation with respect to the characteristic points. In other words, the shaping points will not use the α-values to calculate their time and angle parameters, and will not depend on the time and angle parameters of the characteristic points. This option is only recommended if it is desired to adjust the characteristic points whilst in advanced mode without moving the selected shaping points. Once the adjustments are finished, it is recommended to set either *Option 1* or *Option 2*.

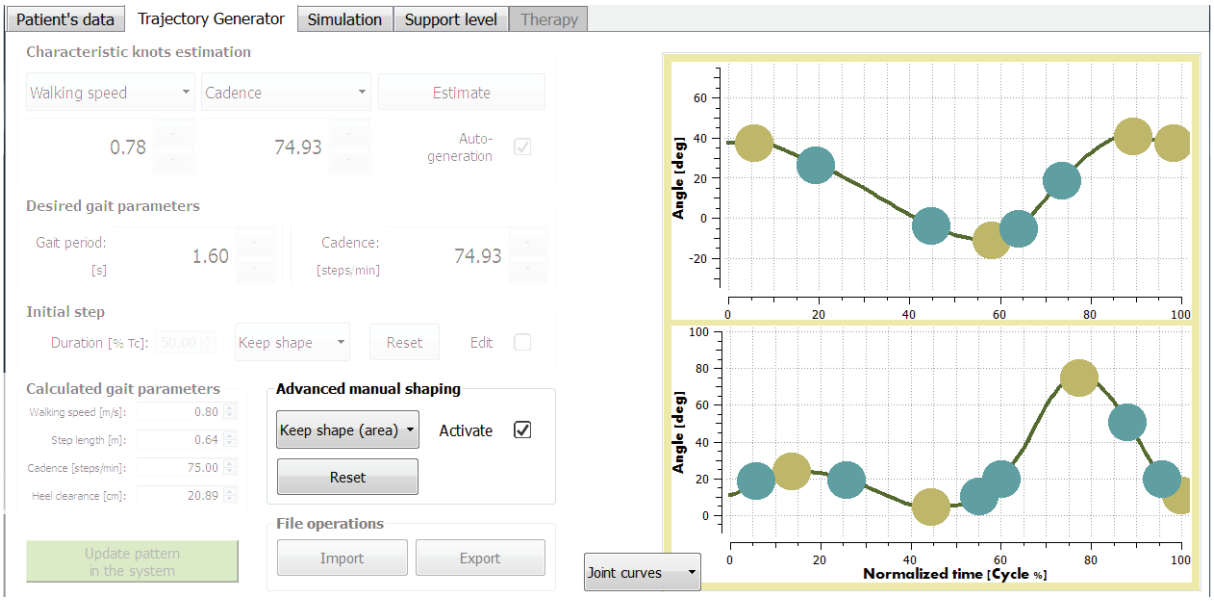

Fig. 129 GUI: trajectory generation and adaptation – advanced mode

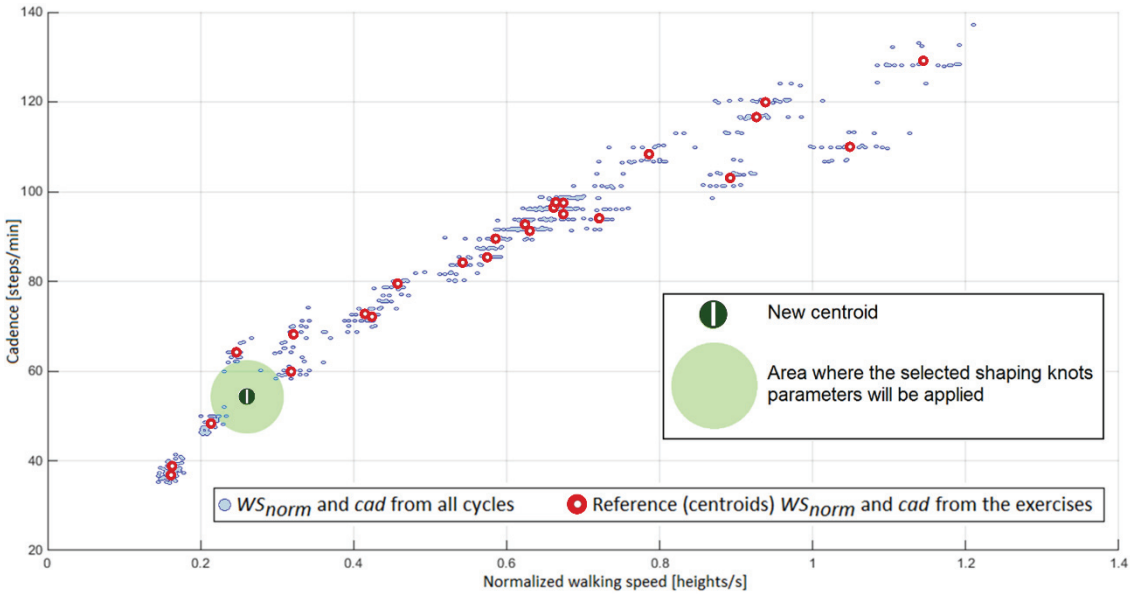

Fig. 130 Operation area of shaping-points' parameters selection during advanced mode for trajectories' shaping using *Option 1*[25]

6.3 Adjustable impedance and haptic tunnel

In section 5.1.2, a method for 'assist as needed' therapy based on an impedance controller with a haptic tunnel was presented. In this method, high values of the spring and damper coefficients in (36) and low radius (size) of haptic tunnels around the reference trajectories will increase the stiffness of the device and hence lead to the exertion of high support forces

[25] Although the area is presented as a circle for simplicity, it might not be the case in the real application where normalized values of cadence and walking speed are used during the mapping. Hence, an oval would fit better the real selection process.

aiming to help the patient to stay closer to the desired pattern. Low impedance parameters and high haptic tunnel sizes, on the other hand, will result in a more compliant behavior of the device with respect to the patients movements, letting him/her deviate from the reference trajectories without exerting high correction forces. A stiff behavior is commonly needed when the level of impairment of the patient is high as well as the level of assistance he/she needs to walk, whereas a compliant behavior is utilized when the patients have some level of movement autonomy and the target of the therapy is to correct, in a low or medium degree, their movements. Hence, it is necessary to give the therapists the tools to easily set these parameters depending on the patient needs. Moreover, it might be desired that the system acts compliant in some phases of the gait cycle, whilst stiff in the others. Thus, different impedance and haptic wall parameters are used in the same exercise depending on the actual phase.

The GUI offers an easy adjustment tool for this purpose, presenting two different options to set the impedance and haptic wall parameters. The first option allows the therapist to set these parameters as continuous profiles throughout the gait cycle dependent on the characteristic points of each of the joints. The therapist will select the levels of compliance and tunnel size for each one of the characteristic points and the system will create smooth profiles containing these values. These support profiles are generated following the same principle of the joint trajectories, where the 'characteristic points' of the compliance and tunnel size profiles can be expressed also as the ordered pairs

$$P_{MC,i} = (t_{MC,i}, c_{MC,i}) \tag{55}$$

and

$$P_{MT,i} = \left(t_{MT,i}, r_{MT,i}\right) \ , \tag{56}$$

respectively, where

$$t_{MC,i} = t_{MT,i} = t_{M,i} \quad ; \quad \forall\, i \ , \tag{57}$$

are the time parameters and are equal to the time parameters of the characteristic points $t_{M,i}$, $c_{MC,i} = [0,1]$ are the compliance level values, $r_{MT,i}$ are tunnel radius values and $i = [1,4]$. By interpolating these points using the BVSIS fitting method together with extra shaping points with the same α-values of the joint trajectories, the resulting compliance and tunnel radius profiles will possess the same shape and extrema moments as the corresponding joint motion profile. To have a better understanding take a look to Fig. 131 and Fig. 132, where the compliance and tunnel radius profiles, respectively, are shown in the right plots together with the reference joint trajectories (dark green lines), and the sliders used to set the corresponding values are located in the left. In these example figures, the support parameters were set so that the system has a stiff behavior near the maximum flexion points of the hip and knee reference profiles, and a compliant behavior near the minimum flexion / maximum extension points.

Note how the therapist can select directly the radius of the haptic tunnel, setting the values in degrees. In the case of the impedance controller coefficients, however, the adjustment is done in an indirect manner. The therapist can select the compliance level of the system, which is translated in a proportional (inverse) way to the impedance parameters K_{IC} and B_{IC}. The proposed method to obtain the desired impedance parameters at a certain moment t follows

$$K_{IC}(t) = (K_{max} - K_{min}) \cdot \big(1 - c(t)\big) + K_{min}$$

$$B_{IC}(t) = (B_{max} - B_{min}) \cdot \big(1 - c(t)\big) + B_{min} \tag{58}$$

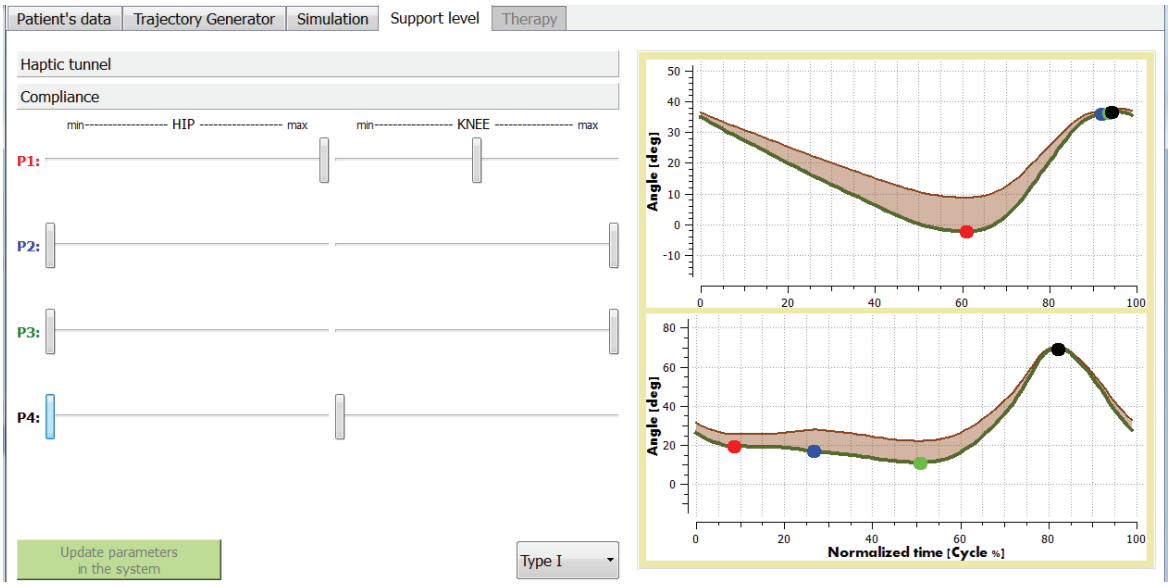

Fig. 131 GUI: compliance profile – type I

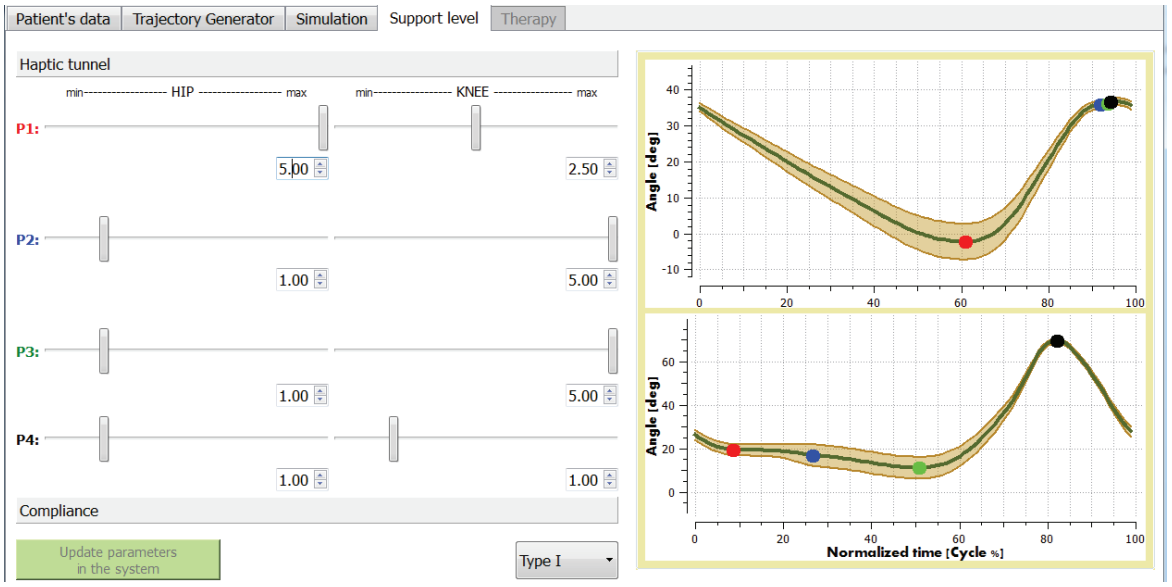

Fig. 132 GUI: haptic wall radius profile – type I

where $c(t)$ =[0,1] is the compliance value set by the therapist, K_{max} and B_{max} are the maximum spring and damper coefficients' values, respectively, and K_{min} and B_{min} are the minimum spring and damper coefficients' values, respectively. The minimum and maximum values are set a priory.

For the second adjustment option the time values of the characteristic points of the support profiles are independent of the joint trajectories' characteristic points. This way, the therapist has the freedom to select the moments in which the extrema of the support profiles are located. Moreover, the interpolation to obtain the profiles is done without adding extra shaping points. An example of this adjustment option is shown in Fig. 133 and Fig. 134, where the compliance and tunnel radius values were selected so that the system has a stiff behavior in the vicinity of the initial contact (IC) to ensure that the patient will follow the desired cadence, whereas in the rest of the gait cycle the system has a compliant behavior. For this second option, a set of (diamond-shaped) markers were added to the plots in order to

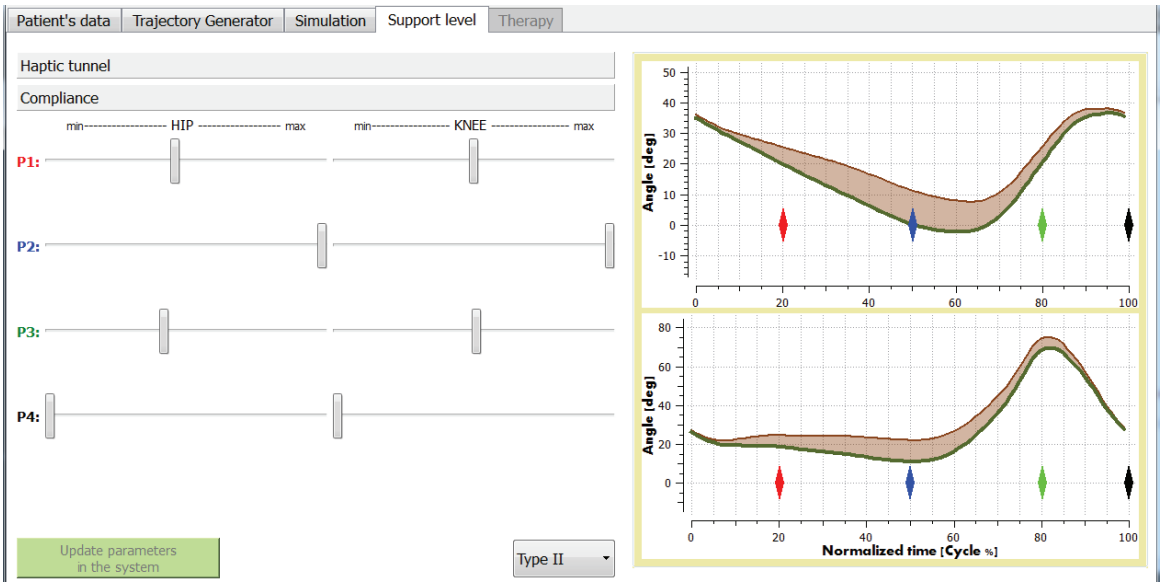

Fig. 133 GUI: compliance profile – type II

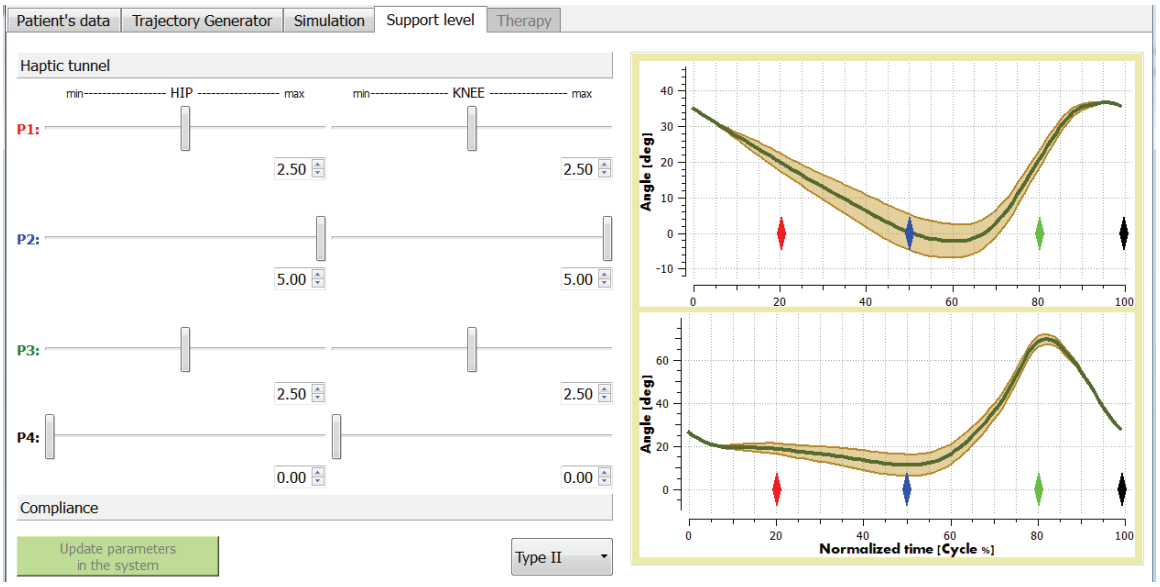

Fig. 134 GUI: haptic wall radius profile – type II

allow the therapist to set the time values of the support profiles' characteristic points in a graphical manner by dragging them and moving them horizontally.

This method for adjustable support levels is presented as a potentially beneficial tool for patient-tailored therapy. For instance, it could be used to train the joints affected by secondary abnormalities avoiding the complementary actions (tertiary abnormalities) that the patient has been using to cope with the primary and secondary deviations. For instance, inadequate knee flexion could be compensated by the patient with abnormal movements in the hip and in the contralateral limb, as explained in section 2.2. Two possible therapy scenarios could be contemplated here using adaptable support profiles. In the first scenario, the knee would be assisted to follow a healthy pattern whereas the hip and contralateral leg move more freely, which would induce the patient to eliminate the compensatory movements while training the affected joint. In the second scenario, the therapist could set a higher support in the hip joint and contralateral limb joints to prevent them to do the compensatory movement, whereas a

little bit more compliant behavior would be set in the affected knee. This way, the system would persuade the patient to train more rigorously the affected joint whilst impeding the coping patterns that he/she has relied on so far to walk. Moreover, because it is possible to set the support level profiles throughout the cycle, the joints can be addressed specifically in the moments where they have deficits.

6.4 Online adaptation of gait parameters

As stated before, the system allows the therapist to change the cadence of the gait pattern (and consequently the walking speed) while performing the walking exercise. As it was discussed in section 4.3, the changes in the cadence and walking speed are reflected in the joint curves, thus when the therapist carry out these changes, the joint trajectories must be adapted correspondingly. To this end, the results gotten from section 4.3 were used to perform the corresponding automatic adjustments to the joint curves depending on the commanded cadence changes. Moreover, because the reference trajectories set by the therapist might differ from the ones estimated by the healthy-like trajectories' estimator for the initially set of walking speed and cadence (i.e. the therapist manually adjusted the curves), these automatic adjustments must also be dependent on the initially set reference trajectories and gait parameters.

The proposed way to tackle this problem is to analyze the difference in the characteristic points' parameters estimated by the neural networks (NN) for the original[26] and adjusted gait parameters, and use them to apply similar changes to the parameters of the characteristic points of the current reference trajectories set by the therapist. Let us introduce a trivial example to have a better understanding of the problem at hand. Imagine that the knee maximum flexion point was set by the therapist to have an angular value of -50° with some initial gait parameters WS_1 and cad_1. However, the NN estimated that value to be -60°. The therapist executes a change in the gait parameters resulting in new values WS_2 and cad_2. For these new parameters, the NN estimated an angular value of -30°. One way to adjust the angle value given this change in the estimated characteristic point is to apply to it the same relative increment/reduction that the estimated values underwent. In this specific case, the estimated angle parameters underwent a reduction of 50%, hence the adjusted reference angle would be equal to -25° after applying the same reduction. Other adjustment options for the angular parameters are presented afterwards. In the case of the characteristic points' time parameters, the changes in the estimated time values are applied directly to the time values set by the therapist. If the therapist had set a time value equal to 80(%) to the characteristic point in the example at (WS_1, cad_1), and the values estimated by the NN for (WS_1, cad_1) and (WS_2, cad_2) were 85(%) and 80(%), respectively, the -5(%) difference would be applied to the original value resulting in a new value equal to 75(%).

A general scheme of the procedure is shown in Fig. 135, where (WS_O, Cad_O) and (WS_{new}, Cad_{new}) are the original and the new (adjusted) gait parameters (walking speed and cadence), respectively; t_O and θ_O are the time and angle values of a given characteristic point set by the therapist before starting the exercise; $t_{O,est}$, $t_{new,est}$, $\theta_{O,est}$ and $\theta_{new,est}$ are the time and angle values estimated by the NN for the original and new gait parameters; and t_{new} and θ_{new} are the new time and angle values of the characteristic point used to generate the adjusted joint

[26] From this point, the reference joint trajectories and gait parameters set by the therapist before the exercise starts are referred to as *original*.

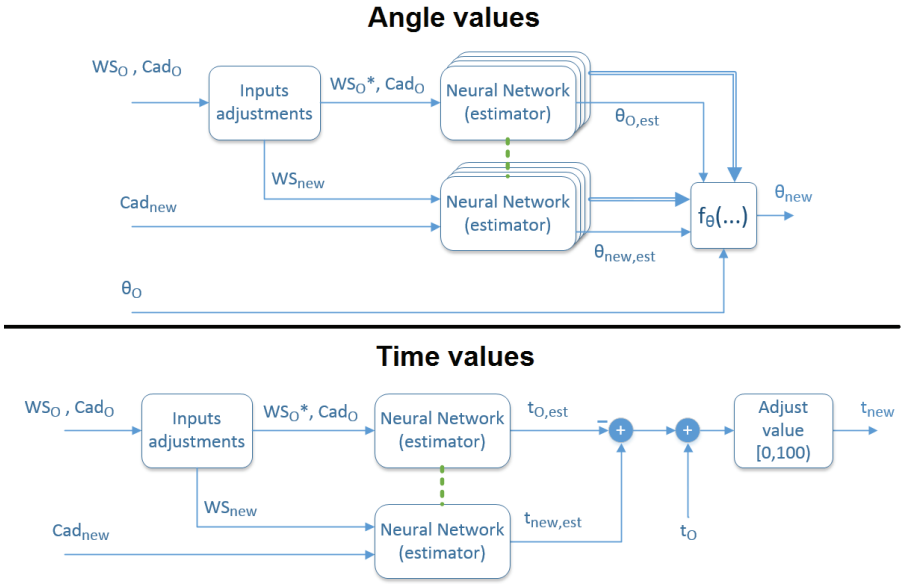

Fig. 135 Scheme for trajectory adjustment due to online adaptation of the cadence

trajectories correspondent to the changes in cadence commanded by the therapist. Different functions f_θ can be used to obtain the new angular values. Three functions are proposed here:

$$f_{\theta 1} = \theta_O + \theta_{new,est} - \theta_{O,est}$$

$$f_{\theta 2} = \theta_O \cdot \frac{\theta_{new,est}}{\theta_{O,est}}$$

$$f_{\theta 3} = (\theta_O - \theta_r) \cdot \frac{\theta_{new,est} - \theta_r}{\theta_{O,est} - \theta_r} + \theta_r \ . \tag{59}$$

All three functions have advantages and disadvantages. $f_{\theta 1}$ maintains a fixed difference between the estimated and the adjusted values, correspondent to the original difference between the value θ_O set by the therapist and the estimated one $\theta_{O,est}$. This constant difference avoids high adjustment changes that might be undesired, but disregards the variable influence of the changes in the gait parameters on the angular parameters of the curves. $f_{\theta 2}$ intends to compute the new angle values taking into account this variable influence in the form of a proportional relation. However, values in the vicinity of 0° will generate high multipliers even if the difference between $\theta_{O,est}$ and $\theta_{new,est}$ is just a couple of degrees. To overcome this issue, $f_{\theta 3}$ includes a new term θ_r, which is a reference value with which $\theta_{O,est}$ and $\theta_{new,est}$ are compared to obtain the multiplier. Note that $f_{\theta 2} = f_{\theta 3}$ when $\theta_r = 0$. The adjustment level is directly influenced by the selection of θ_r. A wrong selection of θ_r will result in a poor performance of the adjustment module. Moreover, values in the vicinity of θ_r might cause the same undesired behavior as when using $f_{\theta 2}$. Two θ_r are proposed here. One, equal to the middle value of the estimated joint trajectory in (WS_O, Cad_O):

$$\theta_{r1} = \frac{\theta_{O,est}^{min} + \theta_{O,est}^{max}}{2} \ , \tag{60}$$

where $\theta_{O,est}^{min}$ and $\theta_{O,est}^{max}$ are the minimum and maximum angular values of the trajectory that was generated with the characteristic points estimated using *(WS_O, Cad_O)* as inputs of the set of NN. For the second option it is proposed to use the angle value of the estimated characteristic point that is the farthest away (in the angular dimension) from the point being adjusted. In other words,

$$\theta_{r2} = \begin{cases} \theta_{O,est}^{min} & ; abs\left(\theta_O - \theta_{O,est}^{min}\right) > abs\left(\theta_O - \theta_{O,est}^{max}\right) \\ \theta_{O,est}^{max} & ; otherwise \end{cases}, \tag{61}$$

Two adjustment blocks are also presented in the scheme. The first one, present only in the time values calculation, is introduced to ensure that the resulting values lie in the range [0%,100%). So, if the value is, for instance, equal to -7(%), the final adjusted value will be 93(%). The second adjustment block is more complex, and is inserted to ensure that the inputs of the NN have valid values, based on the admissible application region from Fig. 40. First of all, take into account that the reference walking speed and cadence selected by the therapist[27] may lie outside the admissible region since he/she is not restricted by it. Hence, the first task of this adjustments' block is to check the validity of the input pair and, if it lies outside of the limit region, it selects an appropriate value of walking speed that fulfills this requirement. Second, note that the therapist is only able to change the cadence of the gait pattern, i.e. only one of the two inputs of the NN. Thus, the second task of the block is to estimate the new value of walking speed to be supplied to the estimators based on the original gait parameters and, of course, lying inside the admissible inputs' area. Additionally, the block will make the corresponding normalization operations which will not be included in the explanations for simplicity.

Let us analyze the first task. Based on the admissible inputs' area for the set of NN shown in Fig. 40, it can be seen that for every value of cadence Cad_i inside the range there exist a valid range of walking speeds limited by [$WS_{i,min}$, $WS_{i,max}$]. If the original value of walking speed is outside this valid range, then a new walking speed WS_O* must be selected to be supplied to the NN. In these cases, the value inside the range that is closest to the original values is selected. If the original value lies in the admissible range, then it can be directly supplied to the NN. There exist a third special case, when it is desired not to use the original walking speed in the calculations; here the value in the middle of the admissible range is selected to be the NN input. All three cases yield

$$WS_O^* = \begin{cases} WS_O & ; WS_{O,min} \leq WS_O \leq WS_{O,max} \\ WS_{O,min} & ; WS_O < WS_{O,min} \\ WS_{O,max} & ; WS_{O,max} < WS_O \\ \dfrac{WS_{O,max} - WS_{O,min}}{2} + WS_{O,min} & ; WS_O \; not \; given \end{cases}. \tag{62}$$

For the second task, the values of WS_O^* and Cad_{new} are used to estimate the new value of walking speed WS_{new} that will be used as input of the NN. It is important to understand that this value is a mere approximation of the new walking speed and it is calculated only to obtain the new characteristic points, and its value will very likely differ from the resulting speed calculated after the new trajectories are generated. As before, Cad_{new} will have a valid range of walking speed values [$WS_{new,min}$, $WS_{new,max}$] associated with it. The idea is that the new

[27] Actually, the therapist only selects the reference cadence, and the reference walking speed is calculated based on that cadence, the selected joint trajectories and the length of the patient's legs. Hence, the therapist selects the reference walking speed in an indirect manner.

value of walking speed possesses the same relation with the limits of the corresponding valid range as the original value WS_O^* had with its corresponding limits. This proportional relation can be expressed as

$$WS_{new} = \left(WS_O^* - WS_{O,min}\right) \cdot \frac{WS_{new,max} - WS_{new,min}}{WS_{O,max} - WS_{O,min}} + WS_{new,min} \ . \tag{63}$$

To observe the performance of the complete adjustment procedure take a look at the example depicted in Fig. 136, where $f_{\theta 2}$ was selected as the function used to compute the adjusted angle values. Fig. 136 shows the reference trajectories (red lines), i.e. the ones corresponding to the original points set by the therapist ('before' side) and the ones resulting from the adjustments done due to a change in the cadence ('after' side). Additionally, it also shows the corresponding estimated trajectories, i.e. the trajectories that the estimator suggests as healthy-like trajectories using the same gait parameters as inputs. Two noticeable differences exist between the reference trajectories set by the therapist and the estimated ones before changing the cadence: one, the hip maximum flexion of the reference trajectories is much higher and sooner that the one suggested by the estimator; and two, the maximum knee flexion angle of the reference trajectories is lower and later that the one suggested by the estimator. The specific gait parameters used in this example were: Cad_O = 45 [steps/min], WS_O = 0.196 [heights/s], Cad_{new} = 70 [steps/min], and WS_{new} = 0.38 [heights/s] [28]. Note how, in the case of the maximum knee flexion, the adjustments done to the original reference trajectory showed small, seemingly appropriate changes in the corresponding characteristic point influenced by both, the initial selection done by the therapist and the estimated change in the curve parameters due to the change in the cadence. In the case of the maximum hip extension, however, the changes in the angle value seem higher than desired. This happened because the estimated angle value for this characteristic point before the changes was too close to zero, and a small change in the estimated angular value of this point resulted in a high adjustment multiplier. This shows the potential improvements brought by $f_{\theta 3}$ over $f_{\theta 2}$ using a reference angle $\theta_r \neq 0$. To corroborate this statement, refer to Fig. 137, where the results in the hip joint from the previous example are shown, with the difference that this time $f_{\theta 3}$ was utilized with $\theta_r = \theta_{r1}$. Note that now the changes in the maximum hip extension are not as abrupt as before.

[28] The values of walking speed are normalized values

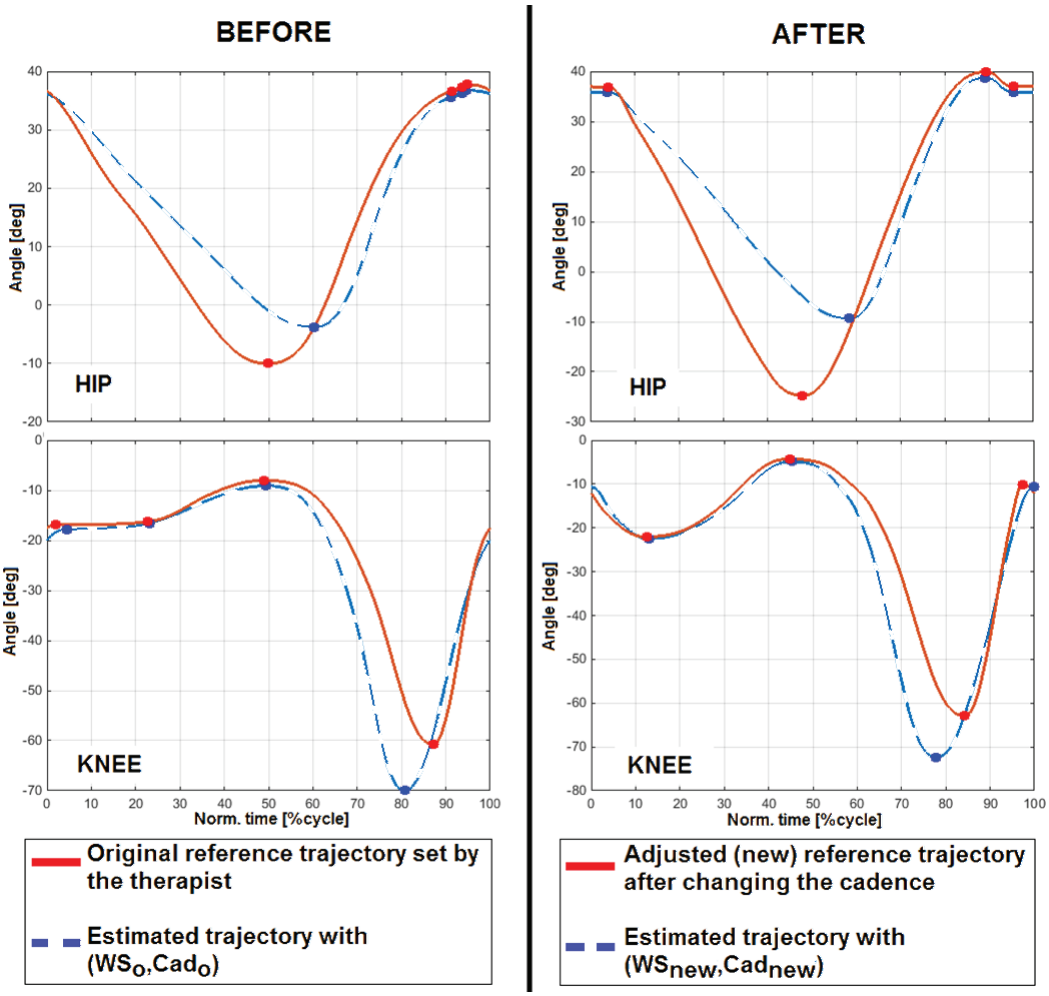

Fig. 136 Example of trajectory adjustment due to adaptation of the cadence

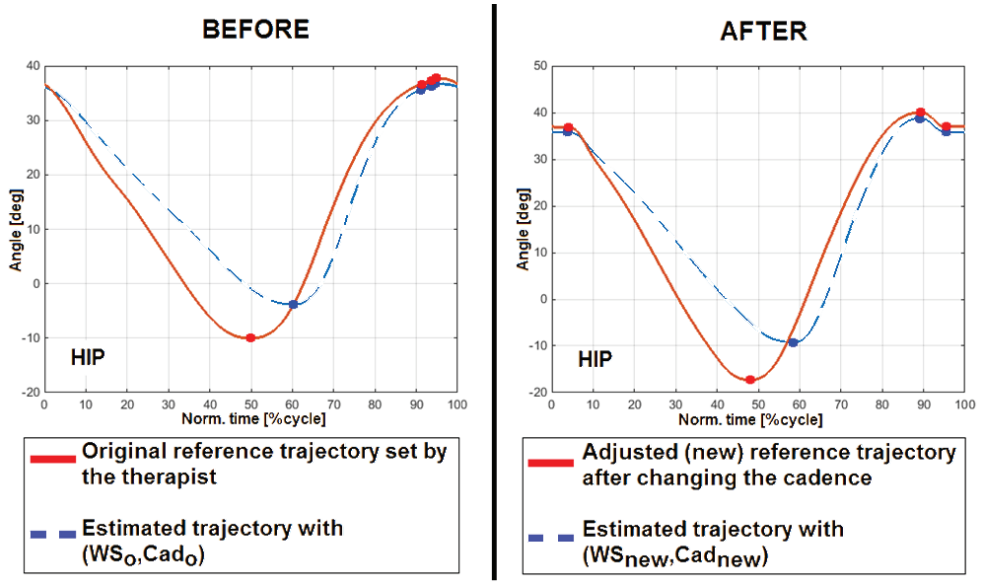

Fig. 137 Example of hip trajectory adjustment due to adaptation of the cadence using $f_{\theta 3}$

7 Conclusions

This dissertation presented a novel approach for hip and knee joints trajectory generation for robot-assisted gait rehabilitation, which was implemented and tested with the *MOPASS* system. First of all, a generator component was developed to estimate healthy-like trajectories based on the height of the patient and the desired walking speed and cadence. This estimation process was divided into the estimation of the characteristic points of the curves (i.e. the points that affect the most the shape and behavior of the curve) and the shaping points (i.e. the points used to shape the curve between the characteristic points). Although it was intended to make the estimation taking into account the data from several subjects with different ages and physical characteristics, it was decided to train the estimators with the data of only one subject: the person who presented the best correlation coefficients between the estimated and experimental characteristic points. This decision was taken due to the high inter-subject variability seen after training the characteristic points' estimators. Although the low predictability might have been caused by the many limitations of the experimental study conducted to train the estimators, low predictability has been also reported by other researchers. Artificial Neural Networks were selected as estimators for the characteristic points, whereas search algorithms and a radial-basis mapping method were developed for the shaping points. At the end, the developed generator component was able to reconstruct healthy-like trajectories as desired. However, these trajectories were generated based on the walking pattern of only one (carefully selected) subject, which raises the following questions. Given the high inter-subject variability in the walking patterns, are state of the art approaches failing in our search for tailoring the trajectories to the specific characteristics of the patient by trying to generalize the key kinematic and spatiotemporal parameters disregarding the variability in the walking preferences of the population? Should data from several subjects be used to generate the healthy-like trajectories or only data from one (or perhaps more than one) subject with very high predictability?

The generator is complemented with the possibility of manually adapting the trajectories in an easy and graphical way, thanks to the novel concept for parametrization and reconstruction of the curves. This not just enables the therapist to search for gait patterns that fit better the preferences of a patient (counteracting, to some extent, the effects of using only one subject for the estimator's training), but also to set reference joint trajectories that can tackle in a more effective way the individual deficiencies and abnormalities (e.g. by training compensatory patterns that might lead to independent walking, even if they are not considered to be normal). As it was seen in chapter 2, there exist sundry kinematic abnormalities in pathological gait that can affect distinctly the patients, which can be addressed in a more efficient way if the therapist has direct access to the generation of the reference trajectories.

The proposed generation process also presents some methods to include the adaptations made by the therapists in further generation and adaptation of the curves. One example is the automatic trajectories' adjustment done when the therapist changes online the cadence of the exercise whilst the patient is walking assisted by the device, taking into account the changes in the gait parameters and the initially selected reference trajectories. The other example is the inclusion of advanced curve shaping tools that allow the therapist to adapt the trajectories in a higher degree, and take the changes into account for the selection of shaping points in different parts of the spectrum of walking speed and cadence. However, the effectiveness of the generation and adaptation process proposed here is subject to the well understanding of the gait principles by the therapists, together with the willingness to step outside the current paradigms of traditional therapy and learn how to properly make use of the emerging technologies.

This thesis also presented a set of improved methods to synchronize the reference gait patterns with the actual pattern of the patient. Desynchronization between these two patterns is a common problem when the system's behavior is not stiff enough to guaranty a close tracking of the reference trajectories, leading to a compliant behavior that allows the patient to deviate from the reference patterns and impose, to some extent, his/her walking pattern. The methods are based on previously presented synchronization strategies that have been used in other devices with success, but include other approaches to current solutions and are complemented by a novel hip trajectory adjustment method to improve the synergy between the device and the patient during training. Moreover, it presents some methods for adjustments of the reference walking speed (i.e. treadmill or mobile platform speed) in order to cope with the synchronization efforts in a smooth and timely manner. The proposed methods were tested in a simulation environment as well as practically with a healthy subject using the *MOPASS* system, showing promising results and exhibiting an upgrade with respect to the previous methods.

A graphical user interface (GUI) was also developed during the course of this research, which includes the several functionalities brought by the presented trajectory generation methods. The GUI also includes a tool to manually adjust the assistance levels (or in other words, the compliance level of the device) throughout the gait cycle. This adjustment tool is based on a proposed 'assist as needed' control strategy that involves an impedance-based controller and a haptic tunnel, strategies used successfully in other state of the art systems. This way, the therapist can not only individualize the reference trajectories targeting the needs of each patient, but also the stiffness of the system and the support given by the device to the patient.

In summary, with the proposed trajectory generator and the proposed method for adjustable support level profiles, the patient-specific secondary and tertiary deviations can be treated in a more optimal manner. Letting the therapist adjust the joint trajectories can help the patients improve or acquire complementary movements to achieve better walking performances. On the other hand, different levels of assistance for each joint throughout the gait cycle allow training only where and when is needed, for example, by assisting the joints affected by secondary abnormalities depending on the moments when their deficits are high, while avoiding the usage of complementary actions in the sounder joints.

Although the overall outcome of this work is promising, there exist a significant number of limitations that affected the effectiveness and functionalities of the proposed methods, mostly regarding the trajectory estimation and generation. Other limitations resulted in the impossibility to properly tests the presented approaches for trajectory generation and motion control, and therefore to reach conclusive results about their clinical effectiveness. One of the hindrances was the power, mechanical and sensory limitations in the *MOPASS* system which, for instance, prevented the practical test of the proposed 'assist as needed' approach. A second limitation, perhaps being the most significant, was the difficulty to test the proposed methods with actual patients. Although many of the concepts were tested in initial clinical trials with the *MOPASS* system, the improvements that resulted from that experience were only tested in simulations and with healthy subjects.

8 Open topics for future work

There exists a wide area for improvement of the proposed methods and continuation of the related research. Only a few topics will be presented next, which to the eyes of the author are mostly related to this work and might enhance the proposed methods and improve the outcomes. These topics will include possible improvements to tackle specific limitations of the methods as well as next steps towards a better rehabilitation experience.

First of all, it is necessary to test the presented methods in a clinical environment with patients with different symptoms and impairment levels, as well as with therapists willing to follow the new trends of technology. This not only would be used to evaluate the effectiveness of the methods, but would also give valuable feedback to target the research efforts to the right direction and make the adjustments and enhancements necessary to come closer to understand the optimal way to use robotic systems in gait rehabilitation.

Let us continue with the estimation of healthy-like walking patterns. As it was seen, the low predictability of the characteristic points when utilizing data from several subjects for the training of the neural networks was one of the limitations faced during the estimation of healthy-like hip and knee joint trajectories. A possible way to improve this with the current experimental setup is to estimate the time and angle values of the characteristic points relative to a specific point of the trajectory (e.g. the point of maximum extension in hip and the point of maximum flexion in knee), instead of doing it with respect to the estimated moment of initial contact of the foot with the ground (for the time values) and the 0° position (for the angle values). The selected reference points would be estimated as it was proposed in section 4.3.2, whereas new neural networks would be trained for the remaining characteristic points with the time and angle values relative to the reference points. It is expected that this would decrease the errors caused by offsets on the angular measurements and increase the predictability of these relative values.

However, many other limitations would remain, mostly related to the methods of data collection. To obtain more reliable results, it is necessary to utilize specialized tools for gait analysis, such as 3D marker-based gait analysis systems. The data collected with these tools could be further used to retrain the estimators presented in this work and obtain better estimation results. Moreover, the inclusion of a much wider spectrum of experimental subjects with different ranges of age, height, weight, fitness condition, etc. could give a better insight on the dependency and variability of the kinematic and spatiotemporal gait parameters. However, this is not an easy task because of the difficulty to set up this kind of experiments with such a high number of participants, organization- and cost-wise.

Regarding the obtainment of the shaping knots of the curves, it would be desired to improve the time consumption of the presented methods without compromising the error performance of the searches. It would be recommended to study the efficiency of setting fixed values to the temporal parameters of the shaping knots to reduce considerably the time-consumption and complexity of the α-values' search. Moreover, depending on the behavior of the obtained angular coefficients following the aforementioned modification, it would be beneficial to implement continues mapping (fitting) methods (such as regression or neural networks) to obtain the angular coefficients of the shaping points depending on the desired gait parameters.

An addition that can be made to the trajectory estimation process is the inclusion of turning. Most state of the art systems are mechanically designed exclusively for straight walking (mostly if using a treadmill), and others that have the potential to be used to train non-straight walking, such as mobile robots, do not possess the methods to appropriately

generate reference trajectories for this task. Studies on how the parameters of the characteristic and shaping points change during turning with respect to straight walking can help in a further implementation of an estimation component capable of estimating the point's parameters of each leg (separately) depending on the straight-walking reference trajectories' parameters and on the desired degree of turn. This would lead to task-oriented training not yet seen in robot-based gait rehabilitation.

There exist some other enhancements related to the generation of trajectories. As it was seen in chapter 2, one of the common symptoms seen in pathological walking is hemiparesis. In these cases, the patients experience impairment in only one of the legs, whilst the other remains sound or almost unaffected. Some research efforts have been put into obtaining reference joint trajectories for the paretic leg based on the motion patterns of the unaffected one. The author proposes the design and implementation of a synergy method based on the same principle. Specifically, it is proposed that the system implements two different compliance profiles for each leg. The therapy would be characterized by a stiff system's behavior in the paretic side, whereas in the unaffected side the system will be more compliant to the movements of the patient. The therapy would start with a healthy reference trajectory. This way, the unaffected side will not be influenced by the paretic side impairments, preventing compensatory movements in the sound leg. With time, the reference trajectory will automatically adapt and progressively come closer to the preferred trajectories in the sound side, following a trajectory adaptation algorithm like the ones presented in [52]. This way, the walking preferences seen in the sound leg can be replicated in the affected leg in a seemingly optimal manner.

Additionally, it is proposed that further efforts are put into the development of 'assist as needed' strategies that involve the proposed trajectory generation concept. Furthermore, a proposal involving the setting of two different reference trajectories for each joint is hereby given. The idea behind this proposal is to have an optimal reference trajectory and a temporal, variable reference trajectory. The former refers to the ultimate target gait pattern that the therapist wants to achieve with the patient, but is out of the reach in the patient's current state. The latter corresponds to the actual reference trajectory delivered to the motion controllers, and hence the one that will be used in the exercises. If the selection of this trajectories is complemented with some algorithms able to measure the level of assistance and/or deviation between actual and reference patterns, it would be possible to automatically adjust the actual reference trajectories towards the optimal trajectories in a progressive manner when it has been recognized that the patient has achieved a certain level of performance (e.g. if the average support torque and/or the average position error in the last cycles is lower that a certain threshold). This adaptation towards the optimal trajectory would be easily implemented thanks to the proposed concept of trajectory parametrization and generation, where the characteristic points of the variable reference trajectories can be moved progressively closer to the ones from the optimal trajectories following the same principle of manual adaptation.

Other enhancements are related to the usage of the graphical user interface (GUI). Future research can make use of the easy and intuitive handling of the GUI-based trajectory generation and adaptation and use it as a tool to learn from the experienced therapists. This means, to utilize the manual adjustments done by the therapist for specific patients as datasets for learning algorithms whose objective will be to suggest appropriate trajectory adjustments based on the therapists experience. This way, the system could be able to automatically infer and suggest which could be the adjustments that an experienced therapist would do for a certain subject based on changes done previously with one or more patients that had similar

limitations and pathological patterns. This ‘learning from the therapist’ approach could benefit greatly the process of patient-tailored therapy.

Additionally, other tools can be added to the GUI. For example, the inclusion of a gait (sub) phases’ estimator would improve the interaction experience of the therapist with the system, for instance, when setting the reference trajectories. Such tool can also be of great benefit during the assessment of the actual patient gait patterns. The inclusion of other feedback signals and evaluation measurements would also facilitate the assessment process.

These are only some ideas for future work related to this dissertation, corresponding to a small part of a very large research topic called rehabilitation robotics, which has many areas yet to be investigated.

References

[1] American Heart Association, "Heart Disease and Stroke Statistics-2016 Update," *Circulation,* vol. 133, no. 4, pp. e38-360, 2016.

[2] S. Mendis, "Stroke disability and rehabilitation of stroke: World Health Organization perspective," *International Journal of Stroke,* vol. 8, no. 1, p. 3–4, 2013.

[3] K. Van Naarden Braun, N. Doernberg, L. Schieve, D. Christensen, A. Goodman and M. Yeargin-Allsopp, "Birth Prevalence of Cerebral Palsy: A Population-Based Study," *Pediatrics,* vol. 56, no. 1, p. 59–65, 2014.

[4] J. Basford, L. Chou, K. Kaufman, R. Brey, A. Walker, J. Malec, A. Moessner and A. Brown, "An assessment of gait and balance deficits after traumatic brain injury," *Archives of Physical Medicine and Rehabilitation,* vol. 84, no. 3, pp. 343-9, 2003.

[5] F. Tagliaferri, C. Compagnone, M. Korsic, F. Servadei and J. Kraus, "A systematic review of brain injury epidemiology in Europe," *Acta Neurochirurgica,* p. 148: 255–268, 2006.

[6] M. Faul, L. Xu, M. M. Wald and V. G. Coronado, "Traumatic Brain Injury in the United States: Emergency Department Visits, Hospitalizations and Deaths 2002–2006," National Center for Injury Prevention and Control, Centers for Disease Control and Prevention, Atranta, USA, 2010.

[7] G. Williams, M. Morris, A. Schache and P. McCrory, "Incidence of gait abnormalities after traumatic brain injury," *Archives of Physical Medicine and Rehabilitation,* vol. 90, no. 4, pp. 587-93, 2009.

[8] T. Lam, J. J. Eng, D. L. Wolfe, J. T. Hsieh, M. Whittaker and SCIRE-Research-Team, "A systematic review of the efficacy of gait rehabilitation strategies for spinal cord injury," *Topics in Spinal Cord Injury Rehabilitation,* vol. 13, no. 1, p. 32–57, 2007.

[9] M. Socie and J. Sosnoff, "Gait variability and multiple sclerosis," *Multiple Sclerosis International,* 2013.

[10] United Nations, "Convention on the Rights of Persons with Disabilities," New York, USA, 2006.

[11] C. Beyaert, R. Vasa and G. Frykberg, "Gait post-stroke: Pathophysiology and rehabilitation strategies," *Clinical Neurophysiology,* vol. 45, no. 4-5, pp. 335-55, 2015.

[12] S. Lambrecht, O. Urra, S. Grosu and S. P. Nombela, "Emerging Rehabilitation in Cerebral Palsy," in *Emerging Therapies in Neurorehabilitation*, Springer, 2013, pp. 23-49.

[13] A. van der Salm, A. Nene, D. Maxwell, P. Veltink, H. Hermens and M. IJzerman, "Gait impairments in a group of patients with incomplete spinal cord injury and their relevance regarding therapeutic approaches using functional electrical stimulation," *Artificial Organs,* vol. 29, no. 1, pp. 8-14, 2005.

[14] N. Larocca, "Impact of walking impairment in multiple sclerosis: perspectives of patients and care partners," *The Patient - Patient-Centered Outcomes Research,* vol. 4, no. 3, pp. 189-201, 2011.

[15] G. A. Prieto, R. Cano de la Cuerda, E. López Larraz, J. Metrot, M. Molinari and L. E. H. van Dokkum, "Emerging Perspectives in Stroke Rehabilitation," in *Emerging Therapies in Neurorehabilitation*, Springer, 2013, pp. 3-21.

[16] K. N. Arya, S. Pandian, R. Verma and R. Garg, "Movement therapy induced neural reorganization and motor recovery in stroke: A review," *Journal of Bodywork & Movement*

Therapies, pp. 15: 528-537, 2011.

[17] P. Langhorne, F. Coupar and A. Pollock, "Motor recovery after stroke: a systematic review," *The Lancet Neurology,* p. 8: 741–54, 2009.

[18] D. L. Damiano, "Rehabilitative Therapies in Cerebral Palsy: The Good, the Not As Good, and the Possible," *Journal of Child Neurology,* vol. 24, no. 9, p. 1200–1204, 2009.

[19] N. Koceska and S. Koceski, "Review: Robot Devices for Gait Rehabilitation," *International Journal of Computer Applications,* vol. 62, no. 13, 2013.

[20] O. Kuzmicheva, S. Focke Martinez, U. Krebs, M. Spranger, S. Moosburner, B. Wagner and A. Gräser, "Overground Robot Based Gait Rehabilitation System MOPASS – Overview and First Results from Usability Testing," *International Conference on Robotics and Automation (ICRA),* 16-21 May 2016.

[21] J. Perry, Gait Analysis: Normal and Pathological Function, SLACK Incorporated, 1992.

[22] M. W. Whittle, Gait Analysis, an introduction, Oxford: Butterworth-Heinemann, 2007.

[23] C. Kirtley, Clinical Gait Analysis, Elsevier, 2006.

[24] K. Götz-Neumann, Gehen verstehen. Ganganalyse in der Physiotherapie, Stuttgart: Thieme, 2006.

[25] D. A. Winter, The Biomechanics and Motor Control of Human Gait: Normal, Elderly and Pathological, Waterloo, Canada: University of Waterloo Press, 1991.

[26] J. Wall, J. Charteris and G. Turnbull, "Two steps equals one stride equals what?: the applicability of normal gait nomenclature to abnormal walking patterns," *Clinical Biomechanics,* vol. 2, no. 3, pp. 119-25, 1987.

[27] M. Murray, "Gait as a total pattern of movement," *American Journal of Physical Medicine & Rehabilitation,* vol. 46, no. 1, pp. 290-333, 1967.

[28] H. Jørgensen, H. Nakayama, H. Raaschou and T. Olsen, "Recovery of walking function in stroke patients: the Copenhagen Stroke Study," *Archives of Physical Medicine and Rehabilitation,* vol. 76, no. 1, pp. 27-32, 1995.

[29] B. Balaban and F. Tok, "Gait disturbances in patients with stroke," *PM&R,* vol. 6, no. 7, pp. 635-42, 2014.

[30] P. Goldie, T. Matyas and O. Evans, "Deficit and change in gait velocity during rehabilitation after stroke," *Archives of Physical Medicine and Rehabilitation,* vol. 77, no. 10, pp. 1074-82, 1996.

[31] M. Brandstater, H. de Bruin, C. Gowland and B. Clark, "Hemiplegic gait: analysis of temporal variables," *Archives of Physical Medicine and Rehabilitation,* vol. 64, no. 12, pp. 583-7, 1983.

[32] K. K. Patterson, I. Parafianowicz, C. J. Danells, V. Closson, M. C. Verrier, W. R. Staines, S. E. Black and W. E. McIlroy, "Gait Asymmetry in Community-Ambulating Stroke Survivors," *Archives of Physical Medicine and Rehabilitation,* vol. 89, no. 2, p. 304–310, 2008.

[33] S. Woolley, "Characteristics of gait in hemiplegia," *Topics in Stroke Rehabilitation,* vol. 7, no. 4, pp. 1-18, 2001.

[34] M. Gaviria, M. D'Angeli, P. Chavet, J. Pelissier, E. Peruchon and P. Rabischong, "Plantar dynamics of hemiplegic gait: a methodological approach," *Gait & Posture,* vol. 4, no. 4, pp. 297-305, 1996.

[35] Cerebral Palsy Fundation (CPF), "Adults with CP," [Online]. Available: http://yourcpf.org/adults-with-cp/. [Accessed Oct 2016].

[36] T. J. Winters, J. Gage and R. Hicks, "Gait patterns in spastic hemiplegia in children and young adults," *The Journal of Bone & Joint Surgery,* vol. 69, no. 3, pp. 437-41, 1987.

[37] C.-J. Lin, L.-Y. Guo, F.-C. Su, Y.-L. Chou and R.-J. Cherng, "Common abnormal kinetic patterns of the knee in gait in spastic diplegia of cerebral palsy," *Gait and Posture,* vol. 11, no. 3, pp. 224 - 232, 2000.

[38] D. Sutherland and J. Davids, "Common Gait Abnormalities of the Knee in Cerebral Palsy," *Clinical Orthopaedics and Related Research,* vol. 288, pp. 139-47, 1993.

[39] traumaticbraininjury.com, "Traumatic Brain Injury," [Online]. Available: http://www.traumaticbraininjury.com/. [Accessed Oct 2016].

[40] A. Esquenazi, "Evaluation and management of spastic gait in patients with traumatic brain injury," *The Journal of Head Trauma Rehabilitation,* vol. 19, no. 2, pp. 109-18, 2004.

[41] B. J. McFadyen, B. Swaine, D. Dumas and A. Durand, "Residual effects of a traumatic brain injury on locomotor capacity: a first study of spatiotemporal patterns during unobstructed and obstructed walking," *The Journal of Head Trauma Rehabilitation,* vol. 18, no. 6, p. 512–525, 2003.

[42] spinalcord.com, "Complete vs. Incomplete Spinal Cord Injuries," [Online]. Available: http://www.spinalcord.com/blog/complete-vs.-incomplete-spinal-cord-injuries. [Accessed Oct 2016].

[43] M. Cameron and J. Wagner, "Gait abnormalities in multiple sclerosis: pathogenesis, evaluation, and advances in treatment," *Current Neurology and Neuroscience Reports,* vol. 11, no. 5, pp. 507-15, 2011.

[44] M. Benedetti, R. Piperno, L. Simoncini, P. Bonato, A. Tonini and S. Giannini, "Benedetti (1999) - Gait abnormalities in minimally impaired multiple sclerosis patients," *Multiple Sclerosis Journal,* vol. 5, no. 5, pp. 363-8, 1999.

[45] National Multiple Sclerosis Society, "What is MS," [Online]. Available: http://www.nationalmssociety.org/What-is-MS. [Accessed Oct 2016].

[46] A. Kalron, A. Achiron and Z. Dvir, "Muscular and gait abnormalities in persons with early onset multiple sclerosis," *Journal of Neurologic Physical Therapy,* vol. 35, no. 4, pp. 164-9, 2011.

[47] J. Sosnoff, B. Sandroff and R. Motl, "Quantifying gait abnormalities in persons with multiple sclerosis with minimal disability," *Gait & Posture,* vol. 36, no. 1, pp. 154-6, 2012.

[48] National Multiple Sclerosis Society, "Walking (Gait) Difficulties," [Online]. Available: http://www.nationalmssociety.org/Symptoms-Diagnosis/MS-Symptoms/Walking-(Gait),-Balance-Coordination. [Accessed Oct 2016].

[49] M. Murray, R. Kory and B. Clarkson, "Walking patterns in healthy old men," *Journal of Gerontology,* vol. 24, no. 2, pp. 169-78, 1969.

[50] G. Colombo, M. Joerg, R. Schreier and V. Dietz, "Treadmill training of paraplegic patients using a robotic orthosis," *Journal of Rehabilitation Research and Development,* pp. 6:693-700, 2000 .

[51] Hocoma, "Lokomat," Hocoma, [Online]. Available: https://www.hocoma.com/usa/us/products/lokomat/. [Accessed July 2016].

[52] S. Jezernik, G. Colombo and M. Manfred, "Automatic gait-pattern adaptation algorithms for rehabilitation with a 4-DOF robotic orthosis," *IEEE Transactions on Robotics and Automation,* pp. 20:574-582, 2004.

[53] A. Duschau-Wicke, T. Brunsch, L. Lünenburger and R. Riener, "Adaptive support for patient-

cooperative gait rehabilitation with the Lokomat," in *IEEE/RSJ International Conference on Intelligent Robots and Systems, 2008. IROS 2008*, Nice, 2008.

[54] Hocoma, "LokomatPro," Hocoma, [Online]. Available: https://www.hocoma.com/usa/us/products/lokomat/lokomatpro/. [Accessed July 2016].

[55] R. Ekkelenkamp, J. Veneman and H. van der Kooij, "LOPES: selective control of gait functions during the gait rehabilitation of CVA patients," *Rehabilitation Robotics, 2005. ICORR 2005. 9th International Conference on,* pp. 361 - 364, 2005.

[56] R. Ekkelenkamp, J. Veneman and H. van der Kooij, "LOPES: a lower extremity powered exoskeleton," in *Robotics and Automation, 2007 IEEE International Conference on*, Roma, 2007.

[57] J. F. Veneman, R. Kruidhof, E. E. G. Hekman, R. Ekkelenkamp, E. H. F. Van Asseldonk and H. van der Kooij, "Design and Evaluation of the LOPES Exoskeleton Robot for Interactive Gait Rehabilitation," *Neural Systems and Rehabilitation Engineering, IEEE Transactions on,* pp. 15(3):379-386, 2007.

[58] J. Meuleman, E. van Asseldonk, G. van Oort, H. Rietman and H. van der Kooij, "LOPES II-Design and Evaluation of an Admittance Controlled Gait Training Robot With Shadow-Leg Approach," *IEEE Transactions on Neural Systems and Rehabilitation Engineering,* vol. 24, no. 3, pp. 352-63, 2016.

[59] D. Reinkensmeyer, D. Aoyagi, J. Emken, J. Galvez, W. Ichinose, G. Kerdanyan, S. Maneekobkunwong, K. Minakata, J. Nessler, R. Weber, R. Roy, R. de Leon, J. Bobrow, S. Harkema and V. Edgerton, "Tools for understanding and optimizing robotic gait training," *Journal of Rehabilitation Research and Developement,* pp. 43(5):657-70, 2006.

[60] D. Aoyagi, W. E. Ichinose, S. J. Harkema, D. J. Reinkensmeyer and J. E. Bobrow, "A robot and control algorithm that can synchronously assist in naturalistic motion during body-weight-supported gait training following neurologic injury," *IEEE Transactions on Neural Systems and Rehabilitation Engineering,* pp. 15(3):387-400, 2007.

[61] K. N. Winfree, P. Stegall and S. K. Agrawal, "Design of a minimally constraining, passively supported gait training exoskeleton - ALEX II," *IEEE International Conference on Rehabilitation Robotics,* 2011.

[62] D. Zanotto, P. Stegall and S. K. Agrawal, "ALEX III: A novel robotic platform with 12 DOFs for human gait training," in *IEEE International Conference on Robotics and Automation (ICRA)*, Karlsruhe, 2013.

[63] D. Zanotto, P. Stegall and S. K. Agrawal, "Adaptive assist-as-needed controller to improve gait symmetry in robot-assisted gait training," in *IEEE International Conference on Robotics and Automation (ICRA)*, Hong Kong, 2014.

[64] M. Pietrusinski, I. Cajigas, G. Severini, P. Bonato and C. Mavroidis, "Robotic Gait Rehabilitation Trainer," *IEEE/ASME Transactions on Mechatronics,* vol. 19, no. 2, pp. 490-499, 2014.

[65] M. Pietrusinski, O. Unluhisarcikli, C. Mavroidis, I. Cajigas and P. Bonato, "Design of human — Machine interface and altering of pelvic obliquity with RGR Trainer," in *IEEE International Conference on Rehabilitation Robotics*, Zurich, 2011.

[66] O. Unluhisarcikli, M. Pietrusinski, B. Weinberg, P. Bonato and C. Mavroidis, "Design and control of a robotic lower extremity exoskeleton for gait rehabilitation," in *IEEE/RSJ International Conference on Intelligent Robots and Systems*, San Francisco, CA, 2011.

[67] HealthSouth, "AutoAmbulator," HealthSouth, [Online]. Available:

http://www.healthsouth.com/experience-healthsouth/the-healthsouth-difference/leading-technology/autoambulator/. [Accessed July 2016].

[68] S. Fisher, L. Lucas and T. Thrasher, "Robot-assisted gait training for patients with hemiparesis due to stroke," *Topics in stroke rehabilitation,* vol. 18, no. 3, pp. 269-76, 2011.

[69] Walkbot, "Walkbot," [Online]. Available: http://walkbot2015.cafe24.com/eng. [Accessed July 2016].

[70] Q. V. Tran, S. Kim, K. Lee, S. Kang and J. Ryu, "Force/torque sensorless impedance control for indirect driven robot-aided gait rehabilitation system," in *IEEE International Conference on Advanced Intelligent Mechatronics (AIM)*, Busan, 2015.

[71] T. Miyoshi, K. Hiramatsu, S.-I. Yamamoto, K. Nakazawa and M. Aka, "Robotic gait trainer in water: Development of an underwater gait-training orthosis," *Disability and Rehabilitation,* vol. 30, no. 2, pp. 81-87, 2008.

[72] C.-Y. Jung, J. Choi, S. Park, J. M. Lee, C. Kim and S.-J. Kim, "Design and control of an exoskeleton system for gait rehabilitation capable of natural pelvic movement," in *IEEE/RSJ International Conference on Intelligent Robots and Systems*, Chicago, IL, 2014.

[73] N. Costa and D. G. Caldwell, "Control of a Biomimetic "Soft-actuated" 10DoF Lower Body Exoskeleton," in *IEEE/RAS-EMBS International Conference on Biomedical Robotics and Biomechatronics (BioRob)*, Pisa, 2006.

[74] J.-h. Han, B. Guo and S.-s. Zhao, "Structure design and trajectory control on gait rehabilitation training robot system driven by pneumatic actuators," in *International Conference on Advanced Mechatronic Systems*, Zhengzhou, 2011.

[75] S. Hesse and D. Uhlenbrock, "A mechanized gait trainer for restoration of gait," *Journal of Rehabilitation Research & Development,* pp. 37(6):701-8, 2000.

[76] H. Schmidt, S. Hesse, R. Bernhardt and J. Krüger, "HapticWalker---a novel haptic foot device," *ACM Transactions on Applied Perception (TAP),* pp. 2(2):166-180, 2005.

[77] H. Schmidt, C. Werner, R. Bernhardt, S. Hesse and J. Krüger, "Gait rehabilitation machines based on programmable footplates," *Journal of NeuroEngineering and Rehabilitation,* p. 4:2, 2007.

[78] J. Yoon, B. Novandy, C.-H. Yoon and K.-J. Park, "A 6-DOF Gait Rehabilitation Robot With Upper and Lower Limb Connections That Allows Walking Velocity Updates on Various Terrains," *IEEE/ASME Transactions on Mechatronics ,* vol. 15, no. 2, pp. 201-215, 2010.

[79] A. Taherifar, M. R. Hadian, M. Mousavi, A. Rassaf and F. Ghiasi, "LOKOIRAN- A novel robot for rehabilitation of spinal cord injury and stroke patients," in *RSI/ISM International Conference on Robotics and Mechatronics (ICRoM)*, Tehran, 2013.

[80] S. Freivogel, J. Mehrholz, T. Husak-Sotomayor and D. Schmalohr, "Gait training with the newly developed 'LokoHelp'-system is feasible for non-ambulatory patients after stroke, spinal cord and brain injury. A feasibility stud," *Brain Injury,* p. 22(7–8):625–632, 2008.

[81] Y. Stauffer, Y. Allemand, M. Bouri, J. Fournier, R. Clavel, P. Metrailler, R. Brodard and F. Reynard, "The WalkTrainer—A New Generation of Walking Reeducation Device Combining Orthoses and Muscle Stimulation," *Neural Systems and Rehabilitation Engineering, IEEE Transactions on,* pp. 17(1):38-45, 2009.

[82] M. Bouri, Y. Stauffer, C. Schmitt, Y. Allemand, S. Gnemmi, R. Clavel, P. Metrailler and R. Brodard, "The WalkTrainer: A Robotic System for Walking Rehabilitation," in *IEEE International Conference on Robotics and Biomimetics*, Kunming, 2006.

[83] P. Métrailler, R. Brodard, Y. Stauffer, R. Clavel and R. Frischknecht, "Cyberthosis: Rehabilitation robotics with controlled electrical muscle stimulation," in *Rehabilitation Robotics*, Intech, 2007, pp. 303-318.

[84] T. P. Luu, K. H. Low, X. Qu, H. B. Lim and K. H. Hoon, "Hardware Development and Locomotion Control Strategy for an Over-Ground Gait Trainer: NaTUre-Gaits," *IEEE Journal of Translational Engineering in Health and Medicine ,* vol. 2, 2014.

[85] P. Wang and K. H. Low, "Modeling and tuning of a subject-loaded mobile gait rehabilitation system," in *Asian Control Conference (ASCC)*, Kaohsiung, 2011.

[86] P. Wang, K. H. Low and A. Tow, "Synchronized walking coordination for impact-less footpad contact of an overground gait rehabilitation system: NaTUre-gaits," in *IEEE International Conference on Rehabilitation Robotics*, Zurich, 2011.

[87] H. Lim, K. Hoon, K. Low, Y. Soh and A. Tow, "Pelvic control and over-ground walking methodology for impaired gait recovery," in *Robotics and Biomimetics, 2008. ROBIO 2008. IEEE International Conference on*, Bangkok, 2009.

[88] H. B. Lim, T. P. Luu, K. H. Hoon, X. Qu, A. Tow and K. H. Low, "Study of body weight shifting on robotic assisted gait rehabilitation with NaTUre-gaits," in *IEEE/RSJ International Conference on Intelligent Robots and Systems*, San Francisco, CA, 2011.

[89] S. Slavnić, D. Ristić-Durrant, R. Tschakarow, T. Brendel, M. Tüttemann, A. Leu and A. Gräser, "Mobile robotic gait rehabilitation system CORBYS - overview and first results on orthosis actuation," in *IEEE/RSJ International Conference on Intelligent Robots and Systems*, Chicago, IL, 2014.

[90] C. Glackin, C. Salge, D. Polani, M. Tüttemann, C. Vogel, C. R. Guerrero, V. Grosu, S. Grosu, A. Olenšek, M. Zadravec, I. Cikajlo, Z. Matjačić, A. Leu and D. Ristić-Durrant, "Learning gait by therapist demonstration for natural-like walking with the CORBYS powered orthosis," in *IEEE/RSJ International Conference on Intelligent Robots and Systems (IROS)* , Hamburg, 2015.

[91] V. Grosu, C. R. Guerrero, S. Grosu, A. Leu, D. Ristic-Durrant, B. Vanderborght and D. Lefeber, " Real-time physical layer architecture for CORBYS gait rehabilitation robot," in *IEEE International Conference on Rehabilitation Robotics (ICORR)*, Singapore, 2015.

[92] S. Slavnic, A. Leu, D. Ristic-Durrant and A. Gräser, "Concept of a mobile robot-assisted gait rehabilitation system — Simulation study," in *IEEE/RSJ International Conference on Intelligent Robots and Systems (IROS)*, Taipei, 2010.

[93] S. Slavnic, A. Leu, D. Ristic-Durrant and A. Gräser, "Modeling and Simulation of Walking with a Mobile Gait Rehabilitation System Using Markerless Motion Data," in *Modeling, Simulation and Optimization of Bipedal Walking*, Berlin, Springer, 2013, pp. 223-232.

[94] B. Hwang and D. Jeon, "A wheelchair integrated lower limb exercise/ rehabilitation system: Design and experimental results on the knee joint," in *IEEE/SICE International Symposium on System Integration (SII)*, Fukuoka, 2012.

[95] M. Sasayama and T. Murakami, "Design of a gait rehabilitation system: Gait analysis and gait trajectory generation algorithm," in *2013 IEEE International Symposium on Industrial Electronics (ISIE)*, Taipei, Taiwan, 2013.

[96] A. Calanca, S. Piazza and P. Fiorini, "Force control system for pneumatic actuators of an active gait orthosis," in *IEEE RAS and EMBS International Conference on Biomedical Robotics and Biomechatronics (BioRob)*, Tokyo, 2010.

[97] K. Kong and D. Jeon, "Design and control of an exoskeleton for the elderly and patients," *IEEE/ASME Transactions on Mechatronics,* vol. 11, no. 4, pp. 428-432, 2006.

[98] K.-H. Seo and J.-J. Lee, "The Development of Two Mobile Gait Rehabilitation Systems," *IEEE Transactions on Neural Systems and Rehabilitation Engineering,* vol. 17, no. 2, pp. 156-166, 2009.

[99] M. Peshkin, D. A. Brown, J. J. Santos-Munne, A. Makhlin, E. Lewis, J. E. Colgate, J. Patton and D. Schwandt, "KineAssist: a robotic overground gait and balance training device," in *International Conference on Rehabilitation Robotics (ICORR)*, Chicago, IL, 2005.

[100] A. Morbi, M. Ahmadi and A. Nativ, "GaitEnable: An omnidirectional robotic system for gait rehabilitation," in *IEEE International Conference on Mechatronics and Automation*, Chengdu, 2012.

[101] ReWalk-Robotics, "ReWalk," ReWalk Robotics, [Online]. Available: http://rewalk.com/. [Accessed July 2016].

[102] M. Talaty, A. Esquenazi and J. E. Briceño, "Differentiating ability in users of the ReWalkTM powered exoskeleton: An analysis of walking kinematics," in *IEEE International Conference on Rehabilitation Robotics (ICORR)*, Seattle, WA, 2013.

[103] E. Strickland, "Good-bye, wheelchair," *IEEE Spectrum,* vol. 49, no. 1, pp. 30-32, 2012.

[104] Ekso-Bionics, "Ekso," Ekso Bionics, [Online]. Available: http://eksobionics.com/. [Accessed July 2016].

[105] P. D. Neuhaus, J. H. Noorden, T. J. Craig, T. Torres, J. Kirschbaum and J. E. Pratt, "Design and evaluation of Mina: A robotic orthosis for paraplegics," in *IEEE International Conference on Rehabilitation Robotics*, Zurich, 2011.

[106] IHMC, "NASA-IHMC X1 Mina Exoskeleton," Florida Institute for Human and Machine Cognition (HIMC), [Online]. Available: http://robots.ihmc.us/x1-mina-exoskeleton/. [Accessed July 2016].

[107] S. Wang, L. Wang, C. Meijneke, E. van-Asseldonk, T. Hoellinger, G. Cheron, Y. Ivanenko, V. La-Scaleia, F. Sylos-Labini, M. Molinari, F. Tamburella, I. Pisotta, F. Thorsteinsson, M. Ilzkovitz, J. Gancet, Y. Nevatia, R. Hauffe, F. Zanow and H. van-der-Kooij, "Design and Control of the MINDWALKER Exoskeleton," *IEEE Transactions on Neural Systems and Rehabilitation Engineering ,* vol. 23, no. 2, pp. 277-286, 2015.

[108] Y. Mori, K. Takayama and T. Nakamura, "Development of straight style transfer equipment for lower limbs disabled," in *IEEE International Conference on Robotics and Automation (ICRA)*, Barcelona, 2004.

[109] Cyberdyne, "HAL," Cyberdyne, [Online]. Available: http://www.cyberdyne.jp/english/products/HAL/index.html. [Accessed July 2016].

[110] T. Hayashi, H. Kawamoto and Y. Sankai, "Control method of robot suit HAL working as operator's muscle using biological and dynamical information," in *IEEE/RSJ International Conference on Intelligent Robots and Systems*, Edmonton, 2005.

[111] H. Kawamoto, S. Lee, S. Kanbe and Y. Sankai, "Power assist method for HAL-3 using EMG-based feedback controller," in *Systems, Man and Cybernetics, 2003. IEEE International Conference on*, 2003.

[112] A. Tsukahara, Y. Hasegawa, K. Eguchi and Y. Sankai, "Restoration of Gait for Spinal Cord Injury Patients Using HAL With Intention Estimator for Preferable Swing Speed," *IEEE Transactions on Neural Systems and Rehabilitation Engineering,* vol. 23, no. 2, pp. 308-318, 2015.

[113] A. Tsukahara, Y. Hasegawa and Y. Sankai, "Gait support for complete spinal cord injury patient

by synchronized leg-swing with HAL," in *IEEE/RSJ International Conference on Intelligent Robots and Systems*, San Francisco, CA, 2011.

[114] H. Kawamoto, H. Kandone, T. Sakurai, R. Ariyasu, Y. Ueno, K. Eguchi and Y. Sankai, "Development of an assist controller with robot suit HAL for hemiplegic patients using motion data on the unaffected side," in *Annual International Conference of the IEEE Engineering in Medicine and Biology Society*, Chicago, IL, 2014.

[115] H. Kawamoto, H. Kadone, T. Sakurai and Y. Sankai, "Modification of hemiplegic compensatory gait pattern by symmetry-based motion controller of HAL," in *Annual International Conference of the IEEE Engineering in Medicine and Biology Society (EMBC)*, Milan, 2015.

[116] H. Kawamoto, T. Hayashi, T. Sakurai, K. Eguchi and Y. Sankai, "Development of single leg version of HAL for hemiplegia," in *Annual International Conference of the IEEE Engineering in Medicine and Biology Society*, Minneapolis, MN, 2009.

[117] A. Zoss, H. Kazerooni and A. Chu, "On the mechanical design of the Berkeley Lower Extremity Exoskeleton (BLEEX)," in *IEEE/RSJ International Conference on Intelligent Robots and Systems*, Edmonton, 2005.

[118] Army-technology, "XOS 2," Army-technology, [Online]. Available: http://www.army-technology.com/projects/raytheon-xos-2-exoskeleton-us/. [Accessed July 2016].

[119] S. Karlin, "Raiding Iron Man's closet," *IEEE Spectrum,* vol. 48, no. 8, p. 25, 2011.

[120] K. Yamamoto, K. Hyodo, M. Ishii and T. Matsuo, "Development of power assisting suit for assisting nurse labor," *JSME International Journal Series C,* vol. 45, no. 3, pp. 703-711, 2002.

[121] K. Yamamoto, M. Ishii, H. Noborisaka and K. Hyodo, "Stand alone wearable power assisting suit - sensing and control systems," in *IEEE International Workshop on Robot and Human Interactive Communication (ROMAN)*, 2004.

[122] W.-s. Kim, S.-h. Lee, H.-d. Lee, S.-n. Yu, J.-s. Han and C.-s. Han, "Development of the heavy load transferring task oriented exoskeleton adapted by lower extremity using qausi - Active joints," in *ICCAS-SICE*, Fukuoka, 2009.

[123] K. H. Low, X. Liu and H. Yu, "Development of NTU wearable exoskeleton system for assistive technologies," in *IEEE International Conference Mechatronics and Automation*, 2005.

[124] C. J. Walsh, D. Paluska, K. Pasch, W. Grand, A. Valiente and H. Herr, "Development of a lightweight, underactuated exoskeleton for load-carrying augmentation," in *IEEE International Conference on Robotics and Automation (ICRA)*, Orlando, FL, 2006.

[125] J. E. Pratt, B. T. Krupp, C. J. Morse and S. H. Collins, "The RoboKnee: an exoskeleton for enhancing strength and endurance during walking," in *IEEE International Conference on Robotics and Automation (ICRA)*, 2004.

[126] C. Fleischer and G. Hommel, "A Human--Exoskeleton Interface Utilizing Electromyography," *Robotics, IEEE Transactions on,* pp. 24(4):872-882, 2008.

[127] R. W. Horst, "A bio-robotic leg orthosis for rehabilitation and mobility enhancement," in *Annual International Conference of the IEEE Engineering in Medicine and Biology Society*, Minneapolis, MN, 2009.

[128] D. P. Ferris, G. S. Sawicki and A. Domingo, "Powered lower limb orthoses for gait rehabilitation," *Topics in Spinal Cord Injury Rehabilitation,* vol. 11, no. 2, pp. 34-49, 2005.

[129] G. S. Sawicki and D. P. Ferris, "A pneumatically powered knee-ankle-foot orthosis (KAFO) with myoelectric activation and inhibition," *Journal of NeuroEngineering and Rehabilitation,* vol. 6, no. 23, 2009.

[130] S. V. Dhule, V. V. Shete and S. B. Somani, "Implementation of adaptive dorsiflexion and plantar flexion in active ankle foot orthosis," in *International Conference on Information Processing (ICIP)*, Pune, 2015.

[131] D. Surdilovic and R. Bernhardt, "STRING-MAN: a new wire robot for gait rehabilitation," in *Robotics and Automation, 2004. Proceedings. ICRA '04. 2004 IEEE International Conference on*, 2004.

[132] D. Surdilovic, J. Zhang and R. Bernhardt, "STRING-MAN: Wire-robot technology for safe, flexible and human-friendly gait rehabilitation," in *Rehabilitation Robotics, 2007. ICORR 2007. IEEE 10th International Conference on*, Noordwijk, 2007.

[133] T. Susko, K. Swaminathan and H. Krebs, "MIT-Skywalker - A Novel Gait Neurorehabilitation Robot for Stroke and Cerebral Palsy," *IEEE Transactions on Neural Systems and Rehabilitation Engineering,* vol. PP, no. 99, 2006.

[134] R. Boian, M. Bouzit, G. Burdea and J. Deutsch, "Dual Stewart platform mobility simulator," in *Engineering in Medicine and Biology Society, 2004. IEMBS '04. 26th Annual International Conference of the IEEE*, San Francisco, CA, 2004.

[135] J. Hollerbach, D. Grow and C. Parker, "Developments in locomotion interfaces," in *International Conference on Rehabilitation Robotics (ICORR)*, 2005.

[136] C. Schmitt, P. Métrailler, A. Al-Khodairy, R. Brodard, J. Fournier, M. Bouri and R. Clavel, "The Motion Make : a Rehabilitation System Combining an Orthosis with Closed-Loop Electrical Muscle Stimulation," in *8th Vienna International Workshop on Functional Electrical Stimulation*, Vienna, 2004.

[137] P. Metrailler, R. Brodard, Y. Stauffer, R. Clavel and R. Frischknecht, "Cyberthosis - Rehabilitation robotics with controlled electrical muscle," in *Rehabilitation Robotics*, INTECH, 2007, pp. 303-319.

[138] J. Hu, Z.-G. Hou, Y. Chen, L. Peng and L. Peng, "Task-oriented active training based on adaptive impedance control with iLeg — A horizontal exoskeleton for lower limb rehabilitation," in *IEEE International Conference on Robotics and Biomimetics (ROBIO)*, Shenzhen, 2013.

[139] L. Saint-Bauzel, V. Pasqui and I. Monteil, "A reactive robotized interface for lower limb rehabilitation - Clinical results," *IEEE Transactions on Robotics,* vol. 25, no. 3, pp. 583-592, 2009.

[140] D. Baiden and O. Ivlev, "Independent torque and stiffness adjustment of a pneumatic direct rotary soft-actuator for adaptable human-robot-interaction," in *International Conference on Robotics in Alpe-Adria-Danube Region (RAAD)*, Smolenice, 2014.

[141] E. Swinnen, D. Beckwée, R. Meeusen, J. Baeyens and E. Kerckhofs, "Does Robot-Assisted Gait Rehabilitation Improve Balance in Stroke Patients? A Systematic Review," *Topics in Stroke Rehabilitation,* vol. 21, no. 2, pp. 87-100, 2014.

[142] B. Fleerkotte, B. Koopman, J. Buurke, E. van Asseldonk, H. van der Kooij and J. Rietman, "The effect of impedance-controlled robotic gait training on walking ability and quality in individuals with chronic incomplete spinal cord injury: an explorative study," *Journal of NeuroEngineering and Rehabilitation,* vol. 11, no. 26, 2014.

[143] L. A. Chernikova and A. S. Klochkov, "The influence of physical training with the use of a lokomat robotic system on the walking ability of the patients with post-stroke hemiparesis," *Vopr Kurortol Fizioter Lech Fiz Kult,* 2014.

[144] D. Varoqui, X. Niu and M. M. Mirbagheri, "Ankle voluntary movement enhancement following

robotic-assisted locomotor training in spinal cord injury," *Journal of NeuroEngineering and Rehabilitation,* vol. 11, no. 46, 2014.

[145] K. Van Kammen, A. Boonstra, H. Reinders-Messelink and R. den Otter, "The combined effects of body weight support and gait speed on gait related muscle activity: a comparison between walking in the Lokomat exoskeleton and regular treadmill walking," *PLOS ONE,* vol. 9, no. 9, 2014.

[146] J. Hidler, W. Wisman and N. Neckel, "Kinematic trajectories while walking within the Lokomat robotic gait-orthosis," *Clinical Biomechanics,* p. 1251–1259, 2008.

[147] N. Lapitskaya, J. Nielsen and A. Fuglsang-Frederiksen, "Robotic gait training in patients with impaired consciousness due to severe traumatic brain injury.," *Brain Injury,* vol. 25, no. 11, pp. 1070-9, 2011.

[148] N. D. Neckel, N. Blonien, D. Nichols and J. Hidler, "Abnormal joint torque patterns exhibited by chronic stroke subjects while walking with a prescribed physiological gait pattern," *Journal of NeuroEngineering and Rehabilitation,* vol. 5, no. 19, 2008.

[149] J. C. Shin, J. Y. K. H. K. Park and N. Y. Kim, "Effect of Robotic-Assisted Gait Training in Patients With Incomplete Spinal Cord Injury," *Annals of Rehabilitation Medicine,* vol. 38, no. 6, p. 719–725, 2014.

[150] I. Schwartz, A. Sajin, I. Fisher, M. Neeb, M. Shochina, M. Katz-Leurer and Z. Meiner, "The effectiveness of locomotor therapy using robotic-assisted gait training in subacute stroke patients - a randomized controlled trial," *PM&R,* vol. 1, no. 6, p. 516–523, 2009.

[151] R. K. Tong, M. F. Ng and L. S. Li, "Effectiveness of gait training using an electromechanical gait trainer, with and without functional electric stimulation, in subacute stroke: a randomized controlled trial," *Archives of Physical Medicine and Rehabilitation,* vol. 87, no. 10, p. 1298–1304, 2006.

[152] U. Dundar, H. Toktas, O. Solak, A. M. Ulasli and S. Eroglu, "A comparative study of conventional physiotherapy versus robotic training combined with physiotherapy in patients with stroke," *Topics in stroke rehabilitation,* vol. 21, no. 6, 2014.

[153] K. P. Westlake and C. Patten, "Pilot study of Lokomat versus manual-assisted treadmill training for locomotor recovery post-stroke," *Journal of NeuroEngineering and Rehabilitation,* vol. 6, no. 18, 2009.

[154] M. van Nunen, K. Gerrits, M. Konijnenbelt, T. Janssen and A. de Haan, "Recovery of walking ability using a robotic device in subacute stroke patients: a randomized controlled study," *Disability and Rehabilitation: Assistive Technology,* vol. 10, no. 2, pp. 141-8, 2015.

[155] C. P. Kelley, J. Childressb, C. Boakec and E. A. Noser, "Over-ground and robotic-assisted locomotor training in adults with chronic stroke: a blinded randomized clinical trial," *Disability and Rehabilitation: Assistive Technology,* vol. 8, no. 2, pp. 161-168, 2013.

[156] M. Wirz, C. Bastiaenen, R. d. Bie and V. Dietz, "Effectiveness of automated locomotor training in patients with acute incomplete spinal cord injury - A randomized controlled multicenter trial," *BMC Neurology,* vol. 11, no. 60, 2011.

[157] Maxon Motor AG, "EC 45 flat, 70 Watt: novel features with proven characteristics," 16 Aug 2011. [Online]. Available: http://www.maxonmotor.com/maxon/view/news/MEDIENMITTEILUNG-EC-45-flat-70-Watt.

[158] Harmonic Drive AG, "HFUS-2A," [Online]. Available: http://harmonicdrive.de/en/products/component-sets/hfus-2a.html. [Accessed Sept 2016].

[159] Elmo Motion Control Ltd., "Gold Solo Whistle," [Online]. Available: http://www.elmomc.com/products/whistle-solo-servo-drive-gold.htm. [Accessed Sept 2016].

[160] AMT Schmid GmbH & Co. KG, "Gearmotor SRG 05: A new type in the SRG-line," [Online]. Available: http://www.amt-schmid.com/en/products/gearmotor_drives/srg_05/srg_05.php. [Accessed Sept 2016].

[161] Schunk GmbH & Co, "PDU 070-101-B," [Online]. Available: https://de.schunk.com/de_en/gripping-systems/#/product/25510-0307352-pdu-070-101-b. [Accessed Sept 2016].

[162] Schunk GmbH & Co., "Motion Control Schunk: Software Manual," [Online]. Available: https://de.schunk.com/fileadmin/pim/docs/IM0010976.PDF. [Accessed Sept 2016].

[163] Orocos, "The Orocos Project," [Online]. Available: http://www.orocos.org/.

[164] H. Lim, K. Hoon, Y. Soh, A. Tow and K. Low, "Effective Gait planning for robotic rehabilitation - From normal gait study to application in clinical rehabilitation," in *IEEE/ASME International Conference on Advanced Intelligent Mechatronics, 2009. AIM 2009.*, Singapore, 2009.

[165] H. Lim, T. P. Luu, K. Hoon and K. Low, "Natural gait parameters prediction for gait rehabilitation via artificial neural network," in *2010 IEEE/RSJ International Conference on Intelligent Robots and Systems (IROS)*, Taipei, 2010.

[166] T. P. Luu, H. Lim, X. Qu and K. Low, "Subject tailored gait pattern planning for robotic gait rehabilitation," in *2010 IEEE International Conference on Robotics and Biomimetics (ROBIO)*, Tianjin, 2010.

[167] T. P. Luu, H. Lim, X. Qu, K. Hoon and K. Low, "Subject-specific lower limb waveforms planning via artificial neural network," in *2011 IEEE International Conference on Rehabilitation Robotics (ICORR)*, Zurich, 2011a.

[168] T. P. Luu, H. Lim, K. Hoon, X. Qu and K. Low, "Subject-specific gait parameters prediction for robotic gait rehabilitation via generalized regression neural network," in *2011 IEEE International Conference on Robotics and Biomimetics (ROBIO)*, Karon Beach, Phuket, 2011b.

[169] N. Tufekciler, E. van Asseldonk and H. van der Kooij, "Velocity-dependent reference trajectory generation for the LOPES gait training robot," in *2011 IEEE International Conference on Rehabilitation Robotics (ICORR)*, Zurich, 2011.

[170] B. Koopman, E. van Asseldonk and H. van der Kooij, "Speed-dependent reference joint trajectory generation for robotic gait support," *Journal of Biomechanics,* vol. 47, no. 6, pp. 1447-58, 2014.

[171] X. Wang, X. Cao, H. Song, T. Lu and K. Yuan, "A gait trajectory measuring and planning method for lower limb robotic rehabilitation," in *Mechatronics and Automation (ICMA), 2015 IEEE International Conference on*, Beijing, 2015.

[172] S. K. Banala, S. H. Kim, S. K. . Agrawal and J. P. Scholz, "Robot assisted gait training with active leg exoskeleton (ALEX)," *IEEE Transactions on Neural Systems and Rehabilitation Engineering,* pp. 17(1):2-8, 2009.

[173] Y. Yang, C. Yang, K.-M. Lee and H. Yu, "Model-based fuzzy adaptation for control of a lower extremity rehabilitation exoskeleton," in *Advanced Intelligent Mechatronics, 2009. AIM 2009. IEEE/ASME International Conference on*, Singapore, 2009.

[174] K. H. Seo, Y. Park, S. Yun and S. Park, "Gait pattern generation for robotic gait rehabilitation system on treadmill," in *Control, Automation and Systems (ICCAS), 2014 14th International*

Conference on, Seoul, 2014.

[175] H. Vallery, E. van Asseldonk, M. Buss and H. van der Kooij, "Reference Trajectory Generation for Rehabilitation Robots: Complementary Limb Motion Estimation," *IEEE Transactions on Neural Systems and Rehabilitation Engineering,* pp. 17(1):23-30, 2009.

[176] H. Vallery, R. Ekkelenkamp, M. Buss and H. v. d. Kooij, "Complementary Limb Motion Estimation based on Interjoint Coordination: Experimental Evaluation," in *IEEE 10th International Conference on Rehabilitation Robotics*, Noordwijk, 2007.

[177] MathWorks, "Spline," MathWorks, [Online]. Available: http://de.mathworks.com/help/matlab/ref/spline.html. [Accessed April 2016].

[178] C. de Boor, A Practical Guide to Splines, Springer, 1978.

[179] MathWorks, "Pchip," MathWorks, [Online]. Available: http://de.mathworks.com/help/matlab/ref/pchip.html. [Accessed April 2016].

[180] F. Fritsch and R. Carlson, "Monotone Piecewise Cubic Interpolation," *SIAM Journal on Numerical Analysis,* pp. 17(2):238-246, 1980.

[181] R. L. Dougherty, A. Edelman and J. M. Hyman, "Nonnegativity-, Monotonicity-, or Convexity-Preserving Cubic and Quintic Hermite Interpolation," *Mathematics of Computation,* pp. 52(86):471-494, 1989.

[182] P. Costantini, "Algorithm 770: BVSPIS—a package for computing boundary-valued shape-preserving interpolating splines," *ACM Transactions on Mathematical Software (TOMS),* pp. 23(2):252-254, 1997b.

[183] P. Costantini, "Boundary-valued shape-preserving interpolating splines," *ACM Transactions on Mathematical Software (TOMS),* pp. 23(2):229-251, 1997a.

[184] P. Costantini, "An algorithm for computing shape-preserving interpolating splines of arbitrary degree," *Journal of Computational and Applied Mathematics,* pp. 22(1):89-136, 1988.

[185] P. Costantini, "Co-Monotone interpolating splines of arbitrary degree—a local approach," *SIAM Journal on Scientific and Statistical Computing,* pp. 8(6):1026-1034, 1987.

[186] G. Wolberg and I. Alfy, "An energy-minimization framework for monotonic cubic spline interpolation," *Journal of Computational and Applied Mathematics,* pp. 143(2):145-188 , 2002.

[187] B. Luong, "Mathworks / Matlab Central / Newsreader," August 2008. [Online]. Available: http://www.mathworks.com/matlabcentral/newsreader/view_thread/173592. [Accessed August 2013].

[188] "Kinovea," [Online]. Available: http://www.kinovea.org/. [Accessed 2014].

[189] M. R. Pierrynowski and V. Galea, "Enhancing the ability of gait analyses to differentiate between groups: scaling gait data to body size," *Gait and Posture,* vol. 13, no. 3, p. 193–201, 2001.

[190] H. L. "FSM-9 Modules," Hillcrest Labs, [Online]. Available: http://hillcrestlabs.com/products/sensor-modules/fsm-9/. [Accessed April 2016].

[191] M. Hagan and M. Menhaj, "Training feedforward networks with the Marquardt algorithm," *Neural Networks, IEEE Transactions on,* vol. 5, no. 6, pp. 989 - 993, 1994.

[192] D. MacKay, Neural Computation, vol. 4, 1992, p. 415–447.

[193] MathWorks, "Neural Network Toolbox," MathWorks, [Online]. Available: http://de.mathworks.com/help/nnet/index.html. [Accessed April 2016].

[194] J. Lelas, G. Merriman, P. Riley and D. Kerrigan, "Predicting peak kinematic and kinetic

parameters from gait speed," *Gait and Posture,* vol. 17, no. 2, pp. 106 - 112, 2003.

[195] B. Pietraszewski, S. Winiarski and S. Jaroszczuk, "Three-dimensional human gait pattern - reference data for normal men," *Acta of Bioengineering and Biomechanics,* vol. 14, no. 3, pp. 9-16, 2012.

[196] M. P. Kadaba, H. K. Ramakrishnan, M. E. Wootten, J. Gainey, G. Gorton and G. V. B. Cochran, "Repeatability of kinematic, kinetic, and electromyographic data in normal adult gait," *Journal of Orthopaedic Research,* vol. 7, no. 6, pp. 849-860, 1989.

[197] M. P. Kadaba, H. K. Ramakrishnan and M. E. Wootten, "Measurement of lower extremity kinematics during level walking," *Journal of Orthopaedic Research,* vol. 8, no. 3, pp. 383-92, 1990.

[198] K. J. Ganley and C. M. Powers, "Gait kinematics and kinetics of 7-year-old children: a comparison to adults using age-specific anthropometric data," *Gait & Posture,* vol. 21, no. 2, pp. 141-145, 2005.

[199] M. Lee, J. Kim, J. Son and Y. Kim, "Kinematic and kinetic analysis during forward and backward walking," *Gait & Posture,* vol. 38, no. 4, p. 674–678, 2013.

[200] L. H. Sloot, M. M. van der Krogt and J. Harlaar, "Self-paced versus fixed speed treadmill walking," *Gait & Posture,* vol. 39, no. 1, pp. 478-484, 2014.

[201] B. Stansfield, S. Hillmana, M. Hazlewooda and J. Robba, "Regression analysis of gait parameters with speed in normal children walking at self-selected speeds," *Gait & Posture,* vol. 23, no. 3, pp. 288-294, 2006.

[202] V. L. Chester, M. Tingley and E. N. Biden, "Comparison of two normative paediatric gait databases," *Dynamic medicine,* vol. 6, no. 8, 2007.

[203] Elmo Motion Control, "CAN DS-402 Implementation Guide," Oct 2013. [Online]. Available: http://www.elmomc.com/support/downloads-operating-manuals-main.htm.

[204] Elmo Motion Control, "Command Reference for Gold Line Drives," Jan 2014. [Online]. Available: http://www.elmomc.com/support/downloads-operating-manuals-main.htm.

[205] N. Hogan, "Impedance Control: An Approach to Manipulation," *Journal of Dynamic Systems, Measurement, and Control,* 1985.

[206] D. Surdilovic and Z. Cojbasic, "Robust robot compliant motion control using intelligent adaptive impedance approach," in *IEEE International Conference on Robotics and Automation (ICRA)*, Detroit, MI, 1999.

[207] B. Siciliano and L. Villani, Robot Force Control, Norwell, MA: Kluwer, 1999.

[208] H. Krebs, J. Palazzolo, L. Dipietro, M. Ferraro, J. Krol, K. Rannekleiv, B. Volpe and N. Hogan, "Rehabilitation Robotics: Performance-Based Progressive Robot-Assisted Therapy," *Autonomous Robots,* vol. 15, no. 1, pp. 7-20, 2003.

[209] R. Riener and G. C. L. Lünenburger, "Human-centered robotics applied to gait training and assessment," *Journal of Rehabilitation Research & Development,* vol. 43, no. 5, pp. 679-94, 2006.

[210] MSC Software, "Adams: The Multibody Dynamics Simulation Solution," [Online]. Available: http://www.mscsoftware.com/product/adams. [Accessed Sept 2016].

[211] D. Aoyagi, W. Ichinose, S. Harkema, D. Reinkensmeyer and J. Bobrow, "An assistive robotic device that can synchronize to the pelvic motion during human gait training," in *International Conference on Rehabilitation Robotics (ICORR)*, Chicago, 2005.

[212] R. Ronsse, S. M. M. De Rossi, N. Vitiello, T. Lenzi, B. Koopman, H. Van Der Kooij, M. C.

Carrozza and A. J. Ijspeert, "Real-time Estimate of Period Derivatives using Adaptive Oscillators: Application to Impedance-Based Walking Assistance," in *IEEE/RSJ International Conference on Intelligent Robots and Systems*, Vilamoura, 2012.

[213] R. Ronsse, T. Lenzi, N. Vitiello, B. Koopman, E. van Asseldonk, S. De Rossi, J. van den Kieboom, H. van der Kooij, M. Carrozza and A. Ijspeert, "Oscillator-based assistance of cyclical movements: model-based and model-free approaches," *Medical & Biological Engineering & Computing,* vol. 49, no. 10, pp. 1173-85, 2011.

[214] G. Chen, P. Qi, Z. Guo and H. Yu, "Gait-Event-Based Synchronization Method for Gait Rehabilitation Robots via a Bio-inspired Adaptive Oscillator," *IEEE Transactions on Biomedical Engineering ,* vol. PP, 2016.

[215] T. Lenzi, M. Carrozza and S. Agrawal, "Powered hip exoskeletons can reduce the user's hip and ankle muscle activations during walking," *IEEE Transactions on Neural Systems and Rehabilitation Engineering,* vol. 21, no. 6, pp. 938-48, 2013.

[216] X. Niu, D. Varoqui, M. Kindig and M. Mirbagheri, "Prediction of gait recovery in spinal cord injured individuals trained with robotic gait orthosis," *Journal of NeuroEngineering and Rehabilitation,* vol. 11, no. 42, 2014.

[217] A. Nardo, F. Anasetti, D. Servello and M. Porta, "Quantitative gait analysis in patients with Parkinson treated with deep brain stimulation: The effects of a robotic gait training," *NeuroRehabilitation,* vol. 35, no. 4, pp. 779-88, 2014.

[218] M. M. Mirbagheri, C. Patel and K. Quiney, "Robotic-assisted locomotor training impact on neuromuscular properties and muscle strength in Spinal Cord Injury," in *Annual International Conference of the IEEE Engineering in Medicine and Biology Society*, Boston, MA, 2011.

[219] M. M. Mirbagheri, X. Niu, M. Kindig and D. Varoqui, "The effects of locomotor training with a robotic-gait orthosis (Lokomat) on neuromuscular properties in persons with chronic SCI," in *Annual International Conference of the IEEE Engineering in Medicine and Biology Society*, San Diego, CA, 2012.

[220] R. S. Calabrò, S. Reitano, A. Leo, R. D. Luca, C. Melegari and P. Bramanti, "Can robot-assisted movement training (Lokomat) improve functional recovery and psychological well-being in chronic stroke? Promising findings from a case study," *Functional Neurology,* vol. 29, no. 2, p. 139–141, 2014.

[221] A. Schück, R. Labruyère, H. Vallery, R. Riener and A. Duschau-Wicke, "Feasibility and effects of patient-cooperative robot-aided gait training applied in a 4-week pilot trial," *Journal of NeuroEngineering and Rehabilitation,* vol. 9, no. 31, 2012.

[222] A. C. Lo, V. C. Chang, M. A. Gianfrancesco, J. H. Friedman, T. S. Patterson and D. F. Benedicto, "Reduction of freezing of gait in Parkinson's disease by repetitive robot-assisted treadmill training - a pilot study," *Journal of NeuroEngineering and Rehabilitation,* vol. 7, no. 51, 2010.

[223] A. J. del Ama, Á. Gil-Agudo, J. L. Pons and J. C. Moreno, "Hybrid gait training with an overground robot for people with incomplete spinal cord injury: a pilot study," *Frontiers in Human Neuroscience,* vol. 8, 2014.

[224] C. Krishnan, R. Ranganathan, Y. Y. Dhaher and W. Z. Rymer, "A Pilot Study on the Feasibility of Robot-Aided Leg Motor Training to Facilitate Active Participation," *PLOS ONE,* vol. 8, no. 10, 2013.

[225] C. Krishnan, R. Ranganathan, S. S. Kantak, Y. Y. Dhaher and W. Z. Rymer, "Active robotic training improves locomotor function in a stroke survivor," *Journal of NeuroEngineering and*

Rehabilitation, vol. 9, no. 57, 2012.

[226] O. Stoller, E. D. de-Bruin, M. Schindelholz, C. Schuster, R. A. de-Bie and K. J. Hunt, "Cardiopulmonary exercise testing early after stroke using feedback-controlled robotics-assisted treadmill exercise - test-retest reliability and repeatability," *Journal of NeuroEngineering and Rehabilitation,* vol. 11, no. 145, 2014.

[227] M. Wu, J. M. Landry, J. Kim, B. D. Schmit, S.-C. Yen and J. MacDonald, "Robotic Resistance/Assistance Training Improves Locomotor Function in Individuals Poststroke: A Randomized Controlled Study," *Archives of Physical Medicine and Rehabilitation,* vol. 95, no. 5, p. 799–806, 2014.

[228] C. Chisari, F. Bertolucci, V. Monaco, M. Venturi, C. Simonella, S. Micera and B. Rossi, "Robot-assisted gait training improves motor performances and modifies Motor Unit firing in post-stroke patients," *European Journal of Physical and Rehabilitation Medicine,* vol. 51, no. 1, pp. 59-69, 2015.

[229] I. Borggraefe, J. S. Schaefer, M. Klaiber, E. Dabrowski, C. Ammann-Reiffer, B. Knecht, S. Berweck, F. Heinen and A. Meyer-Heim, "Robotic-assisted treadmill therapy improves walking and standing performance in children and adolescents with cerebral palsy," *European Journal of Paediatric Neurology,* vol. 14, no. 6, p. 496–502, 2010.

[230] J. M. Hidler and A. E. Wall, "Alterations in muscle activation patterns during robotic-assisted walking," *Clinical Biomechanics,* vol. 20, no. 2, pp. 184-193, 2005.

[231] I. Schwartz, A. Sajin, M. Neeb, I. Fisher, M. Katz-Luerer and Z. Meine, "Locomotor training using a robotic device in patients with subacute spinal cord injury," *Spinal Cord,* vol. 49, p. 1062–1067, 2011.

[232] I. Schwartz, A. Sajin, E. Moreh, I. Fisher, M. Neeb, A. Forest, A. Vaknin-Dembinsky, D. Karusis and Z. Meiner, "Robot-assisted gait training in multiple sclerosis patients - a randomized trial," *Multiple Sclerosis Journal,* vol. 18, no. 6, pp. 881-90, 2012.

[233] A. Mayr, M. Kofler, E. Quirbach, H. Matzak, K. Fröhlich and L. Saltuari, "Prospective, blinded, randomized crossover study of gait rehabilitation in stroke patients using the Lokomat gait orthosis," *Neurorehabilitation and Neural Repair,* vol. 21, no. 4, pp. 307-14, 2007.

[234] M. Drużbicki, W. Rusek, M. Szczepanik, J. Dudek and S. Snela, "Assessment of the impact of orthotic gait training on balance in children with cerebral palsy," *Acta of Bioengineering and Biomechanics,* vol. 12, no. 3, pp. 53-8, 2010.

[235] M. Alcobendas-Maestro, A. Esclarín-Ruz, R. Casado-López, A. Muñoz-González, G. Pérez-Mateos, E. González-Valdizán and J. Martín, "Lokomat robotic-assisted versus overground training within 3 to 6 months of incomplete spinal cord lesion - randomized controlled trial," *Neurorehabilitation and Neural Repair,* vol. 26, no. 9, pp. 1058-63, 2012.

[236] A. Picelli, C. Melotti, F. Origano, A. Waldner, A. Fiaschi, V. Santilli and N. Smania, "Robot-assisted gait training in patients with Parkinson disease - a randomized controlled trial," *Neurorehabilitation and Neural Repair,* vol. 26, no. 4, pp. 353-61, 2012.

[237] S. Beer, B. Aschbacher, D. Manoglou, E. Gamper, J. Kool and J. Kesselring, "Robot-assisted gait training in multiple sclerosis - a pilot randomized trial," *Multiple Sclerosis Journal,* vol. 14, no. 2, pp. 231-6, 208.

[238] B. Husemann, F. Müller, C. Krewer, S. Heller and E. Koenig, "Effects of locomotion training with assistance of a robot-driven gait orthosis in hemiparetic patients after stroke: a randomized controlled pilot study," *Stroke,* vol. 38, no. 2, pp. 349-54, 2007.

[239] M. Gandolfi, C. Geroin, A. Picelli, D. Munari, A. Waldner, S. Tamburin, F. Marchioretto and N.

Smania, "Robot-assisted vs. sensory integration training in treating gait and balance dysfunctions in patients with multiple sclerosis - a randomized controlled trial," *Frontiers in Human Neuroscience,* vol. 8, no. 318, 2014.

[240] C. Vaney, B. Gattlen, V. Lugon-Moulin, A. Meichtry, R. Hausammann, D. Foinant, A. Anchisi-Bellwald, C. Palaci and R. Hilfiker, "Robotic-Assisted Step Training (Lokomat) Not Superior to Equal Intensity of Over-Ground Rehabilitation in Patients With Multiple Sclerosis," *Neurorehabilitation and Neural Repair,* vol. 26, no. 3, pp. 212-21, 2012.

[241] Z.-S. Hou and Z. Wang, "From model-based control to data-driven control: Survey, classification and perspective," *Information Sciences,* vol. 235, p. 3–35, 20 June 2013.

[242] B. Siciliano, L. Sciavicco, L. Villani and G. Oriolo, Robotics: modelling, planning and control, London: Springer, 2009.

[243] M. W. Spong, S. Hutchinson and M. Vidyasagar, Robot Modeling and Control, Wiley, 2006.

[244] N. Sarkar, X. Yun and V. Kumar, "Control of Mechanical Systems With Rolling Constraints. Application to Dynamic Control of Mobile Robots," *The International Journal of Robotics Research,* vol. 13, no. 1, pp. 55-69, February 1994.

[245] H. J. Lee and S. Jung, "Guidance control of a wheeled mobile robot with human interaction based on force control," *International Journal of Control, Automation and Systems,* vol. 8, no. 2, pp. 361-368 , April 2010.

[246] J. Wu, J. Wang and Z. You, "An overview of dynamic parameter identification of robots," *Robotics and Computer-Integrated Manufacturing,* vol. 26, no. 5, p. 414–419, October 2010.

[247] G. Calafiore, M. Indri and B. Bona, "Robot dynamic calibration: Optimal excitation trajectories and experimental parameter estimation," *Journal of Robotic Systems,* vol. 18, no. 2, p. 55–68, February 2001.

[248] F. Benimeli, V. Mata and F. Valero, "A comparison between direct and indirect dynamic parameter identification methods in industrial robots," *Journal Robotica,* vol. 24, no. 5, pp. 579 - 590, 2006.

[249] H. Kawasaki, T. Shimizu and K. Kanzaki, "Symbolic analysis of the base parameters for closed-chain robots based on the completion procedure," in *Robotics and Automation, IEEE International Conference on*, Minneapolis, MN, 1996.

[250] H. Mayeda, K. Yoshida and K. Osuka, "Base parameters of manipulator dynamic models," *Robotics and Automation, IEEE Transactions on,* vol. 6, no. 3, pp. 312 - 321, June 1990.

[251] S. Focke Martinez, O. Kuzmicheva and A. Graeser, "User-friendly hip and knee trajectory generation of healthy gait patterns for robotic rehabilitation systems," in *TAR*, Berlin, 2015.

[252] S. Focke Martinez, O. Kuzmicheva and A. Gräser, "Prediction of characteristic points of hip and knee joint trajectories during overground walking using IMUs and Artificial Neural Networks," in *IEEE International Symposium on Medical Measurements and Applications (MeMeA)*, Benevento, 2016.

[253] S. Focke Martinez, O. Kuzmicheva and A. Graeser, "Joint Trajectory Generation and Control for Overground Robot-based Gait Rehabilitation System MOPASS," in *Augmented Human International Conference*, Geneva, 2016.

[254] H. Sadeghi, "Local or global asymmetry in gait of people without impairments," *Gait & Posture,* vol. 17, no. 3, pp. 197-204, 2003.

[255] K. Ostrosky, J. VanSwearingen, R. Burdett and Z. Gee, "A comparison of gait characteristics in young and old subjects," *Physical Therapy Journal,* vol. 74, no. 7, pp. 644-6, 1994.

[256] T. Oberg, A. Karsznia and K. Oberg, "Joint angle parameters in gait: reference data for normal subjects, 10-79 years of age," *Journal of Rehabilitation Research & Development (JRRD),* vol. 91, no. 3, pp. 199-213, 1994.

[257] A. Frizera, A. Elias, A. J. del Ama, R. Ceres and T. F. Bastos, "Characterization of spatio-temporal parameters of human gait assisted by a robotic walker," in *International Conference on Biomedical Robotics and Biomechatronics (BioRob)* , 2012.

[258] S. Hirokawa, "Normal gait characteristics under temporal and distance constraints," *Journal of Biomedical Engineering,* vol. 11, no. 6, pp. 449-56, 1989.

[259] P. Hageman and D. Blanke, "Comparison of gait of young women and elderly women," *Physical Therapy Journal,* vol. 66, no. 9, pp. 1382-7, 1986.

[260] T. Oberg, A. Karsznia and K. Oberg, "Basic gait parameters: reference data for normal subjects, 10-79 years of age," *Journal of Rehabilitation Research & Development (JRRD),* vol. 30, no. 2, pp. 210-23, 1993.

[261] R. Paróczai, Z. Bejek, Á. Illyés, L. Kocsis and R. Kiss, "Gait parameters of the healthy, elderly people," *Physical Education and Sport,* vol. 4, no. 1, pp. 49 - 58 , 2006.

[262] S. Ko, J. Hausdorff and L. Ferrucci, "Age-associated differences in the gait pattern changes of older adults during fast-speed and fatigue conditions: results from the Baltimore longitudinal study of ageing," *Age and Ageing,* vol. 39, no. 6, pp. 688-94, 2010.

List of abbreviations

1I1O	1-input 1-output
2I1O	2-inputs 1-output
AFO	Ankle-foot orthosis
AMAE	Average mean absolure error
ANN	Artificial Neural Network
AR	Average cross-correlation coefficient
ARMSE	Average root mean square error
ASDAE	Average standard deviation of the absolute errors
AvC	Average curve
BVSIS	Boundary-Valued Shape-preserving Interpolating Spline
BWLL	Body weight / Leg length
BWS	Body-weight support
CAD	Computer-aided design
Cad	cadence
CAN	Controller Area Network
CIMT	Constrained-induced movement therapy
CLME	Complementary limb motion estimation
cov	covariance
CP	Cerebral Palsy
CSHTA	Cyclic synchronization with hip-trajectory adaptation
CVA	Cerebrovascular accident
DCSA	Dynamic-Clustering Search Algorithm
DF	Dorsiflexion
DoF	Degree(s) of freedom
EMG	Electromyografy
FCSSA	Full-Curve-Scanning Search Algorithm
FD	(covered) Foot distance
FES	Functional electric stimulation
FMHD	Foot maximum horizontal displacement
FSM	Finit state-machine
GC	Gait cycle
GRNN	Generalized regression neural networks
GUI	Graphical user interface
IAT	Institute of Automation (U. Bremen)
IMU	Inertial measurement unit

KAFO	Knee-ankle-foot orthosis
MAE	Mean absolure error
MCP	Mopass Communication Protocol
MLPNN	Multi-layer perceptron neural network
MS	Multiple Sclerosis
NN	(Artificial) Neural Network
norm	normalized
PCHIP	Piecewise Cubic Hermite Interpolating Polynomial
PCHTA	Phase-control with hip-trajectory adaptation
PCS	Phase-control synchronization
PF	Plantarflexion
PI	Proportional-Integral
PID	Proportional-Integral-Derivative
P_M	Characteristic point
p-mRep	p most representative curves
PQHI	Piecewise Quintic Hermite Interpolation
PRSA	Progressive-Refinement Search Algorithm
P_S	Shaping point
R	Cross-correlation coefficient
RGRS	Robotic gait rehabilitation systems
RMSE	Root mean square error
ROM	Range of motion
ROMF	Range of motion factor
SCI	Spinal cord injury
SD	Standard deviation
SDAE	Standard deviation of the absolute errors
SL	Step length
SL_{norm}	Normalized step length
SMP	Schunk Motion Protocol
TBI	Traumatic brain injury
TCI	Therapist-controller interface
TF	Time factor
var	variance
VM	Virtual (physical) model
WS	Walking speed
WS_{norm}	Normalized walking speed

List of figures

List of tables

Appendix A: *Assessment of robot-based gait rehabilitation: a summary*

This appendix presents a very superficial summary of the findings of some of the clinical studies that have been carried out with robotic gait rehabilitation systems (RGRS). Table 32 shows some studies that reviewed the differences of walking with and without a RGRS, or the performance of the users before and after using the devices. Table 33, on the other hand, shows some findings of studies that compared robot-based rehabilitation with traditional physiotherapy by analyzing some gait related measurements. Studies that showed disadvantages of robotic rehabilitation are located at the end of the tables.

Table 32 Clinical trials assessing robotic gait rehabilitation

Reference	Subjects	Results
Swinnen, et.al (2014) [141]	9 studies were included (7 true experimental and 2 pre-experimental)	Significant improvements in balance scores measured with the Berg Balance Scale, the Tinetti test, postural sway tests, and the 'Timed Up and Go' test.
Fleerkotte, et.al (2014) [142]	10 individuals with chronic incomplete SCI	Improvements in walking speed, distance, TUG (Timed Up and Go), LEMS (Lower Extremity Motor Scores) and WISCI (Walking Index for Spinal Cord Injury).
		Participants kept the improvements at the eight-week follow-up.
		Slower walkers benefit the most from the training protocol.
Chernikova, et.al (2014) [143]	141 patients with post-stroke hemiparesis	Improvement of kinematic gait parameters (hip flexion/extension and hip abduction/adduction amplitudes, hip abduction/ adduction and knee flexion/extension torque amplitudes).
		Improvement of inter- and intra-joint dynamic interactions.
		Decrease of step asymmetry.
Varoqui, et.al (2014) [144]	15 chronic incomplete SCI subjects	Improvement in the voluntary-movement related active range of motion, maximal velocity and movement smoothness in ankle joint.
		Improvement in the maximal voluntary contraction in ankle dorsi- and plantar-flexor muscles.
		Improvement in the mobility and over-ground gait velocity.
Niu, et.al (2014) [216]	40 SCI subjects with spastic hypertonia at their ankles	Significant improvements in speed and functional mobility in subjects with initial high walking capacity, but no significant change in endurance.
		No significant improvement in subjects with low walking capacity.
Nardo, et.al (2014) [217]	9 patients with Parkinson's Disease	Improvements on spatio-temporal gait parameters.
		Improvements on the Unified Parkinson's Disease Rating Scale motor score.
		Kinematic and kinetic gait parameters did not show significant improvements.
Mirbagheri, et.al (2011) [218]	12 incomplete SCI subjects with different degrees of spasticity	Significant improvement in reflex stiffness and intrinsic (muscular) stiffness.
		Increased isometric maximum voluntary contraction (MVC) of ankle extensor and flexor muscles.
Mirbagheri, et.al (2012) [219]	12 incomplete SCI subjects with spasticity at their ankles	Improvement in patients with a higher reflex stiffness slope and intercept (Class 1).
		Improvement in reflex stiffness parameters in subjects who had lower baseline stiffness.
		Significant decrease in intrinsic intercept.
		No significant changes in intrinsic slope.
Calabro, et.al (2014) [220]	54-year-old female stroke survivor (3 years) with hemiparesis and spastic hypertonia	Moderate improvement in gait and balance.
		Significant increase in the patient's force regarding hip extension.
		Significant improvement both in functional and psychological and cognitive status.
Schueck, et.al (2013) [221]	Two individuals with chronic incomplete spinal cord injury and two with chronic stroke	Significant and relevant increase of gait speed in one subject (no significant changes shown by the other subjects).
		The subjects trained more actively and with more physiological muscle activity when using cooperative control.
Lo, et.al (2010) [222]	4 individuals with Parkinson's disease and freezing of gait (FOG) symptoms	Reduction in FOG (by self-report and clinician-rated scoring).
		Improvements in gait velocity, stride length, rhythmicity, and coordination.
del Ama, et.al (2015) [223]	18 chronic stroke survivors with hemiplegia	Improvements in knee and hip sagittal muscle balance scores.
		Decreased in ankle extensor balance score.
van Nunen, et.al (2014) [154]	30 first-ever stroke patients	Significant increase in walking speed, other walking- and mobility related tests, and strength of the paretic knee extensors relative to baseline at all assessments.

Reference	Subjects	Results
Krishnan, et.al (2013) [224]	6 young adults and 3 male chronic stroke survivors	Increased EMG activity of several lower extremity muscles (the participants were more actively engaged).
		Improvement in target-tracking task and performance with practice (in sound and impaired participants).
Krishnan, et.al (2012) [225]	52-year-old male stroke survivor	Considerable improvement in tracking accuracy and reduction in the kinematic variability of ankle trajectory.
		Improvements in muscle coordination.
		Substantial improvements in several standard clinical and functional parameters.
Stoller, et.al (2014) [226]	20 stroke survivors (<6 month) with severe motor limitations	Good to excellent test-retest reliability and appropriate repeatability for the most important peak cardiopulmonary performance parameters.
Westlake, et.al (2009) [153]	16 stroke survivors with chronic hemiparetic gait	Improvement of self-selected walk speed, paretic step length ratio, and four out of six secondary measures.
Wu, et.al (2014) [227]	30 chronic stroke survivors	Significant increase in walking speed.
		Resistance training was not superior to assistance training.
		Significant improvement in distance and balance for the assistance group but not for the resistance group.
Chisari, et.al (2014) [228]	15 patients with post-stroke hemiparesis	Increase of duration and covered distance.
		Decrease of body weight support and guidance force on the paretic side.
		No increase of force.
		Significant increase of firing rate of Vastus Medialis during asometric knee extension.
Borggraefe, et.al (2010) [229]	20 young patients with cerebral palsy	Significant improvements in dimension D (standing) and dimension E (walking).
van Kammen, et.al (2014) [145]	10 healthy participants	The temporal structure of the stepping pattern was altered when walking with robotic system (relative duration of the double support phase decreased as the single support phase increased).
		The differences between robot- and non-robot-assisted were most prominent at low walking speeds.
Hidler, et.al (2005) [230]	7 healthy people	Significant differences in the spatial and temporal muscle activation patterns.
		Significantly higher activity in the quadriceps and hamstrings during the swing phase while robot-assisted walking.
		Reduction of the activity in the ankle flexor and extensor muscles during robot-assisted walking.
Lapitskaya, et.al (2011) [147]	12 traumatic brain injury patients and 14 healthy controls	Reduction of the DAR (global delta-alpha EEG power ratio) in healthy subjects but not in patients.
		No changes in P300 latencies in neither group.
Neckel, et.al (2008) [148]	10 chronic hemi-paretic stroke subjects and 5 controls with matching age	Abnormal asymmetric joint torque patterns were generated.
		Kinematic patterns of the stroke subjects were similar to those of the control subjects.

Table 33 Clinical trials comparing robotic gait rehabilitation with conventional therapy

Reference	Subjects	Results
Shin, et.al (2014) [149]	60 incomplete SCI patients	Significant improvement in LEMS (lower extremity motor score), AMI (ambulatory motor index), SCIM3-M (Spinal Cord Independence Measure III mobility section), and WISCI-II (walking index for spinal cord injury version II) in both groups.
		Significant improvement for the robotic-assisted gait training group based on WISCI-II (no difference in the remaining variables).
Schwarz, et.al (2009) [150]	67 stroke survivors (mostly < 3 months)	Higher gains in ability to walk independently (functional ambulatory capacity score) and neurological status according to NIHSS (National Institutes of Health Stroke Scale) for robot-assisted group.
		No significant differences between groups after checking the participants who achieved independent walking based on secondary outcome measures of gait parameters.
Schwartz, et.al (2011) [231]	56 subacute SCI patients	Significant improvement in both the FAC (Functional Ambulation Category scale) score and the WISCI (Walking Index for SCI) score for both groups.
		Higher improvements in functional abilities (according to the SCIM score) in robot-assisted group.
Schwarz, et.al (2012) [232]	32 Multiple Sclerosis patients	No difference in improvements between the groups.
		Significant post-treatment improvements in FIM (Functional Independence Measure) and EDSS (Expanded Disability Status Scale) scores for both groups.
Tong, et.al (2006) [151]	46 stroke survivors (<6 weeks)	Significantly higher improvement in the 5-m walking speed test, Motricity Index, EMS (Elderly Mobility Scale), and FAC (Functional Ambulatory Category) for the robot-assisted group.
		Relative duration of stance and swing phase differed between patients and controls, and between robot-assisted and treadmill walking groups.
Dundar, et.al (2014) [152]	107 cases of new cerebral stroke	Significant improvements for all parameters (except lower extremity MASS scores) in both groups.
		Higher improvements in FIM, MMSE, all subparts of SF-36, and lower extremity categories in the BRS in the robot-assisted group.

Reference	Subjects	Results
Mayr, et.al (2007) [233]	16 stroke survivors (mostly < 3 months)	Significantly higher improvement for robot-assisted therapy based on EU-Walking Scale, Rivermead Motor Assessment Scale, 6-minute timed walking distance, Medical Research Council Scale, and Ashworth Scale.
Drużbicki, et.al (2010) [234]	6 to 14 years old children with cerebral palsy	Statistically significant improvement of balance in robot-assisted group, whereas improvement with no statistical significance in control group.
		Significantly higher improvement in robot-assisted group.
Alcobendas-Maestro, et.al (2012) [235]	80 incomplete SCI patients (3 to 6 months)	Walking speed in both groups did not differ.
		Better WISCI II (Walking Index for Spinal Cord Injury) in robot-assisted group.
		Better results in the 6-minute walk test and LEMS (Lower Extremity Motor Score) in robot-assisted group.
Calabro, et.al (2014) [220]	54-year-old female stroke survivor (3 years) with hemiparesis and spastic hypertonia	Improvements regarding mood, cognitive status and coping strategies compared other female patients with chronic stroke undergoing traditional rehabilitation.
Picelli, et.al (2012) [236]	41 patients with PD (Parkinson disease)	No statistical differences between groups based on baseline measures.
		Significant higher improvement in walking speed and distance in robot-assisted group.
Beer, et.al (2008) [237]	35 stable Multiple Sclerosis patients	Increase in walking velocity, walking distance and knee-extensor strength for robot-assisted group, whereas only in walking velocity in control group.
		Outcome values returned to baseline at follow-up after six months for both groups.
Husemann, et.al (2007) [238]	30 acute stroke survivors	Improvements in the walking ability in both groups.
		No significant difference in gain of functional ambulation category parameters between the groups.
		Significantly longer single stance phase on the paretic leg during over-ground walking for the robot-assisted group.
		The robot-assisted group lost fat mass and increased muscle mass, whereas the control group increased the body weight.
Gandolfi, et.al (2014) [239]	22 patients with MS (Multiple sclerosis)	No significant differences on primary and secondary outcome measures between groups.
		Significant improvements in both groups on the Berg Balance Scale.
		Changes approaching significance were found on gait speed (only) for robot-assisted group.
		Significant changes in balance task-related domains during standing and walking conditions for the control group.
Vaney, et.al (2011) [240]	67 patients with Multiple Sclerosis	Nonsignificant higher improvements of gait speed and quality of life in the walking group with respect to the robot-assisted group.
Fischer, et.al (2011) [68]	20 hemiparetic stroke patients	Significant improvement in 8-m walk test, a 3-minute walk test, and the Tinetti balance assessment in both groups.
Westlake, et.al (2009) [153]	16 stroke survivors with chronic hemiparetic gait	No significant differences in primary outcomes.
van Nunen, et.al (2015) [154]	30 first-ever stroke patients	No significant differences in improvements between groups.
Kelley, et.al (2013) [155]	20 adults with chronic stroke	No significant differences between groups.
		Improvements over time of lower extremity motor function and physical functional levels within both groups.
Wirz, et.al (2011) [156]	48 ambulatory chronic stroke survivors	Higher improvements in speed and single limb stance time on the impaired leg in subjects under therapist-assisted therapy.
		Improvement in perceived rating of the effects of physical limitations on quality of life only in subjects with severe gait deficits undergoing therapist-assisted therapy.
Hidler, et.al (2008) [146]	63 stroke survivors (<6 months)	Higher gains in walking speed and distance in conventional therapy.
		Secondary measures were not different between the two groups.
		The diversity of conventional gait training appears to be better for subacute stroke patients with moderate to severe gait impairments.

Appendix B: *Dynamic model of the MOPASS system*

The dynamic models are often used to develop model-based strategies for control and design. Dynamic models play an essential role in many linear and non-linear control systems methodologies, including model-based robust control and Lyapunov-based controller designs. Even though these model-based approaches present controller performance problems (such as robustness) if there exist significant un-modeled dynamics, when the model is accurate it allows the design of model-based controllers with strong capabilities [241]. The procedure to obtain the dynamic model of the *MOPASS* system is presented next.

The dynamic models are obtained based on all the DoF present in a system, both active and passive. In the case of *MOPASS*, the passive DoF have small ranges of motion, hence they were not taken into account in the dynamic model to avoid equations with much higher complexity. Similarly, the caster wheels are assumed to be self-aligning wheels that do not introduce non-holonomic constraints to the system; therefore they are also not part of the modeling process. To have a clearer understanding of the modeling process, a simplified model of *MOPASS* is shown in Fig. 138 with the frames *O* of all the joints that will be taken into account for the modeling.

To model this system, the Euler-Lagrange formulation [242] [243] was selected. The Lagrangian analysis is based on the energy properties of mechanical systems. The equations of motion of these systems are given by the Lagrange equation

$$\frac{d}{dt}\frac{\partial L}{\partial \dot{\boldsymbol{q}}} - \frac{\partial L}{\partial \boldsymbol{q}} = \boldsymbol{\xi} \ , \tag{64}$$

where $\boldsymbol{q}$ is the vector of generalized coordinates, $\boldsymbol{\xi}$ is the vector of generalized forces associated to the coordinates, and L is the Lagrangian defined as the difference between the kinetic (T) and the potential (U) energies

$$L(\boldsymbol{q}, \dot{\boldsymbol{q}}) = T(\boldsymbol{q}, \dot{\boldsymbol{q}}) - U(\boldsymbol{q}). \tag{65}$$

The equation of motion given in (64) can be rewritten in the general form

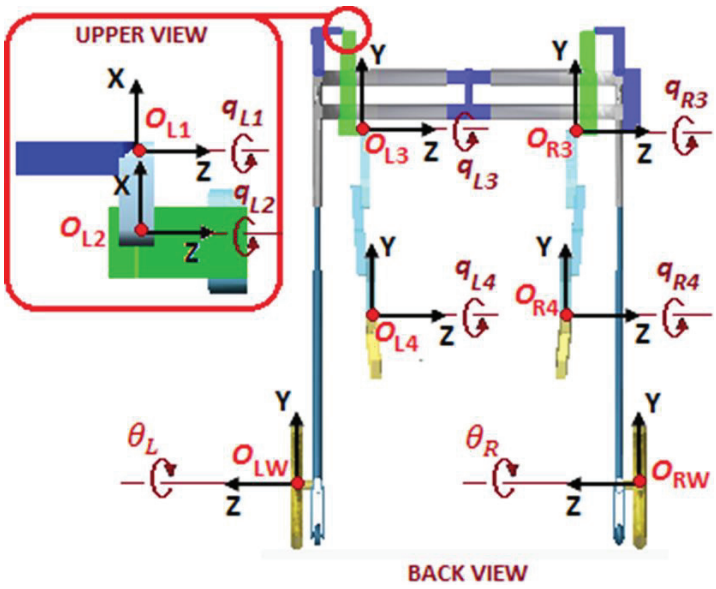

Fig. 138 Simplified model of *MOPASS* with its joint frames.

$$\boldsymbol{M}(\boldsymbol{q})\ddot{\boldsymbol{q}} + \boldsymbol{C}(\boldsymbol{q},\dot{\boldsymbol{q}})\dot{\boldsymbol{q}} + \boldsymbol{F_v}\dot{\boldsymbol{q}} + \boldsymbol{F_s}\mathrm{sgn}(\dot{\boldsymbol{q}}) + \boldsymbol{g}(\boldsymbol{q}) = \boldsymbol{\tau} + \boldsymbol{\tau_e} \ , \tag{66}$$

which represents the joint space dynamic model. In (66), $\boldsymbol{M}$ is the symmetric positive definite inertia matrix, $\boldsymbol{C}$ is the Coriolis/centripetal matrix, $\boldsymbol{g}$ is the gravity vector, and $\boldsymbol{\xi}$ was divided into the actuation torques $\boldsymbol{\tau}$, the viscous friction torques $\boldsymbol{F_v}\dot{\boldsymbol{q}}$, the static friction torques $\boldsymbol{F_s}\mathrm{sgn}(\dot{\boldsymbol{q}})$, and the torques $\boldsymbol{\tau_e}$ resulting from the interaction with the environment. $\boldsymbol{M}$ and $\boldsymbol{C}$ can be calculated in a straight forward way through the rotation and Jacobian matrices obtained from the kinematic analysis of the mechanical system

$$\boldsymbol{M}(\boldsymbol{q}) = \sum_{i=1}^{n} \Big(m_{l_i} \boldsymbol{J}_P^{(l_i)\,T} \boldsymbol{J}_P^{(l_i)} + \boldsymbol{J}_O^{(l_i)\,T} \boldsymbol{R}_i \, \boldsymbol{I}_{l_i}^{\boldsymbol{i}} \boldsymbol{R}_i^T \boldsymbol{J}_O^{(l_i)} + m_{m_i} \boldsymbol{J}_P^{(m_i)\,T} \boldsymbol{J}_P^{(m_i)} + \boldsymbol{J}_O^{(m_i)\,T} \boldsymbol{R}_{m_i} \, \boldsymbol{I}_{m_i}^{m_i} \boldsymbol{R}_{m_i}^T \boldsymbol{J}_O^{m_i} \Big) \ , \tag{67}$$

where n is the number of links (bodies), m_{l_i} and m_{m_i} are the mases of the link i (l_i) and motor rotor i (m_i), respectively, $\boldsymbol{R}_i$ and $\boldsymbol{R}_{m_i}$ are the rotation matrices from the frames of l_i and m_i to the base frame, $\boldsymbol{I}_{l_i}^{\boldsymbol{i}}$ is the inertia (constant) tensor of l_i referred to the link frame, $\boldsymbol{I}_{m_i}^{m_i}$ is the inertia (constant) tensor of m_i referred to the m_i frame, and $\boldsymbol{J}_P$ and $\boldsymbol{J}_O$ are the position and orientation Jacobian matrices relative to the joint velocities and are taken into account from the link at the beginning of the kinematic chain until the link being currently analyzed (i.e. from l_1 to l_i).

Matrix $\boldsymbol{C}$, on the other hand, can be calculated from $\boldsymbol{M}$ following

$$c_{ij} = \sum_{k=1}^{n} c_{ijk} \cdot \dot{q}_k$$

$$c_{ijk} = \frac{1}{2}\left(\frac{\partial b_{ij}}{\partial q_k} + \frac{\partial b_{ik}}{\partial q_j} - \frac{\partial b_{jk}}{\partial q_i} \right) \tag{68}$$

where c_{xy} and b_{xy} are the elements of matrices $\boldsymbol{C}$ and $\boldsymbol{M}$, respectively, in row x and column y, and c_{ijk} are Christoffel symbols of the first type.

The potential energy U can also be calculated using the kinematic relations following

$$U = -\sum_{i=1}^{n} \left(m_{l_i} \boldsymbol{g}_O^T \boldsymbol{p}_{l_i} + m_{m_i} \boldsymbol{g}_O^T \boldsymbol{p}_{m_i} \right) \ , \tag{69}$$

where $\boldsymbol{g}_o$ is the gravity acceleration vector with respect to the base frame, and $\boldsymbol{p}_{l_i}$ and $\boldsymbol{p}_{m_i}$ are the position vectors of l_i and m_i also with respect to the base frame. Finally, it is possible to get the components of the gravity vector from U following

$$g_i(\boldsymbol{q}) = \frac{\partial U}{\partial q_i} \ . \tag{70}$$

To have a more detailed explanation about the obtainment of matrices $\boldsymbol{M}$, $\boldsymbol{C}$ and $\boldsymbol{g}$ refer to [242]. For the modelling of *MOPASS* system, it must be taken into account that there exist two kinematic chains (one per leg) when calculating the Jacobians and, subsequently, the model matrices.

In the specific case of *MOPASS*, the vector of generalized coordinates has 13 items:

$$\boldsymbol{q} = [x_c, y_c, \varphi, \theta_R, \theta_L, q_{1R}, q_{2R}, q_{3R}, q_{4R}, q_{1L}, q_{2L}, q_{3L}, q_{4L}\ ]^T, \tag{71}$$

where the sub-indexes *1, 2, 3, 4, R* and *L* correspond to pelvis active joint, pelvis passive joint, hip, knee, right and left, respectively; (x_c, y_c) is the position of the chassis frame in the transverse plane with respect to the inertial frame (O_O), φ is the angle of rotation of the chassis about the longitudinal axis, and θ_R and θ_L are the wheels' rotation angles. For a better understanding please refer to Fig. 138 and Fig. 139.

Although the computation of (66) is straightforward, two important facts must be taken into account: 1) the actuation and interaction torques associated with x_c, y_c and φ have no physical meaning and therefore are equal to zero; and 2) the mobile platform possesses non-holonomic (kinematic) constraints [244] of the form

$$\boldsymbol{A(q)} \cdot \dot{\boldsymbol{q}} = \boldsymbol{0}. \tag{72}$$

These constraints refer to two basic assumptions introduced by the rolling properties of the driving wheels: 1) the velocity of the chassis frame must be in the direction of the axis of symmetry (i.e. the platform does not move sideward)

$$-\dot{x}_C \cdot \sin(\varphi) + \dot{y}_C \cdot \cos(\varphi) - d_{X1} \cdot \dot{\varphi} = 0 \tag{73}$$

and 2) the wheels do not slip

$$\begin{aligned} -\dot{x}_C \cdot \cos(\varphi) - \dot{y}_C \cdot \sin(\varphi) - b \cdot \dot{\varphi} + r \cdot \dot{\theta}_R = 0 \\ -\dot{x}_C \cdot \cos(\varphi) - \dot{y}_C \cdot \sin(\varphi) + b \cdot \dot{\varphi} + r \cdot \dot{\theta}_L = 0\ , \end{aligned} \tag{74}$$

where r is the radius of the driving wheels, b is the distance between the wheels and the axis of symmetry, and $d_{X1} \neq 0$ is the distance between the chassis frame and the wheels' rotation axis. The kinematic constrains introduce a new term in the dynamic model in (66):

$$\boldsymbol{M\ddot{q}} + \boldsymbol{C\dot{q}} + \boldsymbol{F_v\dot{q}} + \boldsymbol{F_s}\mathrm{sgn}(\dot{\boldsymbol{q}}) + \boldsymbol{g} + \boldsymbol{A^T\lambda} = \boldsymbol{\tau} + \boldsymbol{\tau_e}\ , \tag{75}$$

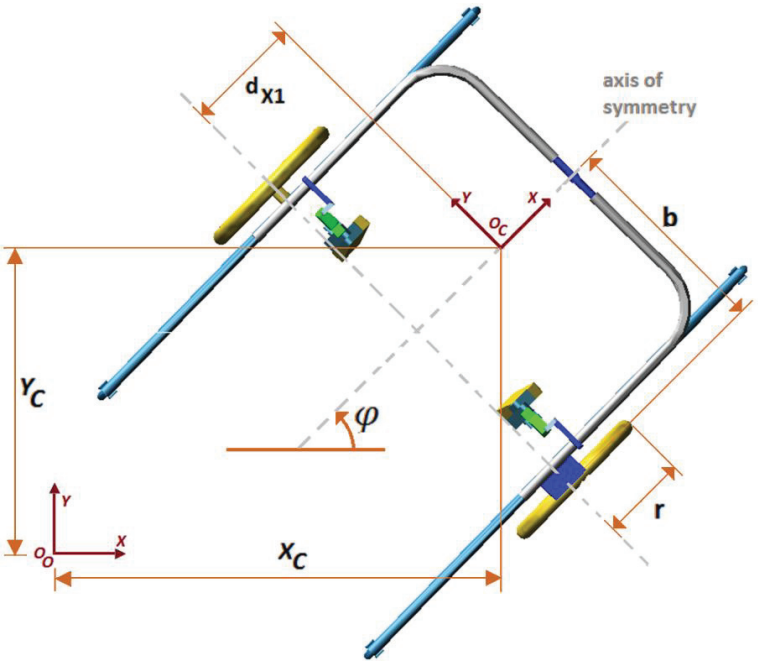

Fig. 139 Simplified model of *MOPASS* (upper view).

where $\boldsymbol{A}$ is the kinematic constraint matrix, $\boldsymbol{\lambda}$ is the vector of Lagrange multipliers, and $\boldsymbol{A^T\lambda}$ is the term related to the constraint forces. Now, it is possible to introduce a matrix $\boldsymbol{S(q)}$ that satisfies $\boldsymbol{A(q)S(q) = 0}$:

$$\boldsymbol{A} = \begin{bmatrix} -\sin(\varphi) & \cos(\varphi) & -d_{X1} & 0 & 0 & \\ -\cos(\varphi) & -\sin(\varphi) & -b & r & 0 & \mathbf{0_{3\times8}} \\ -\cos(\varphi) & -\sin(\varphi) & b & 0 & r & \end{bmatrix} \tag{76}$$

$$\boldsymbol{S} = \begin{bmatrix} \frac{r}{2b}(bc_\varphi - d_{X1}s_\varphi) & \frac{r}{2b}(bc_\varphi + d_{X1}s_\varphi) & \\ \frac{r}{2b}(bs_\varphi + d_{X1}c_\varphi) & \frac{r}{2b}(bs_\varphi - d_{X1}c_\varphi) & \mathbf{0_{3\times8}} \\ \frac{r}{2b} & -\frac{r}{2b} & \\ \multicolumn{3}{c}{\boldsymbol{I_{10\times10}}} & \end{bmatrix}, \tag{77}$$

where c_φ and s_φ stand for $\cos(\varphi)$ and $\sin(\varphi)$, respectively, $\boldsymbol{I}$ is an identity matrix and $\mathbf{0}$ is a null matrix. Noticing that $\boldsymbol{S^TA^T = 0}$ and $\boldsymbol{S^T(\tau + \tau_e) = \tau + \tau_e}$, pre-multiplying both sides of (75) by $\boldsymbol{S^T(q)}$ yields

$$\boldsymbol{S^T(M\ddot{q} + C\dot{q} + F_v\dot{q} + F_s\,\mathrm{sgn}(\dot{q}) + g) = \tau + \tau_e}. \tag{78}$$

This way, the vector of Lagrange multipliers is eliminated. Moreover, it is possible to obtain the kinematic (velocity) relation between x_c, y_c and φ and the generalized coordinates θ_R and θ_L subject to these constraints [245]:

$$\begin{bmatrix} \dot{x}_C \\ \dot{y}_C \\ \dot{\varphi} \end{bmatrix} = \frac{r}{2}\begin{bmatrix} c_\varphi - \frac{d_{X1}}{b}s_\varphi & c_\varphi + \frac{d_{X1}}{b}s_\varphi \\ s_\varphi + \frac{d_{X1}}{b}c_\varphi & s_\varphi - \frac{d_{X1}}{b}c_\varphi \\ 1/b & -1/b \end{bmatrix}\begin{bmatrix} \dot{\theta}_R \\ \dot{\theta}_L \end{bmatrix}, \tag{79}$$

where φ can be gotten by integrating $\dot{\varphi}$ in time and setting the initial value $\varphi(t = 0) = \varphi_0$:

$$\varphi = \frac{r}{2b}[1 \quad -1]\begin{bmatrix} \theta_R \\ \theta_L \end{bmatrix} + \varphi_0. \tag{80}$$

From above explanations, it can be seen that the final model possesses several parameters dependent on the mechanical design and construction, namely masses, inertia tensors, locations of the centers of mass and locations of the link frames. In practice, one might not be able to measure some (or all) of these values, nor to obtain them from the manufacturers. Hence, a parameter identification process is needed to complete the model. An overview of this process is shown in Fig. 140.

The Least Square estimation is the most commonly used method in robotic system identification. It makes use of the inverse dynamic model and estimates the unknown parameter set by minimizing the square error between measured and predicted torques. The dynamic model given in (78) must first be rewritten in the linear regression form

$$\boldsymbol{\tau = \phi(q, \dot{q}, \ddot{q})p}\,, \tag{81}$$

where $\boldsymbol{p}$ is the parameter vector which contains combinations of the unknown parameters and $\boldsymbol{\phi}$ is the regression matrix which contains the known parameters and the joint variables (i.e. positions, velocities and accelerations). In (75), the $\boldsymbol{\tau}_e$ is disregarded since, for the identification, there won't be any interaction torques acting on the system ($\boldsymbol{\tau}_e = \boldsymbol{0}$). By using

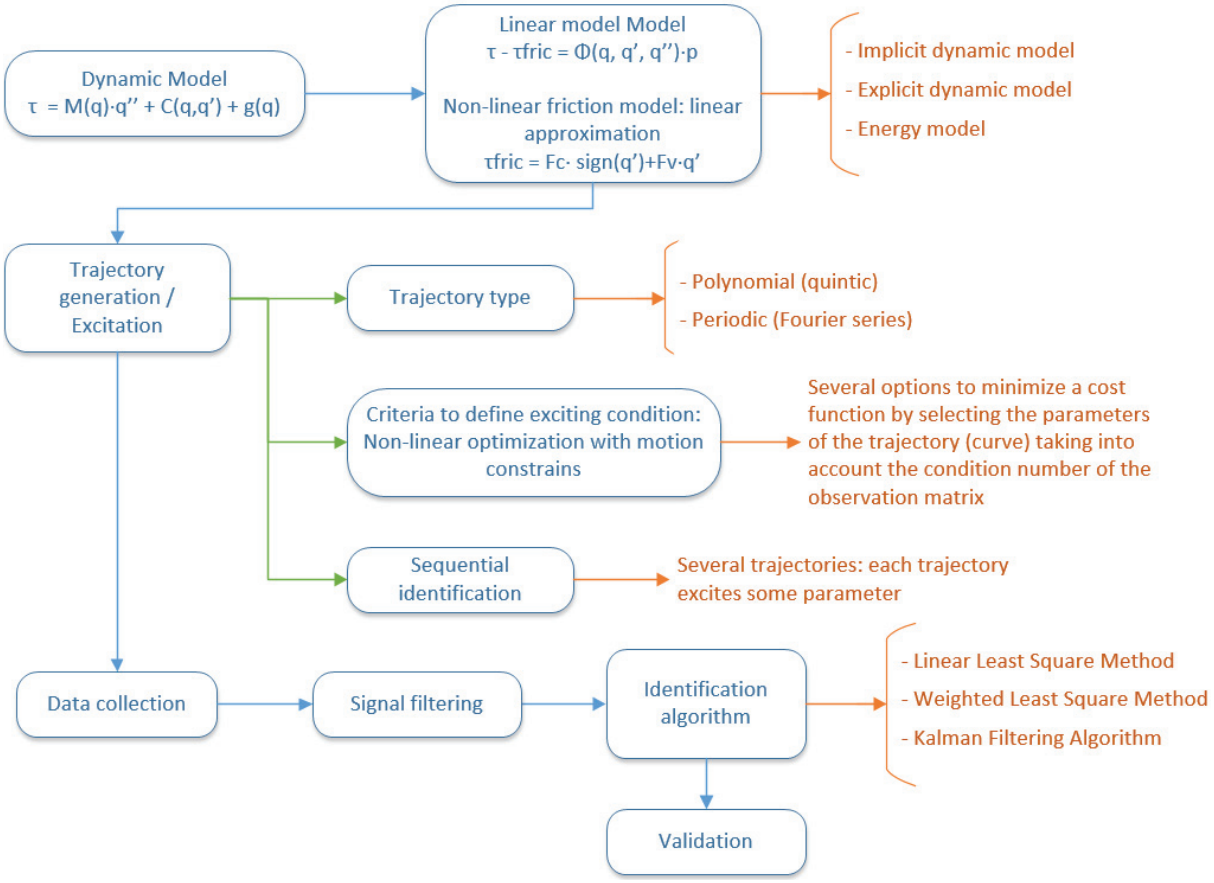

Fig. 140 Overview of the dynamic model's parameter identification process

measured motion data, the parameter set can be estimated from the overdetermined linearized system:

$$\boldsymbol{Y}(\boldsymbol{\tau}) = \boldsymbol{H}(\boldsymbol{q}, \dot{\boldsymbol{q}}, \ddot{\boldsymbol{q}})\boldsymbol{p} + \boldsymbol{e}\ , \tag{82}$$

where $\boldsymbol{Y}$ is the accumulation matrix, $\boldsymbol{H}$ is the observation matrix and $\boldsymbol{e}$ is the vector of residual errors between the predicted and actual input torques. Now, the parameter vector can be obtained [246]:

$$\boldsymbol{p} = (\boldsymbol{H}^{\boldsymbol{T}}\boldsymbol{H})^{-1}\boldsymbol{H}^{\boldsymbol{T}}\boldsymbol{Y}(\boldsymbol{\tau})\ . \tag{83}$$

The selection of the parameter vector $\boldsymbol{p}$ can have a big influence on the identification result. In fact, only the minimum parameter vector that is sufficient to describe the dynamic model, known as the Base Parameter Set, can form reliable and accurate identification results. Moreover, a selection on optimal exciting trajectories (i.e. the trajectories that the robot will follow helped with a non-model-based position controller to obtain the experimental data) must be also done to obtain good identification results. A proper trajectory for identification must 'excite' the dynamics of the system as much as possible while maintaining the motion constraints in all joints. Once the experimental data is obtained and filtered, the estimated elements of the parameter vector can be calculated with (83). To have a more detailed explanation on system identification, including the selection of the parameter vector and the exciting trajectories, refer to [246] [247] [248] [249] [250].

Appendix C: *Step-by-step procedure for automatic extraction of characteristic points*

This appendix contains a detailed explanation of the procedure of the characteristic knots extraction for hip and knee joints, based on the concept for trajectory generation explained in section 4.2, including the selection conditions and thresholds. These are the steps taken after the resampling of the filtered data and the calculation of the normalized time values, the time factor (*TF*), the range of motion (*ROM*) and the ROM factor (*ROMF*).

Steps for the hip joint

1. Extraction of all local and global extrema points.
   1.1. Select the global minimum as the hip characteristic point P_{M2}
   1.2. Select the global maximum as one of the remaining three hip characteristic points, namely P_{M1}, P_{M3} and P_{M4}. Only until the end of the procedure it will be possible to know to which of the three the global maximum will correspond (step 9).
2. If there is more than one local maximum, go to step 3; if not, go to step 5.
3. Select the couple of local extrema (P_{min2} and P_{max2}), different from the global extrema P_{min} and P_{max}, that are more apart from each other and that fulfill the following conditions:
   a. The angular difference, normalized with respect to the ROM, between P_{max2} and P_{min} is higher than a threshold $HTH_{\theta 1} = 80$:

$$(\theta_{max2} - \theta_{min}) \cdot ROMF > HTH_{\theta 1} \tag{84}$$

   This ensures that the selected points are in the higher part of the curve, avoiding noisy local extrema in the lower part.

   b. The absolute normalized time difference between P_{max2} and P_{max} is higher than a threshold $HTH_{t1} = 2$ and lower than a threshold $HTH_{t2} = 30$:

$$HTH_{t2} > |t_{max2} - t_{min}|_m \cdot TF > HTH_{t1} \tag{85}$$

   This ensures that the selected points are in the vicinity of the global maximum, but not to near in order to avoid noisy local extrema. The subscript m is used to indicate that $|t_{max2} - t_{min}|$ corresponds to the minimum time difference between the two points, taking into account that the curve is periodic. This must be borne in mind also for the next conditions.

   c. The absolute normalized time difference between P_{max2} and P_{min2} is higher than a threshold $\alpha \cdot HTH_{t3}$:

$$|t_{max2} - t_{min}|_m \cdot TF > \alpha \cdot HTH_{t3} \tag{86}$$

   where $HTH_{t3} = 2$ and

$$\alpha = \begin{cases} & b < HTH_{b1} \quad \cap \\ 3 \quad ; & P_{min2} \text{ and } P_{min2} \text{ are in opposite sides} \\ & \text{from } P_{min} \text{ in the original curve} \\ & b < HTH_1 \quad \oplus \\ 2 \quad ; & P_{min2} \text{ and } P_{min2} \text{ are in opposite sides} \\ & \text{from } P_{min} \text{ in the original curve} \\ 1 \quad ; & \text{otherwise} \end{cases} \tag{87}$$

where $HTH_{b1} = 0.08$ is a (normalized) velocity threshold, $\cap$ is the *AND* operand, $\oplus$ is the *Exclusive OR* operand, and

$$b = \frac{\theta_{max2} - \theta_{min2}}{|t_{max2} - t_{min2}|_m \cdot TF} \tag{88}$$

4. If a set of local extrema was not found in step 3, go to step 5; if a set was found, set the two local extrema from the set as the two remaining characteristic points and proceed to step 9.
5. Get the cycle samples P_i where the angular difference, normalized with respect to the ROM, between P_i and P_{min} is higher than a threshold $HTH_{\theta 2}$

$$(\theta_{max2} - \theta_{min}) \cdot ROMF > HTH_{\theta 2} \tag{89}$$

where

$$HTH_{\theta 2} = \begin{cases} 80 \quad ; & |t_i - t_{min}|_m \cdot TF < 10 \\ 90 \quad ; & \text{otherwise} \end{cases} \tag{90}$$

6. From the subset of samples gotten in step 5, obtain all couple of samples *(P_i, P_j)* that fulfill the following conditions:

$$(t_j - t_i) \cdot TF > HTH_{t4} \tag{91}$$

$$|b_2| > HTH_{b2} \tag{92}$$

$$b_1/b_2 > HTH_{b3} \tag{93}$$

$$b_3/b_2 > HTH_{b3} \tag{94}$$

where $HTH_{t4} = 2$, $HTH_{b2} = 0.4$, $HTH_{b3} = 2$, and

$$b_1 = \frac{|\theta_{max} - \theta_j| \cdot ROMF}{|t_{max} - t_j|_* \cdot TF} \tag{95}$$

$$b_2 = \frac{|\theta_i - \theta_j| \cdot ROMF}{|t_i - t_j|_* \cdot TF} \tag{96}$$

$$b_3 = \frac{|\theta_i - \theta_{min}| \cdot ROMF}{|t_i - t_{min}|_* \cdot TF} \tag{97}$$

The subscript * is used to indicate that the time difference $|t_x - t_y|$ must be calculated in the interval between t_x and t_y where there are no global extrema in between. If, for instance, $t_i < t_{max} < t_{min}$, $|t_i - t_{min}|_*$ would correspond to $|t_i + T_C - t_{min}|$ and not to $|t_i - t_{min}|$.

7. If no samples were obtained from step 6, go to step 8; if a set of samples was gotten, obtain the couple of samples *(P_{inf1}, P_{inf2})* from that set that minimizes the cost function $C_b = b_1 - b_2 + b_3$ and set them as the two remaining hip characteristic points. The objective behind steps 6 and 7 is to obtain the points in the high part of the hip curves that cause higher bending in the curve's form.
8. If the procedure achieves this step, it means that the hip curve being analyzed has only one set of (significant) extrema (the global minimum and maximum points), without any other prominent change of shape. Therefore, the remaining two characteristic points will correspond to the two samples with time values t_i=t_{max}*-1/TF* and t_i=t_{max}*-2/TF*. Finally, proceed to step 9.
9. Organize, based on the time values, the obtained characteristic points so that they match the points' order introduced in section 4.2. The time value of the resulting points is the one normalized with respect to the cycle period.

Steps for the knee joint

1. Extraction of all local extrema points and the global minimum point.
   1.1. Select the global minimum as the knee characteristic point P_{M3}
2. Get the first sample to the left of the global minimum (P_{M3}) that fulfills the following conditions:
   a. The absolute value of the velocity in the sample is lower that a threshold KTH_{v1} *= 0.1 [Rad/s]*:

$$\left|\frac{\theta_i - \theta_{i-1}}{t_i - t_{i-1}}\right| < KTH_{v1} \tag{98}$$

   b. A lower-resolution velocity in the n^{th} sample ahead is higher than a threshold KTH_{v2} *= -0.2 [Rad/s]*:

$$\frac{\theta_{i-n\_} - \theta_i}{t_{i-n\_} - t_i} > KTH_{v2} \quad ; \quad n = \max(0, i - 50) \tag{99}$$

   c. The sample is at least $0.15 \cdot T_C$ away from the global minimum

$$|t_i - t_{min}|_m \geq 0.15 \cdot T_C \tag{100}$$

   d. The angular difference between the sample and the global maximum, normalized to the ROM of the cycle, is lower than a threshold $KTH_{\theta 1}$ *= 25*:

$$(\theta_i - \theta_{min}) \cdot ROMF > KTH_{\theta 1} \tag{101}$$

The objective of the previous conditions is to find the first point in which the knee curve changes drastically its shape after the maximum flexion point happened.

3. If no sample fulfilled the conditions in step 2, go to step 6; if a sample was found proceed with step 4.
4. Obtain the local/global maximum point to the left of the sample gotten in step 2 (P_{step2}) that is the closest to P_{step2} and fulfills the following condition
   a. The normalized time difference between the extrema and P_{step2} is lower than a threshold $HTH_{t1} = 5$:

$$|t_{step2} - t_i|_m \cdot TF < HTH_{t1} \tag{102}$$

5. If no maximum was found in step 4, set the sample obtained in step 2 as the knee characteristic point P_{M2}; if there was a maximum fulfilling all conditions of step 4, set it as the knee characteristic point P_{M2}. Proceed to step 7.
6. Obtain the local/global maximum point to the left of the global minimum that is closest to the global minimum and fulfills the conditions ***c*** and ***d*** from step 2, and set it as the knee characteristic point P_{M2}.
7. Get the first sample to the right of the global minimum (P_{M3}) that fulfills the following conditions:
   a. The absolute value of the velocity in the sample is lower than a threshold $KTH_{v1} = 0.1$ *[Rad/s]*:

$$\left|\frac{\theta_i - \theta_{i-1}}{t_i - t_{i-1}}\right| < KTH_{v1} \tag{103}$$

   b. A lower-resolution velocity in the n^{th} sample ahead is lower than a threshold $KTH_{v3} = 0.2$ *[Rad/s]*:

$$\frac{\theta_{i-n\_} - \theta_i}{t_{i-n\_} - t_i} < KTH_{v3} \quad ; \quad n = \min(n-1, i+50) \tag{104}$$

   c. The sample is at least $0.15 \cdot T_C$ away from the global minimum

$$|t_i - t_{min}|_m \geq 0.15 \cdot T_C \tag{105}$$

The objective of the previous conditions is to find the first point in which the knee curve changes drastically its shape after the maximum flexion point happened.[29]

8. If no sample fulfilled the conditions in step 7, go to step 11; if a sample was found proceed with step 9.
9. Obtain the local/global maximum point to the right of the sample gotten in step 7 (P_{step7}) that is the closest to P_{step7} and fulfills the following condition
   a. The normalized time difference between the extrema and P_{step7} is lower than a threshold $HTH_{t1} = 5$:

[29] Conditions ***a***. and ***b***. are not considered when the cycle's boundary comes in between the samples taken for the formulations, e.g. when $i = 0$ in condition ***a***., or when $i < 50$ in condition ***b***.

$$(t_i - t_{step7}) \cdot TF < HTH_{t1} \tag{106}$$

10. If no maximum was found in step 9, set the sample obtained in step 7 as the knee characteristic point P_{M4}; if there was a maximum fulfilling all conditions of step 9, set it as the knee characteristic point P_{M4}. Proceed to step 12.
11. Obtain the local/global maximum point to the right of the global minimum that is closest to the global minimum and fulfills the condition $\boldsymbol{c}$ from step 2, and set it as the knee characteristic point P_{M4}. Continue with step 12.
12. Obtain the local minimum that lays in between P_{M2} and P_{M4} (in the region where P_{M3} is not located) that possesses the lowest angular value and that fulfills the following conditions:
    a. Either the absolute value of the angular difference, normalized with respect to the ROM, between the minimum point and P_{M4} is higher that a threshold $KTH_{\theta 2} = 5$:

    $$(\theta_i - \theta_{M4}) \cdot ROMF > KTH_{\theta 2} \ , \tag{107}$$

    or the difference in normalized time between the minimum point and P_{M4} is higher than a threshold $KTH_{t2} = 10$:

    $$|t_i - t_{M4}|_m > KTH_{t2} \tag{108}$$

    b. Either the absolute value of the angular difference, normalized with respect to the ROM, between the minimum point and P_{M2} is higher that a threshold $KTH_{\theta 2} = 5$:

    $$(\theta_i - \theta_{M2}) \cdot ROMF > KTH_{\theta 2} \ , \tag{109}$$

    or the difference in normalized time between the minimum point and P_{M2} is higher than a threshold $KTH_{t2} = 10$:

    $$|t_i - t_{M2}|_m > KTH_{t2} \tag{110}$$

13. If no local minimum was located in step 12, proceed to step 14; it there was a local minimum fulfilling the conditions from step 12, set the selected minimum as the knee characteristic point P_{M1}. Proceed to step 15.
14. Set the sample that is located in the middle of P_{M2} and P_{M4}. Proceed to step 15.
15. Organize, based on the time values, the obtained characteristic points so that they match the points' order introduced in section 4.2. The time value of the resulting points is the one normalized with respect to the cycle period.

Appendix D: *Error measurements between fitted and measured characteristic points*

This appendix contains the tables with the measurements of the mean absolute errors (MAE), standard deviation of the absolute errors and root mean square errors (RMSE) calculated from the experimental data and the estimated values obtained with the neural networks from section 4.3.2. It contains the error measurements from the neural networks trained with the data from all the subjects, as well as the one trained with the data from the selected subject who scored the highest correlation coefficients. The error measurements for the one-subject-based neural networks were computed with respect to the experimental data of the selected subject, as well as to the data of the other subjects.

Training the NN using data from all the subjects

Table 34 Mean absolute errors (MAE) training the NNs with all processed data

	MAE															
	HIP								*KNEE*							
	t_{M1}	θ_{M1}	t_{M2}	θ_{M2}	t_{M3}	θ_{M3}	t_{M4}	θ_{M4}	t_{M1}	θ_{M1}	t_{M2}	θ_{M2}	t_{M3}	θ_{M3}	t_{M4}	θ_{M4}
WS_{norm}	5.99	3.76	1.84	2.72	3.79	3.29	4.55	3.67	1.77	4.08	3.33	5.61	3.55	3.62	1.48	5.49
cad	6.29	4.24	1.61	3.13	3.88	3.68	4.75	4.08	1.74	4.09	3.34	6.39	3.50	3.60	1.53	5.56
SL_{norm}	6.00	3.48	2.35	2.58	3.87	3.17	4.48	3.48	1.85	4.12	3.38	5.51	3.75	3.66	1.60	5.72
WS_{norm} & *cad*	5.80	3.41	1.62	2.54	3.47	3.11	4.44	3.38	1.75	3.96	3.31	5.27	3.48	3.52	1.45	5.41
WS_{norm} & SL_{norm}	5.82	3.41	1.61	2.54	3.48	3.10	4.43	3.39	1.73	3.94	3.30	5.30	3.49	3.52	1.46	5.39
cad & SL_{norm}	5.82	3.40	1.60	2.54	3.47	3.10	4.42	3.39	1.73	3.94	3.30	5.28	3.47	3.50	1.45	5.44

Table 35 Standard deviation of the absolute errors training the NNs with all processed data

	SD absolute error															
	HIP								*KNEE*							
	t_{M1}	θ_{M1}	t_{M2}	θ_{M2}	t_{M3}	θ_{M3}	t_{M4}	θ_{M4}	t_{M1}	θ_{M1}	t_{M2}	θ_{M2}	t_{M3}	θ_{M3}	t_{M4}	θ_{M4}
WS_{norm}	4.24	2.67	1.57	2.22	3.28	2.45	3.29	2.57	3.19	2.77	4.01	4.08	3.58	2.72	1.23	3.89
cad	4.34	3.11	1.43	2.58	3.47	2.79	3.41	2.93	3.27	2.79	4.03	4.76	3.66	2.72	1.25	3.93
SL_{norm}	4.16	2.49	2.05	1.99	3.22	2.26	3.19	2.43	3.16	2.85	4.08	4.16	3.94	2.72	1.39	4.15
WS_{norm} & *cad*	4.20	2.45	1.43	1.94	2.92	2.22	3.05	2.38	3.09	2.76	3.98	3.98	3.59	2.66	1.20	3.84
WS_{norm} & SL_{norm}	4.25	2.45	1.43	1.95	2.93	2.23	3.07	2.37	3.11	2.76	3.97	3.98	3.59	2.68	1.21	3.84
cad & SL_{norm}	4.23	2.44	1.43	1.96	2.94	2.23	3.05	2.37	3.09	2.76	3.96	3.95	3.59	2.65	1.20	3.84

Table 36 Root mean square errors (RMSE) training the NNs with all processed data

	RMSE															
	HIP								*KNEE*							
	t_{M1}	θ_{M1}	t_{M2}	θ_{M2}	t_{M3}	θ_{M3}	t_{M4}	θ_{M4}	t_{M1}	θ_{M1}	t_{M2}	θ_{M2}	t_{M3}	θ_{M3}	t_{M4}	θ_{M4}
WS_{norm}	7.34	4.61	2.42	3.51	5.02	4.10	5.61	4.48	3.65	4.93	5.21	6.94	5.04	4.53	1.93	6.73
cad	7.64	5.26	2.15	4.06	5.21	4.62	5.85	5.02	3.70	4.95	5.23	7.97	5.07	4.51	1.98	6.80
SL_{norm}	7.31	4.28	3.12	3.26	5.03	3.89	5.50	4.24	3.66	5.01	5.29	6.90	5.44	4.56	2.13	7.06
WS_{norm} & *cad*	7.16	4.20	2.16	3.20	4.53	3.82	5.38	4.14	3.55	4.82	5.17	6.60	5.00	4.41	1.88	6.64
WS_{norm} & SL_{norm}	7.21	4.20	2.15	3.20	4.55	3.82	5.39	4.14	3.56	4.81	5.16	6.63	5.00	4.43	1.90	6.61
cad & SL_{norm}	7.19	4.19	2.14	3.20	4.55	3.81	5.38	4.13	3.54	4.81	5.15	6.60	4.99	4.40	1.89	6.66

Training the NN using data from the selected subject

Table 37 Mean absolute errors (MAE) using the selected-subject NNs, calculated with respect to the selected subject's experimental data

	MAE															
	HIP								*KNEE*							
	t_{M1}	θ_{M1}	t_{M2}	θ_{M2}	t_{M3}	θ_{M3}	t_{M4}	θ_{M4}	t_{M1}	θ_{M1}	t_{M2}	θ_{M2}	t_{M3}	θ_{M3}	t_{M4}	θ_{M4}
WS_{norm}	2.28	1.49	1.08	1.27	1.66	1.55	2.15	1.45	1.00	1.31	2.40	2.11	1.56	1.60	1.04	2.25
cad	2.30	1.69	1.01	1.48	1.72	1.71	2.17	1.79	1.00	1.44	2.42	2.41	1.59	1.67	1.10	2.27
SL_{norm}	2.39	1.42	1.23	1.22	1.66	1.45	2.18	1.42	1.05	1.50	2.40	2.20	1.65	1.68	1.15	2.27
WS_{norm} & *cad*	2.18	1.28	1.04	1.11	1.74	1.30	2.08	1.31	1.01	1.40	2.39	2.08	1.56	1.60	1.04	2.14
WS_{norm} & SL_{norm}	2.24	1.25	1.01	1.16	1.60	1.30	2.19	1.21	1.01	1.30	2.38	2.07	1.56	1.65	1.04	2.17
cad & SL_{norm}	2.21	1.31	1.04	1.17	1.77	1.29	2.17	1.22	1.03	1.41	2.36	2.05	1.55	1.58	1.03	2.15

Table 38 Standard deviation of the absolute using the selected-subject NNs, calculated with respect to the selected subject's experimental data

	SD absolute errors															
	HIP								*KNEE*							
	t_{M1}	θ_{M1}	t_{M2}	θ_{M2}	t_{M3}	θ_{M3}	t_{M4}	θ_{M4}	t_{M1}	θ_{M1}	t_{M2}	θ_{M2}	t_{M3}	θ_{M3}	t_{M4}	θ_{M4}
WS_{norm}	2.63	1.16	0.85	1.01	1.87	1.16	1.76	1.25	0.83	1.10	2.72	1.61	1.45	1.22	0.85	1.60
cad	2.58	1.36	0.85	1.15	1.93	1.25	1.74	1.43	0.82	1.09	2.70	1.88	1.47	1.19	0.83	1.54
SL_{norm}	2.74	1.09	0.96	0.97	1.88	1.15	1.77	1.20	0.86	1.22	2.81	1.66	1.52	1.27	0.92	1.54
WS_{norm} & *cad*	2.57	0.97	0.83	0.89	1.91	0.99	1.71	1.06	0.85	1.06	2.71	1.60	1.43	1.22	0.81	1.51
WS_{norm} & SL_{norm}	2.57	0.93	0.85	0.93	1.73	1.02	1.76	1.00	0.82	1.06	2.72	1.59	1.43	1.24	0.81	1.51
cad & SL_{norm}	2.55	0.95	0.84	0.94	1.89	1.02	1.73	1.01	0.83	1.07	2.72	1.60	1.42	1.19	0.81	1.50

Table 39 Root mean square errors (RMSE) using the selected-subject NNs, calculated with respect to the selected subject's experimental data

	RMSE															
	HIP								*KNEE*							
	t_{M1}	θ_{M1}	t_{M2}	θ_{M2}	t_{M3}	θ_{M3}	t_{M4}	θ_{M4}	t_{M1}	θ_{M1}	t_{M2}	θ_{M2}	t_{M3}	θ_{M3}	t_{M4}	θ_{M4}
WS_{norm}	3.48	1.89	1.37	1.62	2.50	1.93	2.78	1.92	1.30	1.71	3.63	2.65	2.13	2.01	1.34	2.76
cad	3.46	2.17	1.32	1.87	2.58	2.11	2.78	2.29	1.29	1.81	3.62	3.06	2.16	2.05	1.37	2.74
SL_{norm}	3.63	1.79	1.56	1.56	2.51	1.85	2.80	1.86	1.35	1.93	3.69	2.76	2.24	2.10	1.48	2.74
WS_{norm} & *cad*	3.37	1.61	1.34	1.42	2.58	1.63	2.69	1.69	1.32	1.75	3.62	2.62	2.12	2.01	1.31	2.62
WS_{norm} & SL_{norm}	3.41	1.56	1.32	1.48	2.35	1.66	2.80	1.57	1.30	1.68	3.61	2.61	2.12	2.07	1.32	2.64
cad & SL_{norm}	3.37	1.62	1.34	1.50	2.58	1.64	2.77	1.59	1.32	1.77	3.60	2.60	2.10	1.98	1.31	2.62

Table 40 Mean absolute errors (MAE) using the selected-subject NNs, calculated with respect to the other subjects' experimental data

	MAE															
	HIP								*KNEE*							
	t_{M1}	θ_{M1}	t_{M2}	θ_{M2}	t_{M3}	θ_{M3}	t_{M4}	θ_{M4}	t_{M1}	θ_{M1}	t_{M2}	θ_{M2}	t_{M3}	θ_{M3}	t_{M4}	θ_{M4}
WS_{norm}	6.08	7.02	2.21	3.13	4.26	7.04	4.73	6.13	1.84	5.44	3.50	8.19	3.65	3.79	1.60	8.85
cad	6.39	8.98	1.76	3.74	4.68	8.42	4.87	7.56	1.90	5.45	3.49	10.38	3.65	3.87	1.66	9.61
SL_{norm}	6.24	5.88	2.95	3.12	4.24	6.18	4.74	5.52	1.96	5.64	3.87	7.20	4.02	3.95	1.97	8.16
WS_{norm} & *cad*	6.29	8.64	1.76	4.07	3.80	8.69	5.72	8.10	1.86	5.73	3.61	8.13	3.70	3.80	1.84	10.33
WS_{norm} & SL_{norm}	6.74	7.60	1.75	3.33	4.95	7.74	4.85	7.30	1.77	5.14	3.97	8.44	3.69	3.86	1.78	9.09
cad & SL_{norm}	6.32	7.86	1.74	3.75	3.81	8.97	4.66	8.39	1.87	5.61	3.78	8.50	3.68	3.90	1.85	8.98

Table 41 Standard deviation of the absolute errors using the selected-subject NNs, calculated with respect to the other subjects' experimental data

	SD absolute errors															
	HIP								*KNEE*							
	t_{M1}	θ_{M1}	t_{M2}	θ_{M2}	t_{M3}	θ_{M3}	t_{M4}	θ_{M4}	t_{M1}	θ_{M1}	t_{M2}	θ_{M2}	t_{M3}	θ_{M3}	t_{M4}	θ_{M4}
WS_{norm}	5.91	4.27	1.82	2.53	3.34	3.80	4.36	3.96	3.50	3.74	4.41	5.94	3.92	3.17	1.35	5.71
cad	6.53	5.27	1.56	2.87	3.43	4.39	4.64	4.55	3.51	3.73	4.37	7.12	3.82	3.35	1.58	6.02
SL_{norm}	5.46	3.83	2.22	2.39	3.33	3.61	4.04	3.76	3.67	3.93	4.61	5.72	4.33	3.23	1.73	5.66
WS_{norm} & *cad*	6.26	5.69	1.53	3.19	3.17	5.72	5.41	5.93	3.48	3.95	4.45	6.01	4.01	3.15	1.48	6.40
WS_{norm} & SL_{norm}	6.74	5.20	1.52	2.76	4.07	4.82	4.60	5.59	3.56	3.59	4.50	6.07	4.01	3.28	1.47	5.90
cad & SL_{norm}	6.27	4.68	1.50	3.07	3.17	5.12	4.14	6.03	3.49	3.80	4.62	6.13	4.01	3.24	1.49	5.86

Table 42 Root mean square errors (RMSE) using the selected-subject NNs, calculated with respect to the other subjects' experimental data

	RMSE															
	HIP								*KNEE*							
	t_{M1}	θ_{M1}	t_{M2}	θ_{M2}	t_{M3}	θ_{M3}	t_{M4}	θ_{M4}	t_{M1}	θ_{M1}	t_{M2}	θ_{M2}	t_{M3}	θ_{M3}	t_{M4}	θ_{M4}
WS_{norm}	8.48	8.21	2.86	4.02	5.41	8.00	6.43	7.30	3.95	6.60	5.63	10.12	5.36	4.94	2.09	10.53
cad	9.14	10.41	2.35	4.71	5.81	9.49	6.73	8.82	3.99	6.61	5.59	12.59	5.29	5.12	2.29	11.34
SL_{norm}	8.29	7.01	3.69	3.93	5.39	7.16	6.23	6.67	4.16	6.88	6.02	9.20	5.91	5.10	2.63	9.93
WS_{norm} & *cad*	8.87	10.35	2.33	5.17	4.95	10.40	7.87	10.04	3.95	6.96	5.73	10.11	5.46	4.94	2.36	12.15
WS_{norm} & SL_{norm}	9.53	9.20	2.32	4.32	6.40	9.12	6.69	9.19	3.98	6.27	6.00	10.39	5.45	5.06	2.31	10.84
cad & SL_{norm}	8.90	9.15	2.30	4.84	4.96	10.33	6.23	10.33	3.96	6.78	5.98	10.48	5.45	5.06	2.37	10.72

Appendix E: *Regenerated trajectories using the characteristic points estimated by the neural networks*

This appendix shows examples of curves generated by interpolating the characteristic knots estimated by the neural networks and some shaping knots (calculated with *Method 1* from section 4.3.3). The first part includes the curves generated using the neural networks that were trained using the data from all the subjects that participated in the experiment, whereas for the second part only the data from the subject that scored the highest correlation coefficients was used. This appendix is complementary to the curves presented in section 4.3.2, where the complete explanations of the figures in given. Two type of figures are shown here: Fig. 141, Fig. 143, Fig. 145 and Fig. 147 show examples of the curves, whereas Fig. 142, Fig. 144, Fig. 146 and Fig. 148 depict the values of the second input depending on the first input used to generate the plots (b), (c) and (d) from the figures showing the examples, respectively.

Using data from all the subjects

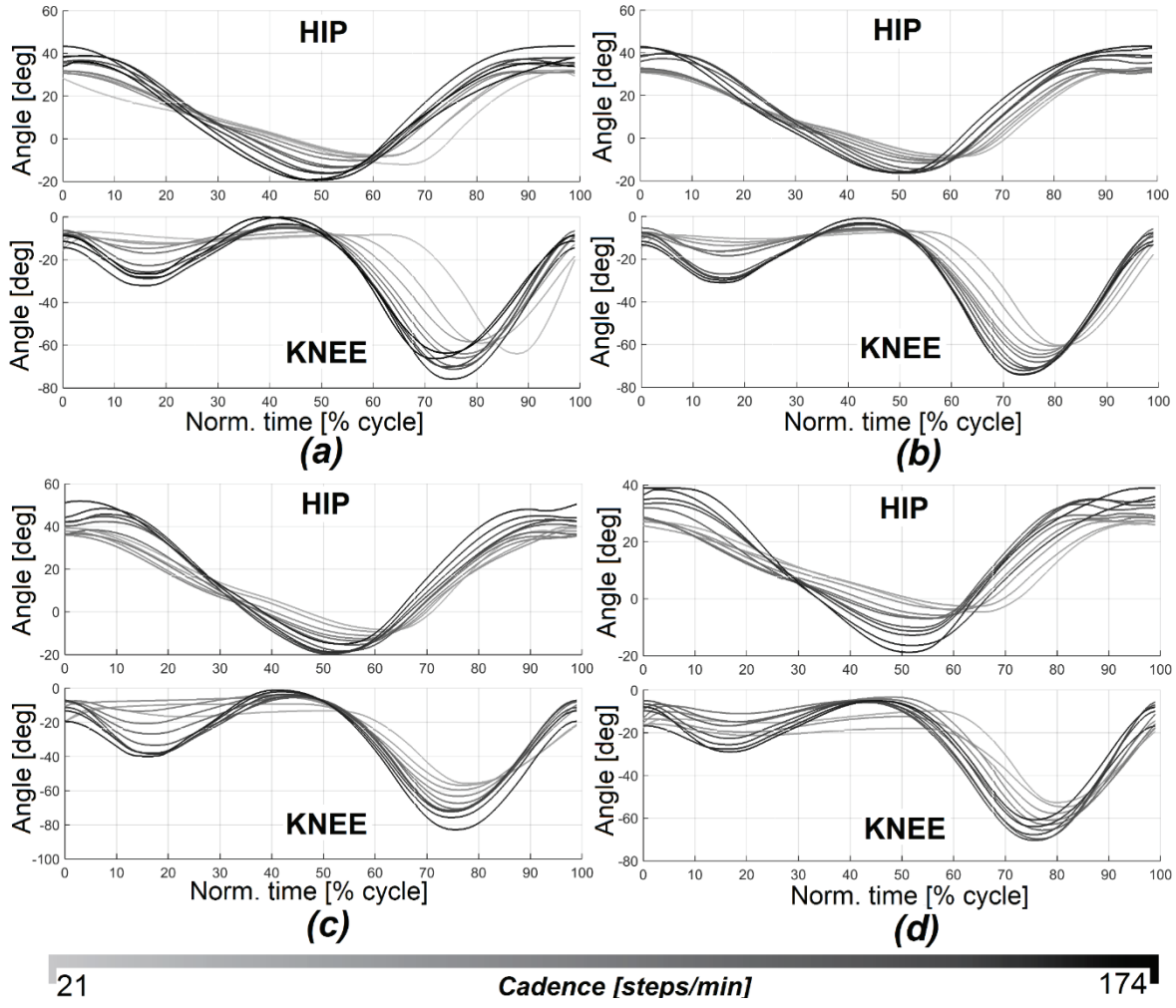

Fig. 141 Generation of hip and knee trajectories depending on *cad* (a) and $cad\&SL_{s,norm}$ (b,c,d) using data from all subjects

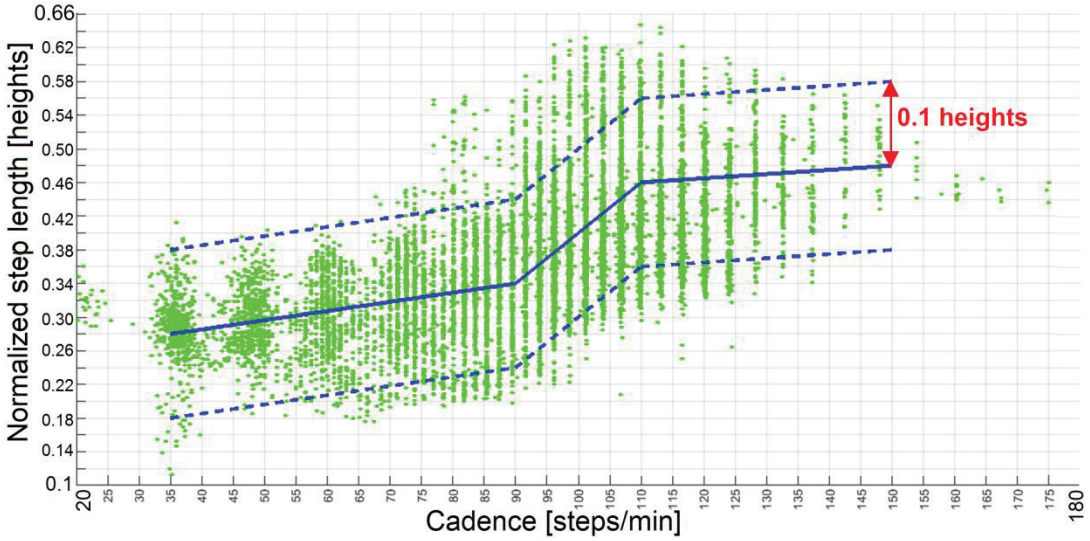

Fig. 142 $SL_{s,norm}$ vs *cad* input values for curve generation using all subjects' data

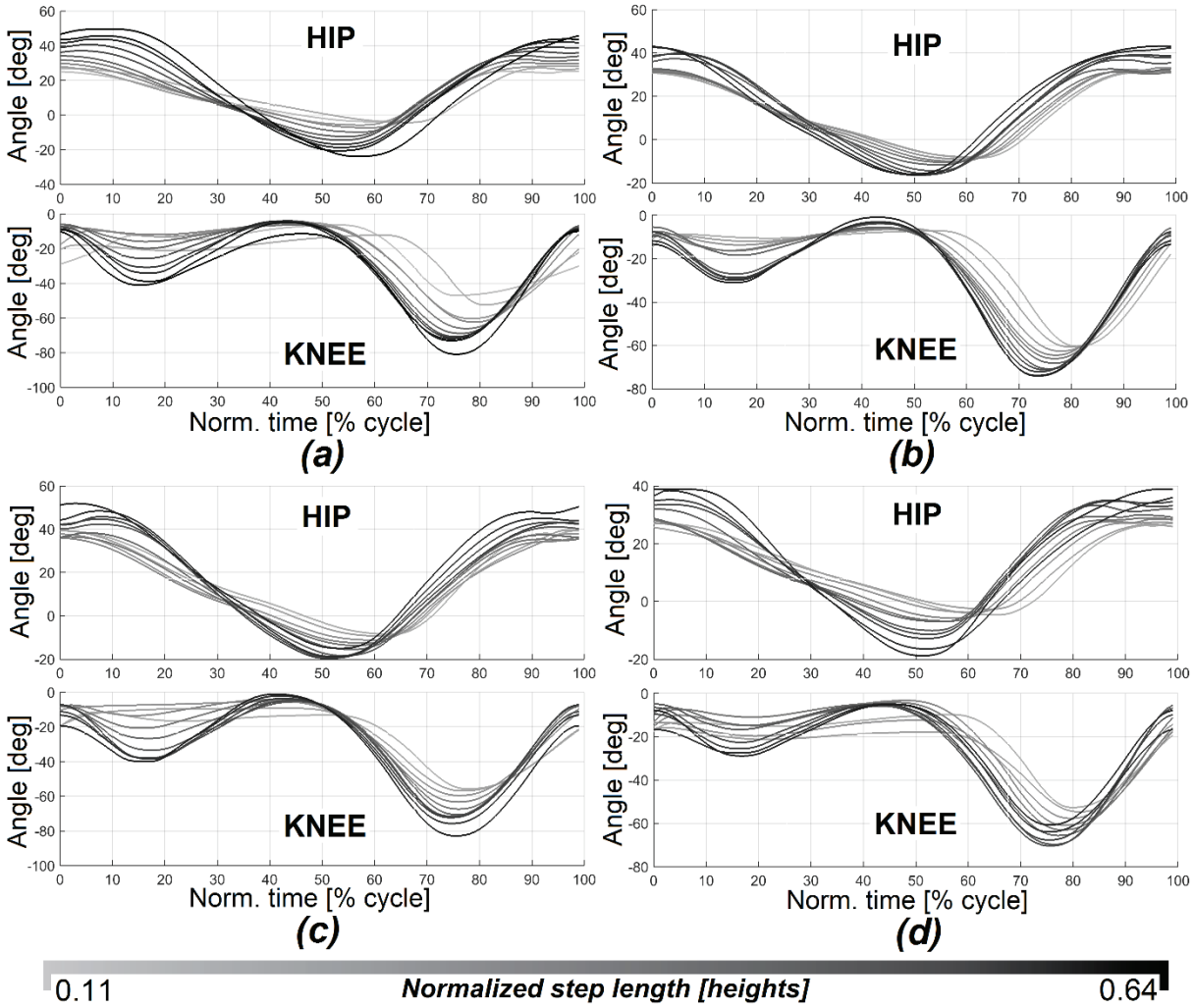

Fig. 143 Generation of hip and knee trajectories depending on $SL_{s,norm}$ (a) and $WS_{s,norm}$& $SL_{s,norm}$ (b,c,d) using data from all subjects

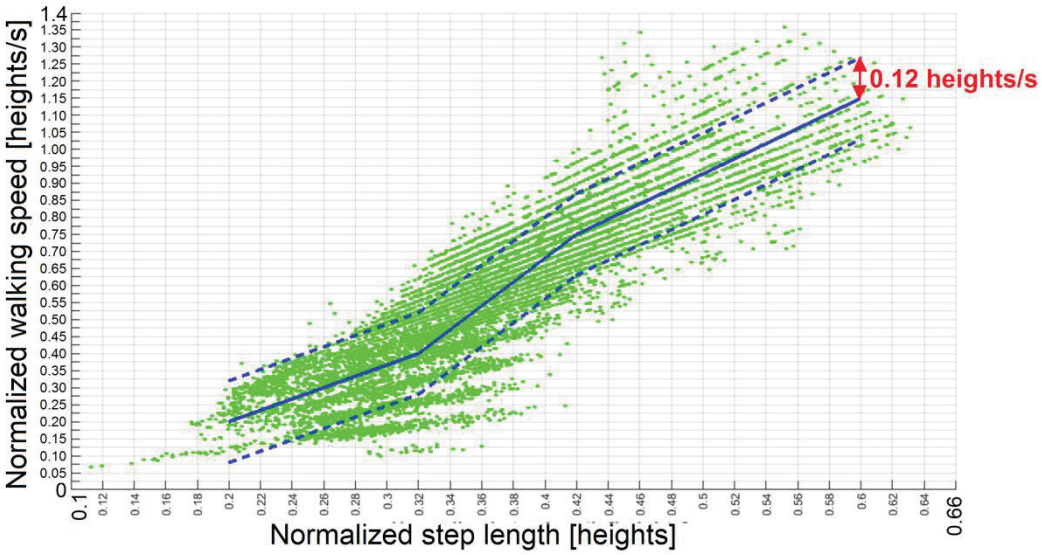

Fig. 144 $WS_{s,norm}$ vs $SL_{s,norm}$ input values for curve generation using all subjects' data

Using data from the selected subject

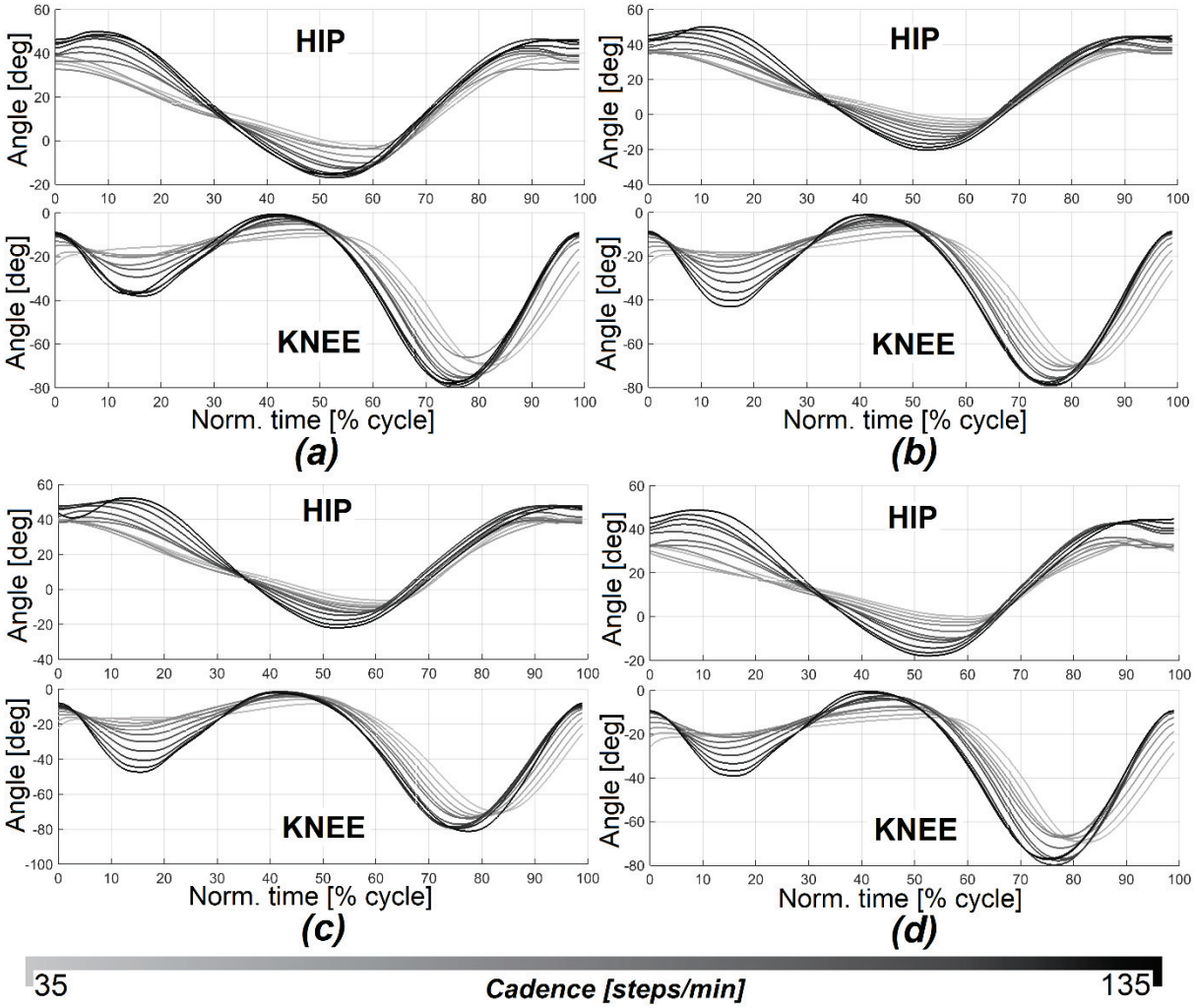

Fig. 145 Generation of hip and knee trajectories depending on *cad* (a) and $cad\&SL_{s,norm}$ (b,c,d) using data from the selected subject

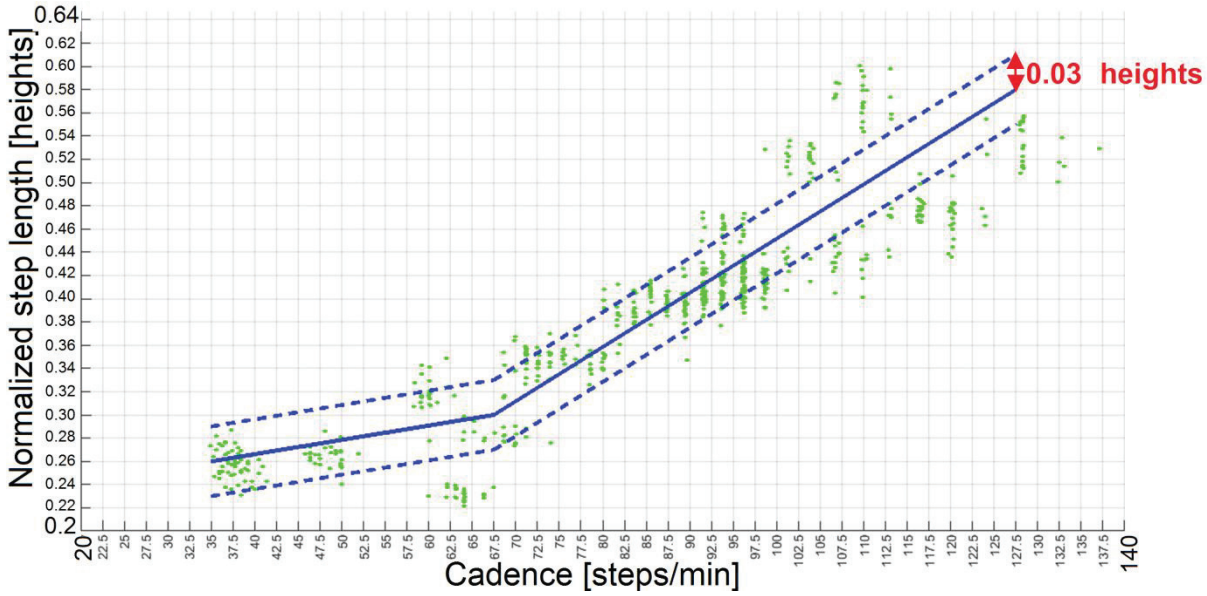

Fig. 146 $SL_{s,norm}$ vs *cad* input values for curve generation using the selected subject's data

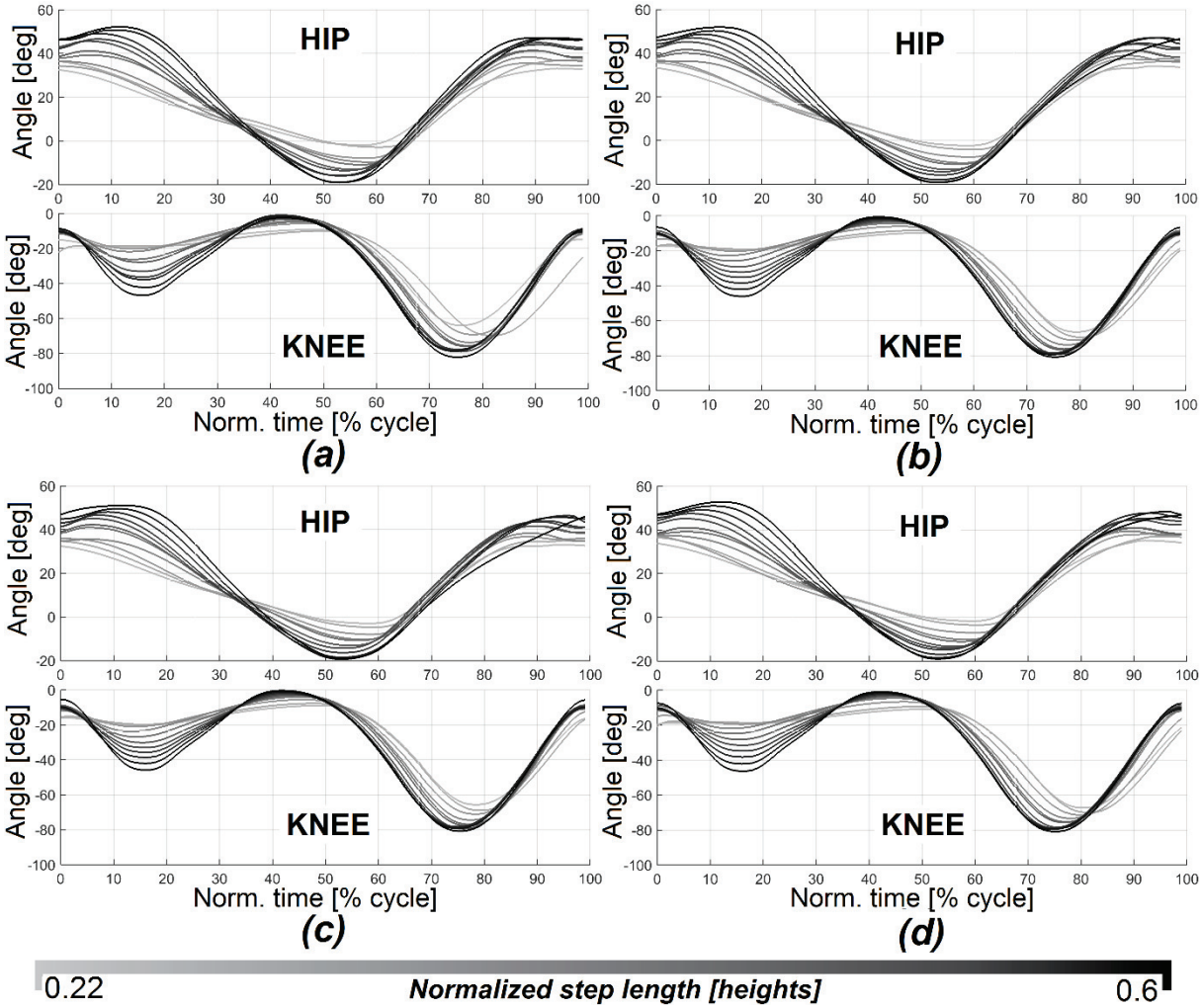

Fig. 147 Generation of hip and knee trajectories depending on $SL_{s,norm}$ (a) and $WS_{s,norm}$& $SL_{s,norm}$ (b,c,d) using data from the selected subject

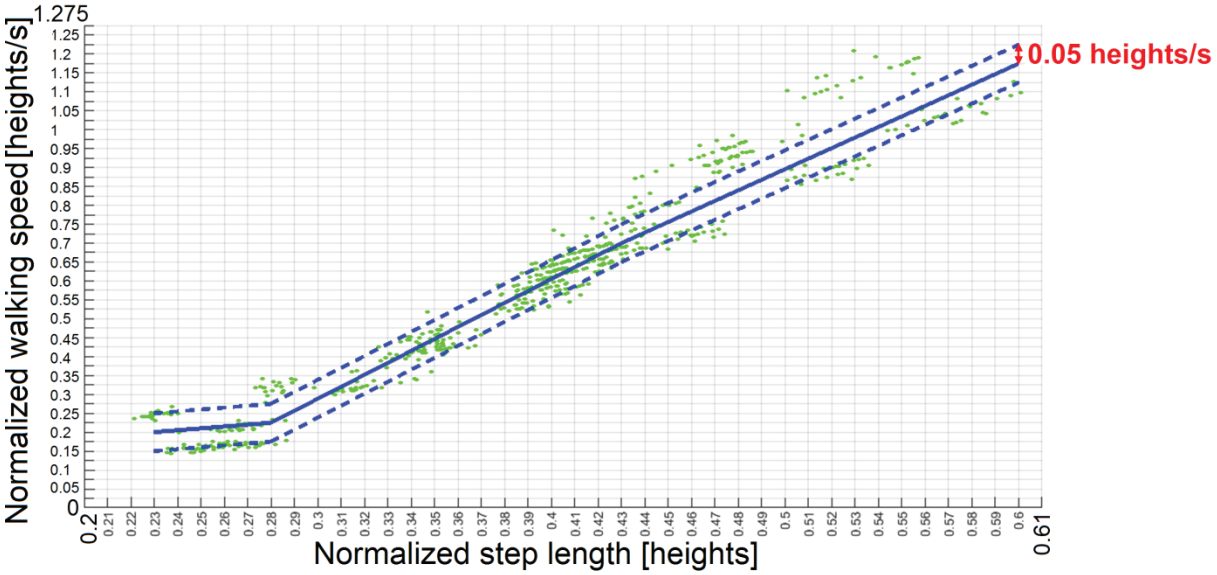

Fig. 148 $WS_{s,norm}$ vs $SL_{s,norm}$ input values for curve generation using the selected subject's data